In-Chain Poly(phosphonate)s:

Synthesis, Degradation and Biomedical Applications

Dissertation

Zur Erlangung des akademischen Grades eines

„Doctor rerum naturalium (Dr. rer. nat.)“

Im Promotionsfach Chemie

des Fachbereiches Chemie, Pharmazie, Geowissenschaften (FB09)

der Johannes Gutenberg-Universität

vorgelegt von

Kristin Bauer

geboren in Heppenheim

JOHANNES GUTENBERG UNIVERSITÄT MAINZ

JG|U Max-Planck-Institut für Polymerforschung

Max Planck Institute for Polymer Research

Dekan:

1. Gutachter:

2. Gutachter:

Die vorliegende Arbeit wurde in der Zeit von Februar 2014 bis November 2017 angefertigt. Hiermit versichere ich, die vorliegende Arbeit selbstständig und ohne Benutzung anderer als der angegebenen Hilfsmittel angefertigt zu haben. Alle Stellen, die wörtlich oder sinngemäß aus Veröffentlichungen oder anderen Quellen entnommen sind, wurden als solche eindeutig kenntlich gemacht. Diese Arbeit ist in gleicher oder ähnlicher Form noch nicht veröffentlicht und auch keiner anderen Prüfungsbehörde vorgelegt worden.

Kristin Bauer

Mainz, November 2017

„Nur wenige wissen,
wie viel man wissen muss, um zu wissen,
wie wenig man weiß.“

-Werner Heisenberg-

Für meine Familie

Danksagung

Abstract

Nature on planet earth is dominated by poly(phosphoester)s (PPEs). They structure and determine life in the form of deoxy- & ribonucleic acid (DNA & RNA), and, as pyrophosphates, they store up chemical energy in organisms. Polymer chemistry, however, is dominated by the non-degradable polyolefins and degradable polycarboxylic esters (PCEs) that are produced on a large scale today. Recent work has illustrated the potential of PPEs for future applications beyond flame-retardancy -the main application of PPEs today-, and provided a coherent vision to implement this classic biopolymer in modern applications that demand biocompatibility and degradability as well as the possibility to adjust the properties to individual needs.

Chapter 1 describes the preparation of in-chain poly(phosphonate)s via acyclic diene metathesis polymerization of three different monomers. Novel unsaturated phosphonate monomers with asymmetric structure have been developed, that are accessible via a three-step synthesis. The prepared poly(phosphonate)s exhibit the stable carbon-phosphorus linkage in the polymer backbone, which changes the nature of the degradation products compared to other poly(phosphoester)s. Polymers with molecular weights up to 28 000 g mol^{-1} were prpared and have been characterized in detail by NMR spectroscopy, size exclusion chromatography, thermogravimetry, and differential scanning calorimetry. They have been also compared to structural analogues polyphosphates with respect to crystallization (SAXS, WAXS) and their rheological behavior. Also solution grown crystals were analyzed rendering some of prepared poly(phosphonate)s as interesting defect poly(ethylene)-like structures.

Chapter 2 focuses on the evaluation of the six-membered cyclic 2-alkyl-1,3,2-dioxaphosphinane-2-oxides as novel monomers for the preparation of poly(phosphoester)s with altered backbone structure by ring-opening polymerization. As representative 2-alkyl-1,3,2-dioxaphosphinane-2-oxides (MPPn) was prepared, which showed increased stability compared to its five-membered analogon facilitating the preparation and further handling. MPPn was attempted to polymerize with standard catalysts, that are well-established for the polymerization of five-membered cyclic phosphoesters. For all applied catalysts no polymerization was observed, which can probably be attributed to the low ring-strain of six-membered cyclic phosphoesters.

Chapter 3 focuses on the introduction of phostones**,** i.e. 2-alkoxy-2-oxo-1,3-oxaphospholanes, as novel monomer class for the preparation of linear PPEs by ring-opening polymerization. Phostones have the stable P-C-bond within the cycle, which leads to a dramatic increase of the

monomer stability towards hydrolysis and long shelf-lives. Two phostone-monomers containing ethoxy or butoxy pendant chains were prepared in a single step synthesis from inexpensive starting materials avoiding the usage of $SOCl_2$ or $POCl_3$. Polymers with ethoxy side chains are water-soluble without a lower critical solution temperature, non-toxic against murine macrophages, and hydrolytically degradable under basic conditions. The polymerization kinetics for different catalyst systems were evaluated for both monomers in order to identify optimal polymerization conditions, resulting in poly(phosphonate)s with molecular weights between 3000 and 25100 g mol^{-1} with reasonable molecular weight dispersities (<1.6).

Chapter 4 focuses on the preparation of PPE-based surfactants for the non-covalent and straightforward surface modification of nanocarriers. For nanocarriers long blood circulation times are crucial for efficient drug delivery. A critical parameter for the circulation time is the so-called protein 'corona', which forms upon exposure to biological fluids by physical adsorption of proteins. An unspecific adsorption of proteins leads to an enhanced recognition by cells of the immune system and to decreased blood circulation times. The typical approach to meet this problem is the decoration of the nanocarrier surface with polymer chains. Recently, hydrophilic PPEs were identified to induce a similar stealth effect like poly (ethylene glycol). In this chapter, the non-covalent adsorption of structurally diverse PPE-surfactants to prepare stealth nanocarriers is exploited. The prepared surfactants were evaluated in detail concerning their toxicity, degradation behavior and interaction with proteins. All considered surfactant-coated nanocarriers showed increased blood circulation times and it was found that the variation of the PPE-structure can influence the protein corona composition formed around polystyrene nanoparticles.

Chapter 5. focuses on the further development of PPE-based surfactants for the modification of nanocarriers. In this chapter functional mannose-moieties were included in the surfactant structure allowing targeting of mannose-receptor presenting cells. PPE-surfactants with altered amount and location of mannose moieties were prepared. The surfactant synthesis was conducted in a two-step protocol starting with the ring-opening polymerization of cyclic phosphoester monomers and subsequent mannosylation by thiol-Michael addition. Subsequently, the surfactants were assembled on the surface of nanocarriers consisting of different materials and the cellular uptake towards mannose-receptor presenting macrophages and dendritic cells was evaluated. Enhanced cellular uptake was observed for nanocarriers coated with PPE-surfactants containing a high amount and density of mannose moieties.

Chapter 6 focuses on the detailed investigation of the hydrolytic degradation of three different PPE-classes, i.e. poly(phosphate)s, in-chain and side-chain poly(phosphonate)s, exhibiting different binding patterns around the central phosphorus atom The degradation studies were conducted in aqueous media under acidic and basic conditions and the degradation process was followed by NMR spectroscopy. Under acidic conditions no degradation was observed while under basic conditions degradation was observed for all considered polymers with distinct different degradation profiles. Detailed NMR spectroscopic investigation indicated a degradation mechanism proceeding by backbiting of the terminal alcohol group similar to the mechanism proposed for the degradation of poly(lactic acid) (PLA) is most likely. Moreover, it was found that the aggregation behavior in aqueous media play a key role in the hydrolytic degradation of the considered polymers.

Zusammenfassung

Der Einsatz von Polymeren als Biomaterialien hat wesentlich zum Fortschritt der modernen Medizin beigetragen. Insbesondere abbaubare Polymere sind von besonderem Interesse für biomedizinische Anwendungen, da sie aus dem Körper ausgeschieden werden können, nachdem sie ihre Aufgabe erfüllt haben. Für Biomaterialien ist es entscheidend, die chemischen und physikalischen Eigenschaften sowie das Abbauverhalten präzise einstellen zu können, um sie den jeweiligen Anforderungen anzupassen

Aufgrund ihrer potentiellen Bioabbaubarkeit und -kompatibilität sind Polyphosphoester (PPEs) in besonderem Maße relevant für den Einsatz als Biomaterialien. Außerdem erlaubt die Pentavalenz des Phosphors eine Vielzahl an Möglichkeiten, um gewünschte Eigenschaften präzise einzustellen: Die Art der organischen „Spacer“ im Polymerrückgrat erlaubt eine Variation der Polarität und ist entscheidend für das Kristallisationsverhalten von PPEs, während das Bindungsmotiv um das zentrale Phosphoratom entscheidend ist, um ihr Abbauprofil zu beeinflussen. Zusätzlich kann die Seitenkette zur Einführung von funktionellen Gruppen verwendet werden.

Im Zuge dieser Arbeit wurden verschiedene Monomere entwickelt, die durch gezielte Strukturveränderungen, die Synthese von PPEs mit variablen Eigenschaften bzgl. Löslichkeit, Abbauverhalten und Stabilität ermöglichen und vereinfachen.

Weiterhin wurden PPEs mit unterschiedlichen Bindungsmotiven hinsichtlich ihrer kürzlich entdeckten „Stealth“-Eigenschaften untersucht, indem PPE-basierte Tenside synthetisiert und zur Oberflächenmodifikation von Nanopartikeln unterschiedlicher Materialien eingesetzt und bezüglich ihrer Blutzirkulationszeiten untersucht wurden. Im nächsten Schritt wurden PPE-Tenside zusätzlich mit Mannose-Einheiten modifiziert, die einen gezielte Adressierung von Zellen des Immunsystems erlauben. Es konnte gezeigt werden, dass die Oberflächenmodifikation von Nanopartikeln mit PPE-Tensiden bei geringem synthetischen Aufwand sowohl zu verlängerten Blutzirkulationszeiten als auch zur zielgerichteten Adressierung bestimmter Zellen geeignet ist. Zum Abschluss wurden PPEs mit unterschiedlichen Bindungsmotiven hinsichtlich ihrer Abbaubarkeit unter basischen Bedingungen untersucht, wobei gezeigt werden konnte, dass schon kleine strukturelle Variationen zu signifikant veränderten Abbauprofilen führen.

Graphical abstract

2. Chapter 1: In-Chain Poly(phosphonate)s via Acyclic Diene Metathesis Polycondensation…….81

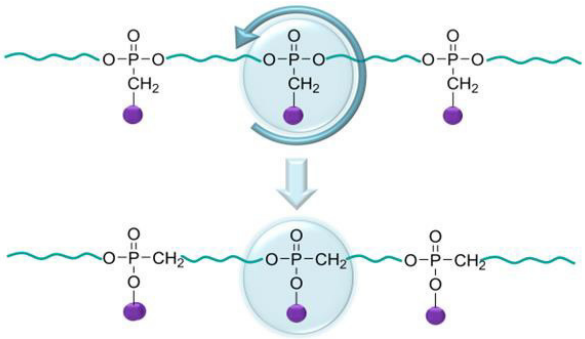

3. 2-Methyl-1,3,2-dioxaphosphinane-2-oxide as new monomer for the preparation of linear poly(phosphoester)s……...119

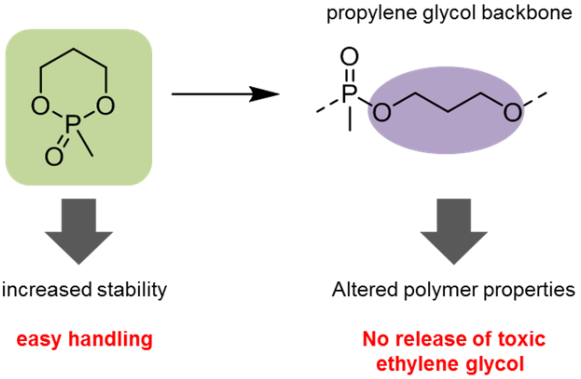

4. Chapter 3: Polymerizing phostones: A fast way to in-chain poly(phosphonate)s with adjustable hydrophilicity……133

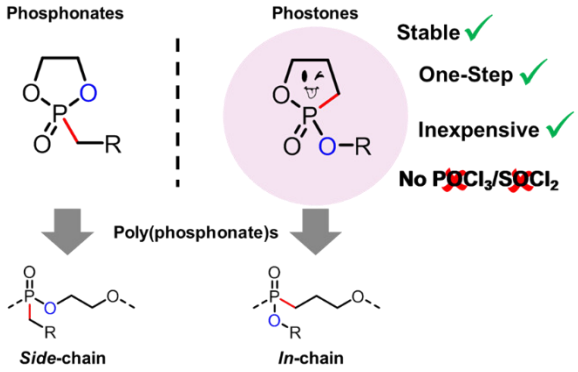

5. Chapter 4: Polyphosphoester stealth surfactants: A general strategy to control the protein corona and the fate of nanocarriers……..179

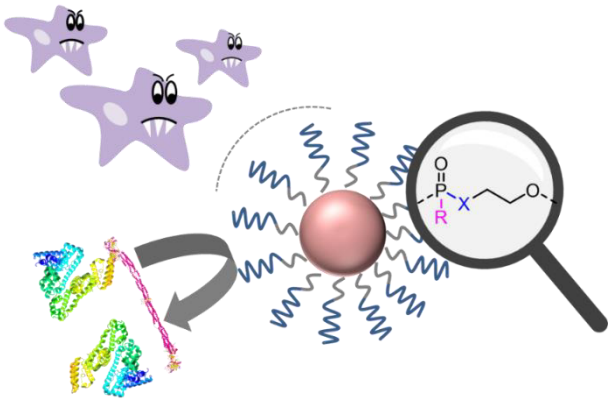

6. Chapter 5: Active targeting of mannose-receptor presenting cells with nanocarriers coated with mannosylated biodegradable polyphosphoester-surfactants……...241

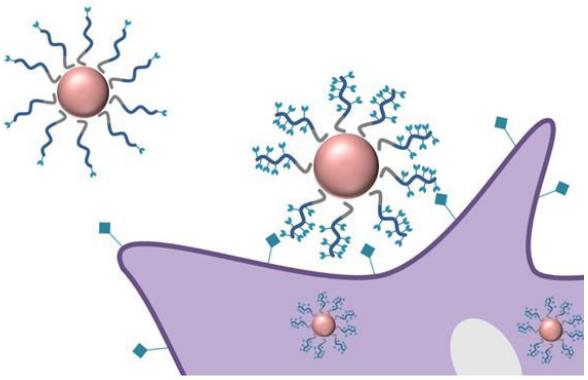

7. Chapter 6: Hydrolytic degradation: poly(phosphate)s *vs.* poly(phosphonate)s……297

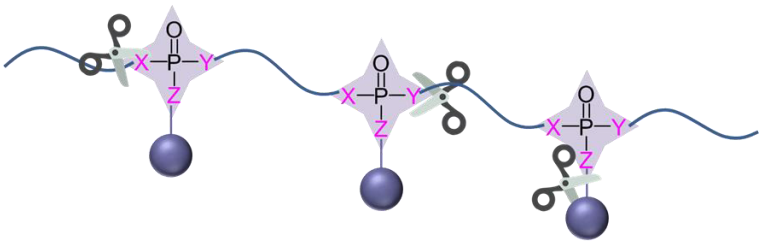

Table of content

	Abstract……	**II**
	Zusammenfassung……..……...……...	**V**
	Motivation…….……...	**1**
1	Introduction…….…….	**5**
2	**Chapter 1**: In-Chain Poly(phosphonate)s via Acyclic Diene Metathesis Polycondensation……...	**81**
3	**Chapter 2:** 2-Methyl-1,3,2-dioxaphosphinane-2-oxide as new monomer for the preparation of linear poly(phosphoester)s……	**119**
4	**Chapter 3:** Polymerizing phostones: A fast way to in-chain poly(phosphonate)s with adjustable hydrophilicity…….…….....	**133**
5	**Chapter 4:** Polyphosphoester stealth surfactants: A general strategy to control the protein corona and the fate of nanocarriers……..……	**179**
6	**Chapter 5:** Active targeting of mannose-receptor presenting cells with nanocarriers coated with mannosylated biodegradable polyphosphoester-surfactants…….....	**241**
7	**Chapter 6:** Hydrolytic degradation: poly(phosphate)s *vs.* poly(phosphonate)s……..	**295**

Motivation

Application of polymers as biomaterials has greatly impacted the progress of modern medicine. Especially, polymers capable of being degraded, provide the tremendous advantage of being removed from the body after fulfilling their intended task. Biodegradable polymers are used in a wide range of applications such as, tissue engineering, protheses or drug delivery. To fulfill functional demands, materials with desired physical, chemical and degradation properties must be designed. One polymer class that is especially appealing for the application as biomaterials are the poly(phosphoester)s (PPEs). They exhibit good biocompatibility and offer several working points for precise adjustment of the desired properties.

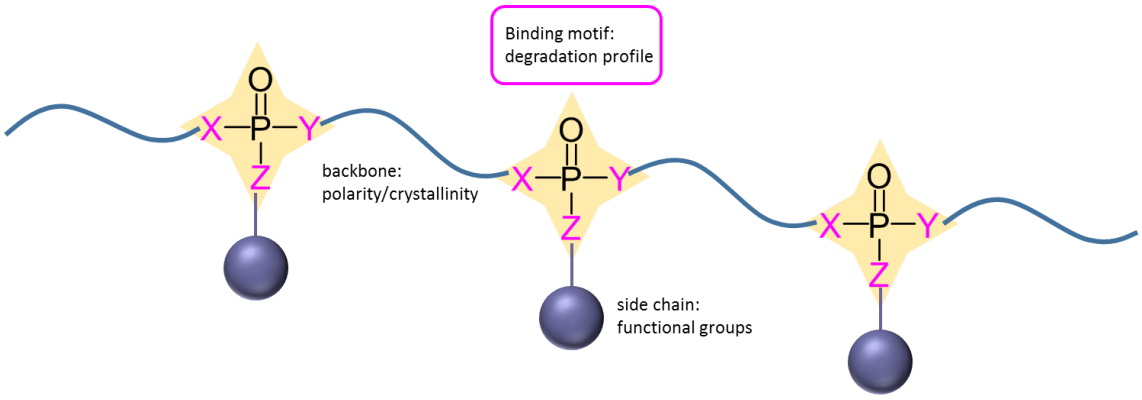

Figure M1. working points for adjusting the properties of poly(phosphoester)s.

The nature of the spacers in the polymer backbone allow a variation of the polarity and is crucial for their crystallization behavior. The binding motif around the central phosphorus atom of each repeating unit is a key parameter to affect their degradation profile. Additionally, the pendant chain can be used for introduction of functional groups. The objective of the following thesis is the preparation and detailed investigation of PPEs from novel monomer types facilitating the PPE synthesis and providing polymers with altered characteristics and degradation profiles.

Development of novel phosphoester monomers (Chapter 1-3)

The implementation of new monomer classes will give access to PPE-based materials with precisely adjustable properties. **Therefore, one aim of the current thesis is the development of new monomers for the preparation of PPEs by ring-opening polymerization (ROP) and acyclic diene metathesis (ADMET) polymerization**.

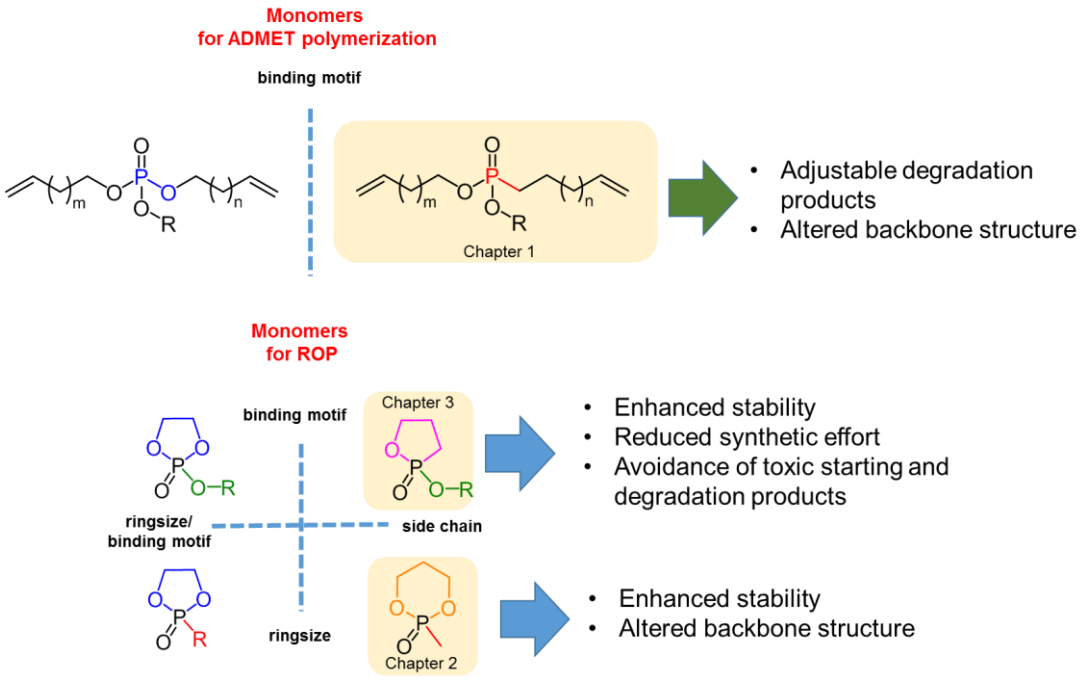

Figure M2. Monomers for the preparation of PPEs by ADMET (left) and ROP (right). The newly established monomers are shaded in yellow.

In chapter 1 a new monomer class suitable for the ADMET polymerization is introduced. The presented monomers exhibit a stable P-C-bond which is located in the backbone of the respective polymer (Figure M2, top). **The aim of this study was the variation of degradation products by altering the binding motif.** The introduced polymers reduce the amount of hydrophobic degradation products compared to the corresponding phosphates.

Chapters 2 & 3 are dedicated to the development of new monomer classes for the ring opening polymerization of cyclic phosphoester monomers. Beside the beginnings of PPE-synthesis by ROP, PPEs are predominantly prepared by ROP of five-membered cyclic phosphoesters (PEs). These monomers are mainly modified by variation of the side chain, while the backbone remains the same. However, the backbone can crucially influence the polymer properties such as the polarity and **thus the objective of Chapter 2 & 3 was the development of new cyclic PE monomers for PPE-preparation by ROP allowing an alteration of the backbone of the respective polymers.**

Six-membered cyclic monomers exhibit reduced ring-strain compared to their five-membered counterparts, which facilitates their preparation and handling and additionally allow the synthesis of PPEs with altered backbone structure. However, six-membered phosphate are known to be poorly polymerizable. Due to the reduced ring strain, cyclic end groups are preferentially formed accompanied by side chain elimination. In Chapter 2, a six-membered cyclic phosphonate, exhibiting the stable P-C-bond in the pendant chain, was prepared. **The objective of this monomer structure was the suppression of side chain elimination and thus facilitating the controlled ring-opening polymerization of six-membered monomers leading to polymers with altered backbone structure.**

In chapter 3 a new five-membered monomer class is introduced, namely the phostones, where one of the inner cyclic ester linkages is replaced by a stable P-C-bond. Beside the possibility of backbone alteration, using phostones as monomers for the ROP of cyclic PEs entails distinct advantages: (i) monomers are accessible by a one-step synthesis from trialkyl phosphites (ii) avoiding toxic $POCl_5$ or $SOCl_2$ respectively and (iii) the monomers show enhanced stability in air and water easing handling and preparation. Additionally, the potential release of toxic ethylene glycol is avoided upon degradation.

PPEs in biomedical applications (Chapter 4 & 5)

Recently, the PPEs were identified to induce a similar stealth effect as PEG, while preventing bioaccumulation due to eventual degradation. Stealth polymers are usually covalently attached to the nanocarrier. Covalent attachment requires certain functionalities on the nanocarrier surface as working point for polymer-attachment as well as several synthesis step. **The objective of chapter 4 was the non-covalent adsorption of a library of structurally diverse degradable PPE-surfactants to facilitate the preparation of stealth nanocarriers. Importantly, this strategy should allow the camouflage of basically any nanocarrier**, which was evaluated with PS, PMMA, and HSA as the carrier materials. The approach of nanocarrier modification by adsorption of PPE-surfactants was advanced in the following chapter 5. **Herein, PPE-surfactants containing mannose moieties were prepared as a straightforward technique for functional surface modification of any kind of particle for targeted drug delivery to dendritic cells.** The applicability of the surfactants wasevaluated for PS-, PMMA- and HES-based nanocarriers as representative model nanocarriers.

Hydrolytic Degradation (Chapter 6)

PPEs are often mentioned as promising biodegradable polymer class due to the inherent cleavable ester linkages along the polymer chain. Although praised in the majority of publications, there are only a few ones dealing with a more detailed investigation of PPE-degradation. Especially in biomedical applications a detailed knowledge about the degradation behavior is crucial for a precise adjustment of degradation time and products and up to now the mode of degradation of PPEs is not yet clarified. **As first step towards better understanding of what effects their degradation, four PPEs exhibiting different binding motifs were evaluated in aqueous media under acidic and basic conditions concerning degradation time and products.** The degradation was constantly followed by NMR spectroscopy and revealed new insights in the degradation behavior of PPEs.

Introduction

Main-chain poly(phosphoester)s: History, Syntheses, Degradation, Bio-and Flame-Retardant Applications

Foreword

The following introduction is based on the publication "Main-chain Poly(phosphoester)s: History, Syntheses, Degradation, Bio- and Flame-Retardant Applications" and is reproduced with permission from *Progress in Polymer Science* **2017**, vol 73. pp.61-122 (Copyright 2017 Elsevier).

The introduction is further based on "Polyphosphoesters: An old biopolymer in a new light." In: "Polymers for Biomedicine: Synthesis, Characterization and Applications", Editor C. Scholz reproduced with permission from John Wiley and Sons Copyright 2017.

Abstract

Nature on planet earth is dominated by poly(phosphoester)s (PPEs). They structure and determine life in the form of deoxy- & ribonucleic acid (DNA & RNA), and, as pyrophosphates, they store up chemical energy in organisms. Polymer chemistry, however, is dominated by the non-degradable polyolefins and degradable polycarboxylic esters (PCEs) that are produced on a large scale today. Recent work has illustrated the potential of PPEs for future applications beyond flame-retardancy -the main application of PPEs today-, and provided a coherent vision to implement this classic biopolymer in modern applications that demand biocompatibility and degradability as well as the possibility to adjust the properties to individual needs. This comprehensive review summarizes synthetic protocols to PPEs, their applications in biomedicine, e.g. as biodegradable drug carrier or in tissue engineering, and their flame retardant properties. We highlighted recent developments that may make phosphorus-based polymers attractive materials for various future applications.

1. Introduction

Poly(phosphoester)s (PPEs), i.e. polyesters based on phosphoric acid derivatives, are omnipresent in nature and all living cells. All life relies on the ability of the C-O-P bond to be stable for a long time but eventually being degradable on demand.[1] The energy-rich phosphorus anhydrides are natures' universal energy storage in the form of adenosine triphosphate (ATP). Controlled cleavage of this bond provides energy for most biochemical reactions. This structure was conserved throughout evolution in all prokaryotes and eukaryotes. Structurally similar but essential for redox-driven bioprocesses, the nicotinamide adenine dinucleotide (NAD^+/NADH + H^+) redox system also carries a diphosphate (Figure 1). Here, a diphosphate is used to link two functionally different parts of a larger molecule together to form a functional unity used in electron transfer processes. Also inorganic polyphosphates play an important role in blood coagulation, inflammation, and bone regeneration.[2-3] Inorganic polyphosphate is structurally very simple, consisting of linear polymers of orthophosphate linked by high-energy phosphoanhydrides bonds (Figure 1). At physiological pH, each internal phosphate unit carries a monovalent negative charge. It is ubiquitous in biology and can vary in polymer length from just a few phosphates to several thousand phosphate units long, depending on the organism and the tissue in which it is synthesized.[4]

PPEs differ from these inorganic polyanhydrides by the organic linker between the phosphorus centers; PPEs can be trivalent, i.e. not charged, or divalent (poly(phosphordiester)s) with a negative charge (*see below*). The most prominent and by far most important examples are the ribonucleic acids and their polymeric forms, DNA and RNA. These macromolecules, as PPEs, encode the genetic information of life and are essential for higher and lower life forms. Both RNA and DNA are PPEs build up from phosphoric acid and derivatives of the carbohydrates ribose or desoxyribose (with the additional nucleobases attached to the anomeric centre), respectively (Figure 1).

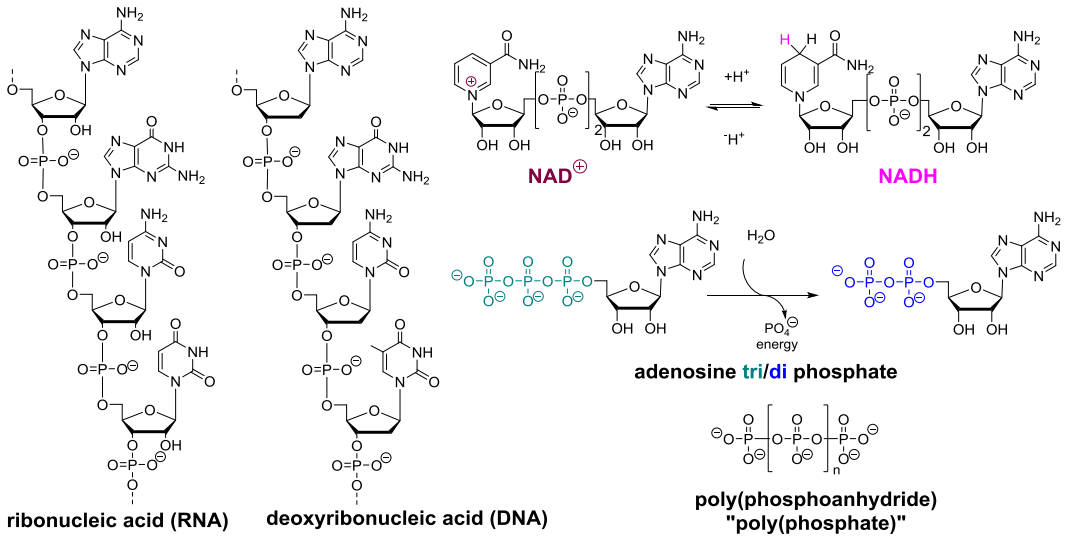

Figure 1. Chemical structures of important phosphorus-containing biomolecules: DNA and RNA sequences, nicotinamide adenine dinucleotide (NADH/NAD+) redox pair containing a diphosphate; adenosine tri/di phosphate (ATP and ADP), essential for the energetic flow in living systems; poly(phosphoanhydride) or inorganic polyphosphate, which is found in platelets.

The negatively charged phosphorus diester in DNA (in combination with the helical double stranded structure) provides long term stability as nucleophilic attacks are unlikely to the anionic charge of the backbone. As natural motif different enzymes are capable of building or degrading phosphoesters. In contrast to DNA, RNA is hydrolyzes much faster, due to the proximity of the additional OH-group on ribose, catalyzing the rapid depolymerization of RNA. The negative charge on the phosphate moiety further allows for interactions with positively charged proteins, the most well-known being histone proteins. These are used for storage and stability purposes.[5] A reduction in positive charge of these proteins plays an important role in the exposing of DNA for other protein-like transcription or translation factors.[5]

Phosphorylation is a general pathway to regulate enzyme activity in cells and hence a multitude of enzymes, the phosphatases, are known with the sole purpose of cleaving several differently substituted phosphoesters.[5] Also synthetic phosphoesters are expected to be enzymatically degraded inside a living system in addition to the intrinsic susceptibility of ester bonds towards (acidic or basic) hydrolysis. Besides phosphates (i.e. with the structural element PO_4^{3-}), also phosphonates (carrying one stable P-C bond, i.e. PRO_3^{2-}, (Figure 4) are important structural elements in nature. Phosphonic acid derivatives have been identified in various plants, fungi, bacteria, and in some animals.[6] Recent ^{31}P NMR spectroscopic studies proved that up to 30% of

the maritime phosphorous reserve is bound in phosphonic acid derivatives.[7] Also many herbicides, such as the currently heavily discussed glyphosate, are based on phosphonates.

The omnipresence and immense biological importance of phosphoric acid esters makes synthetic PPEs a very promising object of research. These polymers are expected to show a high compatibility with biological systems and potentially low toxicity. Compared to the polyesters based on carboxylic acid esters, phosphorus, in phosphoric acid, can form three stable and divergent bonds in addition to the P=O double bond. This makes not only poly(phospho*ester*)s, but also and the respective *amide*s, a versatile platform for main- and side-chain modification of synthetic polymers, a distinct advantage over carboxylic acid esters, for example (Figure 2).[8] Attachment of side-chain functionalities and labels and therefore modification of material properties is possible in a straightforward way via the pendant group. This avoids main-chain functionalization which has to be conducted for other polycarboxylic acid esters or amides, e.g. in functional lactones or lactams. Also the intrinsic biodegradability of PPEs can be adjusted via side-chain (and main-chain) modifications.[9]

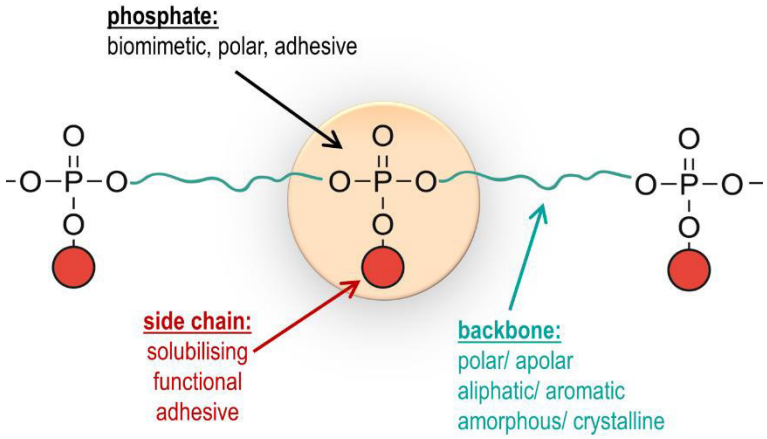

Figure 2. The synthetic platform of poly(phosphoester)s highlighting the handles for the design of future materials.

Polymer chemists have been always taking motifs from nature to synthetics (Figure 3). Polyolefins made it to a commodity material for the modern society with highly efficient catalysts producing polyethylene and polypropylene, for example, on the million ton scale. [10]

Also polyesters and polyamides have made it to commodities in many applications in today's world. Research on these materials[11] is still ongoing with several thousand papers per year covering their synthesis, modification and application in various areas.[12] On the other hand, PPEs - which are the basis for the living world - remain a niche material on industrial scale and

only few research groups are currently interested in these materials.[13-16] To date, only flame retardant plastics or additives are produced industrially (see sections below). The full potential of synthetic PPEs is only touched in academics. This review summarizes the history of the synthetic achievements towards PPEs based on different monomer types and polymerization mechanisms. We will highlight some - rather forgotten - pathways and summarize the recent trends in PPE-chemistry and applications on academic level. The interested reader is also referred to other reviews and books about PPEs including industrial applications.[8, 17-21]

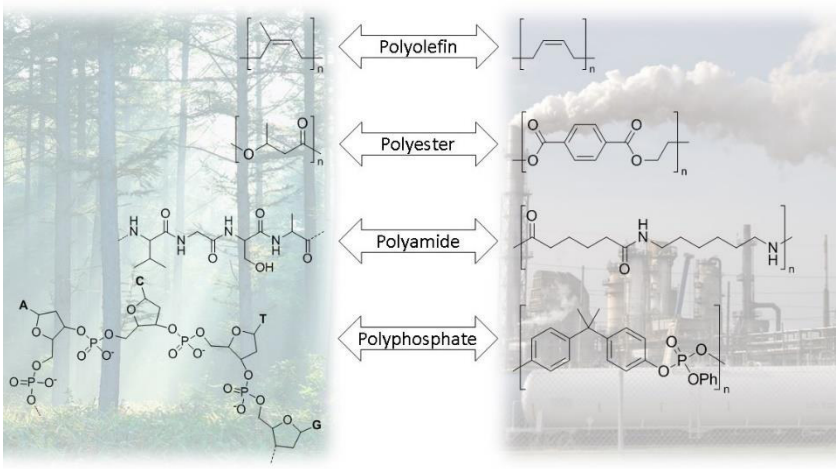

Figure 3. Comparison between the structural motifs of natural occurring polymers (left), and synthetic polymers produced industrially with prominent examples (right)[8] (Reprinted with permission from John Wiley & Sons Inc, Copyright 2015.)

All materials (PPEs) discussed in the actual review carry the phosphorus atoms along the polymer backbone and are separated by organic groups. Polymers with phosphorus in the side-chains, e.g. prepared by the polymerization of vinyl phosphonic acid, will not be touched by this review, however, other recent reviews cover the aspects of those materials.[22] In PPEs, the phosphorus atoms in the polymer backbone are typically in a pentavalent state. , i.e. P(V). Also polymers with trivalent phosphorus, P(III), have been reported and some interesting candidates will be mentioned throughout this review.

In contrast to their carbon analogues, the polycarboxylic acid esters (PCE), the pentavalency of phosphorus provides an additional linkage per repeating unit, which allows the formation of branched structures or the introduction of functional or solubilizing groups. Depending on the nature of this side group which is connected to the phosphorus atom, PPEs are categorized into different subclasses (Figure 4), namely in polyphosphites (or alkylene H-phosphonates),

polyphosphonates, polyphosphates, and polyphosphoramidates with two phosphoesters (P-O-R) building the main chain and P-H, P-C, P-O, or P-N linkages to the side chain, respectively. Only in a very few studies also the linkage motif along the backbone has been altered, for example to generate branched polyphosphoamidates[23] and linear poly(phosphonate)s with the P-C-bonds in the main chain.[24]

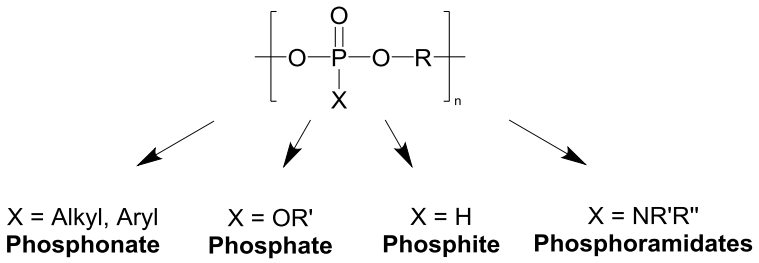

Figure 4. Subclasses of main-chain poly(phosphoester)s.

2. PPEs: Synthesis

PPEs can be prepared by various synthetic routes: step-growth or chain growth polymerization can be chosen. Classical polycondensation of phosphoric acid chlorides and diols or transesterification of phosphoesters with diols is applicable. Also polyaddition and acyclic diene metathesis polycondensation have been reported. In addition, for chain-growth strategies, typically ring-opening polymerization of five- or six-membered cyclic phosphoesters is applied (Scheme 1). The polymers prepared by such methods may carry functional (pendant) groups, which allow further postpolymerization modification by different techniques, which will be discussed in this review. By these techniques, PPEs are accessible ranging from very hydrophobic materials to water-soluble polymers or highly crystalline to amorphous materials with variable molecular weights.[25-26] PPEs with different architectures and polymerization patterns have been prepared, ranging from linear to hyperbranched[27-30] or cyclic[31] homopolymers, copolymers,[32-35] brush copolymers,[36-37] star polymers,[38-40] and segments in block copolymers,[40-45] or sequenced polymers.[46]

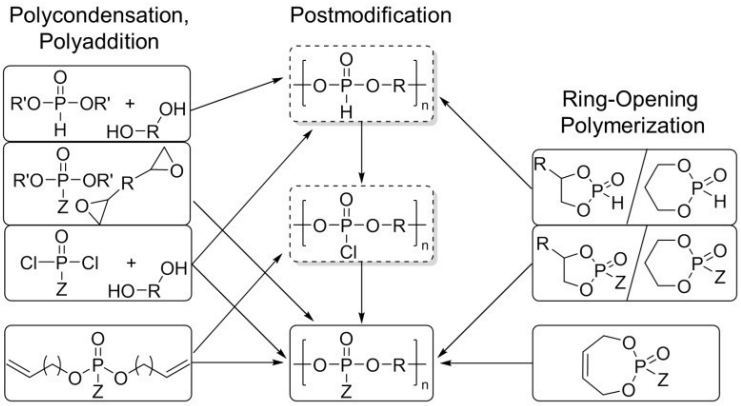

Scheme 1. Overview on the synthetic pathways to PPEs (Z=O-alkyl, O-aryl, alkyl, Cl, H; R= alkyl, aryl).[8] Reprinted with permission from John Wiley & Sons Inc, Copyright 2015.)

1.1 Polycondensation

In 1936 James Arvin reported for the first time the synthesis of aromatic polyphosphates by the polycondensation of phosphorus oxychloride with bisphenol-A.[47] Since then hundreds of reports, especially in the patent literature, on the synthesis of PPEs including polyphosphates,[32, 48] -phosphites, -phosphoramidates,[23, 49] and -phosphonates[50-55] by polycondensation have been published (only a few representative examples are listed here). Also branched and cross-linked materials have been prepared by the use of multifunctional nucleophiles or $POCl_3$.[28, 56] Beside the traditional melt and solution polycondensation the interfacial [50, 52] and the phase-transfer catalyzed[51, 57] polycondensation setups are common techniques.

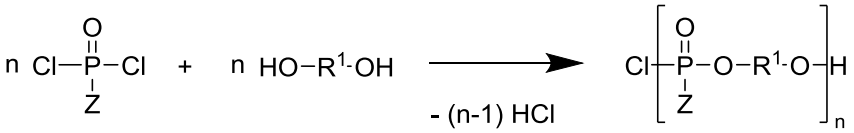

Z = H, O-alkyl, O-aryl, NH_2

R^1 = alkyl, aryl

Scheme 2. General protocol for the polycondensation of phosphoric acid dichlorides with diols.

The interfacial polycondensation can also be used to produce PPE- based nanoparticles. Alexandrino *et al.* reported the successful preparation of PPE nanoparticles by interfacial polycondensation of bisphenol A and dichlorophenylphosphate in miniemulsiom (Figure 5)[57].

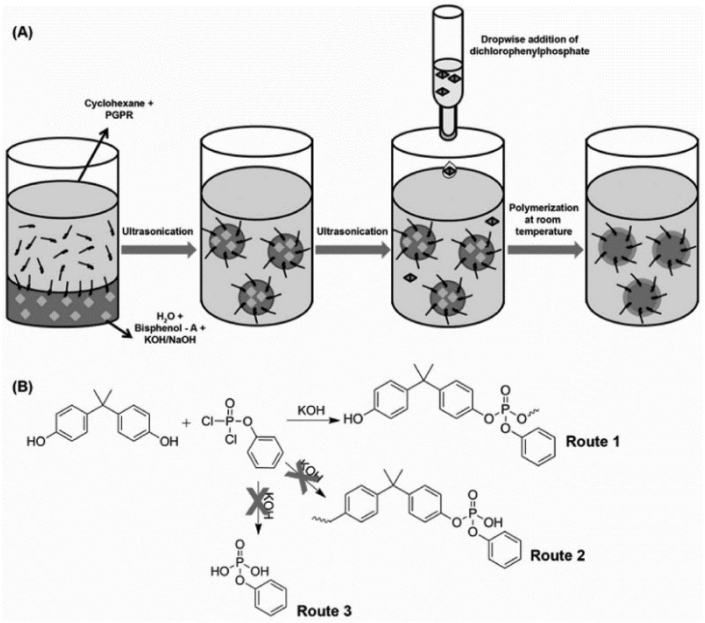

Figure 5: A) Schematic representation of the interfacial polycondensation in inverse miniemulsion applied for the synthesis of PPE colloids. B) Possible side reactions (Routes 2 and 3) that occur during the interfacial polycondensation (Route 1). SEM images of the PPE-articles after redispersion in water/SDS (0.6 wt%): C) KOH or D) NaOH as the osmotic and deprotonation agent. (Reprinted with permission from reference 57. Copyright 2016 Wiley)

The prepared PPE colloids show diameters of 700 - 900 nm and higher molecular weights than PPEs prepared by classical polycondensation reactions. The particles consist of a well-known flame-retardant and are potentially applicable as additives for flame resistant improvement of other polymers compositions.

Although polycondensation is by far the most widely used approach to PPEs, its application is limited due to several side reactions.[19] They restrict the synthesis of high molecular weight polymers (Scheme 3) and the incorporation of functional groups is challenging.[48] Besides the main reactions between monomers or macromolecules (Scheme 3 Pathway 1.1 and 1.2), which lead to the formation of polyesters, various unwanted side reactions take place resulting in the reduction of yield and molecular weight of the polymer. The reaction between the diol and HCl, which evolves within the polycondensation, leads to the deactivation of the diol and to the cessation of the polyester growth. The hydrolysis of acid chloride groups by traces of water results in the formation of acidic groups, which are not able to participate in the polymerization process anymore. Also cyclic (poly)phosphoesters have been observed, depending on the

structure of the diol. In case of pendant ester linkages, transesterification reactions can take place leading to branched polymers.

1. Reactions leading to high molecular weights

1.1 Polyester formation

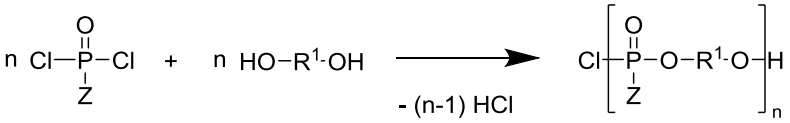

1.2 Reaction between macromolecules

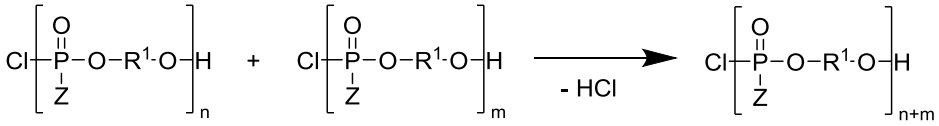

2. Reactions preventing high molecular weights

2.1 Hydrolysis

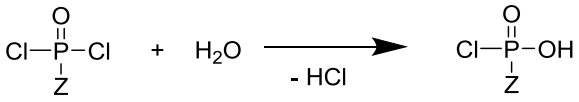

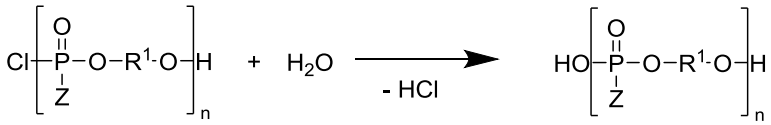

2.2 Deactivation of the diol

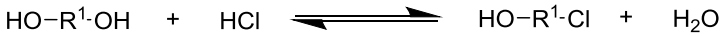

2.3 Formation of cyclic compounds

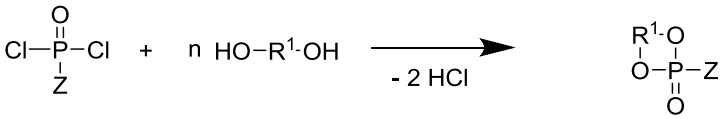

R^1= Alkyl, Aryl

Z = H, alkyl, aryl NR_3

Scheme 3. Reactions during polycondensation of phosphorus dichlorides with diols.[48]

The polycondensation to PPEs also includes the polytransesterification of phosphoric acid diesters with diols (Scheme 4). This strategy is mostly applied for the synthesis of poly(H-phosphonate)s and -(phosphonate)s.

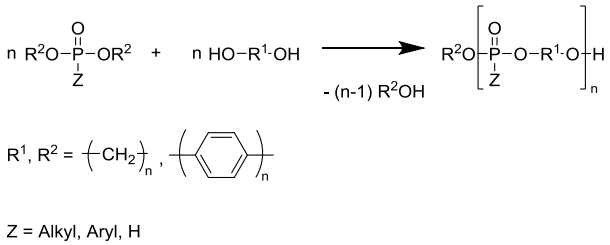

Scheme 4. General scheme of the polytransesterification.[58]

Polytransesterification is not suitable for the direct synthesis of poly(phosphate)s, due to branching., i.e. transesterification with the pendant esters. Nevertheless, poly(phosphates) are also accessible via this method by post polymerization modification of the corresponding poly(H-phosphonate)s.[58-59] The P-H bond is interesting, as it is inert to the polycondensation conditions, however, allows easy access to functional materials by several post polymerization modifications (Scheme 5).

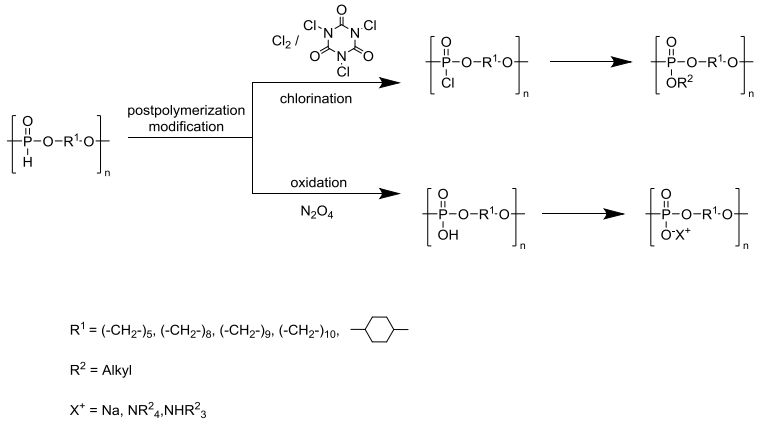

Scheme 5. Post-polymerization modification of poly(H-phosphonate)s.[59-60]

The hydrolytic instability of the poly(H-phosphonate)s allows an easy transformation of the P-H-bond either by oxidation with N_2O_4 or by chlorination with gaseous chlorine or under milder conditions with trichloroiscyanuric acid[60]. The products can then be transferred into further derivatives (Scheme 5).[61-62] Also amphiphilic graft copolymers are accessible via the post-polymerization of the poly(H-phosphonate)s (Scheme 6).

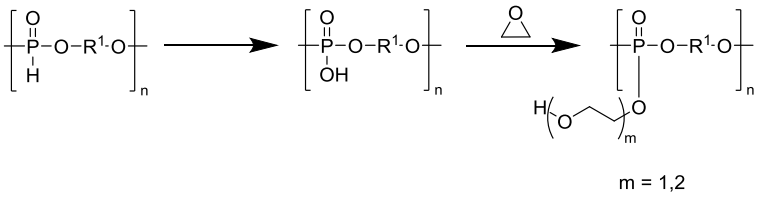

Scheme 6. Synthesis of amphiphilic graft copolymers (PPE-g-PEO).

The addition of ethylene oxide proceeds quantitatively to the PEO grafted PPEs (rather short oligomers are grafted under these conditions). Without the addition of an external acid, the reaction stops when all acidic groups are consumed. Longer PEO-chains can be introduced by usage of an external acid.[59, 63] Another efficient post-polymerization modification was achieved by the application of the Atherton-Todd reaction to poly(H-phosphonate)s (Scheme 7).[64-66] Initially, the Atherton-Todd reaction was applied for the synthesis of phosphoamidates by reaction of dialkyl phosphonate with primary amines in the presence of carbon tetrachloride, but was subsequently extended to different nucleophiles throughout the past years.[67]

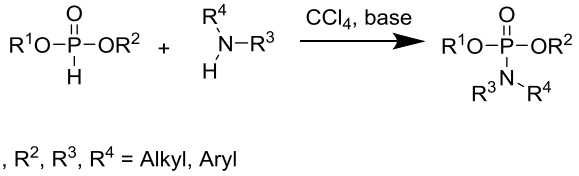

Scheme 7. General scheme of the Atherton-Todd reaction.

Bogomilova *et al.*, for example, used the Atherton-Todd reaction to bind the anticancer drug mephalan to a water-soluble polymer resulting in a reduced toxicity of the cytostatic while maintaining the therapeutic efficacy (Scheme 8).[68]

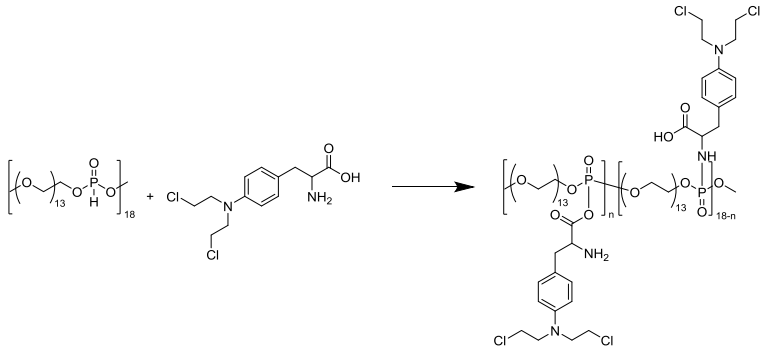

Scheme 8. Reaction pathway for the immobilization of mephalan onto poly(oxyethylene phosphonate) under Atherton-Todd conditions (from Ref 26).

However, the polytransesterification of diesters with diols is plagued with side reactions thus leading to polymers with limited molecular weights. In 1973 Vogt *et al.* reported exhaustively about the side reactions of the polytransesterification of diethyl phosphonate with various diols.[69] Similarly to the side reactions, occurring within the polycondensation reaction between phosphorus dichlorides and diols, the formation of cyclic phosphoesters proceeds also within the polytransesterification process. The reaction of ethylene glycol and dimethyl phosphonate, for example, leads to the formation of oligomers and 2-hydro-2-oxo-1,3,2-dioxaphospholane.[70] Also, the reaction between propylene glycol and dimethyl phosphonate results almost exclusively in the formation of the 2-hydro-2-oxo-1,3,2-dioxaphosphorinane.[71] Beside the formation of cyclic phosphoesters, the formation of cyclic ethers can also be observed within the polytransesterification (Scheme 9).[19, 69]

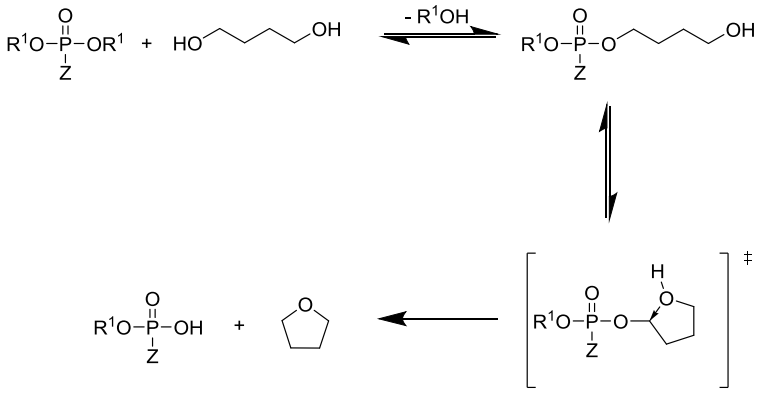

Scheme 9. Formation of tetrahydrofuran during the polytransesterification of phosphorus dialkyls with 1,4-butanediol.[19]

Cyclic ethers are formed by intramolecular cyclization initiated by the nucleophilic attack of the terminal hydroxyl group on the α-carbon. In the course of this ether formation the ester function is transferred into an acidic P-OH-bond, which cannot undergo further condensation reactions. The amount of the ether formation depends on the diol; in case of 1,4-butanediol the corresponding cyclic ether, i.e. tetrahydrofuran, was formed with a yield of 80%, whereas the usage of 1,5-pentanediol leads to the formation of tetrahydropyrane with only 30% yield.[69]
Another side reaction of the polytransesterification is the dealkylation (Scheme 10).

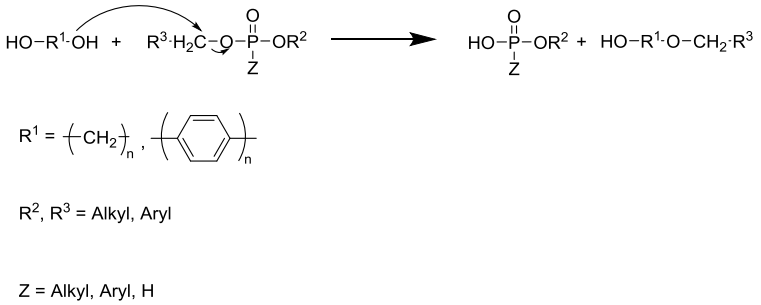

Scheme 10. Dealkylation during the polytransesterification process.

The main side reaction during the polytransesterification is the dealkylation of the phosphorus diester. Dealkylation occurs due to the nucleophilic attack of the oxygen atom on the α-carbon atom, which represents, beside the phosphorus atom, the second electrophilic center within the phosphoric acid esters. Within this reaction one of the ester functionalities is transformed into an acidic P-OH group, which is not able to participate in the polymerization process anymore and thus limiting the molecular weight of the polymer. To date many approaches have been published to eliminate or to reduce the side reactions during the polytransesterification. Petrula *et al.* reported about several modified polytransesterification approaches leading to high molecular weight polyphosphoesters.[58-59, 72-73]

In 1990 they published a two stage protocol providing poly(H-phosphonate)s with molecular weights up to 3.3 x 10^4 g mol^{-1} (determined by VPO) by the polycondensation of dimethyl phosphonate with various diols (Scheme 11).[74]

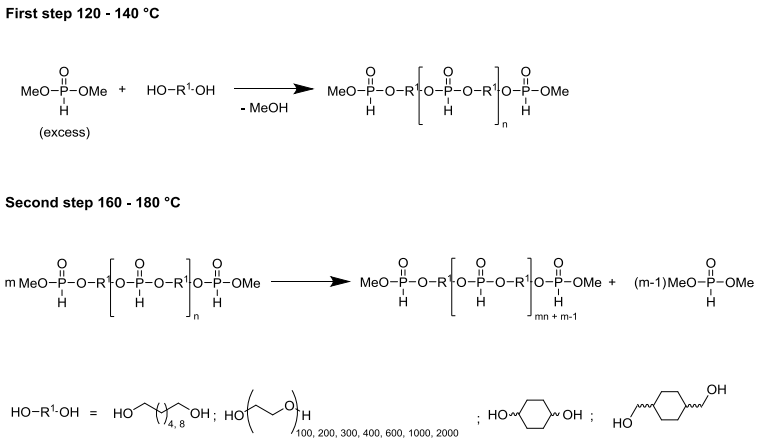

Scheme 11. Synthesis of high molecular weight poly(H-phosphonate)s by a two stage process.[74]

The first stage is conducted with an excess of the dimethyl phosphonate in a temperature range from 120 to 140 °C allowing a complete reaction of the hydroxyl groups with the phosphorus

dimethyl ester. In the first step only oligomers with methyl ester end groups are formed and methanol as side product, which is continuously removed from the reaction mixture by distillation. By this step the side reactions involving hydroxyl groups can be suppressed. After 90% of the theoretical amount of methanol is removed, the temperature is increased to 160- 180 °C. In the second step, high molecular weight polymers are formed by transesterification reactions between the oligomers accompanied by elimination of dialkyl phosphonate.

In 1997 the same group reported about the polycondensation of diphenyl phosphonate with diols such as 1,10-decanediol or tetra(oxyethylene) glycol, leading to high molecular weight poly(H-phosphonate)s with molecular weights up to M_n = 3 x 10^4 g mol^{-1} (determined by membrane osmometry, Scheme 12).[58]

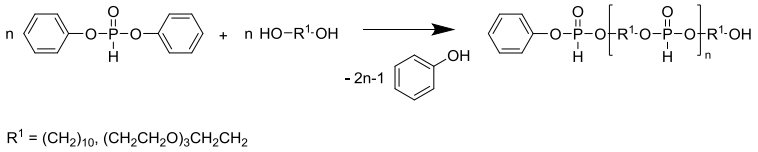

$R^1 = (CH_2)_{10}, (CH_2CH_2O)_3CH_2CH_2$

Scheme 12. Polytransesterification of diphenyl phosphonate with diols.

The usage of aromatic esters reduces the dealkylation of the phosphors to a minimum due to the replacement of the sp^3 by a sp^2 carbon that eliminates the possibility of S_N2 reactions at this position. Furthermore, diphenyl phosphonate reacts almost irreversibly with alcohols.[75] Therefore the removal of phenol, evolving during the polycondensation process, is not necessary for the synthesis of medium-molecular-mass polymers.

Pretula *et al.* also demonstrated that PPEs can be obtained by the polycondensation of phosphoric acid and a diol, avoiding toxic solvents, catalysts or the use of phosphorus oxychloride.[76-78] Unfortunately, the prepared oligomeric phosphoesters by polycondensation of phosphoric acid and ethylene glycol (P_n= 11 determined by MALDI-ToF MS and NMR spectroscopy) were rather ill-defined and exhibited poor mechanical properties (Scheme 13). However, this strategy is promising and may be optimized to produce PPEs directly from inorganic phosphates or phosphoric acid.

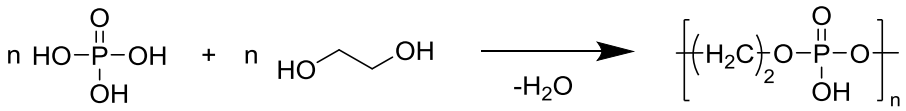

Scheme 13. Direct polycondensation of phosphoric acid with ethylene glycol.

1.2 Polyaddition

Typical approaches to PPEs by polyaddition are reactions of phosphoric acid dichlorides with bisepoxides[79] or bisoxetans[80] using onium salts as catalysts. Poly(phosphates) and -(phosphonates) with reactive pendant chloromethyl groups have been synthesized by Nishikubo *et al.* by polyaddition of aromatic and aliphatic bisepoxides with phosphoric and phosphonic acid dichlorides.[81] Polymers with molecular weights up to 23,000 g mol^{-1} and molecular weight dispersities ranging from M_w/M_n=1.24 to 1.59 were obtained (Scheme 14).

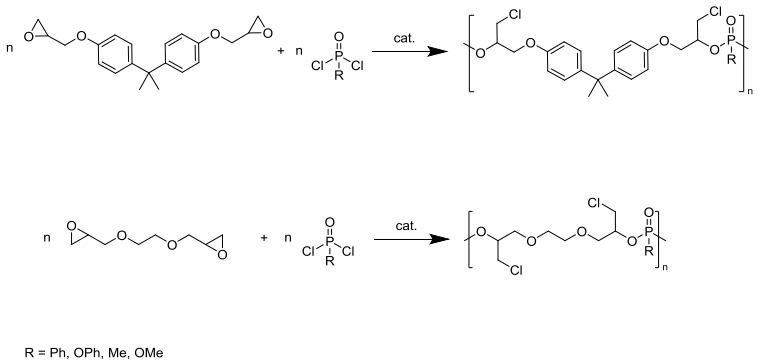

Scheme 14. Synthesis of PPEs by polyaddition of bisepoxides with phosphoric and phosphonic acid dichlorides.

Penczek and co-workers investigated in a series of publications the polyaddition reaction between phosphoric acid and bisepoxides and the associated side reactions [82-85]. The carefully selection of the reactants, namely of 3,4-epoxycyclohexylmethyl-3,4-epoxycyclohexanecarboxylate (ERL) and ethylphosphoric acid allowed the elimination of side reactions and the successful synthesis of PPEs with high molecular weights up to 10^4 g mol^{-1} (determined by VPO, Scheme 15). However, due to the limitation of the starting materials needed for polyadditions, this approach is only of minor relevance. The use of phosphoric acid derivatives is still an attractive idea to omit high-energy intermediates, such as $POCl_3$, and might change the field of PPEs, if new catalysts or synthetic routes are investigated.

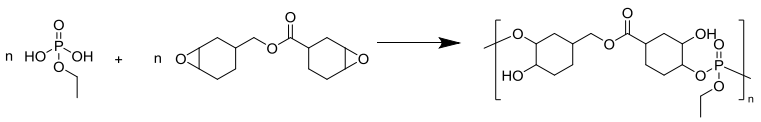

Scheme 15. Synthesis of PPEs by polyaddition of ERL with ethylphosphoric acid.

1.3 Ring-opening polymerization (ROP)

Probably the most versatile approach to PPEs is provided by the ring-opening polymerization (ROP) of cyclic phosphoester monomers (CPM, Scheme 16). The polarity of the polymers obtained by this technique, range from merely water-soluble[86] to very hydrophobic[87-88] depending on the character of the pendant group. Furthermore, due to more recent developments towards controlled (or living) polymerization mechanisms for CPMs, linear,[89-92] branched,[93] and hyperbranched,[27] grafted[14, 94] or cross-linked[95] PPEs have been realized by this protocol.

The ROP can proceed via an anionic, cationic or metal-catalyzed insertion mechanism. In general, to date, the anionic polymerization is by far more relevant than the cationic ROP.

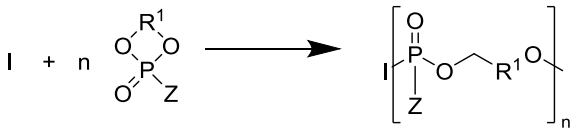

Z = alkyl, aryl, Oalkyl, Oaryl

$R^1 = (-CH_2-)_{2,3}$

Scheme 16. Ring-opening polymerization of cyclic phosphoesters.

Independent from the mechanism, the ideal candidates for the ROP are strained cyclic phosphoesters, with both the phosphorus being tri- or pentavalent. The monomers containing trivalent phosphorus, such as cyclic phosphonates and deoxphostones with variable ring sizes have been intensively studied by Kobayashi *et al.*[96-98] In contrast to the pentavalent monomers, the trivalent phosphorus monomers are exclusively polymerizable by a cationic mechansim.[98] For example the cationic polymerization of 2-phenyl-1,3,2-dioxaphosphephane with methyl iodide as initiator leads to the corresponding poly(phosphonite) with moderate molecular weights (M_n= 3,000 g mol^{-1}, determined by VPO), whereas polymerization under anionic conditions does not proceed at all.[97] The obtained polymers exhibit a wax-like texture and are soluble in polar organic solvents. The monomers based on P(III) have never gained as much attention as their pentavalent counterparts. Nowadays, the interest is focused on the highly strained pentavalent six-membered 2-alkoxy-2-oxo-1,3,2-dioxaphosphorinanes and particularly on the five-membered 2-alkoxy-2-oxo-1,3,2-dioxaphospholanes (see below).[99-100]

The five- and six-membered cyclic phosphates are accessible by the direct condensation of the appropriate diol with phosphorus oxy chloride and subsequent esterification to introduce a side

chain of choice. In practice, this route (pathway 1 in Scheme 17) is only of minor relevance due to low yields and impure monomers, probably by polycondensation as side reaction. In contrast, the three-step protocol (pathway 2 in Scheme 17) starting with the ring closure by condensation of phosphorus trichloride with a suitable diol, followed by the oxidation of the trivalent phosphorus with oxygen and subsequent esterification is the favored method in most literature reports. The third pathway in Scheme 17 for the synthesis of CPMs is the transesterification of dialkylphosphates with diols, which was used for monomers, in which the pendant group is a hydrogen atom.[71, 101] Of course, this approach is not suitable for the synthesis of cyclic phosphates due to unwanted transesterifications and the formation of branched structures.

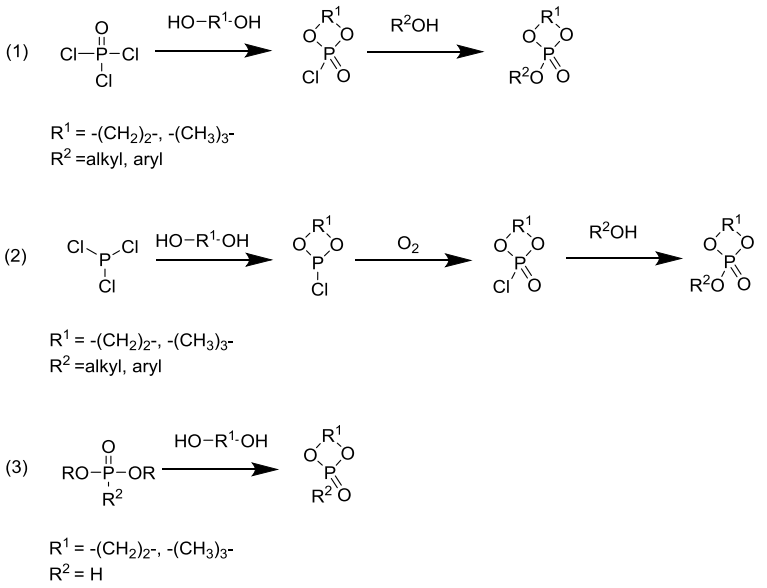

Scheme 17. Different synthetic pathways to cyclic phosphoester monomers.

1.3.1 ROP of Six-Membered Cyclic Phosphates

In the 1960s and 1970s the ROP of six-membered cyclic phosphoesters has been the center of interest.[102-105] Due to their lower ring strain (2.6 kcal/mol[106] for methoxy-2-oxo-1,3,2-dioxaphosphorinane) compared with the five-membered phosphates (6.7 kcal/mol for methoxy-2-oxo-1,3,2-dioxaphospholane [106]) their synthesis is more robust and the monomers are easier to handle but still reactive enough to be polymerized. First attempts to polymerize 2-ethoxy-2-oxo-1.3.2-dioxaphosphorinane have been made by Munoz et al.;[105] the polymerization was conducted thermally at 110-120 °C in the presence of water over several weeks. The polymerization led to viscous polymers with acidic groups soluble in polar solvents such as water or alcohols but

insoluble in diethyl ether or benzene. In the 1970s, the polymerization of cyclic phosphorus-containing compounds has been resumed by Penczek and co-workers, who made intensive progress on elucidating the polymerization mechanism, the thermodynamics and the properties of the final polymers.[107] Two kinds of six-membered cyclic compounds have been investigated in detail, 2-alkoxy- and 2-hydro-2-oxo-1,3,2-dioxaphosphorinanes.[92, 108] The 2-alkoxy-2-oxo-1.3.2-dioxaphosphorinanes can be polymerized either by cationic or anionic ring-opening polymerization.[103-104] The cationic polymerization can be conducted in bulk as well as in solution above 100 °C using typical cationic initiators such as triphenylcarbenium salts (*e.g.* Ph_3CAsF_6 or Ph_3CSbF_6). The cationic polymerization leads to polymers with low molecular weights with $M_n \leq 1{,}200$ g mol^{-1} (determined by VPO). [109]

Intensive investigations on the mechanism of the cationic polymerization have been made by Penczek *et al.* (Scheme 18).[103, 109] The initial step is the nucleophilic attack of the P=O-bond of the monomer at the electrophilic (cationic) initiator and generates a R-O-P-bond leading to a cyclic tetraalkoxy phosphonium cation as the propagating species. In this tetraalkoxy phosphonium cation the C_4- and C_6-atoms are partially positive charged and thus electrophilic enough to be attacked by the oxygen atom of another monomer (Scheme 18).

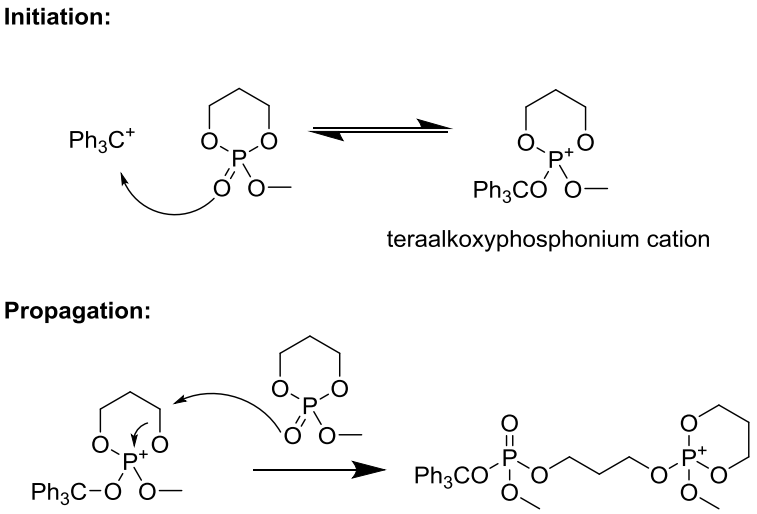

Scheme 18. Mechanism of the cationic polymerization of 2-methoxy-2-oxo-1,3,2-dioxaphosphorinane.

In the propagating step the nucleophilic attack on the partially positive charged carbon atoms results in a transition state that can either lead to a chain growth or to a chain transfer. Chain growth occurs, when an endocyclic CH_2-O-bond is broken (Scheme 19). On the other hand the

passing of the transition state can lead to a chain transfer. In this case an exocyclic O-CH_3-bond is broken resulting in the formation of a macromolecule with a cyclic end group and a new tetraalkoxy phosphonium cation, which can reinitiate the polymerization. According to the proposed mechanism in the ^{1}H NMR spectra signals at 4.5 ppm (Figure 6) can be observed, that are typical for cyclic structures.

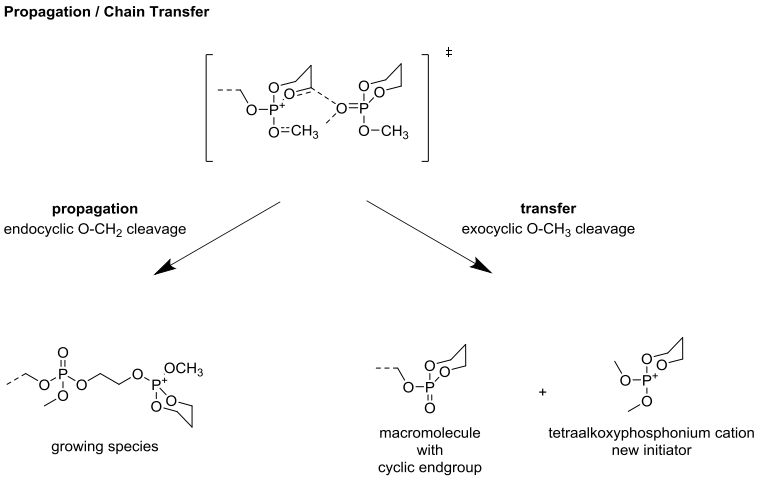

Scheme 19. Proposed mechanism for the propagation and chain transfer step within cationic polymerization of six-membered cyclic phosphoesters. [103, 109] (Adapted with permission from [103]. Copyright 1977 American Chemical Society.)

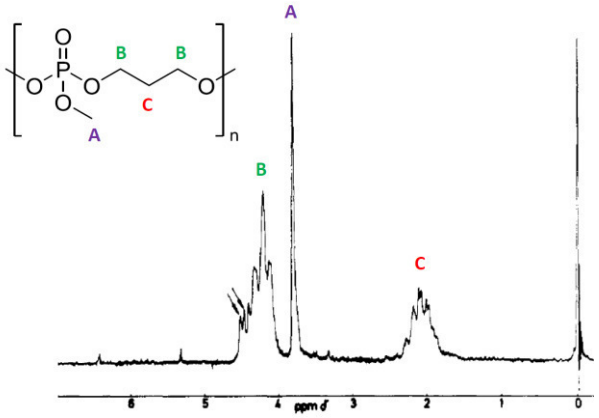

Figure 6. ^{1}H NMR spectrum of poly(2-methoxy-1,3,2-dioxaphosphorinane) showing the presence of some cyclic structures in the macromolecules (the arrows show the region of the contribution of cyclic structures in the linear macromolecule). (Reprinted with permission from reference 109, Copyright 1974 American Chemical Society.)

Besides the chain growth, chain termination can take place: in case of the termination the growing species reacts with a polymer segment, where a non-strained, acyclic teraalkoxyphosphoniumion is built, that cannot initiate further polymerization thus terminating the chain growth (Scheme 20).

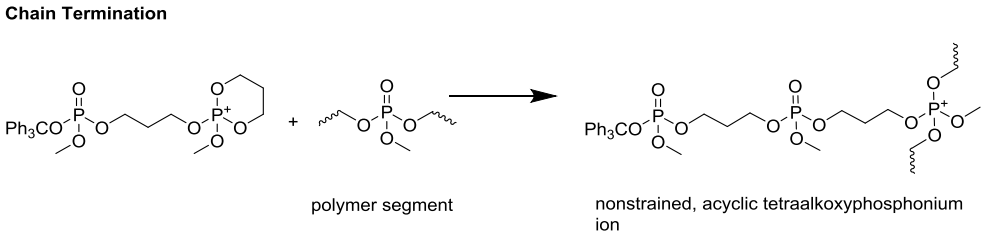

Scheme 20. Branching during the cationic polymerization of 2-methoxy-2-oxo-1.2.3-dioxaphosphorinane.

The only indication of the reaction proposed above comes from the study of the reaction kinetics and from the fact that the measured k_t does not depend on the structure of the anion attached to the growing species.[109] It has to be noted that in most of the older literature molecular weights were determined by VPO, giving no insight in the molar-mass distribution. For many of those systems a modern revival could be possible with detailed SEC or MALDI-TOF analyses. However, PPEs are sometimes not easy to measure on standard GPCs due to interaction with the column material, thus VPO may still be an alternative.

Beside the cationic polymerization, six-membered phosphates can also be polymerized using anionic initiators (e.g. ^{n}BuLi, ^{t}BuOK, etc.). The mechanism of the anionic polymerization has also been investigated in detail by Penczek's group based on the polymerization of 2-methoxy-2-oxo-1.3.2-dioxaphosphorinane. Here again the formation of macromolecules with cyclic end groups can be detected preventing the synthesis of high molecular mass polymers (Scheme 21).[104]

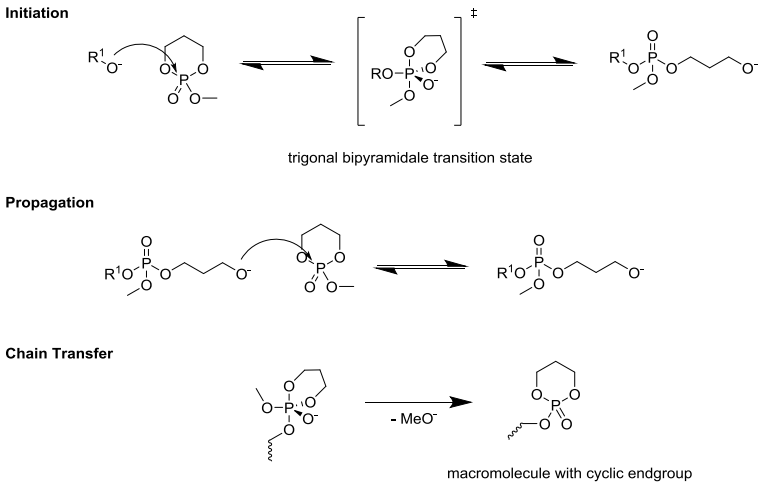

Scheme 21. Proposed mechanism of the anionic polymerization of six-membered cyclic phosphoesters.

The initial reaction is the nucleophilic attack of the initiator at the phosphorus atom, thus leading to a transition state with the geometry of a trigonal bipyramide (Scheme 21). In this transition state the six-membered cycle is still intact and preferably occupies the axial-equatorial position.[11] Although every P-O-bond could be cleaved it is the axial, which is primarily broken resulting in a new alkoxide anion propagating polymerization.

Similar to the cationic polymerization, within the anionic polymerization a terminating chain transfer can occur. This is possible due to the pseudo rotation of the phosphorus compound. It allows a migration of the pendant alkoxy group to the axial position, in which the P-O-bond is preferably cleaved. By this process an alkoxide anion is eliminated, which can again act as initiator, thus leading to macromolecules with cyclic end groups and low molecular mass (M_n < 10^3 g mol^{-1} determined by VPO). [104]

The six-membered 2-hydro-2-oxo-1,3,2-dioxaphosphorinane polymerizes readily to molecular masses up to $M_n = 10^5$ g mol^{-1} (determined by high-speed membrane osmometry) in a temperature range from 45 °C down to -80 °C using common anionic initiators such as ^{t}BuOK, ^{n}BuLi and ^{i}Pr$_3$Al.[92] The obtained polymers show an enhanced susceptibility to hydrolysis, but also allow an easy post-polymerization modification. By replacing the pendant P-H-bond by a P-C or P-N-bond the hydrolytic stability can be altered as described in the previous paragraph for the post-polymerization modification of poly(H-phosphonate)s obtained by polycondensation reactions. In contrast, the cationic polymerization of the 2-hydro-2-oxo-1,3,2-dioxaphosphorinanes was not reported to date.[92] Today the interest in six-membered phosphates has faded due to the efficient polymerization strategies developed for the five-membered

monomers. However, also the 6-membered rings may find a revival with modern polymerization catalysts as one could expect different hydrophilicity, crystallinity, and hydrolysis kinetics with the backbone based on propylene glycol (compared to the backbone based on ethylene glycol for the 5-membered monomers).

Table 1. Six-membered cyclic phosphoesters used for ring-opening polymerization

Monomer	bp [°C] (mbar)	Mp [°C]	Monomer Yield [%]	Polymerization technique	$M_{n,max}$ [g mol^{-1}]	Ref
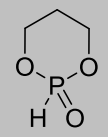	97-98[71] (3.3)	-	79	A,C		[104]
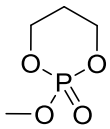	67 (0.01)	-	40	A,C	1.2×10^5	[104, 110]
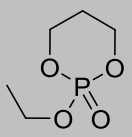	111 (0.9)	-	-	A,C	5×10^4	[103]
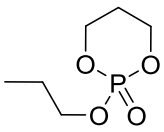	137 (0.7)	-	-	A,C	3.5×10^4	[103]
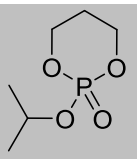	103 (0,01)	-	-	A,C		[103]
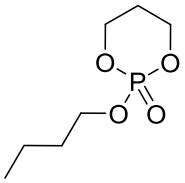	111 (0.03)	-	-	A,C	5.4×10^3	[103]

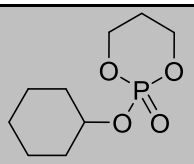		59	-	A,C	1.5 x 10^4	[103]
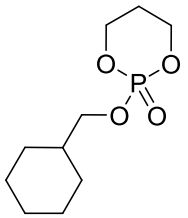		73	-	A,C		[103]
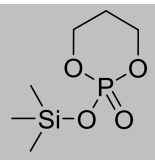		112 (1.5)	-	-	A,C	[103]
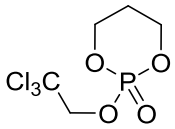		148 (0.07)	-	-	A,C	5.3 x 10^4	[103]
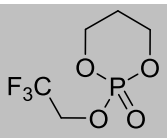		120 (0.4)	-	-	A,C		[103]
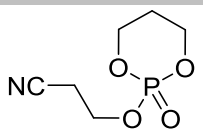		104 (0.07)	-	-	A,C		[103]

A = anionic polymerization, initiators: ^{t}BuOK, ^{n}BuLi and ^{i}Pr$_3$Al, T

C = Cationic polymerization, initiators: Ph_3CAsF_6 or Ph_3CSbF_6

1.4 Ring-opening polymerization of five-membered cyclic phosphates

The usage of the five-membered dioxaphospholanes as monomers for the PPE-synthesis by ROP also started in the 1960 with the first attempts made by Munoz *et al.* leading to brown, viscous oils with undefined molecular masses.[111]

As time went on, the dioxaphospholanes have almost completely displaced the six-membered dioxaphosphorinanes as monomers for ROP and are now the monomers of choice for the

preparation of PPEs. Their cationic polymerization leads to colored, oily oligomers.[86] In contrast, the anionic ROP with alkoxides as initiators proceeds readily within hours at low temperatures to high molecular mass polymers.[112] The mechanistic details of the anionic polymerization have been studied in detail by Penczek and co-workers using the example of 2-methoxy-2-oxo-1,3,2-dioxaphospholane.[99] Thereby, it was revealed that the polymerization of the five-membered phosphates follows a coordination insertion mechanism similar to that proposed by Teyssié *et al.* for the polymerization of L-lactide and ε-caprolactone.[113-114] The initial step is the nucleophilic attack of the P=O oxygen of the phosphate monomer on the aluminum atom of the initiator (Scheme 22). This results in the transfer of an isopropoxy group onto the phosphorus atom and the ring opening of the monomer. Propagation proceeds via a pseudoanionic mechanism by insertion of another monomer into the O-Al-bond. Termination is achieved by the addition of an acidic hydrogen (acidic acid).

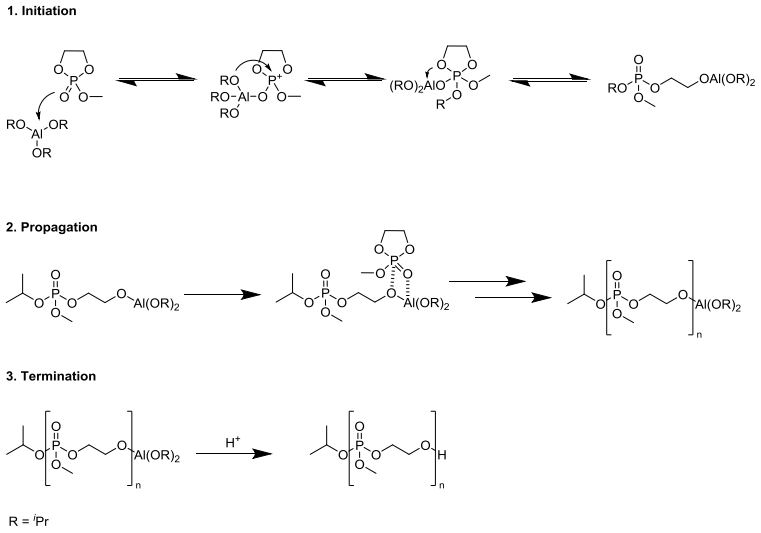

Scheme 22. Mechanism of the anionic ring-opening polymerization of 2-methoxy-2-oxo-1,3,2-dioxaphospholane initiated by aluminum triisopropanolate.

The main difference to the above-mentioned mechanism for the 6-membered analogues is the direct ring-opening after the initiator attack, due to the higher ring strain of the monomer. The high ring-strain of the five-membered monomers suppresses the possible elimination of the side chain attached to the phosphorus atom. Therefore the anionic polymerization of the five-membered in contrast to the six-membered monomers can be conducted under the conditions of a living polymerization, i.e. with absence of transfer and termination reactions. The living nature

of the anionic ROP of the five-membered phosphates was proven by chain extension, i.e. subsequent addition of monomer leading to a restart of the polymerization.[99]

With the anionic ROP established, it was possible to prepare homopolymers of a variety of cyclic phosphoesters with reasonable polymer weights[62, 115-116] and also copolymers leading to materials with altered properties compared to the homopolymers concerning solubility, biodegradability etc.[33-34, 117-119] Furthermore, more sophisticated structures such as block copolymers consisting of PPEs and poly(ε-caprolactone)[120] and block copolymers with a brush-like structure[121] containing PEGylated PPE-segments and poly(ε-caprolactone)-blocks.

Iwasaki *et al.* reported about the synthesis of a copolymer consisting of poly(2-ethoxy-1,3,2-dioxaphospholane) (PEEP) and poly(2-isopropoxy-1,3,2-dioxaphospholane) (PIPP) by anionic ROP using triisobutylaluminum as the initiator.[122] Molecular masses up to 1.2 to 1.5 x 10^4 g mol^{-1} with molecular mass distributions of $Đ < 1.3$ (determined by GPC) were achieved. The copolymers with a composition of 24 % PIPP and 74% PEEP exhibit lower critical solution temperature around 31°C.

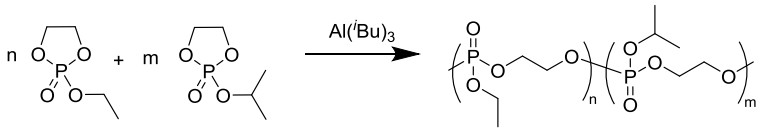

Scheme 23. Synthesis of the thermoresponsive copolymer PIPP-*co*-PEEP.

Furthermore copolymers of PPEs with other biodegradable polymers have been synthesized (Scheme 24). The most thoroughly investigated and widely used biodegradable polymers are aliphatic polyesters such as poly(lactic acid) (PLA) and poly(ε-caprolactone) (PCL). [119, 123] In particular PLA is a suitable material for applications in the biomedical field. Due to its strong mechanical properties and antimicrobial and antioxidant characteristics it is appealing as materials for surgical sutures and reconstructive implants. On the other hand its hydrophobicity and slow degradation limits its application.[119] Leong and associates showed that the copolymerization of lactic acid with phosphoesters allows an adjustability of its hydrophobicity and degradation rate.[119]

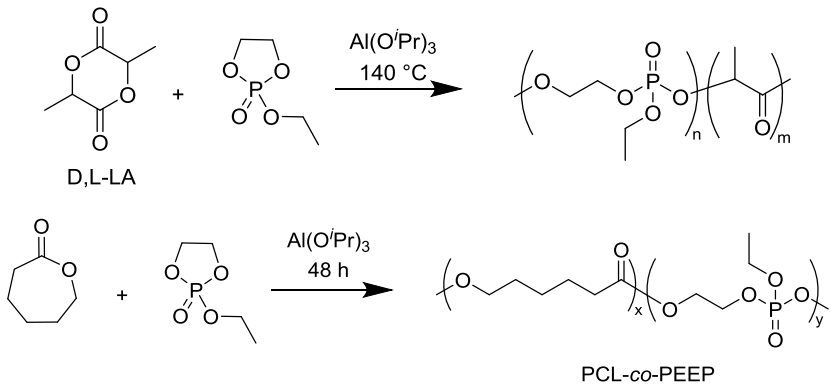

Scheme 24. Top: Synthesis of poly(D,L-lactide-co-2-ethoxy-2-oxo-1,3,2-dioxaphospholane) (PLA-co-PEEP). Bottom: Synthesis of poly(ε-caprolactone-*co*-2-ethoxy-2-oxo-1,3,2-dioxaphospholane) (PCL-*co*-PEEP).

The obtained polymers have been used for the formation of microspheres and were loaded with a model protein, BSA. The incorporation of PEEP led to an accelerated degradation of the microspheres and furthermore eliminated the biphasic degradation behavior of PLA. The microspheres showed a constant release of BSA. Leong *et al.* successfully demonstrated the feasibility of encapsulating human *β*-nerve growth factor, stabilized by bovine serum albumin, in a copolymer of ε-caprolactone and EEP by electrospinning.[118] The copolymer was synthesized by AROP with aluminum triisopropanolate as the initiator.

Furthermore, the formation of block copolymers has been realized by controlled anionic ROP.[120, 124] The first report about block copolymers containing a PPE-block was released by Wang *et al.* in 2006.[120] They reported about the synthesis of block copolymers consisting of poly(ε-caprolactone) (PCL) and either poly(2-isopropoxy)-2-oxo-1,3,2-dioxaphospholane (PIPP) and poly(2-ethoxy-2-oxo-1,3,2-dioxaphospholan) (PEEP) respectively. The block copolymers were synthesized via a one-pot, sequential ROP with Al(^{i}OPr)$_3$ as the catalyst.

The obtained block copolymer exhibit a molecular mass dispersity of $Đ$ = 1.20 determined by GPC. The GPC curves also showed a slight bimodality towards higher molecular mass indicating the formation of branched structures due to transesterification reactions of the pendant group during the polymerization.

A tremendous simplification of the ROP-process of cyclic phosphoesters has been made by Wang *et al*. in 2006 through employing the co-initiation of stannous octoate (Sn(Oct)$_2$) and alcohols, a common initiation system for lactones, on the polymerization of dioxaphospholanes.[125] The polymerization of cyclic phosphoesters with Sn(Oct)$_2$ also provides a certain biocompatibility, due to the rather low amounts and toxicity of Sn(Oct)$_2$ (which is FDA-

approved in many formulations).[126-127] However, alternatives to tin-compounds are a demand for future materials, to rule out any long-term toxicity based on the metal additives. Intensive mechanistic studies using MALDI-TOF mass spectrometry on the polymerization of cyclic carboxylic acid esters with $Sn(Oct)_2$ as catalyst published by Penczek and co-workers indicate a coordination-insertion mechanism starting with the formation of the stannous alkoxide as the active initiating species. This initially formed stannous alkoxide reacts with a monomer by means of coordination-insertion and leads to the active chain end, which propagates polymerization by simple monomer insertion into the -Sn-O- bond.[128] On the basis of these studies, Wang *et al.* suggested an analogues mechanism for the polymerization of cyclic phosphoesters catalyzed by $Sn(Oct)_2$ (Scheme 25).[125]

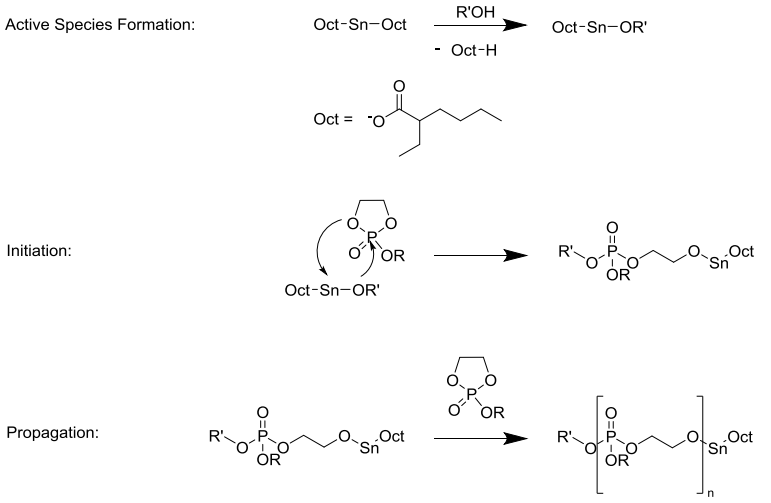

Scheme 25. Proposed mechanism of the ring-opening polymerization of 2-alkoxy-2-oxo-dioxaphospholanes initiated by stannous octoate.[125]

The polymerization can be forced to higher molecular masses by increasing the monomer/initiator ratio. With an increasing monomer conversion the molar-mass dispersity also increases: for conversions less than 70 % M_w/M_n is below 1.2, but increases to 1.5 for monomer conversions up to 95% due to transesterification reactions within the polymerization with $Sn(Oct)_2$. GPC shows besides a shift to higher molar masses, a multimodal molar-mass distribution as well as shoulders towards low molecular masses; the same was also reported for the ROP of cyclic esters.[129-130] The ROP of cyclic phosphoesters is more complex due to the fact that besides the polymer backbone also the side chain can take part in transesterifications (Scheme 26).

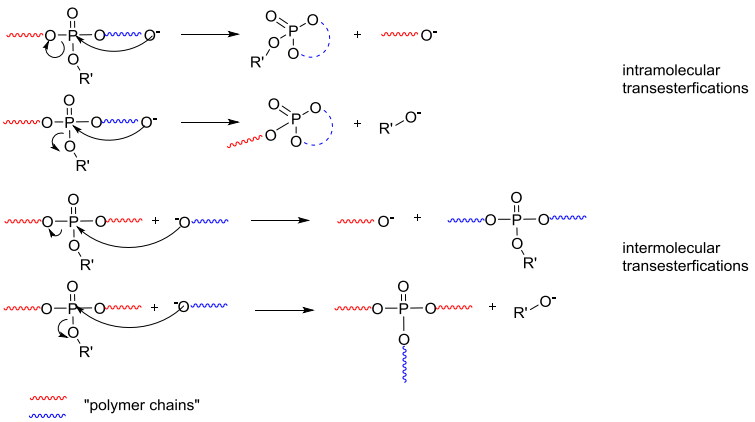

Scheme 26. Schematic depiction of the transesterification reactions of poly(phosphoester)s during ring-opening polymerization (Adapted with permission from[131] Copyright 2012 American Chemical Society.)

This method allows the synthesis of polymers with adjustable molecular masses and $Đ < 1{,}5$.[125] In 2010 Iwasaki et al. reported about a metal-free catalyzed ROP of cyclic phosphoesters by usage of organic superbases as catalysts, namely 1,8-diazabicyclo[5.4.0]undec-7-ene (DBU) and 1,5,7-triazabicyclo[4.4.0]dec-5-ene (TBD) and alcohols as initiators. [13] Here again, it was possible to employ an established initiator/catalyst-system for ROP of cyclic carboxylic esters [132] on the corresponding phosphoesters. Clément *et al.* reduced the amount of transesterifications to a minimum by using a catalyst-system that consists of DBU and organic Lewis acid thiourea (TU).[131] Mechanistic studies indicated an activation of the initiator by formation of hydrogen bonds to the alcohol functionality resulting in a quasi-anionic ring-opening polymerization.[131-133] The catalysts, DBU, TBD and DBU/TU, differ by means of the activation mechanisms. DBU exhibits only one activation site, which functions as hydrogen-bond acceptor and therefore activates only the initiator. In contrast TBD has two activation sites available and can therefore activate the initiator by acting as hydrogen-bond acceptor and simultaneously the CPM by acting as hydrogen-bond donor. The combination of DBU with TU also leads to a catalyst system, which can activate initiator and the cyclic phosphoester monomer (Scheme 34).

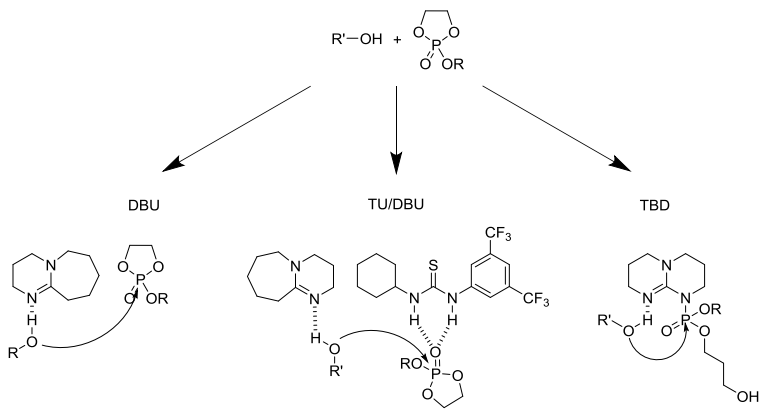

Scheme 27. Activation-mechanism of initiator and/or monomer by DBU, TBD and TU/DBU.(Adapted with permission from Reference 131. Copyright 2012 American Chemical Society.)

For the organocatalytic polymerization molecular masses up to 7×10^4 g mol^{-1} can be achieved with monomodal molar-mass distributions lower than 1.10 and monomer conversion of 98%.[131] Furthermore, by this method metallic catalysts can be avoided, thus making PPEs more attractive as materials for biomedical applications.[134] However, also care has to be taken, to remove unreacted monomer and the also potentially toxic organocatalysts from the final materials.

PPEs have also been synthesized enzymatically in two reports by Wen[135] and Zhuo and coworkers.[136] Porcine pancreas lipase catalyzed the polymerization of ethylene isopropyl phosphate to polymers of about 1 kDa after rather long reaction times (24-120h) and moderate temperatures. The enzymatic synthesis of PPEs is, without doubt, together with the anionic ROP (AROP) the most promising polymerization technique for future applications, meeting the requirements of sustainability.

Our group recently reported on the first living polymerization of cyclic 5-membered phosphonates (Scheme 28).25 In the 2-alkyl-2-oxo-1,3,2-dioxaphospholanes the exocyclic phosphoester is replaced by a phosphonate, whereas the advantageous properties of PPEs such as water-solubility and main chain degradabilitiy are preserved. The monomer was synthesized via a two-step synthesis starting with the preparation of the corresponding alkyl dichloro phosphonate. The following polymerization proceeds with a primary alcohol as initiator and DBU as catalyst.

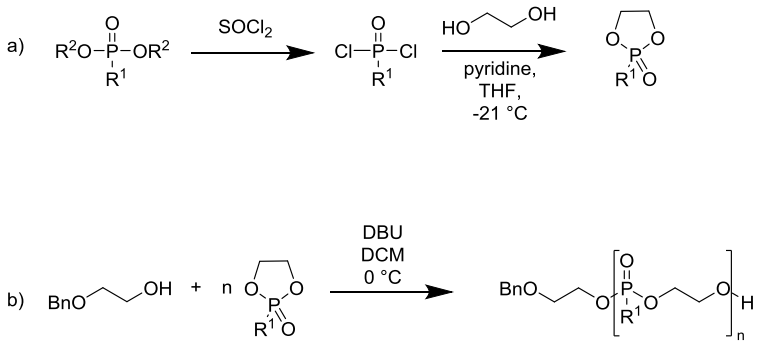

Scheme 28. (a) General synthesis of cyclic phosphonate monomers; (b) polymerization of cyclic phosphonates initiated by 2-(benzyloxy)ethanol and catalyzed by DBU at 0°C in dichloromethane.

Conversions above 90 % can be achieved, while transesterification reactions are reduced to a minimum. In contrast to poly(phosphate)s, within the polymerization process of (phosphonate)s only the main chain can participate in transesterification reactions. It can be distinguished between intra- and intermolecular transesterification resulting in the formation of cycles and termination of the chain growth respectively (
Figure **7**).

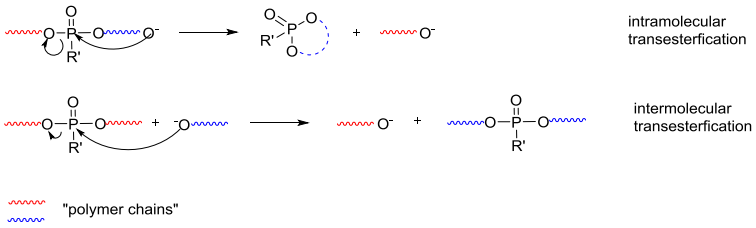

Figure 7. Two possible transesterification reactions during AROP of poly(phosphonate)s.

Very recently we extended the family of cyclic phosphonates to ethyl, propyl, and butyl-substituted structures. They all exhibit an excellent control over polymerization kinetics with full conversion and low molar-mass dispersities.[137] They are currently under deeper investigation concerning their potential in biomedical applications.

With the ROP established and the straightforward synthesis of the five-membered CPMs, it was possible to create more sophisticated polymer architectures especially by varying the pendant group. The thoroughly chosen side chain allows beside a precise adjustability of the hydrophilicity or lipophilicity respectively also a subsequent modification of the polymer.

Iwasaki *et al.*, for example, prepared copolymers consisting of PIPP (Table 2, Entry 9), PChOP (Table 2, Entry 20) and OPBB (Table 2, Entry 27) with adjustable hydrophobicity and functional

side chains.[138] The incorporation of OPBB into the polymer allows a subsequent transformation of the PPE-based linear and hydrophobic copolymer into a grafted and amphiphilic polymer by ATRP of 2-methacryloyloxyethyl phosphorylcholine (MPC). Additionally, the cholesteryl-containing units provide a control over the hydrophobicity and the hydrophobic interactions. So, the nature of the pendant group provides the control over solubility and supramolecular architecture. The CPM-synthesis based on the functionalization of COP provides, besides monomers with pendant ester linkages, also the preparation and direct polymerization of phosphoramidates, i.e. CPMs with amine attached to the phosphorus atom (Scheme 29). Previously, poly(phosphoramidate)s were exclusively accessible by post-polymerization modification of the corresponding poly(H-phosphonate).

Zhang *et al.* reported for the first time about the synthesis of a poly(phosphoamidate)s by direct ROP of the corresponding cyclic phospholane amidate monomer (MOEPA, Table 2, Entry 17).[139] Furthermore, the obtained poly(phosphoramidate)s exhibit acid-labile phosphoramidate-bonds along the backbone, thus providing access to phosphoester ionomers by one further step.

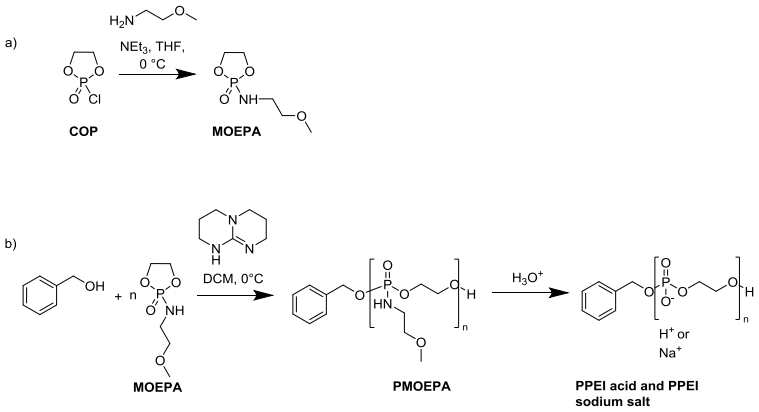

Scheme 29.a) Synthesis of cyclic phospholane amidate monomer and b) Polymerization of MOEPA with TBD as catalyst and benzyl alcohol as initiator and subsequent cleavage of the side chain of PMOEPA.

The presence of functional pendant groups in polymers is of great interest especially for the subsequent modification of polymers. For example, the pendant group in 2-((2,2-dimethyl-1,3-dioxolan-4-yl)methoxy)-1-dioxaphospholane-2-oxide (GEP, 19 Table 2) can be cleaved under acidic conditions releasing two hydroxyl groups, which allow a subsequent polymer modification (Scheme 30).[140]

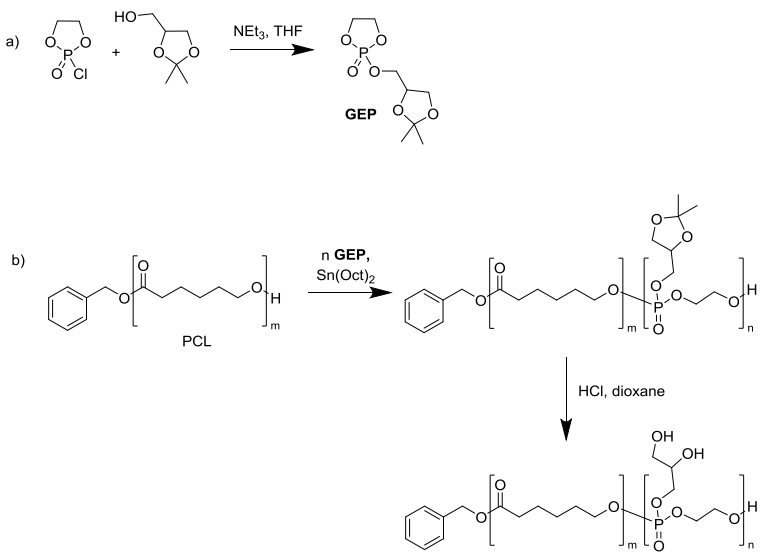

Scheme 30. a) Synthesis of 2-((2,2-dimethyl-1,3-dioxolan-4-yl)methoxy)-1-dioxaphospholane-2-oxide (GEP) and b) polymerization of GEP with Sn(Oct)2 as catalyst and PCL as macroinitiator and subsequent cleavage of the pendant acetal.

Lim *et al.* designed a CPM with a vinyl ether side chain (Scheme 31) as a versatile template for post-polymerization modification allowing beside a functionalization by thiol-ene click reaction also the subsequent introduction of acid labile functionalities, i.e. acetals and thio-acetals respectively.[141] These functionalities are especially appealing for biomedical applications due to their cleavability in acidic environment typical for sites of inflammations, tumors or for the gastrointestinal tract.[142-144]

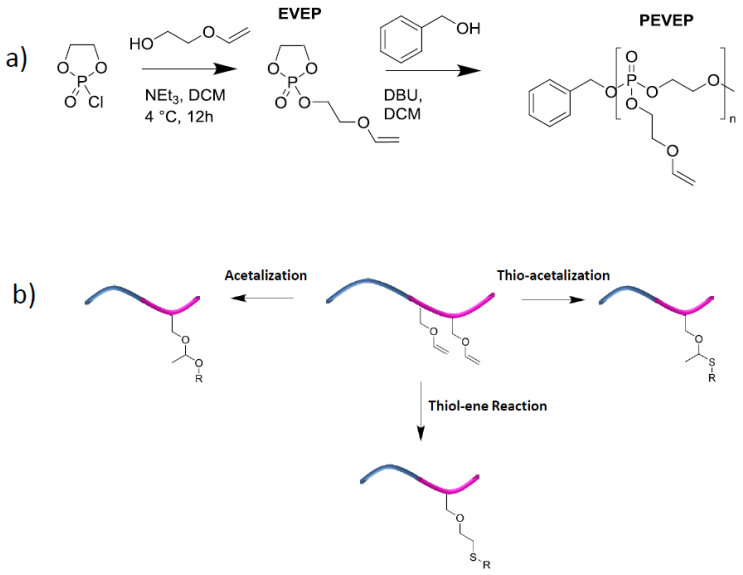

Scheme 31. a) Synthesis of ethylene glycol vinyl ether-1,3,2-dioxaphospholane-2-oxide (EVEP) and b) post-polymerization modification by three different reactions. (Adapted with permission from reference[141]; Copyright 2014 American Chemical Society.)

The post-polymerization of PEVEP by thiol-ene reaction with an excess of 2-(2-methoxyethoxy)ethanethiol leads to a quantitative functionalization of the pendant double bond, whereas the acetalization and thioacetalization are accompanied by transesterification reactions and degradation, thus leading to functionalization degrees of only 18 and 8%, respectively. Another two CPMs, namely 2-(but-3-yne-1-yloxy)- and 2-(but-3-en-1-yloxy)-2-oxo-1,3,2-dioxaphospholane (BYP and BeneP, Table 2 entry 24 and 29) with 'clickable' side chains by thiol-ene/yne or azide-alkyne cycloadditions have also been investigated in depth in the Wooley lab (Scheme 32).

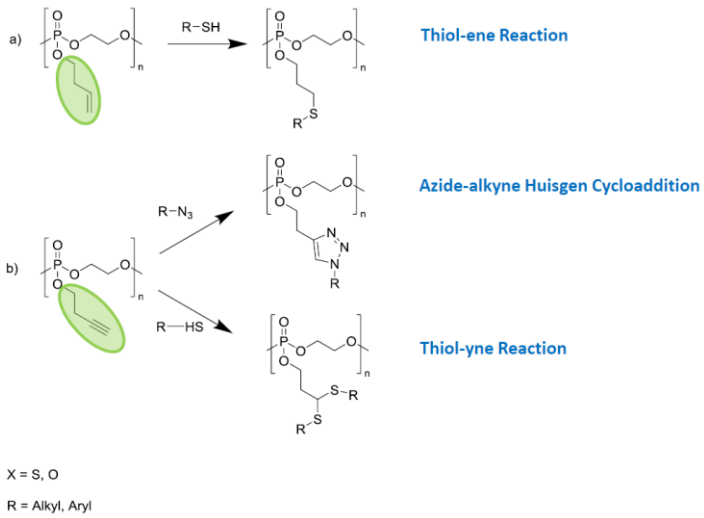

Scheme 32. Post-polymerization modification of poly(2-(but-3-yne-1-yloxy)- and 2-(but-3-en-1-yloxy)-2-oxo-1,3,2-dioxaphospholane) (PBYP and PBeneP, Table 2 entry 24 and 29).

Our group recently reported on the first orthogonally protected PPEs carrying benzyl- and acetal-protected hydroxyl groups in the pendant chains. A new monomer (Table 2, Entry 21) was developed and copolymerized with GEP and EEP (Table 2, Entry 19 and 4). Sequential deprotection under mild acidic conditions or hydrogenation releases the OH-groups selectively.[145] Also hyperbranched PPEs are accessible by ROP of HEEP (Table 2, Entry 22).[27] The inimer HEEP was prepared in high yield and the hyperbranched PPE was obtained by its self-condensing ROP in bulk without catalyst (Scheme 33).

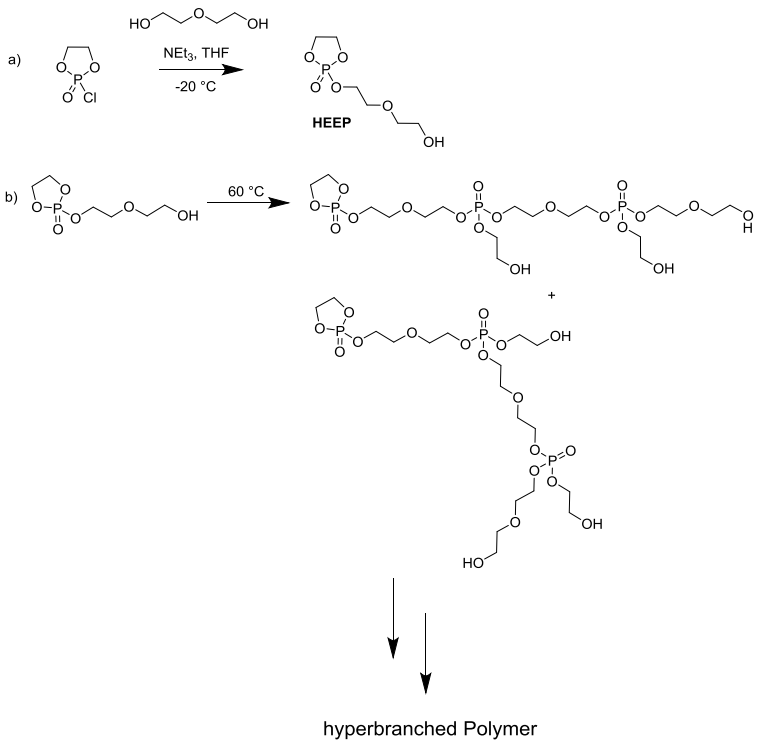

Scheme 33. a) Synthesis of 2-(2-hdroxyethoxy)ethoxy-2-oxo-1,3,2-dioxaphospholane (HEEP) and b) self-condensing ring-opening polymerization at 60 °C.

At 60°C after 14 h the molecular mass of the hyperbranched (hb) *hb*P(HEEP) reached 5,200 g/mol with *Đ*= 1.75. The degree of branching of *hb*P(HEEP) was determined to be 0.47 calculated from quantitative ^{31}P NMR (Figure 8).

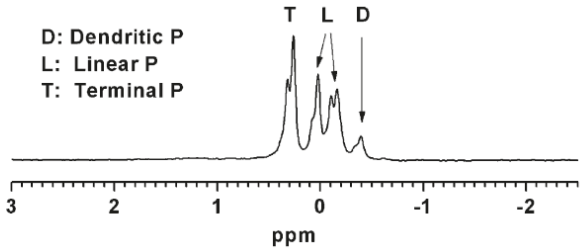

Figure 8. ^{31}P NMR spectra of *hb*PHEEP for the calculation of DB. (Reprinted with permission from reference 27; Copyright 2009 American Chemical Society.)

Table 2 gives an overview of the structures, polymerization techniques (PT), which have already been employed on the individual monomer and their availability.

Table 2. Five-membered cyclic phosphates for the ring-opening polymerization.

#	Monomer	Monomer Yield [%]	PT	Name	Ref
2	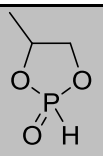 4-methyl-1,3,2-dioxaphospholane 2-oxide	74	A	**- (HMEP)**	[146]
3	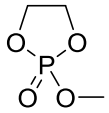 2-methoxy-1,3,2-dioxaphospholane 2-oxide	70	A,O,M	**MEP**	[86]
4	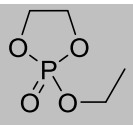 2-ethoxy-1,3,2-dioxaphospholane 2-oxide	65	A,O,M	**EEP**	[86]
5	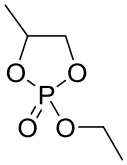 2-ethoxy-4-methyl-1,3,2-dioxaphospholane 2-oxide	51	O	**MEEP**	[147]
6	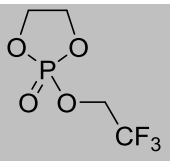 2-(2,2,2-trifluoroethoxy)-1,3,2-dioxaphospholane 2-oxide	55	A	**-**	[86]
7	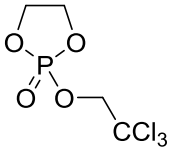 2-(2,2,2-trichloroethoxy)-1,3,2-dioxaphospholane 2-oxide	80	A	**-**	[86]

8	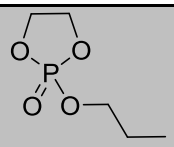 2-propoxy-1,3,2-dioxaphospholane 2-oxide	20	A	**-**	86
9	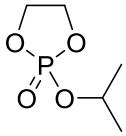 2-isopropoxy-1,3,2-dioxaphospholane 2-oxide	63	A	**IPP**	86, 148
10	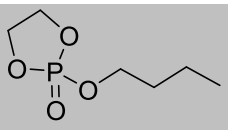 2-butoxy-1,3,2-dioxaphospholane 2-oxide	-	A, O		86
11	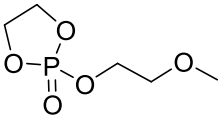 2-(2-methoxyethoxy)-1,3,2-dioxaphospholane 2-oxide	78	A	**MOEEP**	124
12	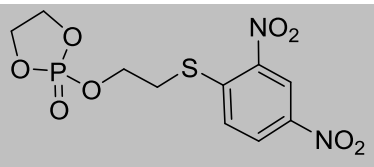 2-(2-((2,4-dinitrophenyl)thio)ethoxy)-1,3,2-dioxaphospholane 2-oxide	36	M	**-**	149
13	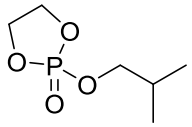 2-isobutoxy-1,3,2-dioxaphospholane 2-oxide	65			131
14	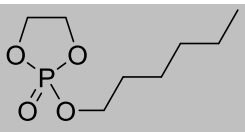 2-(hexyloxy)-1,3,2-dioxaphospholane 2-oxide	-	O	**HEP**	150

15	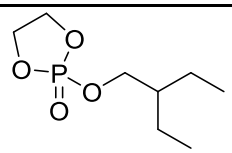 2-(2-ethylbutoxy)-1,3,2-dioxaphospholane 2-oxide	73	O	**EBP**	[15]
17	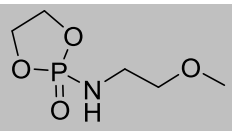 2-((2-methoxyethyl)amino)-1,3,2-dioxaphospholane 2-oxide	63	O	**MOEPA**	[139]
18	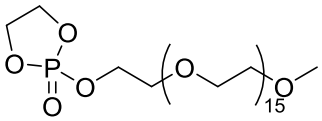 2-(2-(2-methoxyethoxy)ethoxy)-1,3,2-dioxaphospholane 2-oxide	70	A	**PPEG**	[121]
19	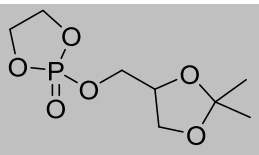 2-((2,2-dimethyl-1,3-dioxolan-4-yl)methox dioxaphospholane 2-oxide	63	M	**GEP**	[140]
20	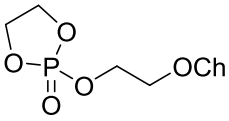 2-cholesteryl-1,3,2-dioxaphospholane 2-oxide	32.5	A	**ChOP**	[138]
21	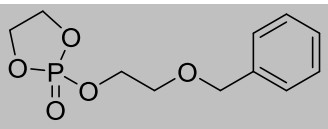 2-(2-(benzyloxy)ethoxy)-1,3,2-dioxaphospholane 2-oxide	87	M	**BnEEP**	[145]
22	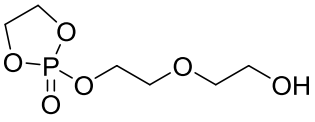 2-(2-(2-hydroxyethoxy)ethoxy)-1,3,2-dioxaphospholane 2-oxide	89.7	Thermal polym.	**HEEP**	[27]

23	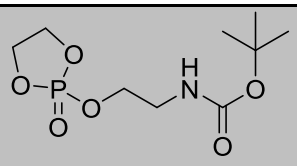	52.5	M	**EEAPBoc**	151
24	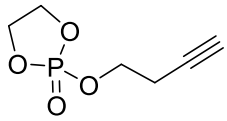 2-(but-3-yn-1-yloxy)-1,3,2-dioxaphospholane 2-oxide	30	M, O	**BYP**	88, 152
25	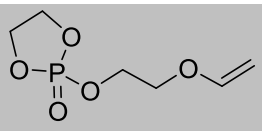 2-(2-(vinyloxy)ethoxy)-1,3,2-dioxaphospholane 2-oxide	76	O	**EVEP**	141
26	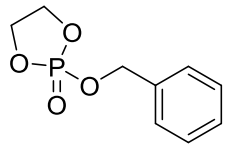 2-(benzyloxy)-1,3,2-dioxaphospholane 2-oxide	-	A	**BP**	153
27	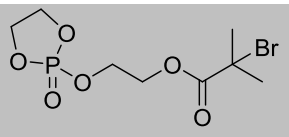 2-((2-oxido-1,3,2-dioxaphospholan-2-yl)oxy)et 2-bromo-2-methylpropanoate	67.1	A	**OPBB**	138
28	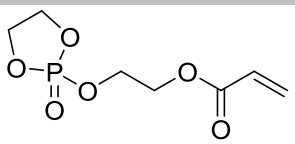 2-((2-oxido-1,3,2-dioxaphospholan-2-yl)oxy) ethyl acrylate	-	A	**OPEA**	154
29	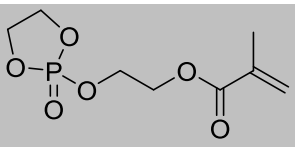 2-((2-oxido-1,3,2-dioxaphospholan-2-yl)o: ethyl methacrylate	97	A	**OPEMA**	155

30	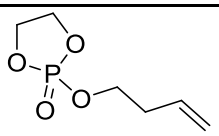 2-(but-3-en-1-yloxy)-1,3,2-dioxaphospholane 2-oxide	52	O	**BEneP**	156
31	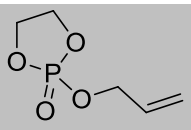 2-(allyloxy)-1,3,2-dioxaphospholane 2-oxide	-	O	**AEP**	157
32	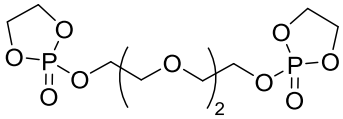 2,2'-((oxybis(ethane-2,1-diyl))bis(oxy))bis(1,3,2-dioxaphospholane 2-oxide)		M	**TEGDP**	95
33	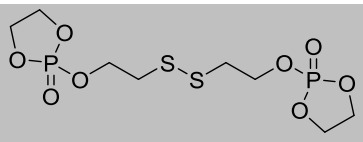 2,2'-((disulfanediylbis(ethane-2,1-diyl))bis(oxy))bis(1,3,2-dioxaphospholane 2-oxi	-	M	**SSDP**	158
34	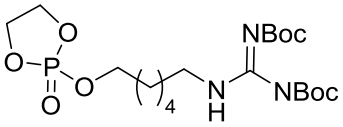 2-(6-*bis*-Boc-guanidino-hexyloxy)-1,3,2,-dioxaphospholane-2-oxide	79	O	**HexPhos**	159

A = anionic polymerization, initiators: ^{t}BuOK, ^{n}BuLi and $^{i}Pr_3Al$,

O = Organocatalysis, initiators: DBU, TBD, DBU/TU

M = Metallic catalysts, iniator: $Sn(Oct)_2$

1.5 Metathesis Polymerization of unsaturated phosphoesters

High molar-mass PPEs can be prepared by chain or step growth olefin metathesis polymerization.[41, 160-165] Cyclic or linear phosphoesters are readily accessible by esterification of $POCl_3$ and its derivatives. A great advantage of the acyclic monomers compared to the highly strained CPMs is their easy handling and long shelf-life also at room temperature. The unique

characteristic of this technique is the combination of the high functional group tolerance of modern ruthenium catalysts with the structural versatility of pentavalent phosphorus, which allows a precise tailoring of the polymer properties and side-chain functionalities.

The acyclic diene (ADMET) and triene metathesis (ATMET) polymerization are polycondensation reactions and follow a step-growth polymerization mechanism.[166] The ADMET is reported so far for acyclic phosphates and phosphonates (with the stable P-C-bond either in the side chain[162] or the polymer backbone[24]) carrying terminal double bonds. Esterification of unsaturated alcohols with phosphoryl chloride (or derivatives) allows access to difunctional or trifunctional monomers with different arm lengths (Figure 9).

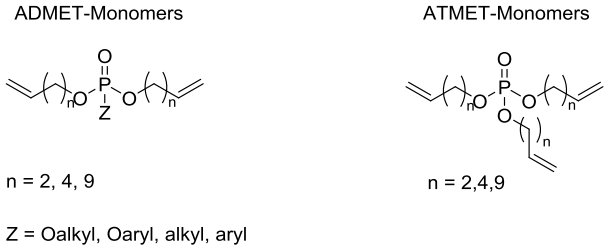

Figure 9. Monomer structures for the acyclic diene (ADMET) and triene (ATMET) metathesis polycondensation.

The polycondensation is promoted by metal carbenes and structurally versatile, linear or branched, unsaturated poly(phosphoester)s (UPPEs) have been prepared with ethylene as the only byproduct (Scheme 34). With the metathesis approach molecular masses ranging from 7 000 up to 50 000 g mol^{-1} can be obtained with molar-mass distributions of $Đ \approx 2$.[161] Also highly reactive P-Cl-containing monomers can be polymerized via the acyclic diene metathesis polymerization of the monomers di-(buten-3-yl) chlorophosphate and di-(undecen-10-yl) chlorophosphate. Molecular masses ranged from 1,000 to ca. 50,000 g/mol. These highly electrophilic phosphochlorides were post-modified with different nucleophiles, i.e. alcohols, amines, water, and thus allowed the synthesis of side chain polyphosphoamidates, -esters, and free acids from the same starting polymer.[164]

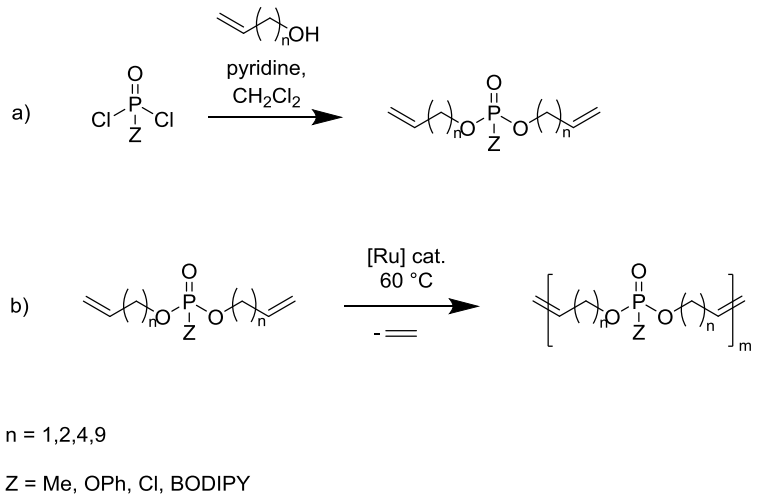

Scheme 34. a) Monomer synthesis for ADMET and ATMET polymerization and b) following ruthenium catalyzed polymerization.

The polymerization of the acyclic dienes can be monitored by NMR spectroscopy, Figure 10 shows this exemplarily for di-(but-3-en-1-yl) chlorophosphate. The polymerization is observed by ^{1}H DOSY NMR spectroscopy: after polymerization the resonances of the terminal double bond protons (a and b) at 5.1 and 5.8 ppm are detected as the end groups of the polymers with a distinct lower diffusion coefficient compared to the monomer. Moreover, as expected, a new peak (c,c') appeared at 5.4 ppm due to formation of internal double bonds. Further, the methylene group next to the phosphorus (d: 4.25 ppm) and the methylene group next to the double bond can be distinguished.

The microstructural adjustability of backbone and side chain allows a facile tailoring of the thermal properties such as melting or glass transition temperatures. The glass transition temperatures decrease with increasing number of methylene groups in the polymer backbone ranging from -30 °C for the poly(phenyl (hex-3-en-1-yl)phosphate) to -70 °C for the poly(phenyl (icos-10-en-1-yl)phosphate). The hydrogenation of the double bonds in the polymer backbone results in a shift of the melting point from -7 °C for the poly(phenyl (icos-10-en-1-yl)phosphate) to 45 °C for the hydrogenated polymer.[161] The respective poly(icos-10-en-1,20-dioxy methylphosphonate)s exhibit melting points up to 70 °C due to the smaller side chain.[162]

The variation of the main chain and thus the distance between the phosphate units (and the P-content) can be adjusted by the length of the unsaturated alcohol used in the monomer synthesis. Due to the „negative neighboring effect" the ADMET polymerization, however, a certain distance between the coordinating oxygen atoms of the phosphate and the double bond is necessary to achieve a reasonable degree of polymerization.[167] It was found that allyl esters do

not undergo ADMET polymerization for linear polymers, however, hyperbranched systems are accessible.[41] Pentavalent phosphorus offers the immediate introduction of three functionalities by esterification of $POCl_3$ with an ω-unsaturated alcohol, making phosphates ideal candidates for ATMET. Hyperbranched PPEs exhibit exceptional scavenging efficiency of singlet oxygen. This system was successfully employed to protect the triplet-triplet annihilation photon upconversion process against singlet oxygen quenching under ambient conditions.[168] They were also investigated as flame-retardant additives for commodity plastics recently.[41]

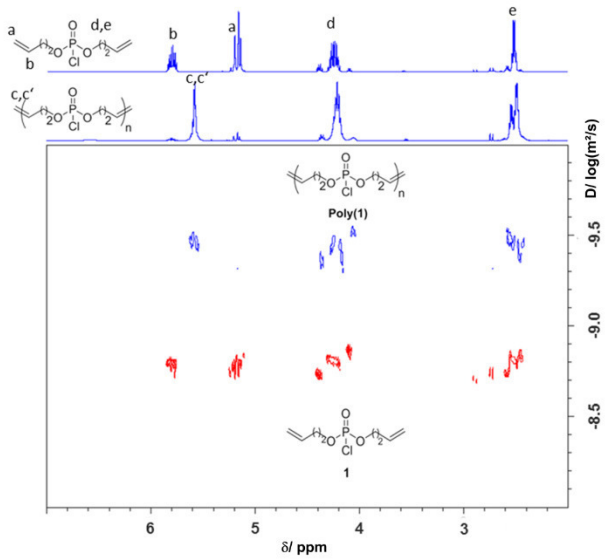

Figure 10. ^{1}H NMR spectrum of monomer 1 (top spectrum of the ^{1}H NMR axis; red signals in the DOSY spectrum) and the respective polymer poly(1) (bottom spectrum of the ^{1}H NMR axis; blue signals of DOSY spectrum) proving the formation of internal double bonds at 5.4 ppm (500 MHz in $CDCl_3$ at 25 °C). (Reprinted with permission from [164]; Copyright 2014 American Chemical Society.)

In our recent work, hydrophobic poly(phosphate)s and poly(phosphonate)s were prepared via ADMET polycondensation. Nanoparticles generated by miniemulsion from the corresponding PPEs exhibited strong binding affinity towards a model bone tissue, making this system potentially useful to deliver drugs to the bones. Fluorescent PPEs are accessible by metathesis by a BODIPY-modified phosphate monomer allowing to follow the pathway of nanoparticular drug carrier via fluorescence microscopy.[169] Another functional ADMET monomer was developed in our group to perform polymer-mediated Horner-Wadsworth-Emmons (HWE) reactions: The

usage of linear poly(phosphonate)s minimizes purification efforts because the polymer is converted into a poly(phosphate) during the HWE reaction which can easily be precipitated from the mixture leaving the raw product in the organic supernatant.[170] By this method, several olefins are accessible in high yields.

Polyesters are rarely synthesized by ring-opening metathesis polymerization (ROMP): strained unsaturated lactones could not be initiated by Grubbs type, i.e. Ruthenium-carbenes, catalysts; considerable polymerization was only observed if a Schrock-type catalyst, i.e. Molybdenum-carbene, was employed. For PPEs, however, ROMP was recently investigated for different monomers. The smallest ring systems, and the only ones that have been studied to date, are unsaturated seven-membered cyclic phosphonates, phosphates[162-163] and the nitrogen-containing counterpart.[171] The alkoxy-4,7-dihydro-1,3,2-dioxaphosphepine-2-oxides are accessible via condensation of *cis*-1,4-butene diol and phosphorus dichlorides; for the 1,3,2-diazaphosphepine 2-oxide, *cis*-1,4-butene diamine was used (Scheme 35). The pendant group, resulting from the third ester linkage, can be introduced prior to ring closure. The ring-closure was performed in a dilute THF solution (*ca.* 10 g L^{-1}) with slow addition of the diol *via* a syringe pump to avoid unwanted oligomerization. The ROMP monomers were obtained in reasonable yield (ca. 50-60%) and high purity. In the ^{1}H NMR, it is noteworthy, that the resonances for the protons of the methylene groups next to the phosphonate split up into two distinct signals as they are diastereotopic. This indicates that the phosphonate ring is conformationally locked.

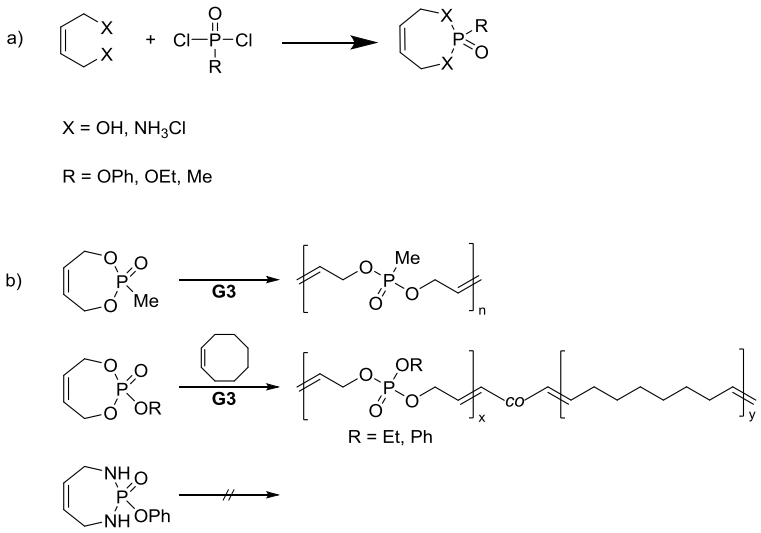

Scheme 35. a) Synthetic approach to 7-membered unsaturated cyclic phosphates and b) homo- and co-polymerization of different ROMP-monomers.

The 1,3,2-diazaphosphepine 2-oxide monomer did not undergo polymerization and was used to terminate a living ROMP of norbornene derivatives.[171] This allows, after acidic hydrolysis of the phosphoamides, the generation of amino-terminated poly(norbornene)s. In the case of the unsaturated seven-membered phosphates (2-phenoxy- and 2-ethoxy-4,7-dihydro-1,3,2-dioxaphosphepine 2-oxide) and phosphonates, polymerization was promoted by the ring-strain in the presence of Grubbs 3rd generation catalyst at ambient temperatures under an argon atmosphere up to 90% monomer conversion. The polymers show a rather broad molecular-mass distribution ($Đ \approx 2$) and molecular masses up to 5,000 g mol^{-1}. They are amorphous materials with glass transition temperature of ca. -45°C. Also, copolymers with cis-cyclooctene have been prepared to adjust the crystallinity of the copolymers.[162-163] ROMP allows to prepare poly(phosphonate)s at room temperature under less strict conditions as the anionic polymerization demands. In order to maximize the hydrophilicity of this polyester, the distance between two ester groups needs to be minimized by introducing short alkyl spacers as a linkage. The polyphosphates, which are accessible by ROMP, close the gap of a hypothetical ADMET polymerization of a diallyl phosphate monomer, which does not undergo ADMET polymerization due to the "negative neighboring group effect" of the phosphate ester.[172]

3. Hydrolytic degradation of PPEs

The degradation behavior of polymeric materials is important for many applications, especially in the biomedical field: for tissue engineering, the degradation rate, for example, needs to be designed in the time of the tissue growth, while drug delivery vehicles or nanocarriers need time-dependent release, which should be adjusted by the chemistry. For PPEs several factors are important to consider: hydrophilicity, crystallinity/ glass transition temperature, binding motif around P, and the architecture of the polymer. The degradation rate of PPEs may be adjusted by controlling the chemical structure of the backbone and/or the pendant groups (Figure 11). For PPEs various enzymes have been reported to degrade phosphoesters in literature,[173-176] depending on their binding motif and their hydrophilicity. In addition often a combination of hydrolytical and enzymatic degradation of PPEs *in vivo* has to be expected making an *in vitro* simulation only partly reasonable. In addition, it has been found, that degradation products may self-catalyze further degradation.[177] Intensive investigations on the kinetics and mechanisms of the hydrolysis of PPEs at different pH-values have been made by Baran and Penczek using the example of poly(2-methoxy-2-oxo-1,3,2-dioxaphospholane).[9]

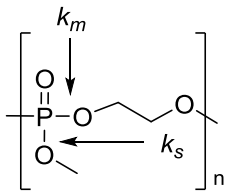

Figure 11. Hydrolysis constants for the phosphoesters in the main chain (k_m) or side chain (k_s) in PPEs.

The investigations revealed that for different pH values the hydrolysis follows different mechanisms: at acidic conditions (pH = 2) the hydrolysis proceeds via a nucleophilic attack of water on the *α*-carbon atom after activation of the phosphoryl (P=O) bond. Due to the higher accessibility of the carbon atom in the side chain, the ester linkage of the pendant group is cleaved faster than the ester linkages in the main chain. Therefore the cleavage of the side chain can be decelerated by using voluminous side groups. Under weak acidic conditions hydrolysis does not occur for most phosphate esters.[178] Under basic conditions the nucleophilic attack of the OH^- takes place on the central phosphorus atom resulting in a trigonal bipyramidal geometry, wherein the axial position is preferentially broken. Due to the pseudo rotation of phosphorus center, the side chain as well as the polymer backbone can occupy this position thus resulting in similar rates for the cleavage of side and main chain (Scheme 36). Due to the simultaneous cleavage of ester linkages in the main chain and side chain, the disruption of the backbone would be accelerated under basic conditions. So the time needed until half of the ester bonds were cleaved have been dramatically faster in basic conditions compared to acidic conditions (6 h at pH 12.30 while 3775 h at pH 3.78). It has to be mentioned that phosphodiesters of phosphoric acid are remarkably stable against hydrolysis,[139] however they may breakdown further by enzymatic degradation.

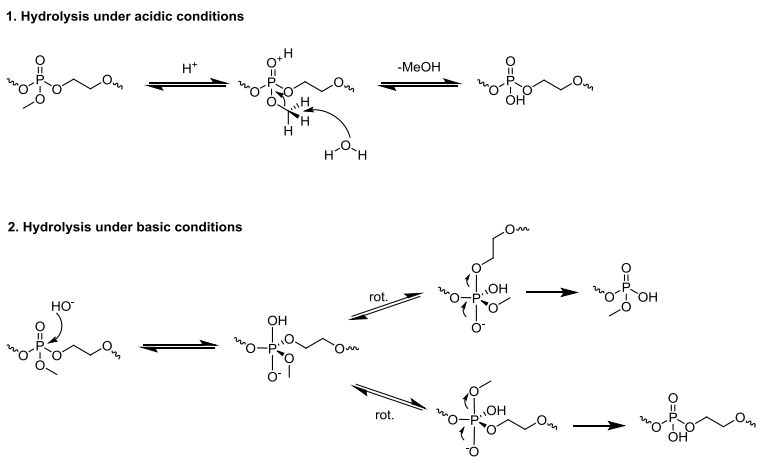

Scheme 36. Hydrolysis of poly(2-methoxy-1,3,2-dioxaphospholane) under 1. acidic and 2. basic conditions.

4. Biomedical applications of poly(phosphoester)s

The major challenges in drug delivery are the poor water-solubility of the majority of drugs, their short blood circulation times and the resulting inability to gain access to the site of action at an appropriate dose.[179-180] The therapeutic effectivity of hydrophobic drugs is often limited by the afore mentioned issues. One possibility to overcome these problems is the usage of nanocarriers, such as polymeric micelles, for the delivery of hydrophobic drugs. Polymeric micelles are formed by amphiphilic block copolymers, which consist in the simplest case of two different polymers covalently attached to each other and are able to self-assemble spontaneously into micelles in aqueous solution. They exhibit core-shell structures with the hydrophobic core serving as environment for hydrophobic drugs and the hydrophilic shell for stabilization in aqueous solution. The sizes of the micelles typically range from 10 to 50 nm. The micelles can be loaded with drugs by a physical entrapment as well as by covalent bonding to the block copolymer. These micelles possess several features such as enhancing the aqueous solubility of drugs, prolonging the blood circulation time, improving the preferential accumulation at tumor sites by the enhanced permeability and retention effect.[181-182] To avoid an accumulation of the carrier materials in the body, biodegradable materials are particularly interesting for the design of micellar nanocarriers. With the development of controlled polymerization techniques, PPEs have attracted the interest of a few working groups as promising materials for drug delivery systems. Especially the controlled synthesis of water-soluble PPEs makes them interesting candidates for drug delivery as a potential substitute for the non-degradable poly(ethylene glycol) (PEG). PEG is the gold standard polymer in today's drug delivery community:

PEGylated drugs (proteins or low molecular mass drugs), PEGylated liposomes or micelles with the hydrophilic corona based on PEG are dominating the scientific literature.[183-185] This is mainly attributed to the extraordinary properties of PEG, such as high water-solubility, low protein affinity and easy access to well-defined structures. The commercially available methoxy-PEGs are typically used and modified with various hydrophobic segments, for example. PPEs, however, are typically biocompatible and degradable materials and by the ROP of EEP, also water-soluble PPEs are accessible with the benefits of a living/ controlled polymerization technique. Further developments, such as clickable PPEs[186] for postpolymerization modification or also water-soluble poly(alkyl alkylene phosphonate)s broaden the potential of these biodegradable materials to replace the stable polyethers in the future.

Just recently, our group successfully demonstrated the "stealth effect", i.e. the inhibition of the unspecific cellular uptake of PEGylated and "PPEylated" nanocarriers.[187] It was shown that the modification of polystyrene nanoparticles with both PEG or PEEP either by covalent[187] or adsorptive[188] attachment of the PPEs to the particle surface resulted in a drastically reduced uptake of the particles by cells of the immune system.

This section will highlight several applications of PPEs for drug delivery; we selected representative and more recent examples for various applications. The interested reader may also refer other excellent reviews about PPEs for additional information.[18, 20-21, 189-190]

To date, several working groups have published PPE-based drug delivery systems ranging from micellar[191-193] to nanoparticulate strucutres.[194-197]

Wang *et al.* demonstrated successfully the delivery of siRNA[151, 198] or siRNA[199] combined with paclitaxel to tumor cells both *in vitro* and *in vivo* without activation of the innate immune response or the generation of carrier associated toxicity. The partially degradable carrier system is based on a triblock copolymer consisting of monomethoxy poly(ethylene glycol), poly(ε-caprolactone) and poly(2-aminoethyl ethylene phosphate) ($mPEG_{45}$-*b*-PCL_{100}-*b*-$PPEEA_{1,}$ Scheme **37**).[151, 198] The triblock copolymer was prepared by sequential ROP of lactide and 2-(*N*-*tert*-butoxycarbonylamino) ethoxy-2-oxo-1,3,2-dioxaphopholane, starting with a PEG macroinitiator and $Sn(Oct)_2$ as the respective catalyst and subsequent careful hydrolysis of the protective group to release the pendant amines.

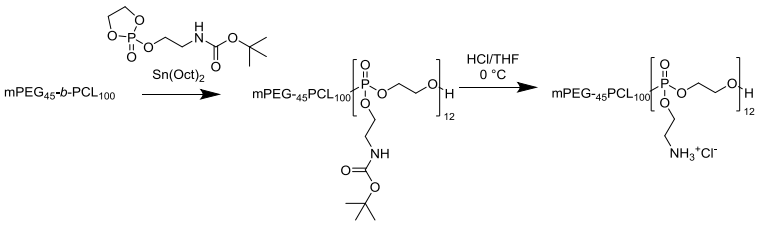

Scheme 37. Synthetic procedure for the synthesis of amphiphilic mPEG45-b-PCL100-PPEEA12 for gene delivery. (Adapted with permission from reference 151. Copyright 2008 American Chemical Society.)

The micellar nanoparticles (MNPs) were prepared by the solvent evaporation method. Wang and coworkers assume a three layered structure for the MNPs with the hydrophobic PCL segment in the inner core and the outer corona consisting of two sublayers (Figure 12). The inner layer of the outer corona includes part of the PEG- and the PPEA-segment and the outer layer is represented by the remaining part of the PEG-block. The siRNA is believed to bind to the cationic layer by electrostatic interaction.

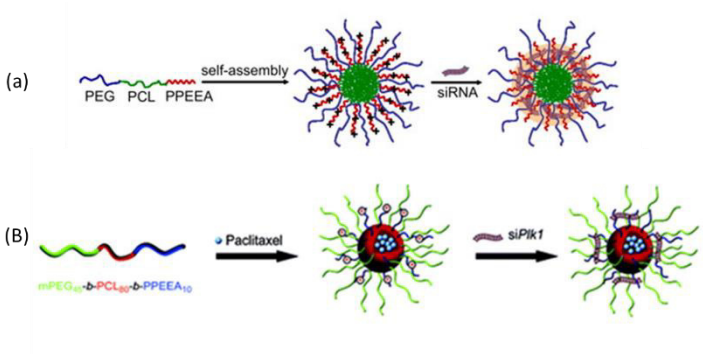

Figure 12. Schematic drawing of self-assembled cationic micellar nanoparticles and loading with (a) siRNA (Reprinted with permission of reference 151. Copyright 2008, with permission from Elsevier.) and (b) siRNA and Paclitaxel (Reprinted with permission from reference 199;Copyright 2011 American Chemical Society.)

The effective internalization of the micellar carrier system by cancer cells and the subsequent siRNA release resulted in a significant down-regulation of protein expression of these cells. Furthermore, the micelles carrying both siRNA and paclitaxel showed remarkably inhibition of tumor growth in a synergistic way.

Furthermore, Wang *et al.* developed an innovative, dual pH-sensitive anti-cancer drug delivery system based on PPEs with enhanced cytotoxicity in drug-resistant cancer stem cells. As proof

of concept, a polymer doxorubicin-conjugate was used that can react to the tumor extracellular and intracellular pH gradients.[200] The nanocarrier was synthesized via a multi-step protocol (Scheme 38). The final drug carrier contains doxorubicin units that are bound to the polymer via an acid-labile hydrazone bond. The remaining amino groups were reacted with 2,3-dimethylmaleic anhydride resulting in an amide bond that can be cleaved under slightly acidic conditions. Therefore, the resulting drug carrier can change its charge by cleavage of the amide bond in the tumor extracellular environment from negative to positive resulting in an enhanced internalization by the tumor cells. Then, in the more acidic intracellular environment the hydrazone bond is cleaved and the doxorubicin is released.

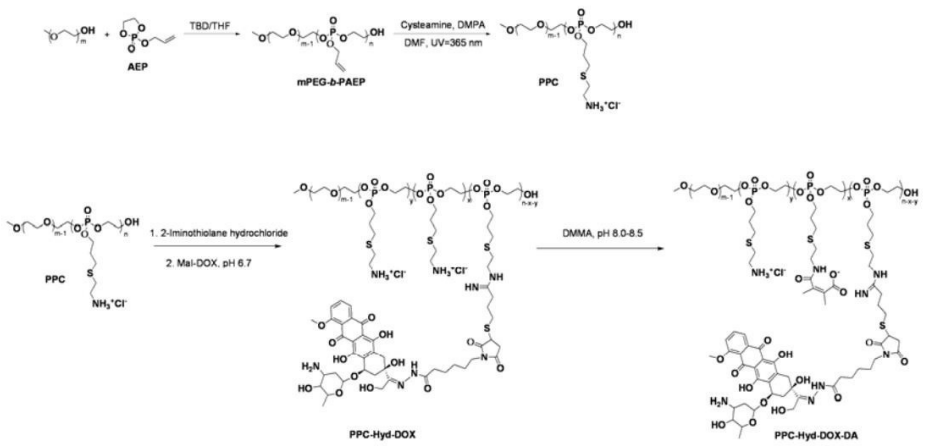

Scheme 38. Synthetic approach to PPC-Hyd-DOX-DA. (Reprinted with permission from reference 200. Copyright 2011 American Chemical Society.)

The final drug carrier contains doxorubicin units that are bound to the polymer via an acid-labile hydrazone bond. The remaining amino groups were reacted with 2,3-dimethylmaleic anhydride resulting in an amide bond that can be cleaved under slightly acidic conditions (Figure 13A) . Therefore, the resulting drug carrier can change its charge by cleavage of the amide bond in the tumor extracellular environment from negative to positive (Figure 13 B) resulting in an enhanced internalization by the tumor cells. Then, in the more acidic intracellular environment, the hydrazone bond is cleaved and the doxorubicin is released (Figure 13C).

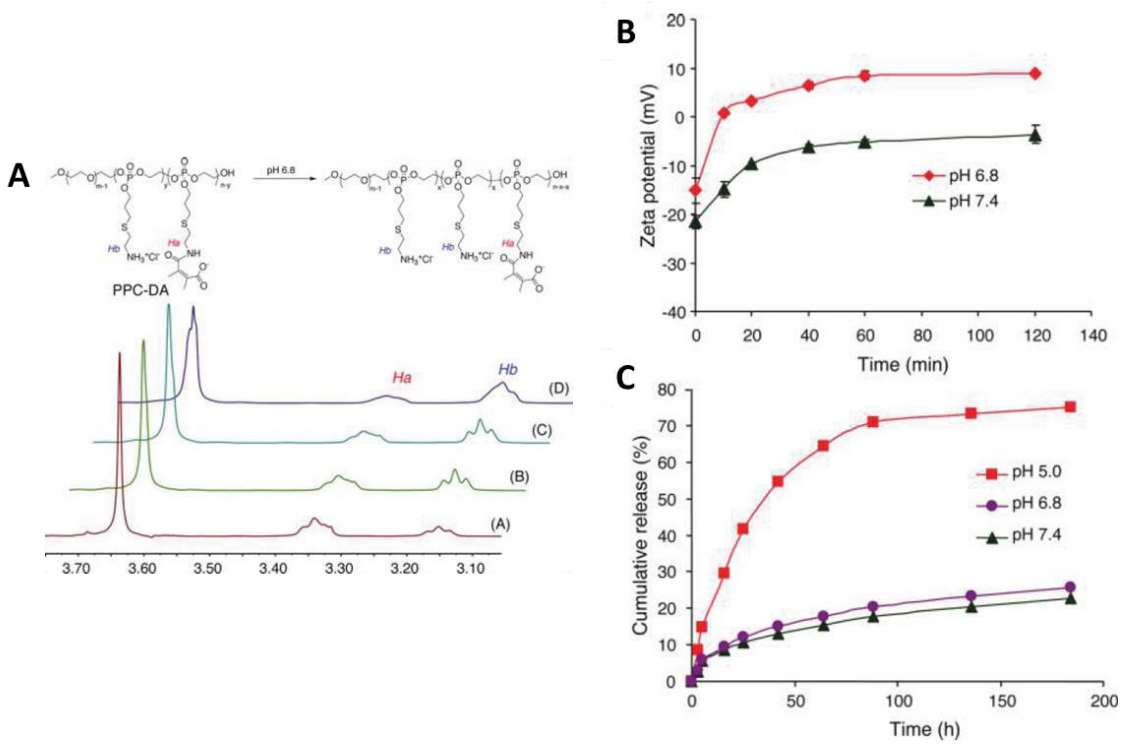

Figure 13. A) ^{1}H NMR spectra of PPC-DA after incubation at pH 6.8 in D_2O/DCl (25°C) for different time periods: (A) 0 min, (B) 10 min, (C) 30 min, (D) 60 min. B) Zeta potential change of PPC-Hyd-DOX-DA nanoparticles after incubation at pH 7.4 or 6.8 for different time periods. C) Time-dependent cumulative release of DOX from PPC-Hyd-DOX-DA NPs at different pH values. (Reprinted with permission from reference 200. Copyright 2011 American Chemical Society)

The successful release of DOX in the tumor cells at pH = 6.8 has been demonstrated by a sphere formation assay in the SK-3rd cancer stem cell line. The treatment of cancer stem cells with the PPC-Hyd-DOX-DA nanoparticles resulted in a significant lower number of cells in the spheres compared to the treatment with free DOX. To conclude, the dual pH responsive nanoparticles represent an interesting platform for further investigations.

The Wooley lab studied in excellent interdisciplinary collaborations block copolymers with one block consisting of either 'clickable' **PBYP** (Table 2, Entry 23) or **PBEneP** (Table 2, Entry 29) as the basic materials for drug delivery systems.[14-15, 94, 152, 201-208] The double/triple bonds in the polymer side chains were subsequently functionalized by click reactions, i.e. the thiol-ene/yne reaction and the azide-alkyne-1,3-dipolar cycloaddition.

These block copolymers have two major intentions: the delivery of the hydrophobic anticancer drug paclitaxel and the delivery of antimicrobial silver for the treatment of lung infections.

In 2013 the 1st generation MNPs was published based on an amphiphilic PEG-*b*-PPE-*g*-PTX block copolymer where the PPE-block consists of PBYP (Table 2 entry 23) serving as anchor point for the Paclitaxel (PTX) grafting.[207] Paclitaxel is a potent microtubule-interfering agent for the treatment of breast, non-small lung and advanced ovarian cancers, which belongs to the class of hydrophobic anticancer drugs. One of the major challenges within the application of paclitaxel is the effective delivery through aqueous environment to intracellular targets. Due to its hydrophobicity it exhibits a strong tendency to aggregate, which can lead to complications such as embolism and local toxicity.[209] One efficient approach to overcome the low water-solubility is the usage of degradable micellar nanoparticle carriers.[210] The pendant alkynes in the PBYP-block ensure the grafting of the azide-functionalized PTX by the azide-alkyne cycloaddition

For the micellar nanoparticle formation, the polymer with a loading capacity of 55 wt% and a high water-solubility of 11.3 mg mL^{-1} was used. However, the polymer showed only a low PTX-release of 5% after four days incubation in 20 mM acetate buffer at pH=6. Thus resulting in an 8-to-63 fold lower cytotoxicity against several cancer cell lines compared to the commercial PTX. The low cytotoxicity can be ascribed to the slow dissociation of PTX from the polymer backbone. Therefore, in 2014 the 2nd generation PEO-*b*-PPE-*g*-PTX (G2) was published (Scheme 39), wherein the hydrophobic PBYP- is replaced by a PBEneP-block (Table 2, entry 29).[14] The PBEneP- in contrast to the PBYP-block allows a thermo-induced thiol-ene reaction for the post polymerization modification proceeding without the usage of potentially toxic metal catalysts.

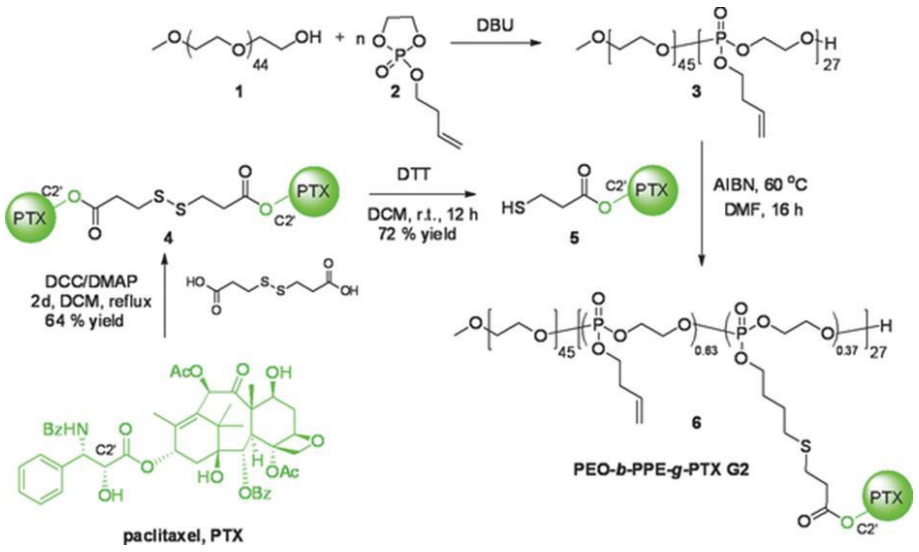

Scheme 39. Synthesis of PEO-*b*-PPE-*g*-PTX G2. (Taken with permission from reference 14. Copyright 2014 Wiley).

In G2 PTX is connected to the polymer backbone via an acid sensitive hydrolytically-labile β-thiopropionate linkage, which ensures a PTX release of 50 wt% after 8 days in PBS buffer at pH=5.5 (under neutral conditions only 25 wt% release). The cytotoxicity of G2 was studied *in vitro* against OVCAR-3 and RAW 264.7 cells. Compared to the first generation PEO-*b*-PPE-*g*-PTX, G2 showed an enhanced, but still 3-to-10 fold lower cytotoxicity compared to the free PTX.

Beside the paclitaxel-conjugates the same group studied different PPE-nanoparticles for the therapy of bacterial infections.[204, 206] Together with the Hunstad lab they prepared silver-bearing degradable nanoparticle consisting of PPE-*block*-poly(L-lactide) and studied the treatment of bacterial infections.[204] The PPE segment in the polymer again consists of PBYP (Table 2 entry 23) that was proven to be suitable for efficient post polymerization modification by thiol-yne reaction. Here, the thiol-yne reaction was performed with 3-mercaptopropanoic acid, which guarantees high water solubility as well as the interaction with silver. Nanoparticles were prepared by direct dissolution in water. The silver loading was performed using three different silver compounds, silver acetate (AgOAc), 1-methyl-3-(3-hydroxypropyl)-4,5-dichloroimidazol-2-ylidene silver(I) acetate (SCC22), or 1-methyl-3-hexyl-4,5-dichloroimidazol-2-ylidene silver(I) acetate (SCC10). It was assumed, that the loading into the nanoparticles occured by three different mechanisms, i.e. electrostatic interaction with the carboxylate groups, coordination by the sulfur atoms and encapsulation by hydrophobic interactions (Figure 14).

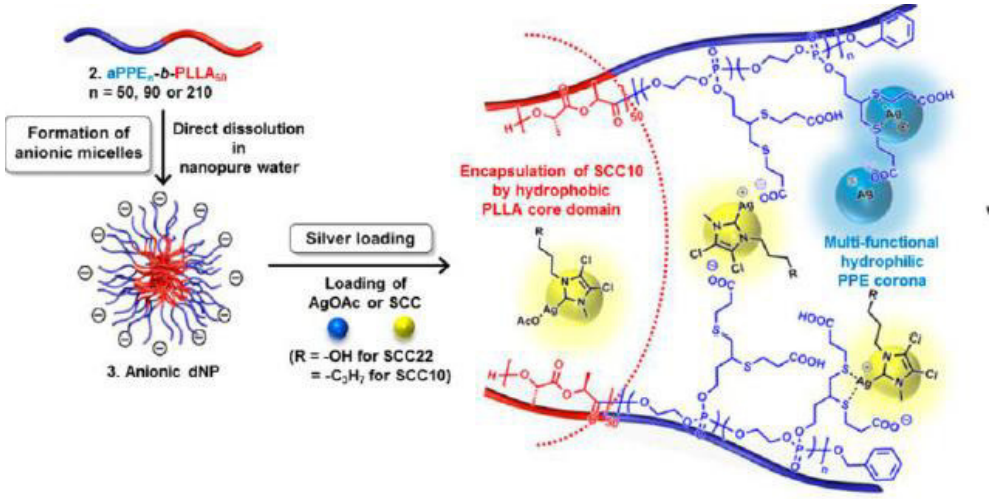

Figure 14. Schematic illustration of the self-assembly of the PPE_n-b-PLLA block copolymer into anionic micelles by direct dissolution in water followed by silver loading. (Reprinted with permission from reference 204. Copyright 2015 American Chemical Society)

The highest loading capacity of 12% was achieved by using SCC22 and a feed ratio of 100 wt % feed amount. For the release kinetics four samples with the highest loading capacities were chosen and all samples showed a plateau with almost complete silver release on the 3rd day. The degradation of the nanoparticles in aqueous buffer solutions at pH 5.0 or 7.4 at 37 °C was evaluated by DLS measurements and ^{31}P NMR spectroscopy. In both cases, after two weeks the hydrodynamic diameters were significantly decreased and after 35 days ^{31}P NMR spectroscopy showed a distinct shift of the signal from the intact backbone to the degradation product, i.e. phosphoric acid. All in all, the fully degradable silver-bearing nanoparticles show high potential for treatment of bacterial infections and are of high interest for further investigation and development.

A straight forward synthesis of new transporter systems based on oligophosphoesters for drug delivery has been developed by McKinlay *et al.*[159] The presented drug delivery systems are based on a new cyclic phosphate monomer (Table 2, Entry 32) exhibiting a guanidine unit in the pendant chain that can facilitate the cell-penetrating properties. The conjugation of drugs and probe molecules respectively can be achieved by two different strategies (Scheme 40). Cargo molecules containing a nucleophilic functional group, i.e. alcohol, thiol or amine group, can be directly used as initiators in the oligomerization reaction resulting in the cargo-transporter system (Scheme 40B, Strategy 1). Cargo molecules that cannot be conjugated to the oligophosphoester directly in the oligomerization process can be attached to the transporter by

postoligomerization strategies. Using this pathway, cargo molecules can attach to be releasable or permanently bound (Scheme 40B, Strategy 2).

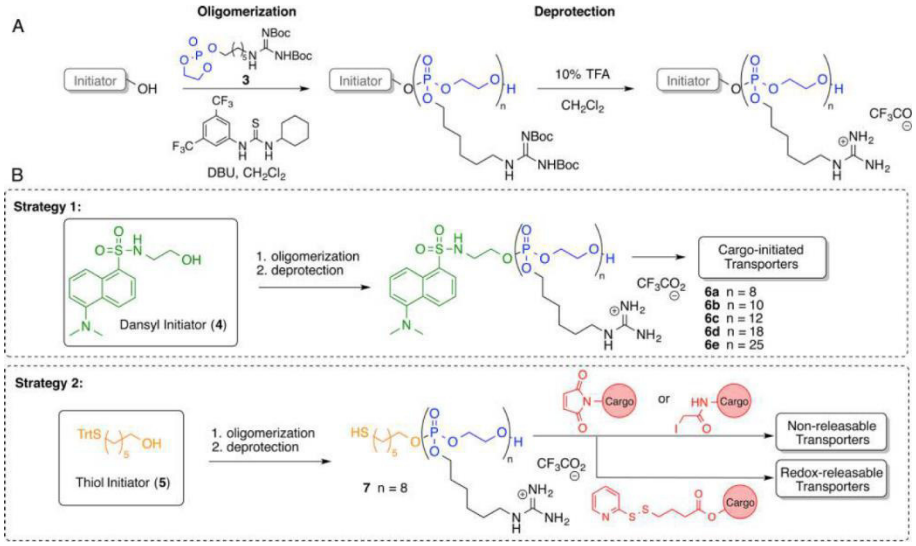

Scheme 40. Overview of synthetic methodologies employed to access guanidinium-rich oligophosphoester transporters. (A) ROP of HexPhos for two step access to guanidinium-functionalized oligophosphoester for drug/probe delivery. (B) Methods of conjugation of drugs or probe molecules to form cell-penetrating oligomeric conjugates. (Reprinted with permission from reference 159. Copyright 2016 American Chemical Society.)

Studies of the length-dependence of the cellular uptake showed a maximum uptake for the HexPhos 10-mer and a in general drastically increased uptake compared to the analogous oligocarbonate (Dansyl-MTC-G_8, Figure 15C) and system and the arginine homopolymer (Dansyl-Arg_8, Figure 15C) (Figure 15A). Cellular uptake was proven in four different cell lines and compared to Dansyl-MTC-G_8 and Dansyl-Arg_8 (Figure 15B).

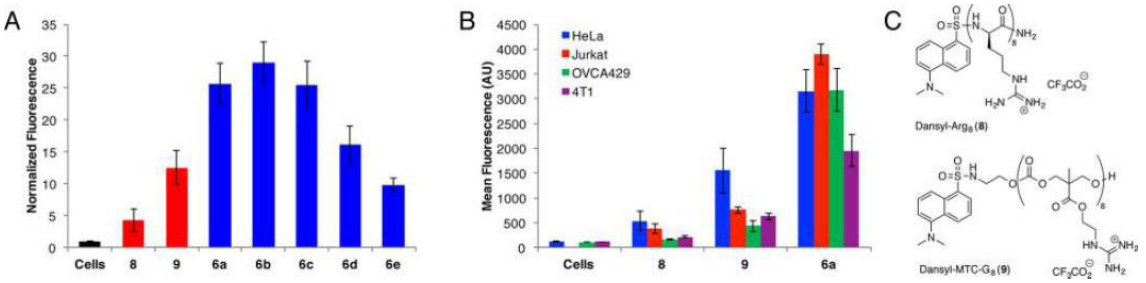

Figure 15.(A) Length dependence of uptake of Dansyl-HexPhos,oligomers 6a−e in HeLa cells compared to Dansyl-Arg8 (8) and Dansyl-MTC-G8 (9). (B) Cell line dependence of uptake of HexPhos8 in HeLa cells (blue), Jurkat cells (red), OVCA429 cells (green), and mouse 4T1 cells (purple). (c) Structures of previously reported transporter systems Dansyl-Arg8 (8) and Dansyl-MTC-G8 (9). (Reprinted with permission from reference 159. Copyright 2016 American Chemical Society.)

Collectively, this study impresses with a plain but clever design of new and efficient drug delivery systems that are accessible via a straightforward synthesis.

Light-responsive amphiphilic hyperbranched PPEs as smart nanocarriers for controlled drug release have been published by Chen *et al*. (Scheme 41) [28, 211] The nanocarriers consist of HPHEEP, (Table 2, entry 22) endcapped with light-sensitive units. The first published polymer contained 2-diazo-1,2-naphthoquinone (DNQ) and the second one contained 1'-(β-carboxyethyl)-3'-3'-dimethyl-6-nitrospiro[indoline-2',2-chromane] (SP-COOH) as light-sensitive unit.

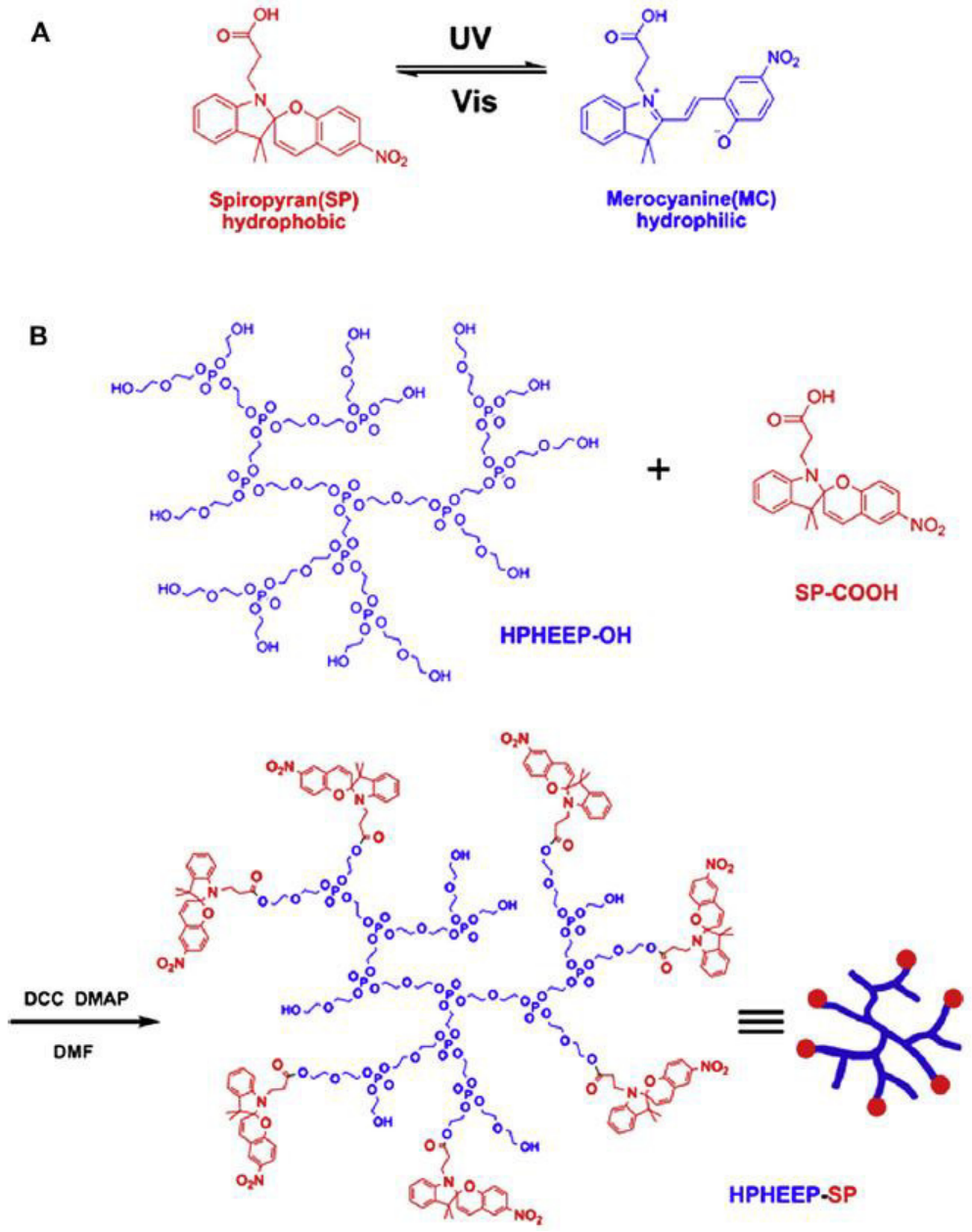

Scheme 41. (A) Photoisomerization of the carboxyl-containing spiropyran. (B) the structure of HPEEP-OH and the synthetic route for HPEEP-SP. (Reprinted from Reference 211 Copyright 2012, with permission from Elsevier)

The next step in the design of smart drug delivery systems is the integration of specific moieties, i.e. for example antigens, proteins or sugars, into the drug carrier which allow a targeted drug delivery to distinct sites in the body. Typical problems associated with systemic drug administration are the even distribution of the pharmaceuticals within the whole body, the lack

of drug specific affinity toward a pathological site, the necessity of high drug doses to achieve sufficient local concentrations and the adverse side-effects due to high drug doses. Smart drug delivery systems allowing a targeted transportation of the drug to the affected site, may resolve many of these problems. Up to date some publications about the usage of poly(phosphoester)s in targeted drug delivery have been published.[212-214] The following paragraph highlights a few of these publications.

The brain is protected against potentially toxic substances by the blood-brain barrier (BBB), which restricts the entry of most pharmaceuticals into the brain. Especially the development of drugs for the treatment of CNS disorders has not kept pace with progress in molecular neurosciences, due to the fact that most new drugs cannot cross the BBB and thus the clinical failure of CNS drugs may be directly linked to a lack of appropriate drug delivery systems. Localized and controlled delivery of drugs at their desired site of action is preferred because it reduces toxicity and increases treatment efficiency.[215]

PPEs are especially appealing as materials for drug delivery to the brain since an enrichment of polymeric drug carriers in the brain can be problematic and PPEs are potentially degradable in this environment. However, up to date there are only a few reports about the usage of PPEs as drug carrier systems for brain targeting.[216-217] The efficient delivery of paclitaxel to the brain by the usage of transferrin-conjugated PPE hybrid micelles has been demonstrated by Yaping Li *et al.*[218] Micelles consisting of PCL-*b*-PEEP and transferrin-conjugated PEG-*b*-PCl block copolymers have been prepared and loaded with paclitaxel. Transferrin (Tf) can facilitate the transcytosis of coupled nanocarriers through Tf receptor mediated pathway. To investigate the brain delivery properties of the TPM *in vitro* primary brain microvascular endothelial cells (BMECs) were used, because they closely represent the barrier property of the BBB. It was shown that the cellular uptake of the TPM nanocarriers in contrast to the unmodified nanocarriers is increased by the factor of two. Furthermore, the cellular uptake of the modified nanocarriers can be inhibited by the addition of free transferrin indicating that the uptake is indeed TfR-mediated (Figure 16A). The anti-glioma activity of the TPM was measured by the survival time of intracranial U-87 MG glioma bearing mice (Figure 16B). Tumor bearing mice were treated either with Taxol®, PM or the modified micelles. Mice treated with PM showed no significantly enhanced survival time compared to those treated with Taxol®, whereas the survival time of those mice treated with the TPM was significantly prolonged.

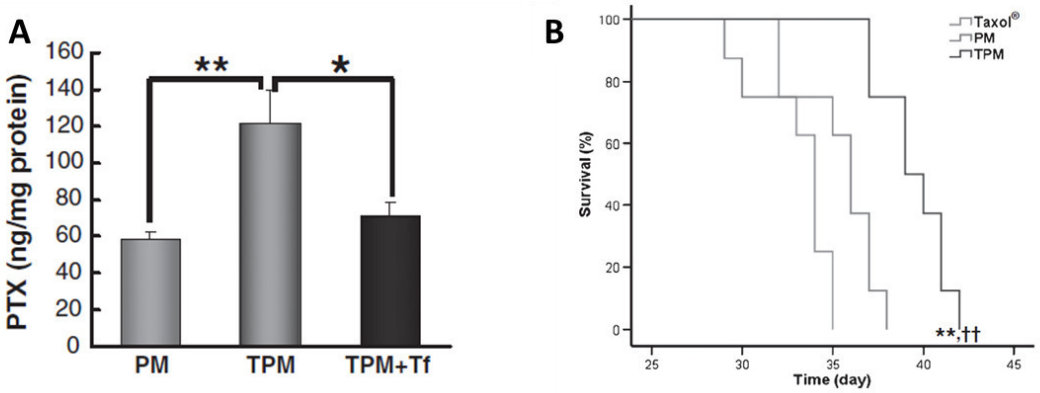

Figure 16. (A) Quantitative determination of the cellular uptake of PTX by BMECs after 1h incubation *p<0.05, **p<0.01. (B) Kaplan-Meiersurvival curve of mice bearing intracranial U-87 MG glioma. (n=8) **p<0.01compared with Taxol®, ††p<0.01compared with Taxol®) (Reprinted from reference 218 Copyright 2012, with permission from Elsevier)

With this work Yaping Li *et al*. have successfully demonstrated the potential of PPE-based targeted delivery and have laid the foundation for further investigations.

A simple, but efficient sheddable ternary acidity-targeted nanoparticular drug delivery system for the delivery of siRNA has been developed by Wang and co-workers.[219] The nanoparticles consist of a ssPEI$_{800}$/siRNA particle core and a ternary negatively charged PEG-*b*-PPE block copolymer that is bound to the particle surface by electrostatic interactions. The outer PEG chain provides a prolonged blood circulation time by minimizing the unspecific interactions of the delivery system with blood components, while the inner PPE-block provides the pH-sensitivity. However, PEGylation also reduces the uptake of the nanoparticle by cancer cells. Therefore, a shedding of the PEG-layer after accumulation at the tumor site is needed which is realized by transferring the PPE-block from a negative to positive charge (Figure 17).

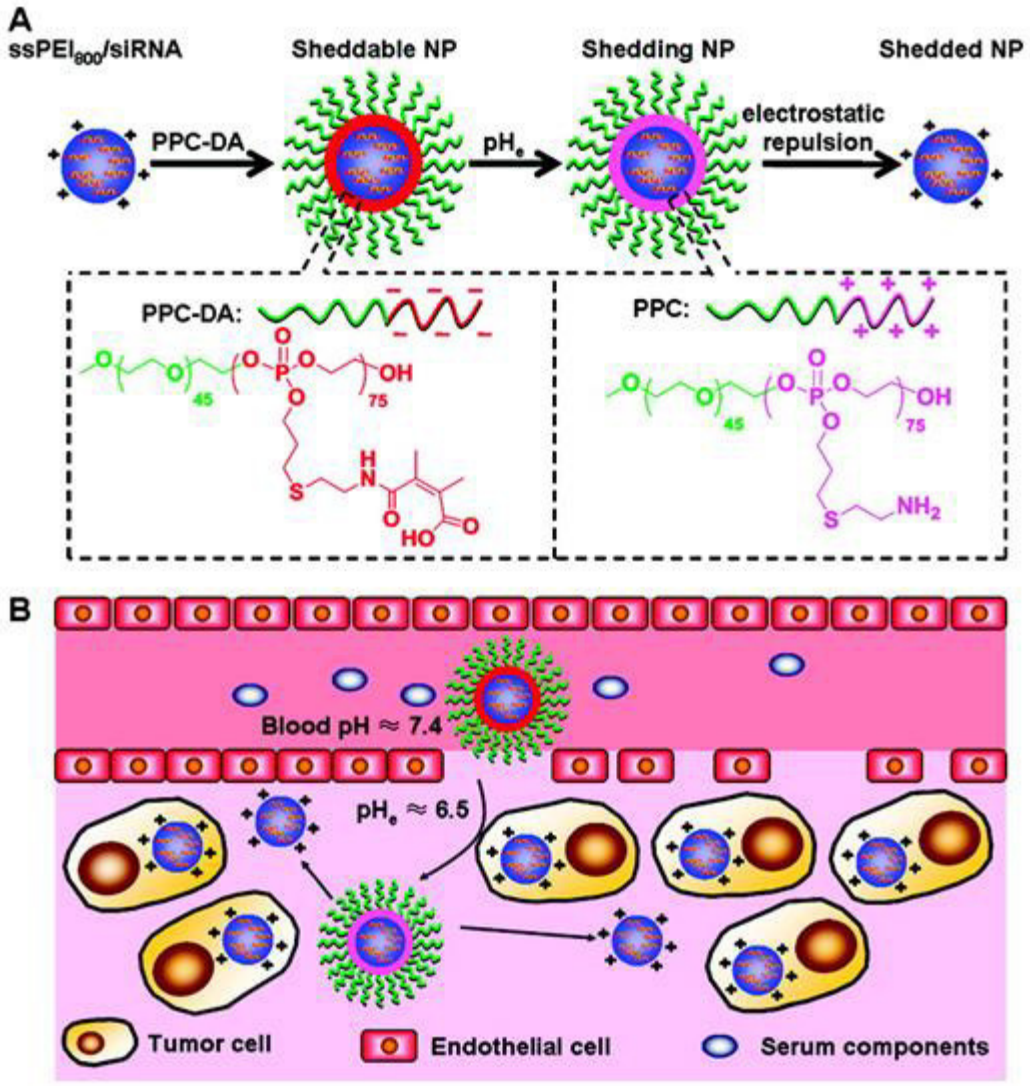

Figure 17: (A) Shielding and deshielding of the positively charged ssPEI800/siRNA nanoparticles by the PEG shell in the acidic environment of the tumor. (B) Schematic illustration of the stealth property and promoted tumoral cell uptake of sheddable nanoparticles. (Taken with permission from reference 219. Copyright 2012 American Chemical Society.)

The deshielding of the of the PEG shell under slightly acidic conditions was demonstrated by the change of the zeta-potential from ca. -12 mV to 8 mV after incubation with PBS at pH 6.8. Furthermore, the increased cellular uptake after deshielding of the PEG shell under acidic conditions by MDA-MB-231 cells has been proven by incubation of sheddable and unsheddable nanoparticles at pH 7.4 and 6.8. The internalization of the unsheddable nanoparticles was not affected by the pH while the sheddable nanoparticles showed an enhanced cellular uptake at pH

6.8 compared to pH 7.4. Finally, the silencing of polo-like kinase 1 (Plk1) expression of MDA-MB-231 cells at different pHs was studied by using sheddable and unsheddable nanoparticles loaded with siRNA targeting. It was found that the incubation of sheddable nanoparticles with MDA-MB-231 cells at pH 6.8 lead to a significantly improved silencing efficiency of Plk1 expression. In conclusion, Wang *et al.* designed a drug delivery system meeting all requirements that are imposed by modern cancer therapy and that is therefore of high interest for further investigation.

5. Conclusions

Main-chain poly(phosphoester)s –and amides have been reviewed comprehensively. With diverse derivatives of phosphoric acid within the polymer backbone those materials are versatile candidates for various future applications. Going back to pioneering works in the 1960s, they are mainly used today in flame retardant additives, but their potential in biodegradable polymers with precise degradation profiles or adjustable adhesion has not been fully explored to date.

The PPE and PPA platform was extended in recent years as novel synthetic techniques were introduced, such as living polymerization techniques to water-soluble polyphosphates and –phosphonates with well-defined architectures. Also the potential of controlling materials properties by variation of the binding patterns around the central phosphorus was used in recent works to further adjust materials properties. This is especially important for biomedical applications, such as drug delivery or tissue engineering and further improved flame retardants.

Today's gold standards in biocompatible polymers have a low chemical functionality, such as poly(ethylene glycol) which is used in drug carriers or biodegradable polyesters, such as PLA and PLGA. In contrast PPEs allow the synthesis of functional polymers using a set of diverse and modular synthetic protocols. Even though PPEs have not found considerable commercial interest in materials science and biomedicine to date, we believe that the current research will lead to considerable innovative materials, which can be commercialized.

The synthesis of PPEs relies on different techniques, depending on the monomer structure, phosphorus center, and the desired polymer properties. Recent advances in controlled polymerization routes, e.g., ROP by organocatalysis and Ruthenium-catalyzed metathesis polymerization, make PPEs readily available on large scale. Also some first approaches were made employing enzyme catalysis, but still being less efficient than classical polymerization techniques. Several groups use polyfunctional PPEs and use postpolymerization functionalization to prepare biodegradable drug-loaded nanocarriers. As most phosphate

monomers are prepared from high-energy products such as phosphoryl chloride, we believe that the next step in the PPE developments is the development of economic and ecological pathways to the monomers and to guarantee their efficient polymerization.

Due to the diverse chemistry of phosphoric acid, the future development of PPEs and PPAs will certainly lead to many fascinating materials.

6. References

1. Westheimer, F., Why nature chose phosphates. *Science* **1987,** *235* (4793), 1173-1178.
2. Morrissey, J. H.; Choi, S. H.; Smith, S. A., Polyphosphate: an ancient molecule that links platelets, coagulation and inflammation. *Blood* **2012**.
3. Schröder, H.; Kurz, L.; Müller, W.; Lorenz, B., Polyphosphate in bone. *Biochemistry (Moscow)* **2000,** *65* (3), 296-303.
4. Brown, M. R. W.; Kornberg, A., Inorganic polyphosphate in the origin and survival of species. *Proc. Natl. Acad. Sci. U. S. A.* **2004,** *101* (46), 16085-16087.
5. Krauss, G., *Biochemistry of signal transduction and regulation*. John Wiley & Sons: 2006.
6. Metcalf, W. W.; van der Donk, W. A., Biosynthesis of phosphonic and phosphinic acid natural products. *Annual review of biochemistry* **2009,** *78* (1), 65-94.
7. L. L. Clark, E. D. I., R. Benner, Marine organic phosphorous cycling; novel insights from nuclear magnetic resonance. *Am. J. Sci* **1999,** *299* (1), 724-737.
8. Steinbach, T.; Wurm, F. R., Poly(phosphoester)s: A New Platform for Degradable Polymers. *Angewandte Chemie International Edition* **2015,** *54* (21), 6098-6108.
9. Baran, J.; Penczek, S., Hydrolysis of polyesters of phosphoric acid. 1. Kinetics and the pH profile. *Macromolecules* **1995,** *28* (15), 5167-5176.
10. Klöpffer, W.; Grahl, B., *Ökobilanz (lca): Ein leitfaden für ausbildung und beruf*. John Wiley & Sons: 2012.
11. Aksnes, G.; Bergesen, K., Rate studies of cyclic phosphinates, phosphonates and phosphates. *Acta chem. scand* **1966,** *20* (9).
12. Thomas, C. M., Stereocontrolled ring-opening polymerization of cyclic esters: synthesis of new polyester microstructures. *Chemical Society Reviews* **2010,** *39* (1), 165-173.
13. Iwasaki, Y.; Yamaguchi, E., Synthesis of Well-Defined Thermoresponsive Polyphosphoester Macroinitiators Using Organocatalysts. *Macromolecules* **2010,** *43* (6), 2664-2666.
14. Zou, J.; Zhang, F.; Zhang, S.; Pollack, S. F.; Elsabahy, M.; Fan, J.; Wooley, K. L., Poly(ethylene oxide)-block-Polyphosphoester-graft-Paclitaxel Conjugates with Acid-Labile Linkages as a pH-Sensitive and Functional Nanoscopic Platform for Paclitaxel Delivery. *Advanced Healthcare Materials* **2014,** *3* (3), 441-448.
15. Zhang, S.; Zou, J.; Zhang, F.; Elsabahy, M.; Felder, S. E.; Zhu, J.; Pochan, D. J.; Wooley, K. L., Rapid and Versatile Construction of Diverse and Functional Nanostructures Derived from a Polyphosphoester-Based Biomimetic Block Copolymer System. *Journal of the American Chemical Society* **2012,** *134* (44), 18467-18474.
16. Wang, J.; Mao, H.-Q.; Leong, K. W., A Novel Biodegradable Gene Carrier Based on Polyphosphoester. *J. Am. Chem. Soc.* **2001,** *123* (38), 9480-9481.
17. Penczek, S.; Pretula, J.; Kubisa, P.; Kaluzynski, K.; Szymanski, R., Reactions of H3PO4 forming polymers. Apparently simple reactions leading to sophisticated structures and applications. *Progress in Polymer Science* (0).
18. Richards, M.; Dahiyat, B. I.; Arm, D. M.; Brown, P. R.; Leong, K. W., Evaluation of polyphosphates and polyphosphonates as degradable biomaterials. *J Biomed Mater Res* **1991,** *25* (9), 1151-1167.
19. Troev, K. D., *Polyphosphoesters: chemistry and application*. Elsevier: 2012.
20. Wang, Y.-C.; Yuan, Y.-Y.; Du, J.-Z.; Yang, X.-Z.; Wang, J., Recent Progress in Polyphosphoesters: From Controlled Synthesis to Biomedical Applications. *Macromolecular Bioscience* **2009,** *9* (12), 1154-1164.
21. Zhao, Z.; Wang, J.; Mao, H.-Q.; Leong, K. W., Polyphosphoesters in drug and gene delivery. *Advanced Drug Delivery Reviews* **2003,** *55* (4), 483-499.

22. Monge, S.; David, G., *Phosphorus-based Polymers: From Synthesis to Applications*. Royal Society of Chemistry: 2014; Vol. 11.
23. Liu, Y.; Yan, N.; Li, F.; Chen, P., Synthesis and properties of a novel hyperbranched polyphosphoramidate using an A2 + CB2 approach. *Polymer International* **2013,** *62* (3), 390-396.
24. Bauer, K. N.; Tee, H. T.; Lieberwirth, I.; Wurm, F. R., In-Chain Poly(phosphonate)s via Acyclic Diene Metathesis Polycondensation. *Macromolecules* **2016,** *49* (10), 3761-3768.
25. Steinbach, T.; Ritz, S.; Wurm, F. R., Water-Soluble Poly(phosphonate)s via Living Ring-Opening Polymerization. *ACS Macro Letters* **2014,** *3* (3), 244-248.
26. Huang, S.-W.; Wang, J.; Zhang, P.-C.; Mao, H.-Q.; Zhuo, R.-X.; Leong, K. W., Water-Soluble and Nonionic Polyphosphoester: Synthesis, Degradation, Biocompatibility and Enhancement of Gene Expression in Mouse Muscle. *Biomacromolecules* **2004,** *5* (2), 306-311.
27. Liu, J.; Huang, W.; Zhou, Y.; Yan, D., Synthesis of hyperbranched polyphosphates by self-condensing ring-opening polymerization of HEEP without catalyst. *Macromolecules* **2009,** *42* (13), 4394-4399.
28. Chen, S.; Zhang, D.; Cheng, X.; Li, T.; Zhang, A.; Li, J., Preparation and characterization of a novel hyperbranched polyphosphate ester. *Materials Chemistry and Physics* **2012,** *137* (1), 154-159.
29. Liu, J.; Huang, W.; Pang, Y.; Zhu, X.; Zhou, Y.; Yan, D., Self-Assembled Micelles from an Amphiphilic Hyperbranched Copolymer with Polyphosphate Arms for Drug Delivery. *Langmuir* **2010,** *26* (13), 10585-10592.
30. Liu, J.; Pang, Y.; Huang, W.; Zhai, X.; Zhu, X.; Zhou, Y.; Yan, D., Controlled Topological Structure of Copolyphosphates by Adjusting Pendant Groups of Cyclic Phosphate Monomers. *Macromolecules* **2010,** *43* (20), 8416-8423.
31. Stukenbroeker, T. S.; Solis-Ibarra, D.; Waymouth, R. M., Synthesis and Topological Trapping of Cyclic Poly(alkylene phosphates). *Macromolecules* **2014,** *47* (23), 8224-8230.
32. Chaubal, M. V.; Wang, B.; Su, G.; Zhao, Z., Compositional analysis of biodegradable polyphosphoester copolymers using nmr spectroscopic methods. *Journal of Applied Polymer Science* **2003,** *90* (14), 4021-4031.
33. Wang, X.-L.; Zhuo, R.-X.; Liu, L.-J., Synthesis and characterization of novel biodegradable poly(carbonate-co-phosphate)s. *Polymer International* **2001,** *50* (11), 1175-1179.
34. Wen, J.; Zhuo, R.-X., Preparation and characterization of poly(D,L-lactide-co-ethylene methyl phosphate). *Polymer International* **1998,** *47* (4), 503-509.
35. Zhu, W.; Sun, S.; Xu, N.; Shen, Z., Synthesis, characterization, and properties of poly(ester-phosphoester)s by lanthanum triphenolate-catalyzed ring-opening copolymerization. *Journal of Polymer Science Part A: Polymer Chemistry* **2011,** *49* (23), 4987-4992.
36. Hao, Y.; He, J.; Zhang, M.; Tao, Y.; Liu, J.; Ni, P., Synthesis and characterization of novel brush copolymers with biodegradable polyphosphoester side chains for gene delivery. *Journal of Polymer Science Part A: Polymer Chemistry* **2013,** *51* (10), 2150-2160.
37. Yuan, Y.-Y.; Du, Q.; Wang, Y.-C.; Wang, J., One-Pot Syntheses of Amphiphilic Centipede-like Brush Copolymers via Combination of Ring-Opening Polymerization and "Click" Chemistry. *Macromolecules* **2010,** *43* (4), 1739-1746.
38. Cheng, J.; Ding, J.-X.; Wang, Y.-C.; Wang, J., Synthesis and characterization of star-shaped block copolymer of poly-(ε-caprolactone) and poly (ethyl ethylene phosphate) as drug carrier. *Polymer* **2008,** *49* (22), 4784-4790.
39. Wu, Q.; Wang, C.; Zhang, D.; Song, X.; Liu, D.; Wang, L.; Zhang, G., Synthesis and micellization of a new amphiphilic star-shaped poly(D,L-lactide)/polyphosphoester block copolymer. *Reactive and Functional Polymers* **2012,** *72* (6), 372-377.

40. Yang, X.-Z.; Wang, Y.-C.; Tang, L.-Y.; Xia, H.; Wang, J., Synthesis and characterization of amphiphilic block copolymer of polyphosphoester and poly(L-lactic acid). *Journal of Polymer Science Part A: Polymer Chemistry* **2008,** *46* (19), 6425-6434.
41. Tauber, K.; Marsico, F.; Wurm, F. R.; Schartel, B., Hyperbranched poly(phosphoester)s as flame retardants for technical and high performance polymers. *Polymer Chemistry* **2014,** *5* (24), 7042-7053.
42. Gao, H.; Tan, Y.; Guan, Q.; Cai, T.; Liang, G.; Wu, Q., Synthesis, characterization and micellization of amphiphilic polyethylene-b-polyphosphoester block copolymers. *RSC advances* **2015,** *5* (61), 49376-49384.
43. Vanslambrouck, S.; Clément, B.; Riva, R.; Koole, L. H.; Molin, D.; Broze, G.; Lecomte, P.; Jérôme, C., Synthesis and tensioactive properties of PEO-b-polyphosphate copolymers. *RSC Advances* **2015,** *5* (35), 27330-27337.
44. Wang, Y.-C.; Li, Y.; Yang, X.-Z.; Yuan, Y.-Y.; Yan, L.-F.; Wang, J., Tunable Thermosensitivity of Biodegradable Polymer Micelles of Poly(ε-caprolactone) and Polyphosphoester Block Copolymers. *Macromolecules* **2009,** *42* (8), 3026-3032.
45. Wu, G.-P.; Darensbourg, D. J., Mechanistic Insights into Water-Mediated Tandem Catalysis of Metal-Coordination CO2/Epoxide Copolymerization and Organocatalytic Ring-Opening Polymerization: One-Pot, Two Steps, and Three Catalysis Cycles for Triblock Copolymers Synthesis. *Macromolecules* **2016,** *49* (3), 807-814.
46. Al Ouahabi, A.; Charles, L.; Lutz, J.-F., Synthesis of Non-Natural Sequence-Encoded Polymers Using Phosphoramidite Chemistry. *J. Am. Chem. Soc.* **2015,** *137* (16), 5629-5635.
47. James, A. A., Resinous compositions. Google Patents: 1936.
48. Maiboroda, V. D.; Datskevich, L. A., Polycondensation of phenylphosphoryl dichloride with diethylene glycol. *Polymer Science U.S.S.R.* **1964,** *6* (10), 2113-2117.
49. Ogawa, T.; Nushimatsu, T.; Minoura, Y., Condensation polymerization of P-phenylphosphonic dichloride with diamines. *Die Makromolekulare Chemie* **1968,** *114* (1), 275-283.
50. Millich, F.; Carraher, C. E., Interfacial syntheses of polyphosphonate and polyphosphate esters. II. Dependence of yield and molecular weight on solvent volumes and concentrations of comers in basic polymerization of hydroquinone and phenylphosphonic dichloride. *Journal of Polymer Science Part A-1: Polymer Chemistry* **1970,** *8* (1), 163-169.
51. Imai, Y.; Sato, N.; Ueda, M., Synthesis of aromatic polyphosphonate by phase-transfer catalyzed polycondensation with quaternary onium salts and crown ethers. *Die Makromolekulare Chemie, Rapid Communications* **1980,** *1* (7), 419-422.
52. Millich, F.; Lambing, L. L., Interfacial sythesis of polyphosphonate and polyphosphate ester. VII. Temperature effects and reaction loci in polycondensations of hydroquinone with phenylphosphonic dichloride and 4-methythiophenyl phosphorodichloridate. *Journal of Polymer Science: Polymer Chemistry Edition* **1980,** *18* (7), 2155-2162.
53. Schmidt, M.; Freitag, D.; Bottenbruch, L.; Reinking, K., Aromatische polyphosphonate: Thermoplastische polymere von extremer brandwidrigkeit. *Die Angewandte Makromolekulare Chemie* **1985,** *132* (1), 1-18.
54. Richards, M.; Dahiyat, B. I.; Arm, D. M.; Lin, S.; Leong, K. W., Interfacial polycondensation and characterization of polyphosphates and polyphosphonates. *Journal of Polymer Science Part A: Polymer Chemistry* **1991,** *29* (8), 1157-1165.
55. Liaw, D.-J.; Shen, W.-C., Synthesis of aromatic polyphosphonate: low temperature solution polycondensation of 4,4′-sulphonyldiphenol with phenoxy dichlorophosphate. *Polymer* **1993,** *34* (6), 1336-1338.
56. Chen, X.; Jiao, C.; Li, S.; Sun, J., Flame retardant epoxy resins from bisphenol-A epoxy cured with hyperbranched polyphosphate ester. *J Polym Res* **2011,** *18* (6), 2229-2237.

57. Alexandrino, E. M.; Wagner, M.; Landfester, K.; Wurm, F. R., Poly(phosphoester) Colloids by Interfacial Polycondensation in Miniemulsion. *Macromolecular Chemistry and Physics* **2016,** *217* (17), 1941-1947.
58. Pretula, J.; Kaluzynski, K.; Szymanski, R.; Penczek, S., Preparation of Poly(alkylene H-phosphonate)s and Their Derivatives by Polycondensation of Diphenyl H-Phosphonate with Diols and Subsequent Transformations. *Macromolecules* **1997,** *30* (26), 8172-8176.
59. Penczek, S.; Pretula, J., High-molecular-weight poly(alkylene phosphates) and preparation of amphiphilic polymers thereof. *Macromolecules* **1993,** *26* (9), 2228-2233.
60. Troev, K.; Naruoka, A.; Terada, H.; Kikuchi, A.; Makino, K., New Efficient Method of Oxidation of Poly(alkylene H-phosphonate)s: A Promising Route to Novel co-Polyphosphoesters. *Macromolecules* **2012,** *45* (14), 5698-5703.
61. Pretula, J.; Kaluzynski, K.; Penczek, S., Synthesis of poly(alkylene phosphates) with nitrogen-containing bases in the side chains. 1. Nitrogen- and carbon-substituted imidazoles. *Macromolecules* **1986,** *19* (7), 1797-1799.
62. Kaluzynski, K.; Libisowski, J.; Penczek, S., A New Class of Synthetic Polyelectrolytes. Acidic Polyesters of Phosphoric Acid (Poly(hydroxyalkylene phosphates)). *Macromolecules* **1976,** *9* (2), 365-367.
63. Biela, T.; Kubisa, P., Oligomerization of oxiranes in the presence of phosphoric acid. Kinetics of model reaction. *Die Makromolekulare Chemie* **1991,** *192* (3), 473-489.
64. Tzevi, R.; Todorova, G.; Kossev, K.; Troev, K.; Georgiev, E. M.; Roundhill, D. M., Immobilization of bioactive substances on poly (alkylene phosphate) s, 1. Immobilization of 2-phenylethylamine. *Die Makromolekulare Chemie* **1993,** *194* (12), 3261-3269.
65. Troev, K.; Tsatcheva, I.; Koseva, N.; Georgieva, R.; Gitsov, I., Immobilization of aminothiols on poly (oxyethylene H-phosphonate) s and poly (oxyethylene phosphate) s—An approach to polymeric protective agents for radiotherapy of cancer. *Journal of Polymer Science Part A: Polymer Chemistry* **2007,** *45* (7), 1349-1363.
66. Troev, K. D.; Mitova, V. A.; Ivanov, I. G., On the design of polymeric 5′-O-ester prodrugs of 3′-azido-2′,3′-dideoxythymidine (AZT). *Tetrahedron Letters* **2010,** *51* (47), 6123-6125.
67. Le Corre, S. S.; Berchel, M.; Couthon-Gourvès, H.; Haelters, J.-P.; Jaffrès, P.-A., Atherton–Todd reaction: mechanism, scope and applications. *Beilstein Journal of Organic Chemistry* **2014,** *10*, 1166-1196.
68. Bogomilova, A.; Höhn, M.; Günther, M.; Herrmann, A.; Troev, K.; Wagner, E.; Schreiner, L., A polyphosphoester conjugate of melphalan as antitumoral agent. *European Journal of Pharmaceutical Sciences* **2013,** *50* (3–4), 410-419.
69. Vogt, W.; Balasubramanian, S., Über die polykondensation von diäthylphosphit mit aliphastischen diolen. *Die Makromolekulare Chemie* **1973,** *163* (1), 111-134.
70. Zwierzak, A., Cyclic organophosphorus compounds. I. Synthesis and infrared spectral studies of cyclic hydrogen phosphites and thiophosphites. *Canadian Journal of Chemistry* **1967,** *45* (21), 2501-2512.
71. Oswald, A. A., SYNTHESIS OF CYCLIC PHOSPHOROUS ACID ESTERS BY TRANSESTERIFICATION. *Canadian Journal of Chemistry* **1959,** *37* (9), 1498-1504.
72. Pretula, J.; Kaluzynski, K.; Szymanski, R.; Penczek, S., Transesterification of oligomeric dialkyl phosphonates, leading to the high-molecular-weight poly-H-phosphonates. *Journal of Polymer Science Part A: Polymer Chemistry* **1999,** *37* (9), 1365-1381.
73. Pretula, J.; Penczek, S., Poly (ethylene glycol) ionomers with phosphate diester linkages. *Die Makromolekulare Chemie, Rapid Communications* **1988,** *9* (11), 731-737.
74. Pretula, J.; Penczek, S., High-molecular-weight poly(alkylene phosphonate)s by condensation of dialkylphosphonates with diols. *Die Makromolekulare Chemie* **1990,** *191* (3), 671-680.

75. Stawinski, J., In Handbook of Organophosphorus Chemistry; Engel, R., Ed. Marcel Dekker: Hoboken, New Jersey: 1992.
76. Pretula, J.; Kaluzynski, K.; Wisniewski, B.; Szymanski, R.; Loontjens, T.; Penczek, S., H3PO4 in a direct synthesis of oligo–poly(ethylene phosphate)from ethylene glycol. *Journal of Polymer Science Part A: Polymer Chemistry* **2006,** *44* (7), 2358-2362.
77. Pretula, J.; Kaluzynski, K.; Wisniewski, B.; Szymanski, R.; Loontjens, T.; Penczek, S., Formation of poly(ethylene phosphates) in polycondensation of H3PO4 with ethylene glycol. Kinetic and mechanistic study. *Journal of Polymer Science Part A: Polymer Chemistry* **2008,** *46* (3), 830-843.
78. Pretula, J.; Kaluzynski, K.; Szymanski, R.; Penczek, S., Polycondensation of H3PO4 with glycerol: From branched structures to hydrolytically reversible gels. *Journal of Polymer Science Part A: Polymer Chemistry* **2014,** *52* (24), 3533-3542.
79. Minegishi, S.; Komatsu, S.; Kameyama, A.; Nishikubo, T., Novel synthesis of polyphosphonates by the polyaddition of bis(epoxide) with diaryl phosphonates. *Journal of Polymer Science Part A: Polymer Chemistry* **1999,** *37* (7), 959-965.
80. Minegishi, S.; Tsuchida, S.; Sasaki, M.; Kameyama, A.; Kudo, H.; Nishikubo, T., Synthesis of polyphosphonates containing pendant chloromethyl groups by the polyaddition of bis(oxetane)s with phosphonic dichlorides. *Journal of Polymer Science Part A: Polymer Chemistry* **2002,** *40* (21), 3835-3846.
81. Nishikubo, T.; Kameyama, A.; Minegishi, S., Novel Syntheses of Poly(phosphonate)s and Poly(phosphate)s by Addition Reactions of Bisepoxides with Phosphonic Dichlorides and Dichlorophosphates. *Macromolecules* **1995,** *28* (14), 4810-4814.
82. Biedron, T.; Kaluzynski, K.; Pretula, J.; Kubisa, P.; Penczek, S.; Loontjens, T., Synthesis of high molar mass poly (alkylene phosphate) s by polyaddition of diepoxides to difunctional phosphoric acids: Unusual elimination of the side reactions. *Journal of Polymer Science Part A: Polymer Chemistry* **2001,** *39* (17), 3024-3033.
83. Nyk, A.; Klosinski, P.; Penczek, S., Water-swelling, hydrolyzable gels through polyaddition of H3PO4 to diepoxides. *Die Makromolekulare Chemie* **1991,** *192* (4), 833-846.
84. Penczek, S.; Kaluzynski, K.; Pretula, J., Addition of H3PO4 to diglycidyl ethers of bisphenol A: Kinetics and product structure. *Journal of Applied Polymer Science* **2007,** *105* (1), 246-254.
85. Kazanskii, K.; Kuznetsova, V.; Pretula, J.; Penczek, S., Ionizable hydrogels of new type based on poly(ethylene glycol) phosphates. *Polymer Gels and Networks* **1996,** *4* (4), 335-349.
86. Libiszowski, J.; Kałużynski, K.; Penczek, S., Polymerization of cyclic esters of phosphoric acid. VI. Poly(alkyl ethylene phosphates). Polymerization of 2-alkoxy-2-oxo-1,3,2-dioxaphospholans and structure of polymers. *Journal of Polymer Science: Polymer Chemistry Edition* **1978,** *16* (6), 1275-1283.
87. Zhai, X.; Huang, W.; Liu, J.; Pang, Y.; Zhu, X.; Zhou, Y.; Yan, D., Micelles from Amphiphilic Block Copolyphosphates for Drug Delivery. *Macromolecular Bioscience* **2011,** *11* (11), 1603-1610.
88. Wang, Y.-C.; Yuan, Y.-Y.; Wang, F.; Wang, J., Syntheses and characterization of block copolymers of poly(aliphatic ester) with clickable polyphosphoester. *Journal of Polymer Science Part A: Polymer Chemistry* **2011,** *49* (2), 487-494.
89. Klosinski, P.; Penczek, S., Synthesis of models of teichoic acids by ring-opening polymerization. *Macromolecules* **1983,** *16* (2), 316-320.
90. Pretula, J.; Kałużyński, K.; Penczek, S., Living reversible anonic polymerization of N,N-diethylamine-1,3,2-dioxaphosphorinan. *Journal of Polymer Science: Polymer Chemistry Edition* **1984,** *22* (6), 1251-1258.

91. Biela, T.; Kłosiński, P.; Penczek, S., Microstructure of poly(alkylene phosphates) related to biopolymers (teichoic acids). *Journal of Polymer Science Part A: Polymer Chemistry* **1989,** *27* (3), 763-774.
92. Kałużynski, K.; Libiszowski, J.; Penczek, S., Poly(2-hydro-2-oxo-1,3,2-dioxaphosphorinane). Preparation and NMR spectra. *Die Makromolekulare Chemie* **1977,** *178* (10), 2943-2947.
93. Yuan, Y.-Y.; Du, J.-Z.; Song, W.-J.; Wang, F.; Yang, X.-Z.; Xiong, M.-H.; Wang, J., Biocompatible and functionalizable polyphosphate nanogel with a branched structure. *Journal of Materials Chemistry* **2012,** *22* (18), 9322-9329.
94. Zhang, F.; Zhang, S.; Pollack, S. F.; Li, R.; Gonzalez, A. M.; Fan, J.; Zou, J.; Leininger, S. E.; Pavía-Sanders, A.; Johnson, R.; Nelson, L. D.; Raymond, J. E.; Elsabahy, M.; Hughes, D. M. P.; Lenox, M. W.; Gustafson, T. P.; Wooley, K. L., Improving Paclitaxel Delivery: In Vitro and In Vivo Characterization of PEGylated Polyphosphoester-Based Nanocarriers. *Journal of the American Chemical Society* **2015,** *137* (5), 2056-2066.
95. Xiong, M.-H.; Wu, J.; Wang, Y.-C.; Li, L.-S.; Liu, X.-B.; Zhang, G.-Z.; Yan, L.-F.; Wang, J., Synthesis of PEG-armed and polyphosphoester core-cross-linked nanogel by one-step ring-opening polymerization. *Macromolecules* **2009,** *42* (4), 893-896.
96. Kobayashi, S.; Hashimoto, T.; Saegusa, T., Alcoholysis Polymerization of Cyclic Acyloxyphosphorane to Polyphosphate Triesters: Polyphosphorylation of Alcohol. *Macromolecules* **1980,** *13* (6), 1650-1654.
97. Kobayashi, S.; Suzuki, M.; Saegusa, T., Cationic ring-opening polymerization of 2-phenyl-1,2-oxaphospholane (deoxophostone). *Polymer Bulletin* **1981,** *4* (6), 315-321.
98. Kobayashi, S.; Tokunoh, M.; Saegusa, T., Cationic ring-opening polymerization of 2-phenyl-1,3,2-dioxaphosphepane, a seven-membered cyclic phosphonite. *Macromolecules* **1986,** *19* (2), 466-469.
99. Penczek, S.; Libiszowski, J., Polymerization of 2-methoxy-2-oxo-1,3,2-dioxaphospholane. Kinetics and polymer microstructure. *Die Makromolekulare Chemie* **1988,** *189* (8), 1765-1785.
100. Sosnowski, S.; Libiszowski, J.; Słomkowski, S.; Penczek, S., Thermodynamics of the polymerization of ethylene methyl phosphate. *Die Makromolekulare Chemie, Rapid Communications* **1984,** *5* (5), 239-244.
101. Maffei, M.; Buono, G., A two step synthesis of 2-oxo-2-vinyl 1,3,2-dioxaphospholanes and -dioxaphosphorinanes. *Tetrahedron* **2003,** *59* (44), 8821-8825.
102. Kałużyński, K.; Penczek, S., Anionic polymerization of 2-Oxo-1,3,2λ5-dioxaphosphorinane. Thermodynamics. *Die Makromolekulare Chemie* **1979,** *180* (10), 2289-2293.
103. Lapienis, G.; Penczek, S., Cationic Polymerization of 2-Alkoxy-2-oxo-1,3,2-dioxaphosphorinanes (1,3-Propylene Alkyl Phosphates). *Macromolecules* **1977,** *10* (6), 1301-1306.
104. Łapienis, G.; Penczek, S., Kinetics and thermodynamics of anionic polymerization of 2-methoxy-2-oxo-1,3,2-dioxaphosphorinane. *Journal of Polymer Science: Polymer Chemistry Edition* **1977,** *15* (2), 371-382.
105. Majoral, J.; Mathis, F.; Munoz, A.; Vives, J.; Navech, J., STUDIES ON CYCLIC ESTERS. 3. POLYMERISATION BY RING OPENING. *BULLETIN DE LA SOCIETE CHIMIQUE DE FRANCE* **1968,** (11), 4455-&.
106. Dudev, T.; Lim, C., Ring Strain Energies from ab Initio Calculations. *Journal of the American Chemical Society* **1998,** *120* (18), 4450-4458.
107. Szymanski, R.; Penczek, S., Complexation of sodium cations by polymeric esters of phosphoric acid. *Die Makromolekulare Chemie* **1993,** *194* (6), 1645-1651.

108. Hu, B.; Zhuo, R.; Fan, C., Synthesis of copolymer of 1,3-dioxan-2-one and 2-hydro-2-oxo-1,3,2-dioxaphosphorinane. *Polymers for Advanced Technologies* **1998,** *9* (2), 145-149.
109. Lapienis, G.; Penczek, S., Kinetics and Thermodynamics of the Polymerization of the Cyclic Phosphate Esters. II. Cationic Polymerization of 2-Methoxy-2-oxo-1,3,2-dioxaphosphorinane (1,3-Propylene Methyl Phosphate). *Macromolecules* **1974,** *7* (2), 166-174.
110. Eliel, E. L.; Chandrasekaran, S.; Carpenter, L. E.; Verkade, J. G., Oxygen-17 NMR spectra of cyclic phosphites, phosphates, and thiophosphates. *Journal of the American Chemical Society* **1986,** *108* (21), 6651-6661.
111. MUNOZ, A.; NAVECH, J.; VIVES, J.; MAJORAL, J., SOME CYCLIC PHOSPHORIC ESTERS. 2. ACTION OF GASEOUS HYDROCHLORIC ACID. *BULLETIN DE LA SOCIETE CHIMIQUE DE FRANCE* **1967,** (9), 3343-&.
112. Vogt, W.; Pflüger, R., Polymere ester von säuren des Phosphors, 3. Polymerisation des 2-Äthoxy-2-oxo-1,3,2-dioxaphospholans. *Die Makromolekulare Chemie* **1975,** *1* (S19751), 97-110.
113. Dubois, P.; Jacobs, C.; Jerome, R.; Teyssie, P., Macromolecular engineering of polylactones and polylactides. 4. Mechanism and kinetics of lactide homopolymerization by aluminum isopropoxide. *Macromolecules* **1991,** *24* (9), 2266-2270.
114. Ouhadi, T.; Stevens, C.; Teyssié, P., Mechanism of ε-Caprolactone polymerization by Aluminum Alkoxides. *Die Makromolekulare Chemie* **1975,** *1* (S19751), 191-201.
115. Wang, J.; Zhang, P.-C.; Lu, H.-F.; Ma, N.; Wang, S.; Mao, H.-Q.; Leong, K. W., New polyphosphoramidate with a spermidine side chain as a gene carrier. *Journal of Controlled Release* **2002,** *83* (1), 157-168.
116. Biela, T.; Penczek, S.; Slomkowski, S.; Vogl, O., Racemic and optically active poly(4-methyl-2-oxo-2-hydro-1,3,2-dioxaphospholane). Synthesis and oxidation to the polyacids. *Die Makromolekulare Chemie, Rapid Communications* **1982,** *3* (10), 667-671.
117. Li, F.; Feng, J.; Zhuo, R., Synthesis and characterization of novel biodegradable poly(p-dioxanone-co-ethyl ethylene phosphate)s. *Journal of Applied Polymer Science* **2006,** *102* (6), 5507-5511.
118. Chew, S. Y.; Wen, J.; Yim, E. K. F.; Leong, K. W., Sustained Release of Proteins from Electrospun Biodegradable Fibers. *Biomacromolecules* **2005,** *6* (4), 2017-2024.
119. Wen, J.; Kim, G. J. A.; Leong, K. W., Poly(d,llactide–co-ethyl ethylene phosphate)s as new drug carriers. *Journal of Controlled Release* **2003,** *92* (1–2), 39-48.
120. Chen, D.-P.; Wang, J., Synthesis and Characterization of Block Copolymer of Polyphosphoester and Poly (ε-caprolactone). *Macromolecules* **2006,** *39* (2), 473-475.
121. Du, J.-Z.; Chen, D.-P.; Wang, Y.-C.; Xiao, C.-S.; Lu, Y.-J.; Wang, J.; Zhang, G.-Z., Synthesis and Micellization of Amphiphilic Brush−Coil Block Copolymer Based on Poly(ε-caprolactone) and PEGylated Polyphosphoester. *Biomacromolecules* **2006,** *7* (6), 1898-1903.
122. Iwasaki, Y.; Wachiralarpphaithoon, C.; Akiyoshi, K., Novel thermoresponsive polymers having biodegradable phosphoester backbones. *Macromolecules* **2007,** *40* (23), 8136-8138.
123. Ozdil, D.; Aydin, H. M., Polymers for medical and tissue engineering applications. *Journal of Chemical Technology & Biotechnology* **2014,** *89* (12), 1793-1810.
124. Wang, Y.-C.; Shen, S.-Y.; Wu, Q.-P.; Chen, D.-P.; Wang, J.; Steinhoff, G.; Ma, N., Block Copolymerization of ε-Caprolactone and 2-Methoxyethyl Ethylene Phosphate Initiated by Aluminum Isopropoxide: Synthesis, Characterization, and Kinetics. *Macromolecules* **2006,** *39* (26), 8992-8998.
125. Xiao, C.-S.; Wang, Y.-C.; Du, J.-Z.; Chen, X.-S.; Wang, J., Kinetics and Mechanism of 2-Ethoxy-2-oxo-1,3,2-dioxaphospholane Polymerization Initiated by Stannous Octoate. *Macromolecules* **2006,** *39* (20), 6825-6831.
126. Garlotta, D., A Literature Review of Poly(Lactic Acid). *Journal of Polymers and the Environment* **2001,** *9* (2), 63-84.

127. Dove, A. P.; Gibson, V. C.; Marshall, E. L.; White, A. J. P.; Williams, D. J., A well defined tin(ii) initiator for the living polymerisation of lactide. *Chemical Communications* **2001,** (3), 283-284.
128. Kowalski, A.; Duda, A.; Penczek, S., Mechanism of Cyclic Ester Polymerization Initiated with Tin(II) Octoate. 2.† Macromolecules Fitted with Tin(II) Alkoxide Species Observed Directly in MALDI−TOF Spectra. *Macromolecules* **2000,** *33* (3), 689-695.
129. Albertsson, A.-C.; Varma, I. K., Recent Developments in Ring Opening Polymerization of Lactones for Biomedical Applications. *Biomacromolecules* **2003,** *4* (6), 1466-1486.
130. Kamber, N. E.; Jeong, W.; Waymouth, R. M.; Pratt, R. C.; Lohmeijer, B. G. G.; Hedrick, J. L., Organocatalytic Ring-Opening Polymerization. *Chemical Reviews* **2007,** *107* (12), 5813-5840.
131. Clément, B.; Grignard, B.; Koole, L.; Jérôme, C.; Lecomte, P., Metal-Free Strategies for the Synthesis of Functional and Well-Defined Polyphosphoesters. *Macromolecules* **2012,** *45* (11), 4476-4486.
132. Pratt, R. C.; Lohmeijer, B. G. G.; Long, D. A.; Waymouth, R. M.; Hedrick, J. L., Triazabicyclodecene: A Simple Bifunctional Organocatalyst for Acyl Transfer and Ring-Opening Polymerization of Cyclic Esters. *Journal of the American Chemical Society* **2006,** *128* (14), 4556-4557.
133. Nederberg, F.; Lohmeijer, B. G. G.; Leibfarth, F.; Pratt, R. C.; Choi, J.; Dove, A. P.; Waymouth, R. M.; Hedrick, J. L., Organocatalytic Ring Opening Polymerization of Trimethylene Carbonate. *Biomacromolecules* **2007,** *8* (1), 153-160.
134. MacMillan, D. W. C., The advent and development of organocatalysis. *Nature* **2008,** *455* (7211), 304-308.
135. Wen, J.; Zhuo, R.-X., Enzyme-catalyzed ring-opening polymerization of ethylene isopropyl phosphate. *Macromolecular Rapid Communications* **1998,** *19* (12), 641-642.
136. He, F.; Zhuo, R. X.; Liu, L. J.; Jin, D. B.; Feng, J.; Wang, X. L., Immobilized lipase on porous silica beads: preparation and application for enzymatic ring-opening polymerization of cyclic phosphate. *Reactive and Functional Polymers* **2001,** *47* (2), 153-158.
137. Wolf, T.; Steinbach, T.; Wurm, F. R., A Library of Well-Defined and Water-Soluble Poly(alkyl phosphonate)s with Adjustable Hydrolysis. *Macromolecules* **2015**.
138. Iwasaki, Y.; Akiyoshi, K., Synthesis and Characterization of Amphiphilic Polyphosphates with Hydrophilic Graft Chains and Cholesteryl Groups as Nanocarriers. *Biomacromolecules* **2006,** *7* (5), 1433-1438.
139. Zhang, S.; Wang, H.; Shen, Y.; Zhang, F.; Seetho, K.; Zou, J.; Taylor, J.-S. A.; Dove, A. P.; Wooley, K. L., A Simple and Efficient Synthesis of an Acid-Labile Polyphosphoramidate by Organobase-Catalyzed Ring-Opening Polymerization and Transformation to Polyphosphoester Ionomers by Acid Treatment. *Macromolecules* **2013,** *46* (13), 5141-5149.
140. Song, W.-J.; Du, J.-Z.; Liu, N.-J.; Dou, S.; Cheng, J.; Wang, J., Functionalized Diblock Copolymer of Poly(ε-caprolactone) and Polyphosphoester Bearing Hydroxyl Pendant Groups: Synthesis, Characterization, and Self-Assembly. *Macromolecules* **2008,** *41* (19), 6935-6941.
141. Lim, Y. H.; Heo, G. S.; Rezenom, Y. H.; Pollack, S.; Raymond, J. E.; Elsabahy, M.; Wooley, K. L., Development of a Vinyl Ether-Functionalized Polyphosphoester as a Template for Multiple Postpolymerization Conjugation Chemistries and Study of Core Degradable Polymeric Nanoparticles. *Macromolecules* **2014,** *47* (14), 4634-4644.
142. Tang, R.; Ji, W.; Panus, D.; Palumbo, R. N.; Wang, C., Block copolymer micelles with acid-labile ortho ester side-chains: Synthesis, characterization, and enhanced drug delivery to human glioma cells. *Journal of Controlled Release* **2011,** *151* (1), 18-27.
143. Lee, E. S.; Shin, H. J.; Na, K.; Bae, Y. H., Poly(l-histidine)–PEG block copolymer micelles and pH-induced destabilization. *Journal of Controlled Release* **2003,** *90* (3), 363-374.

144. Jain, R.; Standley, S. M.; Frechet, J. M., Synthesis and degradation of pH-sensitive linear poly (amidoamine) s. *Macromolecules* **2007,** *40* (3), 452-457.
145. Muller, L. K.; Steinbach, T.; Wurm, F. R., Multifunctional poly(phosphoester)s with two orthogonal protective groups. *RSC Advances* **2015,** *5* (53), 42881-42888.
146. Oussadi, K.; Montembault, V.; Belbachir, M.; Fontaine, L., Ring-opening bulk polymerization of five- and six-membered cyclic phosphonates using maghnite, a nontoxic proton exchanged montmorillonite clay. *Journal of Applied Polymer Science* **2011,** *122* (2), 891-897.
147. Wurm, F.; Steinbach, T.; Klok, H.-A., One-pot squaric acid diester mediated aqueous protein conjugation. *Chem. Commun.* **2013,** *49* (71), 7815-7817.
148. Iwasaki, Y.; Akiyoshi, K., Design of Biodegradable Amphiphilic Polymers: Well-Defined Amphiphilic Polyphosphates with Hydrophilic Graft Chains via ATRP. *Macromolecules* **2004,** *37* (20), 7637-7642.
149. Wang, Y.-C.; Li, Y.; Sun, T.-M.; Xiong, M.-H.; Wu, J.; Yang, Y.-Y.; Wang, J., Core–Shell–Corona Micelle Stabilized by Reversible Cross-Linkage for Intracellular Drug Delivery. *Macromolecular Rapid Communications* **2010,** *31* (13), 1201-1206.
150. Sun, C.-Y.; Ma, Y.-C.; Cao, Z.-Y.; Li, D.-D.; Fan, F.; Wang, J.-X.; Tao, W.; Yang, X.-Z., Effect of Hydrophobicity of Core on the Anticancer Efficiency of Micelles as Drug Delivery Carriers. *ACS Applied Materials & Interfaces* **2014,** *6* (24), 22709-22718.
151. Sun, T.-M.; Du, J.-Z.; Yan, L.-F.; Mao, H.-Q.; Wang, J., Self-assembled biodegradable micellar nanoparticles of amphiphilic and cationic block copolymer for siRNA delivery. *Biomaterials* **2008,** *29* (32), 4348-4355.
152. Zhang, S.; Li, A.; Zou, J.; Lin, L. Y.; Wooley, K. L., Facile Synthesis of Clickable, Water-Soluble, and Degradable Polyphosphoesters. *ACS Macro Letters* **2012,** *1* (2), 328-333.
153. Iwasaki, Y.; Kawakita, T.; Yusa, S.-i., Thermoresponsive Polyphosphoesters Bearing Enzyme-cleavable Side Chains. *Chemistry Letters* **2009,** *38* (11), 1054-1055.
154. Shao, H.; Zhang, M.; He, J.; Ni, P., Synthesis and characterization of amphiphilic poly(ε-caprolactone)-b-polyphosphoester diblock copolymers bearing multifunctional pendant groups. *Polymer* **2012,** *53* (14), 2854-2863.
155. Ishihara, K.; Ueda, T.; Nakabayashi, N., Preparation of Phospholipid Polylners and Their Properties as Polymer Hydrogel Membranes. *Polym J* **1990,** *22* (5), 355-360.
156. Baeten, E.; Vanslambrouck, S.; Jérôme, C.; Lecomte, P.; Junkers, T., Anionic flow polymerizations toward functional polyphosphoesters in microreactors: Polymerization and UV-modification. *European Polymer Journal* **2016,** *80*, 208-218.
157. Clément, B.; Molin, D. G.; Jérôme, C.; Lecomte, P., Synthesis of polyphosphodiesters by ring-opening polymerization of cyclic phosphates bearing allyl phosphoester protecting groups. *Journal of Polymer Science Part A: Polymer Chemistry* **2015,** *53* (22), 2642-2648.
158. Xiong, M.-H.; Li, Y.-J.; Bao, Y.; Yang, X.-Z.; Hu, B.; Wang, J., Bacteria-Responsive Multifunctional Nanogel for Targeted Antibiotic Delivery. *Advanced Materials* **2012,** *24* (46), 6175-6180.
159. McKinlay, C. J.; Waymouth, R. M.; Wender, P. A., Cell-Penetrating, Guanidinium-Rich Oligophosphoesters: Effective and Versatile Molecular Transporters for Drug and Probe Delivery. *Journal of the American Chemical Society* **2016,** *138* (10), 3510-3517.
160. Malzahn, K.; Marsico, F.; Koynov, K.; Landfester, K.; Weiss, C. K.; Wurm, F. R., Selective Interfacial Olefin Cross Metathesis for the Preparation of Hollow Nanocapsules. *ACS Macro Letters* **2013,** *3* (1), 40-43.
161. Marsico, F.; Wagner, M.; Landfester, K.; Wurm, F. R., Unsaturated Polyphosphoesters via Acyclic Diene Metathesis Polymerization. *Macromolecules* **2012,** *45* (21), 8511-8518.

162. Steinbach, T.; Alexandrino, E. M.; Wahlen, C.; Landfester, K.; Wurm, F. R., Poly(phosphonate)s via Olefin Metathesis: Adjusting Hydrophobicity and Morphology. *Macromolecules* **2014,** *47* (15), 4884-4893.
163. Steinbach, T.; Alexandrino, E. M.; Wurm, F. R., Unsaturated poly(phosphoester)s via ring-opening metathesis polymerization. *Polymer Chemistry* **2013,** *4* (13), 3800-3806.
164. Steinmann, M.; Markwart, J.; Wurm, F. R., Poly(alkylidene chlorophosphate)s via Acyclic Diene Metathesis Polymerization: A General Platform for the Postpolymerization Modification of Poly(phosphoester)s. *Macromolecules* **2014,** *47* (24), 8506-8513.
165. Peres, L. B.; Preiss, L. C.; Wagner, M.; Wurm, F. R.; de Araújo, P. H. H.; Landfester, K.; Muñoz-Espí, R.; Sayer, C., ALTMET Polymerization of Amino Acid-Based Monomers Targeting Controlled Drug Release. *Macromolecules* **2016,** *49* (18), 6723-6730.
166. Opper, K. L.; Wagener, K. B., ADMET: metathesis polycondensation. *Journal of Polymer Science Part A: Polymer Chemistry* **2011,** *49* (4), 821-831.
167. Wagener, K. B.; Brzezinska, K.; Anderson, J. D.; Younkin, T. R.; Steppe, K.; DeBoer, W., Kinetics of Acyclic Diene Metathesis (ADMET) Polymerization. Influence of the Negative Neighboring Group Effect. *Macromolecules* **1997,** *30* (24), 7363-7369.
168. Marsico, F.; Turshatov, A.; Peköz, R.; Avlasevich, Y.; Wagner, M.; Weber, K.; Donadio, D.; Landfester, K.; Baluschev, S.; Wurm, F. R., Hyperbranched Unsaturated Polyphosphates as a Protective Matrix for Long-Term Photon Upconversion in Air. *Journal of the American Chemical Society* **2014,** *136* (31), 11057-11064.
169. Marsico, F.; Turshatov, A.; Weber, K.; Wurm, F. R., A Metathesis Route for BODIPY Labeled Polyolefins. *Org. Lett.* **2013,** *15* (15), 3844-3847.
170. Steinbach, T.; Wahlen, C.; Wurm, F. R., Poly (phosphonate)-mediated Horner–Wadsworth–Emmons reactions. *Polymer Chemistry* **2015**.
171. Nagarkar, A. A.; Crochet, A.; Fromm, K. M.; Kilbinger, A. F. M., Efficient Amine End-Functionalization of Living Ring-Opening Metathesis Polymers. *Macromolecules* **2012,** *45* (11), 4447-4453.
172. Steinbach, T.; Schroder, R.; Ritz, S.; Wurm, F. R., Microstructure analysis of biocompatible phosphoester copolymers. *Polymer Chemistry* **2013,** *4* (16), 4469-4479.
173. Tanaka, K.; Kitamura, N.; Chujo, Y., Biodegradable main-chain phosphate-caged fluorescein polymers for the evaluation of enzymatic activity. *Macromolecules* **2010,** *43* (14), 6180-6184.
174. Wachiralarpphaithoon, C.; Iwasaki, Y.; Akiyoshi, K., Enzyme-degradable phosphorylcholine porous hydrogels cross-linked with polyphosphoesters for cell matrices. *Biomaterials* **2007,** *28* (6), 984-993.
175. Wang, Y.-C.; Tang, L.-Y.; Sun, T.-M.; Li, C.-H.; Xiong, M.-H.; Wang, J., Self-assembled micelles of biodegradable triblock copolymers based on poly (ethyl ethylene phosphate) and poly (ϵ-caprolactone) as drug carriers. *Biomacromolecules* **2007,** *9* (1), 388-395.
176. Xiang, D. F.; Bigley, A. N.; Ren, Z.; Xue, H.; Hull, K. G.; Romo, D.; Raushel, F. M., Interrogation of the Substrate Profile and Catalytic Properties of the Phosphotriesterase from Sphingobium sp. Strain TCM1: An Enzyme Capable of Hydrolyzing Organophosphate Flame Retardants and Plasticizers. *Biochemistry* **2015,** *54* (51), 7539-7549.
177. Wang, Y.-C.; Tang, L.-Y.; Li, Y.; Wang, J., Thermoresponsive Block Copolymers of Poly(ethylene glycol) and Polyphosphoester: Thermo-Induced Self-Assembly, Biocompatibility, and Hydrolytic Degradation. *Biomacromolecules* **2009,** *10* (1), 66-73.
178. Whiteside, T.; Carreira, L.; Hilal, S., Estimation of phosphate ester hydrolysis rate constants. II. Acid and general base catalyzed hydrolysis. *QSAR & Combinatorial Science* **2007,** *26* (5), 587-595.
179. Haag, R.; Kratz, F., Polymer Therapeutics: Concepts and Applications. *Angewandte Chemie International Edition* **2006,** *45* (8), 1198-1215.

180. Mitragotri, S.; Burke, P. A.; Langer, R., Overcoming the challenges in administering biopharmaceuticals: formulation and delivery strategies. *Nat Rev Drug Discov* **2014,** *13* (9), 655-672.
181. Torchilin, V., Tumor delivery of macromolecular drugs based on the EPR effect. *Advanced Drug Delivery Reviews* **2011,** *63* (3), 131-135.
182. Maeda, H.; Bharate, G. Y.; Daruwalla, J., Polymeric drugs for efficient tumor-targeted drug delivery based on EPR-effect. *European Journal of Pharmaceutics and Biopharmaceutics* **2009,** *71* (3), 409-419.
183. Greenwald, R. B.; Choe, Y. H.; McGuire, J.; Conover, C. D., Effective drug delivery by PEGylated drug conjugates. *Advanced Drug Delivery Reviews* **2003,** *55* (2), 217-250.
184. Harris, J. M.; Chess, R. B., Effect of pegylation on pharmaceuticals. *Nat Rev Drug Discov* **2003,** *2* (3), 214-221.
185. Veronese, F. M.; Pasut, G., PEGylation, successful approach to drug delivery. *Drug Discovery Today* **2005,** *10* (21), 1451-1458.
186. Elsabahy, M.; Zhang, S.; Zhang, F.; Deng, Z. J.; Lim, Y. H.; Wang, H.; Parsamian, P.; Hammond, P. T.; Wooley, K. L., Surface Charges and Shell Crosslinks Each Play Significant Roles in Mediating Degradation, Biofouling, Cytotoxicity and Immunotoxicity for Polyphosphoester-based Nanoparticles. *Scientific Reports* **2013,** *3*, 3313.
187. Schöttler, S.; Becker, G.; Winzen, S.; Steinbach, T.; Mohr, K.; Landfester, K.; Mailänder, V.; Wurm, F. R., Protein adsorption is required for stealth effect of poly (ethylene glycol)-and poly (phosphoester)-coated nanocarriers. *Nature nanotechnology* **2016,** *11* (4), 372-377.
188. Müller, J.; Bauer, K. N.; Prozeller, D.; Simon, J.; Mailänder, V.; Wurm, F. R.; Winzen, S.; Landfester, K., Coating nanoparticles with tunable surfactants facilitates control over the protein corona. *Biomaterials* **2017,** *115*, 1-8.
189. Tian, H.; Tang, Z.; Zhuang, X.; Chen, X.; Jing, X., Biodegradable synthetic polymers: preparation, functionalization and biomedical application. *Progress in Polymer Science* **2012,** *37* (2), 237-280.
190. Huang, Y.; Wang, D.; Zhu, X.; Yan, D.; Chen, R., Synthesis and therapeutic applications of biocompatible or biodegradable hyperbranched polymers. *Polymer Chemistry* **2015**.
191. Li, Y.; Wang, F.; Sun, T.; Du, J.; Yang, X.; Wang, J., Surface-modulated and thermoresponsive polyphosphoester nanoparticles for enhanced intracellular drug delivery. *Sci. China Chem.* **2014,** *57* (4), 579-585.
192. Liu, J.; Huang, W.; Pang, Y.; Zhu, X.; Zhou, Y.; Yan, D., Hyperbranched Polyphosphates for Drug Delivery Application: Design, Synthesis, and In Vitro Evaluation. *Biomacromolecules* **2010,** *11* (6), 1564-1570.
193. Zhu, W.; Du, H.; Huang, Y.; Sun, S.; Xu, N.; Ni, H.; Cai, X.; Li, X.; Shen, Z., Cationic poly(ester-phosphoester)s: Facile synthesis and antibacterial properties. *Journal of Polymer Science Part A: Polymer Chemistry* **2013,** *51* (17), 3667-3673.
194. Wang, F.; Wang, Y.-C.; Yan, L.-F.; Wang, J., Biodegradable vesicular nanocarriers based on poly(ε-caprolactone)-block-poly(ethyl ethylene phosphate) for drug delivery. *Polymer* **2009,** *50* (21), 5048-5054.
195. Yuan, Y.-Y.; Mao, C.-Q.; Du, X.-J.; Du, J.-Z.; Wang, F.; Wang, J., Surface Charge Switchable Nanoparticles Based on Zwitterionic Polymer for Enhanced Drug Delivery to Tumor. *Advanced Materials* **2012,** *24* (40), 5476-5480.
196. Tang, L.-Y.; Wang, Y.-C.; Li, Y.; Du, J.-Z.; Wang, J., Shell-Detachable Micelles Based on Disulfide-Linked Block Copolymer As Potential Carrier for Intracellular Drug Delivery. *Bioconjugate Chemistry* **2009,** *20* (6), 1095-1099.

197. Sun, C.-Y.; Dou, S.; Du, J.-Z.; Yang, X.-Z.; Li, Y.-P.; Wang, J., Doxorubicin Conjugate of Poly(Ethylene Glycol)-Block-Polyphosphoester for Cancer Therapy. *Advanced Healthcare Materials* **2014,** *3* (2), 261-272.
198. Mao, C.-Q.; Du, J.-Z.; Sun, T.-M.; Yao, Y.-D.; Zhang, P.-Z.; Song, E.-W.; Wang, J., A biodegradable amphiphilic and cationic triblock copolymer for the delivery of siRNA targeting the acid ceramidase gene for cancer therapy. *Biomaterials* **2011,** *32* (11), 3124-3133.
199. Sun, T.-M.; Du, J.-Z.; Yao, Y.-D.; Mao, C.-Q.; Dou, S.; Huang, S.-Y.; Zhang, P.-Z.; Leong, K. W.; Song, E.-W.; Wang, J., Simultaneous Delivery of siRNA and Paclitaxel via a "Two-in-One" Micelleplex Promotes Synergistic Tumor Suppression. *ACS Nano* **2011,** *5* (2), 1483-1494.
200. Du, J.-Z.; Du, X.-J.; Mao, C.-Q.; Wang, J., Tailor-Made Dual pH-Sensitive Polymer–Doxorubicin Nanoparticles for Efficient Anticancer Drug Delivery. *Journal of the American Chemical Society* **2011,** *133* (44), 17560-17563.
201. Aweda, T. A.; Zhang, S.; Mupanomunda, C.; Burkemper, J.; Heo, G. S.; Bandara, N.; Lin, M.; Cutler, C. S.; Cannon, C. L.; Youngs, W. J., Investigating the pharmacokinetics and biological distribution of silver-loaded polyphosphoester-based nanoparticles using 111Ag as a radiotracer. *Journal of Labelled Compounds and Radiopharmaceuticals* **2015**.
202. Gustafson, T. P.; Lonnecker, A. T.; Heo, G. S.; Zhang, S.; Dove, A. P.; Wooley, K. L., Poly (d-glucose carbonate) Block Copolymers: A Platform for Natural Product-Based Nanomaterials with Solvothermatic Characteristics. *Biomacromolecules* **2013,** *14* (9), 3346-3353.
203. Lim, Y. H.; Heo, G. S.; Cho, S.; Wooley, K. L., Construction of a Reactive Diblock Copolymer, Polyphosphoester-block-Poly(l-lactide), as a Versatile Framework for Functional Materials That Are Capable of Full Degradation and Nanoscopic Assembly Formation. *ACS Macro Letters* **2013,** *2* (9), 785-789.
204. Lim, Y. H.; Tiemann, K. M.; Heo, G. S.; Wagers, P. O.; Rezenom, Y. H.; Zhang, S.; Zhang, F.; Youngs, W. J.; Hunstad, D. A.; Wooley, K. L., Preparation and in Vitro Antimicrobial Activity of Silver-Bearing Degradable Polymeric Nanoparticles of Polyphosphoester-block-Poly(l-lactide). *ACS Nano* **2015,** *9* (2), 1995-2008.
205. Shen, Y.; Zhang, S.; Zhang, F.; Loftis, A.; Pavía-Sanders, A.; Zou, J.; Fan, J.; Taylor, J. S. A.; Wooley, K. L., Polyphosphoester-Based Cationic Nanoparticles Serendipitously Release Integral Biologically-Active Components to Serve as Novel Degradable Inducible Nitric Oxide Synthase Inhibitors. *Advanced Materials* **2013,** *25* (39), 5609-5614.
206. Zhang, F.; Smolen, J. A.; Zhang, S.; Li, R.; Shah, P. N.; Cho, S.; Wang, H.; Raymond, J. E.; Cannon, C. L.; Wooley, K. L., Degradable polyphosphoester-based silver-loaded nanoparticles as therapeutics for bacterial lung infections. *Nanoscale* **2015,** *7* (6), 2265-2270.
207. Zhang, S.; Zou, J.; Elsabahy, M.; Karwa, A.; Li, A.; Moore, D. A.; Dorshow, R. B.; Wooley, K. L., Poly (ethylene oxide)-block-polyphosphester-based paclitaxel conjugates as a platform for ultra-high paclitaxel-loaded multifunctional nanoparticles. *Chemical Science* **2013,** *4* (5), 2122-2126.
208. Gustafson, T. P.; Lim, Y. H.; Flores, J. A.; Heo, G. S.; Zhang, F.; Zhang, S.; Samarajeewa, S.; Raymond, J. E.; Wooley, K. L., Holistic Assessment of Covalently Labeled Core–Shell Polymeric Nanoparticles with Fluorescent Contrast Agents for Theranostic Applications. *Langmuir* **2014,** *30* (2), 631-641.
209. Owen, S. C.; Doak, A. K.; Wassam, P.; Shoichet, M. S.; Shoichet, B. K., Colloidal Aggregation Affects the Efficacy of Anticancer Drugs in Cell Culture. *ACS Chemical Biology* **2012,** *7* (8), 1429-1435.
210. Sun, T.; Zhang, Y. S.; Pang, B.; Hyun, D. C.; Yang, M.; Xia, Y., Engineered Nanoparticles for Drug Delivery in Cancer Therapy. *Angewandte Chemie International Edition* **2014,** *53* (46), 12320-12364.

211. Chen, C.-J.; Jin, Q.; Liu, G.-Y.; Li, D.-D.; Wang, J.-L.; Ji, J., Reversibly light-responsive micelles constructed via a simple modification of hyperbranched polymers with chromophores. *Polymer* **2012,** *53* (17), 3695-3703.
212. Wu, J.; Sun, T.-M.; Yang, X.-Z.; Zhu, J.; Du, X.-J.; Yao, Y.-D.; Xiong, M.-H.; Wang, H.-X.; Wang, Y.-C.; Wang, J., Enhanced drug delivery to hepatocellular carcinoma with a galactosylated core-shell polyphosphoester nanogel. *Biomaterials Science* **2013,** *1* (11), 1143-1150.
213. Wang, Y.-C.; Liu, X.-Q.; Sun, T.-M.; Xiong, M.-H.; Wang, J., Functionalized micelles from block copolymer of polyphosphoester and poly(ε-caprolactone) for receptor-mediated drug delivery. *Journal of Controlled Release* **2008,** *128* (1), 32-40.
214. Tao, Y.; He, J.; Zhang, M.; Hao, Y.; Liu, J.; Ni, P., Galactosylated biodegradable poly(?-caprolactone-co-phosphoester) random copolymer nanoparticles for potent hepatoma-targeting delivery of doxorubicin. *Polymer Chemistry* **2014,** *5* (10), 3443-3452.
215. Patel, M. M.; Goyal, B. R.; Bhadada, S. V.; Bhatt, J. S.; Amin, A. F., Getting into the Brain. *CNS Drugs* **2009,** *23* (1), 35-58.
216. Zhang, G.; Zhang, M.; He, J.; Ni, P., Synthesis and characterization of a new multifunctional polymeric prodrug paclitaxel-polyphosphoester-folic acid for targeted drug delivery. *Polymer Chemistry* **2013,** *4* (16), 4515-4525.
217. Zhang, P.; Hu, L.; Yin, Q.; Feng, L.; Li, Y., Transferrin-Modified c[RGDfK]-Paclitaxel Loaded Hybrid Micelle for Sequential Blood-Brain Barrier Penetration and Glioma Targeting Therapy. *Molecular Pharmaceutics* **2012,** *9* (6), 1590-1598.
218. Zhang, P.; Hu, L.; Yin, Q.; Zhang, Z.; Feng, L.; Li, Y., Transferrin-conjugated polyphosphoester hybrid micelle loading paclitaxel for brain-targeting delivery: synthesis, preparation and in vivo evaluation. *Journal of controlled release* **2012,** *159* (3), 429-434.
219. Yang, X.-Z.; Du, J.-Z.; Dou, S.; Mao, C.-Q.; Long, H.-Y.; Wang, J., Sheddable Ternary Nanoparticles for Tumor Acidity-Targeted siRNA Delivery. *ACS Nano* **2012,** *6* (1), 771-781.

Chapter 1

In-Chain Poly(phosphonate)s via Acyclic Diene Metathesis Polycondensation

Foreword

This chapter is reproduced with permission from "*Macromolecules*, **2016**, *49* (10), pp 3761–3768" American Chemical Society Copyright 2016.

Authors: Kristin N. Bauer, Hisaschi T. Tee, Ingo Lieberwirth, Frederik R. Wurm.

Abstract

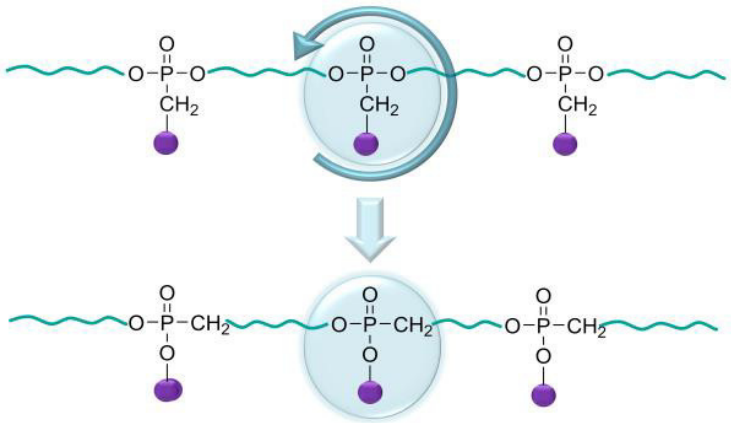

In-chain poly(phosphonate)s have been prepared via acyclic diene metathesis polymerization of three different monomers. Novel unsaturated phosphonate monomers with asymmetric structure have been developed. The monomers are accessible via a three-step synthesis that can be easily scaled up. This is the first report on poly(phosphonate)s by olefin metathesis where the stable carbon-phosphorus linkage is localized in the polymer backbone. This changes the nature of the degradation products compared to other poly(phosphoester)s. Polymers with molecular weights up to 28 000 g mol^{-1} can be achieved and have been characterized in detail by NMR spectroscopy, size exclusion chromatography, thermogravimetry, and differential scanning calorimetry. They have been also compared to structural analogues polyphosphates with respect to crystallization (SAXS, WAXS) and their rheological behavior. Also solution grown crystals

were analyzed rendering some of the herein reported poly(phosphonate)s as interesting defect poly(ethylene)-like structures.

1 Introduction

Degradable polymers - natural or synthetic- have become a major research area in polymer science, ranging from everyday plastics to complex nanostructures.[1] Polymers with a merely carbon-based backbone are resilient against environmental influences (hydrolysis, enzymes, most UV light) and typically do not degrade *in vivo* and in many cases show long half-life times also in the natural environment.[2] In contrast, polymers with heteroatoms in the backbone, such as polyesters, -amides, -anhydrides, polyurethanes and -ureas show a strong structure-degradation relation depending on the conditions, e.g. hydrolysis and/or enzymatic cleavage.[3-4] During the last decades degradable polymers have attracted tremendous interest for the development of therapeutic devices such as temporary prostheses,[5] porous structures as scaffolds for tissue engineering,[6] or as vehicles for sustained drug release[7]. Each of these applications demands high standards concerning physical, chemical, biochemical, and degradation properties to guarantee efficient therapy. Beside the biodegradability, especially the biocompatibility of the polymer and the degradation products is crucial for the usage of a polymeric material in the biomedical field. One class of biodegradable polymers which is especially appealing for the application in the biomedical field are main-chain poly(phosphoester)s (PPEs) not only due to their similarity to biomacromolecules such as the most prominent PPE, deoxyribose nucleic acid (DNA), but also due to their high structural and chemical versatility.[8-9] The pentavalency of phosphorus enables -in contrast to carboxylic polyesters- the introduction of pendant functional and/or solubilizing groups in every repeat unit, and at the same time is a direct handle for adjusting the degradation profile.[10] Under physiological conditions PPEs can be degraded due to the hydrolytically and enzymatically degradable phosphoester bonds along the polymer backbone into phosphates, diols and alcohols as the final breakdown products.[3] PPEs are known since the 1930s, but compared to conventional polyesters, the interest in these polymers faded because of the expensive synthesis and low molecular weights combined with mostly ill-defined structures. However, since the 1970s PPEs have been studied sporadically in academia mainly based on the pioneering works of Penczek[11-14]; later the groups of Wang,[15-18] Leong,[19-20] and Iwasaki[21] have paved the way to PPEs with control over structure and molecular weights. Typical approaches to PPEs are first and foremost the polycondensation of phosphorus

dichlorides or diesters with diols,[22-24] the polyaddition[25-26] and the ring-opening polymerization of cyclic phosphorus compounds.[27-28] During the past few years the acyclic diene metathesis (ADMET) polymerization has proven to be a reliable method for the preparation of (unsaturated) PPEs ((U)PPEs) with diverse thermal properties due to the precise adjustability of main- and side-chains.[29-30]

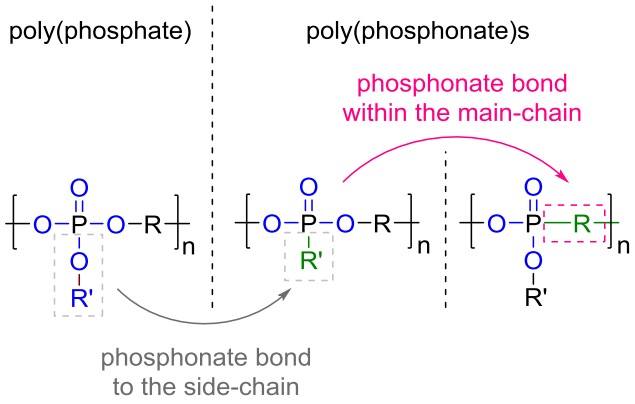

Figure 1.1. Structure of poly(phosphate)s (*left*) and main-chain poly(phosphonate)s with the P-C-bond as pendant group (*middle*) or as part of the PPE-backbone. (*right*).

Furthermore, the high functional group tolerance of the ruthenium catalysts allows the synthesis of polymers with functional groups.[31] However, the usage of these materials in biomedical applications is still limited due to the hydrophobic long-chain diols, which are part of the final degradation products of the PPEs and reduce the degradation kinetics. To date, the ADMET protocol was used to prepare poly(phosphate)s[29, 32] and main-chain poly(phosphonates)s with the stable P-C-bond as side chain (cf. Figure 1.1).[33] Poly(phosphonate)s are an almost forgotten subclass of PPEs, consisting of two ester linkages and one alkyl- or aryl-group, which is directly attached to the phosphorus atom. The degradation profiles of poly(phosphonate)s and poly(phosphate)s differ due to the stable P-C-bonds, however, for both systems hydrolytic and enzymatic cleavage has been reported. In the so far reported main-chain poly(phosphonate)s the two phosphoesters build up the polymer backbone, while the P-C-bond is the pendant group.[34] Especially aliphatic poly(phosphonate)s are interesting materials for usage in the biomedical field, since they are potentially biodegradable and biocompatible. Nevertheless, beside some recently published approaches to aliphatic phosphonates,[28, 35] to date, mainly aromatic poly(phosphonate)s are known for their flame retardant properties.

Herein, we describe the first synthesis of a main-chain poly(phosphonate)s by ADMET polycondensation with the P-C-bond as a part of the polymer backbone ("in-chain", Figure 1.1 right) and compare them to structural analogues poly(phosphate)s. Different monomers and polymers have been prepared with varying the hydrophilicity and the phosphorus content. The monomer syntheses were performed in three to four steps yielding difunctional phosphonates with the polymerizable double bond in the stable phosphonate chain. The polycondensation was conducted in bulk or in solution leading to a quantitative polymer-formation. This new class of (U)PPEs allows the reduction of the hydrophobic degradation products to a minimum: by "rotating" the P-C-bond from the pendant chain into the polymer backbone, the degradation product remains attached to the charged phosphonates and thus should allow their easy body clearance.

2 Results and Discussion

Monomer synthesis. To date, difunctional or trifunctional phosphate or phosphonates monomers with different chain lengths were accessible via esterification of terminal unsaturated alcohols with phosphoryl chloride or derivatives.[32, 36] In contrast, the protocol for the corresponding phosphonate monomers for the synthesis of in-chain poly(phosphonate)s needed to be designed. To generate a phosphonate monomer suitable for ADMET polymerization, the Michaelis-Arbuzov reaction between triethyl phosphite and an alkenyl-bromide or -iodide was applied to install the terminal double bond for olefin metathesis at the phosphorus center (Scheme 1.1, synthesis of **1'**,**2'**,**3'**). The usage of either the alkenyl-bromide or -iodide is dependent on the reactivity: for the synthesis of the "short"- chain phosphonates, i.e. **1',** the bromide is sufficient, while for the synthesis of the derivatives with longer alkyl chain (**2'**, and **3'**), the more reactive iodides were necessary. The alkenyl-halides are commercially available or can be synthesized by the reaction of the corresponding alcohol with imidazole and iodine according to literature.[37-38] After the formation of the diethyl-alkenyl phosphonates (**1'**,**2'**,**3'**), one phosphoester was cleaved with trimethylsilylbromide. The final difunctional monomer was then prepared by the esterfication of the crude precursor hydrogen-alkenyl-phosphonate with an alkenyl-halide of choice using Cs_2CO_3 in DMF (Scheme 1.1).

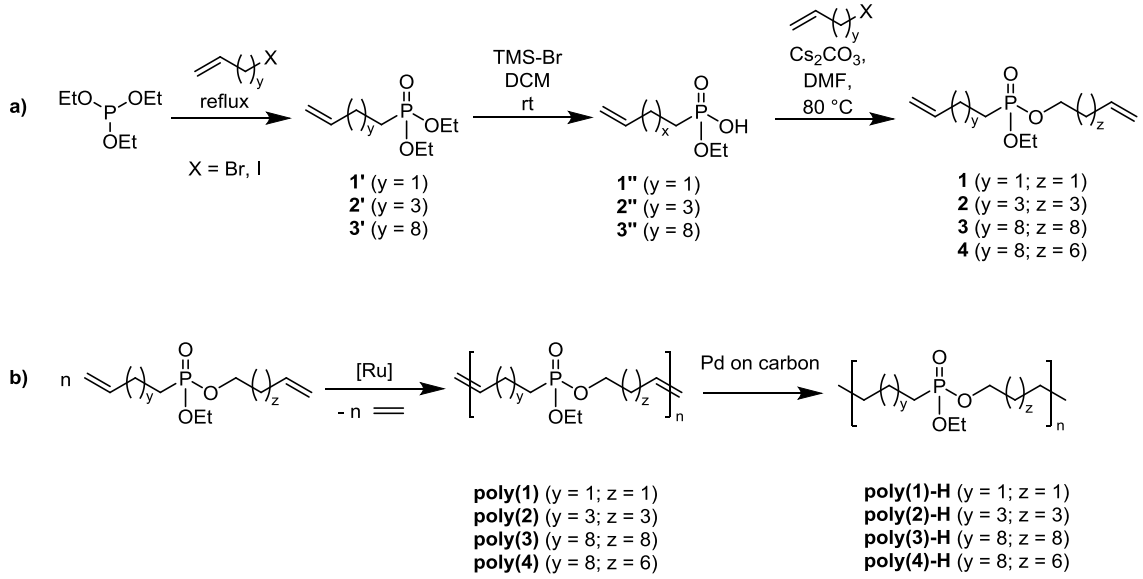

Scheme 1.1. a) Synthesis of in-chain phosphonate-monomers b) ADMET polycondensation of monomers 1-4 and subsequent hydrogenation.

This protocol allows the synthesis of symmetrical and unsymmetrical phosphonates monomers, which was also not reported for the respective phosphates. The monomers were purified by column chromatography as colorless liquids in moderate yields (compare Experimental Section). For comparison, bis-(undec-10-en-1-yl) ethylphosphate (**5**), a so far not reported ADMET monomer, was prepared in high yields from ethyl dichlorophosphate and undecenol. All monomers were stable at room temperature at least for several months. This general protocol allows the variation of the phosphorus-content and thus the hydrophilicity of the materials easily. The pendant group could be varied by changing from triethyl phosphite to other precursors. Spectral characterization of all monomers is listed in the experimental section Figures 1.6-1.17.

ADMET-Polycondensation. The polycondensation reactions of the monomers **1-4** were carried out according to the conditions developed by our group recently[32] for the polymerization of the phosphates and phosphonates. The monomers **1-4** have been polymerized in a ruthenium-catalyzed acyclic diene metathesis reaction at reduced pressure at 60 °C using the Grubbs catalyst 1st generation. Variation of molecular weights was achieved by conducting the reaction

in the high boiling solvent 1-chloronaphthalene (20 wt%) to guarantee continuous mixing during the polymerization process. The obtained polymers **poly(1)-(4)** are viscous materials with molecular weights up to 4 x 10^4 g mol^{-1} and molecular weight dispersities of $Đ \approx 2$ for **poly(3)** and **(4),** which are in good agreement with the theoretically predicted distribution by the Carothers equation (compare Table 1.2). **Poly(2)** could not be analyzed by SEC, due to strong interactions with the column material (different conditions were tested, but in all cases no elution was detected). As the successful polymerization of **2** was proven by NMR spectroscopy, this is an interesting finding and distinct difference to the analogues phosphate, which eluted under the same conditions from the SEC column. Vapor pressure osmometry let us at least estimate a molecular weight of ca 8,000 g mol^{-1}. For monomer **1** only oligomers were produced which can be attributed to the 'negative neighboring group effect'. The proximity of the phosphonate enter to the double bond and thus to the ruthenium carbene after catalyst attachment probably hinders the propagation due to complexation, which was reported previously for diallyl-phenyl-phosphate.[39] This effect can also be seen with the naked eye as the color of the catalyst changed from violet to brown within a few minutes indicating the formation of metathesis-inactive species. For all other polycondensations, after ceasing of the ethylene evolution, the polymers were precipitated into hexane three times to remove the catalyst (and 1-chloronaphthalene for solution polycondensations).

The obtained polymers exhibit irregular structures due to the asymmetric architectures of the monomers allowing hyphenated structures as well as tail to tail and head to head attachment (see Scheme 1.2). The structural irregularity results in varying distances between the phosphonate units. Compared to the corresponding poly(phosphate)s this characteristic leads to slightly altered properties such as a lower degree of crystallinity and the presence of several melting endotherms (*see below*). In a next step, saturated PPEs were synthesized from the obtained polymers via catalytic hydrogenation of the double bonds using Pd on carbon under a H_2-atmosphere. After hydrogenation the viscous UPPE changed into resin-like (for **poly(4)-H**) or solid (for **poly(3)-H**) materials. Only **poly(2)-H** remained a viscous oil after hydrogenation. The SEC results of the hydrogenated polymers are in good agreement with the results of the UPPEs, proving –in combination with NMR- the stability of the P-C- as well as the P-O-linkage under hydrogenation conditions (cf. Figures 1.24-1.25). Figure 1.2 shows an overlay of the ^{1}H NMR spectra of the monomer (**2**), the polymer after ADMET (**poly(2)**), and the hydrogenated PPE (**poly(2)-H**). It is obvious that the terminal double bonds at 4.9 and 5.7 ppm disappear after the ADMET process and internal double bonds (5.3 ppm) can be detected, which disappear after

hydrogenation (other NMR spectra of polymer cf. Figures 1.18-1.23). The resulting polymers contain the expected high amount of trans olefins, around 80% (determined by NMR spectroscopy), since the stereochemistry is controlled thermodynamically. The polymers are readily soluble in organic solvents such as CH_2Cl_2, toluene and THF, but insoluble in hexane or methanol, for example.

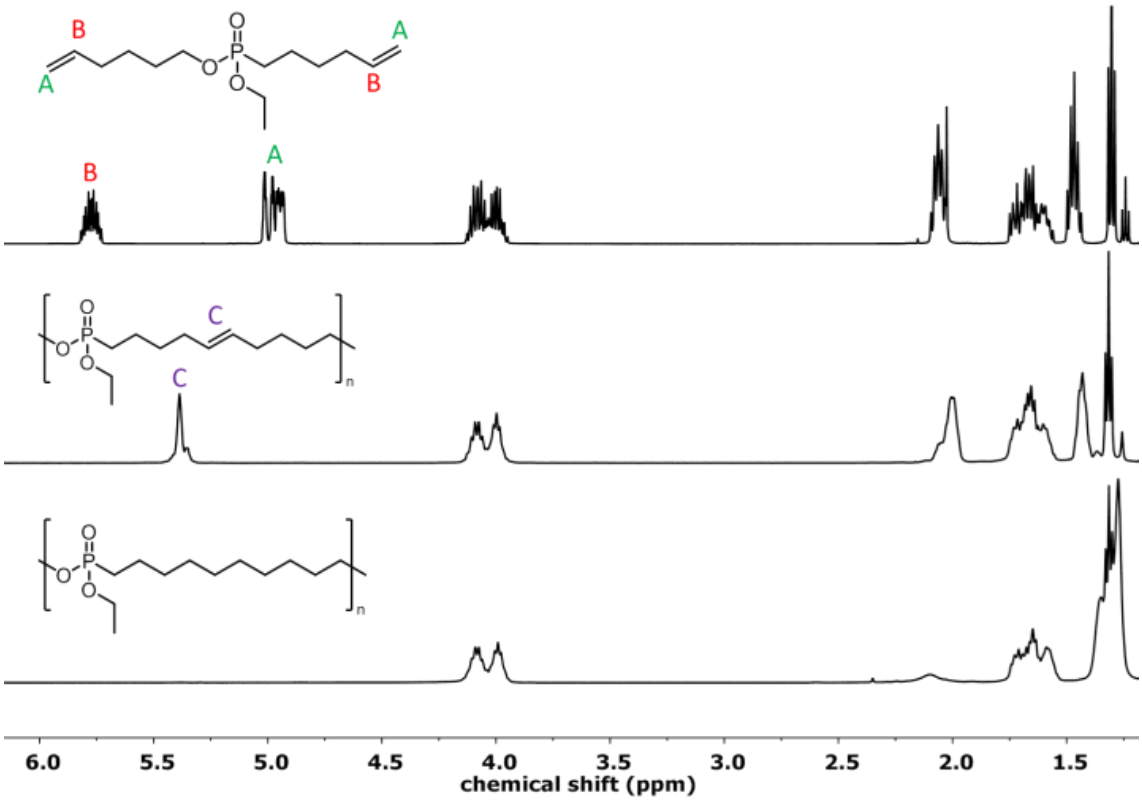

Figure 1.2. ^{1}H NMR (500 MHz at 298.3 K) of monomer 2 and the corresponding polymers poly(2) and poly (2)-H after hydrogenation.

Solid State Characterization. The UPPEs synthesized in this study are all sticky viscous materials, while the hydrogenated polymers range from sticky liquids to resin-like solids. The thermal stability of all synthesized polymers was examined by thermal gravimetric analysis (TGA), indicating a thermal stability comparable with the respective poly(phosphate)s (Ton between 260-300°C). However, two degradation steps are detected in TGA, probably due to the stable P-C bond in the backbone (cf. Figure 1.27). The glass transition temperatures (T_g) and the melting points (T_m) were determined by differential scanning calorimetry (DSC) under nitrogen. Table 1 summarizes the thermal properties of the synthesized polymers. The poly(phosphonate)s

show the expected low glass transitions ranging from -55 °C for **poly(3)** to -65 °C for **poly(2)** and -66 °C for **poly(4),** respectively, which are similar to the poly(phosphate)s (Figures 1.3, 1.28-1.30). Interestingly, the poly(phosphonate)s with the longer alkyl chains, especially the hydrogenated samples (**poly(3)-H** and **poly(4)-H**, exhibit additional thermal transitions at low temperature at ca. -45°C, which could be due to the presence of different crystallite structures within the polymer matrix due to the asymmetry of the monomers. For poly(5)-H – the polyphosphate analogue – a glass transition of -47°C and a melting endotherm of ca 51°C is detected (Figure 1.30).

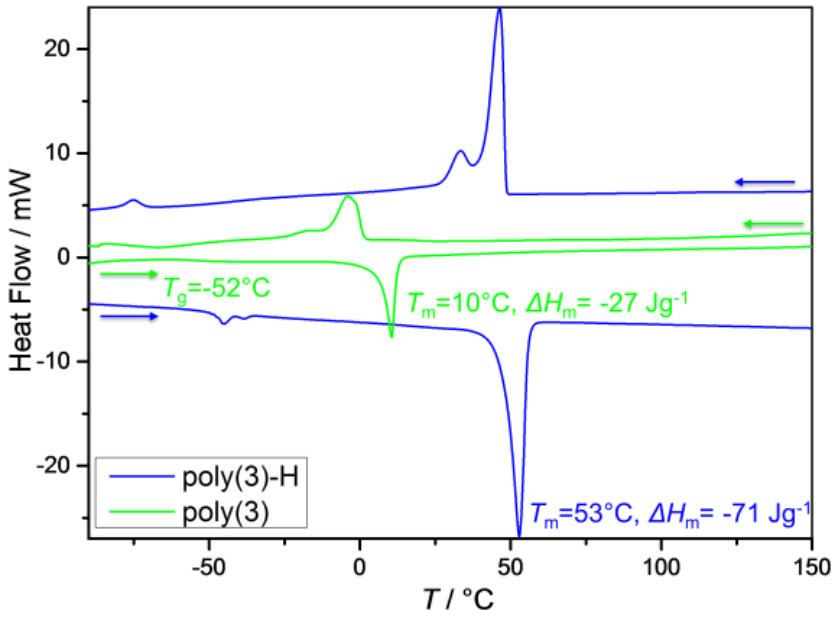

Figure 1.3. DSC thermograms of poly(3) and poly(3)-H (heating and cooling rate 10 Kmin^{-1} (2nd run), the main melting endotherm are labelled, details see main text.).

The hydrogenation of the double bonds in the polymer backbone causes a slight shift of the glass transitions but a distinct change of the melting behavior especially of the polymers with longer alkyl-chains in the backbone. The hydrogenation of **poly(3)** to **poly(3)-H,** for example**,** leads to a shift of the main melting temperature from 10 °C to 53 °C and an increase in the melting enthalpy from ca. -27 J g^{-1} to -71 J g^{-1}(Figure 1.3). **Poly(4)** is amorphous, but after hydrogenation a melting endotherm at ca. 12°C can be detected (Figure 1.29). In contrast, the short-chain **poly(2)** exhibit neither as unsaturated nor as hydrogenated polymer **poly(2)-H** crystalline areas.

Table 1. Thermal properties (determined by DSC) of the UPPEs and the corresponding PPEs.

Polymer	M_n /gmol^{-1}	$Đ$	T_g /°C	T_m /°C	ΔH_m /Jg^{-1}
poly(2)	8700	-	-66	-	-
poly(3)	27900	1.66	-52	10	-27.52
poly(4)	27600	1.68	n.d.	-45	-0.9
poly(5)	9300	2.5	-61	14	-35.21
poly(2)-H	-	-	-61	-	-
poly(3)-H	31000	1.69	n.d.	-48, -40, 53	-71.20
poly(4)-H	14600	1.99	n.d.	-47, -39, 10	-17.9
poly(5)-H	9900	2.33	-47	51	-70.5

The crystalline UPPEs synthesized by ADMET polymerization are considered to have a similar lamellar crystalline structure as polyethylene, in which the phosphate units as well as the double bonds, that can be either *cis* or *trans*, with the cis part acting as defects and thus reducing the melting points and enthalpies dramatically. By hydrogenation of the double bonds one defect can be eliminated and materials with higher degree of crystallinity can be obtained. Recently, the crystallization behavior of poly(phosphate)s and side-chain poly(phosphonate)s has been studied.[40] Poly(3)-H was dissolved in hot n-octane and crystallized slowly during cooling from solution. Drop-cast TEM (Figures 1.4 and 1.33) shows the resulting crystals. The corresponding electron diffraction pattern (inset Figure 1.4) indicates that the crystal packing is similar to the pseudohexagonal crystal phase of polyethylene with a lattice spacing of 4.1 Å. The WAXS

measurement (Figure 1.5) yields a similar finding. In the respective angular range only one distinct peak at a position corresponding to a lattice spacing of 4.1 Å appears. Furthermore, the WAXS diffractogram reveals another noticable feature at low angular position, which corresponds to a structure having a periodicity of 2.6 nm. This structural feature is found in the SAXS measurements as well with a structural periodicity of 2.4 nm (Figure 1.32). It is straight forward to assign this periodicity to the all-trans length of the 19 methylene groups that form the crystalline stem of one crystal lamellae. However, the thickness of the solution grown crystals exceeds this one-fold thickness by far, as demonstrated from the EELS thickness measurements (Figure 1.31). Accordingly, the **poly(3)-H** crystals are assembled like a stack of folded chain lamellae.

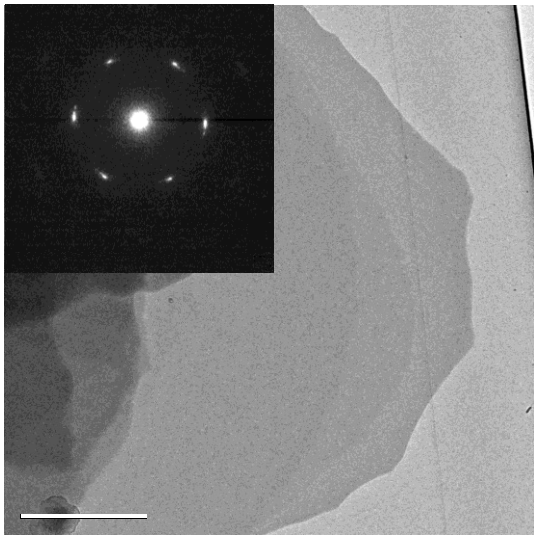

Figure 1.4. TEM brightfield micrograph and the ED pattern (inset) of solution grown crystals of poly(3)-H from n-octane solution.

The crystallization behavior of **poly(3)-H** was also compared to a structural similar poly(phosphate) (Figure 1.5). X-ray diffractogramm of the two polymers shows similar degrees of crystallinity and a similar crystal structure as well. Even the feature at low scattering angles in WAXS is noticeable for both materials, which indicates the presence of polymer folded chain crystals with a typical thickness as expected from the length of the methylene groups between the phosphonate units.

The investigation of the mechanical properties was accomplished by dynamic mechanical analysis (DMA) (Figure 1.5 (3)). To evaluate the mechanical properties of the in-chain

poly(phosphonate)s, again the poly(phosphate)s were used as comparison. Figure 1.5 shows the progression of the storage (G') and the loss (G'') modulus with increasing temperature of **poly(3)-H** and the corresponding poly(phosphate). The DMA analysis reveals the similar viscoelastic properties of both polymers. Below the glass transition, the storage moduli of both polymers are relatively high due to the nearly elastic properties at low temperatures. Above the T_g, the storage modulus decreases significantly and the loss moduli increases due to the softening of the material. By achieving the melting temperatures, the storage as well as the loss moduli decrease since the polymers lost their rigidity. Below the melting point the polymers differ in their behavior. The storage and the loss moduli of the poly(phosphate) are significantly lower and diffuse indicating that this material is significantly softer than the in-chain poly(phosphonate).

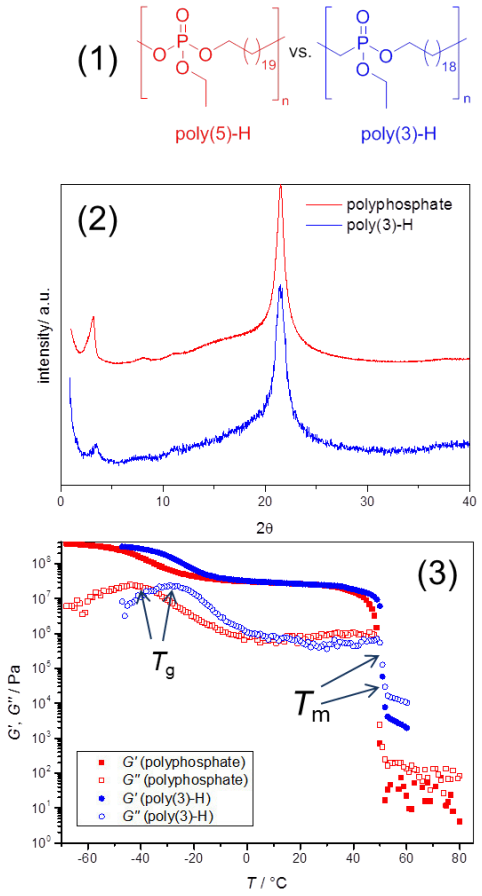

Figure 1.5. (1) structural comparison of poly(3)-H and poly(phosphate). (2) X-ray diffractograms of poly(3)-H and the corresponding poly(phosphate). (3) Temperature dependence of the shear moduli G and G'' of poly(3)-H and the corresponding polyphosphate.

3 Conclusion

This study is the first report on main-chain poly(phosphonate)s with the P-C-bond in the polymer backbone, i.e. *in-chain* poly(phosphonate)s. Several structurally different monomers with varying P-content have been prepared and their ADMET polycondensation was studied. The resulting polymers exhibit molecular weights up to 28 000 g/mol and show distinct different thermal properties, depending on the length of the alkyl spacers. The mechanical analysis of the materials reveals similar properties to the already established poly(phosphate)s making the in-chain poly(phosphonate)s interesting materials for biomedical applications and as potential tissue engineering scaffold. Many postpolymerization reactions on the internal and external

double bonds might be carried out in order to vary their mechanical properties. Furthermore, the exchange of one ester linkage by a stable P-C-linkage inside the polymer backbone reduces the amount of hydrophobic degradation products. In conclusion, the in-chain poly(phosphonate)s are a further step to complete the wide range of biomedically interesting polyphosphonates with various architectures and properties.

4 Experimental

4.1 General information

Materials. Solvents and chemicals were purchased from Acros Organics, Sigma Aldrich, or Fluka and used as received, unless otherwise stated. Triethylphosphite was used as received from Sigma Aldrich. Deuterated solvents were purchased from Sigma Aldrich and kept over molecular sieves.

4.2 Instrumentation and characterization techniques.

SEC. For the poly(phosphonate)s size exclusion chromatography (SEC) measurements were performed in THF with an Agilent 1100 Series as an integrated instrument, including a MZ-Gel SD plus e5/e3/100 column, a UV (Spectra System UV 2000), and a refractive index (RI) detector (Agilent Technologies 1260 Infinity). Calibration was carried out using polystyrene standards provided by Polymer Standards Service. For the poly(phosphate) SEC measurements were performed in THF with a PSS SecCurity system (Agilent Technologies 1260 Infinity). Sample injection was performed by a 1260-ALS auto sampler (Waters) at 30 °C. SDV columns (PSS) with dimensions of 300 × 80 mm, 10 µm particle size and pore sizes of 106, 104 and 500 Å were employed. The DRI Shodex RI-101 detector (ERC) and UV-Vis 1260-VWD detector (Agilent) was used for detection. Calibration was achieved using poly(styrene) standards provided by Polymer Standards Service.

NMR. For nuclear magnetic resonance analysis ^{1}H, ^{13}C and ^{31}P NMR spectra of the monomers were recorded on a Bruker AVANCE III 500 MHz or 700MHz spectrometer. All spectra were measured either in CD_2Cl_2 or $CDCl_3$ at 298 K. The spectra were calibrated against the solvent signal and analyzed using MestReNova 8 from Mestrelab Research S.L.

DSC. The thermal properties of the synthesized polymers have been measured by differential scanning calorimetry (DSC) on a Mettler Toledo DSC 823 calorimeter. Three scanning cycles of heating-cooling were performed in a N_2-atmosphere 30 mL/min) with a heating and cooling rate of 10 °C/min.

TGA. TGA was measured on a Mettler Toledo ThermoSTAR TGA/SDTA 851-Thermowaage in nitrogen atmosphere. The heating rate was 10 °C/min in a range of temperature between 25 °C and 600 – 900 °C. **VPO.** Vapor pressure osmometry (VPO) was measured on a Knaur vapor

pressure osmometer K-7000 in chloroform at 30 °C. Calibration was carried out using poly(ethylene glycol) methyl ether.

DMA. Dynamic Mechanical Analysis (DMA) was performed using an Advanced Rheometric Expansion System (ARES) equipped with a force-rebalanced transducer. Plate-plate geometry was used with plate diameters of 6 mm. The gap between plates was around 1 mm. Experiments were performed under dry nitrogen atmosphere. The isochronal temperature dependencies of *G*' and *G*'' were determined for ω = 10 rad/s.

WAXS/SAXS. For wide angle x-ray scattering (WAXS) and small angle x-ray scattering (SAXS) experiments the sample was prepared by hot pressing an approximately 200 - 400 µm thick film on a hot stage. In order to achieve a well crystallized specimen, we prepared an annealed sample by heating the sample well above the melting point to 120°C and kept it at this temperature for 10 min. Subsequently, it was cooled from the melt to 42°C and kept at this temperature for 48 h. SAXS was recorded using Cu Kα radiation (wavelength 1.54 Å) from a rotating anode source (Rigaku MicroMax 007 x-ray generator) with curved multilayer optics (Osmic Confocal Max-Flux). Polymer foils were measured in transmission geometry. The scattered intensity was recorded on a 2D detector (Mar345 image plate) with a sample-detector distance of 2 m. For WAXS measurements the sample-detector distance was set to 20 cm.

TEM. For TEM examination solution grown crystals were prepared from a 0.05 % solution in *n*-octane. The solution was heated to 85 °C in a temperature controlled oil bath and slowly cooled down to room temperature to achieve a turbid dispersion. One drop of this dispersion was applied to a carbon coated TEM grid, excess liquid was blotted of with a filter paper and the specimen was allowed to dry under ambient conditions. A FEI Tecnai F20 transmission electron microscope operated at an acceleration voltage of 200 kV was used to determine the crystal morphology, thickness and crystal structure. Bright field (BF) and energy-filtered transmission electron microscopy (EFTEM) techniques were used for measurements.

4.3 Synthetic Procedures

Synthesis of 6-iodohex-1-ene. This compound was synthesized by a literature procedure[37] from hex-5-en-1-ol (20.48 mL, 17 g, 169.73 mol) with triphenylphosphine (53.42 g, 203.7 mmol), imidazole (13.87 g, 203.7 mmol) and iodine (51.7g , 203.7 mmol) in dichloromethane to yield after distillation 6-iodohex-1-ene as a colorless oil (29.3 g, 82%).^{1}H NMR (250 MHz,

chloroform-*d*) δ 5.72 (ddt, *J* = 16.9, 10.2, 6.7 Hz, 1H), 5.02 – 4.84 (m, 2H), 3.12 (t, *J* = 7.0 Hz, 2H), 2.10 – 1.93 (m, 2H), 1.86 – 1.69 (m, 2H), 1.52 – 1.36 (m, 2H).

Synthesis of 11-iodoundec-1-ene. This compound was synthesized according to a literature procedure.[38] 11-bromoundec-1-ene (10 g, 42.9 mmol) was treated with NaI (12.86 g, 85.8 mmol) in 50 mL acetone under reflux over 16 h. Acetone was removed under reduced pressure and water was added to the residue. The mixture was extracted with diethyl ether and the combined organic layers were dried with sodium sulfate and concentrated under reduced pressure to yield known 11-iodoundec-1-ene as slight yellow oil (11.35 g, 94%).[1]H NMR (300 MHz, chloroform-*d*) δ 5.74 (ddt, *J* = 16.9, 10.1, 6.7 Hz, 1H), 5.02 – 4.82 (m, 2H), 3.12 (td, *J* = 7.0, 2.9 Hz, 2H), 2.06 – 1.91 (m, 2H), 1.75 (p, *J* = 7.1 Hz, 2H), 1.27 (d, *J* = 30.4 Hz, 12H).

General procedure for the synthesis of diethyl alkyl phosphonates. The diethyl alkyl phosphonates were synthesized by a Michaelis-Arbuzov reaction of the corresponding alkyl halides with triethyl phosphite. For the synthesis of diethyl but-3-en-1-yilphosphonate **(1')** 4-bromobut-1-ene was used whereas 6-iodohex-1-ene and 11-iodoundec-1-ene were used as alkyl halides for the syntheses of diethyl hex-5-en-1-ylphosphonate **(2')** and diethyl undec-10-en-1-ylphosphonate **(3')**. A mixture of the alkyl halide (1 eq) and triethyl phosphate were mixed and heated up to 100-140 °C until the alkyl halide was consumed completely (the consumption of the alkyl halide was monitored by NMR measurements since no solvent is used for the reaction). The diethyl alkyl phosphonates are obtained in 75-85% yield.

(1') [1]H NMR (300 MHz, chloroform-*d*) δ 5.79 (ddt, *J* = 16.6, 10.1, 6.3 Hz, 1H), 5.07 – 4.89 (m, 2H), 4.10 – 3.99 (m, 4H), 2.28 (ddtt, *J* = 11.1, 9.4, 6.4, 1.5 Hz, 2H), 1.85 – 1.67 (m, 2H), 1.31 – 1.24 (m, 6H). **(2')** [1]H NMR (300 MHz, chloroform-*d*) δ 5.72 (ddt, *J* = 16.9, 10.1, 6.6 Hz, 1H), 4.99 – 4.85 (m, 2H), 4.02 (dqd, *J* = 7.7, 7.1, 3.5 Hz, 4H), 2.07 – 1.94 (m, 2H), 1.73 – 1.47 (m, 4H), 1.47 – 1.35 (m, 2H), 1.25 (t, *J* = 7.1 Hz, 6H). **(3')** [1]H NMR (250 MHz, chloroform-*d*) δ 5.74 (ddt, *J* = 16.9, 10.2, 6.7 Hz, 1H), 5.01 – 4.79 (m, 2H), 4.17 – 3.87 (m, 4H), 1.96 (qt, *J* = 6.6, 1.4 Hz, 2H), 1.75 – 1.41 (m, 4H), 1.25 (t, *J* = 7.1 Hz, 18H).

General procedure for the synthesis of ethyl hydrogen alkenylphosphonates. The compounds were synthesized according to literature.[41] Briefly, a solution of the diethyl alkenylphosphonate (1 eq) was treated dropwise with trimethylsilyl bromide (1.2 eq) at room temperature. After stirring for a further hour at room temperature, the reaction was quenched with 5% $KHSO_4$-solution and stirred vigorously for five minutes. The phases were separated and the water phase

was washed with ethyl acetate. The organic layers were combined and dried with sodium sulfate. After removal of the solvent under reduced pressure the crude ethyl hydrogen alkenylphosphonates were obtained and used without further purification.

(1'') ^{1}H NMR (300 MHz, chloroform-*d*) δ 10.25 (s, 1H), 5.89 – 5.64 (m, 1H), 5.15 – 4.84 (m, 2H), 4.16 – 3.91 (m, 2H), 2.43 – 2.18 (m, 2H), 1.86 – 1.70 (m, 2H), 1.27 (td, *J* = 7.1, 2.0 Hz, 3H). **(2'')** ^{1}H NMR (300 MHz, chloroform-*d*) δ 9.93 (s, 1H), 5.72 (ddt, *J* = 16.9, 10.2, 6.7 Hz, 1H), 5.03 – 4.81 (m, 2H), 4.17 – 3.91 (m, 2H), 2.00 (q, *J* = 7.1 Hz, 2H), 1.80 – 1.33 (m, 6H), 1.26 (td, *J* = 7.1, 1.3 Hz, 3H). **(3'')** ^{1}H NMR (250 MHz, chloroform-*d*) δ 7.61 (s, 1H), 7.20 (s, 1H), 5.75 (ddt, *J* = 16.9, 10.1, 6.7 Hz, 2H), 5.01 – 4.74 (m, 2H), 4.14 – 3.91 (m, 2H), 2.04 – 1.87 (m, 4H), 1.45 – 1.09 (m, 15H).

General Procedure for the synthesis of in-chain phosphonate ADMET monomers. The respective hydrogen alkenylphosphonate (1 eq) was mixed with Cs_2CO_3 (1.1 eq) in DMF at room temperature. After stirring for 30 minutes the alkenyliodide was added dropwise and the reaction mixture was allowed to react for 12 h. The reaction mixture was filtrated and the filtration residue was washed thrice with DMF. The filtrate was concentrated under reduced pressure and the crude product was purified by column chromatography over silica using ethyl acetate/petroleum ether as eluent. The ADMET-monomers are obtained in 30-40% yield.

(1) ^{1}H NMR (500 MHz, chloroform-*d*) δ 5.87 – 5.70 (m, 2H), 5.14 – 4.92 (m, 4H), 4.14 – 3.97 (m, 4H), 2.39 (qt, *J* = 6.7, 1.4 Hz, 2H), 2.31 (ddtt, *J* = 11.3, 9.5, 6.5, 1.5 Hz, 2H), 1.79 (ddt, *J* = 20.0, 11.7, 4.4 Hz, 2H), 1.29 (t, *J* = 7.1 Hz, 3H). ^{13}C NMR (126 MHz, chloroform-*d*) δ 137.18, 133.60, 117.55, 115.10, 77.26, 64.54, 61.56, 34.95, 26.49, 25.54, 24.42, 16.44. ^{31}PH NMR (202 MHz, chloroform-*d*) δ 31.59. **(2)** ^{1}H NMR (500 MHz, chloroform-*d*) δ 5.78 – 5.67 (m, 2H), 4.99 – 4.86 (m, 4H), 4.10 – 3.88 (m, 4H), 2.06 – 1.94 (m, 5H), 1.71 – 1.49 (m, 6H), 1.41 (p, *J* = 7.5 Hz, 4H), 1.25 (t, *J* = 7.0 Hz, 3H). ^{13}C NMR (176 MHz, chloroform-*d*) δ 138.27, 138.18, 114.82, 114.80, 65.21, 65.17, 61.45, 61.42, 53.41, 33.17, 29.97, 29.94, 29.88, 29.79, 29.69, 25.87, 25.07, 24.80, 21.92, 21.89, 16.50, 16.46. ^{31}PH NMR (283 MHz, chloroform-*d*) δ 32.36. **(3)** ^{1}H NMR (700 MHz, chloroform-*d*) δ 5.82 (ddd, *J* = 16.8, 10.4, 5.3 Hz, 2H), 4.98 (dd, *J* = 43.4, 13.6 Hz, 4H), 4.07 (dddd, *J* = 59.0, 28.2, 15.3, 7.9 Hz, 4H), 2.06 (q, *J* = 7.5, 7.1 Hz, 4H), 1.68 (ddq, *J* = 57.5, 43.3, 8.6, 7.7 Hz, 7H), 1.44 – 1.21 (m, 29H). ^{13}C NMR (176 MHz, chloroform-*d*) δ 139.13, 114.11, 65.44, 65.40, 61.38, 61.34, 33.77, 30.63, 30.58, 30.54, 29.44, 29.39, 29.37, 29.30, 29.14, 29.07, 28.89, 28.71, 26.01, 25.52, 25.21, 22.41, 22.38, 16.50, 16.46. ^{31}PH NMR (283 MHz, chloroform-*d*) δ 32.62. **(4)** ^{1}H NMR (700 MHz, chloroform-*d*) δ 5.85 – 5.73 (m, 2H), 5.03 – 4.89

(m, 4H), 4.14 – 3.93 (m, 5H), 2.07 (q, *J* = 7.2, 6.7 Hz, 2H), 2.05 – 2.00 (m, 3H), 1.74 – 1.64 (m, 4H), 1.61 – 1.54 (m, 2H), 1.49 – 1.44 (m, 2H), 1.35 (qd, *J* = 7.0, 3.5 Hz, 4H), 1.30 (td, *J* = 7.1, 1.3 Hz, 3H), 1.29 – 1.23 (m, 8H). ^{13}C NMR (176 MHz, Chloroform-*d*) δ 139.17, 138.30, 114.83, 114.12, 65.19, 65.15, 61.42, 61.39, 60.37, 33.79, 33.19, 30.64, 30.55, 29.40, 28.90, 26.03, 25.23, 24.82, 22.43, 22.40, 16.52, 16.49, 14.19. ^{31}PH NMR (283 MHz, Chloroform-*d*) δ 32.66.

Synthesis of Bis-(undec-10-en-1-yl) ethylphosphate (5). A schlenk flask, equipped with a dropping funnel, was charged with ethyl dichlorophosphate (1 eq.), dissolved in dry CH_2Cl_2 (1.9 mol/L) under an argon atmosphere. The solution was cooled to 0 °C with an ice-bath. DMAP (0.01 eq.), Et_3N (1.8 eq.) and 10-Undecen-1-ol (1.8 eq.) were dissolved in dry CH_2Cl_2 (10 mol/L) and dropped over a period of 1 h via the dropping funnel. After the addition the reaction was stirred overnight at room temperature. The crude mixture was concentrated at reduced pressure, dissolved in diethylether and filtered. The organic phase was washed twice with 10 % aqueous hydrochloric acid solution and twice with brine. The organic layer was dried over sodium sulfate, filtered, concentrated at reduced pressure, and purified by flash chromatography over neutral alumina using dichloromethane as eluent to give a clear yellowish liquid. ^{1}H NMR (300 MHz, chloroform-*d*) δ 5.79 (ddt, J_1= 15 Hz, J_2 = 9 Hz, J_3 = 6 Hz, 2H), 4.97 (ddt, J_1 = 17.1 Hz, J_2 = 3.6 Hz, J_3 = 1.5 Hz, 2H), δ 4.91 (ddt, J_1 = 9.9 Hz, J_2 = 2.1 Hz, J_3 = 1.2 Hz, 2H), δ 4.14-4.04 (m, 2H), δ 4.01 (td, J_1 = 9 Hz, , J_2 = 4.5 Hz, 4H), δ 2,06-1.98 (m, 4H), δ 1.70-1.63 (m, 4H), δ 1.38-1.27 (m, 24H).

General Procedure for the ADMET Bulk Polymerization. In a glass Schlenk tube the respective monomer (1eq) and the Grubbs catalyst first generation (0.03 eq) were combined under an argon atmosphere. Polymerization was carried out at reduced pressure (to remove the ethylene gas evolving during the metathesis polymerization) at 60 °C for 24h. The polymers are obtained as brown viscous materials in quantitative yield.

General Procedure for the ADMET Solution Polymerization. In a glass Schlenk tube the respective monomer (1eq) and the Grubbs catalyst first generation (0.03 – 0.06 eq) were dissolved in 1-chloronaphthalene under an argon atmosphere. Polymerization was carried out at reduced pressure (to remove the ethylene gas evolving during the metathesis polymerization) at 60 °C for 24 - 48h. To remove 1-chloronaphthalene the obtained polymers were precipitated three times from hexane. The polymers are obtained as brown viscous materials in quantitative

yield. **Poly(2)** ^{1}H NMR (500 MHz, chloroform-*d*) δ 5.46 – 5.31 (m), 4.17 – 3.91 (m), 2.13 – 1.93 (m), 1.68 (dtd, *J* = 33.7, 18.7, 17.4, 10.5 Hz), 1.44 (qd, *J* = 7.6, 3.5 Hz), 1.32 (t, *J* = 7.0 Hz). ^{13}C NMR (126 MHz, Methylene Chloride-d_2) δ 75.37, 75.11, 74.86, 63.37, 63.32, 59.56, 59.51, 30.10, 28.66, 28.53, 28.25, 28.15, 28.10, 24.80, 24.11, 23.69, 23.53, 23.52, 22.99, 20.22, 20.08, 20.04. ^{31}P{H} NMR (202 MHz, Chloroform-*d*) δ 32.38. **Poly(3)** ^{1}H NMR (500 MHz, chloroform-*d*) δ 5.43 – 5.34 (m), 4.19 – 3.95 (m), 2.07 – 1.94 (m), 1.80 – 1.55 (m), 1.43 – 1.26 (m). ^{13}C NMR (126 MHz, chloroform-*d*) δ 65.31, 65.26, 61.42, 61.37, 32.62, 32.60, 32.03, 30.71, 30.58, 30.05, 29.67, 29.62, 29.51, 29.47, 29.39, 29.20, 29.18, 29.13, 28.50, 26.18, 25.50, 25.46, 25.07, 22.45, 22.41. ^{31}P{H} NMR (202 MHz, chloroform-*d*) δ 32.59. **Poly(4)** ^{1}H NMR (500 MHz, chloroform-*d*) δ 5.46 – 5.29 (m), 4.17 – 3.93 (m), 2.01 (tdd, *J* = 25.3, 13.3, 6.7 Hz), 1.82 – 1.53 (m), 1.43 (dt, *J* = 10.0, 6.6 Hz), 1.40 – 1.23 (m). ^{13}C NMR (126 MHz, Methylene Chloride-d_2) δ 75.40, 75.15, 74.89, 63.54, 63.48, 59.46, 59.41, 30.68, 30.28, 30.13, 28.76, 28.69, 28.64, 27.84, 27.80, 27.73, 27.57, 27.53, 27.50, 27.44, 27.36, 27.26, 27.24, 27.18, 26.91, 26.25, 25.29, 25.04, 24.39, 24.25, 23.77, 23.62, 23.13, 20.51, 20.47. ^{31}P{H} NMR (202 MHz, Methylene Chloride-d_2) δ 30.74 (d, *J* = 4.4 Hz).

General Procedure for the Catalytic Hydrogenation of ADMET Polymers. The polymers Poly(2), Poly(3) and Poly(4) were charged into a schlenk flask and dissolved in toluene (ca. 12 wt%). To remove the disturbing oxygen the flask was evacuated and flushed with argon again. 10 wt% of 5 % Pd/C catalyst were added followed by the removal of argon under reduced pressure and flushing with hydrogen. Hydrogen was bubbled into the solution via septum and syringe. Hydrogenation was then performed with a hydrogen balloon under vigorous stirring at room temperature until NMR showed no signals of double bonds. The solution was filtered over Celite and the solid polymer isolated after removal of the solvent in quantitative yield.

Poly(2)-H: ^{1}H NMR (500 MHz, Chloroform-*d*) δ 4.03 (ddt, *J* = 38.3, 13.6, 7.4 Hz), 2.10 (s), 1.65 (ddq, *J* = 39.1, 32.3, 8.1 Hz), 1.33 (ddt, *J* = 28.9, 14.8, 6.1 Hz). ^{13}C NMR (126 MHz, Chloroform-*d*) δ 77.20, 65.47, 65.42, 61.42, 61.37, 30.69, 30.63, 30.59, 30.56, 30.54, 29.69, 29.51, 29.47, 29.45, 29.33, 29.28, 29.17, 29.09, 28.90, 26.22, 25.54, 25.52, 25.10, 22.45, 22.41, 16.53, 16.49. ^{31}P{H} NMR (202 MHz, Chloroform-*d*) δ 32.12. **Poly(3)-H** ^{1}H NMR (500 MHz, Methylene Chloride-d_2) δ 4.03 – 3.82 (m), 1.58 (dddd, *J* = 21.5, 14.8, 11.8, 7.0 Hz), 1.47 (ddt, *J* = 15.7, 11.2, 7.2 Hz), 1.32 – 1.13 (m). ^{13}C NMR (126 MHz, Methylene Chloride-d_2) δ 65.31, 65.26, 61.26, 61.21, 53.84, 53.63, 53.41, 53.19, 52.98, 30.62, 30.57, 30.52, 29.72, 29.71, 29.68, 29.63, 29.60, 29.55, 29.42, 29.20, 29.12, 26.01, 25.57, 24.90, 22.44, 22.40. ^{31}P{H} NMR (202

MHz, Methylene Chloride-d_2) δ 32.12. **Poly(4)-H** ^{1}H NMR (500 MHz, Methylene Chloride-d_2) δ 4.03 – 3.81 (m), 1.67 – 1.41 (m), 1.36 – 1.10 (m). ^{13}C NMR (126 MHz, Methylene Chloride-d_2) δ 65.47, 61.47, 61.42, 54.00, 53.78, 53.57, 53.35, 53.14, 30.78, 30.73, 30.68, 29.88, 29.83, 29.79, 29.76, 29.71, 29.61, 29.59, 29.36, 29.33, 29.28, 26.16, 25.72, 25.05, 22.59, 22.55. ^{31}P{H} NMR (202 MHz, Methylene Chloride-d_2) δ 32.19.

Table 1.2. Synthetic results for in-chain poly(phosphonate)s prepared by ADMET polymerization in solution using 1-chloronaphthalene as solvent or in bulk.

#	catalyst	Cat. / eq	$V_{solvent}$/mL	t / h	M_n /gmol^{-1}	M_w/M_n
Poly(1)-a	Grubbs 1st Gen.	0,06	-	4	-	-
Poly(1)-b	Grubbs 2nd Gen.	0,06	-	4	-	-
Poly(2)-a	Grubbs 1st Gen.	0,09	2	48	8700*	-
Poly(2)-b	Grubbs 1st Gen.	0,06	2	48	8000*	-
Poly(3)-a	Grubbs 1st Gen.	0,09	2	48	27900	1.67
Poly(3)-b	Grubbs 1st Gen.	0,06	2	48	20600	1.84
Poly(3)-c	Grubbs 1st Gen.	0,03	-	24	5030	1.41
Poly(4)-a	Grubbs 1st Gen.	0,09	2	48	27600	1.68
Poly(4)-b	Grubbs 1st Gen.	0,06	2	48	6700	2.49
Poly(4)-c	Grubbs 1st Gen.	0,03	-	24	3640	8.4

* determined by vapor pressure osmometry

4.4 ^{1}H, ^{13}C, ^{31}P NMR spectra

4.4.1 Monomer Spectra:

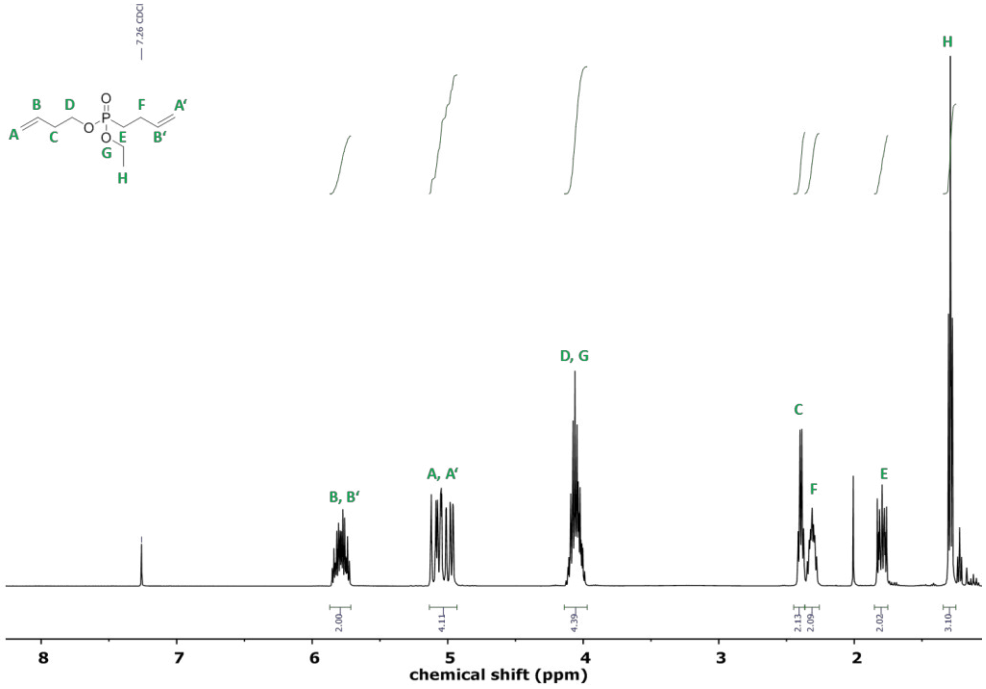

Figure 1.6. ^{1}H NMR of compound 1 at 500 MHz in $CDCl_3$ at 298 K.

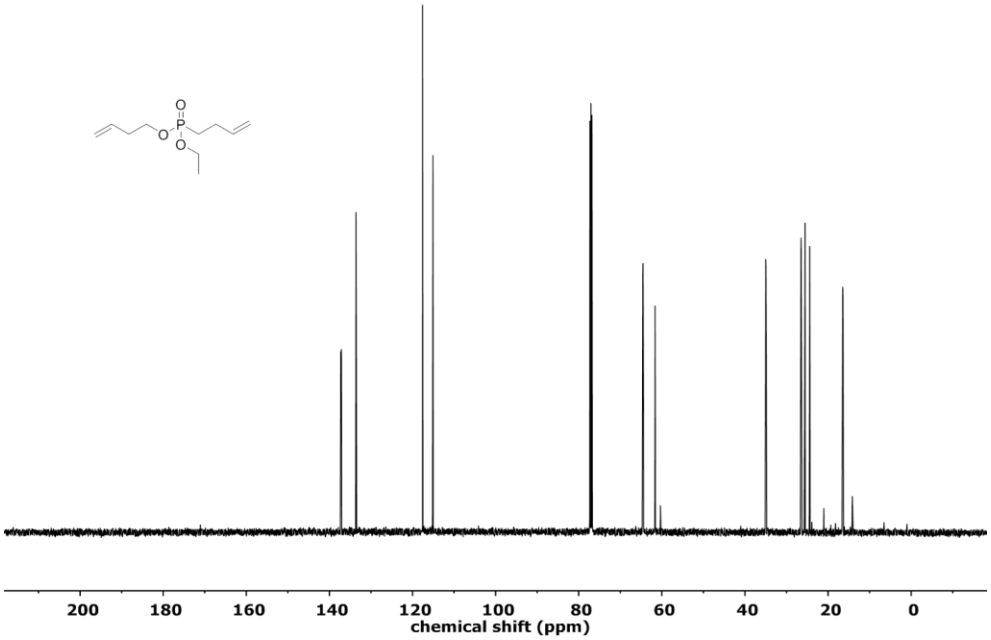

Figure 1.7. ^{13}C NMR of compound 1 at 126 MHz in $CDCl_3$ at 298 K.

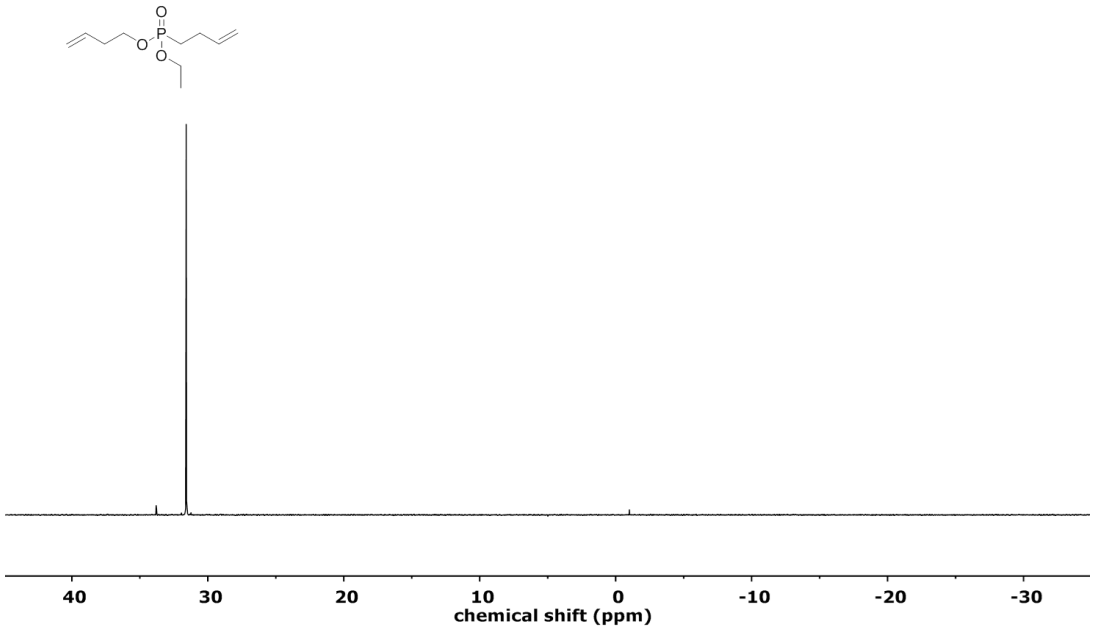

Figure 1.8. $^{31}P\{H\}$ NMR of compound 1 at 202 MHz in $CDCl_3$ at 298 K.

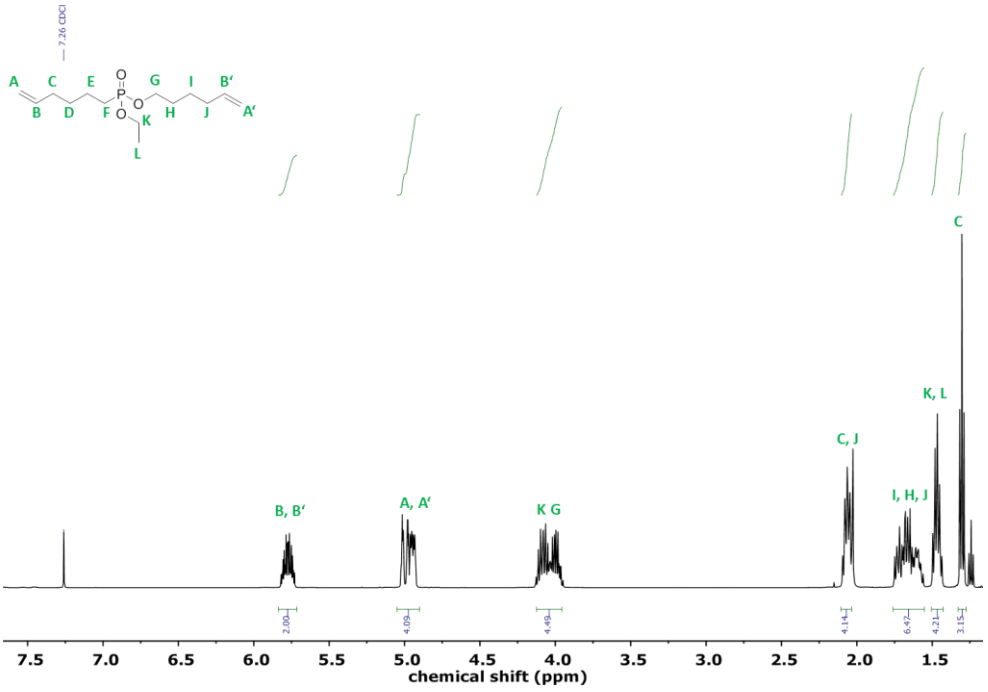

Figure 1.9. ^{1}H NMR of compound 2 at 500 MHz in $CDCl_3$ at 298 K.

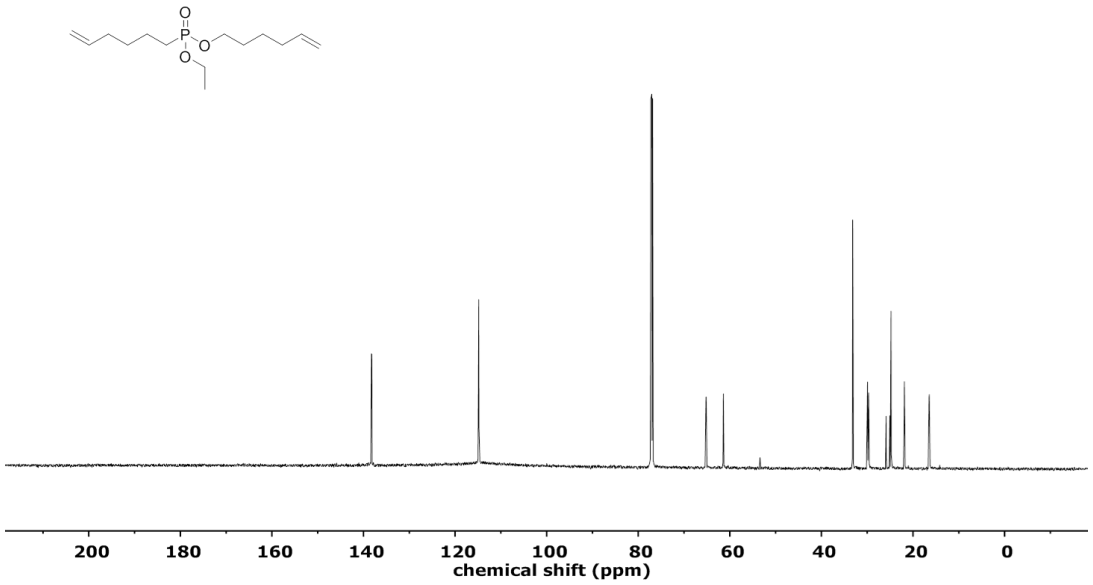

Figure 1.10. ^{13}C NMR of compound 2 at 176 MHz in $CDCl_3$ at 298 K.

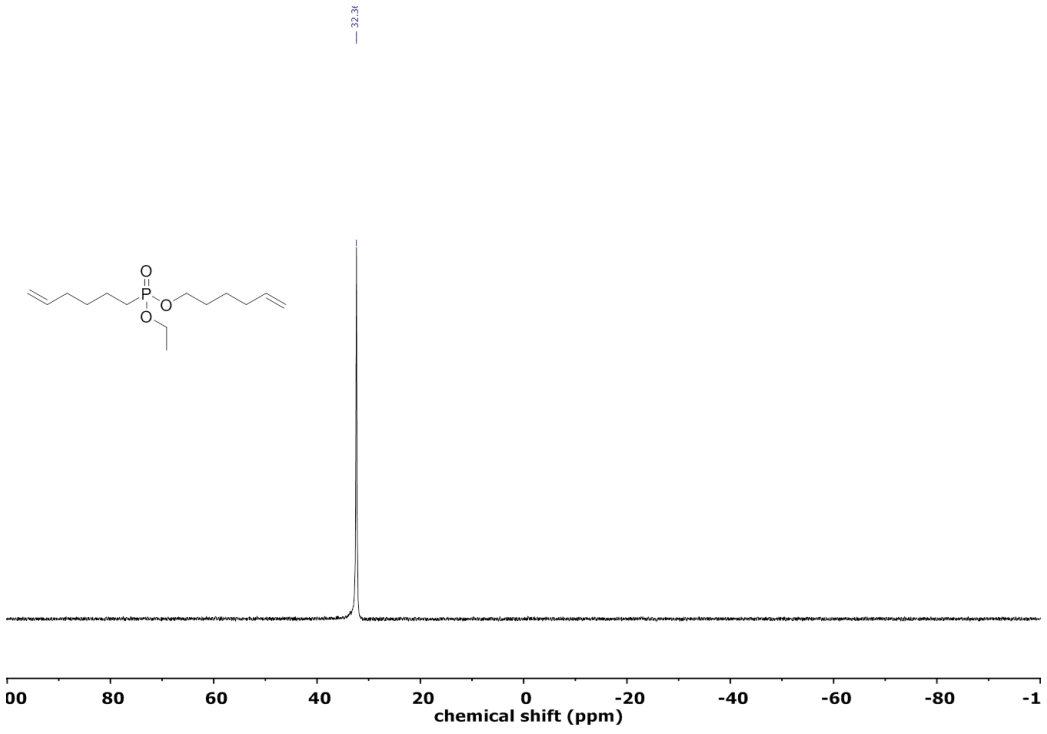

Figure 1.11. $^{31}P\{H\}$ NMR of compound 2 at 283 MHz in $CDCl_3$ at 298 K.

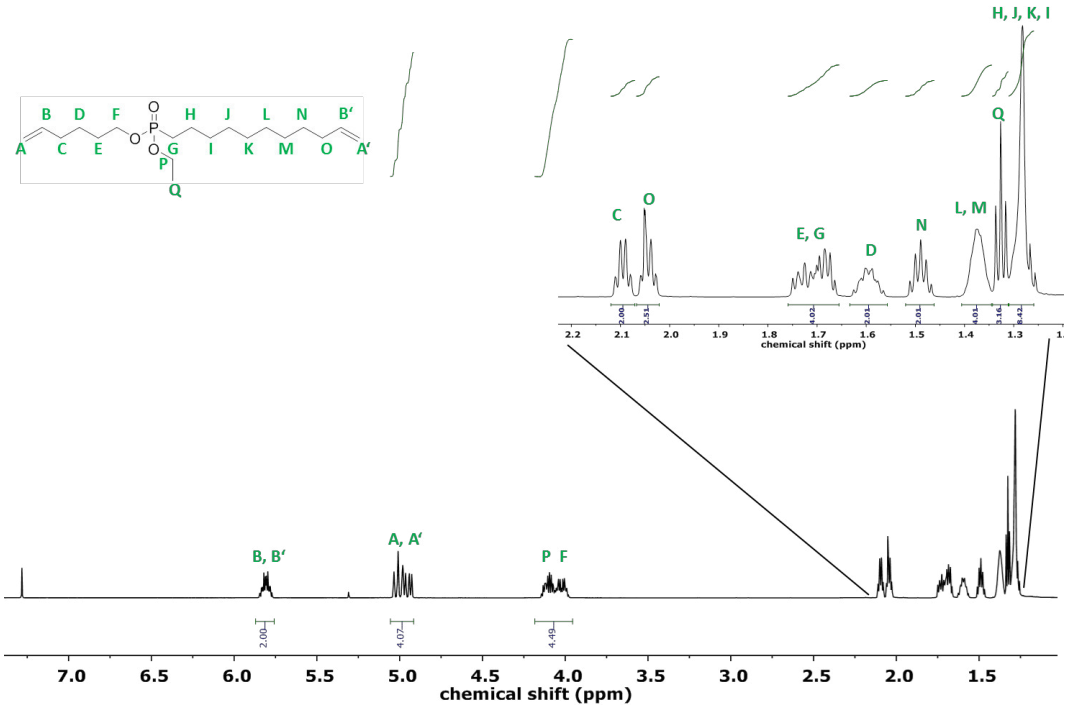

Figure 1.12. ^{1}H NMR of compound 4 at 700 MHz in $CDCl_3$ at 298 K.

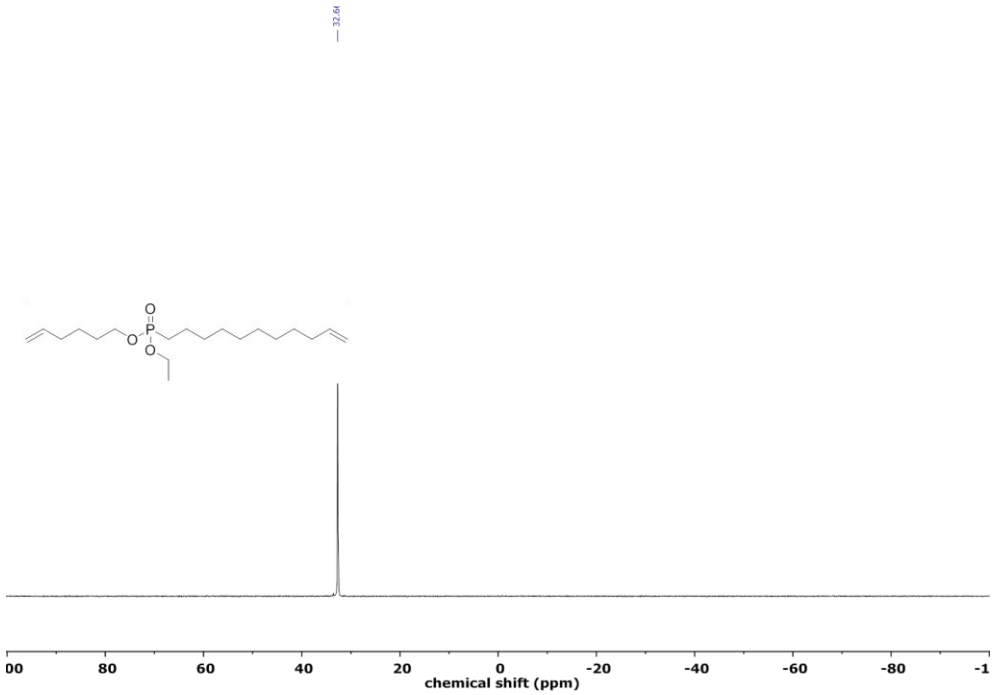

Figure 1.13.^{31}P{H} NMR of compound 4 at 283 MHz in $CDCl_3$ at 298 K.

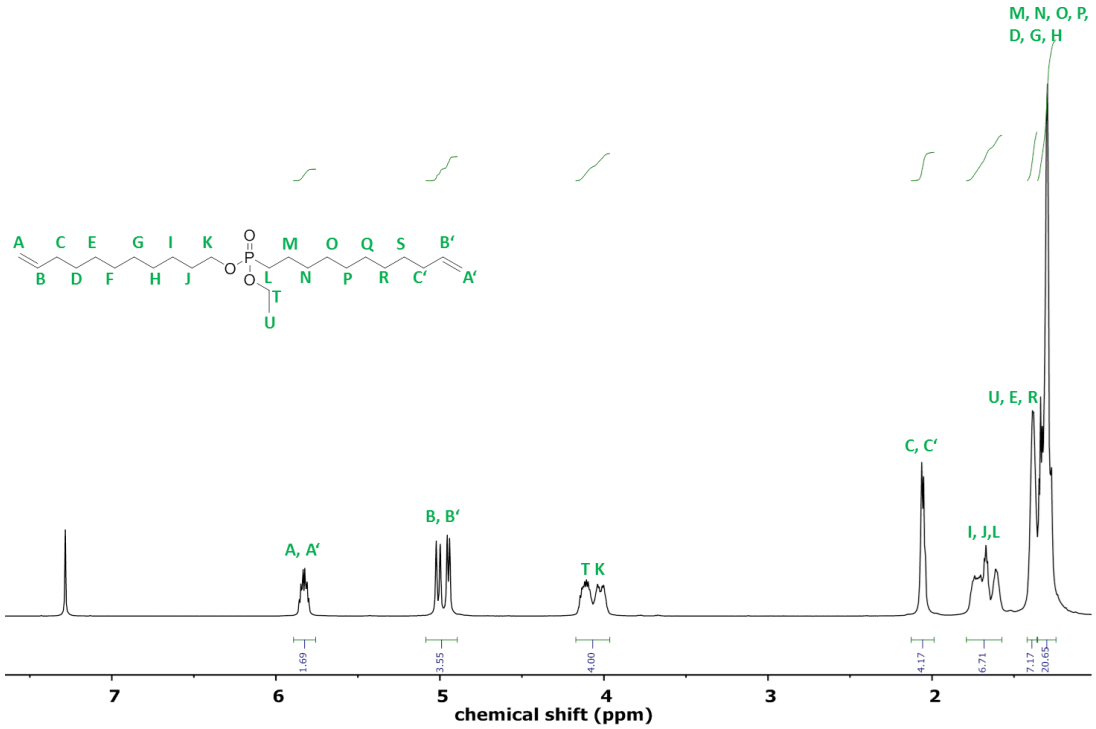

Figure 1.14. ^{1}H NMR of compound 3 at 700 MHz in $CDCl_3$.

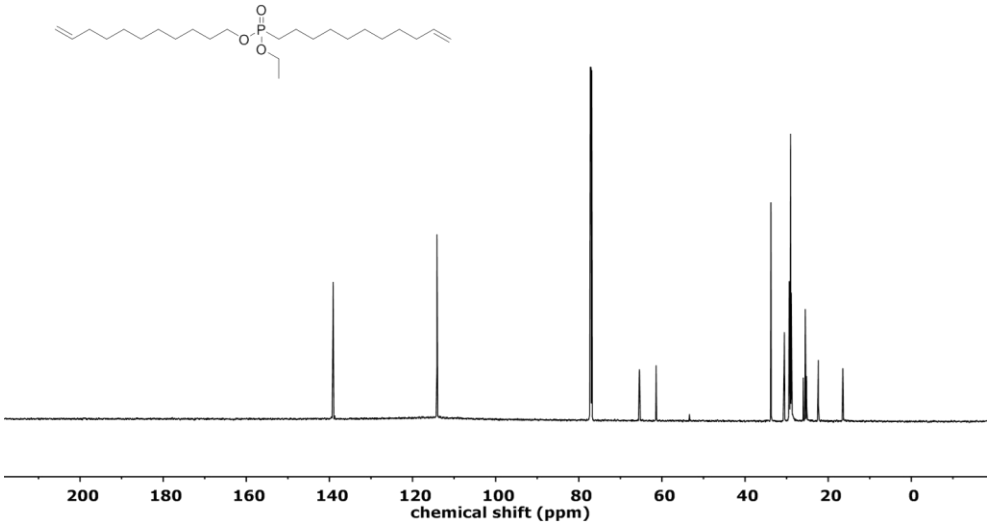

Figure 1.15.^{13}C NMR of compound 3 at 176 MHz in $CDCl_3$ at 298 K.

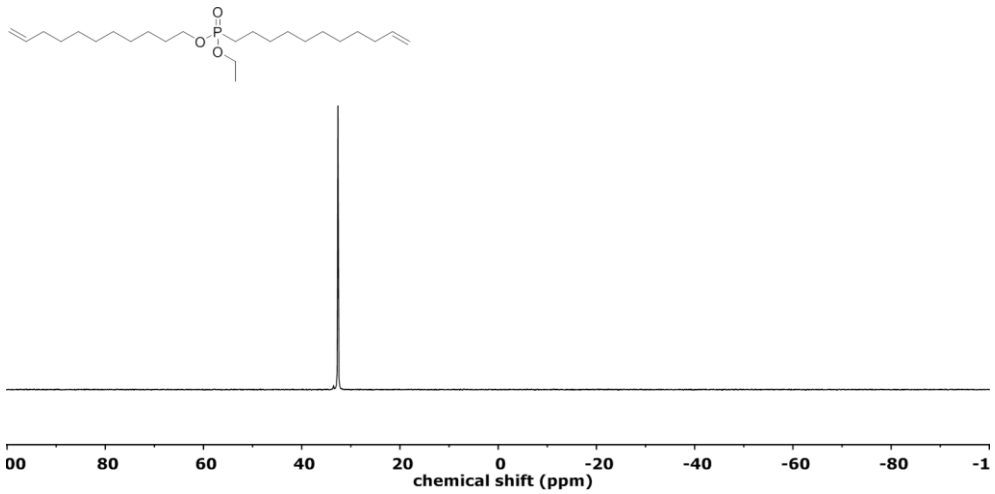

Figure 1.16. $^{31}P\{H\}$ NMR of compound 3 at 283 MHz in $CDCl_3$ at 298 K.

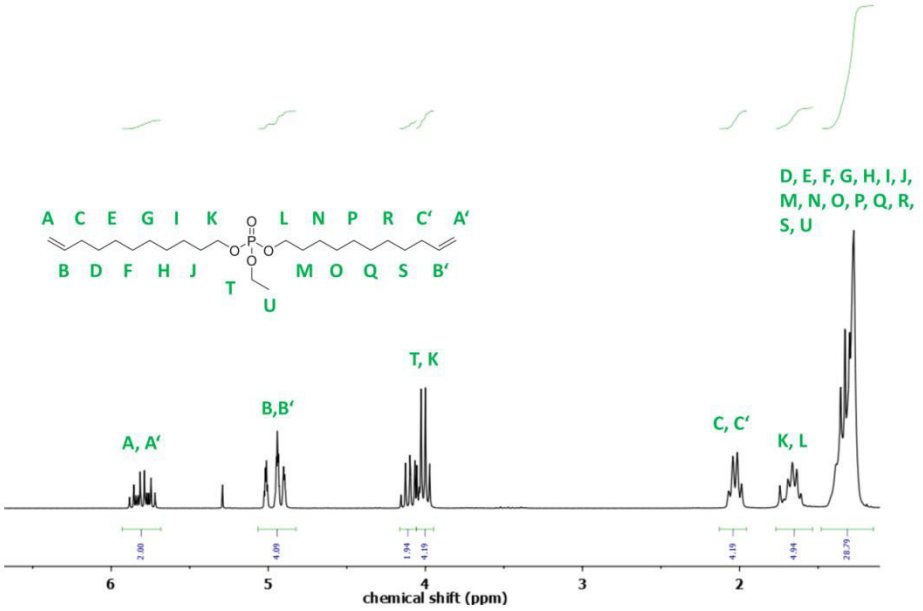

Figure 1.17. ^{1}H NMR of compound 5 at 300 MHz in $CDCl_3$.

4.4.2 Polymer NMR Spectra

The monomer architecture allows three different types of conjunction, i.e. head to tail, tail to tail and head to head (see **Scheme S1**), all contained in the obtained polymers. In the following, the polymer structures are presented in the simplified head to tail structure.

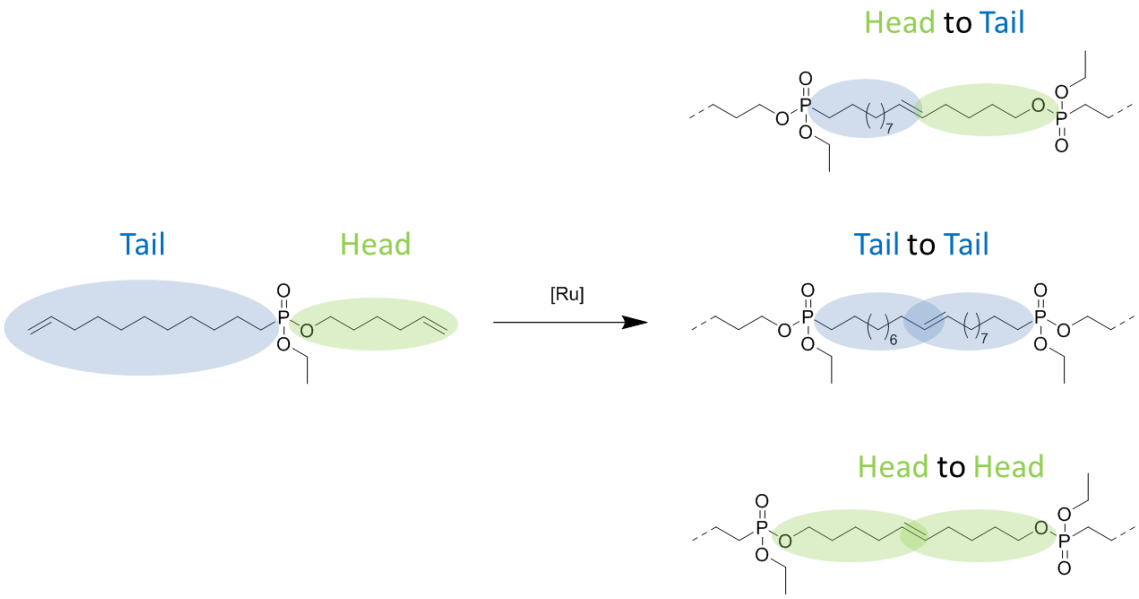

Scheme 1.2. Possible conjunctions within the polymer structure.

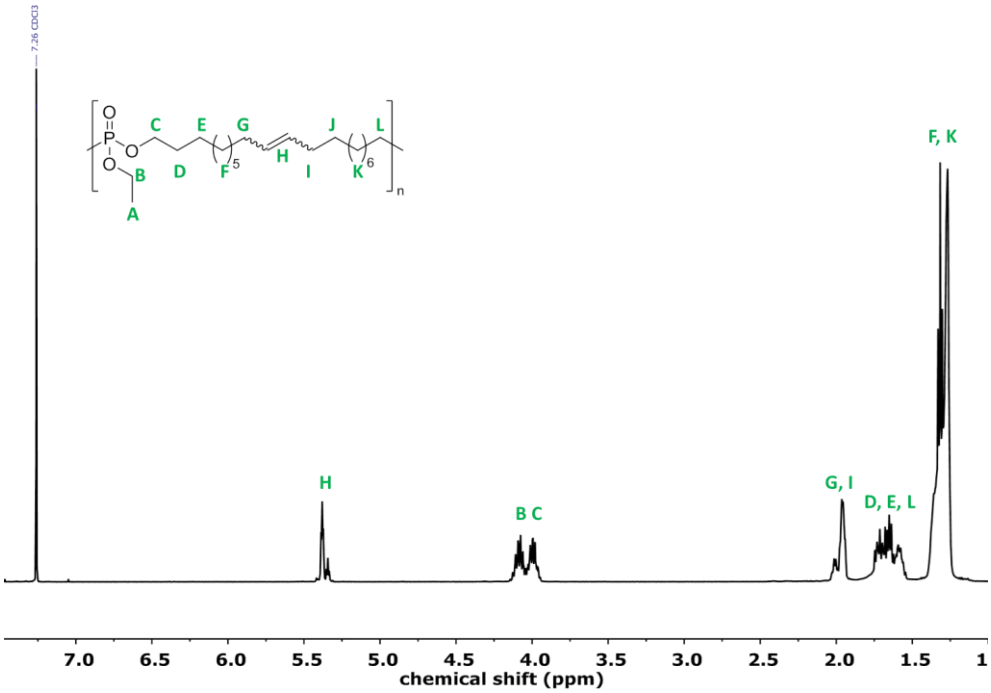

Figure 1.18. ^{1}H NMR of poly(3) at 500 MHz in $CDCl_3$.

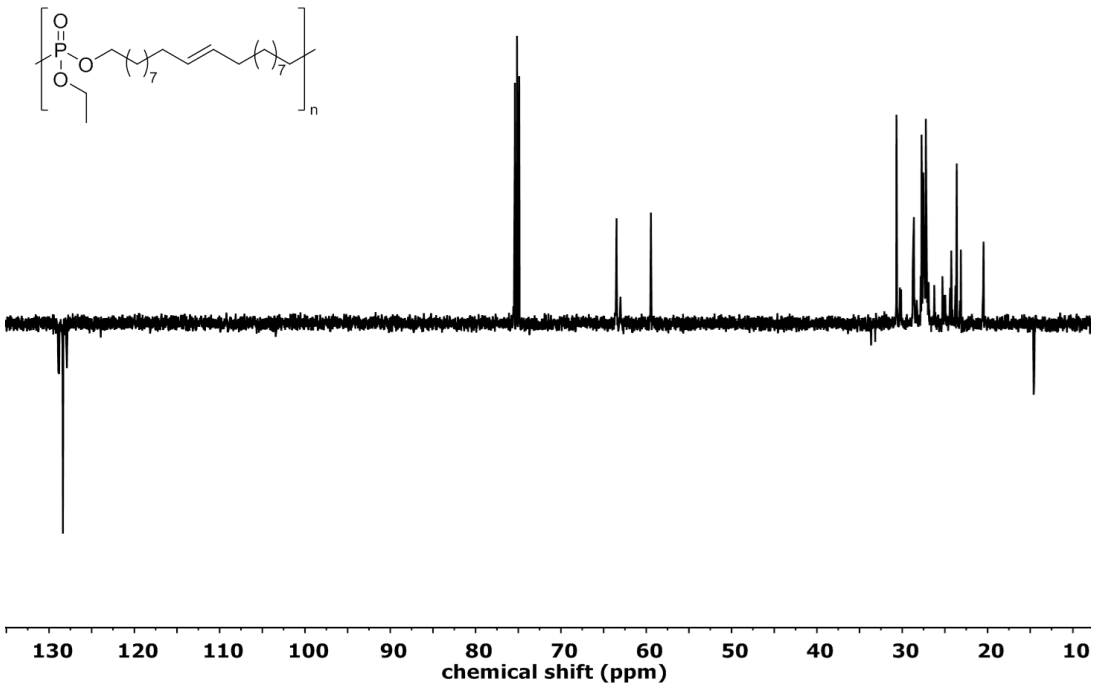

Figure 1.19. ^{13}C NMR of poly(3) at 126 MHz in $CDCl_3$ at 298 K.

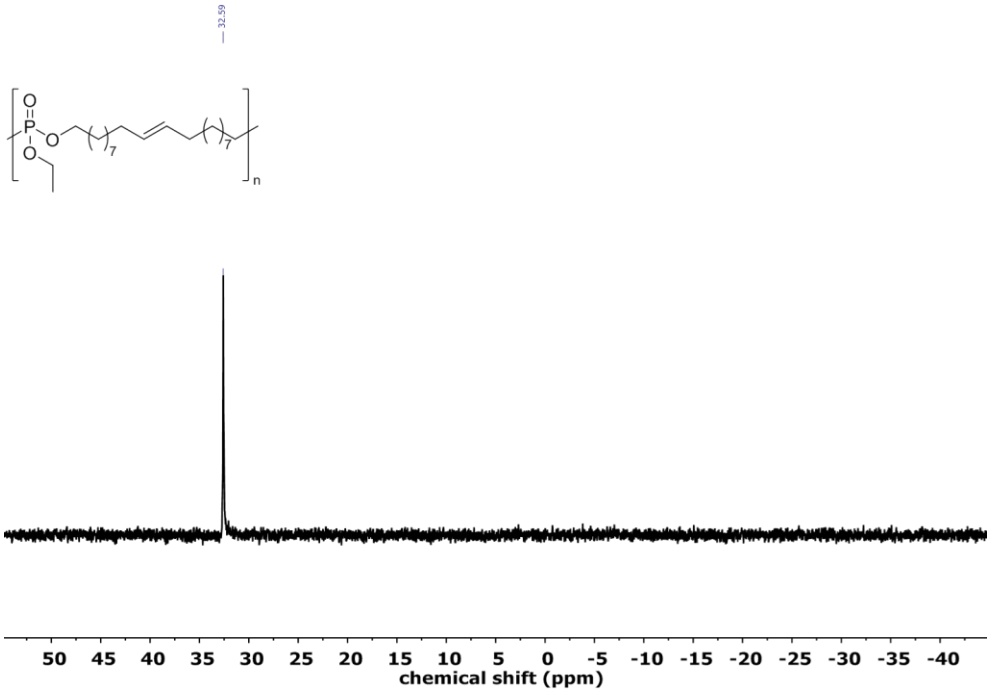

Figure 1.20. $^{31}P\{H\}$ NMR of poly(3) at 202 MHz in $CDCl_3$.

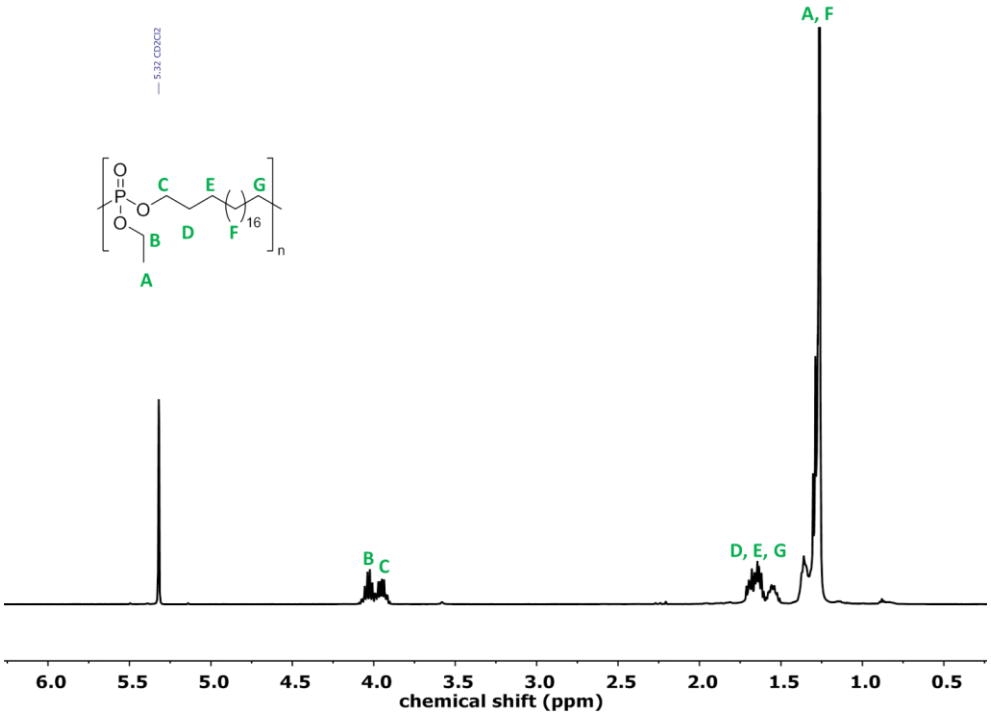

Figure 1.21. ^{1}H NMR of poly(3)-H at 500 MHz in CD_2Cl_2

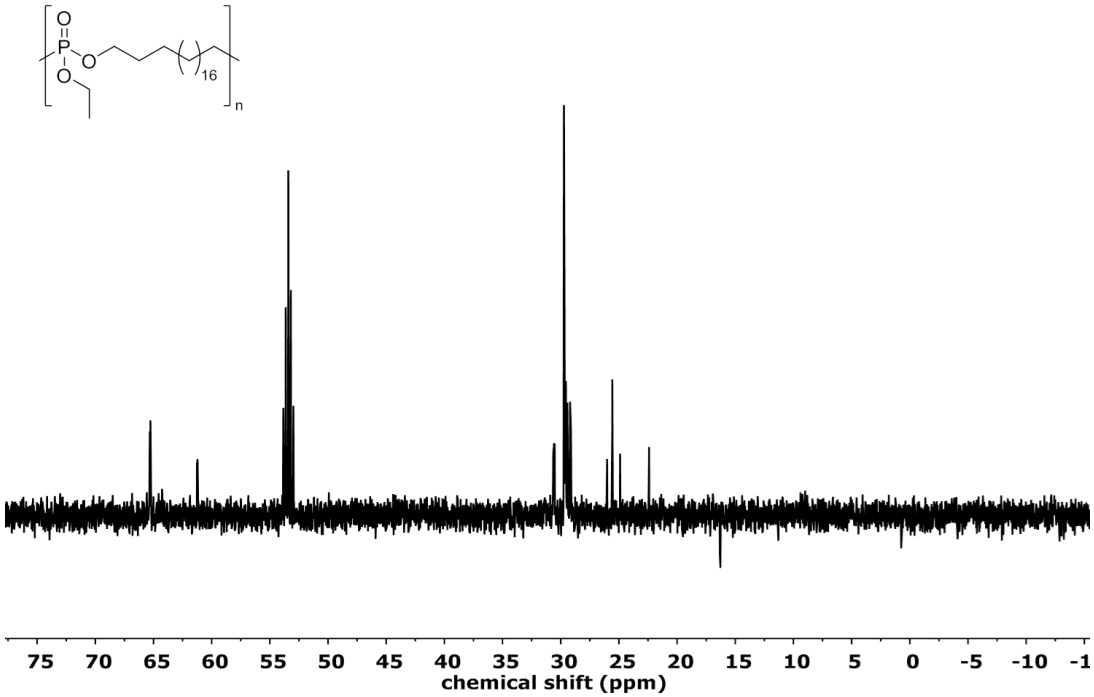

Figure 1.22. ^{13}C NMR of poly(3)-H at 126 MHz in CD_2Cl_2 at 298 K.

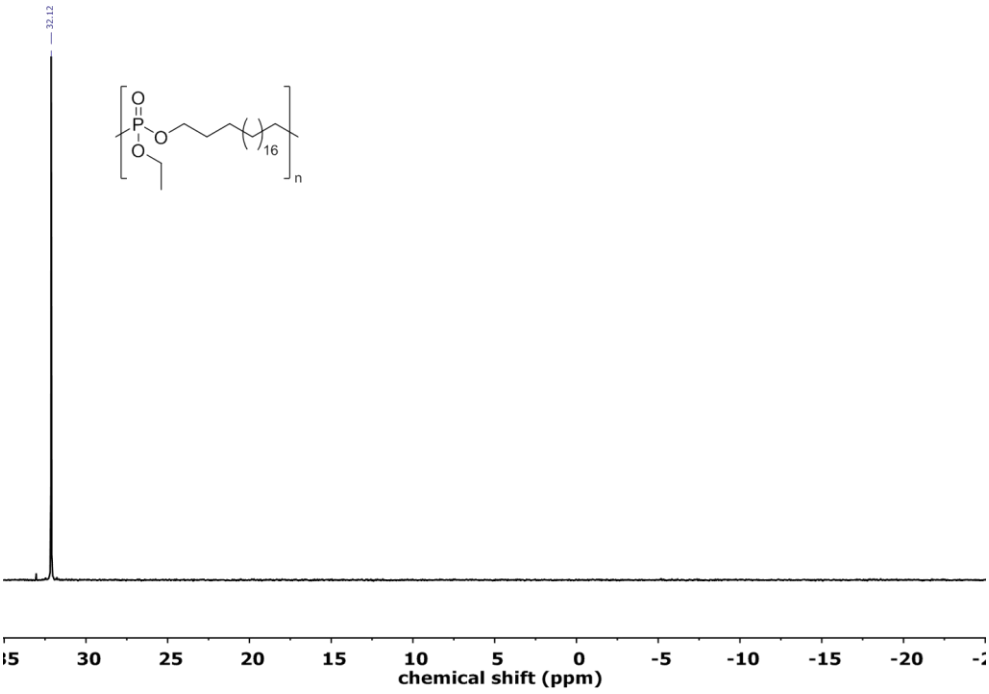

Figure 1.23. $^{31}P\{H\}$ NMR of poly(3)-H at 202 MHz in CD_2Cl_2.

4.4.3 Size exclusion chromatography

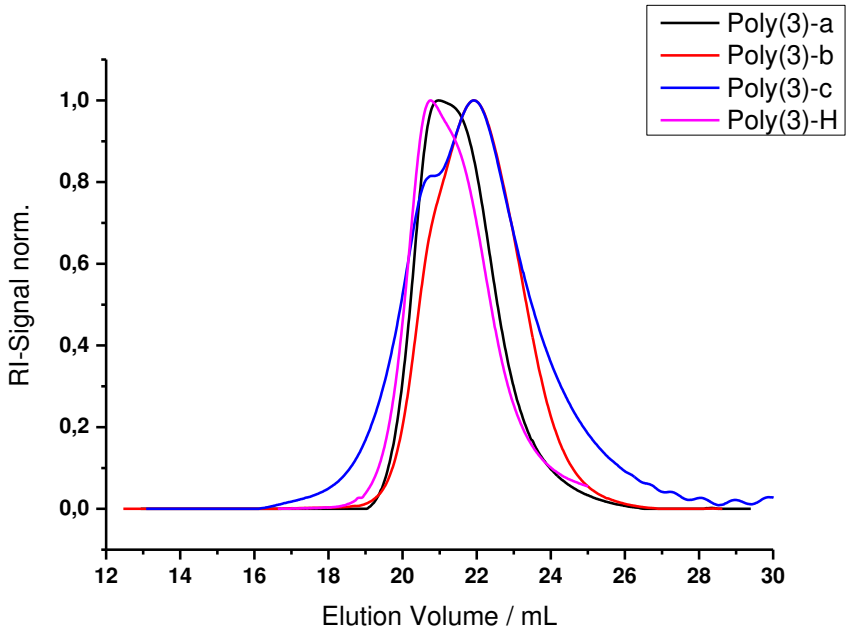

Fiure 1.24. SEC elugrams of poly(3)s prepared ADMET polymerization.

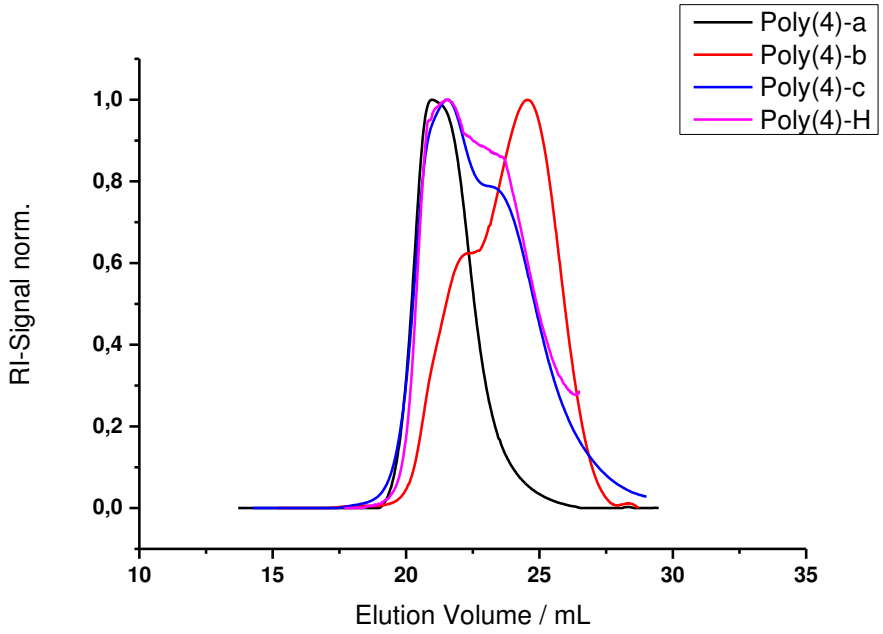

Figure 1.25. SEC elugrams of poly(4)s prepared ADMET polymerization.

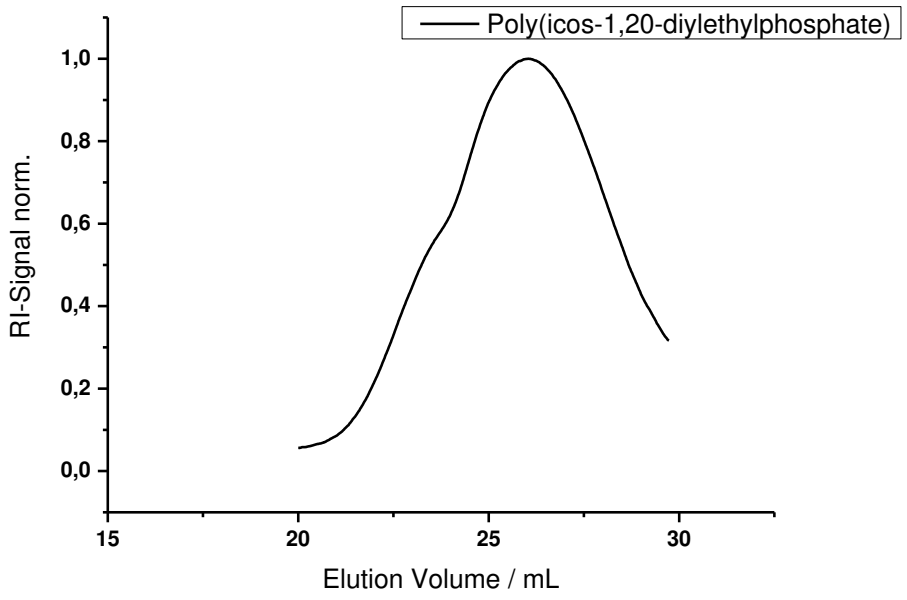

Figure 1.26. SEC elugrams of poly(5) prepared ADMET polymerization.

4.4.4 DSC, TGA

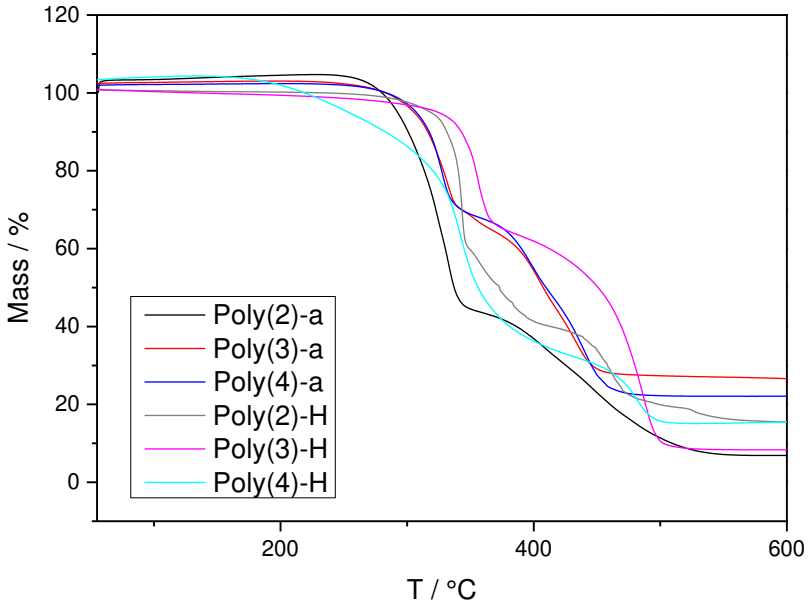

Figure 1.27. TGA thermogram of poly(4)-a and the corresponding hydrogenated polymer poly(4)-H.

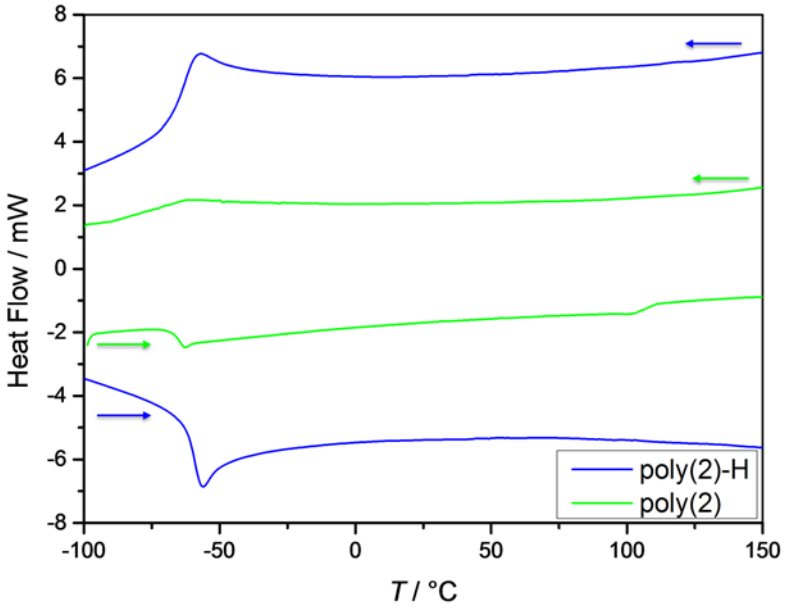

Figure 1.28. DSC thermogram of Poly(2)-a and the corresponding hydrogenated polymer Poly(2)-H.

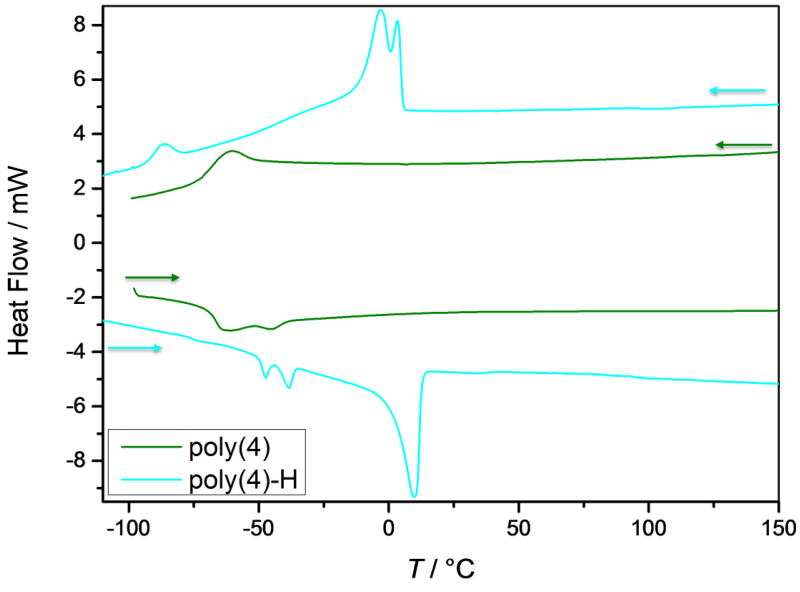

Figure 1.29. DSC thermogram of Poly(4)-a and the corresponding hydrogenated polymer Poly(4)-H.

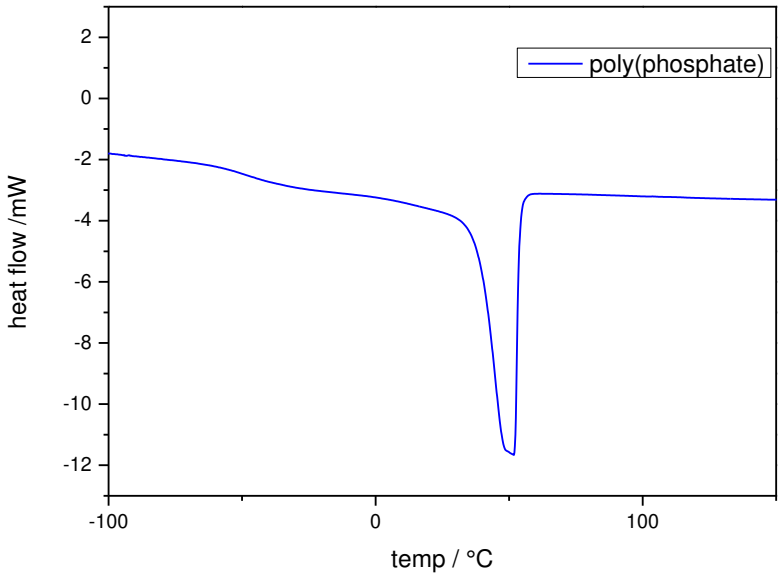

Figure 1.30. DSC thermogram (heating curve) of poly(5)-H .

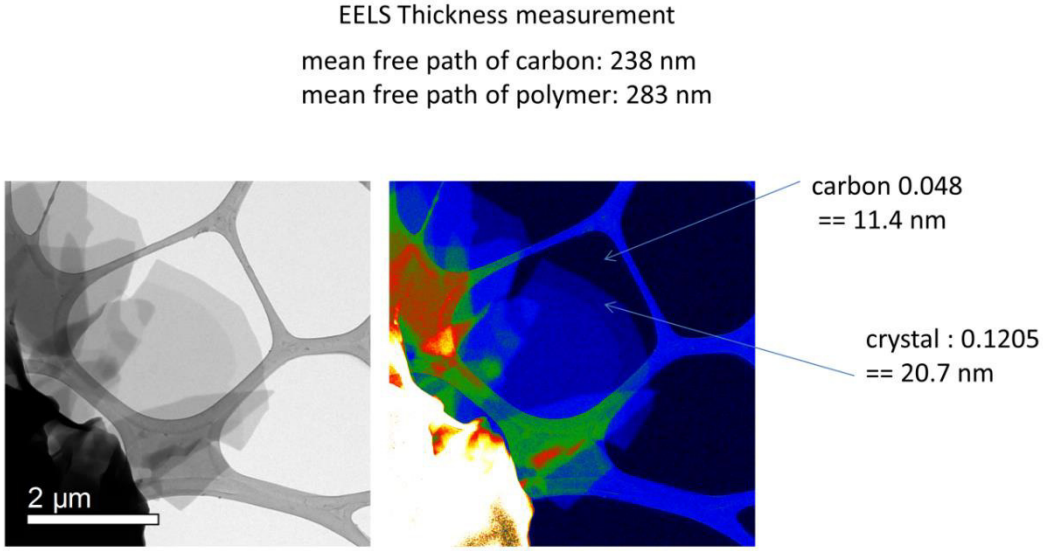

Figure 1.31. EELS thickness measurements for solution grown crystals of poly(3)-H.

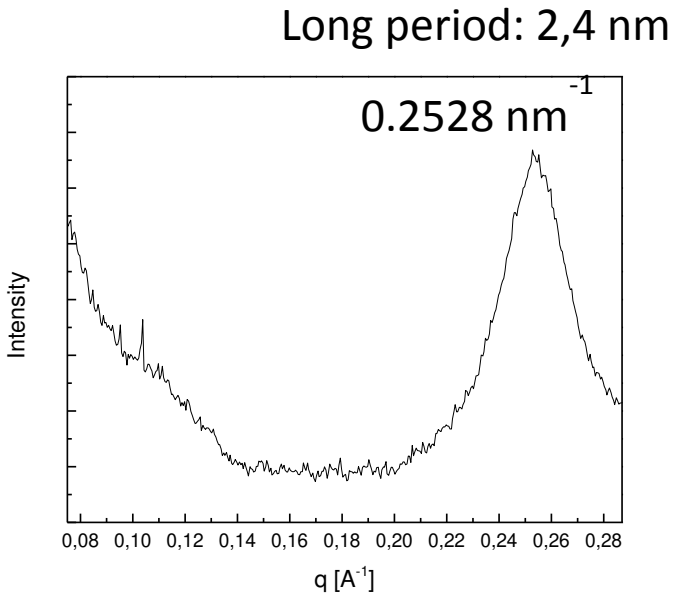

Figure 1.32. SAXS measurements of poly(3)-H.

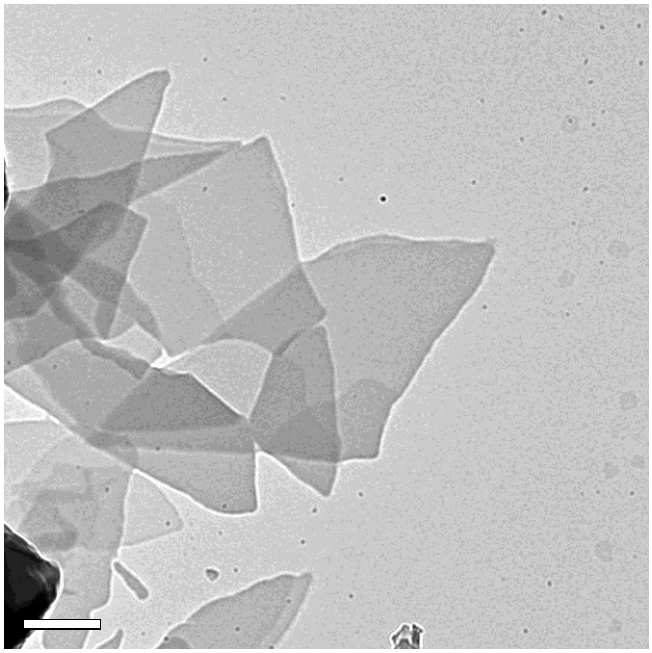

Figure 1.33. TEM BF micrograph of solution grown crystals of poly(3)-H from *n*-octane solution.

5 References

1. Ulery, B. D.; Nair, L. S.; Laurencin, C. T., Biomedical Applications of Biodegradable Polymers. *Journal of polymer science. Part B, Polymer physics* **2011,** *49* (12), 832-864.
2. Mueller, R.-J., Biological degradation of synthetic polyesters—Enzymes as potential catalysts for polyester recycling. *Process Biochemistry* **2006,** *41* (10), 2124-2128.
3. Nair, L. S.; Laurencin, C. T., Biodegradable polymers as biomaterials. *Progress in polymer science* **2007,** *32* (8), 762-798.
4. Uhrich, K. E.; Cannizzaro, S. M.; Langer, R. S.; Shakesheff, K. M., Polymeric systems for controlled drug release. *Chemical reviews* **1999,** *99* (11), 3181-3198.
5. Vert, M., Polymeric biomaterials: Strategies of the past vs. strategies of the future. *Progress in Polymer Science* **2007,** *32* (8–9), 755-761.
6. Rezwan, K.; Chen, Q. Z.; Blaker, J. J.; Boccaccini, A. R., Biodegradable and bioactive porous polymer/inorganic composite scaffolds for bone tissue engineering. *Biomaterials* **2006,** *27* (18), 3413-3431.
7. Jeong, B.; Bae, Y. H.; Lee, D. S.; Kim, S. W., Biodegradable block copolymers as injectable drug-delivery systems. *Nature* **1997,** *388* (6645), 860-862.
8. Zhao, Z.; Wang, J.; Mao, H.-Q.; Leong, K. W., Polyphosphoesters in drug and gene delivery. *Advanced Drug Delivery Reviews* **2003,** *55* (4), 483-499.
9. Steinbach, T.; Wurm, F. R., Polyphosphoester: eine neue Plattform für abbaubare Polymere. *Angewandte Chemie* **2015,** *127* (21), 6196-6207.
10. Mao, H. Q.; Leong, K. W., Design of Polyphosphoester-DNA Nanoparticles for Non-Viral Gene Delivery. In *Advances in Genetics*, Academic Press: 2005; Vol. Volume 53, pp 275-306.
11. Lapienis, G.; Penczek, S., Kinetics and Thermodynamics of the Polymerization of the Cyclic Phosphate Esters. II. Cationic Polymerization of 2-Methoxy-2-oxo-1,3,2-dioxaphosphorinane (1,3-Propylene Methyl Phosphate). *Macromolecules* **1974,** *7* (2), 166-174.
12. Lapienis, G.; Penczek, S., Cationic Polymerization of 2-Alkoxy-2-oxo-1,3,2-dioxaphosphorinanes (1,3-Propylene Alkyl Phosphates). *Macromolecules* **1977,** *10* (6), 1301-1306.
13. Łapienis, G.; Penczek, S., Kinetics and thermodynamics of anionic polymerization of 2-methoxy-2-oxo-1,3,2-dioxaphosphorinane. *Journal of Polymer Science: Polymer Chemistry Edition* **1977,** *15* (2), 371-382.
14. Penczek, S.; Duda, A.; Kaluzynski, K.; Lapienis, G.; Nyk, A.; Szymanski, R., Thermodynamics and kinetics of ring-opening polymerization of cyclic alkylene phosphates. *Makromolekulare Chemie. Macromolecular Symposia* **1993,** *73* (1), 91-101.
15. Xiao, C.-S.; Wang, Y.-C.; Du, J.-Z.; Chen, X.-S.; Wang, J., Kinetics and Mechanism of 2-Ethoxy-2-oxo-1,3,2-dioxaphospholane Polymerization Initiated by Stannous Octoate. *Macromolecules* **2006,** *39* (20), 6825-6831.
16. Du, J.-Z.; Du, X.-J.; Mao, C.-Q.; Wang, J., Tailor-Made Dual pH-Sensitive Polymer–Doxorubicin Nanoparticles for Efficient Anticancer Drug Delivery. *Journal of the American Chemical Society* **2011,** *133* (44), 17560-17563.
17. Sun, T.-M.; Du, J.-Z.; Yao, Y.-D.; Mao, C.-Q.; Dou, S.; Huang, S.-Y.; Zhang, P.-Z.; Leong, K. W.; Song, E.-W.; Wang, J., Simultaneous Delivery of siRNA and Paclitaxel via a "Two-in-One" Micelleplex Promotes Synergistic Tumor Suppression. *ACS Nano* **2011,** *5* (2), 1483-1494.

18. Yuan, Y.-Y.; Mao, C.-Q.; Du, X.-J.; Du, J.-Z.; Wang, F.; Wang, J., Surface Charge Switchable Nanoparticles Based on Zwitterionic Polymer for Enhanced Drug Delivery to Tumor. *Advanced Materials* **2012,** *24* (40), 5476-5480.
19. Chew, S. Y.; Wen, J.; Yim, E. K. F.; Leong, K. W., Sustained Release of Proteins from Electrospun Biodegradable Fibers. *Biomacromolecules* **2005,** *6* (4), 2017-2024.
20. Li, Q.; Wang, J.; Shahani, S.; Sun, D. D. N.; Sharma, B.; Elisseeff, J. H.; Leong, K. W., Biodegradable and photocrosslinkable polyphosphoester hydrogel. *Biomaterials* **2006,** *27* (7), 1027-1034.
21. Iwasaki, Y.; Yamaguchi, E., Synthesis of Well-Defined Thermoresponsive Polyphosphoester Macroinitiators Using Organocatalysts. *Macromolecules* **2010,** *43* (6), 2664-2666.
22. Baran, J.; Klosinski, P.; Penczek, S., Poly(alkylene phosphate)s by polycondensation of phosphonic diamides with diols. *Die Makromolekulare Chemie* **1989,** *190* (8), 1903-1917.
23. Ogawa, T.; Nushimatsu, T.; Minoura, Y., Condensation polymerization of P-phenylphosphonic dichloride with diamines. *Die Makromolekulare Chemie* **1968,** *114* (1), 275-283.
24. Penczek, S.; Pretula, J., High-molecular-weight poly(alkylene phosphates) and preparation of amphiphilic polymers thereof. *Macromolecules* **1993,** *26* (9), 2228-2233.
25. Biedron, T.; Kaluzynski, K.; Pretula, J.; Kubisa, P.; Penczek, S.; Loontjens, T., Synthesis of high molar mass poly (alkylene phosphate) s by polyaddition of diepoxides to difunctional phosphoric acids: Unusual elimination of the side reactions. *Journal of Polymer Science Part A: Polymer Chemistry* **2001,** *39* (17), 3024-3033.
26. Liu, Z.; Wang, L.; Bao, C.; Li, X.; Cao, L.; Dai, K.; Zhu, L., Cross-Linked PEG via Degradable Phosphate Ester Bond: Synthesis, Water-Swelling, and Application as Drug Carrier. *Biomacromolecules* **2011,** *12* (6), 2389-2395.
27. Clément, B.; Grignard, B.; Koole, L.; Jérôme, C.; Lecomte, P., Metal-Free Strategies for the Synthesis of Functional and Well-Defined Polyphosphoesters. *Macromolecules* **2012,** *45* (11), 4476-4486.
28. Steinbach, T.; Ritz, S.; Wurm, F. R., Water-Soluble Poly(phosphonate)s via Living Ring-Opening Polymerization. *ACS Macro Letters* **2014,** *3* (3), 244-248.
29. Marsico, F.; Turshatov, A.; Peköz, R.; Avlasevich, Y.; Wagner, M.; Weber, K.; Donadio, D.; Landfester, K.; Baluschev, S.; Wurm, F. R., Hyperbranched Unsaturated Polyphosphates as a Protective Matrix for Long-Term Photon Upconversion in Air. *Journal of the American Chemical Society* **2014,** *136* (31), 11057-11064.
30. Steinbach, T.; Alexandrino, E. M.; Wurm, F. R., Unsaturated poly(phosphoester)s via ring-opening metathesis polymerization. *Polymer Chemistry* **2013,** *4* (13), 3800-3806.
31. Steinmann, M.; Markwart, J.; Wurm, F. R., Poly(alkylidene chlorophosphate)s via Acyclic Diene Metathesis Polymerization: A General Platform for the Postpolymerization Modification of Poly(phosphoester)s. *Macromolecules* **2014,** *47* (24), 8506-8513.
32. Marsico, F.; Wagner, M.; Landfester, K.; Wurm, F. R., Unsaturated Polyphosphoesters via Acyclic Diene Metathesis Polymerization. *Macromolecules* **2012,** *45* (21), 8511-8518.
33. Steinbach, T.; Alexandrino, E. M.; Wahlen, C.; Landfester, K.; Wurm, F. R., Poly(phosphonate)s via Olefin Metathesis: Adjusting Hydrophobicity and Morphology. *Macromolecules* **2014,** *47* (15), 4884-4893.
34. Opper, K. L.; Fassbender, B.; Brunklaus, G.; Spiess, H. W.; Wagener, K. B., Polyethylene functionalized with precisely spaced phosphonic acid groups. *Macromolecules* **2009,** *42* (13), 4407-4409.
35. Wolf, T.; Steinbach, T.; Wurm, F. R., A Library of Well-Defined and Water-Soluble Poly(alkyl phosphonate)s with Adjustable Hydrolysis. *Macromolecules* **2015**.

36. Täuber, K.; Marsico, F.; Wurm, F. R.; Schartel, B., Hyperbranched poly (phosphoester) s as flame retardants for technical and high performance polymers. *Polymer Chemistry* **2014,** *5* (24), 7042-7053.
37. Tannert, R.; Milroy, L.-G.; Ellinger, B.; Hu, T.-S.; Arndt, H.-D.; Waldmann, H., Synthesis and Structure−Activity Correlation of Natural-Product Inspired Cyclodepsipeptides Stabilizing F-Actin. *Journal of the American Chemical Society* **2010,** *132* (9), 3063-3077.
38. Cho, J.-Y.; Domercq, B.; Barlow, S.; Suponitsky, K. Y.; Li, J.; Timofeeva, T. V.; Jones, S. C.; Hayden, L. E.; Kimyonok, A.; South, C. R.; Weck, M.; Kippelen, B.; Marder, S. R., Synthesis and Characterization of Polymerizable Phosphorescent Platinum(II) Complexes for Solution-Processible Organic Light-Emitting Diodes. *Organometallics* **2007,** *26* (19), 4816-4829.
39. Wagener, K. B.; Brzezinska, K.; Anderson, J. D.; Younkin, T. R.; Steppe, K.; DeBoer, W., Kinetics of Acyclic Diene Metathesis (ADMET) Polymerization. Influence of the Negative Neighboring Group Effect. *Macromolecules* **1997,** *30* (24), 7363-7369.
40. Zheng, Y.-R.; Tee, H. T.; Wei, Y.; Wu, X.-L.; Mezger, M.; Yan, S.; Landfester, K.; Wagener, K.; Wurm, F. R.; Lieberwirth, I., Morphology and Thermal Properties of Precision Polymers: The Crystallization of Butyl Branched Polyethylene and Polyphosphoesters. *Macromolecules* **2016**.
41. Yang, J.; Chaurand, P.; Norris, J. L.; Porter, N. A.; Caprioli, R. M., Activity-Based Probes Linked with Laser-Cleavable Mass Tags for Signal Amplification in Imaging Mass Spectrometry: Analysis of Serine Hydrolase Enzymes in Mammalian Tissue. *Analytical Chemistry* **2012,** *84* (8), 3689-3695.

Chapter 2

2-Methyl-1,3,2-dioxaphosphinane-2-oxide as new monomer for the preparation of linear poly(phosphoester)s

Foreword

This project was started in the course of Torben Herrmann's bachelor thesis and he prepared the monomer as well as (5,10,15,20-tetraphenylporphinato)aluminum methoxide ((TPP)AlOMe) and attempted the polymerization with (TPP)AlOMe.

Abstract

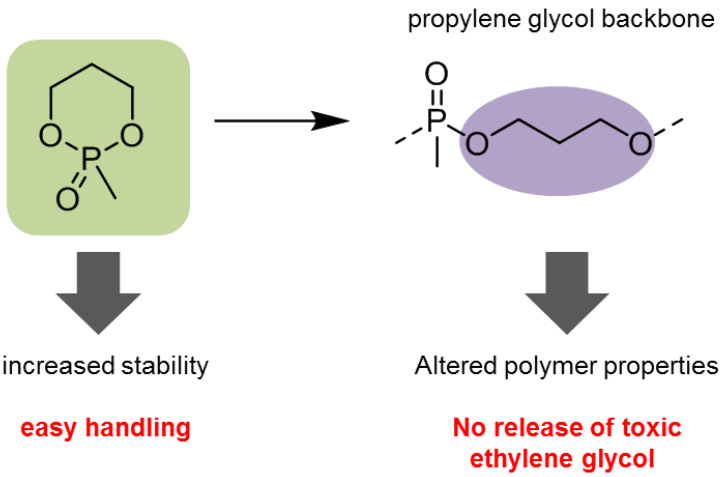

The six-membered cyclic 2-methyl-1,3,2-dioxaphosphinane-2-oxide (MPPn) was prepared as new monomer for the preparation of poly(phosphoester)s with altered backbone structure by ring-opening polymerization. MPPn showed increased stability compared to its five-membered analogon facilitating the preparation and further handling. MPPn was attempted to polymerize with standard catalysts, that are well-established for the polymerization of five-membered cyclic phosphoesters. For all applied catalysts no polymerization was observed. For the very reactive TBD particle partial ring opening was observed.

1 Introduction

First attempts to produce linear PPEs by the anionic ring-opening polymerization were mainly made by Penzcek's group in the 1960s and 1970s using the six-membered 2-alkoxy-1,3,2-dioxaphosphorinane-2-oxides.[1-3] Due to the lower ring strain of these monomers, they exhibit no tendency towards spontaneous polymerization and are therefore easier in handling. However, several attempts to polymerize these monomers either by cationic[2] or anionic[3] polymerization only led to colored, ill-defined materials with low molecular weights. Based on intensive kinetic studies, Penzcek and co-workers concluded that the poor polymerizability of these compounds by anionic polymerization is due to the formation of cyclic end groups during the propagation step (Scheme 2.1). Cyclic end groups can be built by nucleophilic attack of the propagating chain end on the last phosphorus atom. Usually, the high ring strains prevent the formation of cyclic end groups. However, the decreased ring-strain of six-membered cycles can lead to stabilization by several mechanisms. In the easiest case, the cyclic end group is opened again (Scheme 2.1, **1**) and polymerization can continue. Furthermore, the cyclic end group can lead to the elimination of the main chain releasing a monomer molecule and the propagating species (Scheme 2.2, **3**). Both possibilities do not lead to a final termination of the chain growth. However, in the third case, the cyclic end group can also be stabilized by eliminating the side chain producing a "dead" polymer chain with a cyclic end group and an alcoholate anion that can act as initiator (Scheme 2.1, **2**) resulting in the presence of polymeric species initiated by the actual initiator as well as by the eliminated side chain. Thus, elimination of the side chain can lead to low molecular weights and broad molecular weight distributions. They concluded that due to the low ring strain, during the propagation step of the polymerization the cleavage of an inner cyclic ester linkage is as likely as the cleavage of the ester linkage in the side.

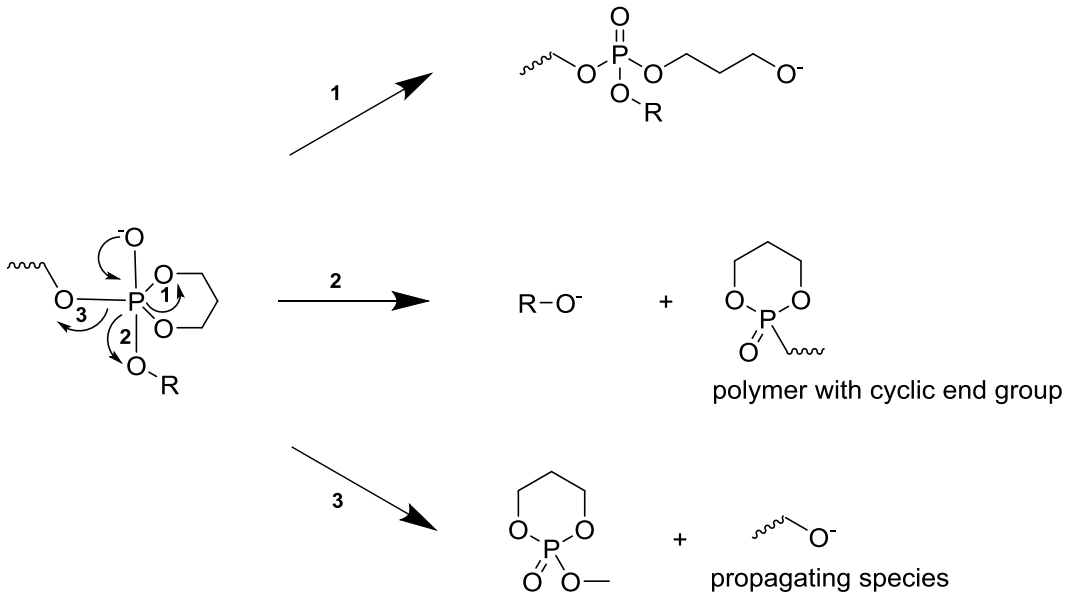

Scheme 2.1. Cyclic end group formation within the polymerization of 2-alkoxy-1,3,2-dioxaphosphorinane-2-oxides.

The aim of this project was the development of a new polymerizable six-membered monomer class for the preparation of linear PPEs by ring-opening polymerization. From the kinetic studies made by Penczek and coworkers, it was concluded that the poorly polymerizable 2-alkoxy-1,3,2-dioxaphosphinane-2-oxides might be transferred into polymerizable monomers by the replacement of the ester linkage in the pendant chain by a stable P-C-bond (Figure 2.1). The introduction of hydrolytically stable P-C-bond avoids the formation of polymer chains with dead, cyclic end groups formed upon elimination of the pendant alkoxy chain.

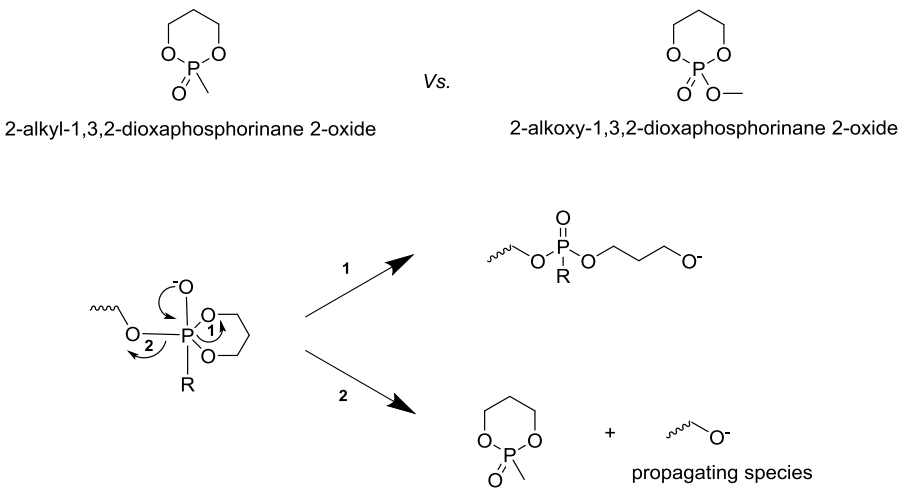

Figure 2.1. Structures of the established 2-alkoxy-1,3,2-dioxaphosphorinane-2-oxide and the alternative 2-alkoxy-1,3,2-dioxaphosphorinane-2-oxide

Furthermore, the preparation of poly(phosphoester)s by ring-opening-polymerization is up to date almost entirely limited to five-membered monomers. These monomers allow the introduction of a plethora of functional groups in the pendant chain while the spacer between the phosphorus atoms along the polymer chain is more or less limited to ethylene glycol. In contrast, polymerization of six-membered monomers leads to PPEs with a propylene glycol-based backbone and therefore the potential release of toxic ethylene glycole upon degradation can be avoided. Since altering the character of the pendant chain in PPEs prepared from five-membered monomers can significantly influence the polymer properties[4], the variation of the backbone is also supposed to influence the polymer properties significantly concerning their thermal characteristics as well as their water-solubility.

2 Results & Discussion

Monomer Synthesis. For a first evaluation of the suitability of the 2-alkyl-1,3,2-dioxaphosphorinane-2-oxides as new monomer class for the preparation of linear PPEs by ring-opening polymerization 2-methyl-1,3,2-dioxaphosphorinane-2-oxide (MPPn) was prepared. The preparation of MPPn has been reported in literature before[5] and several preparation methods were evaluated, but to the best of our knowledge, MPPn was never used as a monomer for the preparation of PPEs by ROP. The synthesis of MPPn was conducted similarly to the preparation of the analog five-membered cyclic phosphonate (Scheme 2.2).[4, 6] The first step of the two-stage synthesis protocol comprises the chlorination of commercially available dimethyl methyl

phosphonate with thionyl chloride leading to dichloro methyl phosphonate. The cyclization to the monomer was achieved by reaction of the dichloride with 1,3-propandiol. Purification of the monomer was achieved by sublimation of the crude product.

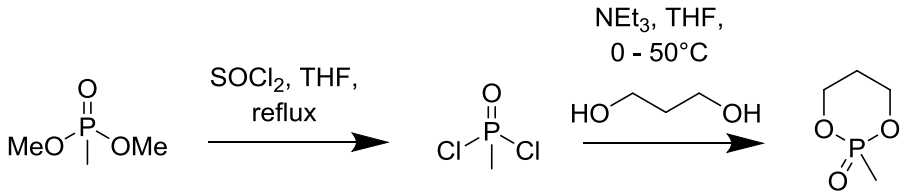

Scheme 2.2. Synthesis of 2-methyl-1,3,2-dioxaphosphorinane-2-oxide. Methylphosphonic dichloride was synthesized from the commercial dimethyl methylphosphonate with thionyl chloride under reflux and transferred into the monomer by cyclization with propane-1,3-diol.

The purity of the monomer was confirmed by ^{1}H NMR spectroscopy (Figure 2.2). The spectrum shows a characteristic duplet at 1.56 ppm that can be ascribed to the pendant methyl group. The splitting into a duplet results from the J-coupling with the adjacent phosphorus atom. Furthermore, the spectrum shows four signals for the inner cyclic protons. The appearance of four signals for the cyclic protons indicates that the monomer exists in a non-planar conformation, which leads to a separation of the cyclic protons into axial and equatorial protons distinguishable by NMR spectroscopy. The multiplets at 4.52 ppm and 4.21 ppm respectively can be ascribed to the methylene groups adjacent to the ester groups while the signals at 2 ppm result from the protons C (Figure 2.2).

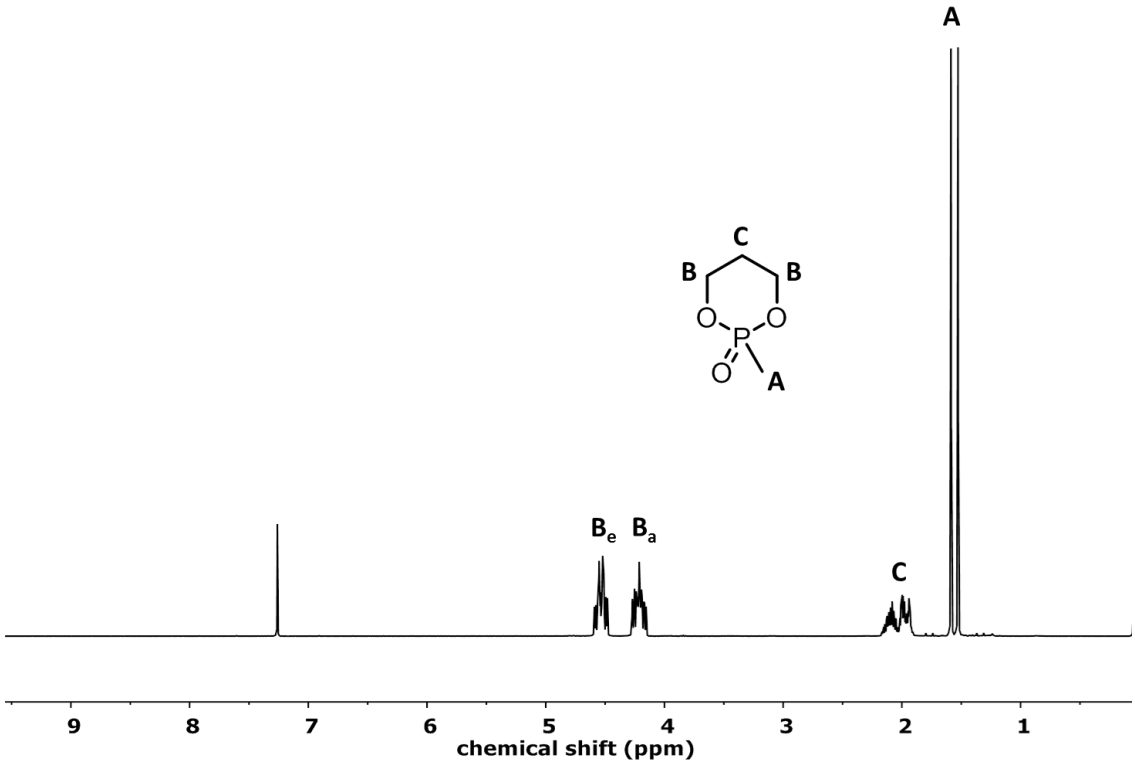

Figure 2.2. ^{1}H NMR of 2-methyl-1,3,2-dioxaphosphorinane-2-oxide in $CDCl_3$ at 298 K and 300 MHz.

However, MPPn existing in non-planar conformation already indicates an increased stability and therefore a lower ring-strain that allows the atoms to deviate from the planar conformation. Another indication of the decreased ring-strain of the six-membered MPPn is the chemical shift of the compound in the ^{31}P NMR spectrum appearing at 28.2 ppm (Figure 2.3 (C)). The signal of the analog strained five-membered cyclic phosphonate, 2-methyl-1,3,2-dioxaphospholane 2-oxide, appears at 48.71 ppm (Figure 2.3 (B)) and shifts to 32 ppm upon ring-opening. Similar observations were made for 2-ethoxy-1,2-oxaphospholane-2-oxide, a cyclic phosphonate monomer which carries the stable P-C-bond within the ring. The signal of the cyclic compound appears at 49.25 ppm (Figure 2.3 (A)) and shifts upon ring-opening to 31.8 ppm. Therefore, MPPn appears already as a cyclic compound in the region of strain-free phosphonate compounds, indicating a ring structure with very low strain. Additionally, the prepared monomer is stable in air at ambient temperature for several months in contrast to its five-membered analog. These finding might be an indication for an aggravated polymerizability of MPPn since the thermodynamic driving force for ring-opening polymerizations is typically the relief of ring strain, which enables the unfavorable entropy to be overcome.[7-8]

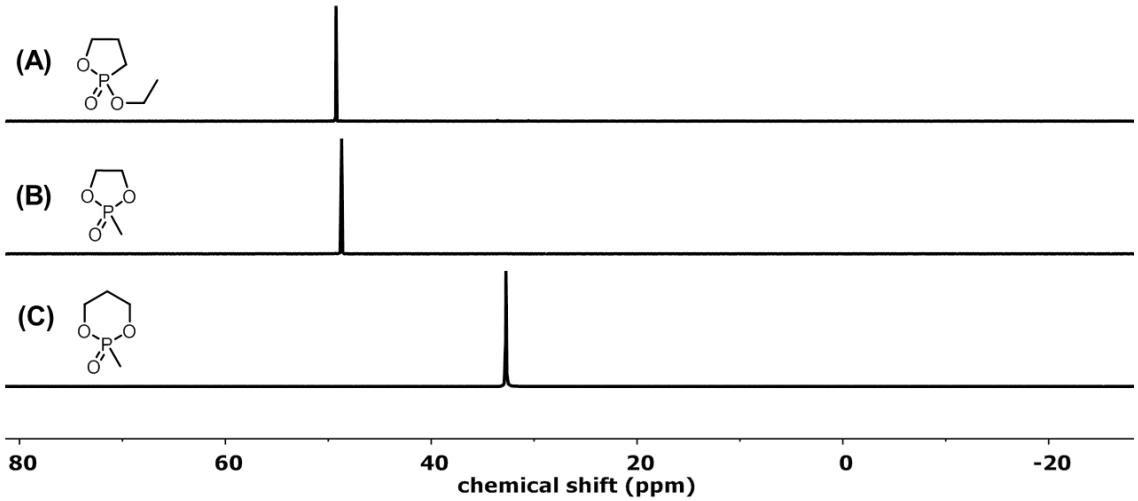

Figure 2.3. ^{31}P NMR spectra of cyclic phosphonate compounds. (A) ^{31}P NMR spectra (121 MHz, $CDCl_3$, 298K) 2-ethoxy-1,2-oxaphospholane-2-oxide. (B) ^{31}P NMR spectra (121 MHz, $CDCl_3$, 298K) of 2-methyl-1,3,2-dioxaphospholane 2-oxide. (C) ^{31}P NMR spectra (202 MHz, $CDCl_3$, 298K) of 2-methyl-1,3,2-dioxaphosphorinane-2-oxide (MPPn)

Polymerization. The only attempts to polymerize six-membered cyclic phosphonates were made by Penzcek and co-workers in the 1970s using alkoxides, namely sodium ethoxide and potassium butoxide, as initiators. Due to the ill-defined materials and the low molecular weights achieved by these attempts, the six-membered monomers are more or less forgotten in the academic world to date. However, in the last decades various, more sophisticated approaches to polyesters by ROP have been developed including organocatalytic ROP as well as metal catalyzed ROP following a coordination-insertion mechanism.[9-10] Both methods allow a good control over molecular weight and molecular weight distribution and have been successfully transferred to the polymerization of cyclic phosphoester monomers. Table 2.1 provides an overview of the conditions applied for the polymerization of MPPn.

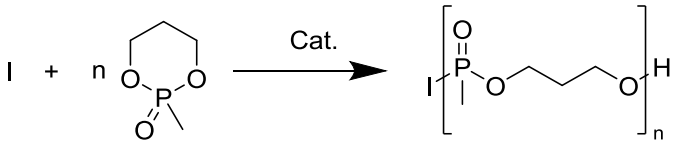

Figure 2.4. General scheme for the polymerization of 2-methyl-1,3,2-dioxaphosphorinane-2-oxide

Table 2.1. Conditions tested for the polymerization of MPPn

#	Catalyst	[M]:[I]:[cat.]	solvent	T / °C	t / h	polymer
1	$Sn(Oct)_2$	50:1:5	toluene	r.t.	24	x
2	$Sn(Oct)_2$	50:1:5	toluene	90	24	x
3	DBU	50:1:5	toluene	r.t.	24	x
4	DBU	50:1:5	toluene	90	24	x
5	TBD	50:1:5	toluene	r.t.	24	x
6	sec-BuLi	50:1	toluene	r.t.	48	x
7	(TPP)AlOMe	50:1	-	98	500	x

For the polymerization of cyclic esters by a coordination-insertion mechanism tin(II) 2-ethyl hexanoate is one of the standard catalysts and has proven to be a suitable catalyst for the polymerization of cyclic five-membered phosphoester monomers with various pendant chains.[10] Thus, attempts to polymerize MPPn were conducted at ambient temperature. After 24 h the progress of the polymerization was checked by NMR spectroscopy showing that no polymerization took place at all. Thus, the reaction temperature was increased to 90 °C for further 24 h. NMR spectroscopy showed exclusively signals of MPPn proving that no polymerization took place. Today, ROP of five-membered phosphoester monomers is usually performed using organocatalysts. Especially for biomedical applications, metal-free polymers are necessary. The typical catalyst is 1,5,7-Triazabicyclo[4.4.0]dec-5-ene (TBD) for cyclic phosphates and 1,8-diazabicyclo[5.4.0]undec-7-ene (DBU) for the cyclic phosphonates which can be seen as the five-membered analog of MPPn. The polymerization of MPPn with DBU was conducted at ambient temperature analogously to the polymerization of the five-membered monomers. Polymerizations of the five-membered monomers are typically completed after 17 h. In case of MPPn, NMR spectroscopy showed no conversion at all after 24 h. A significantly more active catalyst for the ROP is TBD. In contrast to DBU, TBD exhibits two activation sites.

For the initiating species, TBD reacts as hydrogen acceptor while it acts as a hydrogen donor for the activation of the monomer. Combining both activation sites in one catalyst molecule leads to an immediate proximity of both reaction partners resulting in short reaction times. For the cyclic five-membered phosphates, reaction times are typically in the range of a few minutes at 0°C while for phostones reaction times are in the range of a few hours. However, polymerization of MPPn with TBD as catalyst was conducted at ambient temperature and the progress after 24 h was monitored by ^{31}P NMR spectroscopy (Figure 2.5). The ^{31}P NMR spectrum showed beside the main signal that can be ascribed to MPPn a second signal that was slightly shifted to the high field compared to the MPPn-signal. A slight shift to the high field is expected for the ring-opening of MPPn indicating that MPPn was partially opened when using TBD as a catalyst. However, after 24 h the main signal still resulted from MPPn indicating that TBD is not suitable for the polymerization with TBD. Furthermore, MPPn was treated with *sec*-BuLi but did not result in the formation of the polymer. The failed polymerization using sec-BuLi might be attributed in part to the fact that phosphoesters are preferentially polymerized using oxygen-based nucleophiles.

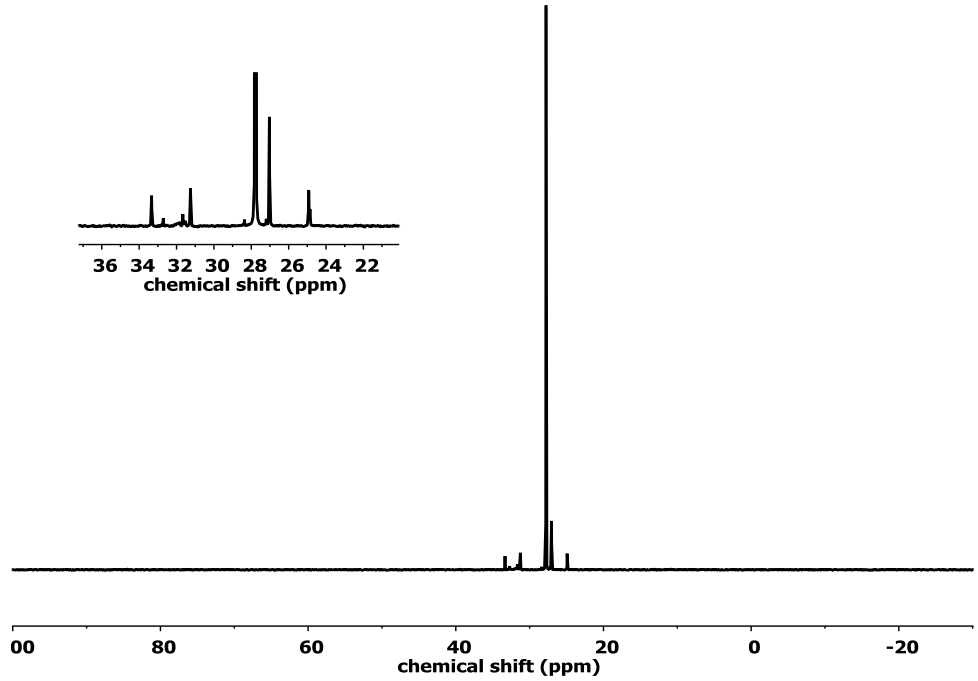

Figure 2.5. 31P NMR (121 MHz, $CDCl_3$, 298K) spectrum of the polymerization of MPPn after 24 h

Additionally, (5,10,15,20-Tetraphenylporphinato)aluminum methoxide ((TPP)AlOMe) was used as initiator. (TPP)AlOMe showed excellent results for the polymerization of δ-valerolactone.

However, treating MPPn over a period of 500 h with (TPP)AlOMe did not lead to polymerization.

3 Conclusion & Outlook

2-methyl-1,3,2-dioxaphosphorinane-2-oxides was prepared as a new monomer for the preparation of linear PPEs by ring-opening polymerization. However, this study shows that the new monomer was not successful at polymerizing under the conditions and catalysts well-established for the polymerization of five-membered cyclic phosphates, phosphonates, and phostones. It may be possible that MPPn is capable of polymerizing using other known catalysts, outside the scope of this study. The reason for the unsuccessful polymerization of MPPn using well-established conditions can probably be attributed to the decreased ring-strain compared to its five-membered cyclic counterparts. The decreased ring-strain of MPPn was indicated by its enhanced stability in air at ambient temperature, the non-planar structure seen in the ^{1}H NMR and the chemical shift in the ^{31}P NMR spectrum. Penczek and coworkers already suggested the increased stability of the six-membered ring as a reason for the poor polymerizability of six-membered phosphoesters compared to their five-membered counterparts. They proposed the formation of cyclic structures at the end of the growing polymer chain stabilizing itself by elimination of the pendant alkoxy chain. The objective of this study was the replacement of the eliminable alkoxy-side chain by an ineliminable alkyl side chain. However, cyclic end groups formed upon back biting can still lead to elimination of the polymer main chain leading to the release of a monomer molecule (Scheme 2.3). If this reaction is favored complete depolymerization can occur preventing the formation of a polymer.

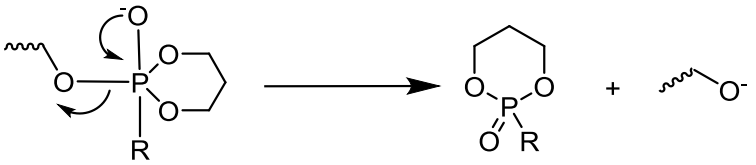

Scheme 2.3. Depolymerization of PMPPn

Another reason of the failed polymerizations of MPPn might simply be the low ring-strain which makes the initial ring-opening thermodynamically unfavorable.

However, so far copolymerization of MPPn with other monomers, such as the well-polymerizable five-membered phosphoesters, was not yet attempted. Copolymerization might lead to an incorporation of MPPn into the polymer structure.

4 Experimental

NMR. ^{1}H and ^{31}P NMR spectra were recorded on a Bruker AVANCE III 300 MHz. The spectra were measured in $CDCl_3$ at 298 K. The spectra were calibrated against the solvent signal and analyzed using MestReNova 8 from Mestrelab Research S.L.

4.1 Synthetic procedures

Synthesis of methylphosphonic dichloride. The dichloride was synthesized according to a well-established literature procedure.[11] Briefly, O, O-Dimethylmethylphosphonic acid diester (100.0 g, 0.8 mol) and DMF (2 mL) were added dropwise to refluxing thionyl chloride (146 mL, 2 mol) and stirred for further 18 h at 120 °C after complete addition of the phosphonate. The product was obtained by fractionated distillation of the crude reaction mixture (62.3 g, 0.47 mol, 58%)

Synthesis of 2-methyl-1,3,2-dioxaphosphorinane-2-oxide (MPPn). A flame-dried three-necked round-bottom flask, equipped with a magnetic stirring bar and two dropping funnels, was charged with 500 mL of dry THF and cooled to 0 °C. One dropping funnel contained methyl phosphonic acid dichloride (46.8 g, 0.3 mol) in 250 mL of dry THF (250 mL) and the other contained 1,3-propanediol and triethylamine dissolved in 230 ml THF. Both solutions were added with approximately the same dropping speed. After complete addition, the reaction mixture was stirred for one further hour at 50 °C. Subsequently, the reaction mixture was filtered and THF was removed under reduced pressure. Sublimation of the crude product yielded MPPn as colorless crystals (12.4 g, 0.09 mol, 30.2%).
^{1}H NMR (300 MHz, Chloroform-*d*) δ 4.54 (dddd, *J* = 11.8, 9.2, 8.4, 3.6 Hz, 2H), 4.21 (dddd, *J* = 13.3, 11.6, 5.8, 4.1 Hz, 2H), 2.21 – 1.88 (m, 2H), 1.56 (d, *J* = 17.6 Hz, 3H). **^{31}P{H} NMR** (202 MHz, Chloroform-*d*) δ, 32.74.

Synthesis of (TPP)AlOMe. The catalyst was synthesized according to a literature procedure.[12] Just briefly, 5,10,15,20-Tetraphenylporphine (615 mg, 1 mmol, 1eq) was dissolved in 20 mL of dry DCM and triethyl aluminum (0.16 mL, 1.2 mmol, 1.2 eq) was added and stirred for 2.5 h. Subsequently, the reaction mixture was heated to reflux for further 30 min, methanol (40.5 µL, 1 mmol, 1 eq) was added and heated under reflux for 18 h. The solvents were removed under reduced pressure. (TPP)AlOMe was obtained as a purple powder.

Polymerization of MPPn using TBD as catalyst. The reaction was conducted in dry toluene with 2-(benzyloxy) ethanol as the initiator. All Schlenk-tubes were flame-dried prior to use. MPPn (103 mg, 0.8 mmol, 50 eq with respect to the initiator) and TBD (11.5 mg, 76 µmol, 5 eq with respect to the initiator) were charged into a Schlenk-tube and dried by lyophilization with benzene. After lyophilization 1 mL of dry toluene was added and the reaction was started at ambient temperature by the rapid addition of 230µL (2.3 mg, 15 µmol, 1 eq) of initiator stock solution. The reaction was stirred for 24 h at ambient temperature. The reaction was quenched by addition of acetic acid in toluene (20 mg mL^{-1}).

Polymerization of MPPn using DBU/Sn(Oct)$_2$ as catalyst. The reaction was conducted in dry toluene with 2-(benzyloxy) ethanol as the initiator. The Schlenk-tube was flame-dried prior to use. MPPn (103 mg, 0.8 mmol, 50 eq with respect to the initiator) and was charged into a Schlenk-tube and dried by lyophilization with benzene. After lyophilization 230µL (2.3 mg, 15 µmol, 1 eq) of initiator stock solution were added and 1 mL of dry toluene. The reaction was started at ambient temperature by the addition of DBU (11.5 mg, 76 µmol, 5 eq with respect to the initiator) or Sn(Oct)$_2$ (30.61 mg, 76 µmol, 5 eq with respect to the initiator) respectively via a Hamilton syringe. The reaction was stirred for 24 h at ambient temperature. After 24h the reaction progress was monitored by NMR spectroscopy and showed that no polymerization took place. Subsequently, the reaction temperature was increased to 90 °C and stirred for further 24 h. No polymer was obtained.

Polymerization of MPPn using (TPP)AlOMe. The Schlenk-tube was flame-dried prior to use. MPPn (211 mg, 1.6 mmol, 50 eq with respect to the initiator) and (TPP)AlOMe (20.8 mg, 31µmol, 1eq) were charged into a Schlenk-tube and heated to 98°C. To avoid crystallization at the cold top, the whole reaction vessel was plunged into the oil bath. The reaction was conducted for 500 h and the reaction progress was followed by NMR spectroscopy. No polymer was obtained.

Polymerization of MPPn using sec-BuLi. The Schlenk-tube was flame-dried prior to use. MPPn (850 mg, 6.2 mmol, 50 eq) was charged into a Schlenk-tube and dried by lyophilization. Subsequently, MPPn was dissolved in 4 mL of THF. The reaction was started at ambient temperature by the addition of a 1.4 M sec-BuLi solution (89.2 µL 125 µmol) and stirred for 48 h. No polymer was obtained.

5 References

1. Lapienis, G.; Penczek, S., Kinetics and Thermodynamics of the Polymerization of the Cyclic Phosphate Esters. II. Cationic Polymerization of 2-Methoxy-2-oxo-1,3,2-dioxaphosphorinane (1,3-Propylene Methyl Phosphate). *Macromolecules* **1974,** *7* (2), 166-174.
2. Lapienis, G.; Penczek, S., Cationic Polymerization of 2-Alkoxy-2-oxo-1,3,2-dioxaphosphorinanes (1,3-Propylene Alkyl Phosphates). *Macromolecules* **1977,** *10* (6), 1301-1306.
3. Łapienis, G.; Penczek, S., Kinetics and thermodynamics of anionic polymerization of 2-methoxy-2-oxo-1,3,2-dioxaphosphorinane. *Journal of Polymer Science: Polymer Chemistry Edition* **1977,** *15* (2), 371-382.
4. Wolf, T.; Steinbach, T.; Wurm, F. R., A Library of Well-Defined and Water-Soluble Poly(alkyl phosphonate)s with Adjustable Hydrolysis. *Macromolecules* **2015**.
5. Yuan, C.; Li, S.; Cheng, Z., Studies on Organophosphorus Compounds XXVI. New Aspects on the Synthetic Study of Some Cyclic Esters of Alkylphosphonic Acids. *Synthesis* **1988,** *1988* (03), 186-189.
6. Steinbach, T.; Ritz, S.; Wurm, F. R., Water-Soluble Poly(phosphonate)s via Living Ring-Opening Polymerization. *ACS Macro Letters* **2014,** *3* (3), 244-248.
7. Thomas, C. M., Stereocontrolled ring-opening polymerization of cyclic esters: synthesis of new polyester microstructures. *Chemical Society Reviews* **2010,** *39* (1), 165-173.
8. Duda, A.; Kowalski, A.; Penczek, S.; Uyama, H.; Kobayashi, S., Kinetics of the Ring-Opening Polymerization of 6-, 7-, 9-, 12-, 13-, 16-, and 17-Membered Lactones. Comparison of Chemical and Enzymatic Polymerizations. *Macromolecules* **2002,** *35* (11), 4266-4270.
9. Iwasaki, Y.; Yamaguchi, E., Synthesis of Well-Defined Thermoresponsive Polyphosphoester Macroinitiators Using Organocatalysts. *Macromolecules* **2010,** *43* (6), 2664-2666.
10. Muller, L. K.; Steinbach, T.; Wurm, F. R., Multifunctional poly(phosphoester)s with two orthogonal protective groups. *RSC Advances* **2015,** *5* (53), 42881-42888.
11. Maier, L., ORGANIC PHOSPHORUS COMPOUNDS 90.1 A CONVENIENT, ONE-STEP SYNTHESIS OF ALKYL- AND ARYLPHOSPHONYL DICHLORIDES. *Phosphorus, Sulfur, and Silicon and the Related Elements* **1990,** *47* (3-4), 465-470.
12. Shimasaki, K.; Aida, T.; Inoue, S., Living polymerization of .delta.-valerolactone with aluminum porphyrin: trimolecular mechanism by the participation of two aluminum porphyrin molecules. *Macromolecules* **1987,** *20* (12), 3076-3080.

Chapter 3

Polymerizing phostones: A fast way to in-chain poly(phosphonate)s with adjustable hydrophilicity

Foreword

The following chapter is based on unpublished results.

DFT calculations were performed by Dr. Denis Andrienko[1] and the toxicity tests were conducted by Johanna Simon[1].

[1]*Max Planck Institute for Polymer Research, Ackermannweg 10, 55128 Mainz, Germany*

Abstract

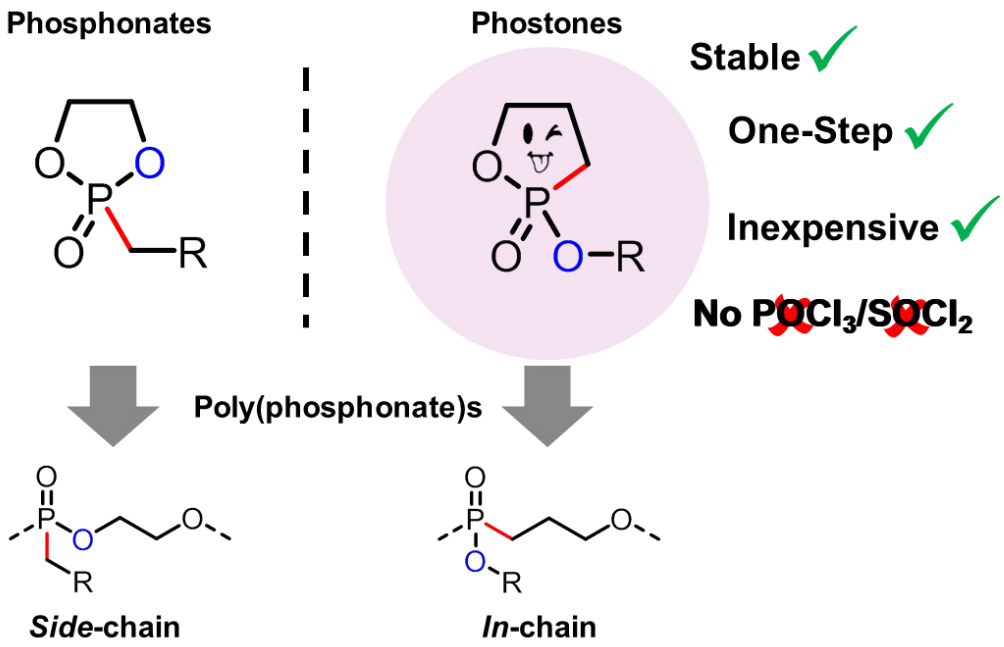

Phostones, i.e. 2-alkoxy-2-oxo-1,3-oxaphospholanes, are accessible in a one-pot reaction from commercially available 1,3-dibromopropane and alkyl phosphites. These 5-membered cyclic phosphonic acid esters are used for the preparation of linear poly(phosphonate)s via ring-opening polymerization resulting in polymers with a hydrolytically stable P-C bond in the

polymer backbone. Phostones have the stable P-C-bond within the cycle, which leads to a dramatic increase of the monomer stability towards hydrolysis and long shelf-lives. Two phostone-monomers containing ethoxy or butoxy pendant chains were prepared in a single step synthesis from inexpensive starting materials avoiding the usage of $SOCl_2$ or $POCl_3$. Polymers with ethoxy side chains are water-soluble without a lower critical solution temperature, non-toxic against murine macrophages, and hydrolytically degradable under basic conditions. The polymerization kinetics for different catalyst systems were evaluated for both monomers in order to identify optimal polymerization conditions, resulting in polyphosphonates with molecular weights between 3000 and 25100 g mol^{-1} with reasonable molecular weight dispersities (<1.6). Due to the ease of synthesis and distinct different hydrolysis kinetics compared to side-chain polyphosphonates, we believe that these new polyphostones represent a valuable addition to water-soluble biopolymers for future biomedical applications.

1 Introduction

Phosphorus-containing polymers, and especially poly(phosphoester)s (PPEs), are promising materials for biomedical applications.[1-2] The pentavalency of the phosphorus atom allows the design of modular structures and the inherent ester bonds in the polymer backbone make them hydrolytically degradable. Furthermore, water-soluble PPEs are promising candidates for drug delivery vehicles,[3-5] due to their "stealth effect", similar to poly(ethylene glycol) (PEG), while their degradability prevents any potential bioaccumulation.[6-7] Through precise control of their chemistry, the physical properties, degradation products, and time can be tuned. [8-10]

In recent years, we have been studying PPEs and developing both novel synthetic protocols and potential applications. We have focused our efforts on an almost forgotten subclass of PPEs: the poly(phosphonate)s. They contain a chemically stable P−C bond, replacing one of the P−O−C bonds of poly(phosphate)s, which has strong influence on hydrolysis rates, as the P-C-bond itself is stable against hydrolysis, but microorganisms can cleave the phosphonate linkage.[11] However, poly(phosphonate)s are mainly found as aromatic oligomers prepared by step-growth polymerization and very few water-soluble, well-defined examples have been reported.[12-14] In poly(phosphonate)s the P-C bond is commonly installed as a pendant group, however rare in-chain P-C linkages have been reported.[10, 15-16]

Herein, the first ring-opening polymerization (ROP) of 2-alkoxy-2-oxo-1,3-oxaphospholanes is reported with both ethyl and butyl side chains, carrying the P-C-bond within the ring structure and thus forming in-chain poly(phosphonate)s upon polymerization. These so-called phostones

have been of some interest in the past, due to their potential application as glycomimetics.[17-19] While the 2-ethoxy-2-oxo-1,3-oxaphospholane heterocycle has been known for a long time,[20-21] it has never been used in ROP to the best of our knowledge. The phostone monomers offer several advantages: The P-C bond in the ring reduces monomer synthesis to a single step from inexpensive, less-toxic starting materials, avoiding $SOCl_2$ and $POCl_3$; and the resulting monomers are stable towards hydrolysis and therefore have an extended shelf-life (>12 months) even at room temperature, and avoid undue precautions over the presence of water. We report an optimization of the polymerization of this new class of monomers, exploring different catalysts and monomer:initiator ratios, providing well-controlled and rapid access to PPEs with tunable hydrophilicity and improved hydrolytic stability compared to the analogous poly(phosphonate)s.

2 Results & Discussion

Monomer synthesis. A preparative route to the target phostones, alkoxy-2-oxo-1,2-oxaphospholanes, was developed. Two monomers with different pendant chains (ethoxy (**M1**) and butoxy (**M2**)) were prepared in order to adjust the hydrophilicity of the resulting polymers. A one-pot reaction of the commercially available 1,3-dibromopropane and the corresponding trialkyl phosphite via consecutive Michaelis-Arbuzov and ring-closing reaction (Scheme 3.1) avoided use of the traditional toxic reagents used to prepare cyclic phosphate or phosphonate monomers.

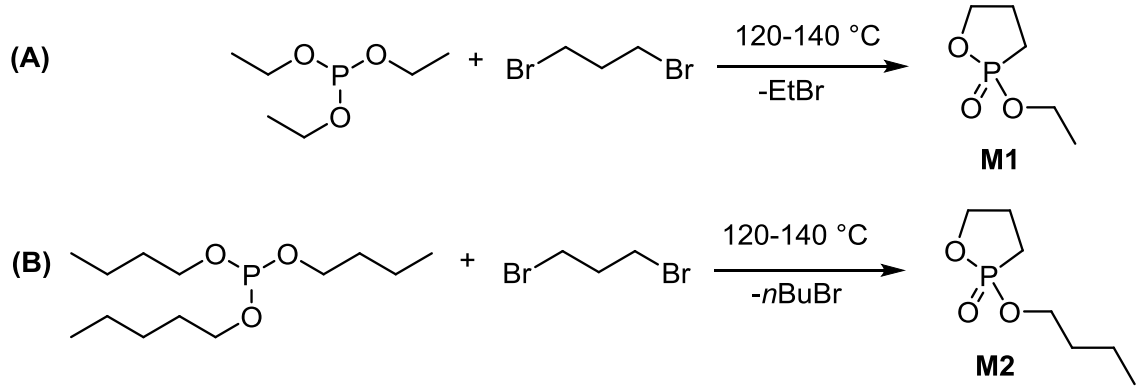

Scheme 3.1. One-pot synthesis of monomers M1 (A) and M2 (B).

The formation of the phostone monomers from 1,3-dibromopropane and the trialkyl phosphite proceeds in two stages. First, the P-C bond is formed via a Michaelis-Arbuzov reaction accompanied by elimination of alkyl bromide.[21] The cyclization proceeds within the second

stage via intramolecular nucleophilic substitution and elimination of further alkyl bromide to yield the monomers. Purification is required prior to polymerization, with fractional distillation providing highest quality, albeit in reduced isolated yields of ca. 20%. The yields are limited because of the presence of side reactions, such as the formation of oligomers by intermolecular nucleophilic substitution reactions or the reaction of the evolving alkyl bromide with the trialkyl phosphite. While further optimization of the synthesis could target improved yields, the focus for in this study was in the polymerization behavior of the phostones so this was not pursued. Purification of the monomers requires two successive distillations, first to remove the oligomeric side product and second a subsequent fractional distillation or column chromatography on the multi-gram scale.

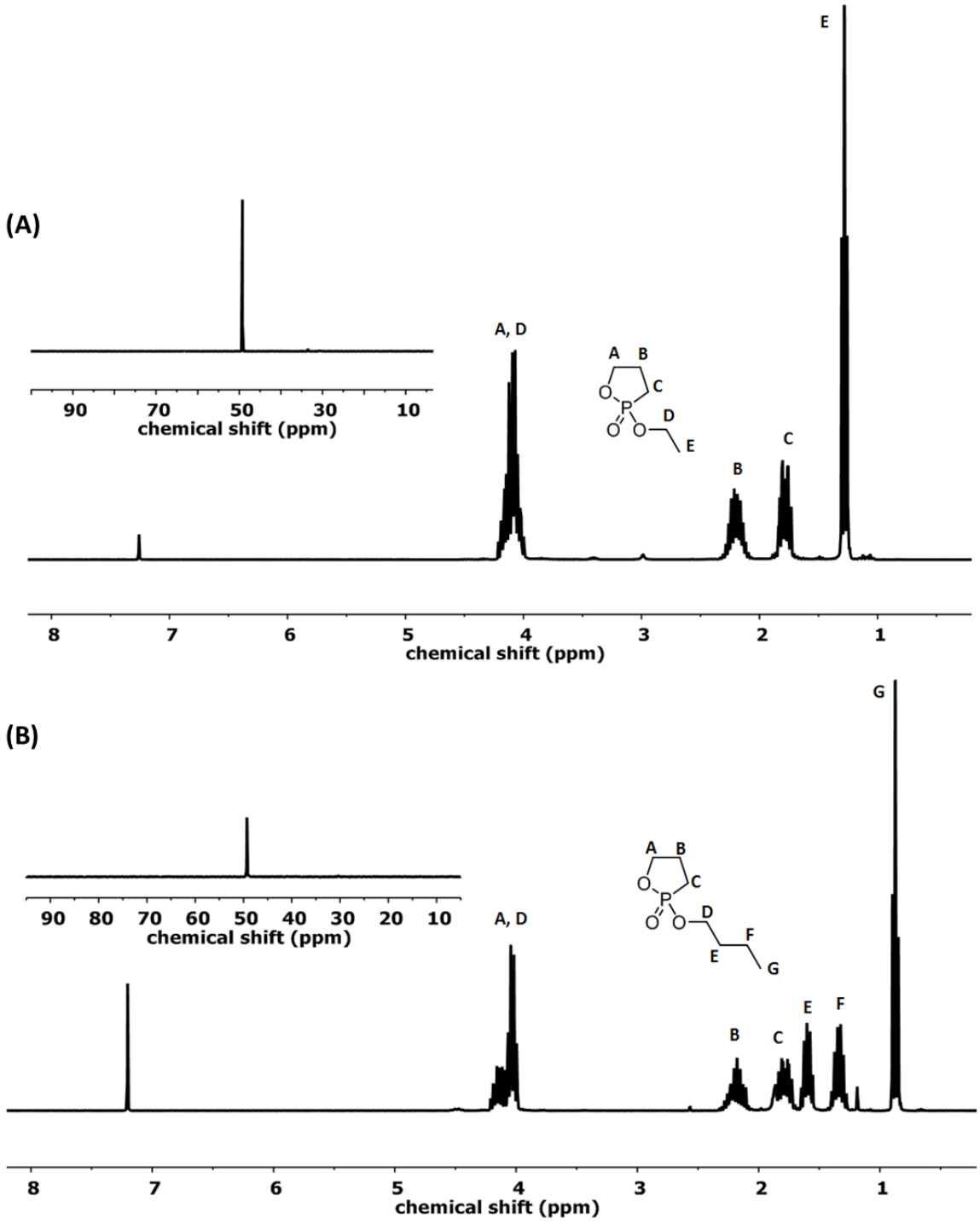

Figure 3.1. ^{1}H NMRs of (A) M1 and (B) M2 ($CDCl_3$, 298 K, 300 MHz); ^{31}P NMRs ($CDCl_3$, 298 K, 121 MHz

The ^{1}H NMR spectra of both compounds exhibit two distinctly separated signals for the cyclic methylene groups B and C (Figure 3.1) typical for the rigid ring structure and complex splitting pattern due to J coupling to the phosphorus atom. The ^{31}P NMR spectra show a single resonance at 49.24 ppm for **M1** and at 49.28 ppm for **M2**, similar to the resonances of the cyclic phosphonates with the P-C-bond as pendant chain.[10, 16] However, a distinct difference between phostones and the cyclic phosphate (EEP) and phosphonate (EtEPn) was observed concerning their stability. While, the cyclic phosphonates with the P-C-bond in the pendant chain as well as the phosphates must be stored under inert gas at low temperatures (-20°C) to avoid ring-opening degradation or spontaneous polymerization, the phostones show no such tendencies. ^{31}P NMR spectroscopy in deuterium oxide showed immediate ring-opening for the cyclic phosphates and side chain phosphonates by a distinct signal shift to the high field, while the phostone stayed intact upon contact with deuterium oxide at least two days (Figure 3.36). This increased stability of the phostone monomers can be attributed to a reduced ring-strain compared to the phosphates and side chain phosphonates. Higher ring strain energy is often indicative of a better polymerization in cyclic phosphoesters.[22] The ring strain energy can be evaluated as the difference between the formation enthalpy and the enthalpy of a strain free model reference compound (see experimental section for calculation details).[23] Here we compare the ring-strain energy of one representative compound of each five-membered monomer class, i.e. the phosphates, phosphonates, and phostones. The six-membered 2-ethoxy-1,3,2-dioxaphosphorinane-2-oxide (**M5**) was used as a reference compound (Figure 3.2).[22]

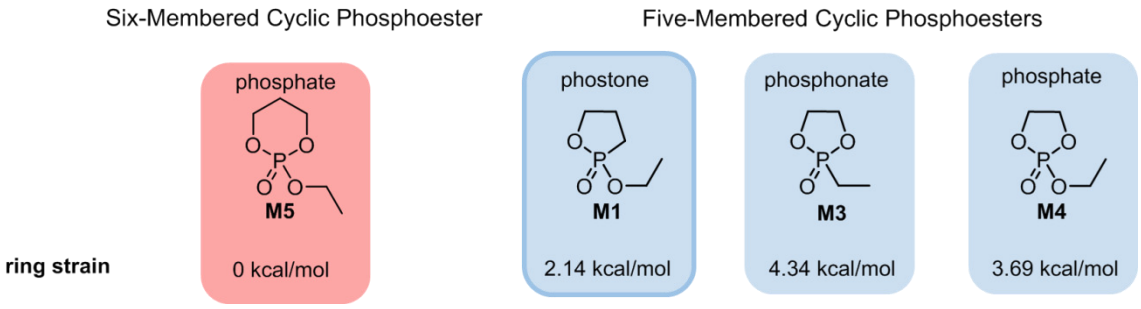

Figure 3.2. DFT (B3LYP functional and aug-cc-pVTZ basis set) calculations of the ring strain energies (kcal/mol) of six-membered cyclic phosphoester (M5) and of five-membered cyclic phostone (M1), phosphate (M3) and phosphonate (M4) heterocycles.

The calculations show significantly reduced ring-strain energy of 2.14 kcal mol^{-1} for the phostone monomer (**M1**) compared to the phosphate (**M3**) and phosphonate (**M4**) monomer with

ring-strain energies of 3.69 and 4.34 kcal mol^{-1}, respectively. The decreased ring-strain energy of **M1** can be rationalized by the replacement of one P-O-bond in the ring structure by a longer P-C-bond.

Ring-opening polymerization of phostones. A range of catalysts were investigated for the ROP of alkoxy-2-oxo-1,2-dioxaphospholanes (Scheme 3.2); monomer purity is crucial for efficient ROP. Table 3.1 shows that **M1** polymerized readily with 1,5,7-triazabicyclo[4.4.0]undec-7-ene (TBD) as single catalyst in several hours, while the polymerization of **M1** with DBU (1,8-diazabicyclo[5.4.0]undec-7-ene) as single catalyst, which is an effective catalyst for the polymerization of other phosphoester monomers,[24] did not produce any polymer in the case of **M1** under these conditions (after 24 h, at 0°C or room temperature). In contrast, the combination of DBU with urea-derived co-catalysts turned out to be suitable for the polymerization of phostones. The combination of DBU and 1-(3,5-bis(trifluoromethyl)phenyl)-3-cyclohexylthiourea (TU) as catalyst system[25] was already established for the polymerization of other phosphoester monomers and turned out to be also effective for the polymerization of phostones leading to high monomer conversions above 90% (determined by ^{31}P NMR spectroscopy) within reaction times of up to 5 days.

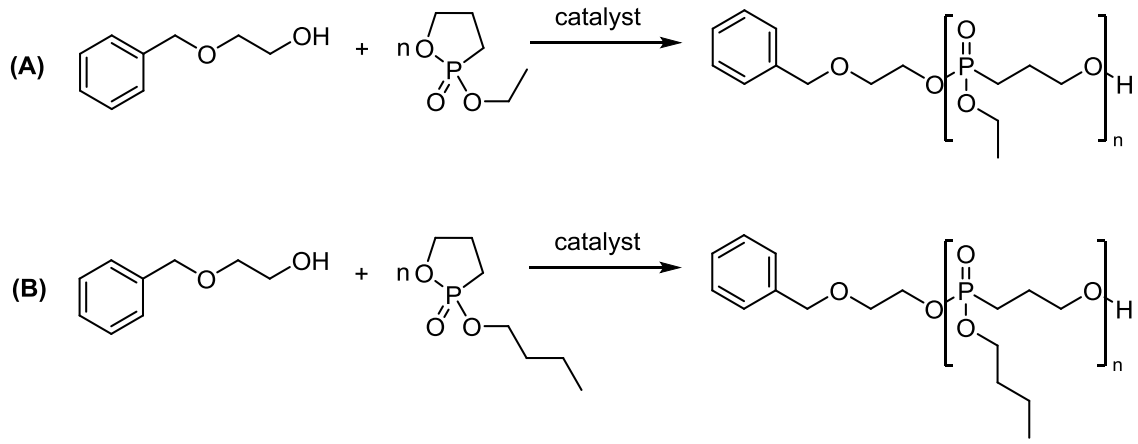

Scheme 3.2. Ring-opening polymerization of M1 (A) and M2 (B) to main-chain and in-chain polyphosphonates.

As second dual catalyst system DBU combined with 1,1',1"-(nitrilotris(ethane-2,1-diyl))tris(3-(3,5-bis(trifluoromethyl)phenyl)urea) (Tris-Urea) was applied for the polymerization of **M1**. The high efficacy of the Tris-Urea cocatalyst for the ROP of lactones within short reaction times and

low transesterification rates was recently reported by Kiesewetter et al. [26] This catalyst system was not used for the polymerization of cyclic phosphoester monomers before. But indeed, the combination of DBU/Tris-Urea turned out to be an effective catalyst system for the polymerization of phostones with high monomer conversions of ca. 90% and significantly decreased reaction times to ~24 h compared to DBU/TU. Furthermore, tin(II) 2-ethylhexanoate ($SnOct_2$) was attempted to polymerize **M1**, but led to lower monomer conversions of ca. 69% and rather ill-defined materials (Figure 3.11). Finally, the Lewis acidic ^{tBu}[salen]AlMe polymerized **M1**, albeit to lower conversions than other systems. While the Al catalyst was capable of polymerizing monomers at lower concentrations than the organocatalysts, the resulting ill-defined materials indicated organocatalysts are better suited for these systems, contrasting results for phosphonates where Al salen systems were excellent mediators of ROP.[27]

Table 3.1. Overview over polymerization conditions tested for the polymerization of M1.

#	catalyst	$[M1]_0$:$[I]_0$	$[M1]_0$: [cat]	solvent	T (°C)	time	conv. (%)
1	$SnOct_2$	50	6	tol.	95	18 h	69
2	DBU	40	5	tol.	0 /r.t.	24 h	0
3	TBD	100	5	tol.	0	4.5 h	87
4	DBU/TU	100	5	tol.	0	5 d	>90
5	DBU/Tris-Urea	100	2	tol.	0	30 h	87
6	Al(Salen)	50	2	tol.	100	18 h	24

For the polymerization with TBD, DBU/TU, or DBU/Tris-Urea (Table 3.1 entries 3, 4, and 5) detailed kinetic investigations were conducted (Figure 3.3). For the kinetic studies, monomer conversions as well as molecular weight and molecular weight distributions at different time points were determined by removing aliquots from the reaction mixture at defined reaction times and terminating in acidic $CDCl_3$. Due to the stability of the phostones, the acetic acid only terminates the polymerization without hydrolyzing the remaining monomer, making analysis of monomer conversion (by ^{31}P NMR) and molecular weight distribution (by SEC in DMF) straightforward. During the polymerization, the ^{31}P NMR resonance of the cyclic monomer shifts from 49 ppm to 31 ppm for the linear polymer, allowing a quantification of the amount of

polymer and residual monomer (see example for **M1** in Figure 3.3 (A)). For determination of M_n, the reaction aliquots were purified by precipitation into diethyl ether to remove residual monomer. M_n was calculated via ^{1}H NMR spectroscopy by comparing the integrals of the initiator with the integrals of the polymer.

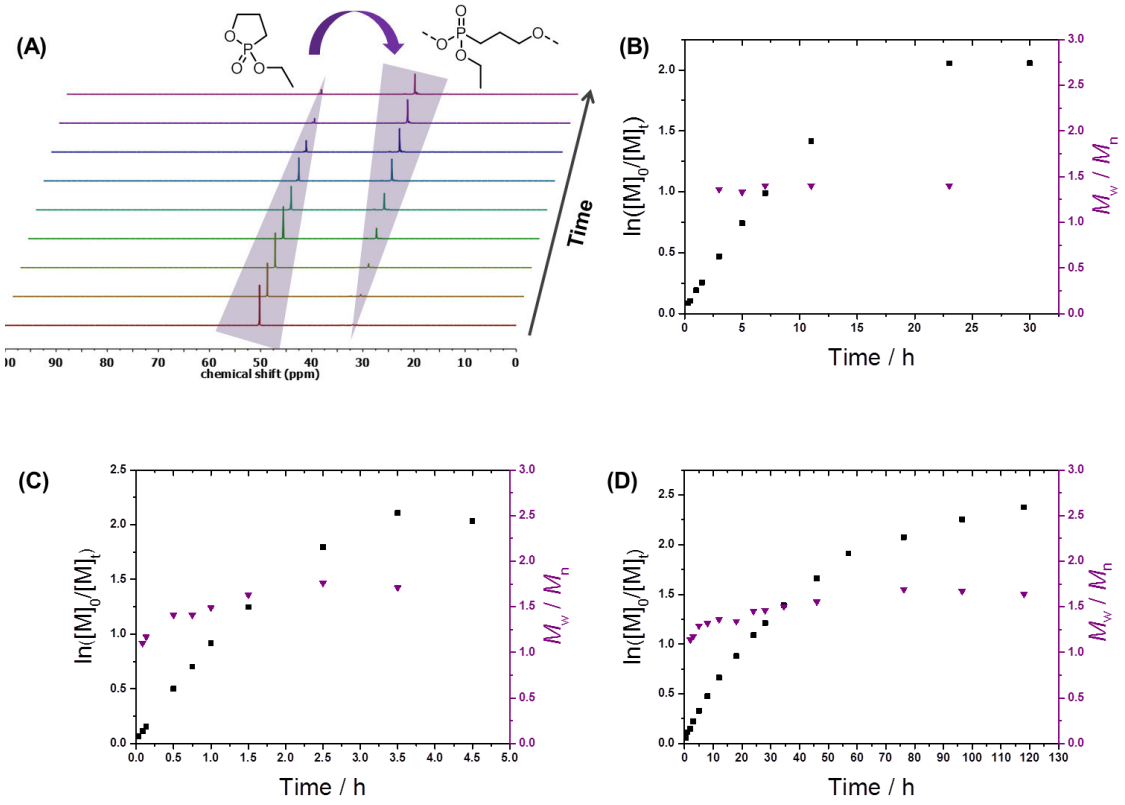

Figure 3.3. (A) ^{31}P NMR spectra of the polymerization of M1 at different time points. Plots of monomer conversion ($\ln([M]_0/[M]_t)$) *vs* time obtained from ^{31}P NMR spectra for the polymerization of EPP with DBU/Tris-Urea (B), TBD (C) and DBU/TU (D). The ratio of monomer : initiator : catalyst was 100 : 1 : 2 for (A) and 100 : 1 : 5 for (C), (D)

The plots of $\ln([M]_0/[M]_t)$ *vs* time follow first order kinetics for all catalysts, suggesting a controlled polymerization of **M1**. The polymerization of **M1** with DBU/Tris-Urea proceeded within 24 h with reasonable molecular weight dispersities of $Đ \approx 1.3$-1.4 (Figure 3.3 (B)). In contrast, the exchange of Tris-Urea for TU as a cocatalyst leads to a distinct increase of the reaction time from 1 day to 5 days, albeit with similar molecular weight distributions (Figure 3.3 (D)). The increased reaction time might be attributed to the lower activity of the TU cocatalyst,

previously observed for the ring-opening polymerization of lactones.[26] With TBD as single dual-functioning catalyst, the polymerization of **M1** was accelerated and final monomer conversion was reached after 4-5 h (Table 3.1, entry 3). However, the high activity of TBD is associated with a broadening of the molecular weight distribution to $Đ \approx 1.7$, probably due to competing transesterfication. Reduction of the temperature from r.t. to 0°C or -20°C resulted in decreased propagation kinetics (Figure 3.4 (A)) and in increased maximum monomer conversion from 86% at room temperature to 93% at -20°C. The change of the temperature also influenced the molecular weight distributions to some extent (1.60 and 1.89), probably due to the increased reaction time of 9.5 h at -20 °C (Figure 3.4(A)). Figure 3.4(B) shows the SEC traces for the polymerization of **M1** with TBD at -20 °C. A distinct broadening of the elution peak can be observed from 60 min (corresponding to a conversion of 38%) onwards that can be attributed to transesterification reactions.

The polymerization conditions established for **M1** were transferred to **M2** with similar observations concerning reaction time, monomer conversion, and molecular weight distribution. The polymerization of **M2** at 0 °C with TBD proceeded within ca. 4.5 h to 86% conversion and broad molecular weight distributions of $Đ$ = 1.5-2.0 (Figure 3.29, Figure 3.30). The change to Tris-Urea and DBU as catalyst system led to narrower molecular weight distributions of $Đ \approx 1.5$, while the reaction time increased but remained reasonable (36 h, Figure 3.29). Conversions >90% were achieved with Tris-Urea/DBU.

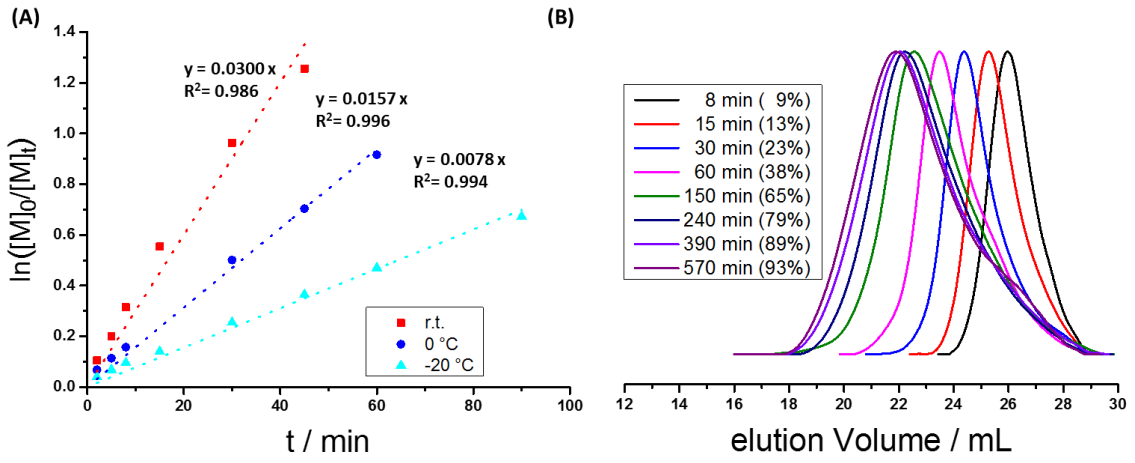

Figure 3.4. Temperature variation for the polymerization of M1 with TBD as catalyst at r.t., 0 °C, -20 °C. The ratio of monomer : initiator : catalyst was 100 : 1 : 5. (A) Plots of monomer conversion ($\ln([M]_0/[M]_t)$) *vs* time obtained from ^{31}P NMR spectra. (B) SEC traces for the polymerization of M1 with TBD at -20 °C with Đ=1.89.

Polymers **P(1)** and **P(2)** are readily soluble in common organic solvents such as THF, DCM or $CDCl_3$, while **P(1)** is water-soluble up to concentrations of at least 10 mg mL^{-1}. Like the corresponding polyphosphate (PEEP) and side-chain polyphosphonate (**P(3)**), **P(1)** shows no macroscopic phase separation from aqueous solution, even at high concentrations of 10 mg mL^{-1} in milliQ water or PBS. However, turbidity measurements of **P(1)** in water showed a slight but constant transmission drop during the measurement, until a transmission of roughly 90% is reached, while for the 'naked eye' the polymer solution remained transparent (Figure 3.24 (a)). Temperature-dependent dynamic light scattering measurements of the aqueous solution of **P(1)-4** (c=5 mg mL^{-1} in water) showed the formation of temperature independent aggregates with hydrodynamic radii R_h of ca. 120 nm (Figure 3.24 (b)). In contrast, DLS measurements of the corresponding side-chain-phosphonate **P(3)** (M_n=6000 g mol^{-1}, DP=50 (Figure 3.25)) only exhibited molecularly dissolved polymer with R_h=2 nm (Figure 3.25) and no aggregates at least up to 10 mg mL^{-1}. Solution properties of water-soluble PPEs are currently a focus of deeper investigation for our group.

Thermal Properties. All PPEs synthesized in this study are colorless, viscous, honey-like materials with low glass transition temperatures from -48 to -58°C for **P(1)** and -60 to -65°C for **P(2)**. Such values are comparable to other aliphatic PPEs prepared by ROP (Table 3.2).[10] Thermal gravimetric analysis shows a single mass loss starting at T_{on} between 260-300°C, which is again comparable to structural similar poly(phosphate)s (Figure 3.20 and Figure 3.21).

Table 3.2. Polymer properties of P(1) and P(2) prepared by ring-opening polymerization

Entry	initiator	catalyst	DP_{theo}	DP[a]	M_n / g mol^{-1}[a]	T_g / °C[b]	M_w/M_n[c]
P(1)-1	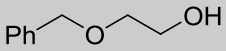	TU/DBU	20	19	3000	-48	1.25
P(1)-2	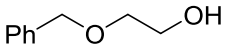	TU/DBU	50	49	7500	n.d.	1.47
P(1)-3	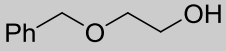	TU/DBU	60	54	8300	-56	1.24
P(1)-4	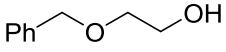	TU/Tris-Urea	170	166	25100	-58	1.56
P(1)-5	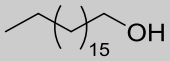	TU/DBU	40	40	6300	-50	1.50
P(2)-1	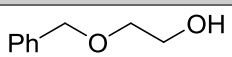	TBD	20	21	3900	-65	1.56
P(2)-2	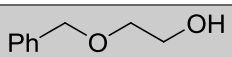	TBD	50	47	8500	-64	1.61
P(2)-3	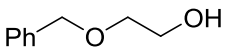	TBD	100	73	12800	-60	1.55
P(3)-1	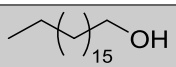	DBU	40	40	5900	-46	1.10

[a]: Determined via ^{1}H NMR. [b]: Determined by differential scanning calorimetry. [c]: Determined via SEC in DMF.

Toxicity. PPEs are currently regarded as promising materials for biomedical applications. However, phosphorus-containing compounds and especially phosphonates with good leaving groups attached to phosphorus gained notoriety, due to their application as chemical warfare agents. Many phosphonates are known to inhibit acetylcholinesterase (AChE) irreversibly, which is the typical mode of action of nerve agents.[28] AChE is an enzyme that hydrolyzes the neurotransmitter acetylcholine (ACh), terminating incoming nervous signals and serving as a regulator of neurotransmission by ACh hydrolysis. Irreversible inhibition of AChE results in accumulation of acetylcholine in cholinergic receptors and continuous stimulation of the nerve fiber leading to, among other symptoms, bronchospasm and respiratory failure.[29] As the phostones hydrolyze slowly in water, the effect of both monomers **M1** and **M2** on AChE was

investigated and no significant influence on the AChE activity up to concentrations of 0.4 g L^{-1} was found. The positive control, tacrine, led to almost complete AChE inhibition even at the lowest concentration of 25 mg L^{-1}. In addition, the cytotoxicity of **M1** and **M2** and the water-soluble polymers **P(1)** with different degrees of polymerization were evaluated *in vitro* against murine macrophages (RAW264.7). Concentrations ranging from 37.5 to 1000 µg mL^{-1} after 48 h of incubation at 37 °C in Dulbecco's modified eagle medium (DMEM), supplemented with 10% FBS were investigated (Figure 3.5**,** 20 % DMSO was used as positive control.). Cell viability was monitored as a function of ATP concentration, which was dependent on the amount of living cells. **M1** and **P(1)** showed no toxicity toward murine macrophages even at high concentrations, while **M2** showed a slight and dose-dependent cytotoxicity under these conditions (Figure 3.5 B&C).

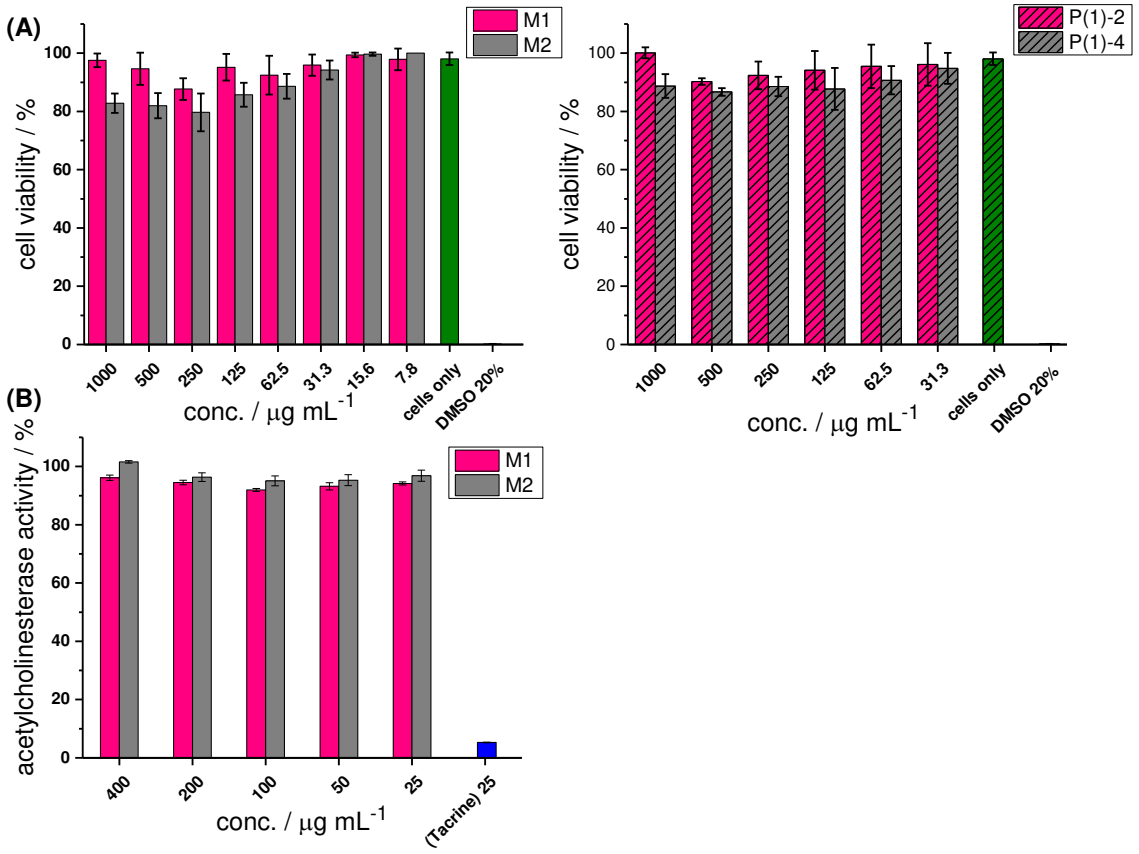

Figure 3.5. (A) ***In vitro*** **cell-viability of murine macrophages (RAW264.7) treated with M1, M2 (left) and P(1)-2,P(1)-4 (right) after 48 h of incubation. The experiments were carried out as triplicates. (B) Acetylcholinesterase assay of M1 and M2 with tacrine as positive control**

Degradation. The location of the hydrolysis-stable P-C-linkage in the PPE backbone was expected to influence the hydrolytic degradation of **P(1)** compared to other structurally similar PPEs (**P(3)** and **P(4)**). In general, degradation of PPEs follows different mechanisms under acidic or basic conditions. In acidic media the phosphoryl bond is activated by protonation allowing nucleophilic attack of water on the α-carbon atoms.[30] As the α-carbons in the pendant chains are more accessible, the pendant chains are cleaved faster than the polymer backbone. Under acidic conditions, no or slow degradation has been reported for most PPEs.[30] In contrast, under basic conditions, the degradation of PPEs is induced by nucleophilic attack of hydroxyl anions on the central phosphorus atom leading to a trigonal bipyramidal geometry, wherein the axial position is preferably cleaved. Due to the pseudo rotation of phosphorus, the main chain as well as the pendant chain can occupy this position and are therefore cleaved with approximately same rates (for low molecular weight compounds).[30-31]

The degradation of polymer **P(1)** was investigated at three different pH values (pH 1, 10, 12) and the degradation at pH 10 was compared to the side-chain analog **P(3)-1** (Figure 3.6 (B)). For polymers **P(1)** at pH 10 and 12, the degradation proceeded in two phases. In the first phase, a fast degradation was observed, which slows down and reaches a plateau with different degrees of degradation within the second phase. The degradation of **P(1)** can be accelerated with increasing pH. While the degradation at pH 10 proceeded slowly and did not exceed 10%, even after 10 days, a significantly acceleration was observed at pH 12. After 5 days, degradation of ca. 35%, and after 12 days of 40% was observed. The cleavage of the pendant chain was confirmed by the appearance of ethanol signals in the ^{1}H NMR spectra (Figure 3.6 (C) signals at 1.06 and 3.53 ppm), whereas cleavage of the main-chain is indicated by the evolution of resonances at 3.79 and 1.14 ppm (Figure 3.6).

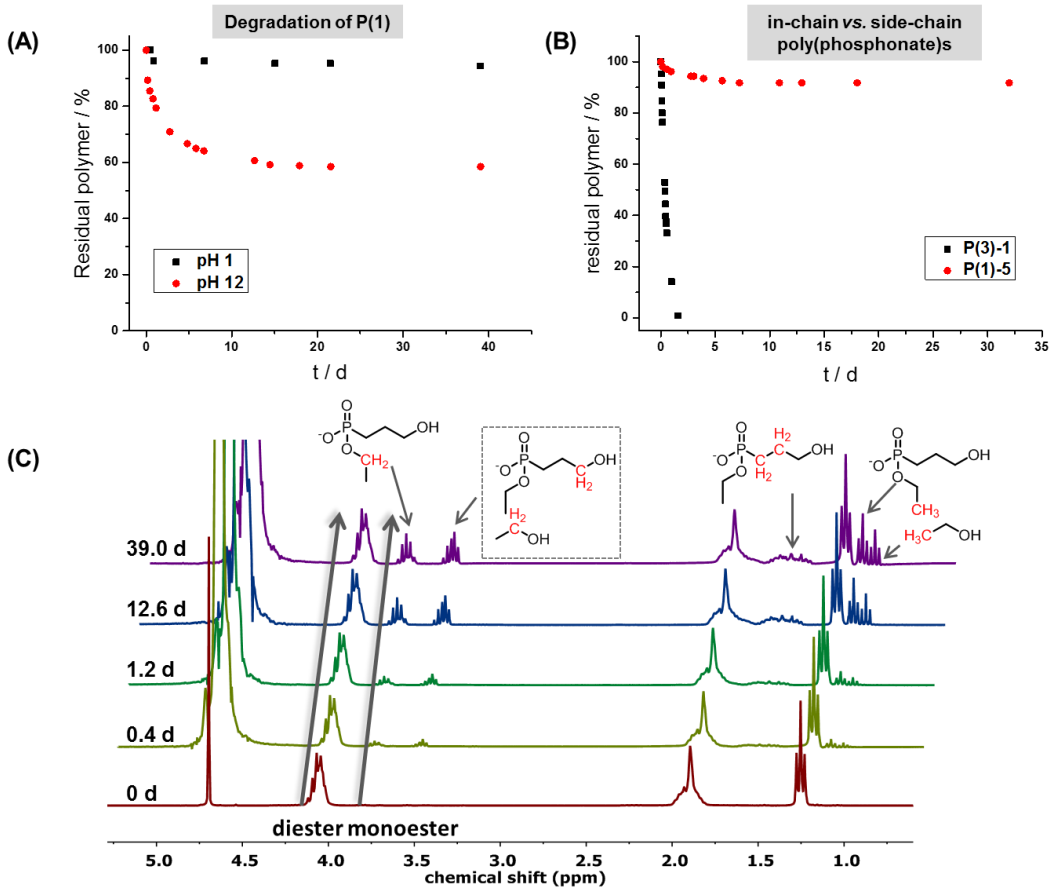

Figure 3.6. (A) Degradation of polymer P(1) pH 1 (0.1 M HCl containing 10% D_2O) and at pH 12 (0.01 M KOH containing 10% D_2O) . (B) Degradation of P(1) compared to the analogue side-chain phosphonate P(3) at pH 10 (borate buffer containing 10% D_2O) (Data depicted in (B) are also presented in chapter 4 Figure4.4) . (C) ^{1}H NMR spectra (300 MHz, H_2O/ D_2O 9:1, 298K) of the degradation of P(1)-4 at pH12.

Under acidic conditions (pH 1), only 4% degradation was observed over a period of 40 d. The dramatically decelerated degradation of **P(1)** observed under acidic conditions is in good agreement with the previously reported degradation studies of poly(phosphate)s and side-chain poly(phosphonate)s.16, 30 In contrast to **P(1)**, the side-chain poly(phosphonate) degraded at pH 10 within two days completely leading to selective degradation and only one break down product, 2-hydroxyethyl phosphonic acid, as confirmed by ^{1}H NMR spectroscopy. The dramatic different degradation behavior of the two poly(phosphonate)s may be attributed to their different behavior in water. While polymers **P(1)** aggregate in water, as described above, the side-chain polyphosphonate **P(3)** are molecularly dissolved under these conditions (Figure 3.25). The

aggregate formation probably leads to a shielding of the polymer from nucleophilic attacks of the hydroxyl anions thus leading to increased stability compared to **P(3)**. However, this unique degradation behavior of different PPEs is currently under further detailed investigation.

3 Conclusion

In summary, the first in-chain poly(phosphonate)s prepared by ring-opening polymerization is rported. In contrast to previously reported phosphate and phosphonate monomers, the unique phostone-monomers were prepared by a single-step protocol from inexpensive phosphites and dibromopropane, avoiding toxic reagents. Due to a significantly lower ring-strain of the phostones compared to the phosphate or phosphonate analogs they can be stored at room temperature and show significantly improved resistance to degradation by water. The phostones are thus a powerful alternative to other water-soluble PPEs due to easy monomer handling. However, monomer purification is still crucial to efficient polymerization. Both hydrophilic and hydrophobic materials are accessible by variation of the pendant chains. The controlled nature of the polymerization was shown in detailed kinetic studies with different catalyst systems and different monomer to initiator ratios. The Tris-Urea/DBU catalyst combination was preferred, with significantly reduced reaction times of 24 h and molecular weight dispersities of ca. 1.2-1.6. Initial studies on the biocompatibility were carried out by treating macrophages with various concentrations of the hydrophilic polymer **P(1)** and cell viabilities of above 88% were observed for polymer concentrations up to 1 g L^{-1}. The degradation of the hydrophilic polymer in aqueous media was investigated at different pH values and was found to be significantly slower than the degradation of the corresponding side-chain phosphonate, proving that a slight structural difference can lead to different polymer properties. In all, these new polymers offer an intriguing complement to other phosphorus monomers thanks to their ease of monomer synthesis, tunable hydrophilicity, biocompatibility and unique degradation behavior.

4 Experimental

4.1 General Information

All chemicals and solvents were purchased from Sigma-Aldrich, Acros Organics or Fluka and used as received unless otherwise stated. Monomers and Initiator were distilled from $MgSO_4$ and stored over molecular sieves. Deuterated solvents were purchased from Sigma-Aldrich and used as received. ^{tBu}[salen]AlMe was synthesized according to well established literature procedures.[32-33]

4.2 Instrumentation and Characterization Techniques

NMR. ^{1}H ^{13}C and ^{31} P NMR spectra were recorded using a Bruker Avance III 250, a Bruker Avance 300 or a Bruker Avance III 500. All spectra were referenced internally to residual proton signals of the deuterated solvent. All ^{31}P NMR spectra were recorded proton decoupled.

FTIR. FT-IR spectra were recorded using a Thermo Scientific iS10 FT-IR spectrometer, equipped with a diamond ATR unit.

SEC. For the size exclusion chromatography (SEC) measurements two different methods were used. ***Method a***: SEC measurements of standard polymers were performed in DMF (containing 1 gL^{-1} of lithium bromide as an additive) at 60 °C and a flow rate of 1 mL min^{-1} with a PSS SECurity as an integrated instrument, including a set of 3 PSS GRAM columns (porosity of 100 Å and 1000 Å) and a refractive index (RI) Detector. Calibration was carried out using polyethylene glycol standards provided by Polymer Standards Service. ***Method b***: SEC measurements were performed in DMF (containing 1 gL^{-1} of lithium bromide as an additive) at 50 °C with an Agilent 1100 Series as an integrated instrument, including a HEMA column (300/100/40) from MZ Analysentechnik, a UV (275 nm), and a refractive index (RI) detector. Calibration was carried out using poly(ethylene glycol) standards provided by Polymer Standards Service.

DSC. The thermal properties of the synthesized polymers were measured by differential scanning calorimetry (DSC) on a Mettler Toledo DSC 823 calorimeter. Three scanning cycles of heating-cooling were performed in a N_2-atmosphere 30 mL/min) with a heating and cooling rate of 10 °C/min.

TGA. Thermal gravimetric analysis (TGA) was measured on a Mettler Toledo ThermoSTAR TGA/SDTA 851-Thermowaage in nitrogen atmosphere. The heating rate was 10 °C/min in a range of temperature between 25 °C and 600 – 900 °C.

DLS. Dynamic light scattering (DLS) measurements were performed on an ALV spectrometer consisting of a goniometer and an ALV-5004 multiple-tau full-digital correlator(320 channels) which allows measurements over an angular range from 30° to 150. A He-Ne Laser (wavelength of 632.8 nm) is used as light source. For temperature controlled measurements the light scattering instrument is equipped with a thermostat from Julabo.

Acetylcholinesterase Assay. Inhibition of acetylcholinesterase was tested with the colorimetric Acetylcholinesterase Activity Assay Kit from Sigma Aldrich. The tests were performed according to the general protocol.

Determination of the cloud point. Cloud points were determined in MilliQ water and detected by optical transmittance of a light beam (λ = 500 nm) through a sample cell with 1 cm cell width. The measurements were performed in a Jasco V-630 photo spectrometer with a Jasco ETC-717 Peltier element. The intensity of the transmitted light was recorded dependent on the temperature of the sample cell. The heating/ cooling rate was 1 °C min^{-1}, and values were recorded every 0.1 °C.

Density functional calculations. Ring strain energies were calculated as a difference between energies of cyclic molecules and its strain-free, linear counterparts. All calculations were performed using the B3LYP density functional aug-cc-pVTZ basis set, and the Gaussian 09 package. Results are given in Table 3.3.

Table 3.3. Formation energies (Hartree) of cyclic compounds and their linear counterparts, their differences, and relative with respect to M5 strain energies.

compound	cyclic/ Hartree	linear/Hartree	difference/ kcal mol^{-1}	relative strain/ kcal mol^{-1}
M1	-764.462657486	-840.937554072	47988.68588178427	2.14
M3	-725.130710275	-801.609109812	47990.88401506339	4.34
M4	-800.401795679	-876.879155007	47990.231274553975	3.69
M5	-839.73594868	-916.207427025	47986.54090479263	0

4.3 Synthetic Procedures

2-Ethoxy-1,2-oxaphospholane 2-oxide (M1). **M1** was synthesized according to a literature procedure.[20] Triethyl phosphite (131 g, 0.8 mol, 2 eq) and 1,3-dibromopropane (80 g, 0.4 mol,

1 eq) were combined in a round bottom flask equipped with a distillation apparatus to remove evolving ethyl bromide. The mixture was heated up to 120 °C until 1,3-dibromopropane was consumed completely (the consumption of the alkyl halide was monitored by NMR measurements since no solvent is used for the reaction). The crude monomer was separated from the oligomeric side product by distillation (55-60 °C, 0.1 mbar) and purified by fractional distillation. 12.5 g (0.08 mol, 20%) 2-ethoxy-1,2-oxaphospholane-2-oxide is obtained as colorless liquid.

^{1}H NMR (300 MHz, chloroform-*d*) δ 4.25 – 3.96 (m, 4H, -P-O-C***H*****$_2$**-), 2.37 – 2.06 (m, 2H), 1.90 – 1.65 (m, 2H, -P-C***H*****$_2$**-), 1.28 (t, *J* = 7.1 Hz, 3H, -C***H*****$_3$**). **^{13}C NMR** (176 MHz, chloroform-*d*) δ 67.26 (-O-***C***H$_2$-CH$_2$-), 62.18 (-O-***C***H$_2$-CH$_3$), 23.92 (-P-***C***H$_2$-), 18.49 (-P-CH$_2$-***C***H$_2$-), 16.47 (-***C***H$_3$). **^{31}P{H} NMR** (121 MHz, chloroform-*d*) δ 49.25. **FTIR** (cm^{-1}): 2988, 2904, 1451, 1415 (P-CH$_2$-), 1392, 1364, 1266, 1235 (P=O), 1160, 1043 (P−O−C), 980 (P−O−C), 960, 894, 807, 775

2-butoxy-1,2-oxaphospholane 2-oxide (M2). Tributyl phosphite (198 g, 0.8 mol, 2 eq) and 1,3-dibromopropane (80 g, 0.4 mol, 1 eq) were combined in a round bottom flask equipped with a distillation aparatus to remove evolving butyl bromide. The mixture was heated up to 120 °C until 1,3-dibromopropane was consumed completely (the consumption of the alkyl halide was monitored by NMR measurements since no solvent is used for the reaction). The crude monomer was separated from the oligomeric side product by distillation and purified by column chromatography using ethyl acetate as eluent to remove side products. The product can be removed from the column by using acetone as eluent to yield 15.6 g (21%) of a colorless liquid.

^{1}H NMR (300 MHz, chloroform-*d*) δ 4.24 – 3.94 (m, 4H, -P-O-C***H*****$_2$**-), 2.34 – 2.02 (m, 2H), 1.92 – 1.69 (m, 2H), 1.71 – 1.52 (m, 2H), 1.46 – 1.23 (m, 2H), 0.87 (t, *J* = 7.4 Hz, 3H, -C***H*****$_3$**). **^{13}C NMR** (176 MHz, chloroform-*d*) δ 67.24 (-O-***C***H$_2$-CH$_2$-), 66.16 (-O-***C***H$_2$-C$_3$H$_7$), 32.71 (-O-CH$_2$-***C***H$_2$-), 29.83 (-***C***H$_2$-CH$_3$), 24.12(-P-***C***H$_2$-), 19.10(-P-CH$_2$-***C***H$_2$-), 13.73 (-***C***H$_3$). **^{31}P{H} NMR** (122 MHz, chloroform-*d*) δ 49.28. FTIR (cm^{-1}): 2959, 2867, 1458, 1413(P-CH$_2$-), 1379, 1358, 1269 (P=O), 1235, 1151, 1062, 1020 (P−O−C), 978 (P−O−C), 897, 851, 796, 737

General Procedure for the ROP of M1 and M2 using TBD as catalyst. The reaction was conducted either in dry dichloromethane or dry toluene at different temperatures with 2-(benzyloxy) ethanol as the initiator and TBD as the catalyst. All Schlenk-tubes were flame-dried prior to use. **M1/M2** and a stock solution of 2-(benzyloxy) ethanol (65.7 mmol L^{-1}) were

introduced into a tube via syringe. TBD was freeze-dried with benzene before use and a stock solution (0.36 mol L^{-1}) in dry solvent was prepared. The initiator stock solution was added to the monomer and the concentration was adjusted to an overall concentration of 2 mol L^{-1} of monomer with the respective solvent. The reaction tube as well as the TBD stock solution were cooled down to 0 °C and the polymerization was initiated by the rapid addition of the TBD solution (5 equivalents in respect to the initiator) to the stirred monomer/initiator solution via syringe. Polymerizations were quenched by addition of an excess of acetic acid (20 mg mL^{-1}) in the respective solvent. The polymers were purified by precipitation into diethyl ether or hexane (for (**P(2)**) and subsequent dialysis.

General Procedure for the ROP of M1 and M2 using TU/DBU or Tris-Urea/TU. All Schlenk-tubes were flame-dried prior to use. 2-(benzyloxy) ethanol was used as initiator. TU/Tris-Urea was introduced into a flame-dried Schlenk-tube, dissolved in dry benzene, and dried by lyophilization. **M1/M2** was introduced into the Schlenk-tube. A Stock solution of the initiator (65.7 mmol L^{-1}) in the respective dry solvent was prepared. A calculated amount of the initiator stock solution was added to the stirred solution of monomer and co-catalyst. In all cases a certain amount of dry solvent was added to the monomer/co-catalyst solution to give a total reaction concentration of 2 mol L^{-1}. The temperatures were adjusted and the polymerization was started by rapid addition of DBU to the reaction mixture by a microliter syringe. The polymerizations of **M1** with TU/DBU as catalyst were conducted with 5 equivalents in respect to the initiator. The polymerizations with Tris-Urea/DBU as catalyst were conducted with 2 equivalents in respect to the initiator for **M1** and with 4 equivalents for the polymerization of **M2**. Polymerizations were quenched by addition of an excess of acetic acid in the respective solvent. The polymers were purified by precipitation into diethyl ether or hexane (for (**P(2)**) and subsequent dialysis.

Representative NMR data for **P(1)**

^{1}H NMR (300 MHz, Methylene Chloride-d_2) δ 7.27 (d, J = 3.9 Hz, aromatic C***H***), 4.47 (s, benzyl -C***H***$_2$-), 4.15 – 3.81 (m, backbone /side chain –P-O-C***H***$_2$-), 2.00 – 1.60 (m, backbone –P-C***H***$_2$-C***H***$_2$-), 1.23 (t, J = 7.0 Hz, side chain –C***H***$_3$). **^{13}C NMR** (126 MHz, Chloroform-*d*) δ 64.91 (-P-C$_2$H$_4$-***C***H$_2$-), 62.00 (-O-***C***H$_2$-CH$_3$), 23.88(-P-***C***H$_2$-CH$_2$-), 21.32 (-P-CH$_2$-***C***H$_2$-), 16.48, (-***C***H$_3$). **^{31}P{H} NMR** (121 MHz, Methylene Chloride-d2) δ 31.29, 30.87.

Representative NMR data for **P(2)**

^{1}H NMR (300 MHz, Methylene Chloride-d_2) δ 7.26 (d, J = 4.0 Hz, aromatic C***H***), 4.47 (s, benzyl -C***H***$_2$-), 4.17 – 3.77 (m, backbone /side chain –P-O-C***H***$_2$-), 1.96 – 1.44 (m, backbone –P-

C***H***$_2$-C***H***$_2$– and side chain –C***H***$_2$-C_2H_5), 1.32 (dq, *J* = 14.4, 7.3 Hz, side chain -C***H***$_2$-CH_3), 0.86 (t, *J* = 7.3 Hz, side chain –C***H***$_3$). **^{13}C NMR** (126 MHz, Chloroform-*d*) 65.68 (backbone -O-***C***H_2-), 65.01(side chain -O-***C***H_2-CH_3), 32.58(side chain –O-CH_2-***C***H_2-), 23.94 (backbone –P-***C***H_2-) 21.28 (backbone –CH_2-***C***H_2-CH_2-), 18.74 (side chain –***C***H_2–CH_3), 13.61 (side chain –***C***H_3).**^{31}P{H} NMR** (121 MHz, Methylene Chloride-d_2) δ 31.42, 30.83.

Synthesis of P(1)-5. Octadecanol and TU were dried by lyophilization with benzene. **M1** (490 mg, 3.26 mmol, 40 eq) was added to the dried TU. A stock solution of octadecanol in dry toluene was prepared with a concentration of 0.07 mol L^{-1}. 1.1mL (22.0 mg, 0.084 mmol, 1 eq) of the initiator stock solution was added to the monomer resulting in a monomer concentration of 3 mol L^{-1}. The polymerization was initiated by the addition of 60 µL of DBU (62 mg, 0.41 mmol, 5eq). Polymerization was conducted at 0 °C and terminated after 20 h by the rapid addition of an excess of acetic acid dissolved in dichloromethane with a concentration of 20 mg mL^{-1}. The polymer was obtained by three-times precipitation in cold diethyl ether and subsequent dialysis against water to yield 396 mg (77%) of a colorless amorphous polymer.
^{1}H NMR (500 MHz, chloroform-*d*) δ 4.22 – 3.83 (m), 1.99 – 1.69 (m), 1.27 (t, *J* = 7.0 Hz), 0.81 (t, *J* = 6.9 Hz, 3H). **^{31}P{H} NMR** (202 MHz, chloroform-*d*) δ 31.43. **^{13}C NMR** (126 MHz, chloroform-*d*) δ 64.99, 61.71, 29.68, 22.50, 21.36, 16,51.

General Procedure for the kinetic studies of the ROP of M1/M2. All reaction kinetics were conducted at a monomer concentration of 2 mol L^{-1}. At different time points 100 µL of the reaction mixture was removed and terminated in 1 mL $CDCl_3$ containing 20 mg acetic acid. These solutions were divided in two parts each containing 0.5 mL. One part was freed from solvent under reduced pressure and analyzed without further purification by SEC. The other part was directly analyzed by ^{31}P NMR spectroscopy without purification to determine the conversion. M_n was determined by ^{1}H NMR spectroscopy of the purified polymer sample. The reaction mixture was purified by three-times precipitation into diethyl ether (3x) and vacuum dried.

Synthesis of P(3)-1. 2-ethyl-1,3,2-dioxaphospholane-2-oxide (457 mg, 3.36 mmol, 40 eq) was placed in a flame-dried Schlenk tube. A stock solution of octadecanol in dry toluene was prepared with a concentration of 0.07 mol L^{-1}. 1.13mL (22.7 mg, 0.084 mmol, 1 eq) of the initiator stock solution was added to the monomer resulting in a monomer concentration of 3

mol L^{-1}. The polymerization was initiated by the addition of 62 µL of DBU (64 mg, 0.42mmol, 5eq). Polymerization was conducted at room temperature and terminated after 19 h by the rapid addition of an excess of acetic acid dissolved in dichloromethane with a concentration of 20 mg mL^{-1}. The polymer was obtained by three-times precipitation in cold diethyl ether and subsequent dialysis against water to yield 448mg (93%) of a colorless amorphous polymer.

^{1}H NMR (500 MHz, chloroform-*d*) δ 4.38 – 4.09 (m), 1.83 (dq, *J* = 18.4, 7.7 Hz), 1.19 (dt, *J* = 20.5, 7.6 Hz, 126H), 0.86 (t, *J* = 6.9 Hz). **^{13}C NMR** (126 MHz, chloroform-*d*) δ 64.50, 29.69, 19.36, 18.22**. ^{31}P{H} NMR** (202 MHz, chloroform-*d*) δ 35.23.

4.4 Spectra

4.4.1 Monomer spectra

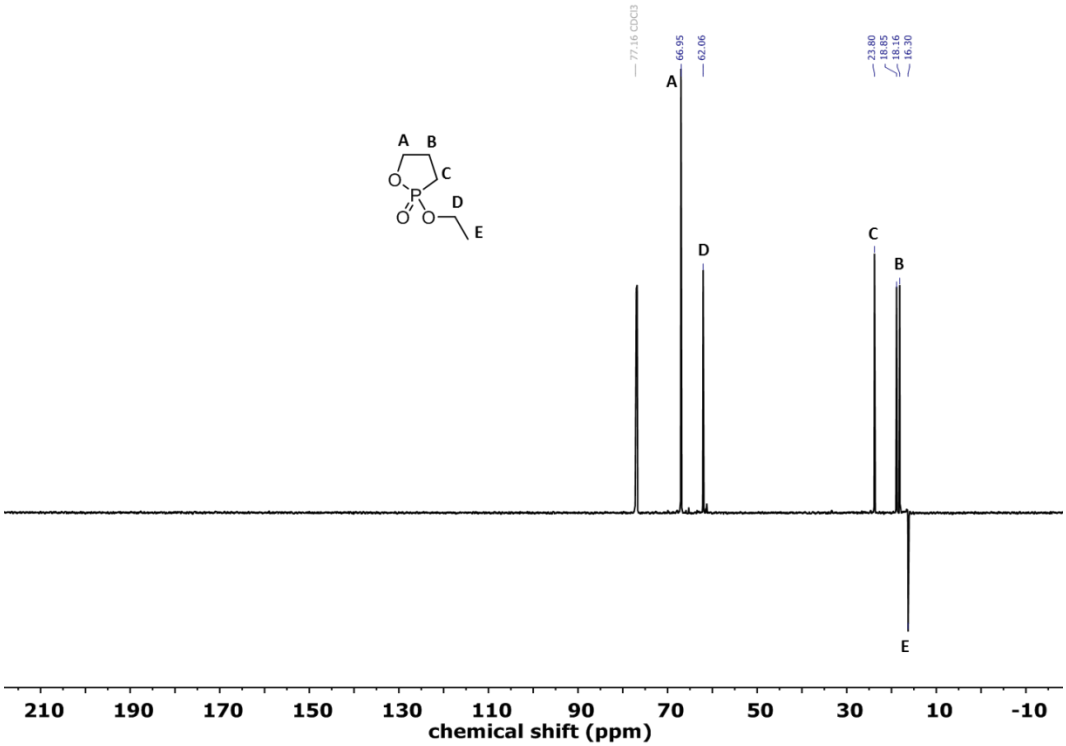

Figure 3.7. ^{13} C NMR (J MOD) (176 MHz) of M1 in $CDCl_3$ at 298 K.

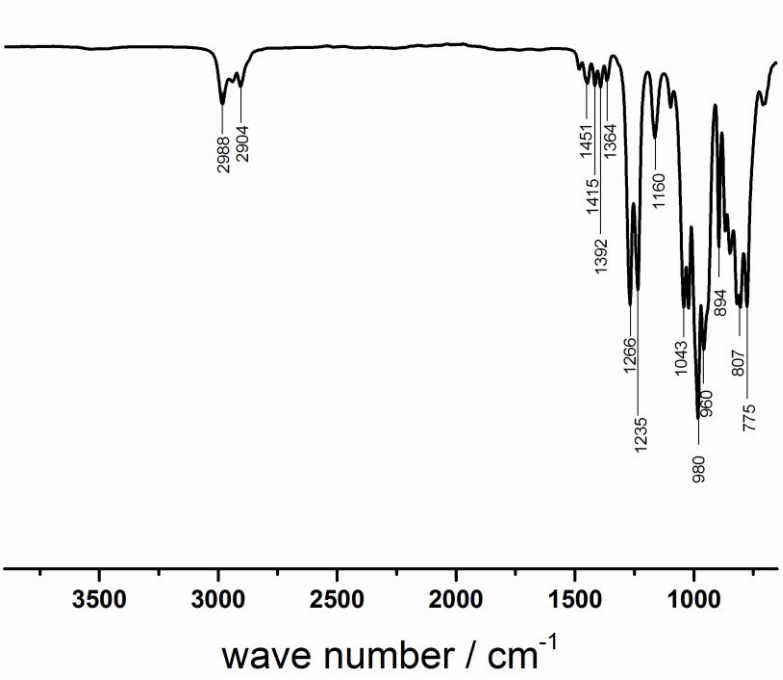

Figure 3.8: IR spectrum of M1.

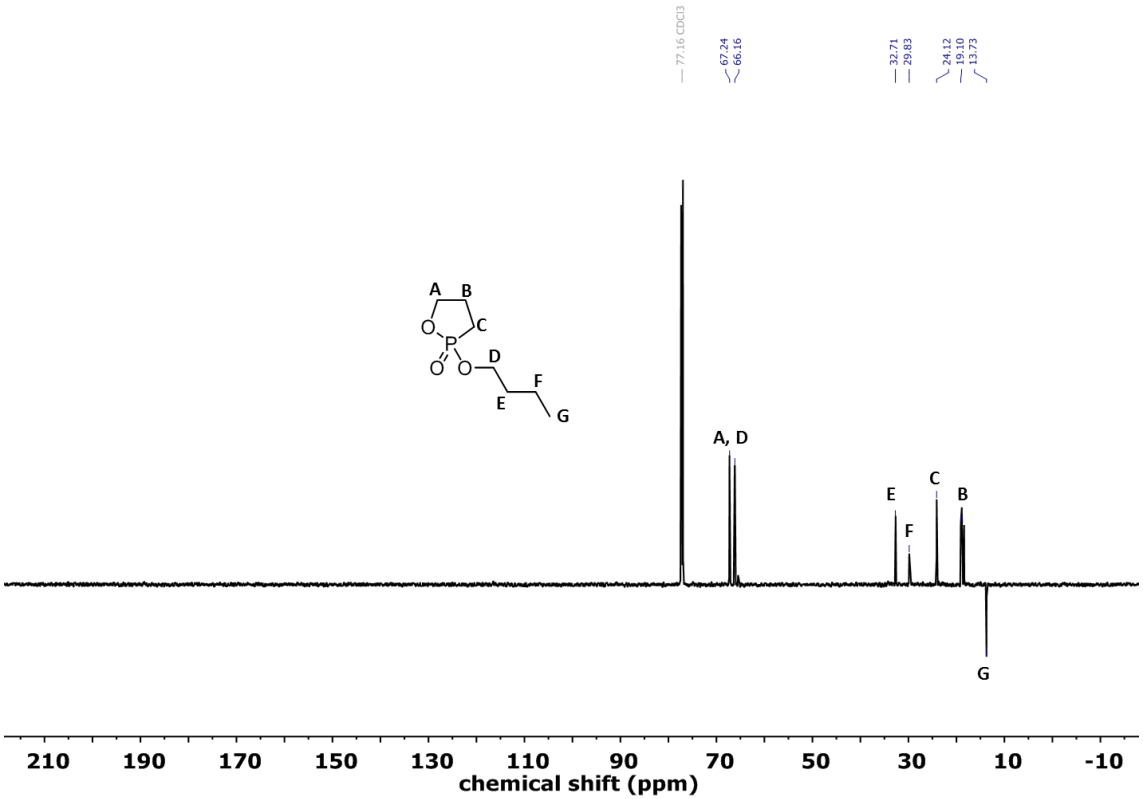

Figure 3.9.[13] C NMR (J MOD) (176 MHz) of M2 in $CDCl_3$ at 298 K.

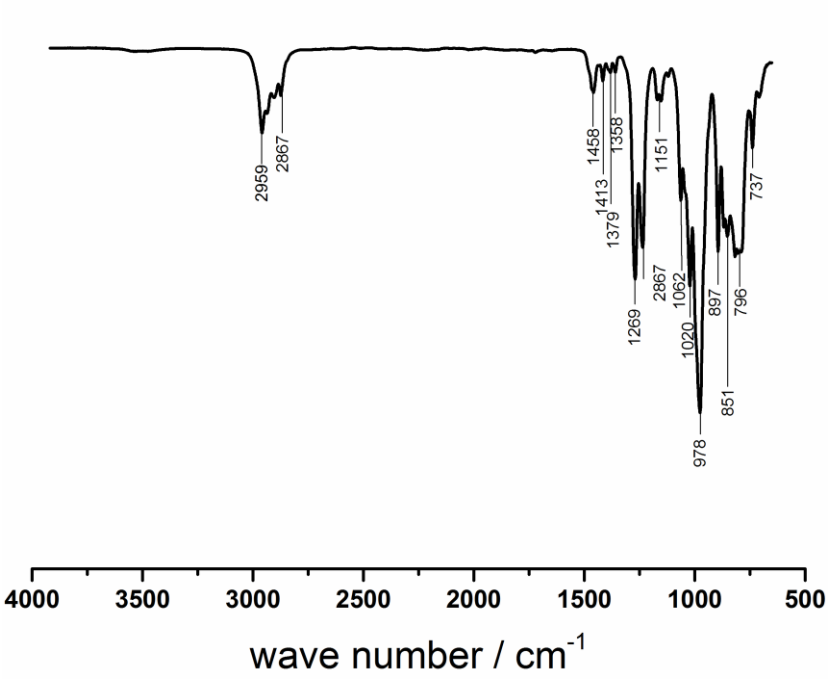

Figure 3.10. IR spectrum of M2**.**

4.4.2 Polymer spectra

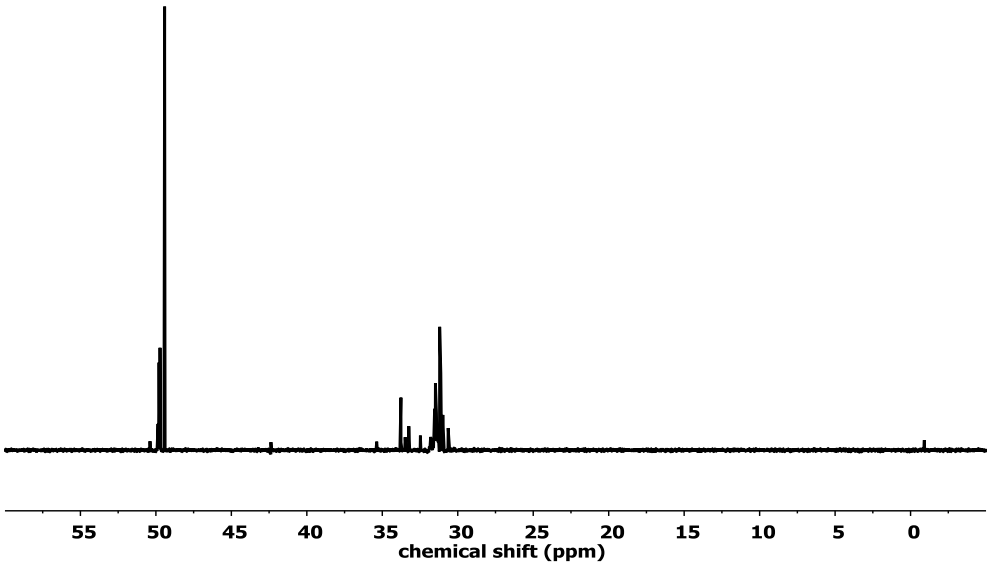

Figure 3.11. $^{31}P\{H\}$ NMR (121 MHz) in $CDCl_3$ at 298 K of the polymerization of M1 with $Sn(Oct)_2$ after 18 h at 95°C in toluene with a ratio $[M]_0$:$[I]_0$:[cat.] 50:1:5.7

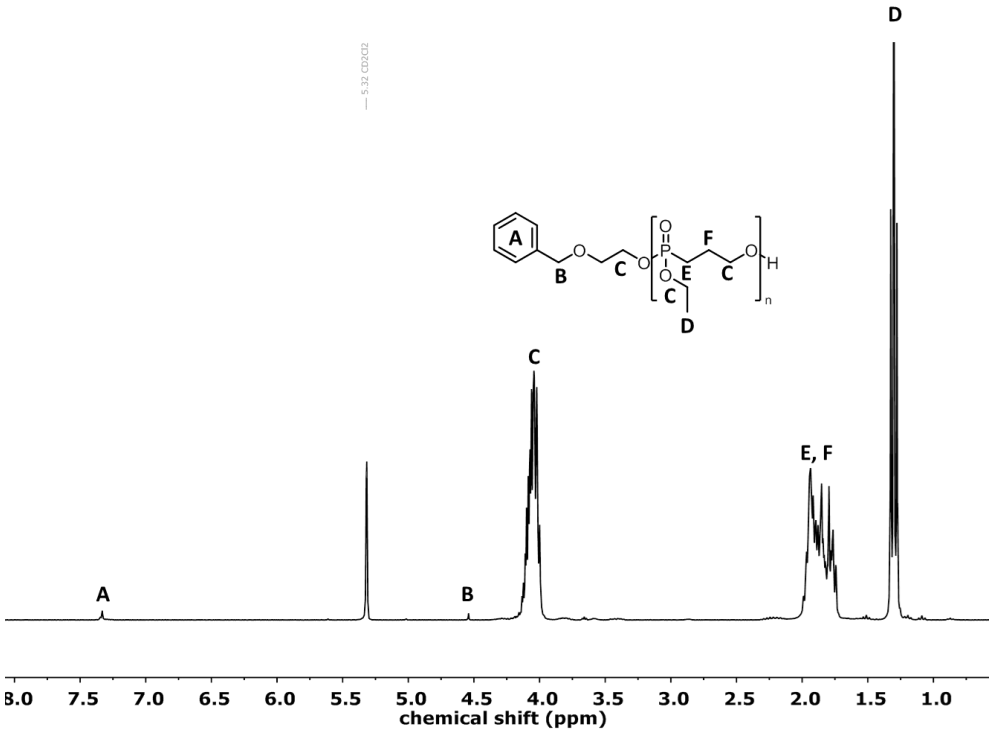

Figure 3.12. ^{1}H NMR (300 MHz) of P(1)-4 in CD_2Cl_2 at 298 K.

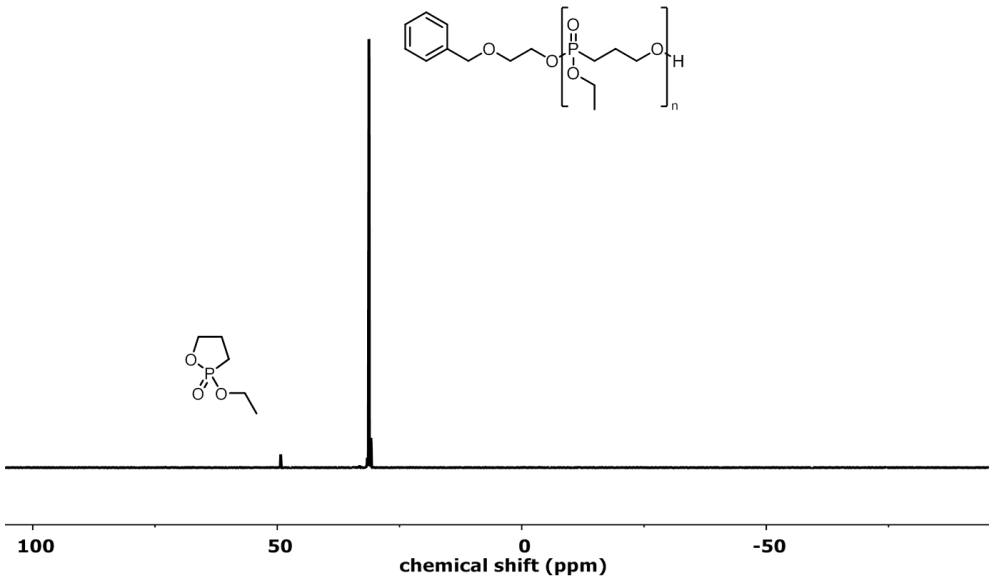

Figure 3.13. ^{31}P{H} NMR (202 MHz) of P(1)-4 in CD_2Cl_2 at 298 K. The spectra shows 2% of residual monomer at 49.3 ppm.

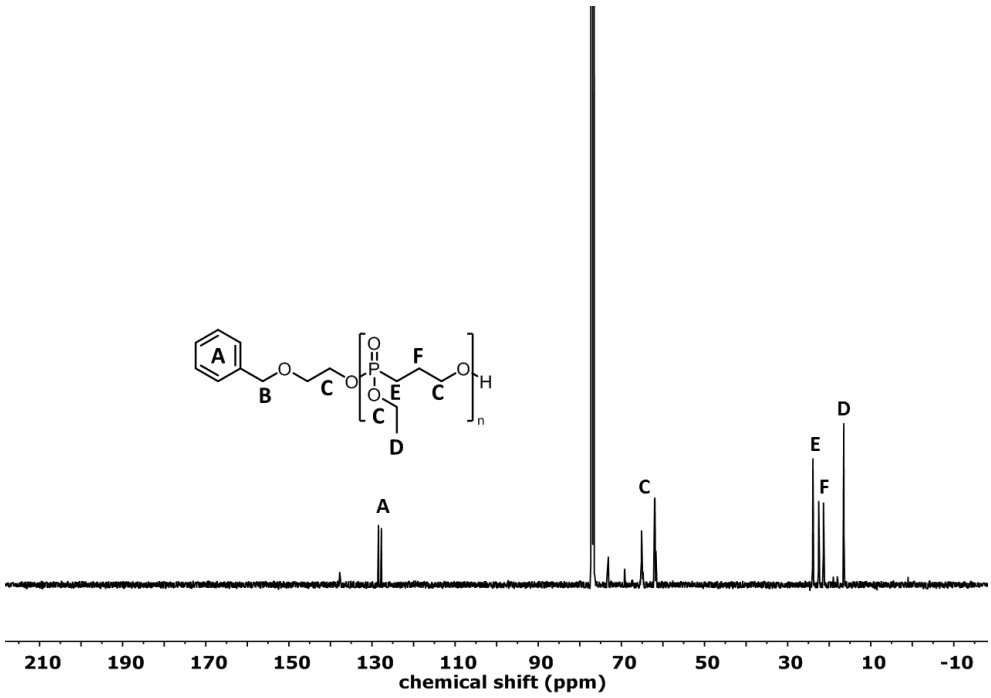

Figure 3.14. ^{13}C NMR (126 MHz) of P(1)-1 in $CDCl_3$ at 298 K.

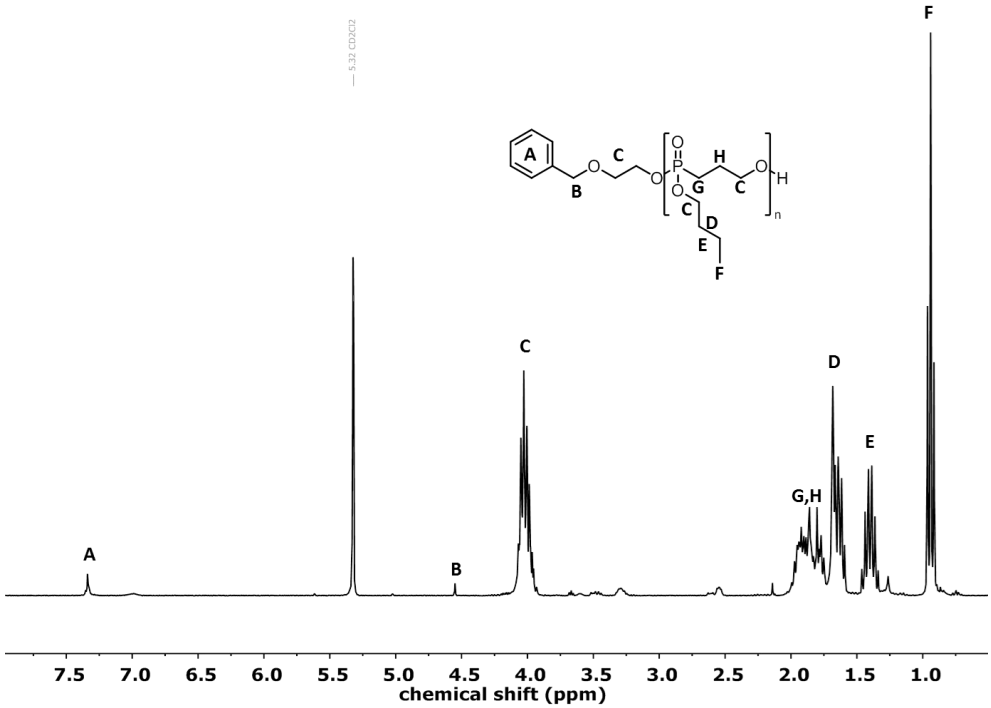

Figure 3.15. ^{1}H NMR (300 MHz) of P(2)-3 in CDCl3 at 298 K.

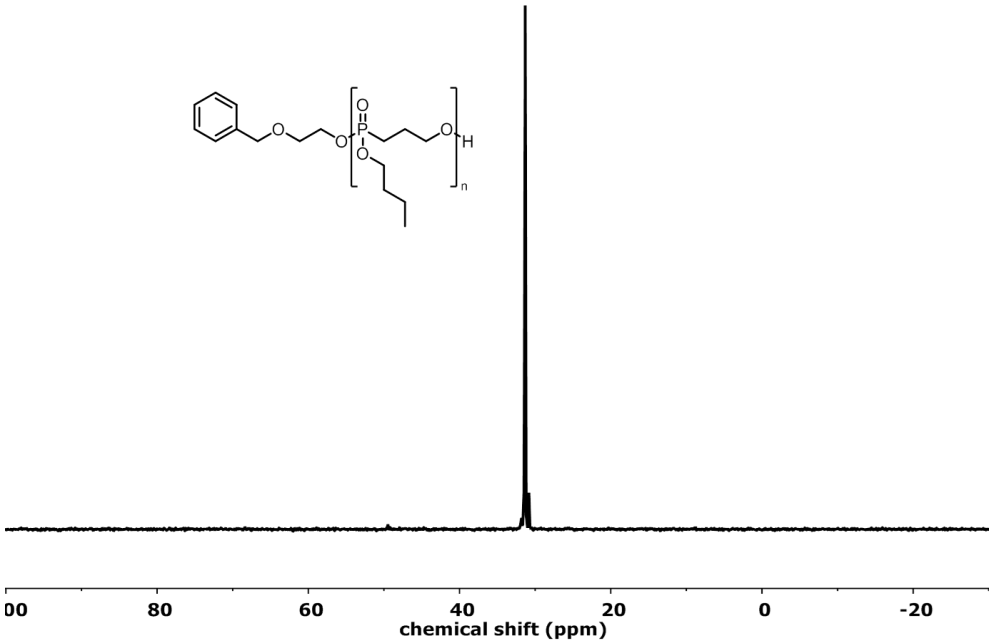

Figure 3.16. $^{31}P\{H\}$ NMR (121 MHz) of P(2) with DP=75 (product of the reaction kinetic with Tris-Urea/DBU) in CD_2Cl_2 at 298 K.

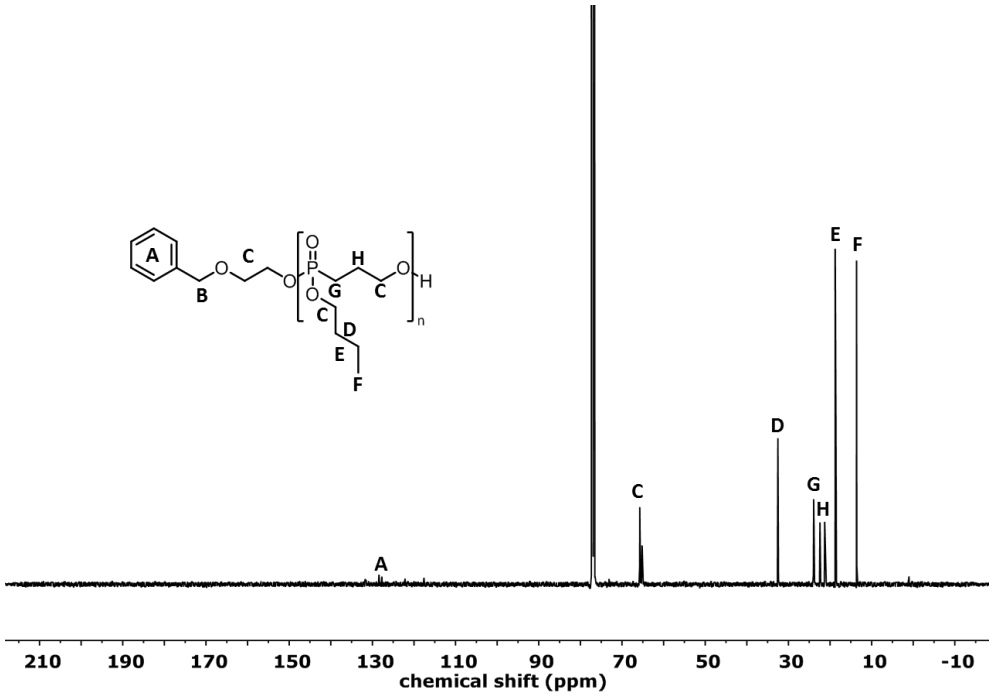

Figure 3.17.^{13}C NMR (126 MHz) of P(2)-3 in $CDCl_3$ at 298 K.

4.5 SEC-Elugrams

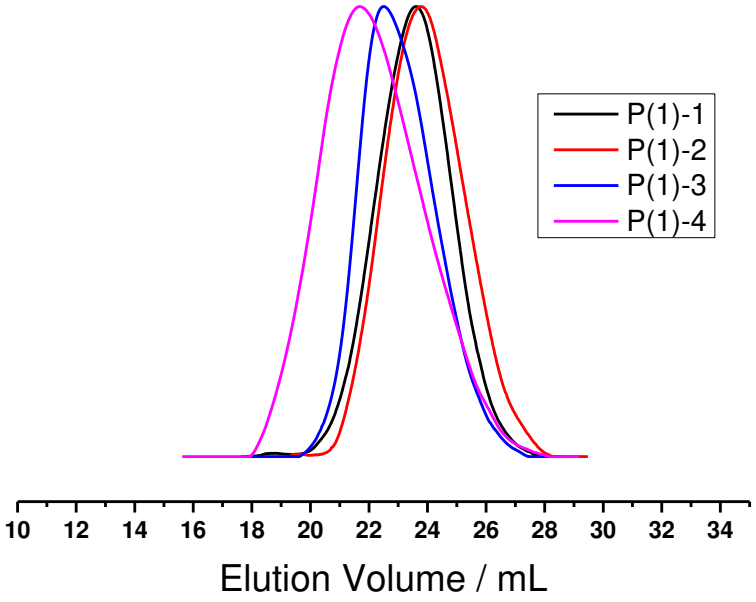

Figure 3.18. SEC-elugrams of polymers P(1)-1in DMF at 50°C (*method b*).

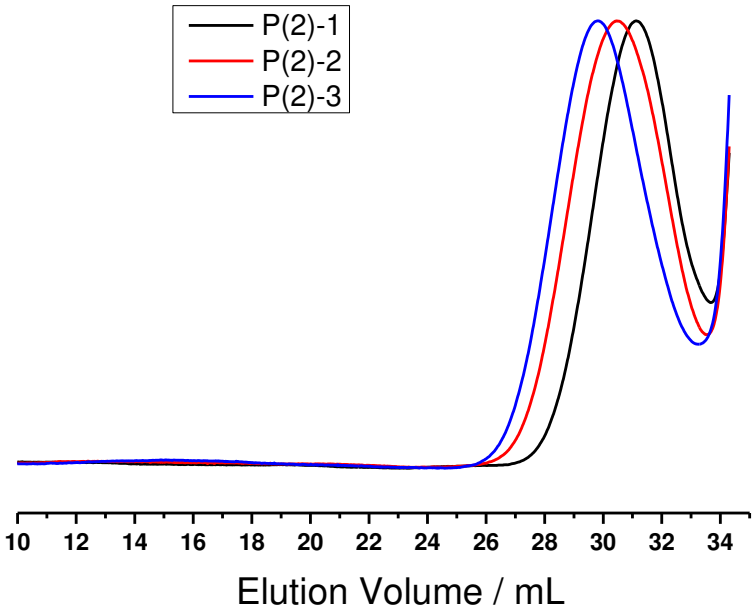

Figure 3.19. SEC-elugrams of polymers P(2) in DMF at 60°C (*method a*).

4.6 Thermal Characterization

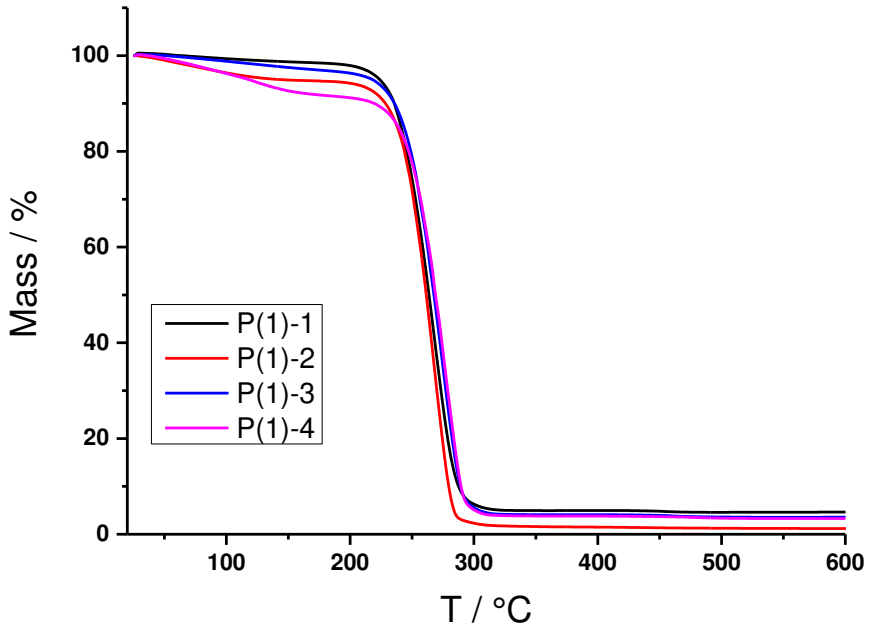

Figure 3.20. TGA measurements of polymers P(1).

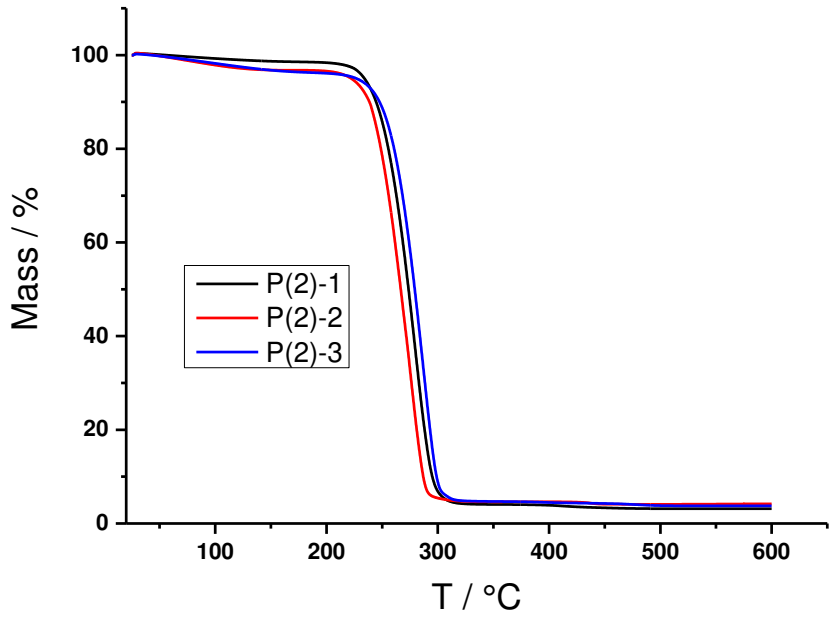

Figure 3.21. TGA thermograms of polymers P(2).

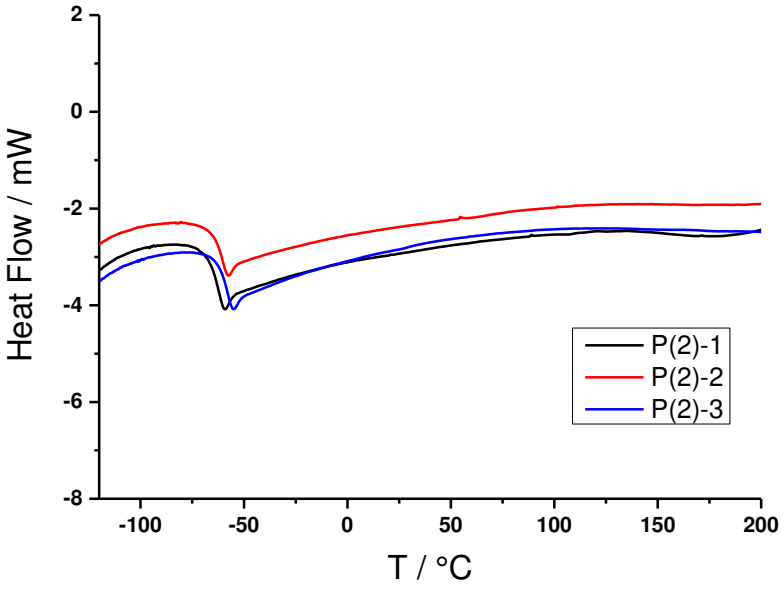

Figure 3.22. DSC thermograms of polymers P(2) at a heating rate of 10 K min^{-1} (depicted is the second heating phase).

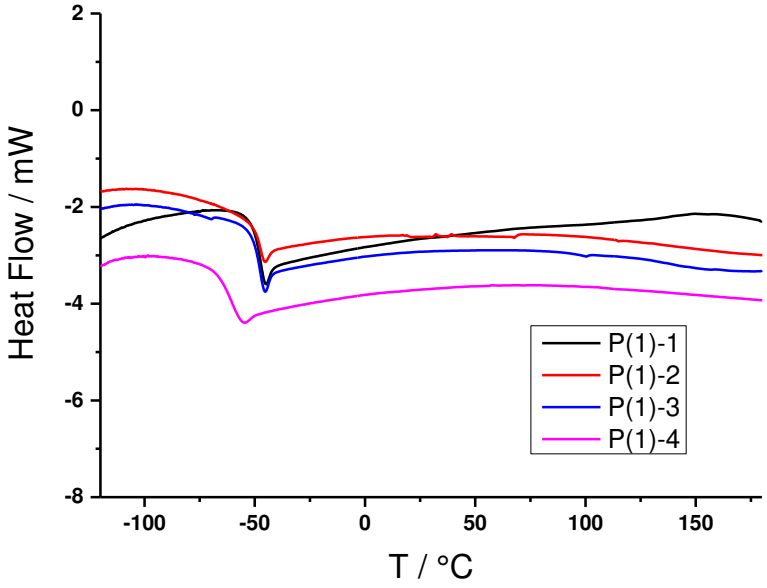

Figure 3.23. DSC thermograms of Poly(2)-polymers P(1) at a heating rate of 10 K min^{-1} (depicted is the second heating phase second heating).

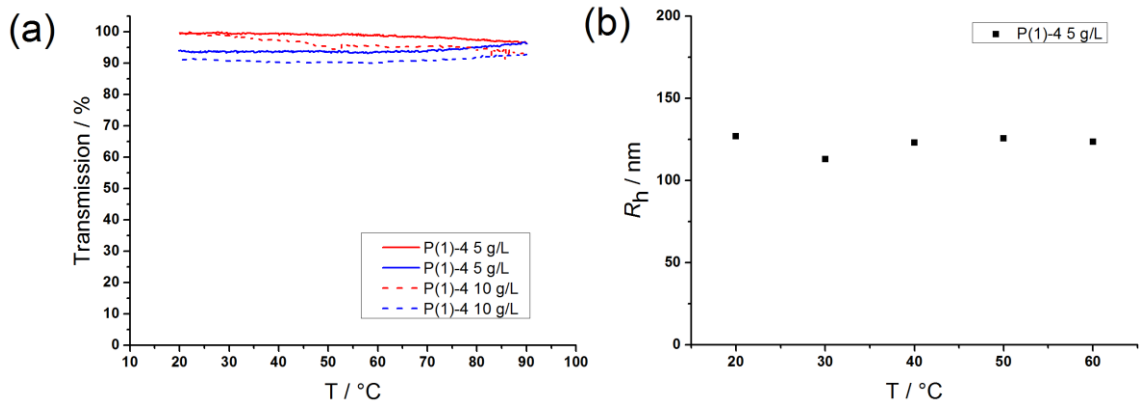

Figure 3.24. (a) Turbidity measurements of P(1)-4 in H_2O at a heating rate of 1°C min^{-1} .Transmission was measured at 500 nm for two concentrations (5, 10 g L^{-1}). (b) DLS measurements for P(1)-4 in H_2O at a concentration of 5 g L^{-1} showed the formation of aggregates with hydrodynamic radii of ~120 nm.

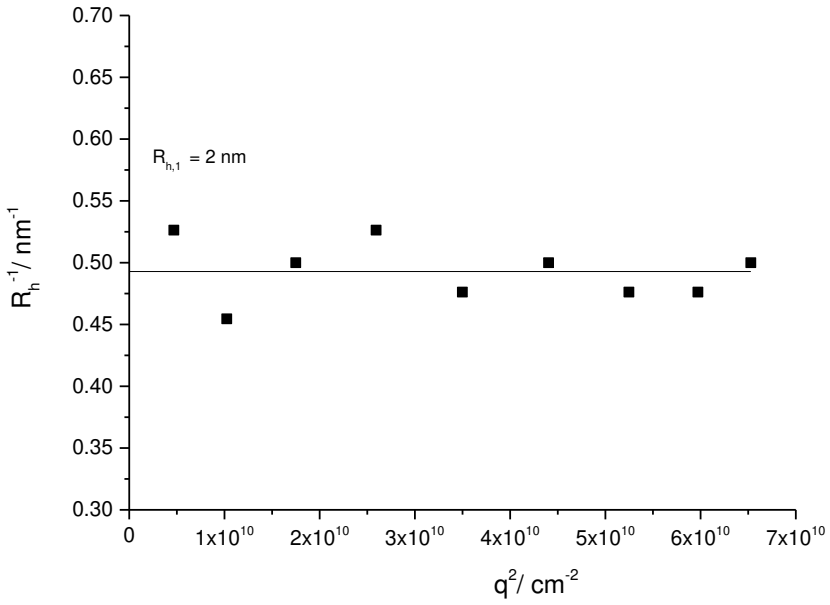

Figure 3.25. DLS measurements for P(3) DP=50 in H_2O at a concentration of 10 g L^{-1}.

4.7 Kinetic studies for the polymerization of M1

4.7.1 Kinetic studies with TBD

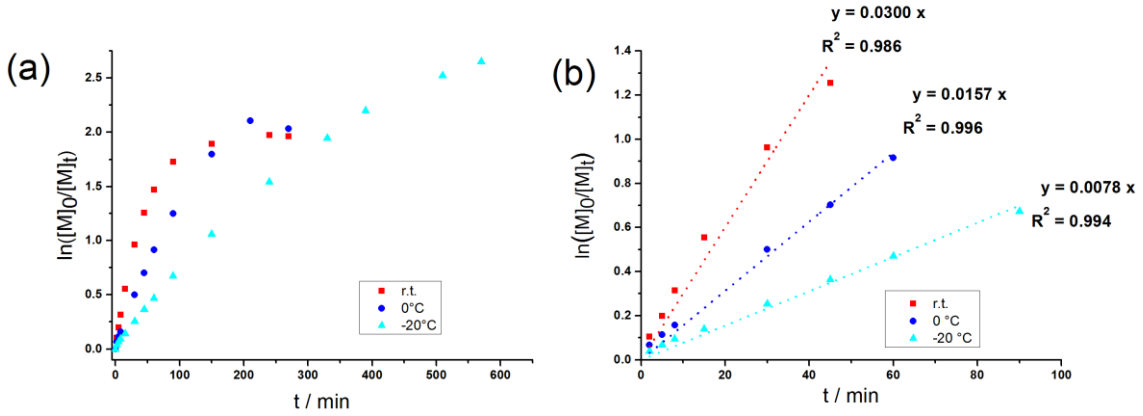

Figure 3.26. (a) Kinetic plots of ($\ln([M]_0/[M]_t)$) *vs* time obtained from ^{31}P NMR spectra for the polymerization of M1 with TBD as catalyst at r.t., 0 °C, -20 °C. The ratio of monomer : initiator : catalyst was 100 : 1 : 5 (data listed in Table 3.4). (b) Linear area of the conversion ($\ln([M]_0/[M]_t)$) *vs* time.

Table 3.4. Kinetic data for the polymerization of M1 by organocatalytic ROP using 2-(benzyloxy)ethanol as initiator and TBD as catalyst at different temperatures. Polymerizations were conducted at a monomer concentration of 2 mol L^{-1}.

#	$[M]_0/[I]_0/[cat.]$	T / °C	solvent	Time / min	Conv. [a] / %	DP [b]	M_n [a]	M_n [b] / gmol^{-1}	Đ [c]
1	100:1:5	0	tol	2	7	n.d.	1200	n.d.	n.d.
2	100:1:5	0	tol.	5	12	n.d.	2000	n.d.	1.10
3	100:1:5	0	tol.	8	15	n.d.	2400	n.d.	1.17
4	100:1:5	0	tol.	30	40	53	6200	8100	1.41
5	100:1:5	0	tol.	45	52	n.d.	8000	n.d.	1.41
6	100:1:5	0	tol.	60	60	71	9200	10800	1.49
7	100:1:5	0	tol.	90	71	82	10800	12500	1.63
8	100:1:5	0	tol.	150	84	n.d.	12800	n.d.	1.76
9	100:1:5	0	tol.	210	88	93	13400	14100	1.71
10	100:1:5	0	tol.	270	87	n.d.	13200	n.d.	n.d.

11	100:1:5	r.t.	tol.	2	10	n.d.	1700	n.d.	1.12
12	100:1:5	r.t.	tol.	5	18	n.d.	2900	n.d.	1.23
13	100:1:5	r.t.	tol.	8	27	37	4200	5700	1.22
14	100:1:5	r.t.	tol.	15	43	52	6600	8000	1.32
15	100:1:5	r.t.	tol.	30	62	67	9500	10200	1.43
16	100:1:5	r.t.	tol.	45	72	75	11000	11410	1.46
17	100:1:5	r.t.	tol.	60	77	78	11700	11900	1.44
18	100:1:5	r.t.	tol.	90	82	81	12500	12300	1.52
19	100:1:5	r.t.	tol.	150	85	86	12900	13100	1.58
20	100:1:5	r.t.	tol.	240	86	86	13100	13100	n.d.
21	100:1:5	r.t.	tol.	270	86	n.d.	13100	n.d.	1.60
22	100:1:5	-20	tol.	2	4	n.d.	800	n.d.	1.05
23	100:1:5	-20	tol.	5	6	n.d	1100	n.d	1.08
24	100:1:5	-20	tol.	8	9	n.d.	1500	n.d.	1.09
25	100:1:5	-20	tol.	15	13	n.d.	2100	n.d.	1.12
26	100:1:5	-20	tol.	30	23	n.d.	3600	n.d.	1.19
27	100:1:5	-20	tol.	45	31	34	4800	5300	n.d.
28	100:1:5	-20	tol.	60	38	53	5900	8100	1.29
29	100:1:5	-20	tol.	90	49	n.d.	7500	n.d.	1.37
30	100:1:5	-20	tol.	150	65	67	9900	10200	1.60
31	100:1:5	-20	tol.	240	79	79	12000	12000	1.65
32	100:1:5	-20	tol.	330	85	n.d.	12900	n.d.	1.75
33	100:1:5	-20	tol.	390	89	n.d.	13500	n.d.	1.83
34	100:1:5	-20	tol.	510	92	n.d.	14000	n.d.	1.81
35	100:1:5	-20	tol.	570	93	n.d.	14100	n.d.	1.89

Conv.[a]: monomer conversions were obtained from ^{31}P NMR spectra on aliquots taken from the polymerization mixtures. DP, M_n[a] were calculated from the monomer conversion obtained by ^{31}P

NMR spectroscopy. M_n [b] was calculated from the monomer to initiator ratio based on 1H NMR of the purified aliquots. Đ [c] was measured by SEC calibrated using PEG standards.

4.7.2 Kinetic studies with TU/DBU

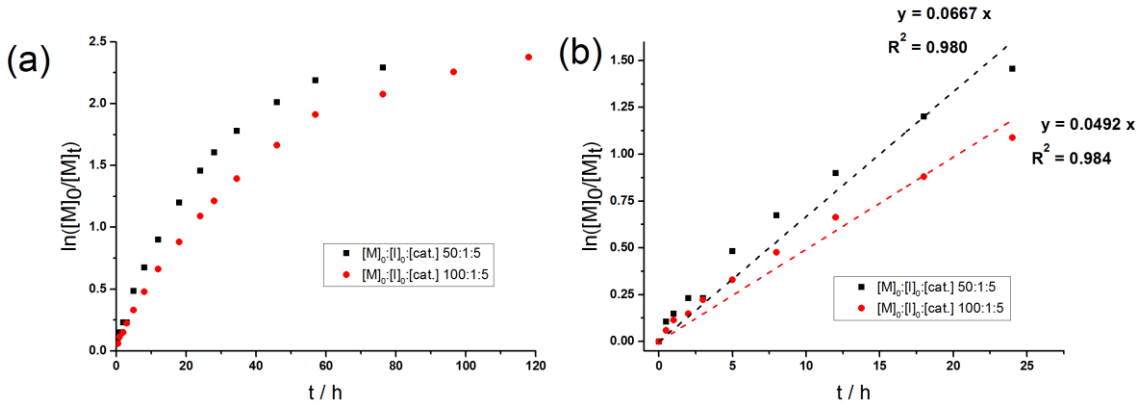

Figure 3.27. (a) Kinetic plots of ($\ln([M]_0/[M]_t)$) *vs* time obtained from ^{31}P NMR spectra for the polymerization of M1 with TU/DBU as catalyst system with different ratios of $[M]_0/[I]_0/[cat.]$ (data listed in Table 3.5). (b) Linear fit of the conversion ($\ln([M]_0/[M]_t)$) *vs* time.

Table 3.5. Kinetic data for the polymerization of M1 by organocatalytic ROP using 2-(benzyloxy) ethanol as initiator and a DBU/TU as catalyst with different ratios of $[M]_0/[I]_0/[cat.]$. Polymerizations were conducted at a monomer concentration of 2 mol L^{-1}.

#	$[M]_0$:$[I]_0$:[cat.]	T / °C	solvent	Time / h	Conv. [a] / %	DP[a]	M_n[a] / gmol^{-1}	M_n[b] / gmol^{-1}	Đ[c]
1	50:1:5	0	tol.	0.5	10	n.d.	900	n.d.	n.d.
2	50:1:5	0	tol.	1	14	n.d.	1200	n.d.	1.05
3	50:1:5	0	tol.	2	21	23	1800	3600	1.14
4	50:1:5	0	tol.	5	38	23	3000	3600	1.23
5	50:1:5	0	tol.	8	49	27	3900	4200	1.28
6	50:1:5	0	tol.	12	59	n.d.	4700	n.d.	1.35
7	50:1:5	0	tol.	18	70	n.d.	5400	n.d.	1.39
8	50:1:5	0	tol.	24	77	n.d.	6000	n.d.	1.45

9	50:1:5	0	tol.	28	80	39	6200	6000	1.45
10	50:1:5	0	tol.	34.5	83	n.d.	6500	n.d.	1.48
11	50:1:5	0	tol.	46	87	n.d.	6600	n.d.	1.48
12	50:1:5	0	tol.	57	89	n.d.	6900	n.d.	n.d.
13	50:1:5	0	tol.	76.25	90	n.d.	6900	n.d.	n.d.
14	100:1:5	0	tol.	0.5	6	n.d.	1100	n.d.	n.d.
15	100:1:5	0	tol.	1	11	n.d.	1800	n.d.	n.d.
16	100:1:5	0	tol.	2	14	n.d.	2300	n.d.	1.14
17	100:1:5	0	tol.	3	20	31	3200	4800	1.18
18	100:1:5	0	tol.	5	28	n.d.	4400	n.d.	1.29
19	100:1:5	0	tol.	8	38	n.d.	5900	n.d.	1.32
20	100:1:5	0	tol.	12	48	43	7400	6600	1.36
21	100:1:5	0	tol.	18	59	60	9000	9200	1.34
22	100:1:5	0	tol.	24	66	n.d.	10100	n.d.	1.45
23	100:1:5	0	tol.	28	70	n.d.	10700	n.d.	1.46
24	100:1:5	0	tol.	34.5	75	n.d.	11400	n.d.	1.50
25	100:1:5	0	tol.	46	81	80	12300	12200	1.55
26	100:1:5	0	tol.	57	85	n.d.	12900	n.d.	n.d.
27	100:1:5	0	tol.	76.25	87	n.d.	13200	n.d.	1.69
28	100:1:5	0	tol.	96.5	90	n.d.	13700	n.d.	1.67
29	100:1:5	0	tol.	118	91	n.d.	13800	n.d.	1.64

Conv.[a]: monomer conversions were obtained from 31P NMR spectra on aliquots taken from the polymerization mixtures. M_n[a] was calculated from the monomer conversion obtained by ^{31}P NMR spectroscopy. M_n[b] was calculated from the monomer to initiator ratio based on ^{1}H NMR of the purified aliquots. Đ[c] was measured by SEC calibrated using PEG standards.

4.7.3 Kinetic studies with Tris-Urea/DBU

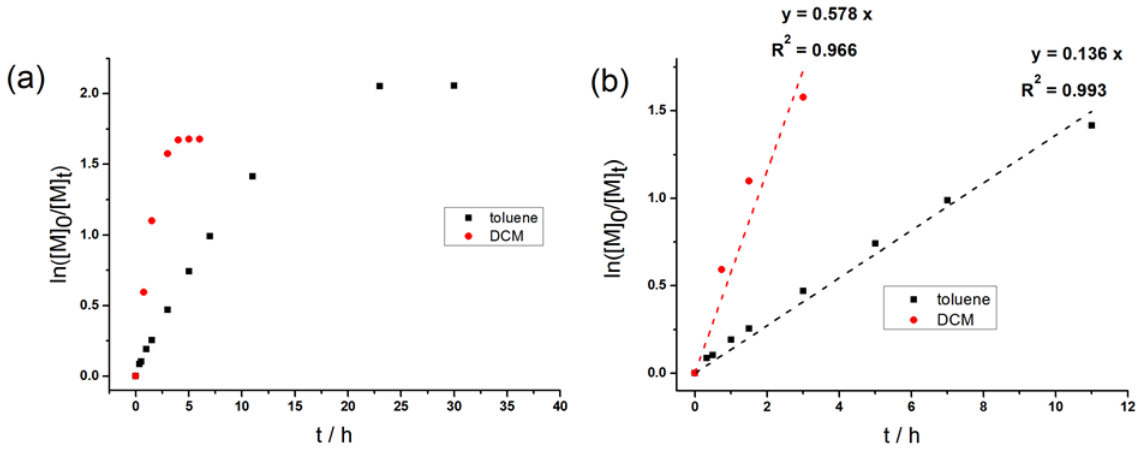

Figure 3.28. Kinetic plots of ($\ln([M]_0/[M]_t)$) *vs* time obtained from ^{31}P NMR spectra for the polymerization of M1 with Tris-Urea/DBU as catalyst system with different in different solvents (data listed in Table 3.6). (B) Linear fit of the conversion ($\ln([M]_0/[M]_t)$) *vs* time.

Table 3.6. Kinetic data for the polymerization of M1 by organo catalytic ROP using 2-(benzyloxy)ethanol as initiator and a DBU/TU as catalyst with different ratios of $[M]_0/[I]_0/[cat.]$

#	$[M]_0/[I]_0/[cat.]$	T / °C	solvent	Time / h	Conv. [a] / %	DP[a]	M_n[a] / gmol^{-1}	M_n[b] / gmol^{-1}	Đ[c]
1	100:1:2	0	tol	0.33	8	n.d.	1400	n.d.	n.d.
2	100:1:2	0	tol	0.5	10	n.d.	1700	n.d.	n.d.
3	100:1:2	0	tol	1	17	n.d.	2700	n.d.	n.d.
4	100:1:2	0	tol	1.5	22	n.d.	3500	n.d.	n.d.
5	100:1:2	0	tol	3	38	44	5900	6800	n.d.
6	100:1:2	0	tol	5	52	58	8000	8900	n.d.
7	100:1:2	0	tol	7	63	69	9600	10500	1.36
8	100:1:2	0	tol	11	76	79	11600	12000	1.33
9	100:1:2	0	tol	23	87	87	13200	13200	1.40
10	100:1:2	0	tol	30	87	n.d.	13200	n.d.	1.40

11	100:1:2	0	DCM	0.75	45	52	6900	8000	1.26
12	100:1:2	0	DCM	1.5	67	71	10200	10810	1.46
13	100:1:2	0	DCM	3	79	77	12000	11700	1.53
14	100:1:2	0	DCM	4	81	78	12300	11900	1.53
15	100:1:2	0	DCM	5	81	n.d.	12300	n.d.	1.38
16	100:1:2	0	DCM	6	81	81	12300	12300	1.44
17	170:1:2	0	tol.	14.5	63	n.d.	9600	n.d.	n.d.
18	170:1:2	0	tol.	20	73	147	18800	22200	n.d.
19	170:1:2	0	tol.	26.5	82	150	21200	22700	n.d.
20	170:1:2	0	tol.	38.5	88	166	22700	25100	1.56

Conv.[a]: monomer conversions were obtained from ^{31}P NMR spectra on aliquots taken from the polymerization mixtures. M_n[a] was calculated from the monomer conversion obtained by ^{31}P NMR spectroscopy. M_n[b] was calculated from the monomer to initiator ratio based on ^{1}H NMR of the purified aliquots. Đ[c] was measured by SEC calibrated using PEG standards.

4.8 Kinetic studies for the polymerization of M2

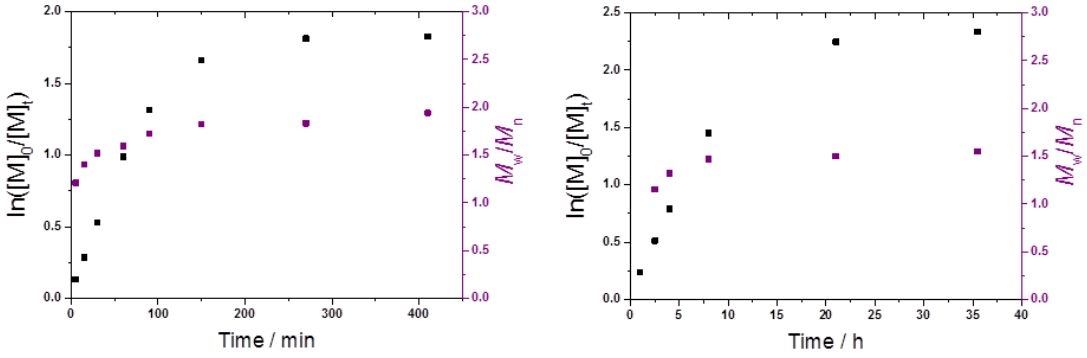

Figure 3.29. Plots of monomer conversion ($\ln([M]_0/[M]_t)$) *vs* time obtained from ^{31}P NMR spectra for the polymerization of M2 with TBD (A) and DBU/Tris-Urea (B). The ratio of monomer : initiator : catalyst was 100 : 1 : 5 for (A) and 100 : 1 : 4 for (B).

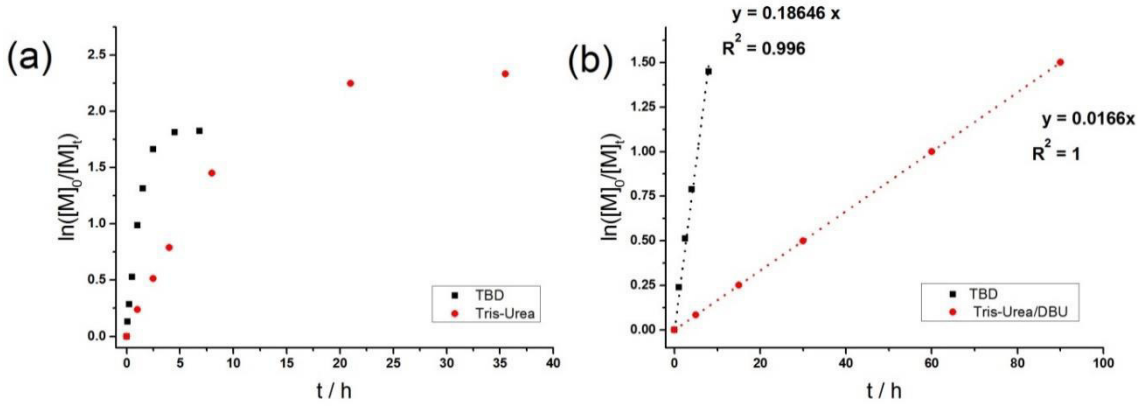

Figure 3.30. Kinetic plots of ($\ln([M]_0/[M]_t)$) *vs* time obtained from ^{31}P NMR spectra for the polymerization of M2 with Tris-Urea/DBU and TBD as catalyst. The ratio of monomer : initiator : catalyst was 100 : 1 : 5 for the polymerization with TBD and 100:1:4 for the polymerization with Tris-Urea/DBU (data listed in Table 3.7). (b) Linear fit of the conversion ($\ln([M]_0/[M]_t)$) *vs* time.

Table 3.7. Kinetic data for the polymerization of M2 by organo catalytic ROP using 2-(benzyloxy)ethanol as initiator.

#	cat	$[M]_0$:$[I]_0$:[cat]	T / °C	solvent	Time / h	Conv.[a] / %	DP[a]	M_n[a] /gmol^{-1}	M_n[b] / gmol^{-1}	Đ[c]
1	TrisU/DBU	100:1:4	0	tol.	1	21	n.d.	3900	n.d.	n.d.
2	TrisU/DBU	100:1:4	0	tol.	2,5	40	n.d.	7300	n.d.	1.15
3	TrisU/DBU	100:1:4	0	tol.	4	55	n.d.	10000	n.d.	1.32
4	TrisU/DBU	100:1:4	0	tol.	8	77	n.d.	13900	n.d.	1.47
5	TrisU/DBU	100:1:4	0	tol.	21	90	94	16200	16900	1.50
6	TBD	100:1:5	0	DCM	0.08	12	n.d.	2300	n.d.	1.21
7	TBD	100:1:5	0	DCM	0.25	25	n.d.	4600	n.d.	1.40
8	TBD	100:1:5	0	DCM	0.5	41	48	7500	8700	1.52
9	TBD	100:1:5	0	DCM	1	63	60	11400	10800	1.59
10	TBD	100:1:5	0	DCM	1.5	73	68	13200	12300	1.82
11	TBD	100:1:5	0	DCM	2.5	84	86	15100	15500	1.83
12	TBD	100:1:5	0	DCM	6.8	84	86	15100	15500	1.94

Conv.[a]: monomer conversions were obtained from ^{31}P NMR spectra on aliquots taken from the polymerization mixtures. M_n[a] was calculated from the monomer conversion obtained by ^{31}P NMR spectroscopy. M_n[b] was calculated from the monomer to initiator ratio based on ^{1}H NMR of the purified aliquots. Đ[c] was measured by SEC calibrated using PEG standards.

4.9 Degradation studies

Degradation studies were conducted in NMR tubes and followed by ^{1}H and ^{31}P NMR spectroscopy. For the degradation at pH 12 a 0.01 M KOH solution was prepared containing 10% D_2O. The polymer (3.5 mg) was dissolved in 0.7 mL 0.01 M KOH and incubated at r.t.

For the degradation at pH 1 a 0.1 M HCl solution was prepared containing 10% D_2O and 3.5 mg of polymer were incubated in 0.7 mL at r.t.

The degradation at pH 10 was conducted in 0.15 M $Na_2B_4O_7$/NaOH buffer. 3.5 mg of polymer were incubated in 0.7 mL buffer at r.t.

4.9.1 Degradation of P(1) at pH 1

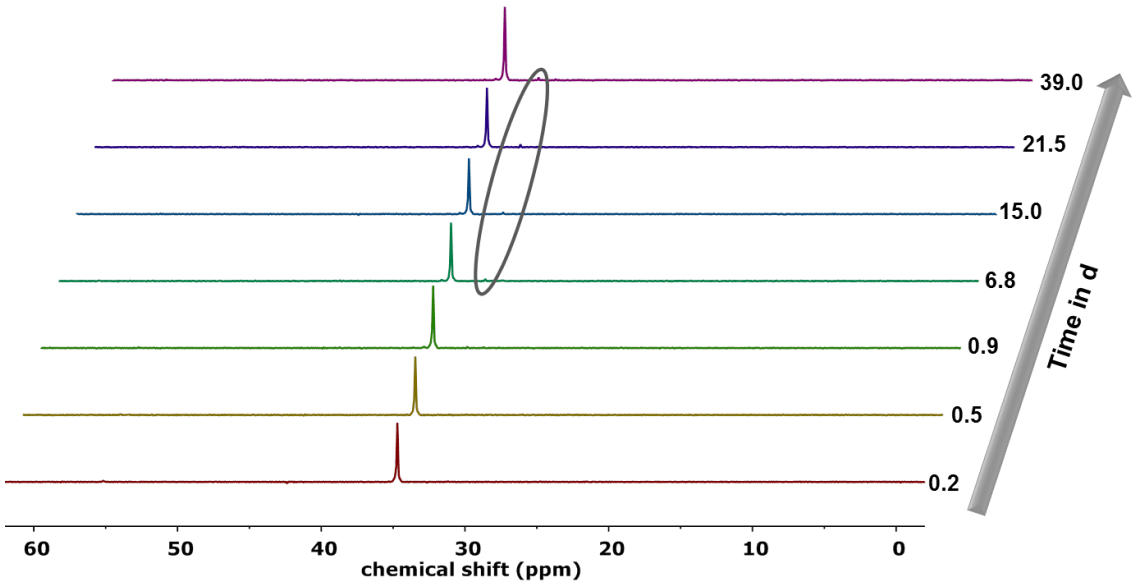

Figure 3.31. ^{31}P NMR spectra (H_2O/ D2O (9:1), 121 MHz, 298K) of the degradation of P(1)-4 at pH 1 at different time points. After 6 days the evolution of a signal at 32.36 ppm indicates starting degradation.

4.9.2 Degradation of P(1) at pH 12

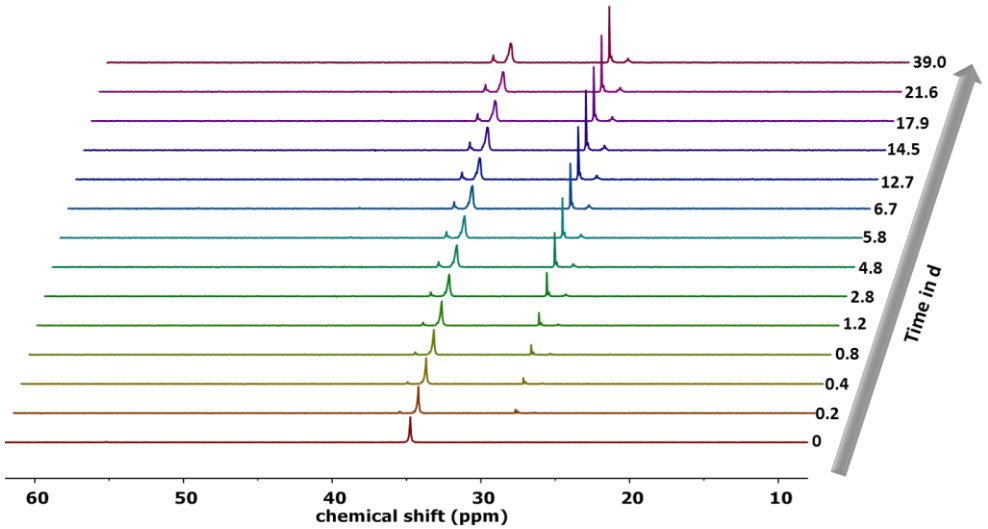

Figure 3.32. Overlay of the ^{31}P NMR spectra (H_2O/ D2O (9:1), 121 MHz, 298K) during the degradation of P(1)-4 at pH 12 at different time points.

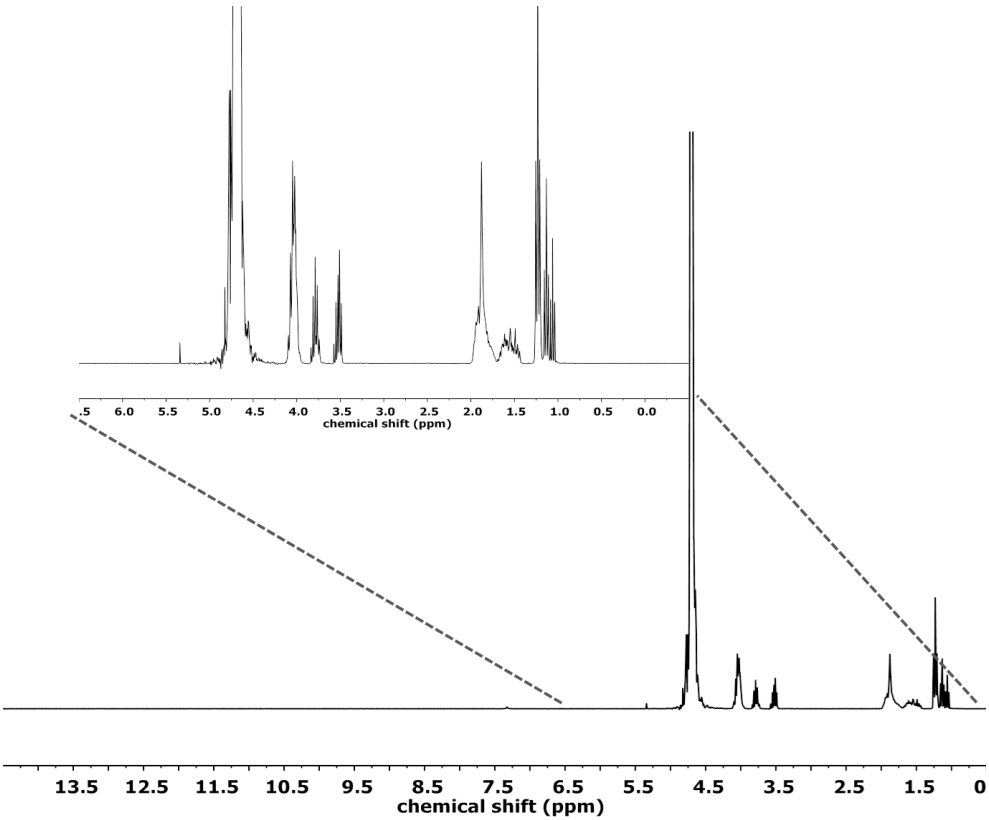

Figure 3.33. ^{1}H NMR spectrum (300MHz) of the degradation of P(1)-4 after 39 days in D_2O at 298K.

4.10 Degradation of P(3) at pH 10

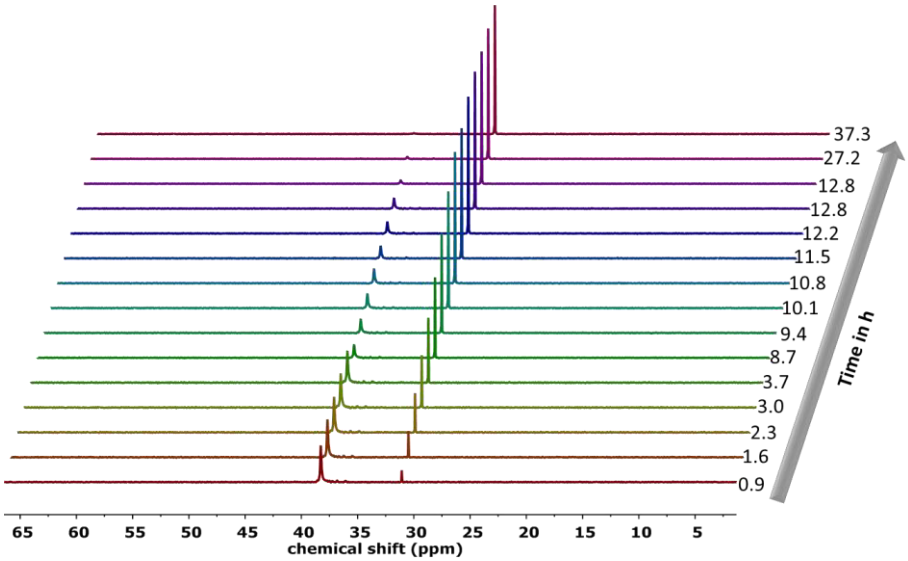

Figure 3.34. ^{31}P NMR spectra (H_2O/ D2O (9:1), 121 MHz 298K) of the degradation of polymer P(3) at pH 10

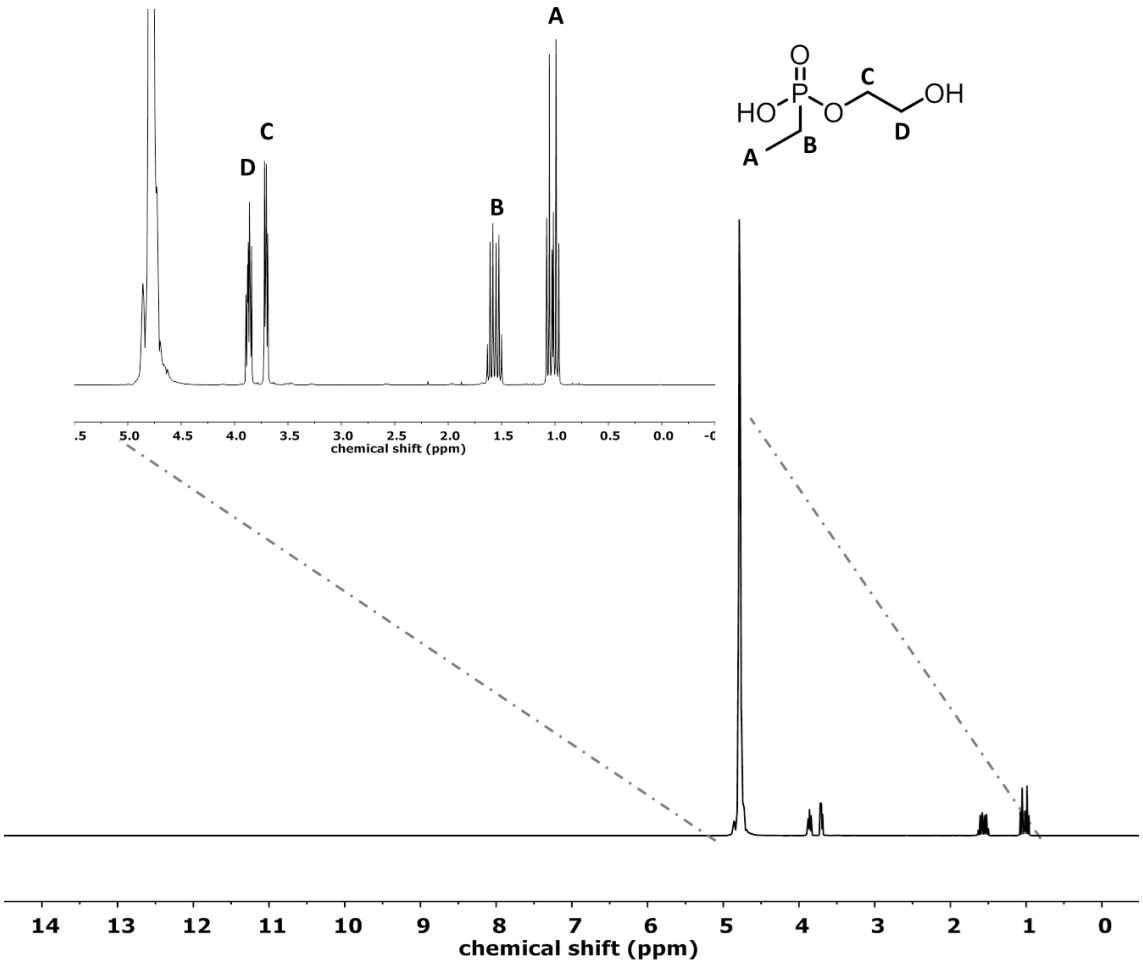

Figure 3.35. ^{1}H NMR spectrum (300MHz) of the final breakdown product of P(3) at pH 10 in D_2O at 298K

4.11 Monomer stability in D_2O

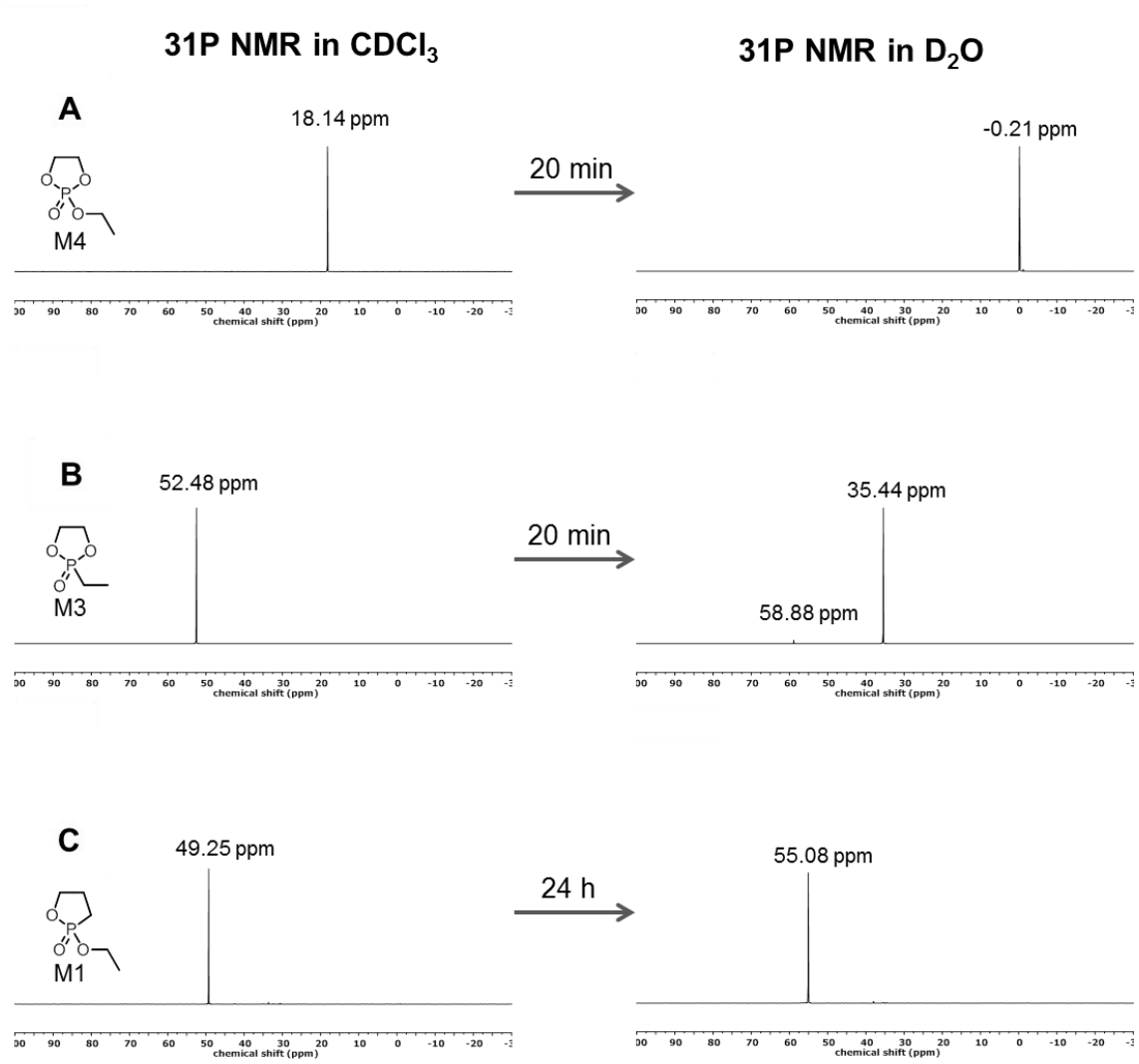

Figure 3.36: ^{31}P NMRs M4 (A), M3 (B), M1(C) in $CDCl_3$ and D_2O MHz

5 References

1. Steinbach, T.; Wurm, F. R., Poly(phosphoester)s: A New Platform for Degradable Polymers. *Angewandte Chemie International Edition* **2015,** *54* (21), 6098-6108.
2. Bauer, K. N.; Tee, H. T.; Velencoso, M. M.; Wurm, F. R., Main-chain poly(phosphoester)s: History, syntheses, degradation, bio-and flame-retardant applications. *Progress in Polymer Science*.
3. Du, J.-Z.; Du, X.-J.; Mao, C.-Q.; Wang, J., Tailor-Made Dual pH-Sensitive Polymer–Doxorubicin Nanoparticles for Efficient Anticancer Drug Delivery. *Journal of the American Chemical Society* **2011,** *133* (44), 17560-17563.
4. Mao, C.-Q.; Du, J.-Z.; Sun, T.-M.; Yao, Y.-D.; Zhang, P.-Z.; Song, E.-W.; Wang, J., A biodegradable amphiphilic and cationic triblock copolymer for the delivery of siRNA targeting the acid ceramidase gene for cancer therapy. *Biomaterials* **2011,** *32* (11), 3124-3133.
5. Sun, T.-M.; Du, J.-Z.; Yao, Y.-D.; Mao, C.-Q.; Dou, S.; Huang, S.-Y.; Zhang, P.-Z.; Leong, K. W.; Song, E.-W.; Wang, J., Simultaneous Delivery of siRNA and Paclitaxel via a "Two-in-One" Micelleplex Promotes Synergistic Tumor Suppression. *ACS Nano* **2011,** *5* (2), 1483-1494.
6. Schöttler, S.; Becker, G.; Winzen, S.; Steinbach, T.; Mohr, K.; Landfester, K.; Mailänder, V.; Wurm, F. R., Protein adsorption is required for stealth effect of poly (ethylene glycol)-and poly (phosphoester)-coated nanocarriers. *Nature nanotechnology* **2016,** *11* (4), 372-377.
7. Müller, J.; Bauer, K. N.; Prozeller, D.; Simon, J.; Mailänder, V.; Wurm, F. R.; Winzen, S.; Landfester, K., Coating nanoparticles with tunable surfactants facilitates control over the protein corona. *Biomaterials* **2017,** *115*, 1-8.
8. Steinmann, M.; Wagner, M.; Wurm, F. R., Poly(phosphorodiamidate)s by Olefin Metathesis Polymerization with Precise Degradation. *Chemistry – A European Journal* **2016,** *22* (48), 17329-17338.
9. Wang, H.; Su, L.; Li, R.; Zhang, S.; Fan, J.; Zhang, F.; Nguyen, T. P.; Wooley, K. L., Polyphosphoramidates That Undergo Acid-Triggered Backbone Degradation. *ACS Macro Letters* **2017,** *6* (3), 219-223.
10. Wolf, T.; Steinbach, T.; Wurm, F. R., A Library of Well-Defined and Water-Soluble Poly(alkyl phosphonate)s with Adjustable Hydrolysis. *Macromolecules* **2015**.
11. Horsman, G. P.; Zechel, D. L., Phosphonate Biochemistry. *Chemical Reviews* **2017,** *117* (8), 5704-5783.
12. Ogawa, T.; Nushimatsu, T.; Minoura, Y., Condensation polymerization of P-phenylphosphonic dichloride with diamines. *Die Makromolekulare Chemie* **1968,** *114* (1), 275-283.
13. Pretula, J.; Kaluzynski, K.; Szymanski, R.; Penczek, S., Preparation of Poly(alkylene H-phosphonate)s and Their Derivatives by Polycondensation of Diphenyl H-Phosphonate with Diols and Subsequent Transformations. *Macromolecules* **1997,** *30* (26), 8172-8176.
14. Pretula, J.; Kaluzynski, K.; Szymanski, R.; Penczek, S., Transesterification of oligomeric dialkyl phosphonates, leading to the high-molecular-weight poly-H-phosphonates. *Journal of Polymer Science Part A: Polymer Chemistry* **1999,** *37* (9), 1365-1381.
15. Bauer, K. N.; Tee, H. T.; Lieberwirth, I.; Wurm, F. R., In-Chain Poly(phosphonate)s via Acyclic Diene Metathesis Polycondensation. *Macromolecules* **2016,** *49* (10), 3761-3768.
16. Steinbach, T.; Ritz, S.; Wurm, F. R., Water-Soluble Poly(phosphonate)s via Living Ring-Opening Polymerization. *ACS Macro Letters* **2014,** *3* (3), 244-248.
17. Stoianova, D. S.; Hanson, P. R., A Ring-Closing Metathesis Strategy to Phosphonosugars. *Organic Letters* **2001,** *3* (21), 3285-3288.

18. Roy, R., *Glycomimetics: Modern Synthetic Methodologies*. American Chemical Society: 2005; Vol. 896, p 206.
19. Hanessian, S.; Galéotti, N.; Rosen, P.; Oliva, G.; Babu, S., Synthesis of carbohydrate phostones as potential glycomimetics. *Bioorganic & Medicinal Chemistry Letters* **1994,** *4* (23), 2763-2768.
20. Phosphonic acid phostones. Google Patents: 1960.
21. Ragulin, V., ω-haloalkylphosphoryl compounds: Synthesis and properties. *Russian Journal of General Chemistry* **2012,** *82* (12).
22. Tsao, Y.-Y. T.; Wooley, K. L., Synthetic, Functional Thymidine-Derived Polydeoxyribonucleotide Analogues from a Six-Membered Cyclic Phosphoester. *Journal of the American Chemical Society* **2017,** *139* (15), 5467-5473.
23. Bach, R. D.; Dmitrenko, O., Strain Energy of Small Ring Hydrocarbons. Influence of C−H Bond Dissociation Energies. *Journal of the American Chemical Society* **2004,** *126* (13), 4444-4452.
24. Wolf, T.; Rheinberger, T.; Wurm, F. R., Thermoresponsive coacervate formation of random poly(phosphonate) terpolymers. *European Polymer Journal* **2017**.
25. Clément, B.; Grignard, B.; Koole, L.; Jérôme, C.; Lecomte, P., Metal-Free Strategies for the Synthesis of Functional and Well-Defined Polyphosphoesters. *Macromolecules* **2012,** *45* (11), 4476-4486.
26. Fastnacht, K. V.; Spink, S. S.; Dharmaratne, N. U.; Pothupitiya, J. U.; Datta, P. P.; Kiesewetter, E. T.; Kiesewetter, M. K., Bis- and Tris-Urea H-Bond Donors for Ring-Opening Polymerization: Unprecedented Activity and Control from an Organocatalyst. *ACS Macro Letters* **2016,** *5* (8), 982-986.
27. K., M. E.; P., S. M., An expanded range of catalysts for synthesising biodegradable polyphosphonates. *Green Materials* **2016,** *4* (2), 81-88.
28. Kim, K.; Tsay, O. G.; Atwood, D. A.; Churchill, D. G., Destruction and Detection of Chemical Warfare Agents. *Chemical Reviews* **2011,** *111* (9), 5345-5403.
29. Eddleston, M.; Buckley, N. A.; Eyer, P.; Dawson, A. H., Management of acute organophosphorus pesticide poisoning. *The Lancet* **2008,** *371* (9612), 597-607.
30. Baran, J.; Penczek, S., Hydrolysis of polyesters of phosphoric acid. 1. Kinetics and the pH profile. *Macromolecules* **1995,** *28* (15), 5167-5176.
31. Du, J.-Z.; Sun, T.-M.; Weng, S.-Q.; Chen, X.-S.; Wang, J., Synthesis and characterization of photo-cross-linked hydrogels based on biodegradable polyphosphoesters and poly (ethylene glycol) copolymers. *Biomacromolecules* **2007,** *8* (11), 3375-3381.
32. Berry, M. T.; Castrejon, D.; Hein, J. E., Oxidative Esterification of Aldehydes Using Mesoionic 1,2,3-Triazolyl Carbene Organocatalysts. *Organic Letters* **2014,** *16* (14), 3676-3679.
33. Atwood, D. A.; Hill, M. S.; Jegier, J. A.; Rutherford, D., The Use of Five-Coordinate Aluminum Alkyls To Prepare Molecules Containing a Single Al−O−Si Linkage. *Organometallics* **1997,** *16* (12), 2659-2664.

Chapter 4

Polyphosphoester stealth surfactants: A general strategy to control the protein corona and the fate of nanocarriers

Foreword

The following project was accomplished in cooperation with Johanna Simon[1], who did the biological evaluation of the prepared nanoparticle dispersions.
Protein structures depicted in the graphic below were obtained as free download from RCSB Protein Data Bank and are based on reference 1 for fibrinogen and on reference 2 for albumin.

[1]*Max Planck Institute for Polymer Research, Ackermannweg 10, 55128 Mainz, Germany*

Abstract

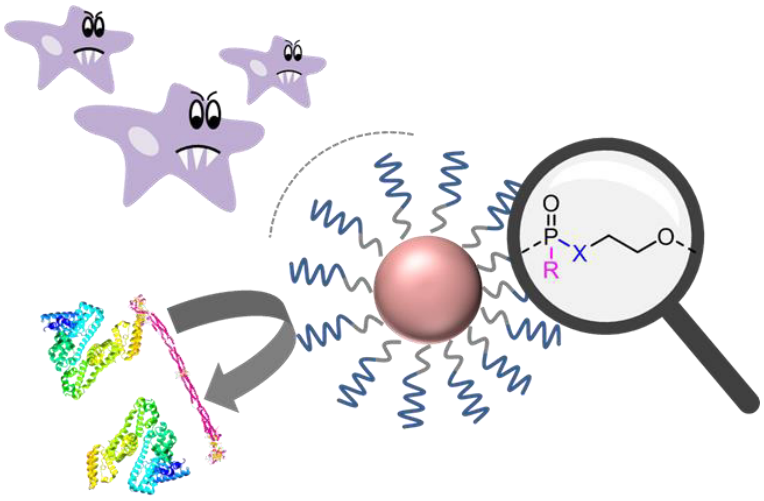

Nanoparticles with long blood circulation times are crucial for efficient drug delivery. A critical parameter for the circulation time is the so-called protein 'corona', which forms upon exposure to biological fluids by physical adsorption of proteins. An unspecific adsorption of proteins leads to an enhanced recognition by cells of the immune system and to decreased blood circulation times. The typical approach to meet this problem is the decoration of the nanocarrier surface with polymer chains. Herein, the non-covalent adsorption of structurally diverse PPE-surfactants

is exploited to prepare stealth nanocarriers and to tailor their protein corona. Four PPE-surfactants exhibiting different binding patterns around the central phosphorus atom of each repeat unit were prepared and assembled on the surface of nanocarriers consisting of different materials, i.e. polystyrene, poly(methyl methacrylate) and human serum albumin. The surfactant coated nanocarriers were evaluated with regard to their protein corona composition and cellular uptake against murine macrophages. The prepared PPE-surfactants were investigated in detail concerning their biocompatibility and hydrolytic degradation under basic conditions.

1 Introduction

The intended use of nanomaterials as drug carriers requires precise control of their biological 'fate' after administration. A long blood circulation time of the nanomaterials is crucial for an efficient targeted delivery.[3] A critical parameter for the circulation time is the so-called protein 'corona', which forms immediately around the nanocarrier upon exposure to biological fluids by physical adsorption of proteins.[4] An unspecific adsorption of proteins leads to an enhanced recognition by cells of the immune system thus leading to enhanced blood clearance and lower blood circulation times.[5] The typical approach to meet this problem is the decoration of the nanocarrier surface with polymer chains, typically poly(ethylene glycol) (PEG).[6] It is thought that PEG can reduce the protein adsorption, which lowers the recognition of the nanocarriers by immune cells and thus prolongs their blood circulation time.[7] Prolongation of the blood circulation by reducing the amount of unspecific protein adsorption is known as the 'stealth effect'.[8]

However, since PEG is non-biodegradable, accumulation has been reported causing unpredictable risks.[9-10] The use of biodegradable polymers can meet the problem of unwanted accumulation. Polyphosphoesters (PPE) are a class of biodegradable polymers, which are especially appealing as alternatives to PEG since they are not only biodegradable but also provide the possibility of precisely tailored characteristics due to the pentavalency of the phosphorus atom.[11-12] Recently, poly(phosphoester)s were identified to induce a similar stealth effect as PEG.[13] In recent studies, the PPE- or PEG-chains were covalently attached to the nanocarrier. The covalent attachment of such water-soluble polymers to the nanoparticles surface was achieved via grafting-to techniques of suitable end functionalized polymers. However, the covalent attachment of polymer chains to the nanocarrier surface requires careful preparation in order to retain the stability of the dispersion and achieve a high grafting density.

More importantly, every nanocarrier requires a tailored strategy for its surface modification, depending on the functional groups on the surface.

Recently, first experiments demonstrated that polystyrene nanoparticles stabilized with PPE-surfactants exhibited a similar protein corona compared to the polystyrene nanoparticles modified by covalent attachment of PPEs.[3]

Herein, we exploit the non-covalent adsorption of a library of structurally diverse PPE-surfactants to prepare stealth nanocarriers. The non-covalently modified nanocarriers were analyzed with regard to their cellular uptake against murine macrophages and the composition of their protein corona. Macrophages are cells of the immune system and responsible for the detection and efficient clearing of foreign molecules from the blood. For nanoparticles, therefore, it is important to be well-camouflaged against the recognition by macrophages to avoid rapid blood clearance. Importantly, this strategy should allow the camouflage of basically any nanocarrier, which is demonstrated here with PS, PMMA, and HSA as the carrier materials. Furthermore, the PPE platform allows the synthesis of hydrophilic polymers with striking different properties, regarding degradation rates and products. Different PPE-surfactants were used to influence the composition of the protein corona and control the stability of the PPEs. Surfactant is an acronym for *surface active agent* and literally means active at surfaces.[14] Here, they act to reduce and control the protein adsorption from human blood plasma on nanocarriers. Surfactants adsorb on hydrophobic surfaces from aqueous solutions via hydrophobic interactions. In case of the nanoparticle coating, the hydrophobic part of the surfactant (long alkyl chain) adsorbs to the particle surface while the hydrophilic part is extended into the aqueous surrounding producing a hydrophilic particle surface by a simple means.

2 Results & Discussion

Surfactant Preparation. Four different nonionic poly(phosphoester)-surfactants were prepared and were assembled on the surface of different polymer nanoparticles. The surfactants were prepared in a single step by the anionic ring-opening polymerization (ROP) of different cyclic phosphoester monomers (producing water-soluble polymers), initiated by octadecanol as the hydrophobic tail. The PPE surfactants differ in their hydrophilic part, exactly in the binding pattern around the central phosphorus atom of each repeating unit (Scheme 4.1). Here, the synthesized PPEs belong to two different PPE-subclasses, i.e. the poly(phosphate)s (Scheme 4.1, **S1** and **S4**) and the poly(phospho*n*ate)s while it has to be distinguished between *in-chain* (Scheme 4.1, **S2**) and *side-chain* poly(phosphonate)s (Scheme 4.1, **S3**). The different binding

motifs influence the hydrophilicity/hydrophobicity of the PPEs and especially influence the degradation behavior dramatically.[15-16] In this study, the influence of the different binding patterns on the surfactant properties is evaluated in detail concerning their stabilizing ability, toxicity, protein interaction, stealth and degradation behavior and compared to the well-established Lutensol® AT50.

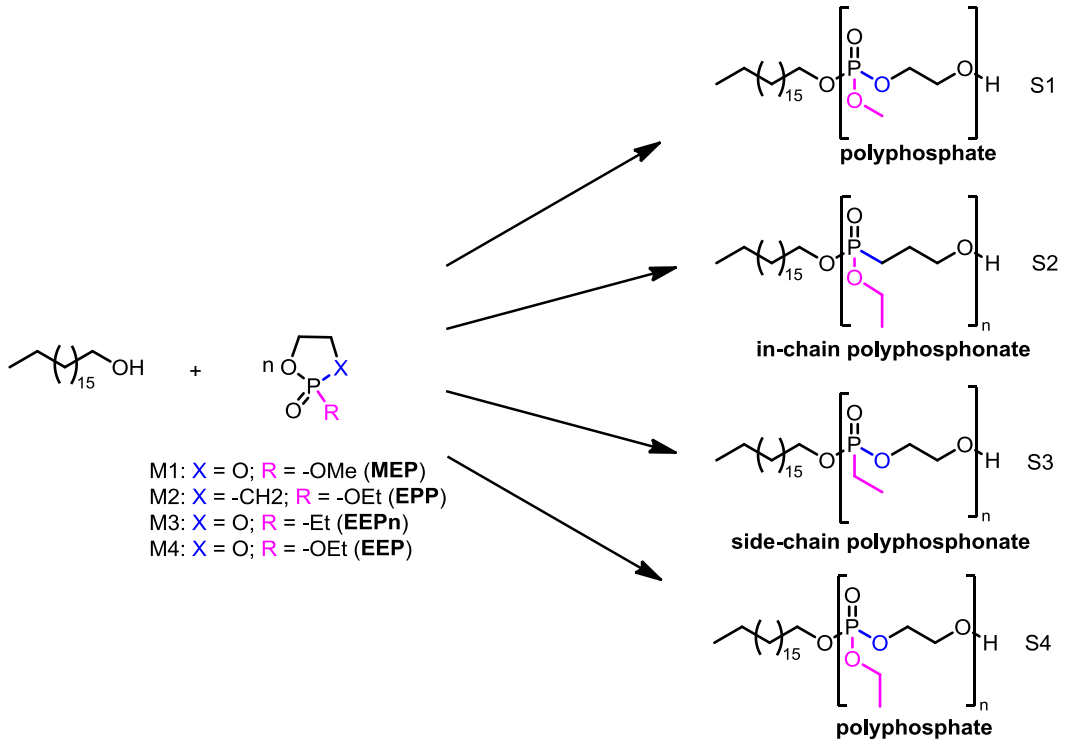

Scheme 4.1. General scheme for the synthesis of polyphosphoester-surfactants with different binding motifs.

5-membered cyclic phosphates, phosphonates and phostones are the monomers used herein. In case of the cyclic phosphates, two different monomers were used one carrying a methyl ester (MEP) and the other one an ethyl ester (EEP) as pendant chain. Polymers of EEP have been used previously for the covalent surface modification of polystyrene nanoparticles and were the first polymers to demonstrate the stealth properties of PPEs. However, surfactant **S4** prepared from EEP exhibited a temperature dependent solubility in water and PBS, due to the C_{18}- tail. Especially the cloud point of the surfactants in PBS is pertinent since it has a similar ionic strength as cell culture medium used for all cellular uptake studies performed within this study. In PBS, a cloud point for **S4** of T_{cp}= 29 °C (Figure 4.33) was determined that is below the

physiological temperature of 37 °C. For cellular experiments, lower critical solution temperatures (LCST) above 37 °C are needed to prevent precipitation of the surfactant. In order to increase the hydrophilicity of the polyphosphate 'head', MEP was used. Due to its more hydrophilic pendant chain it was supposed to show no or at least a higher LCST compared to PEEP-surfactants. Indeed, temperature dependent turbidity measurements showed no precipitation of **S1** upon heating (**Figure 4.**32). The usage of phostones - cyclic phosphonates with the stable P-C-bond within the ring-structure - as monomers for the synthesis of PPEs was established in the course of this dissertation. The prepared polymers were found to be highly water-soluble up to concentration of at least 10 g L^{-1} and thus are potentially suitable for biomedical applications. Furthermore, the changed backbone structure in the PEPP-polymers avoids the potential release of toxic ethylene glycol upon degradation. We also prepared side-chain phosphonates recently which exhibit faster kinetics compared to the other two PPE-classes: 2-ethyl-1,2-oxaphospholane 2-oxide (EEPn) was used herein as representative of the phosphonates.

All monomers were polymerized via organocatalytic ROP. Polymerizations of the cyclic phosphates and the phostone were conducted using a combination of 1,8-diazabicyclo[5.4.0]undec-7-ene (DBU) and N-cyclohexyl-N′- (3,5-bis(trifluoromethyl)phenyl)thiourea (TU) as the catalyst. Polymerizations were initiated at 5 °C to avoid initiator precipitation and were subsequently cooled down to 0 °C. For the phosphates and the phostone molecular weight distributions of Đ ≈ 1.2-1.5 were obtained. In contrast, polymerization of the phosphonate EEPn was carried out at ambient temperature over a period of 17 h using DBU as single catalyst yielding polymers with narrow molecular weight distributions (Đ ≈ 1.10). Typically, polymerizations of phosphonates lead to narrow molecular weight distributions due to stable P-C-bond in the pendant chain avoiding a high amount of transesterfication. All surfactants were purified by precipitation from diethyl ether and subsequent dialysis against water. Molecular weight distributions of the surfactants were determined by size exclusion chromatography (SEC) while ^{1}H NMR spectroscopy (Figure 4.1) was used to determine the number of repeat units.

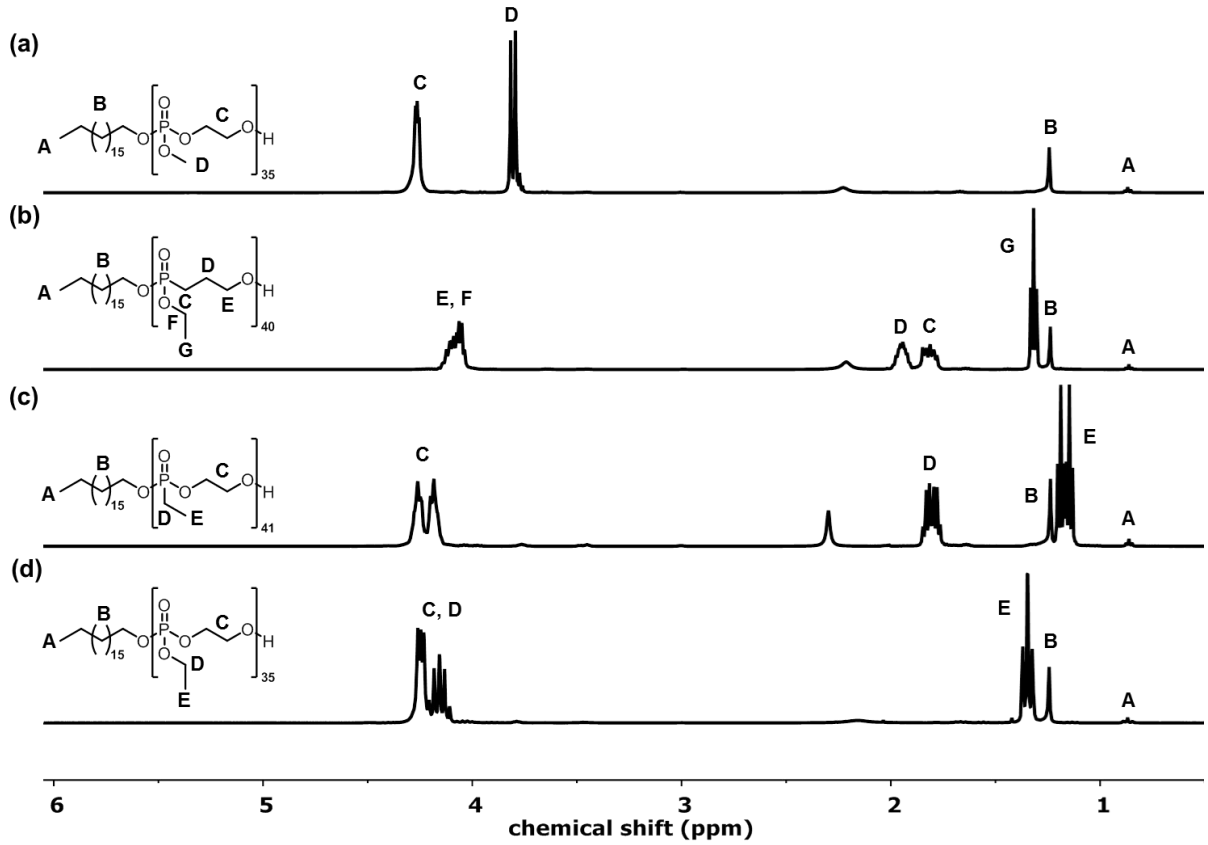

Figure 4.1. ^{1}H NMRs of the surfactants 1-4. (a) ^{1}H NMR of S1 (500 MHz, $CDCl_3$, 298 K). (b) ^{1}H NMR of S2 (500 MHz, $CDCl_3$, 298 K). (c) ^{1}H NMR of S3 (500 MHz, $CDCl_3$, 298 K). (a) ^{1}H NMR of S4 (300 MHz, $CDCl_3$, 298 K).

The number of repeat units was determined by comparison of the integration of the initiator signals with signals that can be ascribed to the PPE part. The initiator shows a characteristic triplet at 0.86 ppm (Figure 4.1) that can be ascribed to the terminal methyl group and was thus normalized to three. For the determination of the amount of repeat units, this signal was compared with distinct resonances for the PPE-part. For **S1** (Figure 4.1(a)) the signal at 3.81 ppm was used which belongs to the pendant methoxy group. For **S2** (Figure 4.1 (b)) the signal at 1.32 ppm, which belongs to the methyl group in the pendant chain and the analogous signal at 1.34 ppm was used for **S4** (Figure 4.1(d)). The repeat units in **S3** (Figure 4.1 (c)) were determined by comparison of the initiator signals with the signal at ppm that can be attributed to the methylene group in the pendant chain adjacent to the phosphorus atom. Table 4.1 provides an overview over the properties of the prepared PPE-surfactants. The critical micelle concentrations (CMC) of the PPE-surfactants were determined by ring-tensiometry and were in

the range between 4.2 and 5.8 µmol L^{-1}. Thus, the determined CMCs are in the same order like the CMC of Lutensol® AT50. Surface tensions above the CMC were found to be in the range between 37 and 45 mN m^{-1}.

Table 4.1. Overview over synthesized surfactants

Surfactant	Monomer	Repeat Units[a]	M_n[a] / gmol^{-1}	CMC[b] / µmol L^{-1}	γ / mN m^{-1}
S1	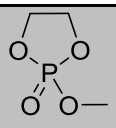	35	5100	5.3 ± 1.8	44[b]
S2	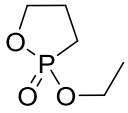	40	6300	4.8 ± 0.9	37[b]
S3	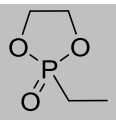	41	5850	5.8 ± 1.5	45[b]
S4	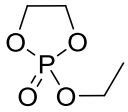	35	5600	4.2 ± 1.3	44[b]
Lutensol® AT50[c]		50	2500	2.5	48[c]

[a]: Determined by ^{1}H NMR spectroscopy. [b]: Determined by ring tensiometry. [c]: surface tension for c=1 gL^{-1} (data was retrieved from the data sheet provided by BASF).

The aim of this project was the modification of polymeric nanoparticles with the prepared PPE-surfactants to prolong their blood circulation time for potential *in vivo* applications. However, for polymers used in biomedical applications it is necessary to show no toxic side effects. Surfactants are known to target effectively cell membranes leading to membrane damage and in the worst case to cell lysis.[17-18] In general, their cytotoxicity is dependent on the nature and the structure of the surfactant and it was found that nonionic surfactants show the least cytotoxicity in the order as cationic > anionic > zwitterionic > nonionic.[19] However, the cytotoxicity of the

prepared PPE-surfactants **S1-S4** was evaluated *in vitro* against murine macrophages (RAW 264.7) and compared to the commercial surfactants, Lutensol® AT50 and SDS (Figure 4.2). Macrophages were used to evaluate the cytotoxicity of the prepared surfactants since they were used for all following cellular uptake studies. The cells were incubated for 12 h at 37 °C with the surfactants at concentrations ranging from 1.88 to 240 µmol L^{-1}. The results of the toxicity test are depicted in Figure 4.2.

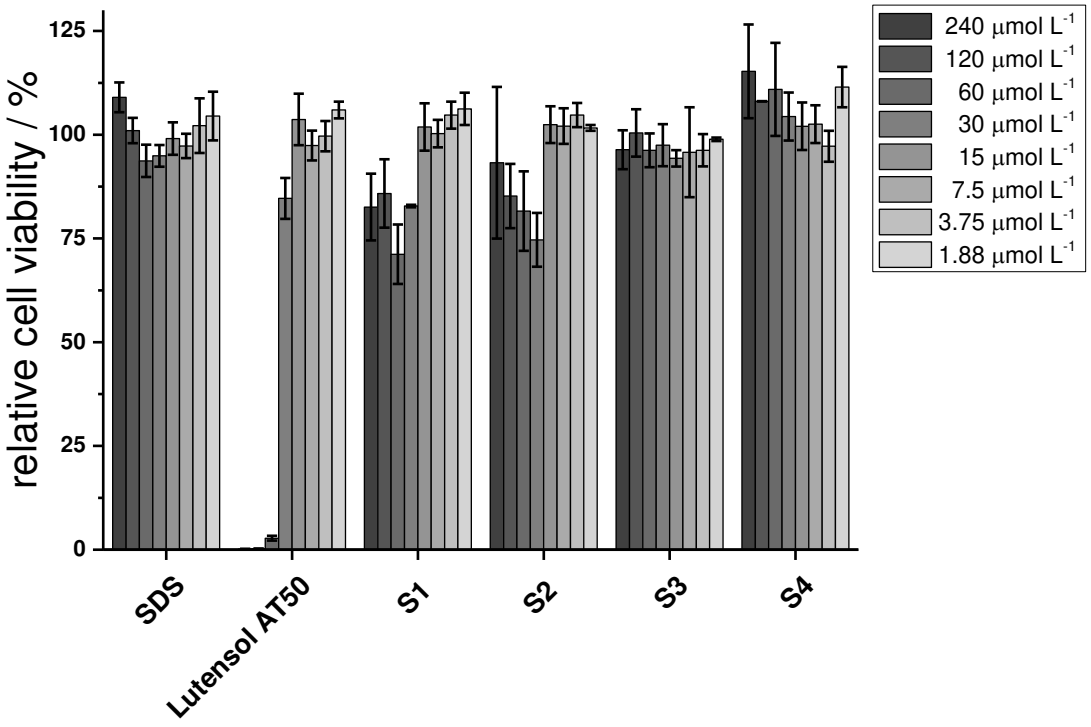

Figure 4.2. In vitro cell-viability assay of RAW 264.7 cells treated with surfactants S1-4, SDS and Lutensol® AT50 after 12 h of incubation. The experiments were carried out as three independent replicates. (*Experiments depicted in this figure were conducted by Johanna Simon.*)

For SDS no cytotoxic effects were observed in the evaluated concentration range. This observation is probably due to the fact that the considered concentrations are below the critical micelle concentration of SDS which amounts to 7-10 mmol L^{-1}. In contrast, Lutensol® AT50 showed the highest cytotoxicity of the evaluated surfactants. Lutensol® AT50 has a low CMC of 2.5 µmol L^{-1} which is exceeded by far in the conducted test. The low cell viabilities for the highest concentrations were expected since it is known, that surfactants far above their CMC can

induce cell lysis.[20] At high concentrations of 240 - 60 µmol L^{-1} nearly entire cell death was observed, while abruptly increased cell viabilites were observed upon 30 µmol L^{-1}. Surfactants **S1** and **S2** showed in concentrations ranging from 240 – 30 µmol L^{-1} slightly toxic effects, while high cell viabilities were observed for concentrations from 30 µmol L^{-1} on. Surfactants **S3** and **S4** showed not cytotoxic effects in all considered concentrations. However, in case of **S4** the low cytotoxicity can probably be ascribed to partial precipitation of the surfactant during the incubation at 37 °C. **S3** showed no toxic effects up to the highest concentration of 240 µmol L^{-1}.

Nevertheless, a major aspect of this project was the characterization of the surfactant coated nanoparticles with regard to their behavior in biological fluids, herein in human blood plasma. Surfactants are known to effectively denature proteins that can influence the particle protein interaction when getting in contact.[21] Thus, the interactions of the PPE-surfactants with blood proteins were evaluated and compared with SDS and Lutensol® AT50. Two proteins were chosen to evaluate the interactions, i.e. human serum albumin as the most abundant protein in human blood and fibrinogen being the most abundant protein in the corona of unmodified polystyrene nanoparticles.[3, 13] For the cellular uptake studies in presence of proteins, the nanoparticles are incubated in human blood plasma for 1 h at 37 °C containing 0.03 - 0.1 µmol PPE-surfactants. To simulate the incubation step as accurately as possible, protein concentrations were applied according to their concentration in human blood plasma. Thus, HSA was applied in a concentration of 60 mg mL^{-1} while fibrinogen was applied in a lower concentration of 10 mg mL^{-1}.[22] The proteins were separately incubated with the surfactants at 37 °C in a concentration range of 0.02 – 0.1 µmol mL^{-1} according to the concentration range used for the particle modification. The protein/surfactant interaction for different surfactant concentrations, was determined by label-free differential scanning fluorimetry (nanoDSF).[23] Depending on the protein structure the thermal unfolding process led to changes in fluorescence emission properties which are monitored at two wavelengths (350 nm and 330 nm). The shift in fluorescence emission was plotted as the ratio of 350 nm and 330 nm against the heating temperature. As references, the distance between the curve of the native and the fully denatured protein was used and the other measurements are normalized to this value. Figure 4.3 depicts the results of the surfactant/protein interaction determined by nanoDSF.

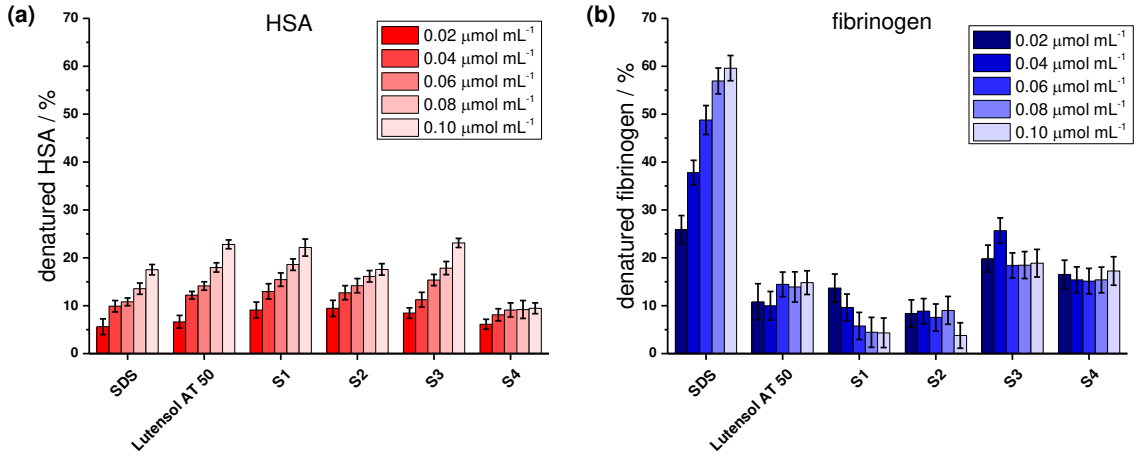

Figure 4.3. Protein surfactant interaction. Interaction of HSA (A) and fibrinogen (B) with SDS, Lutensol and the PPE-surfactants S1-S4.

Figure 4.3 (a) shows for all considered surfactants a concentration dependent denaturation of HSA with the highest amount of denatured protein for the highest surfactant concentration. However, for HSA the highest denaturation was observed for Lutensol® AT50 and **S3** with ~23% of denatured protein for the highest concentrations. SDS and **S2** showed lower effects on the protein denaturation with a maximum denaturation of ~15% for the highest concentration. In contrast, for **S4** significantly lower amounts of denatured protein were observed. This can probably be attributed to its T_{cp}= 29 °C, which probably led to precipitation of the surfactant during the incubation step at 37°C and therefore causes only slight denaturation of HSA. The same measurement was conducted for fibrinogen (Figure 4.3 (b)) with significantly different results. In case of SDS, an almost linear increase of denatured protein was observed with increasing concentration culminating in a maximum denaturation of ~60 %. The highest interaction of fibrinogen with SDS was expected since it is the most abundant protein in the corona of SDS-stabilized nanoparticles. In contrast, the polymeric PPE-surfactants and Lutensol® AT50 showed no concentration-dependent denaturation of fibrinogen. For the surfactants **S1** and **S2,** very low amount of denatured fibrinogen can be detected.

Surfactant degradation. The objective of the degradation study in this project was the evaluation of the influence of the different polymer structures on the degradation rate. Detailed investigations on the degradation of different PPEs, concerning their degradation products and degradation mechanism, were conducted using non-amphiphilic homopolymers and are discussed in chapter 6. Polyesters are known to degrade faster with increasing pH.[24] Therefore,

degradation of the surfactants was performed under basic conditions in order to keep the degradation studies in a reasonable time fame. Upon ester cleavage within the degradation process phosphoric or phosphonic acids are formed which lead to a decrease of the pH. Therefore, to guarantee a constantly basic pH throughout the whole degradation time, a borate buffer at pH 10 (0.15 M) was applied. The degradation for each surfactant was conducted at ambient temperature in a NMR tube and the degradation progress was monitored by ^{1}H and ^{31}P NMR spectroscopy. The quantitative evaluation of the degradation was performed using the ^{31}P NMR spectra by comparing the integrals of the polymer signal with the integrals of the newly evolved signals. For surfactants **S1**, **S2**, and **S4**, ester cleavage can occur either in the side chain or in the main chain, while for **S3** ester cleavage can only occur in the polymer backbone. For surfactants **S1** and **S4** phosphoric diesters are formed upon ester cleavage and can be distinguished from the triester (polymer) by ^{31}P NMR spectroscopy. Analogously, for **S2** and **S3** a phosphonic monoester is built upon ester cleavage that can also be distinguished from the phosphonic diester (polymer) by ^{31}P NMR spectroscopy. Quantification of the degradation was achieved by comparing the integrals of the degradation product (diester/monoester) signals with the polymer (triester/diester) signals (Figure 4.4).

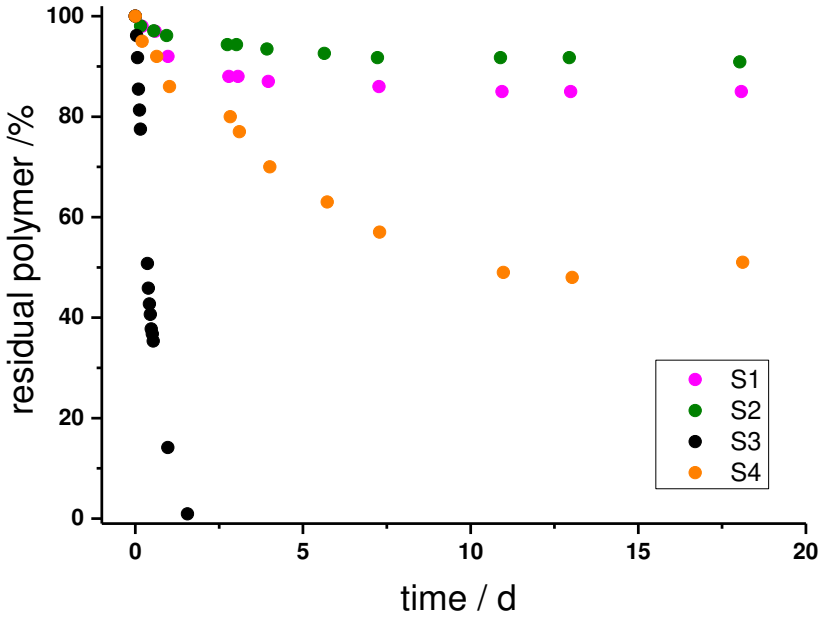

Figure 4.4. Degradation of PPE-surfactants S1-S4 at pH 10. The degradation was quantified by $^{31}P\{H\}$ NMR spectra recorded at different time points over a period of 18 days. The degradation curve was obtained by integration of the phosphorus triester/diester (polymer) and diester/monoester (degradation product) signal and comparison of the integrals. (The data presented for the degradation of S2 and S3 is the same data presented in chapter 3 Figure 3.6(B)).

Figure 4.4 shows distinct different degradation behavior for the different surfactant structures. For **S3** the fastest degradation was observed which proceeded within less than two days. For the other surfactants a significantly slower degradation was observed. The degradation of **S1**, **S2**, and **S4** was found to proceed in two phases with an initial rapid degradation followed by a second slower degradation phase. In general, for all surfactants distinct different degradation times were observed. While for **S4** initially rapid degradation lasted until day 11, after then it reached a plateau with a residual amount of polymer of ~51%, **S2** showed only for the first 4 days significant degradation that did not exceed 10% even after 18 days. For **S1** a degradation of 13 % was observed within the first three days and reached 15 % within the considered time. However, it need to be considered that surfactants far above their CMC were used for the degradation study and thus not only structural differences between the surfactants but also aggregation effects need to be taken into account when evaluating the results. ^{1}H NMR spectra of **S4**, recorded throughout the degradation study, clearly showed that aggregates where formed at the beginning of the study which changed with increasing degradation. At the beginning of the degradation study, the signals of the initiator, such as the signal of the methyl group with a

resonance at 0.86 ppm, were not visible (Figure 4.5). The missing initiator signals indicate the formation of aggregates, where the hydrophobic initiator is located in the center of the aggregate and is therefore shielded by the outer sphere. The shielding of the hydrophobic tail by the outer sphere prevents its detection by NMR spectroscopy. However, after 14 days the initiator signals appeared again in the ^{1}H NMR spectra (Figure 4.5), indicating that the aggregates have rearranged. Furthermore, after 14 days the quantitative analysis of the ^{31}P NMR spectra showed an increasing polymer signal, which is a further indication of rearrangements within the surfactant solution – at the beginning, a part of the polymer was shielded due to its location in the inner part of the aggregates. Therefore, the amount of degradation was overestimated at the beginning. After rearranging, the polymer parts close to the initiator were no longer shielded by the outer sphere and thus the signal of the residual polymer increased again. However, the differences in the degradation behavior can probably be attributed to the formation of aggregates beside spheric micelles above the CMC exhibiting different structures for the different polymers. Therefore, significantly different degradation rates were observed for the considered surfactants. The degradation study showed that for the evaluation of the hydrolytic degradation of the polymers several factors have to be taken into account.

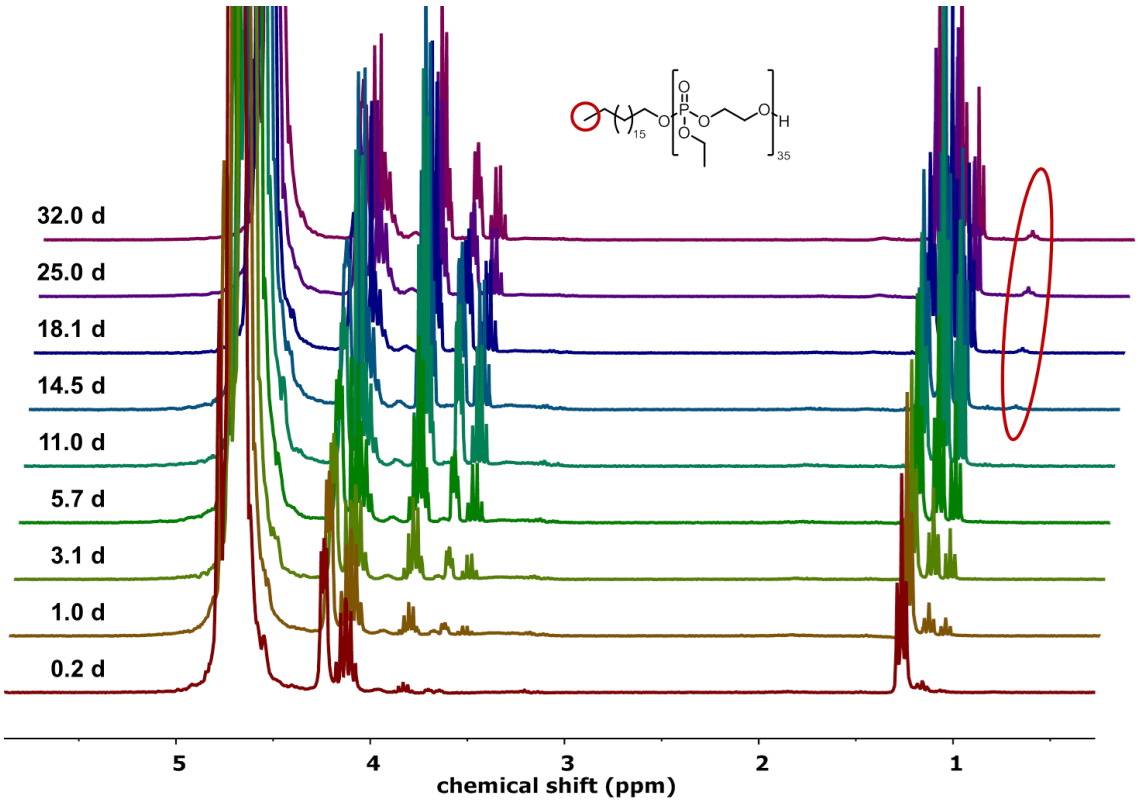

Figure 4.5. ^{1}**H NMRs (300 MHz, D_2O/H_2O (1:9), 298K) of the degradation of S4 at pH 10.**

Particle preparation. To evaluate the applicability of the prepared surfactants for the surface modification of nanoparticles prepared from different materials, two polymer nanoparticles were prepared by minimemulsion polymerization, i.e. polystyrene (PS) and poly(methyl methacrylate). PS-NPs are well-established model nanocarriers that have been intensively studied by our group concerning their interactions with proteins and have been modified with PPEs before.[3, 13] PMMA was chosen as further material since it is one of the most widely explored materials for biomedical applications and is widely used in bone cements[25] or surgical implants due to its good biocompatibility.[26-27] Additionally, PMMA nanoparticles can be prepared analogously to PS-NPs via miniemulsion polymerization by exchanging the monomer. Thus, evaluation of the influence of the particle material on the interaction with blood proteins is possible. However, PS and PMMA are not biodegradable and might accumulate in the body. As an example for a fully biodegradable nanocarrier, human serum albumin (HSA) nanoparticles were prepared with incorporated doxorubicin by a surfactant-free precipitation method. HSA is the most abundant protein in human blood plasma with concentrations up to 50 g L^{-1} and is furthermore among the most studied proteins[28] and is widely used as biodegradable material in

therapeutic applications.[22] HSA exhibits a high binding capacity to a variety of substrates including therapeutic substrates.[29] The high binding affinity and abundance have made HSA an attractive material for the preparation of drug carriers and furthermore albumin based nanocarriers were found to be well-tolerated without showing any serious side effects.[22] Table 4.2 provides an overview over the prepared nanoparticles.

Table 4.2. Overview of the prepared nanoparticles.

Particle	Ø / nm[a]	ζ-Potential[b] / mV	m [c] / g	V [c] / m^3	A [c] / nm^2
PS	103 ± 7	-55 ± 15	$6.01 \cdot 10^{-16}$	$5.72 \cdot 10^{-22}$	33300
PMMA	114 ± 13	-45 ± 12	$9.15 \cdot 10^{-16}$	$7.76 \cdot 10^{-22}$	40800
HSA-A	153 ± 15	-45.3	-	$1.88 \cdot 10^{-21}$	73500
HSA-B	193 ± 22	-43.9	-	$3.76 \cdot 10^{-21}$	117000
HSA-C	195 ± 28	-43.6	-	$3.88 \cdot 10^{-21}$	119500

[a]: *d*eterminde by DLS, [b] : determined by electrophoresis, [c]: calculated assuming the nanoparticles are perfect spheres.

For the calculation of the mass, volume and surface of the nanoparticles, the following equations were used, assuming the nanoparticles are perfect spheres.

$$A_s = 4\,\pi\,r^2 \quad \textbf{(4.1)}$$

$$V_s = \frac{4}{3}\,\pi\,r^3 \quad \textbf{(4.2)}$$

$$m_s = \rho_{PS} \cdot V_s \quad \textbf{(4.3)}$$

A_s= spherical surface, V_s= spherical volume; r: radius of nanoparticles; m_s= mass of particle; ρ_{PS}= density of polystyrene (1.05 g cm^{-3}); ρ_{PMMA}= density of poly(methyl methacrylate) (1.18 g/cm^{-3})

All prepared nanoparticles were subsequently coated with PPE-surfactants and Lutensol® AT50 as a PEGylated reference and analyzed with regard to their cellular uptake against murine macrophages and the composition of their protein corona. In order to coat the nanocarriers with the polymeric surfactants, two different techniques were applied. For the NPs prepared by miniemulsion polymerization, SDS was exchanged in the presence of polymeric surfactants by dialysis against water using a dialysis tube with a MWCO permeable for SDS but impermeable for the polymeric surfactant (Figure 4.6). As SDS has a CMC which is 3 orders of magnitude higher compared to the polymeric surfactants, it can easily be exchanged by dialysis. In contrast, HSA nanoparticles were coated with polymeric surfactant by redispersion in the respective surfactant solution (1wt%) and incubation for 24 h similar to the procedure reported by Kreuter *et al.*[30]

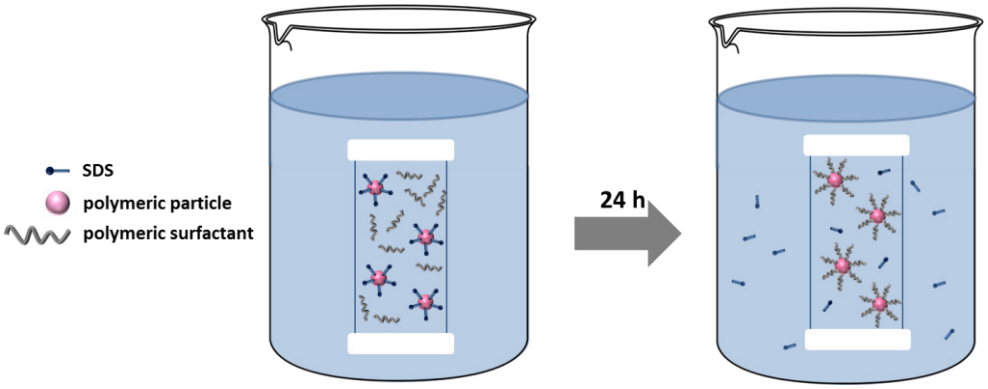

Figure 4.6. Schematic depiction of the coating process for the nanoparticles prepared by miniemulsion polymerization using SDS as surfactant.

To evaluate the amount of surfactant needed for an entire coverage of the PS- and PMMA-NP surface, surface tension measurements of the dispersions were conducted. Therefore, defined amounts of surfactant were dissolved in the particle dispersion and the surface tension was determined by ring tensiometry. The measurement was conducted for Lutensol® AT50 and **S1** as representative PPE-surfactant. The surface tension was plotted as a function of the surfactant concentration of a 2wt% dispersion (Figure 4.7). The critical micelle formation concentration of surfactants in the dispersions (CMC_d) differs from the CMC in water – the surfactant interacts with the additional nanoparticle/water interface, thus the point of micellization is reached at much higher concentrations.[31] However, the obtained graphs showed an analog shape like for the CMC determination of surfactants – with increasing amount of added surfactant the surface

tension of the dispersion decreased until a plateau was reached where further addition of surfactant did not lead to further surface tension decrease. Achieving the plateau indicated a full coverage of the particle surface with surfactant molecules and the formation of micelles upon exceedance. The results are depicted in Figure 4.7.

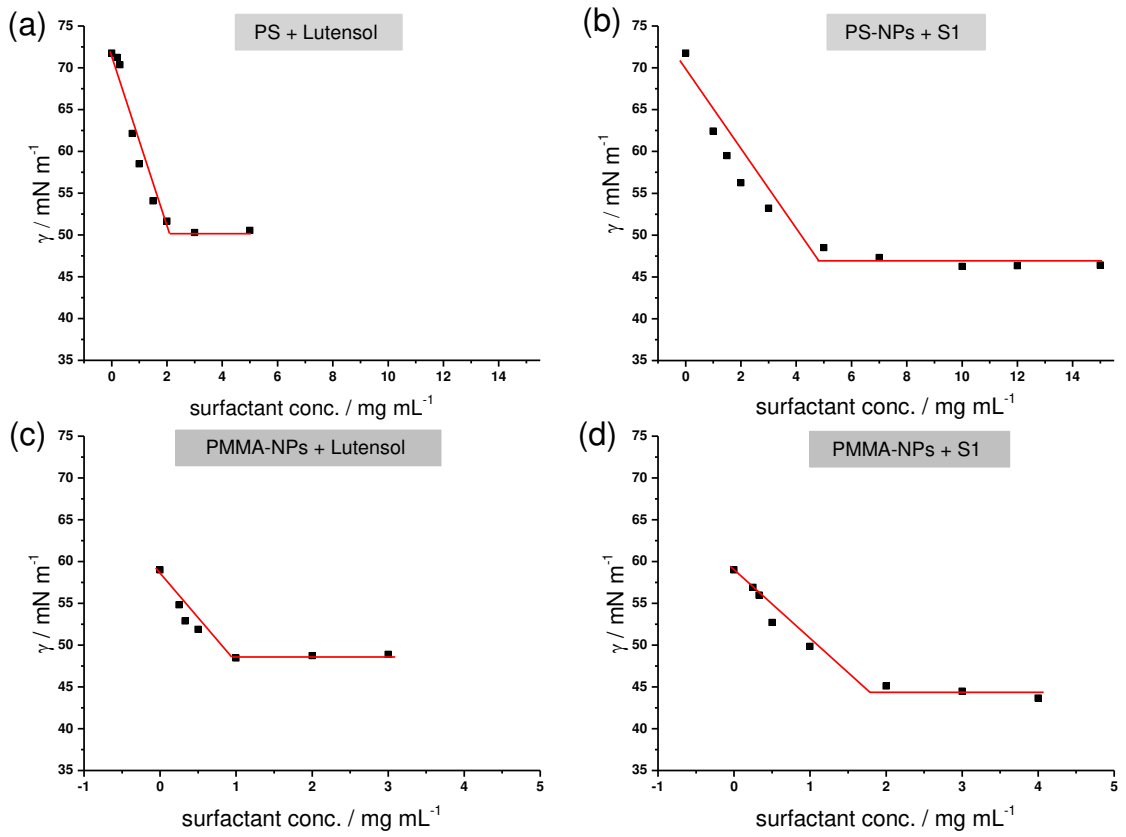

Figure 4.7. CMC determination. The CMCs of Lutensol AT50 and S1 were determined in 2wt% polystyrene particle dispersion. Different amounts of the respective surfactant were dissolved in the particle dispersion and the surface tension was determined by ring tensiometry.

Figure 4.7 (a) and (b) shows the results for the surface tension measurements of the PS-NPs. For Lutensol® AT 50 the plateau is reached upon a concentration of c≈ 1.9 mg mL^{-1}, while for **S1** a constant surface tension was reached upon c≈ 4.4 mg mL^{-1}. The higher amount of PPE-surfactant needed for reaching a constant surface tension was expected due to the higher molecular masses. However, distinct lower concentrations were observed for the PMMA-NPs (Figure 4.7 (c) and (d)). For Lutensol® AT no further surface tension decrease was observed upon c≈ 0.9 mg mL^{-1} and for **S1** a constant surface tension was observed for c≈ 1.7 mg mL^{-1}. The surface of the PMMA-NPs is slightly larger than the surface of PS-NPs (Table 4.2), thus

slightly higher or at least similar surfactant concentrations were expected to be required to reach a constant surface tension for both NP-dispersions. However, the lower concentration observed for the PMMA-NP dispersion probably indicated a lower affinity of the surfactants to enrich at the particle surface. Due to the lower interaction with the PMMA-NPs, surfactants enrich preferably at the water/air interface leading to a constant surface tension upon lower surfactant concentrations. Upon complete occupancy of the air/water interface, the surfactant molecules are forced to either accumulate at the nanoparticle surface or to form micelles.

A further indication of the lower interaction of the hydrophobic surfactant tail with PMMA compared to PS is the lower surface tension of the PMMA-NP dispersion containing no additional polymeric surfactant. For PMMA-NPs the surface tension was γ= 59 mN m^{-1} while the surface tension of the PS-NP dispersion was found to be γ= 71 mN m^{-1}, matching the surface tension of water (γ= 72.8 mN m^{-1}) indicating almost no free SDS in the dispersion. In contrast, the surface tension of the PMMA dispersion is distinctly below the surface tension of water indicating the presence of free SDS in the particle dispersion. However, the CMC determination in PMMA-NP dispersion indicated a lower interaction of the polymeric surfactants with PMMA compared to PS and thus higher amounts of surfactant were applied for coating PMMA-NPs to guarantee a sufficient surface coverage.

For PS-NPs the amount of surfactant needed for an entire surface coverage was additionally evaluated by cellular uptake studies against murine macrophages. Therefore, nanoparticles coated with different amounts of surfactant were incubated with murine macrophages in the presence and absence of proteins and the cellular uptake was determined. With increasing amount of surfactant, the cellular uptake was expected to decreased due to increasing shielding of the hydrophobic particle surface. Thus, a full surface coverage was indicated by minimum cellular uptake (recognition) by the macrophages. Here, again Lutensol® AT 50 as well as **S1** as representative PPE-surfactant were applied. Figure 4.8 shows the cellular uptake for PS-NPs coated with different amounts of surfactant.

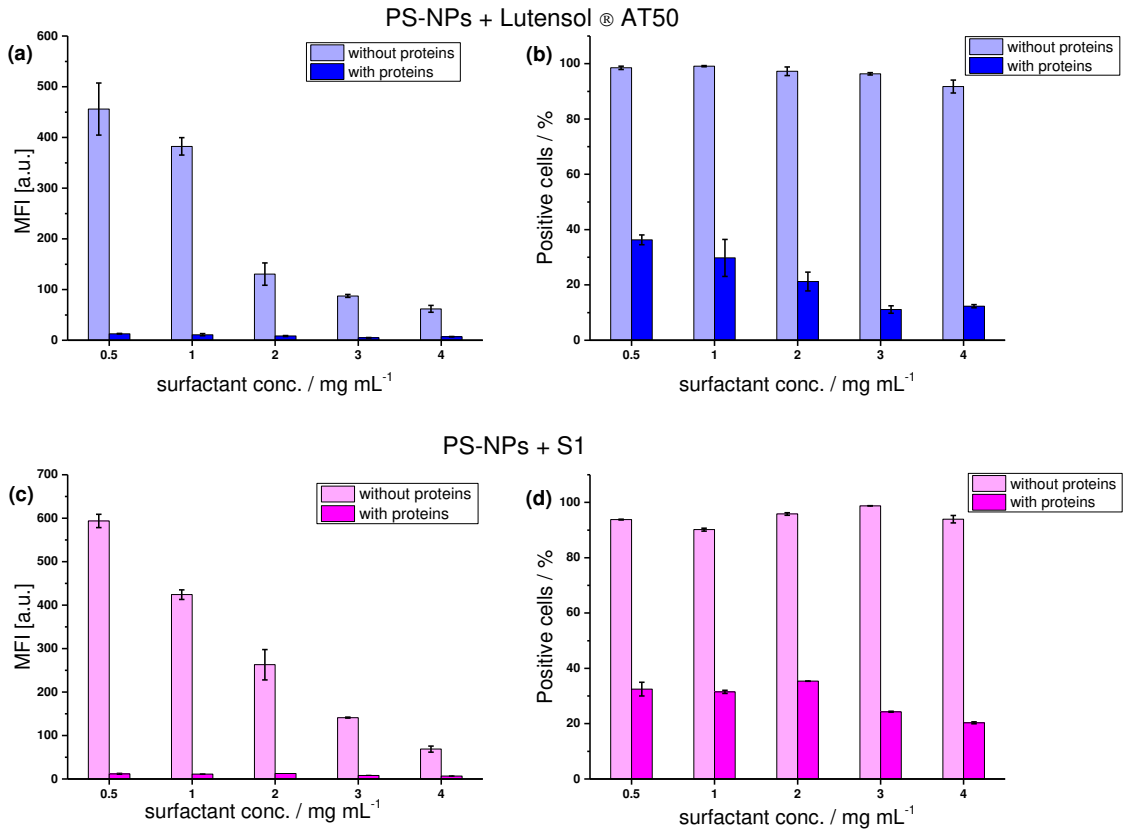

Figure 4.8. Flow cytometry analysis of RAW264.7 cells incubated with polystyrene nanoparticles coated with different amounts of Lutensol® AT 50 or S1 for 2 h. The nanoparticles were incubated in human plasma (with proteins) or in water (without proteins) for 1 h at 37 °C and separated from residual proteins by centrifugation before incubation with macrophages. (*Experiments depicted in this figure were conducted by Johanna Simon.*)

Figure 4.8(b) shows a decreasing cellular uptake for PS-NPs coated with Lutensol® AT50 up to a surfactant concentration of c=3 mg mL^{-1} indicating a full coverage of the particle surface. For a surfactant concentration of c=4 mg mL^{-1}, no further decrease of the cellular uptake was observed indicating a full coverage. For **S1** (Figure 4.8 (b)) slightly higher concentrations are needed to reach minimum cellular uptake by macrophages. The lowest cellular uptake was found for a concentration of c=4mg mL^{-1} dispersion. Taking the results obtained by the CMC determination and the cellular uptake studies with different surfactant amount into account, PS-NPs (2wt%) were coated with 3 mg surfactant per mL nanoparticle dispersion while for the PMMA-NPs (2wt%) higher amounts of 10 mg surfactant per mL NP dispersion were used. Table 4.3 provides an overview over the calculated theoretical maximum amount of surfactant molecules per particle calculated using equations **(4.4)** and **(4.5)** .

$$N(particle) = \frac{solid\ cotent}{m\ (particle)} \quad \textbf{(4.4)}$$

$$N(surf.)/particle = \frac{N(surf.)}{N(particle)} \quad \textbf{(4.5)}$$

Table 4.3. Calculations of the theoretical maximum number of surfactant molecules per nanoparticle.

	m (surf.)/ mg	n(surf.) / mol	N(surf.)	$N_{theo,\ max}$ surfactant molecules per particle
Lutensol® AT50 (PS)	3	$1.20 \cdot 10^{-6}$	$7.23 \cdot 10^{17}$	21700
Lutensol® AT50 (PMMA)	10	$4.00 \cdot 10^{-6}$	$2.41 \cdot 10^{18}$	110000
S1(PS)	3	$5.88 \cdot 10^{-7}$	$3.54 \cdot 10^{17}$	10600
S1 (PMMA)	10	$1.96 \cdot 10^{-6}$	$1.18 \cdot 10^{18}$	54000
S2 (PS)	3	$4.76 \cdot 10^{-7}$	$2.87 \cdot 10^{17}$	8600
S3 (PS)	3	$5.12 \cdot 10^{-7}$	$3.08 \cdot 10^{17}$	9250
S3 (PS)	3	$5.34 \cdot 10^{-7}$	$3.21 \cdot 10^{17}$	9640

The nanoparticles were coated with the polymeric surfactants by the dialysis method subsequently analyzed with regard to their size and ζ-potential. For the characterization in presence of proteins, the nanoparticles were incubated in human blood plasma for 1h at 37°C. Subsequently, the nanoparticles were centrifuged thrice in order to remove the excess of proteins and also analyzed with regard to their size and ζ-potential. The amount of proteins bound to nanoparticles were determined by a Pierce assay (Table 4.4).

Table 4.4. Diameter, ζ-potential for the surfactant coated nanoparticles in the absence and presence of proteins.

Particle	Ø[a] / nm		ζ-Potential[b] / mV		m(protein)[c] / ng cm^{-2}
	- proteins	+ proteins	- proteins	+ proteins	
PS(SDS)	103	250± 115	-55 ± 15	-20 ± 4	2,59 ± 0,06
PS+S1	112 ± 16	160 ± 30	-36 ± 10	-25 ± 5	0.41 ± 0.02
PS+S2	109 ± 9	131 ± 24	-34 ± 8	-20 ± 4	0.45 ± 0.04
PS+S3	113 ± 29	140 ± 17	-22 ± 9	20 ± 5	0.40 ± 0.07
PS+S4	109 ± 8	127 ± 44	-35 ± 9	-22 ± 5	0.52 ± 0.04
PS+Lutensol AT 50	104 ± 16	146 ± 32	-9 ± 8	20 ± 4	0.51± 0.14
PMMA(SDS)	114 ± 13	150 ± 8	-46 ± 12	-26 ± 5	1.20
PMMA+S1	121 ± 26	157 ± 32	-28 ± 8	-26 ± 7	0.79
PMMA+Lutensol AT 50	110 ± 13	146 ± 32	-30 ± 9	-20 ± 5	0.49

[a]*:* Determined by DLS. [b]*:* Determined by electrophoresis. [c]*:* Determined by Pierce protein assay.

The qualitative analysis of the composition of the hard corona of the SDS-stabilized PS- and PMMA-NPs as well as the surfactant-coated nanoparticles was analyzed by sodium dodecyl sulfate polyacrylamide gel electrophoresis (SDS-PAGE). PS-NPs modified with PPE on the particle surface have been investigated before.[3, 13] It was found that upon attaching PPE- or PEG-chains on the particle surface, the composition of the protein corona changed significantly compared to the unmodified nanoparticles. For the unmodified nanoparticles, fibrinogen was found to be the predominant protein, while clusterin and ApoAI were the predominant proteins in the corona of the polymer-modified nanoparticles. Thus, a similar change was expected for coating the nanoparticles with the different PPE-surfactants. SDS-PAGE analysis for PS-and PMMA-NPs are depicted in Figure 4.9.

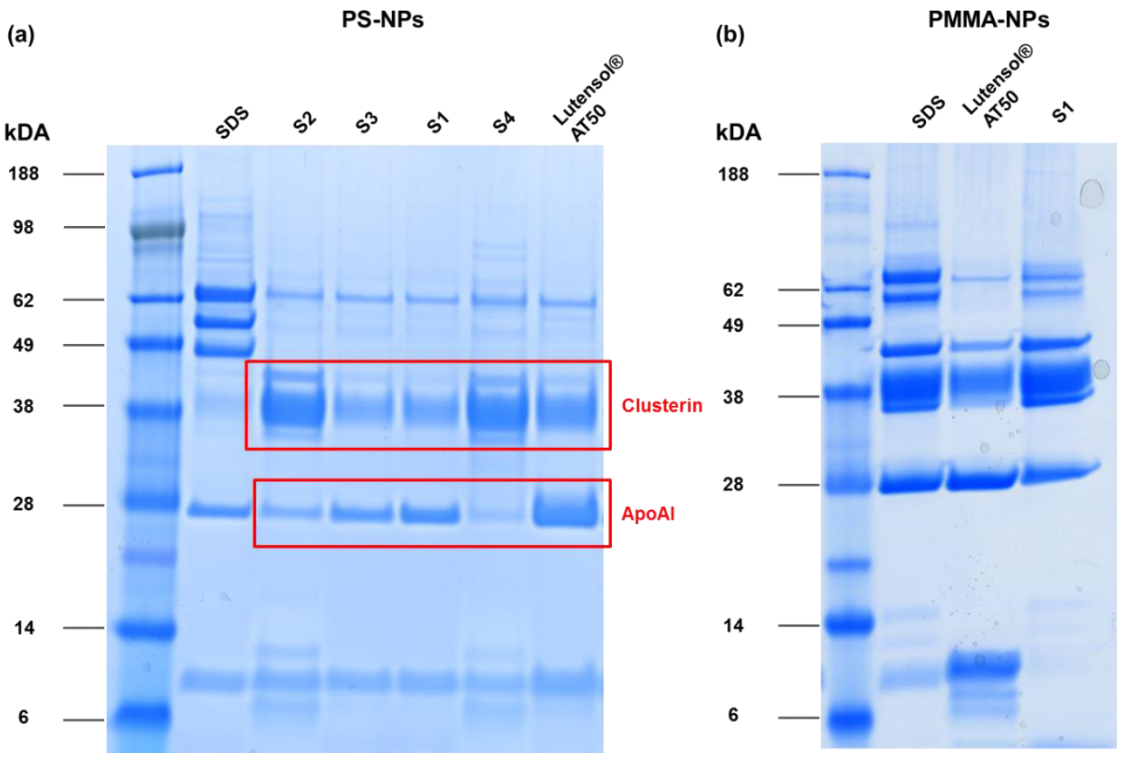

Figure 4.9. (a) SDS-PAGE analysis of (a) SDS-stabilized and surfactant coated (S1-S4, Lutensol® AT50) PS-NPs and (b) SDS-stabilized and surfactant coated (S1 and Lutensol® AT50) PMMA-NPs. (*Experiments depicted in this figure were conducted by Johanna Simon.*)

Figure 4.9 (a) shows the expected protein corona change from fibrinogen as the dominant protein in the corona of the SDS-stabilized nanoparticles to clusterin and ApoA1 as the dominant proteins in the corona of the surfactant coated nanoparticles. However, the SDS-PAGE further showed that the different binding patterns of the PPE-surfactants indeed had an influence on the protein corona. It can be distinguished between two different corona-types, i.e. a PEG-like corona for PS-NPs coated with **S1**, **S3** and Lutensol® AT50 and a second slightly different corona upon coating with surfactants **S2** and **S4**. While the PEG-like corona showed two main bands at 28 kDa and 38 kDa which can be assigned to ApoA1 and Clusterin respectively, the protein corona of nanoparticles coated with **S2** and **S4** was dominated by the clusterin-band. Figure 4.9 (b) shows the SDS-PAGE analysis of the PMMA-NPs. For the SDS-stabilized PMMA-NPs distinct bands at 28 and 38 kDa that can be attributed to Clusterin and ApoA1 respectively and two further bands at 62 kDa were observed. Upon coating with Lutensol® AT 50 a change of the protein corona was observed – the two bands at 62 kDa disappeared and in the region between 6-14 kDa new bands emerged. Upon coating with **S1** the intensity of the

bands at 62 kDa decreased significantly, but in general the protein corona of the **S1** coated PMMA-NPs resembled strongly the protein corona of the SDS-stabilized nanoparticles. The slight change of the protein corona upon coating with **S1** indicates that the NP surface is probably not entirely covered with surfactant. Furthermore, the protein corona of the SDS-stabilized PMMA-NPs showed no fibrinogen-band at all, while the protein corona of the SDS-stabilized PS-NPs was dominated by fibrinogen. Besides the differences in the protein corona, SDS-stabilized polystyrene and poly(methyl methacrylate) nanoparticles furthermore showed significantly different behavior when incubated in human blood plasma. While polystyrene nanoparticles are known to aggregate upon plasma incubation[32], PMMA nanoparticles were rather stable in plasma and formed only small aggregates (Figure 4.45). The distinct different observation made for PS- and PMMA-NPs can probably be attributed to the different particle materials and their different protein interaction. The presence of fibrinogen on the bare PS-NPs and its absence on the analogue PMMA-NPs might indicate that the different particle properties, concerning protein corona and stability in blood plasma, can be attributed to the different interactions with fibrinogen. Fibrinogen is a fibrous protein that plays a crucial role in haemostasis and wound healing by forming fibrous networks that reinforce blood clotting.[33] In 2014, Hahm *et al.* reported about the self-assembly characteristics of fibrinogen on chemically different surfaces.[34] Among others, they investigated the structure of fibrinogen on polystyrene and PMMA surfaces. And indeed, they found unambiguously different structures of fibrinogen on the two surfaces – on polystyrene they found significantly elongated structures for fibrinogen compared to the structure on PMMA. A direct investigation of the interaction of polystyrene nanoparticles of different size and surface modification with fibrinogen was done by Kendall et al.[35] Dynamic light scattering measurements showed a distinctly increasing particle size for all examined PS-NPs upon exposure to fibrinogen. These observations were confirmed by environmental scanning electron microscopy that showed particle aggregates exhibiting bridges between the nanoparticles that were attributed to fibrinogen. Thus, the high amount of fibrinogen in the protein corona of SDS-stabilized PS-NPs may be ascribed to the specific interaction of polystyrene with fibrinogen that is suppressed upon coating of the polystyrene surface with polymeric surfactants. Furthermore, different amounts of SDS, present on the particle surface, might influence the interaction of the nanoparticles with fibrinogen. NanoDSF measurements showed that SDS – as the only considered surfactant – led to a high denaturation of fibrinogen. The surface tension measurements indicated a lower amount of free SDS in the PS-NP

dispersion compared to the PMMA-NP dispersion and therefore a higher concentration on the particle surface that can influence the protein/particle interaction.

For the coated PS- and PMMA-NPs, the cellular uptake against murine macrophages was evaluated. PS-NPs were coated with all PPE-surfactants **S1-S4** and Lutensol® AT50 to evaluate the provided stealth behavior. In contrast, PMMA-NPs were coated with Lutensol® AT50 and **S1** as representative PPE-surfactant. The results of the cellular uptake studies are depicted in Figure 4.10.

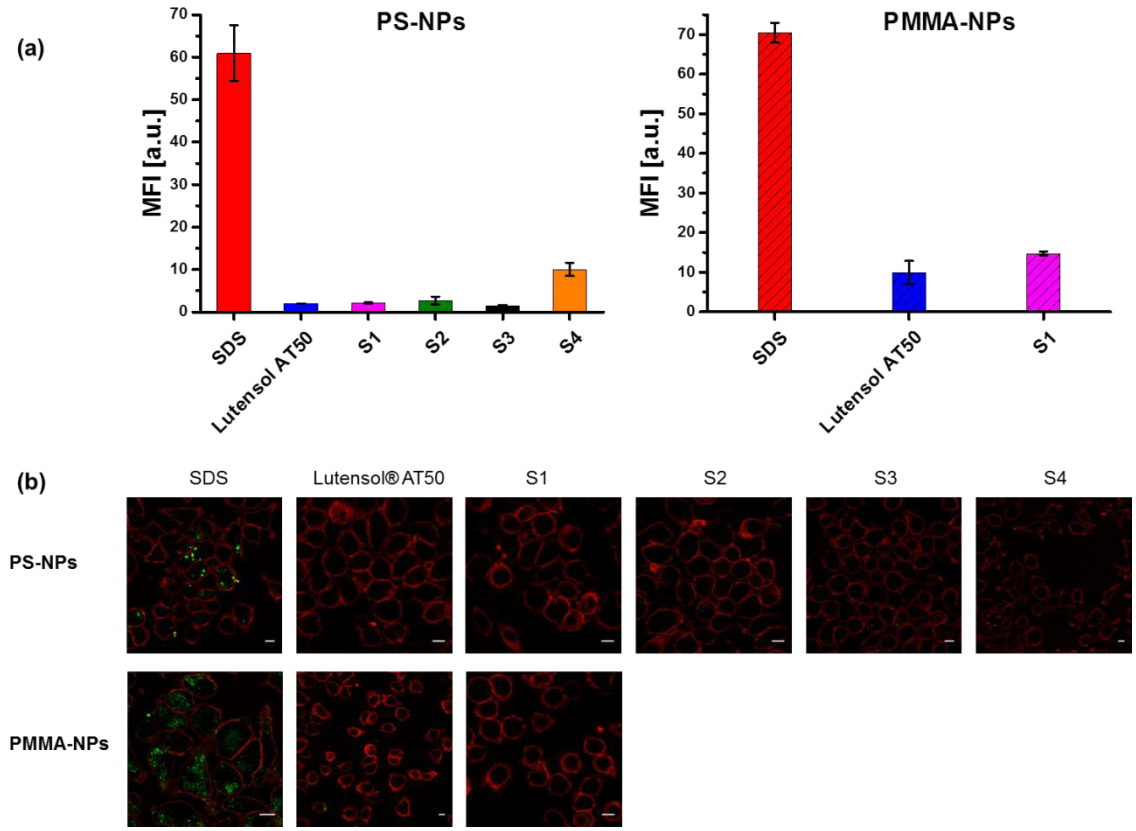

Figure 4.10. Flow cytometry analysis of RAW264.7 cells incubated with polystyrene and poly(methyl methacrylate) nanoparticles coated with PPE-surfactants S1-S4 and Lutensol AT 50. The nanoparticles were incubated in human plasma for 1 h at 37 °C and separated from residual proteins by centrifugation before incubation with macrophages for 2h. (b) laser scanning microscopy images of RAW264.7 cells incubated with SDS-stabilized and surfactant-coated PS-and PMMA-NPs, scale bars, 10 µm. (*Experiments depicted in this figure were conducted by Johanna Simon.*)

As depicted in Figure 4.10 (a) (*left*) for all surfactant coated PS-NPs distinctly reduced cellular uptake by murine macrophages was observed compared to the SDS-stabilized PS-NPs. For PPE-surfactants **S1-S3** as well as for Lutensol® AT50 a reduction of 95-97% compared to the SDS-stabilized particle was observed. Slightly higher cellular uptake was observed for PS-NPs coated with **S4**. Coating PS-NPs with **S4** led to a decrease of the cellular uptake by 85%. The higher cellular uptake of the **S4** coated nanoparticles can probably be attributed to aggregation of the nanoparticles during the incubation step at 37°C due to partial precipitation of the surfactant. For surfactant coated PMMA-NPs, a significantly decreased cellular uptake was also observed upon surfactant-coating (Figure 4.10 (a) *right*). For PMMA-NPs coated with Lutensol® AT50 a reduction of 86% and upon coating with **S1** a reduction of 80% was observed. In general, the cellular uptake for the surfactant coated PMMA-NPs were found to be higher than the cellular uptake of the surfactant coated PS-NPs that probably indicated an incomplete coverage of the PMMA-NP surface. However, the cellular uptake studies clearly showed a successful transfer of stealth behavior to NPs consisting of different materials upon surfactant-coating. Confocal laser scanning microscope (CLSM) imaging clearly confirmed the reduced cellular uptake of both nanoparticles upon coating with polymeric surfactants (Figure 4.10(b)).

Human Serum Albumin Nanoparticles. In order to prepare a fully degradable drug delivery system, consisting of a degradable nanocarrier and a degradable surfactant, HSA nanoparticles were prepared and subsequently coated with **S1** as degradable PPE-surfactant and Lutensol® AT50. HSA-NPs were prepared by a surfactant-free precipitation method according to a well-established literature procedure and subsequently cross-linked by the addition of a 8% glutaraldehyde (GA) solution.[36] Doxorubicin (DOX) was incorporated as dye to track the nanoparticles in biological experiments. HSA-NPs were prepared with varying amount of cross-linker to achieve surfaces with different permeability for the incorporated DOX. Table 4.5 provides an overview over the properties of the obtained nanoparticles concerning size, ζ-potential and drug incorporation.

Table 4.5. Summary of diameter, ζ-potential, and drug incorporation of the prepared HSA-NPs

#	Ø[a] / nm	µL GA/ mg HSA	DOX-incorporation
HSA-A	153 ± 15	2.1	94.2 ± 0.4
HSA-B	193 ± 22	0.4	87.9 ± 0.1
HSA-C	195 ± 28	0.294	88.9 ± 0.8

[a]*:* determined by DLS.

Due to the high hydrophilicity of HSA, a weaker interaction of the hydrophobic tail of the polymeric surfactants with the HSA-NPs was expected. And thus, less effective surface modification was expected compared to PMMA- and PS-NPs. SDS-PAGE analysis of the protein corona of HSA-NPs **HSA-A- HSA-C** showed a strong dependence of the amount of added cross-linker on the composition of the protein corona (Figure 4.11 (a)). For **HSA-C** with the lowest degree of crosslinking, SDS-PAGE analysis showed one predominant band at ca. 62 kDa that can be attributed to albumin. However, with increasing amount of added cross-linker, the protein corona composition changes significantly. On the nanoparticles **HSA-A** and **HSA-B**, cross-linked with a higher amount of GA, a high amount of protein bands was observed that can be attributed to complement proteins. These observations indicate particle surfaces with significantly different characteristics for the prepared HSA-NPs, which influence the interaction with proteins and surfactants. The increased protein interaction of **HSA-A** indicates a higher hydrophobicity of the surface compared to HSA-NPs prepared with lower amounts of GA. Thus, **HSA-A** was used for subsequent coating with Lutensol® AT50 and **S1** as representative PPE-surfactant. For coating of the HSA nanoparticles, a different strategy was applied compared to the polymeric nanoparticles prepared by miniemulsion polymerization. Since they were prepared by a surfactant-free precipitation technique, no surfactant-exchange is necessary. Therefore, HSA-NPs were centrifuged, the supernatant was removed and the obtained pellet was redispersed in a surfactant solution, containing 1wt% of the respective surfactant. The surfactant coated HSA-NPs were analyzed analogously to the PS-and PMMA-NPs with regard to their cellular uptake by murine macrophages and the qualitative composition of the protein corona was evaluated by SDS-PAGE. The results are depicted in Figure 4.11 (b) and (c).

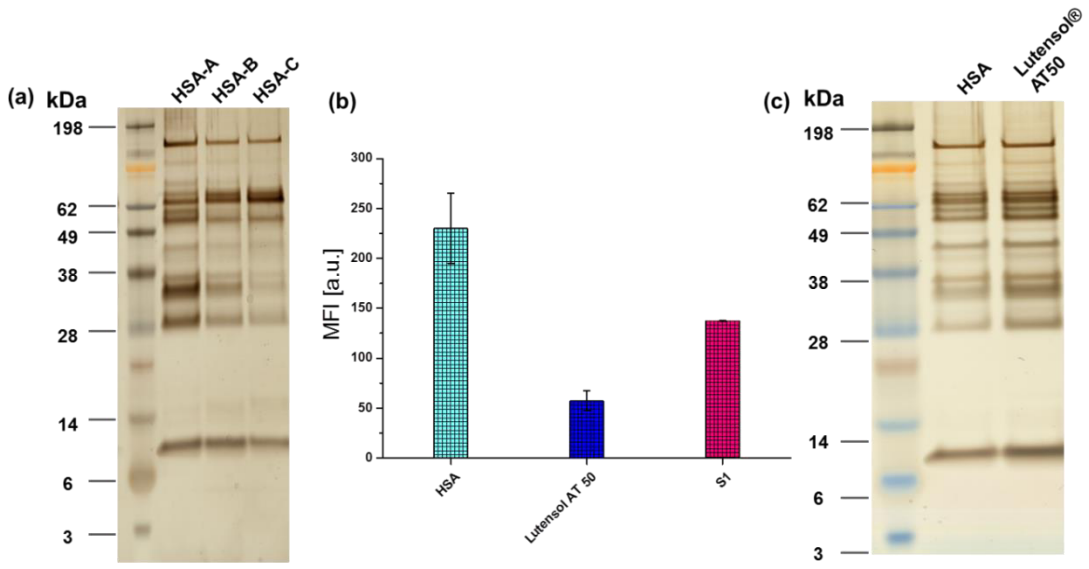

Figure 4.11. (a) Cellular uptake studies of surfactant coated HSA nanoparticles against murine macrophages (b) Qualitative SDS-PAGE analysis of the HSA nanoparticles (c) Qualitative SDS-PAGE analysis of the protein corona of HSA-NPs with different degrees of crosslinking (*Experiments depicted in this figure were conducted by Johanna Simon.*)

Figure 4.11 (b) shows that the cellular uptake of the HSA-NPs by macrophages can be reduced upon coating with Lutensol® AT50 and **S1**. For HSA-NPs, the cellular uptake can be reduced by 75% when coated with Lutensol® AT 50 while the coating with **S1** led to a reduction of the cellular uptake by 40%. In general, coating of HSA-NPs with polymeric surfactants, **S1** and Lutensol® AT50, led to less decreased cellular uptake by murine macrophages compared to surfactant-coated PS- and PMMA-NPs. This can probably be attributed to less interaction of the surfactants with HSA compared to the other particle materials. HSA is hydrophilic and thus interaction with the hydrophobic surfactant tail is less likely compared to the more hydrophobic PMMA and PS. Furthermore, the low interaction between the mere surfactants and HSA observed by nanoDSF measurement (Figure 4.3) is probably a further indication for the weaker interaction of the surfactants with HSA-NPs compared to PS- and PMMA-NPs. The qualitative protein corona analysis by SDS-PAGE of the bare and Lutensol® AT 50 coated HSA-NPs (Figure 4.11 (c)) showed that the coating of the HSA-NPs with surfactants had no significant influence on the corona composition. The almost identical protein corona of the bare and surfactant coated HSA-NP is a further indication of less effective surface modification compared to the polymeric nanoparticle prepared by miniemulsion polymerization.

3 Conclusion

A facile strategy for the non-covalent surface modification of different polymer nanocarriers with PPE-surfactants was presented. PPE-surfactants with altered binding pattern around the phosphorus of each repeat unit were prepared and characterized concerning their toxicity, protein interaction, and degradation under basic conditions. PPE-surfactants were found to be less toxic than the commercial Lutensol® AT50 and proved no significant protein denaturation in the considered concentration range. Degradation studies showed significantly different degradation rates for the PPE-surfactants with different binding patterns, allowing precisely tailored degradation behavior by variation of the PPE-structure. The surfactants were assembled on the surface of three different nanocarriers, i.e. PS-, PMMA- and HSA-NPs, and their ability to shield the modified nanocarriers from the recognition by cells of the immune system (macrophages) was evaluated. Cellular uptake studies against macrophages showed, that the cellular uptake can be decreased for all considered nanocarriers upon coating with PPE-surfactants, while the effectivity is also dependent on the particle material. The amount and types of proteins identified on the PPE-surfactant-coated PS-NPs after incubation in human plasma resembled previously reported nanocarriers modified with PPEs. Furthermore, it was found that the protein corona composition can be influenced by small changes in the PPE-structure of the applied surfactants. In conclusion, the presented study demonstrates that non-covalent coating of nanocarriers with PPE-surfactants facilitates the surface modification of nanocarriers and allows a tailoring of the protein adsorption on nanoparticles and their behavior in a biological environment.

4 Experimental

4.1 General Information

All chemicals and solvents were purchased from Sigma-Aldrich, Acros Organics or Fluka and used as received unless otherwise stated. Monomers and Initiator were distilled from $MgSO_4$ and stored over molecular sieves. Deuterated solvents were purchased from Sigma-Aldrich and used as received. Human serum albumin was purchased from Sigma-Aldrich and used as received. Fibrinogen (Haemocomplettan® P 1 g / 2 g) was used as received. Whole human blood was obtained form 10 healty donors. Sodium citrate was added as anticoagualant to generate human blood plasma. For serum preparation, blood from 6 healty donors was taken and allowed to clot overnight according to the standard procedure.

NMR. ^{1}H ^{13}C and ^{31} P NMR spectra were recorded using a Bruker Avance III 250, a Bruker Avance 300, a Bruker Avance III 500 or a Bruker Avance700. All spectra were referenced internally to residual proton signals of the deuterated solvent. All ^{31}P NMR spectra are recorded proton decoupled.

SEC. Size exclusion chromatography (SEC) measurements of the surfactants were performed in DMF (containing 1 gL^{-1} of lithium bromide as an additive) at 60 °C and a flow rate of 1 mL min^{-1} with a PSS SECurity as an integrated instrument, including a set of 3 PSS GRAM columns (porosity of 100 Å and 1000 Å) and a refractive index (RI) Detector. Calibration was carried out using polyethylene glycol standards provided by Polymer Standards Service.

ξ-potential. The zeta potential of the prepared nanoparticles was measured with a Zeta Sizer Nano Series (Malvern Instruments, U.K.) at 25 °C. The samples were prepared by diluting 10 µL of the nanoparticle dispersion in 1 mL of a 10^{-3} M potassium chloride solution

DLS. Dynamic light scattering (DLS) measurements of the surfactants were performed on an ALV spectrometer consisting of a goniometer and an ALV-5004 multiple-tau full-digital correlator (320 channels) which allows measurements over an angular range from 30° to 150. A He-Ne Laser (wavelength of 632.8 nm) is used as light source. For temperature controlled measurements the light scattering instrument is equipped with a thermostat from Julabo. The average size and the size distribution of the nanoparticles were measured by means of DLS at 23 °C using a PSS NicompTM Submicron Particle Sizer 380 (Nicomp Particle Sizing Systems) equipped with a detector for a scattering angle of 90° to the incident beam. The samples were diluted in demineralized water to be hardly cloudy.

For evaluation of the stability of nanoparticles in human blood plasma the method by Rausch *et al.*[37] was applied.

T_{cp} determination. Cloud points (T_{cp}) were determined either in MilliQ water or Dulbecco's PBS from Sigma-Aldrich and detected by optical transmittance of a light beam (λ = 500 nm) through a 1 cm sample cell. The measurements were performed in a Jasco V-630 photo spectrometer with a Jasco ETC-717 Peltier element. The intensity of the transmitted light was recorded versus the temperature of the sample cell. The heating/cooling rate was 1 °C min^{-1}, and values were recorded every 0.1 °C.

DSC. The thermal properties of the synthesized polymers have been measured by differential scanning calorimetry (DSC) on a Mettler Toledo DSC 823 calorimeter. Three scanning cycles of heating-cooling were performed in a N_2-atmosphere 30 mL/min) with a heating and cooling rate of 10 °C/min.

SFT Measurements. Surface tension measurements to determine the critical micelle concentration (CMC) of the surfactants in MilliQ water were performed using a DCAT 11 EC tensiometer (Dataphysics, Filderstadt, Germany) equipped with a TV 70 temperature control unit, a LDU 1/1 liquid dosing and a refill unit, as well as a RG 11 Du Nouy ring. The Du Nouy ring was washed with water and annealed prior to use. CMCs were determined using a standard program, where defined amounts of a surfactant solution (0.375 mg mL^{-1}) were added into 16 mL of MilliQ water. After each addition, the solution was stirred for 60 s and the surface tension was determined as average value of three measurements. Surface tension data were processed using SCAT v3.3.2.93 software. The CMC was determined by linear regression of the slopes at high and at low concentration. The point of intersection was the CMC. For the surface tension measurements in particle dispersions samples were prepared by dissolving a defined amount of surfactant in the particle dispersion. The surface tension of each sample was determined as average value of ten measurements.

SEM. Scanning electron microscopy (SEM) of the prepared nanoparticles was performed using a Zeiss 1530 LEO Gemini microscope with an accelerating voltage of 0.2 kV and a working distance of ~3 mm. The nanoparticles were prepared by dilution of the respective nanoparticle dispersion in MilliQ water. The diluted dispersion was dropped onto a silica wafer, and dried at ambient temperature.

Confocal Laser Scanning Microscopy (CLSM).RAW264.7 (80.000 cells per well) were seeded in Ibidi iTreat μ-dishes (IBIDI, Germany) overnight, washed with PBS and kept in DMEM without additional proteins. Cellular uptake experiments were conducted as described

above (flow cytometry). For confocal images, the cell membrane was stained with CellMask Orange (CMO, stock solution: 5 mg mL^{-1} in DMSO, Thermo Fisher, USA). Images were taken on a Leica TCS SP5 II microscope with an HC PL APO CS 63x/1.4 oil objective using the software LAS AF 3000 software and the fluorescence signals of nanoparticles (excitation: 488 nm) and CMO (excitation: 561 nm) were detected.

Flow Cytometry. For cellular uptake analysis, 150.000 cells per well (RAW 264.7) were seeded out in 24-well plates. After overnight incubation at 37°C, cells were washed with PBS and kept in cell culture medium additional proteins. Prior to cellular uptake experiments, nanoparticles were incubated with plasma/serum (see protein corona preparation above) and added to cells at a concentration of 75 µg/mL for 2h. Further, cells were washed wit PBS to remove free nanoparticles and detached with 2.5% trypsin (Gibco, Germany). Measurements were conducted on a CyFlow ML Cytometer and data analysis was analyzed with FCS Express V4 software. Cells were selected on a forward/sideward scatter plot, eluding cell debris and gated events were as median fluorescence intensity (MFI) or percentage of fluorescent positive cells (%).

Toxicity. The toxicity of the surfactants and Lutensol© AT50 were evaluated using a Cell Titer-Glo® Luminescent Cell viability assay from Promega. Tests were performed according to the provided protocol.

Protein Corona Preparation. A constant ratio between nanoparticle surface are (0.05 m^2) and human citrate plasma or human serum (1 mL) was chosen. Nanoparticles were incubated at 37°C for 1h to allow corona formation. To remove unbound proteins, nanoparticles were centrifuged for 1h, 20.000 g (4°C) and redispersed in 1 mL PBS (Sigma Aldrich, USA). This step was repeated three times. To elude the bound proteins, the nanoparticle pellet was resuspended in 2% (w/v) SDS (Carl Roth GmbH, Germany) with 62.5 mM Tris*HCl (Sigma Aldrich, USA) and incubated at 95°C (5 min). Nanoparticles were centrifuged (20.000g, 1h, 4°C) and the supernatant contained desorbed corona proteins.

Pierce 660 nm Protein Assay. The protein concentrations were determined by Pierce 660 nm protein assay (Thermo Scientific, USA) according to the manufacturer's instructions.

Sodium Dodecyl Sulfate Polyacrylamide Gel Electrophoresis (SDS-PAGE). Protein samples (26 µL) were diluted with 10 µL of NuPAGE LDS Sample Buffer, 6 µL NuPAGE Sample Reducing Agent and incubated 70°C (10 min). Samples were applied to a NuPAGE® 10% Bis-Tris gel and electrophoresis was carried out 100 V (1 h) in NuPAGE MES SDS Running Buffer. SeeBlue Plus2 Pre-Stained Standard was used as protein marker. Protein (1 µg) bands were visualized by Pierce Silver Stain kit according to the manufactures´ instruction. For high protein

amounts (6 µg per lane) the ready to use Coomassie solution (Simple Blue Safe Stain) was chosen. All reagents were obtained from Thermo Fischer Scientific, USA.

Cell Culture. The murine macrophage cell line RAW264.7 was cultured in Dulbecco's modified eagle medium (DMEM), supplemented with 10% fetal bovine serum (FBS), 100 U/mL penicillin, 100 mg/mL streptomycin and 2 mM glutamine. All reagents were obtained from Gibco, USA.

Particle coating. For coating of polystyrene nanoparticles **S1-S4** and Lutensol® AT50 were dissolved at a concentration of 3 mg mL^{-1} in the particle dispersion (2wt%) and charged into a dialysis tube with MWCO of 1 kDa and dialyzed against deionized water for 24 h. For coating of poly (methyl methacrylate) nanoparticles **S1** and Lutensol® AT50 were dissolved at a concentration of 10 mg mL^{-1} in the particle dispersion (2wt%) and charged into a dialysis tube with MWCO of 1 kDa and dialyzed against deionized water for 24 h. For coating of human serum albumin nanoparticles with **S1** and Lutensol® AT50 the dispersion was centrifuged, the supernatant was removed and the obtained nanoparticle pellet was redispersed in 1wt% solution of the respective surfactant.

4.2 Synthetic Procedures

4.2.1 Monomer synthesis

Synthesis of 2-Ethyl-2-oxo-1,3,2-dioxaphospholane (EEPn).[16] A flame-dried three-necked round-bottom flask, equipped with a magnetic stirring bar and two dropping funnels, was charged with 250 mL of dry THF and cooled to -21 °C. Ethylphosphonic acid dichloride (64 g, 0.44 mol, 1 eq) was dissolved in dry THF (250 mL) and transferred into one dropping funnel. A solution of dry ethylene glycol (27 g, 0.44 mol, 1 eq) and dry pyridine (69 g, 0.87 mol, 2 eq) in THF (250 mL) was transferred into the second dropping funnel. The dropping speed was adjusted to be approximately equal for both dropping funnels. After complete addition the reaction mixture was stirred for further 3 h and kept overnight at −28 °C to facilitate the precipitation of the pyridinium hydrochloride byproduct. The precipitate was removed by filtration via a Schlenk funnel, and the solvent was removed at reduced pressure. Fractionated distillation yielded the desired product as colorless oil. (50.4 g, yield 85%, bp 95 °C/2.6 × 10^{-2} mbar).

^{1}H NMR (300 MHz, Chloroform-*d*) δ 4.58 – 4.38 (m, 2H, -P-O-C***H*$_2$**-), 4.36 – 4.15 (m, 2H, -P-O-C***H*$_2$**-), 2.08 – 1.88 (m, 2H, 2H, -P-C***H*$_2$**-), 1.29 – 1.10 (m, 3H, -C***H*$_3$**). ^{31}P{H} NMR** (121 MHz, Chloroform-*d*) δ 52.52.

Synthesis of 2-methoxy-1,3,2-dioxaphospholane 2-oxide (MEP). A flame-dried three-neck flask, equipped with a dropping funnel, was charged with a solution of dry methanol (11.24 g, 0.35 mol) and dry triethylamine (39.1 g, 0.39 mol, 1.1 eq) in dry THF (250 mL) and cooled down to 0 °C. A solution of 2-chloro-2-oxo-1,3,2-dioxaphospholane (50 g, 0.35 mol, 1 eq) dissolved in dry THF (50 mL) was added to the trimethylamine/methanol mixture under constant stirring. After complete addition of COP the reaction mixture was stirred for 2 more hours at 0 °C. The precipitated salt was removed by filtration and the filtrate was concentrated *in vacuo*. The residue was purified by distillation under reduced pressure. The product was obtained as colorless, liquid (30.8 g, 0.27 mol, yield: 80%, bp.: 62 °C, 10^{-2} mbar).

^{1}H NMR (300 MHz, Chloroform-*d*) δ 4.54 – 4.26 (m, 4H, -O-C***H*$_2$**-C***H*$_2$**-O-), 3.82 (d, 3H, *J* = 11.7 Hz, -C***H*$_3$**). ^{31}P{H} NMR** (121 MHz, Chloroform-*d*) δ 18.57

2-Ethoxy-2-oxo-1,3,2-dioxaphospholane (EEP). A flame-dried three-neck flask, equipped with a dropping funnel, was charged with a solution of dry ethanol (10.8 g, 0.23 mol 1.0 eq) and dry triethylamine (23.7 g, 0.23 mol, 1.0 eq) in dry THF (250 mL) and cooled down to 0 °C. A solution of 2-chloro-2-oxo-1,3,2-dioxaphospholane (33.4 g, 0.23 mol, 1 eq) dissolved in dry THF (50 mL) was added to the trimethylamine/methanol mixture under constant stirring. After complete addition of COP the reaction mixture was stirred for 2 more hours at 0 °C. The precipitated salt was removed by filtration and the filtrate was concentrated *in vacuo*. The residue was purified by distillation under reduced pressure. The product was obtained as colorless, liquid (37.3g, 0.27mol, yield: 77%, bp.: 83°C, 10^{-2} mbar).

^{1}H NMR (300 MHz, Chloroform-*d*) δ 4.51 – 4.30 (m, 4H, O-C***H*$_2$**-C***H*$_2$**-O), 4.29-4.13 (m, 2H, O-C***H*$_2$**-CH$_3$), 1.37 (t, 3H, O-CH$_2$-C***H*$_3$**). ^{31}P{H} NMR** (121 MHz, Chloroform-*d*) δ 17.50.

Synthesis of 2-ethoxy-1,2-oxaphospholane-2-oxide (EPP). EPP was synthesized according to a literature procedure.[38] Triethyl phosphite (131 g, 0.8 mol, 2 eq) and 1,3-dibromopropane (80 g, 0.4 mol, 1 eq) were combined in a round bottom flask equipped with a distillation apparatus to remove evolving ethyl bromide. The mixture was heated up to 120 °C until 1,3-dibromopropane

was consumed completely (the consumption of the alkyl halide was monitored by NMR measurements since no solvent is used for the reaction). The crude monomer was separated from the oligomeric side product by distillation (55-60 °C, 0.1 mbar) and purified by fractional distillation. 12.5 g (0.08 mol, 20%) 2-ethoxy-1,2-oxaphospholane-2-oxide was obtained as colorless liquid.

^{1}H NMR (300 MHz, chloroform-*d*) δ 4.25 – 3.96 (m, 4H, -P-O-C***H₂***-), 2.37 – 2.06 (m, 2H, P-O-CH_2-C***H₂***-), 1.90 – 1.65 (m, 2H, -P-C***H₂***-), 1.28 (t, *J* = 7.1 Hz, 3H, -C***H₃***). ^{13}C NMR (176 MHz, chloroform-*d*) δ 67.26 (-O-***C***H_2-CH_2-), 62.18 (-O-***C***H_2-CH_3), 23.92 (-P-***C***H_2-), 18.49 (-P-CH_2-***C***H_2-), 16.47 (-***C***H_3). **^{31}P{H} NMR** (121 MHz, chloroform-*d*) δ 49.25.

4.2.2 Surfactant synthesis

Representative Synthesis of S1. Octadecanol and TU were dried by lyophilization with benzene. MEP (511 mg, 3.71 mmol, 40 eq) was added to the dried TU. A stock solution of octadecanol in dry dichloromethane was prepared with a concentration of 0.07 mol L^{-1}. 1.25 mL (25.0 mg, 0.084 mmol, 1 eq) of the initiator stock solution was added to the monomer resulting in a monomer concentration of 3 mol L^{-1}. The polymerization was initiated by the addition of 60 µL of DBU (62 mg, 0.41 mmol, 5eq). Polymerization was conducted at 5 °C and terminated after 1 h by the rapid addition of an excess of acetic acid dissolved in dichloromethane with a concentration of 20 mg mL^{-1}. The polymer was obtained by three-times precipitation in cold diethyl ether and subsequent dialysis against water to yield 396 mg (75%) of a colorless amorphous polymer.

Representative NMR data.

^{1}H NMR (500 MHz, Chloroform-*d*) δ 4.29 – 4.21 (m, -O-C***H₂***-C***H₂***-O- polymer backbone), 3.81 (d, *J* = 11.3 Hz, -O-C***H₃***), 1.67 (m, -O-CH_2-C***H₂***- initiator) 1.24 (s, -(***CH₂***)$_{15}$-CH_3 initiator) 0.87 (t, J = 6.8 Hz, -C***H₃*** initiator). **^{31}P{H} NMR** (202 MHz, Chloroform-d) δ 1.11, -0.18, -1.50. ^{13}C NMR (126 MHz, Chloroform-d) δ 66.34 (-O-***C***H_2-***C***H_2-O- polymer backbone), 54.68 (-O***C***H_3 side chain) , 29.69, 29.68 (-***C***H_2- initiator), 29.65, 29.52, 29.35, 29.16, 14.06 (-***C***H_3 initiator).

Table 4.6. Analytical results for surfactants S1.

#	DPn	M_n[a] / g mol^{-1}	M_w/M_n[b]	CMC[c] / µmol L^{-1}	T_{cp}/ °C (PBS)
S1-1	35	5100	1.36	5.3 ± 1.8	-
S1-2	35	5100	1.33	7.45 ± 2.5	-
S1-3	35	5100	1.24	n.d.	n.d.

[a]: determined by [1b]: determined by SEC in DMF. [c]: determined by ring-tensiometry. (n.d. = not determined).

Synthesis of surfactant S2. Octadecanol and TU were dried by lyophilization with benzene. EPP (490 mg, 3.26 mmol, 40 eq) was added to the dried TU. A stock solution of octadecanol in dry toluene was prepared with a concentration of 0.07 mol L^{-1}. 1.1mL (22.0 mg, 0.084 mmol, 1 eq) of the initiator stock solution was added to the monomer resulting in a monomer concentration of 3 mol L^{-1}. The polymerization was initiated by the addition of 60 µL of DBU (62 mg, 0.41 mmol, 5 eq). Polymerization was conducted at 0 °C and terminated after 20 h by the rapid addition of an excess of acetic acid dissolved in dichloromethane with a concentration of 20 mg mL^{-1}. The polymer was obtained by three-times precipitation in cold diethyl ether and subsequent dialysis against water to yield 396 mg (77%) of a colorless amorphous polymer.

^{1}H NMR (500 MHz, Chloroform-*d*) δ 4.18 – 4.02 (m, -CH_2-***CH_2***-O- polymer backbone, -O-C***H_2***- side chain), 1.95 (ddt, *J* = 14.9, 11.0, 6.2 Hz, -O-*C*H_2-***CH_2***- polymer backbone), 1.82 (ddt, *J* = 16.7, 11.7, 7.2 Hz, -O-CH_2-CH_2-***CH_2***- polymer backbone), 1.32 (t, *J* = 7.0 Hz, -C***H_3*** side chain), 1.24 (s, -(***CH_2***)$_{15}$-CH_3 initiator), 0.86 (t, *J* = 6.9 Hz, -C***H_3*** initiator). **^{13}C NMR** (126 MHz, Chloroform-*d*) δ 64.99 (-CH_2-***C***H_2-O- polymer backbone) 61.71(-O-***C***H_2- side chain), 29.68 (-(***C***H_2)$_{15}$- initiator), 23.91 (-O-CH_2-***C***H_2- polymer backbone), 22.50, 21.36 (-O-CH_2-CH_2-***C***H_2- polymer backbone), 16,51(-***C***H_3 side chain), 14.12 (-***C***H_3 initiator). **^{31}P{H} NMR** (202 MHz, Chloroform-*d*) δ 31.78, 31.43, 31.19.

Table 4.7. Analytical results for surfactants S2.

#	DP	M_n[a] / g mol^{-1}	M_w/M_n[b]	CMC[c] / g L^{-1}	T_{cp}/ °C (PBS)
S2	40	6300	1.50	4.8 ± 0.9	-

[a]: determined by [1b]: determined by SEC in DMF. [c]: determined by ring-tensiometry

Synthesis of S3. 2-ethyl-1,3,2-dioxaphospholane-2-oxide (457 mg, 3.36 mmol, 40 eq) was placed in a flame-dried Schlenk tube. A stock solution of octadecanol in dry toluene was prepared with a concentration of 0.07 mol L^{-1}. 1.13 mL (22.7 mg, 0.084 mmol, 1 eq) of the initiator stock solution was added to the monomer resulting in a monomer concentration of 3 mol L^{-1}. The polymerization was initiated by the addition of 62 µL of DBU (64 mg, 0.42mmol, 5eq). Polymerization was conducted at room temperature and terminated after 19 h by the rapid addition of an excess of acetic acid dissolved in dichloromethane with a concentration of 20 mg mL^{-1}. The polymer was obtained by three-times precipitation in cold diethyl ether and subsequent dialysis against water to yield 448mg (93%) of a colorless amorphous polymer.

^{1}H NMR (500 MHz, Chloroform-*d*) δ 4.38 – 4.09 (m, -O-C***H₂***-C***H₂***-O- polymer backbone), 1.83 (dq, *J* = 18.4, 7.7 Hz, P-C***H₂***-CH_3 side chain), 1.26 (s, -(C***H₂***)$_{15}$- initiator), 1.19 (dt, *J* = 20.5, 7.6 Hz, P-CH_2-C***H₃*** side chain), 0.86 (t, *J* = 6.9 Hz, -C***H₃*** initiator). **^{13}C NMR** (126 MHz, Chloroform-*d*) δ 64.50(-O-***C***H_2-***C***H_2-O- polymer backbone), 29.69 (-(***C***H_2)$_{15}$- initiator), 19.36, 18.22 (P-***C***H_2-CH_3 side chain), 14.12(-***C***H_3 initiator), 6.44 (P-CH_2-***C***H_3 side chain). **^{31}P{H} NMR** (202 MHz, Chloroform-*d*) δ 35.23.

Table 4.8. Analytical results for surfactants S3.

#	DPn	M_n[a] / g mol^{-1}	M_w/M_n[b]	CMC[c] / g L^{-1}	T_{cp}/ °C (PBS)
S3	41	5700	1.10	5.8 ± 1.5	-

[a]: determined by [1b]: determined by SEC in DMF. [c]: determined by ring-tensiometry

Representative Synthesis of surfactants **S4.** 2-ethoxy-1,3,2-dioxaphospholane-2-oxide (457 mg, 3.36 mmol, 40 eq) was placed in a flame-dried Schlenk tube. A stock solution of octadecanol in dry toluene was prepared with a concentration of 0.07 mol L^{-1}. 1.13 mL (22.7 mg, 0.084 mmol, 1 eq) of the initiator stock solution was added to the monomer resulting in a monomer concentration of 3 mol L^{-1}. The polymerization was initiated by the addition of 62 µL of DBU (64 mg, 0.42 mmol, 5eq). Polymerization was conducted at room temperature and terminated after 19 h by the rapid addition of an excess of acetic acid dissolved in dichloromethane with a concentration of 20 mg mL^{-1}. The polymer was obtained by three-times precipitation in cold diethyl ether and subsequent dialysis against water to yield 448 mg (93%) of a colorless amorphous polymer.

Representative NMR data

^{1}H NMR (300 MHz, Chloroform-*d*) δ 4.39 – 3.95 (m, -O-C***H*****$_2$**-C***H*****$_2$**-O- polymer backbone, -O-C***H*****$_2$**- side chain), 1.35 (t, *J* = 7.1 Hz, -C***H*****$_3$** side chain), 1.24 (s, -(C***H*****$_2$**)$_{15}$- initiator), 0.86 (t, *J* = 6.9 Hz, -C***H*****$_3$** initiator). **^{13}C NMR** (126 MHz, Chloroform-*d*) δ 66.56 (-O-***C***H$_2$-***C***H$_2$-O- polymer backbone), 64.86 (-O-***C***H$_2$- side chain), 29.69(-(***C***H$_2$)$_{15}$- initiator), 16.12 (-***C***H$_3$ side chain). **^{31}P{H} NMR** (202 MHz, Chloroform-d) δ -1.31.

Table 4.9. Analytical results for surfactants S4

#	DP	M_n[a] / g mol^{-1}	M_w/M_n[b]	CMC[c] / g L^{-1}	T_{cp}/ °C (H_2O / PBS)
S4-1	35	5500	1.22	4.2 ± 1.3	n.d.
S4-2	35	5500	1.22	6.6 ± 6.1	57/28

[a]: determined by [1b]: determined by SEC in DMF. [c]: determined by ring-tensiometry

Synthesis of polystyrene and poly (methyl methacrylate) nanoparticles.

The nanoparticles were prepared according to a well-established method.[39] Briefly, a macroemulsion was prepared with the continuous phase containing sodium dodecyl sulfate (SDS) (60 mg) as surfactant in 24 g Milli-Pore water and a dispersed phase containing distilled styrene or methyl methacrylate (6 g), hexadecane (250 mg) as ultrahydrophobe, BODIPY methacrylate (6 mg) as fluorescent dye and azoisobutyronitrile (AIBN) (100 mg, 0.6 mmol) as oil soluble initiator. Both phases were homogenized by mechanical stirring and subsequently, the organic phase was added slowly to the stirring aqueous phase. The macroemulsion was stirred for 1 h at highest speed. Subsequently, the macroemulsion was ultrasonicated with a Branson Sonifier (1/2“ tip) for 3 min (program: 10 s puls and 3 s pause) 70% amplitude under ice cooling to obtain a miniemulsion. The miniemulsion was directly transferred into a 50 mL flask, heated to 72 °C and stirred overnight. In this study two different batches of PS-NPs were used. PS-2 was used for the surface tension measurements depicted in Figure 4.7. Table 4.10 provides an overview over the prepared particles.

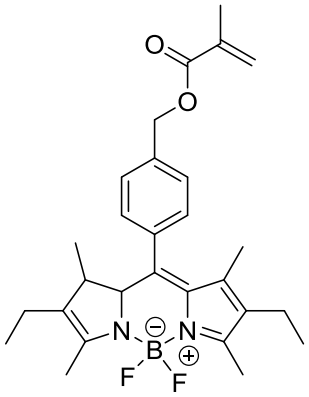

Bodipy

Figure 4.12. Structure of the applied BODIPY methacrylate dye.

Table 4.10. Analytical results for PS and PMMA particles

#	Ø / nm	ζ-Potential
PS-1	103 ± 7	-55 ± 15
PS-2	108 ± 8	-51
PMMA	114 ± 15	-46 ± 12

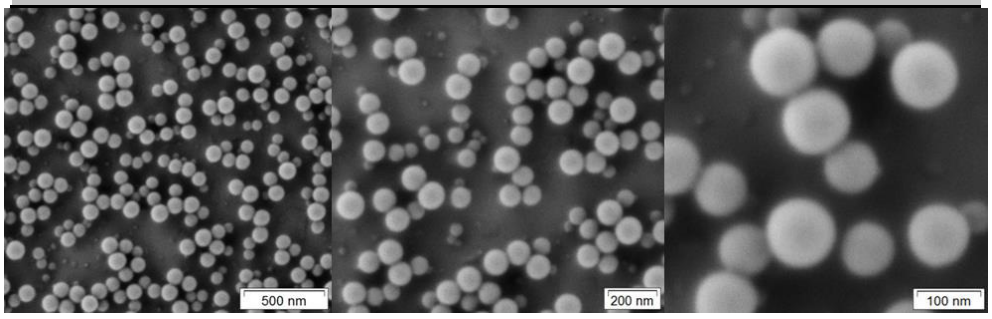

Figure 4.13. Representative SEM pictures of PS-NPs.

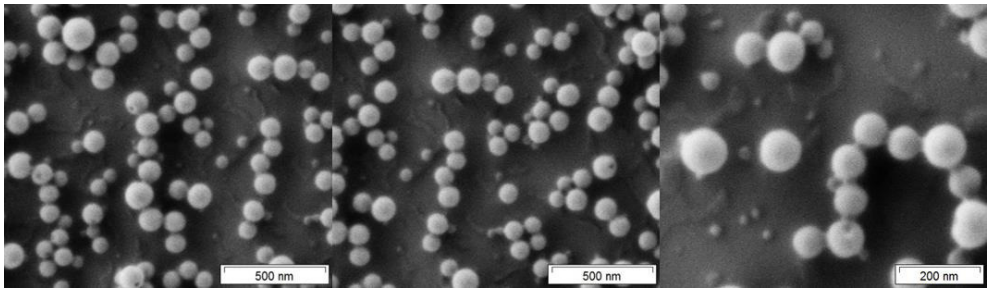

Figure 4.14. SEM pictures of PMMA-NPs.

HSA nanoparticles. HSA particle **HSA-A** was prepared according to a literature procedure.[36, 40] HSA was dissolved at a concentration of 100 mg mL^{-1} in 10 mM NaCl solution and the pH was adjusted to 8 by addition of 10 mM NaOH solution. Aliquots of 1 mL of the HSA solution were taken and mixed with 1 mg of doxorubicin hydrochloride and stirred for 2 h to achieve adsorption of doxorubicin to HSA. Subsequently, nanoparticles were formed by addition of 4 mL of ethanol by using a syringe pump with a dropping rate of 1 mL min^{-1}. The nanoparticles were crosslinked by subsequent addition of 118 µL of a 8% glutaraldehyde solution. The preparation of **HSA-B** and **HSA-C** was conducted analogously using 0.5 mg doxorubicin hydrochloride and crosslinking was achieved by addition of 24.6 µL (**HSA-B**) and 18 µL (**for HSA-C**) of an aqueous 8% glutaraldehyde solution respectively.

Table 4.11. overview over prepared HSA nanoparticles

#	Ø / nm	ζ-Potential /mV	µL GA/ mg HSA	Dox-incorporation
HSA-A	173 ± 15	-45.4	2.1	94.2 ± 0.4
HSA-B	193 ± 22	-43.9	0.4	87.9 ± 0.1
HSA-C	195 ± 28	-43.6	0.294	88.9 ± 0.8

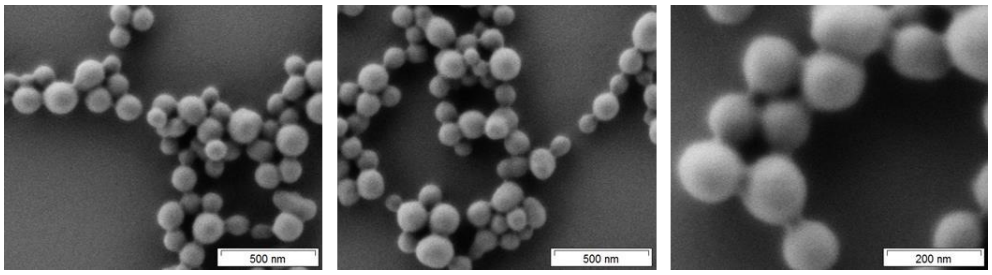

Figure 4.15. Representative SEM pictures of nanoparticles HSA-NPs (HSA-B).

4.3 NMR Spectra

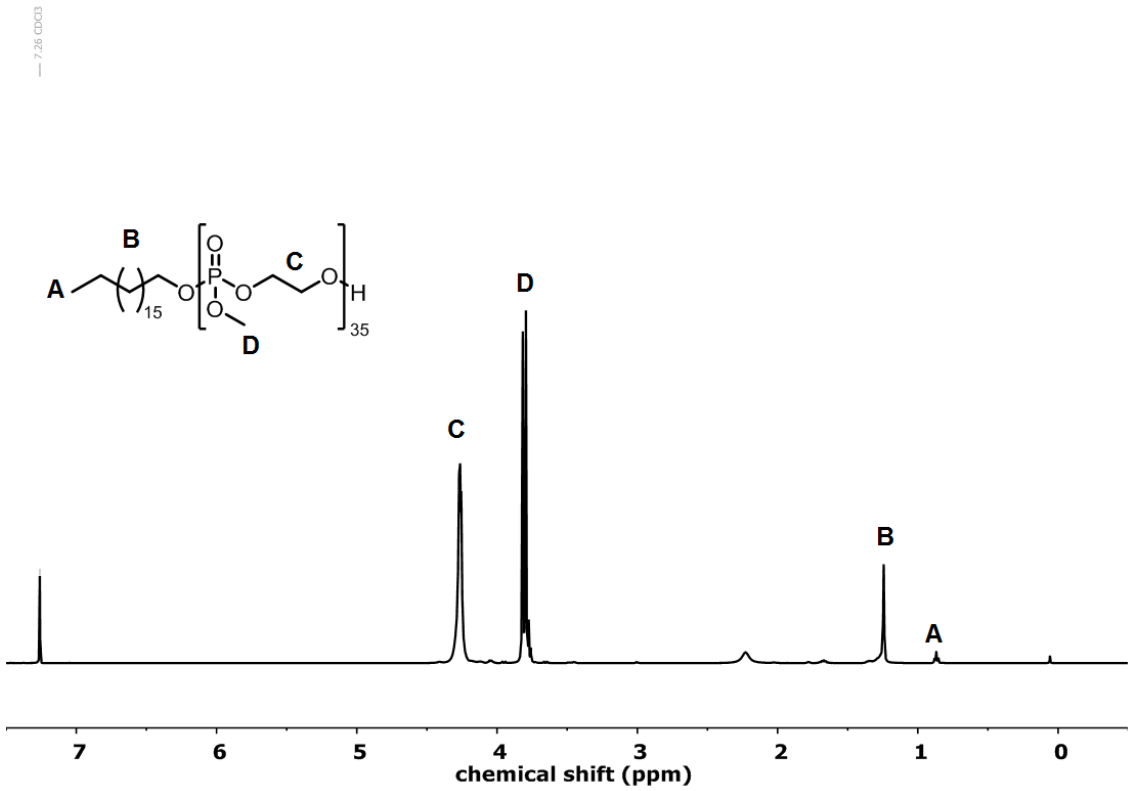

Figure 4.16. Representative ^{1}H NMR (500 MHz) of S1 in $CDCl_3$ at 298 K.

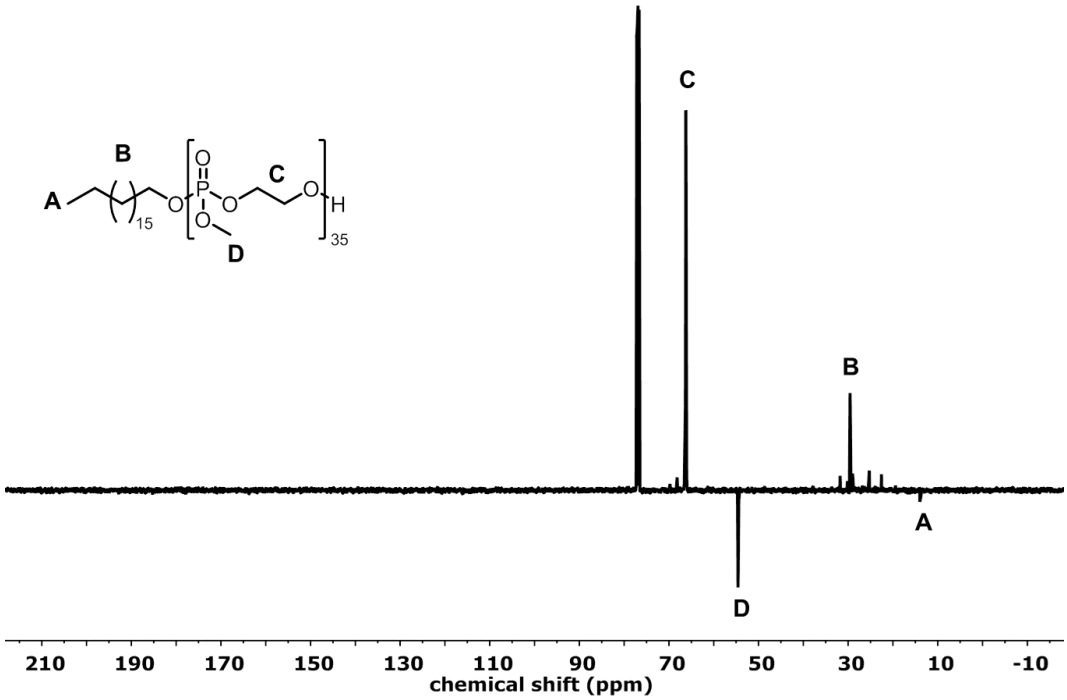

Figure 4.17. Representative ^{13}C NMR (126 MHz) of S1 in $CDCl_3$ at 298 K.

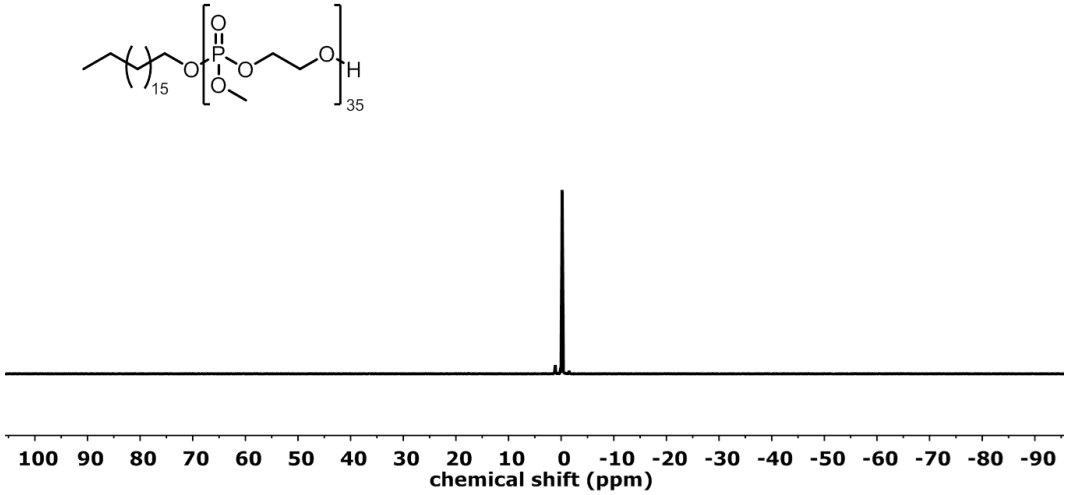

Figure 4.18. Representative $^{31}P\{H\}$ NMR (202 MHz) of S1 in $CDCl_3$ at 298 K.

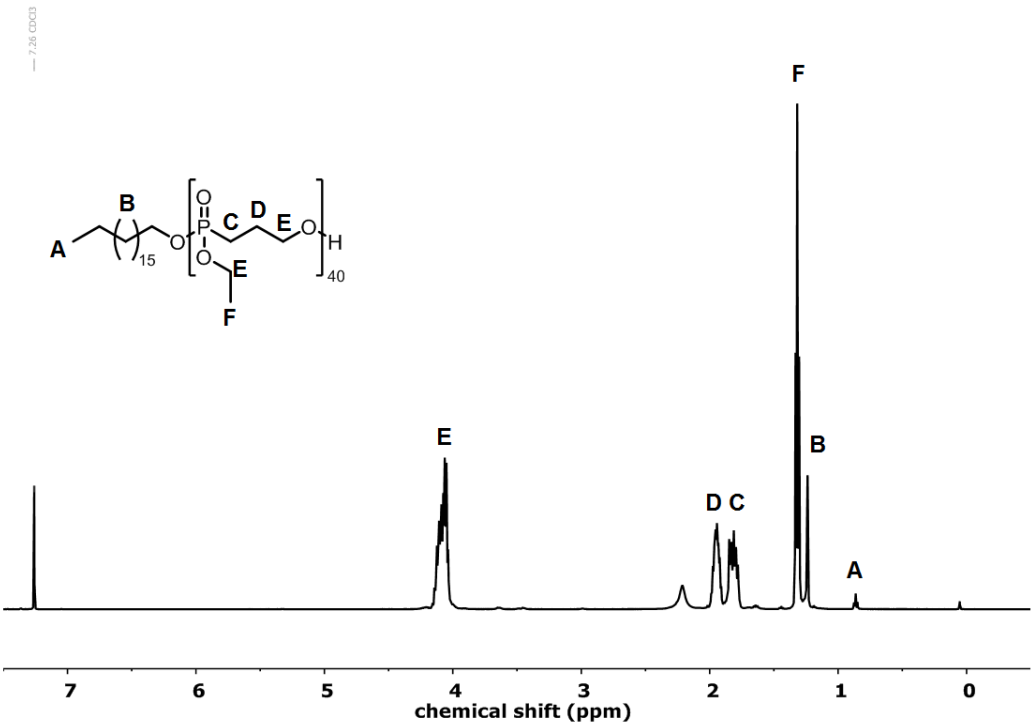

Figure 4.19. Representative ^{1}H NMR (500 MHz) of S2 in $CDCl_3$ at 298 K

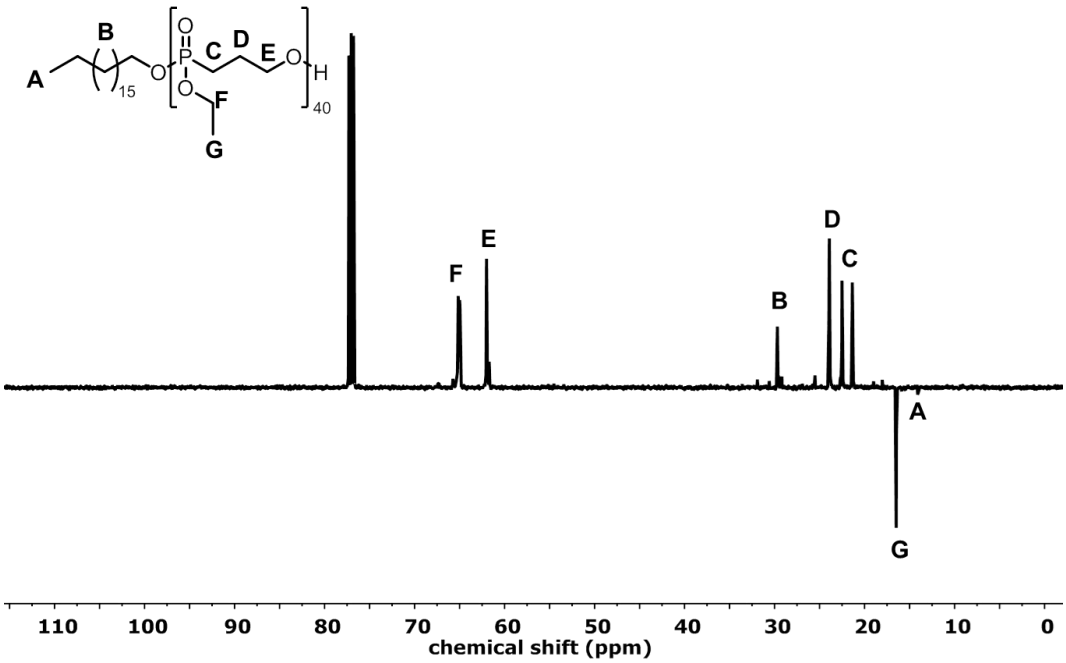

Figure 4.20. Representative ^{13}C NMR (126 MHz) of S2 in $CDCl_3$ at 298 K.

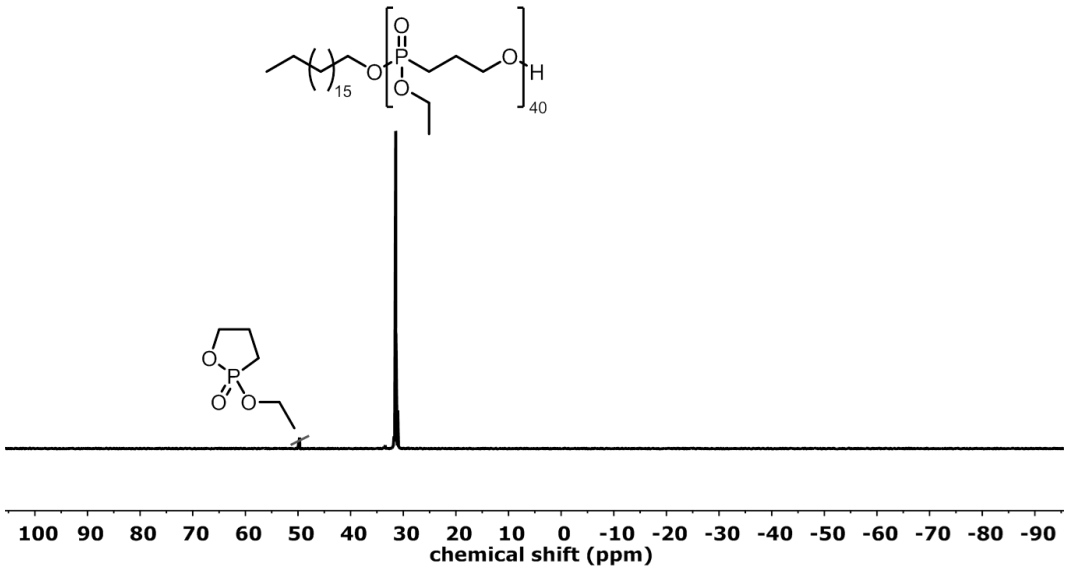

Figure 4.21. Representative $^{31}P\{H\}$ NMR (202 MHz) of S2 in $CDCl_3$ at 298 K.

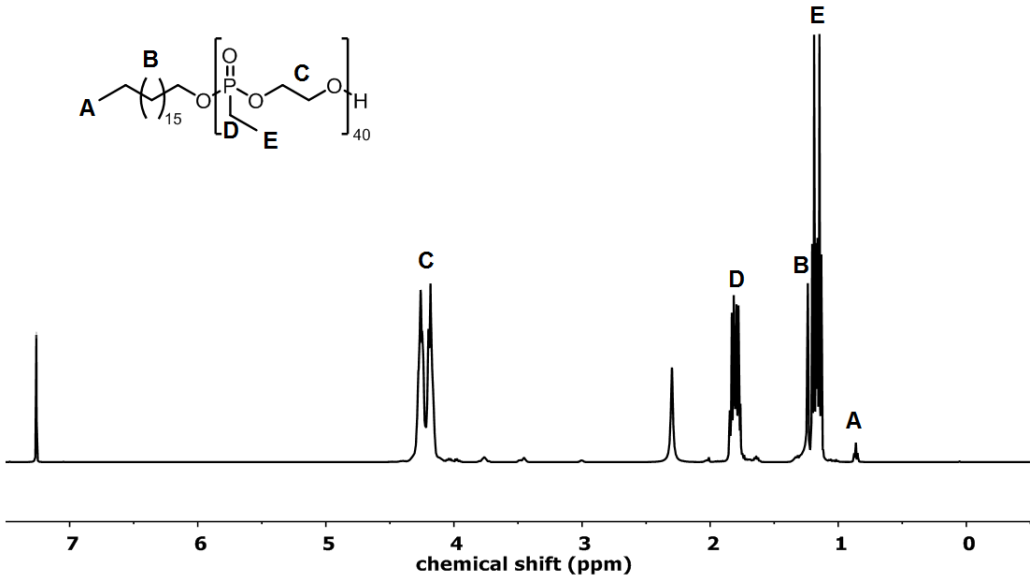

Figure 4.22. Representative ^{1}H NMR (500 MHz) of S3 in $CDCl_3$ at 298 K.

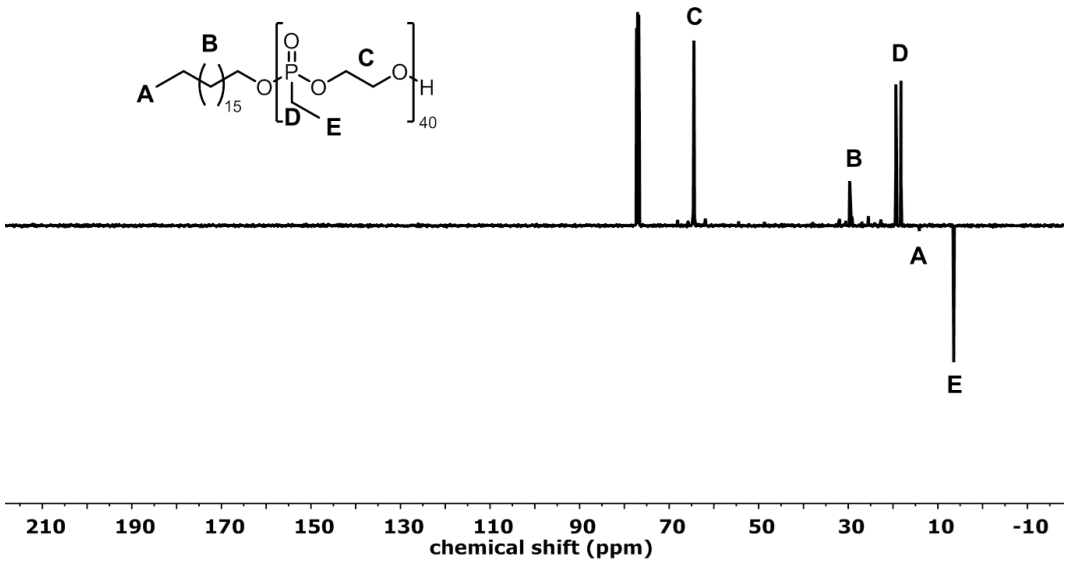

Figure 4.23. Representative ^{13}C NMR (126 MHz) of S2 in $CDCl_3$ at 298 K.

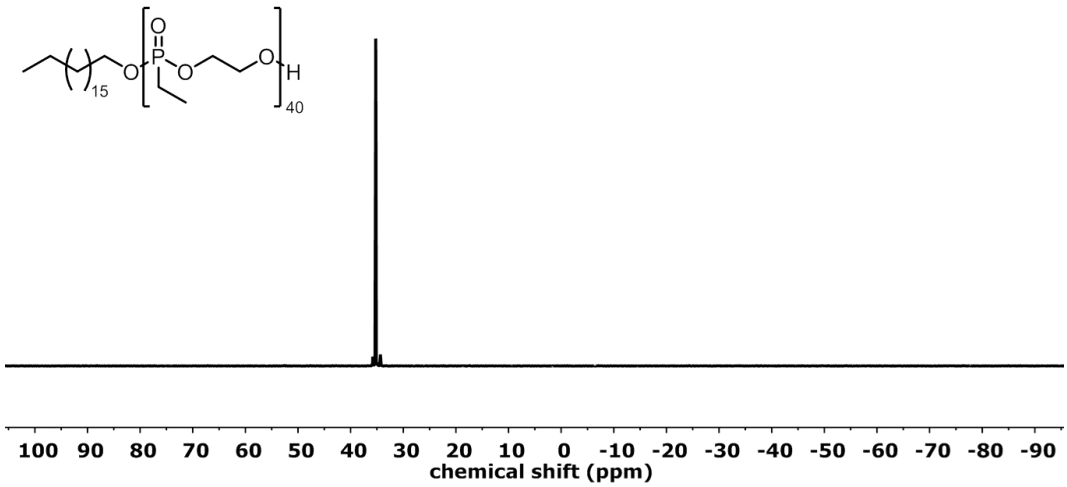

Figure 4.24. Representative $^{31}P\{H\}$ NMR (202 MHz) of S3 in $CDCl_3$ at 298 K.

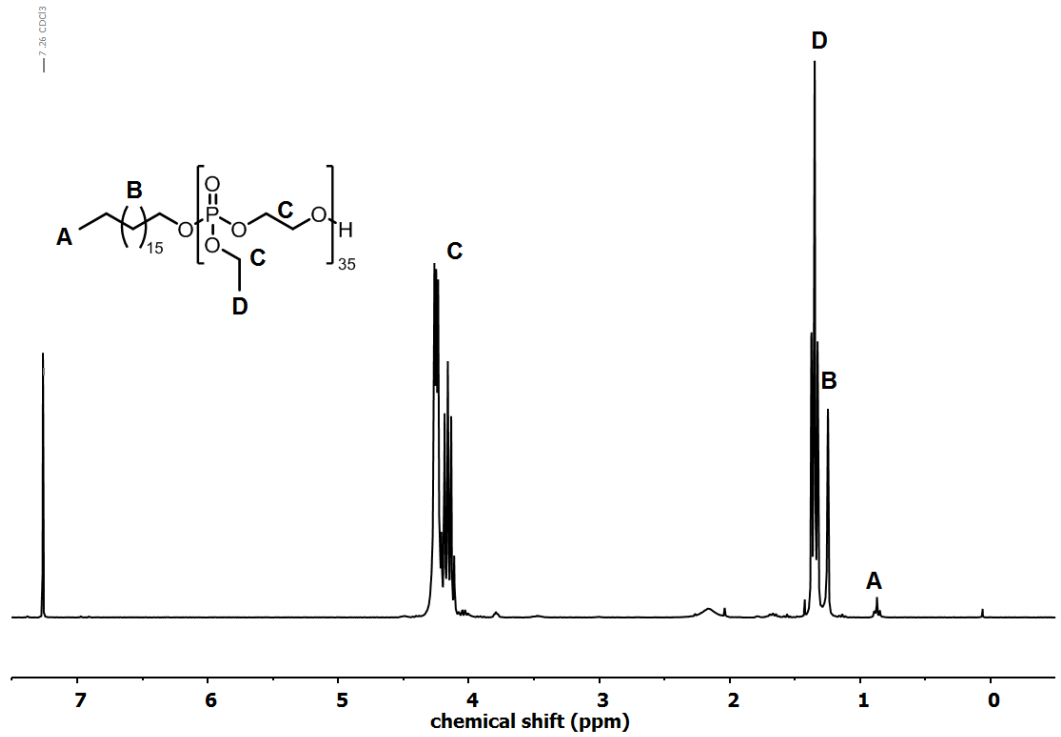

Figure 4.25. Representative ^{1}H NMR (300 MHz) of S4 in $CDCl_3$ at 298 K

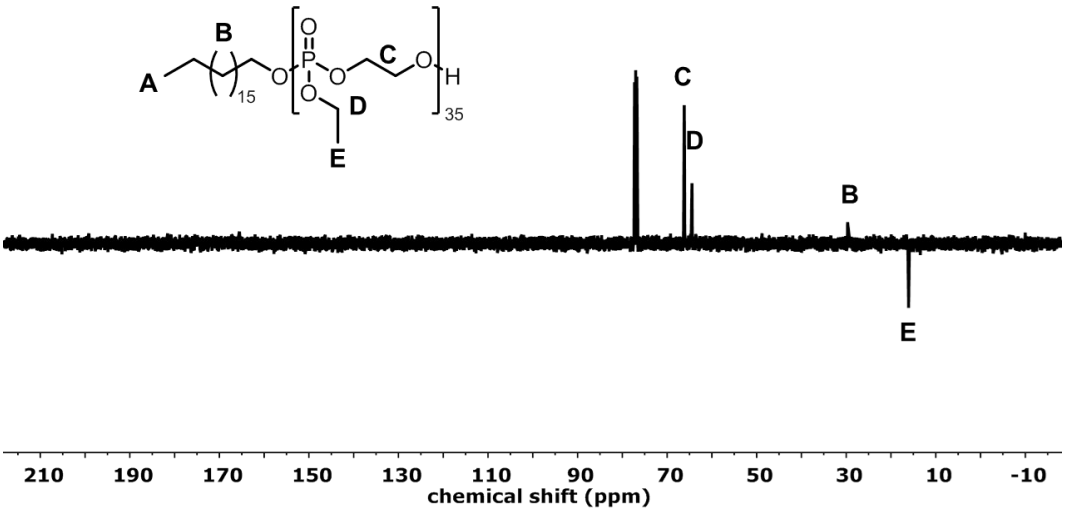

Figure 4.26. Representative ^{13}C NMR (126 MHz) of S4 in $CDCl_3$ at 298 K.

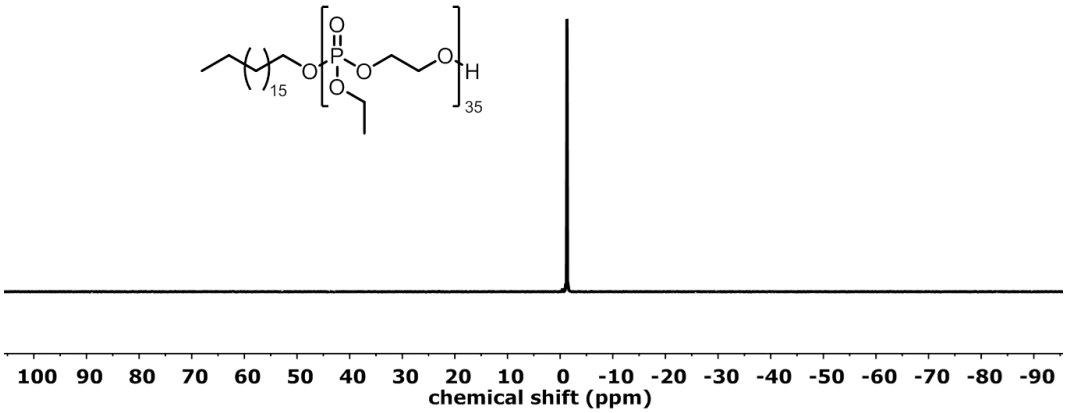

Figure 4.27. Representative $^{31}P\{H\}$ NMR (202 MHz) of S4 in $CDCl_3$ at 298 K.

4.4 SEC

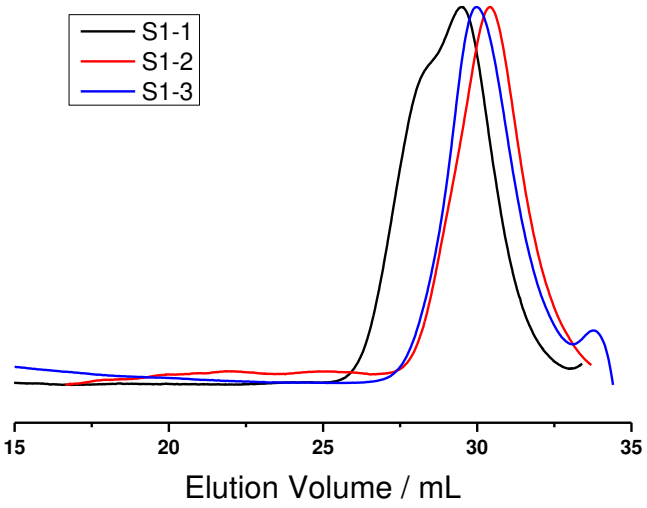

Figure 4.28. SEC traces (RI detection) of surfactants S1 in DMF at 60 °C

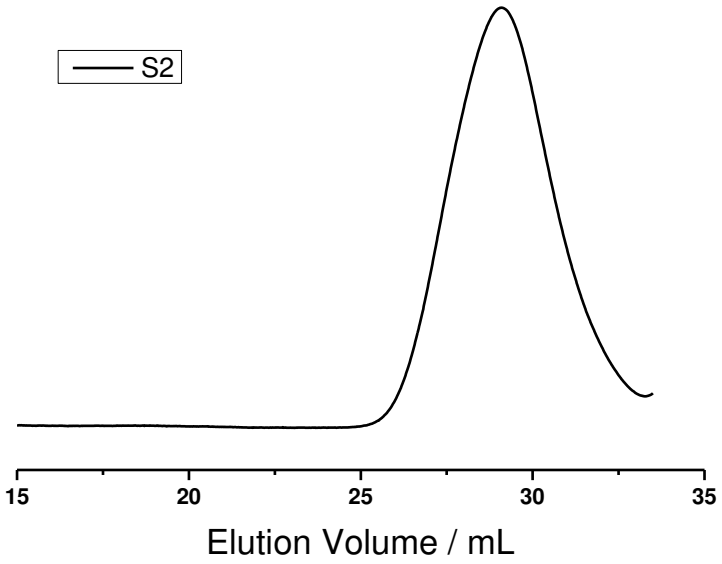

Figure 4.29. SEC traces (RI detection) of surfactant S2 in DMF at 60 °C

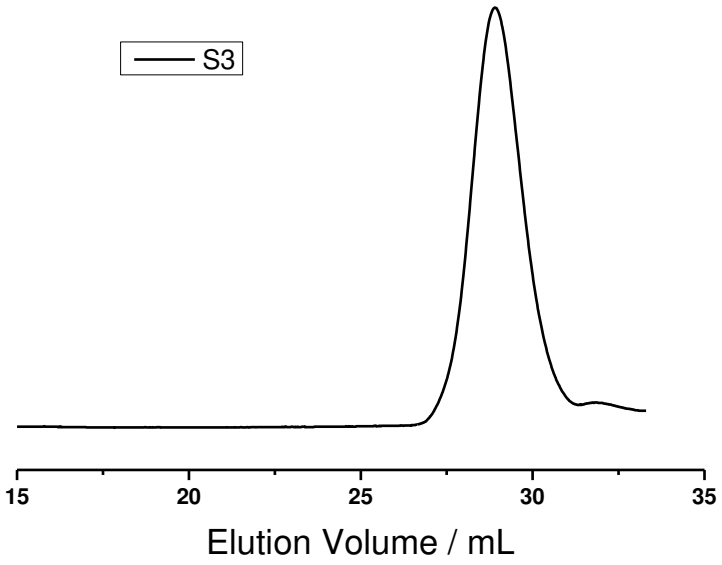

Figure 4.30. SEC traces (RI detection) of S3 in DMF at 60 °C

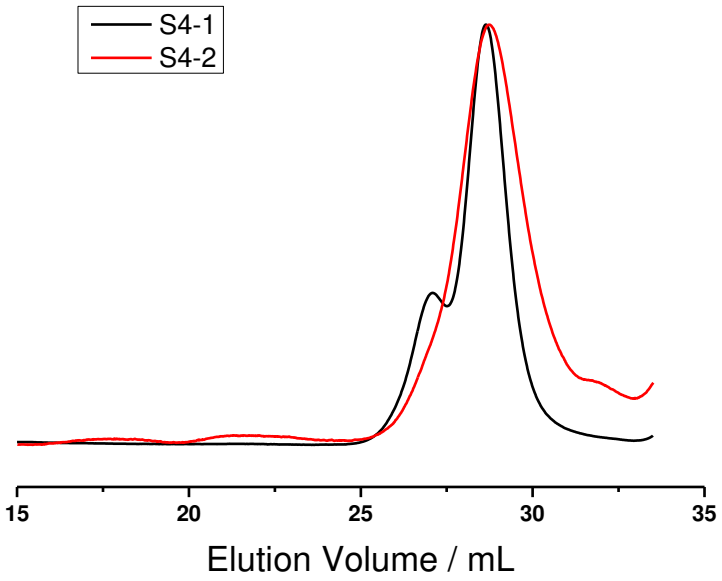

Figure 4.31. SEC traces (RI detection) of S4 in DMF at 60 °C

4.5 LCST

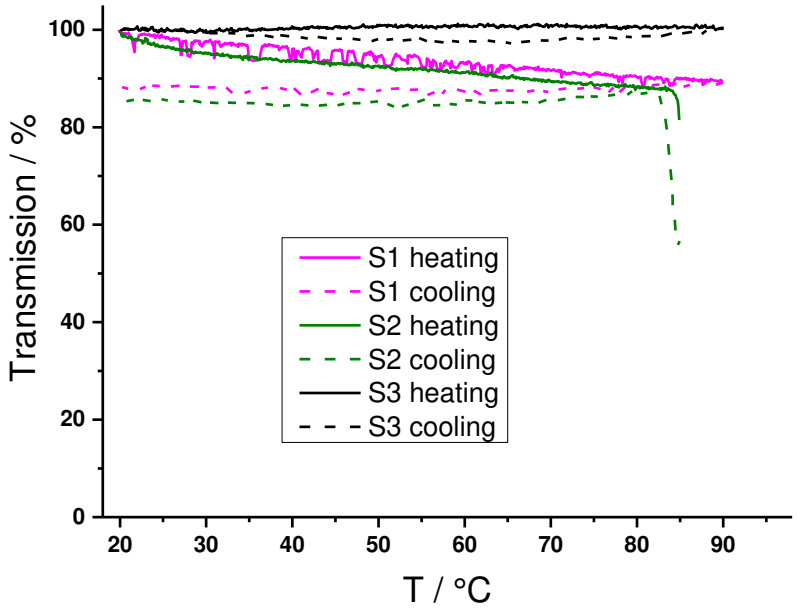

Figure 4.32. Turbidity measurements of S1, S2 and S3 in PBS at a concentration of 5 g L-1 and a heating rate of 1°C min-1. Transmission was measured at 500 nm

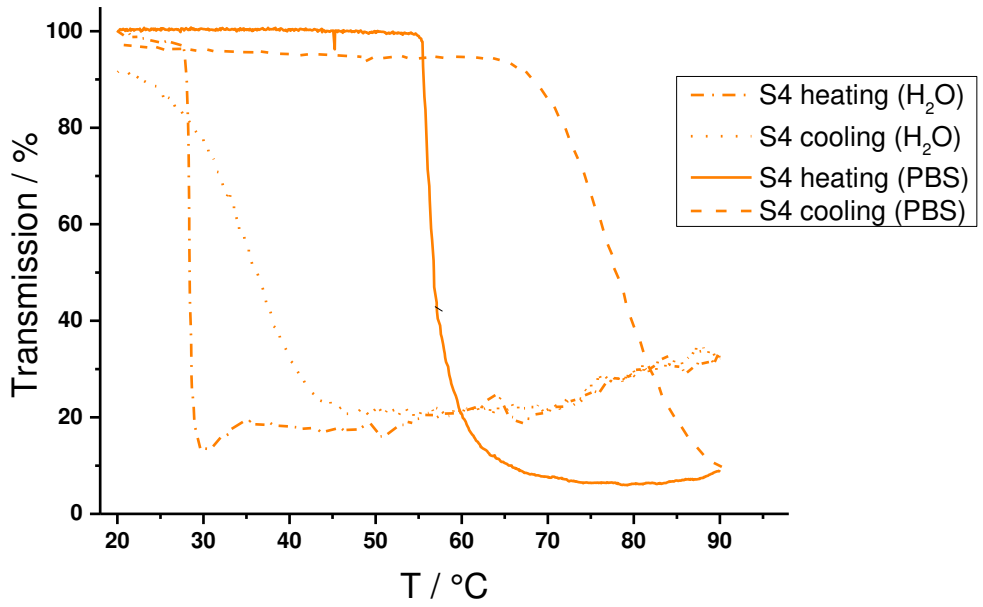

Figure 4.33. Turbidity measurements of S4-2 in MilliQ water and PBS at a concentration of 5 g L^{-1} and a heating rate of 1°C min^{-1}. Transmission was measured at 500 nm. Cloud point temperature (Tcp) was measured at the inflection of the heating curve. The occurrence of phase separation was observed at 29 °C (PBS) and 57 °C (H2O), respectively.

4.6 DSC

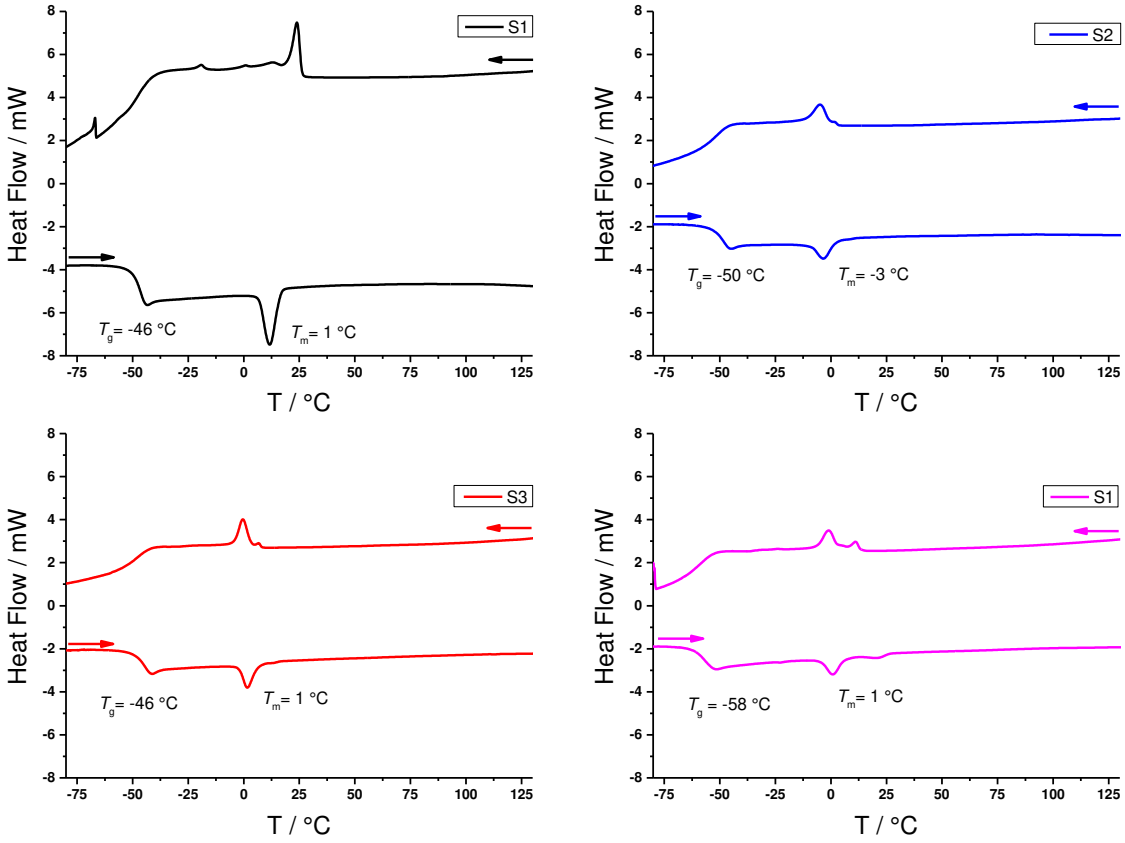

Figure 4.34. DSC thermograms of surfactants S1-S4 (heating and cooling rate 10 K min^{-1} (2nd run).

4.7 Surfactant Degradation

Degradation studies at pH 10 were conducted by incubating 3.5 mg of the respective surfactant in 0.7 mL of a 0.15 M borate buffer ($Na_2B_4O_7$/NaOH) at r.t.. The surfactants were applied in concentrations c= 0.8 - 1µmol L^{-1} corresponding to c= 0.04 - 0.05 mol L^{-1} of repeat unit.

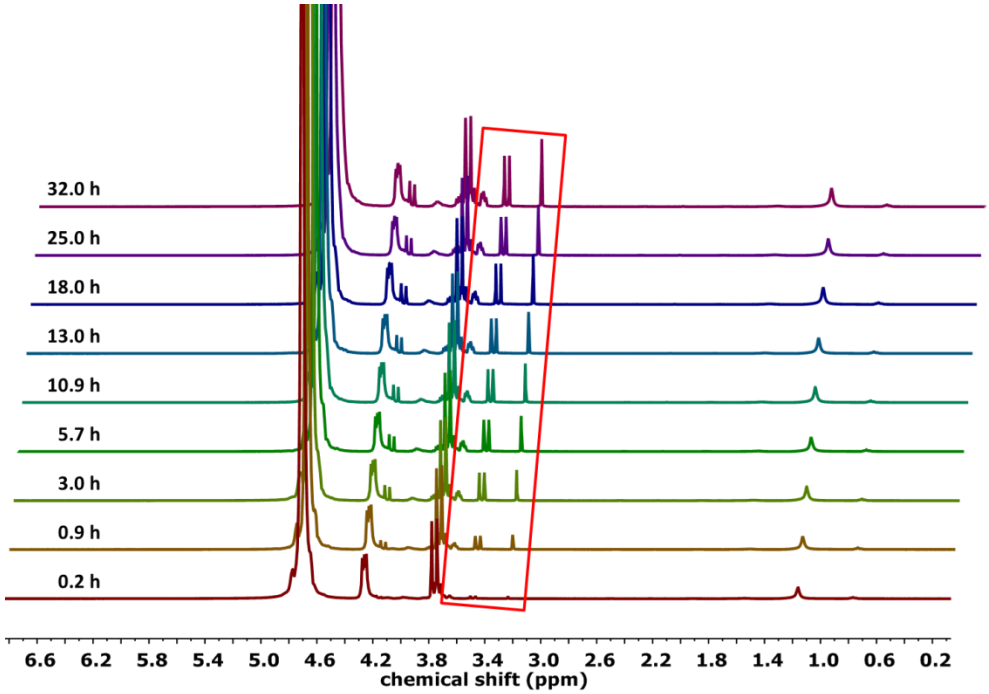

Figure 4.35. ^{1}**H NMRs (300 MHz, H_2O/D_2O (9/1), 298 K) of the degradation of S1 at pH10. Signals of the degradation products are marked in red.**

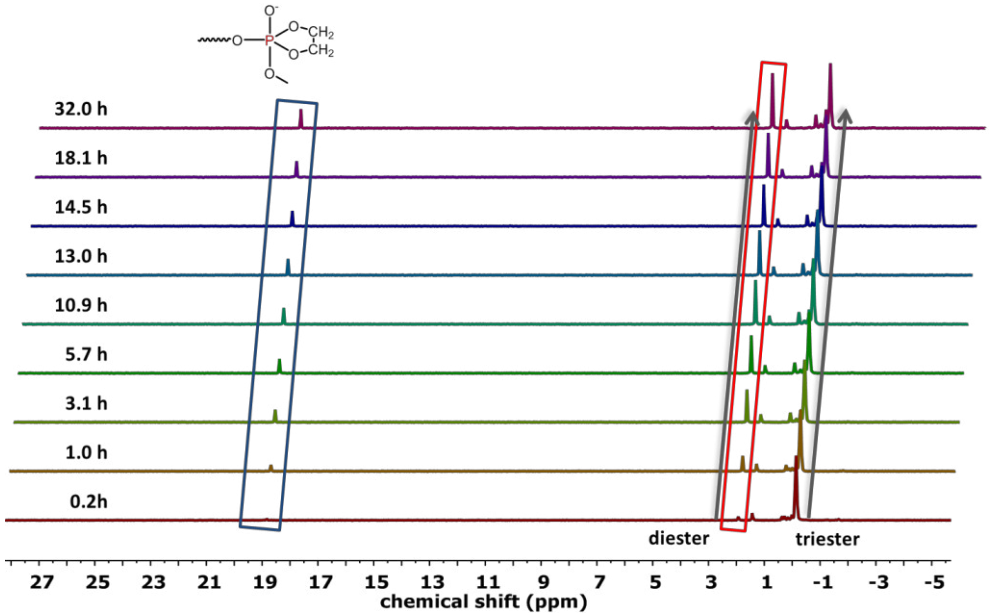

Figure 4.36. ^{31}**P{H} NMRs (121 MHz, H_2O/D_2O (9/1), 298 K) of the degradation of S1 at pH10. Signals of the degradation products are marked in red.**

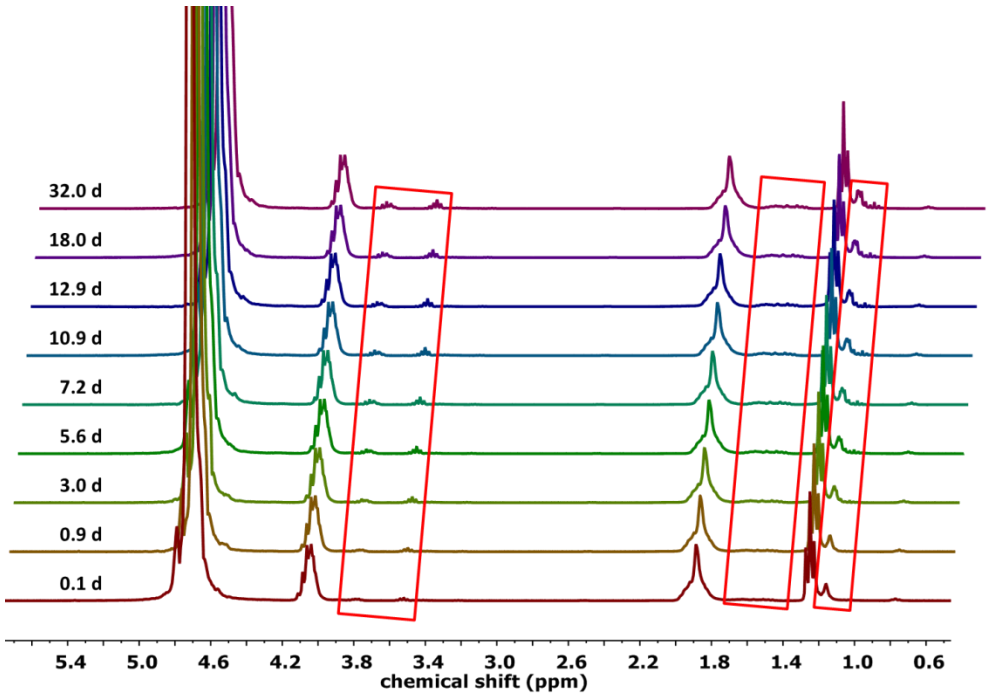

Figure 4.37. ^{1}H NMRs (300 MHz, H_2O/D_2O (9/1), 298 K) of the degradation of S2 at pH10. Signals of the degradation products are marked in red. (Data depicted in this figure was also used in chapter 3)

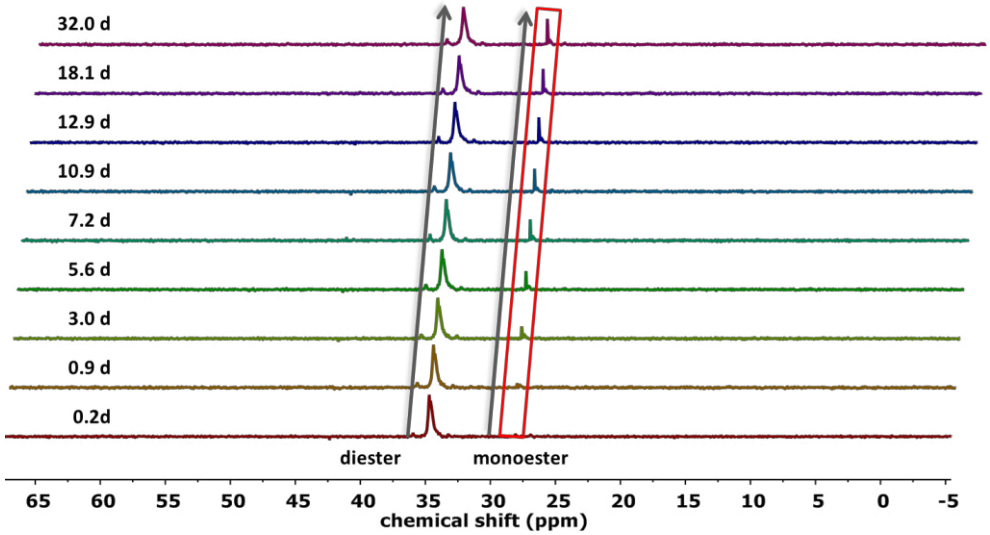

Figure 4.38. $^{31}P\{H\}$ **NMRs (121 MHz,** H_2O/D_2O **(9/1), 298 K) of the degradation of S2 at pH10. Signals of the degradation products are marked in red. (Data depicted in this figure was also used in chapter 3)**

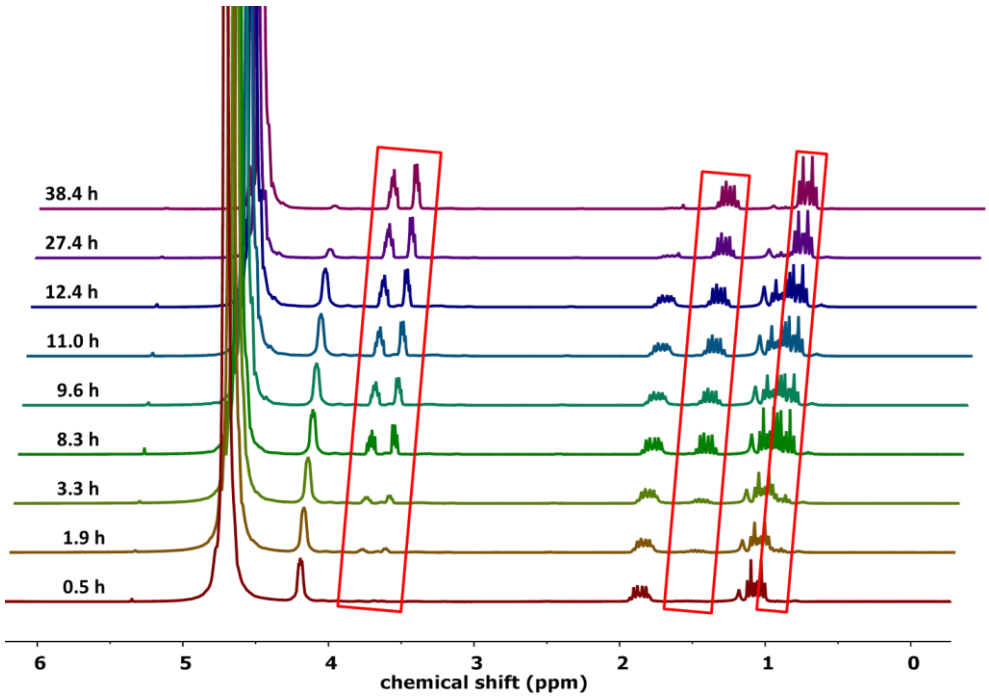

Figure 4.39. ^{1}**H NMRs (300 MHz,** H_2O/D_2O **(9/1), 298 K) of the degradation of S3 at pH10. Signals of the degradation products are marked in red. (Data depicted in this figure was also used in chapter 3)**

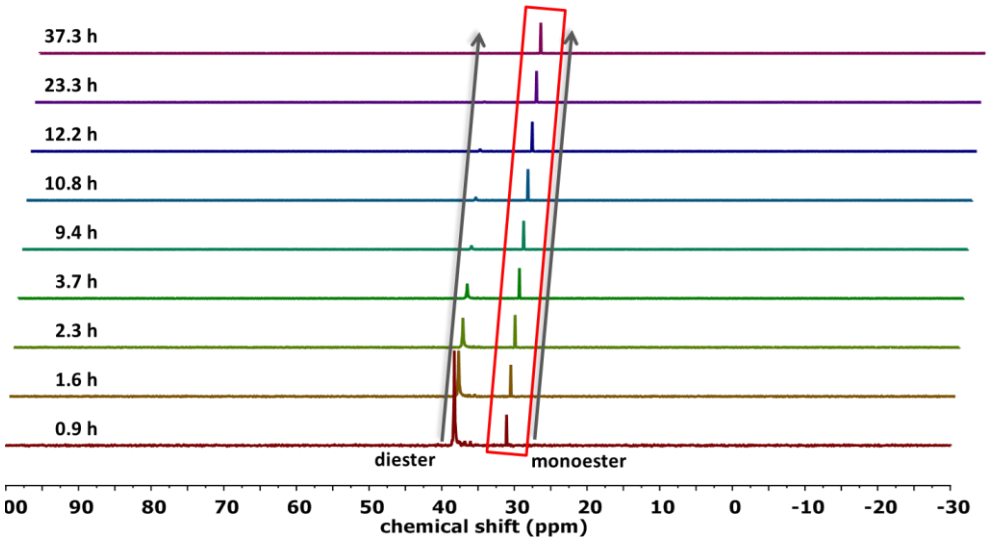

Figure 4.40. ^{31}P{H} NMRs (121 MHz, H_2O/D_2O (9/1), 298 K) of the degradation of S3 at pH10. Signals of degradation products are marked in red. (Data depicted in this figure was also used in chapter 3)

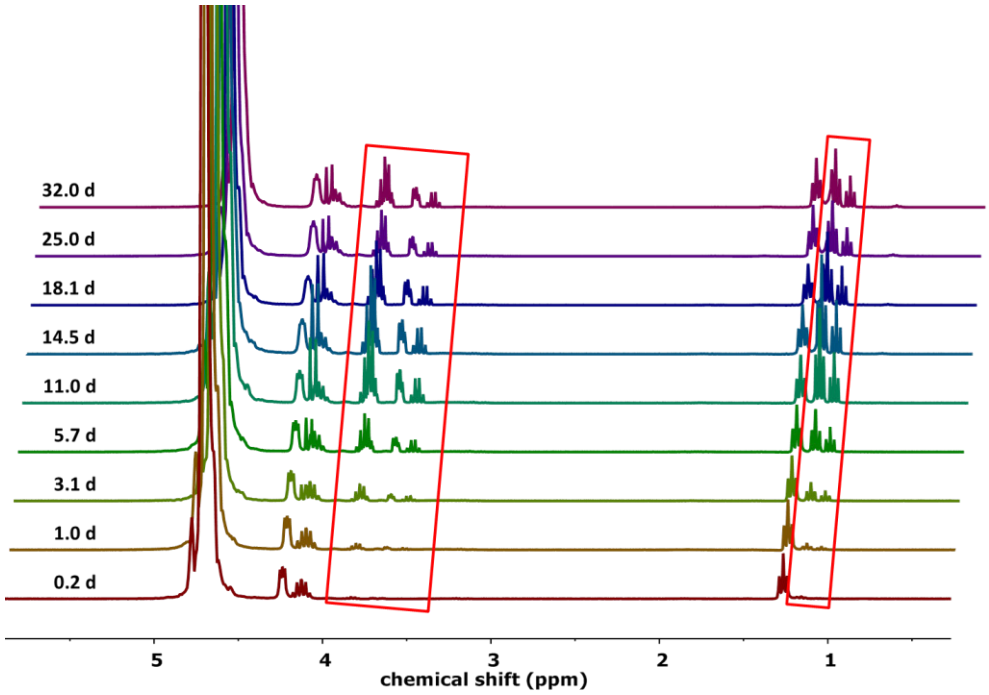

Figure 4.41. ^{1}H NMRs (300 MHz, H_2O/D_2O (9/1), 298 K) of the degradation of S4 at pH10. Signals of degradation products are marked in red.

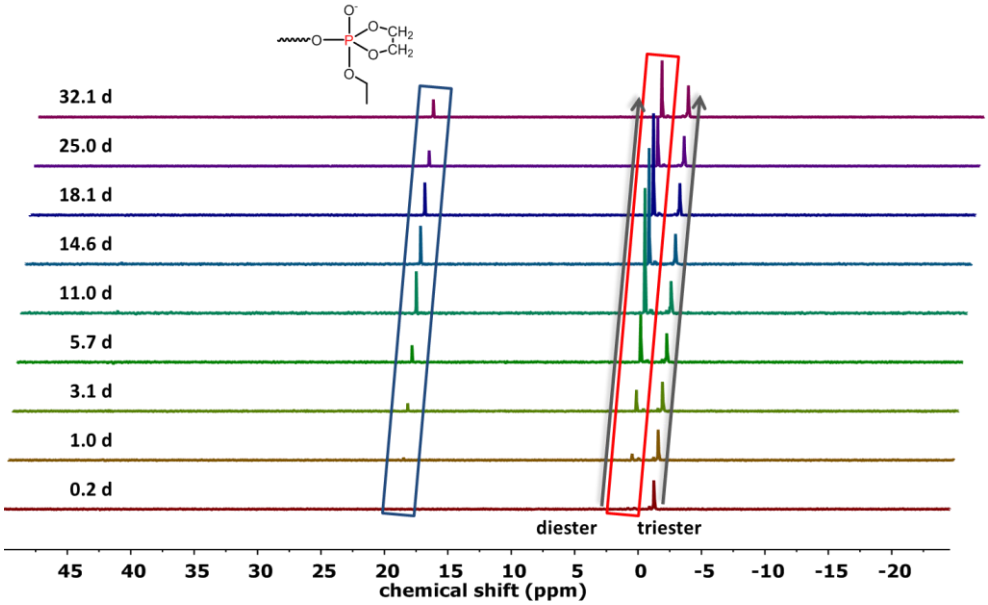

Figure 4.42. $^{31}P\{H\}$ NMRs (121 MHz, H_2O/D_2O (9/1), 298 K) of the degradation of S4 at pH10. Signals of degradation products are marked in red.

4.8 Surfactant Protein interaction

4.8.1 Interaction with human serum albumin (HSA)

A stock solution of HSA in MilliQ water at a concentration of 60 mg mL^{-1} was prepared and solutions of each surfactant in MilliQ water at a concentration of 4 µmol L^{-1} were prepared. To evaluate the concentration dependent interaction 200 µL of HSA stock solution were treated with 5, 10, 15, 20, 25 µL of the surfactant stock solutions and the amount of denatured protein was evaluated by NanoDSF measurements. As reference the native protein and the denatured protein were used. Denaturing of the protein was achieved by incubation of the protein in a SDS solution at a concentration of 2 wt% for 30 min at 95°C. The amount of denatured protein was determined by label-free differential scanning fluorimetry (nanoDSF). Depending on the protein structure the thermal unfolding process led to changes in fluorescence emission properties monitored at to wavelengths (350 nm and 330 nm). Here, the fluorescence emission is plotted as the ratio of 350/330 nm. As references the native protein and the denatured protein were used. Denaturing of the protein was achieved by incubation of the protein in a SDS solution at a concentration of 2 wt% for 30 min at 95°C. The distance between the plots for the native and the

denatured protein was assumed as maximum deviation. The percentage of denaturation of HSA at different surfactant concentrations was determined by referencing the deviation for each surfactant concentration to the maximum deviation. Here, the first six values were used to determine the deviation from the plot of the native protein.

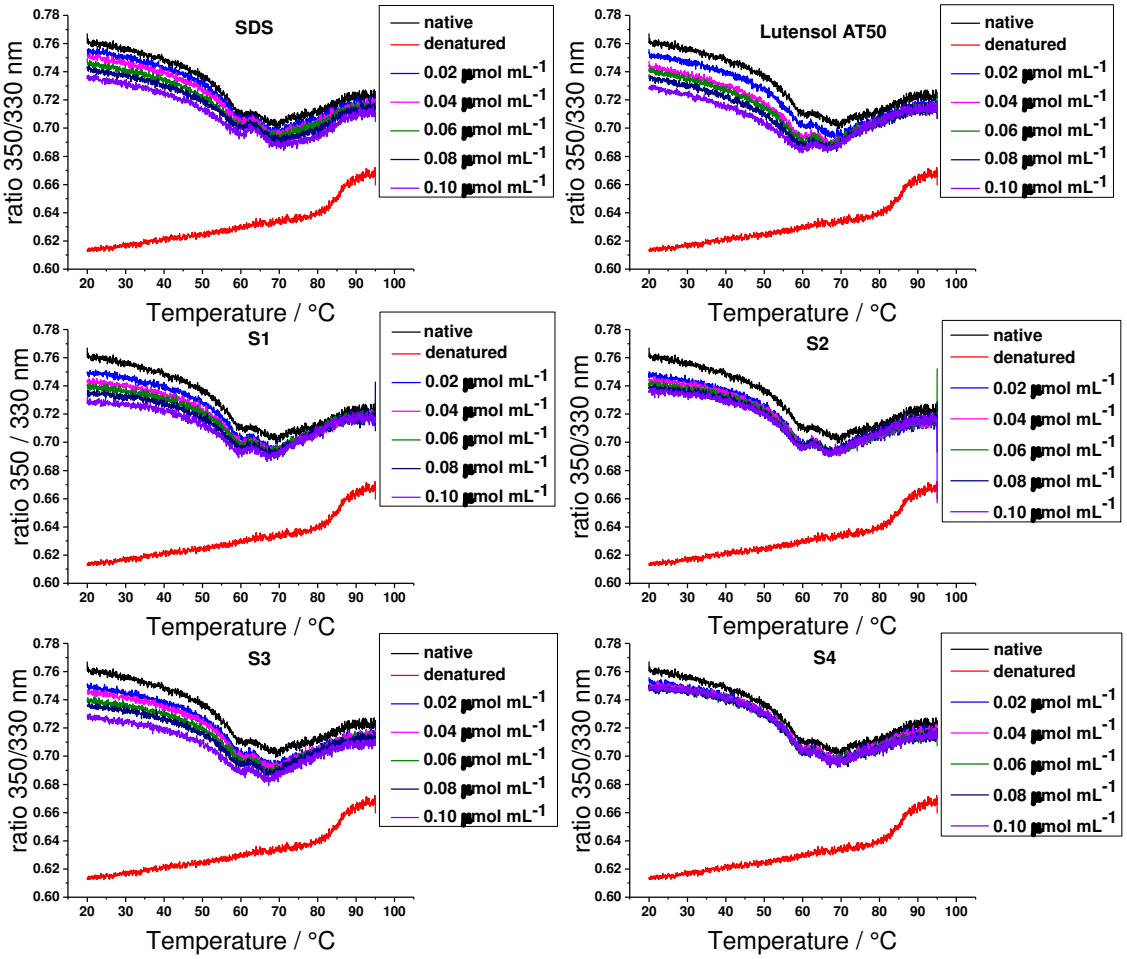

Figure 4.43. Thermal unfolding curves of HSA in a temperature range between 20 and 95 °C plotted as the ratio between 350/330 nm. Each graph shows the plot for the native and denatured protein as well as the plots for HSA treated with different amounts of SDS (A), Lutensol AT50 (B), S1 (C), S2 (D), S3 (E) and S4(F).

4.8.2 Interaction with fibrinogen

The interaction between the surfactants and fibrinogen was evaluated analogously to the procedure for HSA. For fibrinogen a stock solution at a lower concentration of 10 mg mL^{-1} in MilliQ water was prepared.

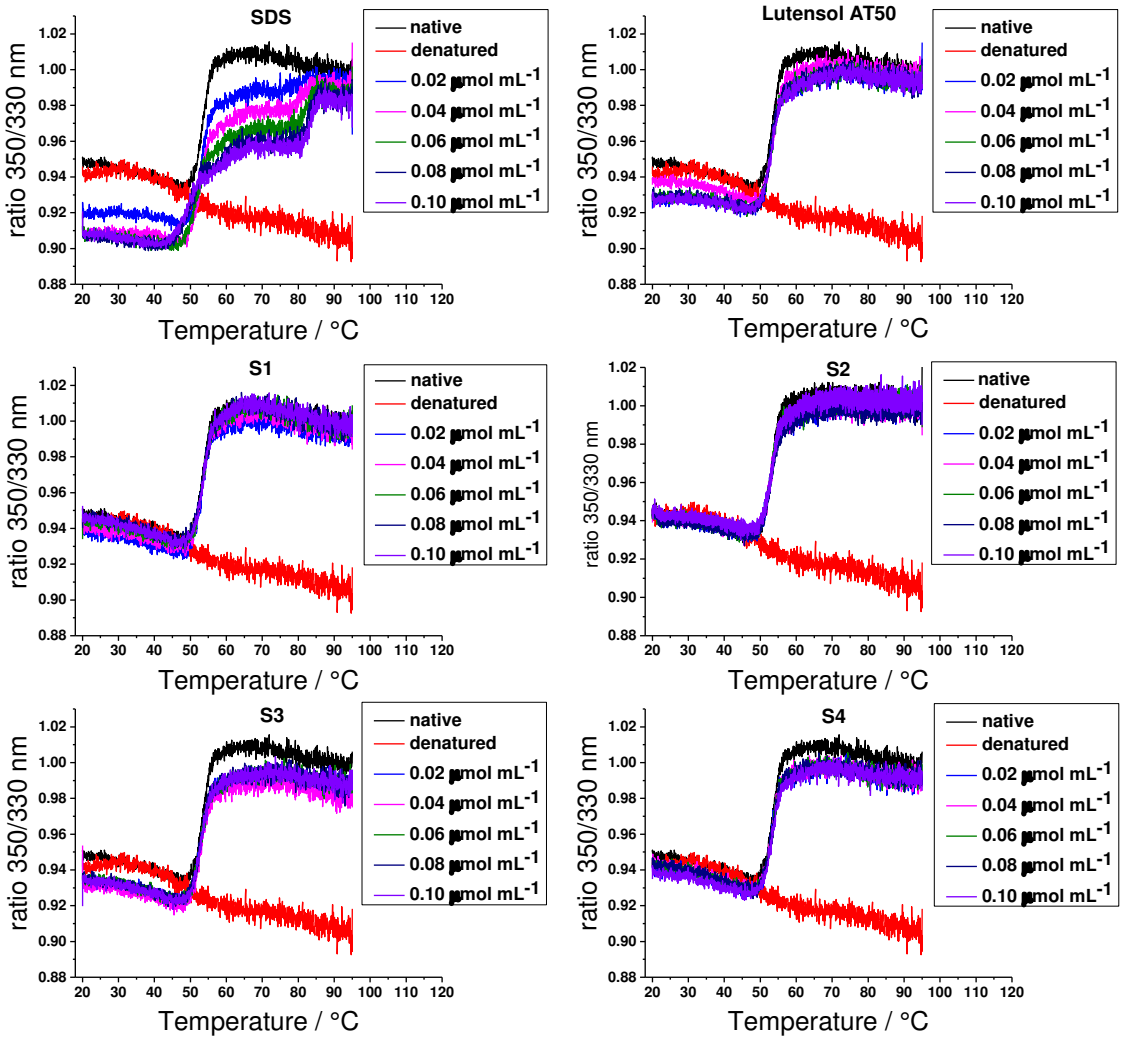

Figure 4.44. Thermal unfolding curves of fibrinogen in a temperature range between 20 and 95 °C plotted as the ratio between 350/330 nm. Each graph shows the plot for the native and denatured protein as well as the plots for fibrinogen treated with different amounts of SDS (A), Lutensol AT50 (B), S1 (C), S2 (D), S3 (E) and S4(F).

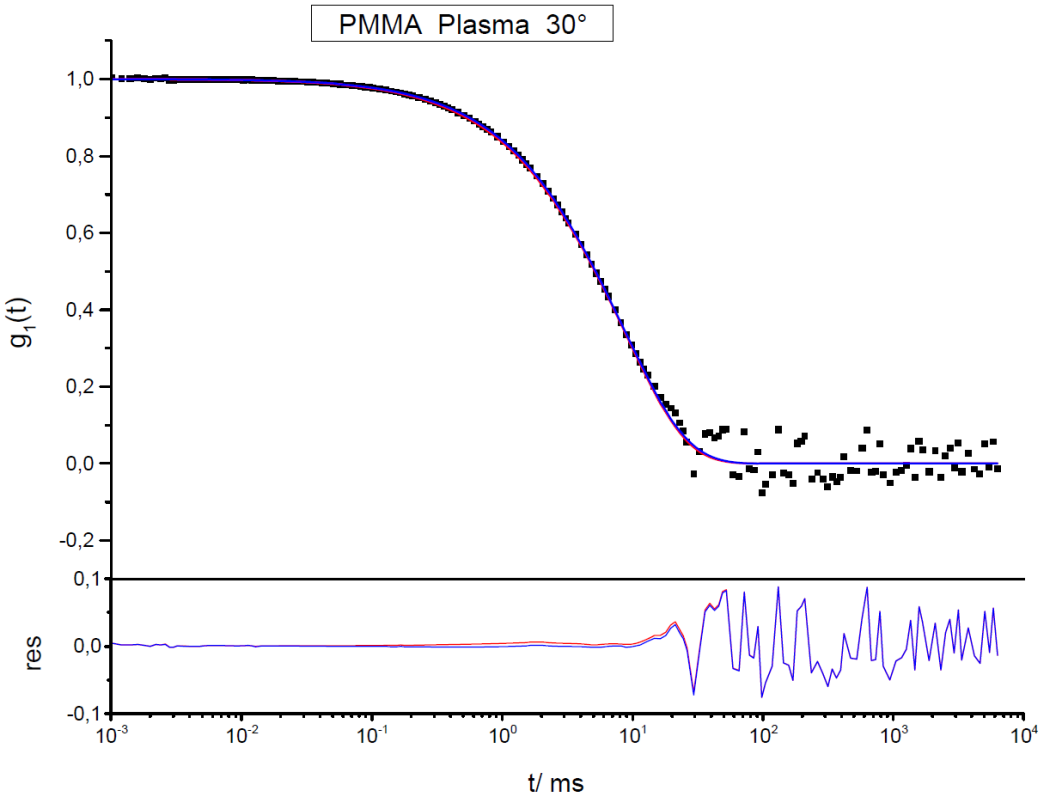

Figure 4.45. Autocorrelation functions (ACFs) for PMMA-NPs stabilized with SDS. Upper graphs: ACF $g_1(t)$ (black dots) for a scattering angle of 30 ° with a forced fit consisting of the sum of the two individual components (red line −) and a fit with an additional aggregate function where necessary (blue line −). Lower graphs: Residuals resulting from the difference of the data and the corresponding fits.

5 References

1. Kollman, J. M.; Pandi, L.; Sawaya, M. R.; Riley, M.; Doolittle, R. F., Crystal Structure of Human Fibrinogen. *Biochemistry* **2009,** *48* (18), 3877-3886.
2. Zhang, Y.; Lee, P.; Liang, S.; Zhou, Z.; Wu, X.; Yang, F.; Liang, H., Structural Basis of Non-Steroidal Anti-Inflammatory Drug Diclofenac Binding to Human Serum Albumin. *Chemical Biology & Drug Design* **2015,** *86* (5), 1178-1184.
3. Müller, J.; Bauer, K. N.; Prozeller, D.; Simon, J.; Mailänder, V.; Wurm, F. R.; Winzen, S.; Landfester, K., Coating nanoparticles with tunable surfactants facilitates control over the protein corona. *Biomaterials* **2017,** *115*, 1-8.
4. Caracciolo, G.; Palchetti, S.; Colapicchioni, V.; Digiacomo, L.; Pozzi, D.; Capriotti, A. L.; La Barbera, G.; Laganà, A., Stealth Effect of Biomolecular Corona on Nanoparticle Uptake by Immune Cells. *Langmuir* **2015,** *31* (39), 10764-10773.
5. Mirshafiee, V.; Kim, R.; Park, S.; Mahmoudi, M.; Kraft, M. L., Impact of protein pre-coating on the protein corona composition and nanoparticle cellular uptake. *Biomaterials* **2016,** *75* (Supplement C), 295-304.
6. Knop, K.; Hoogenboom, R.; Fischer, D.; Schubert, U. S., Poly(ethylene glycol) in Drug Delivery: Pros and Cons as Well as Potential Alternatives. *Angewandte Chemie International Edition* **2010,** *49* (36), 6288-6308.
7. Allen, T. M.; Cullis, P. R., Drug delivery systems: entering the mainstream. *Science* **2004,** *303* (5665), 1818-1822.
8. Schöttler, S.; Landfester, K.; Mailänder, V., Controlling the Stealth Effect of Nanocarriers through Understanding the Protein Corona. *Angewandte Chemie International Edition* **2016,** *55* (31), 8806-8815.
9. Carpenter, C. P.; Woodside, M. D.; Kinkead, E. R.; King, J. M.; Sullivan, L. J., Response of dogs to repeated intravenous injection of polyethylene glycol 4000 with notes on excretion and sensitization. *Toxicology and Applied Pharmacology* **1971,** *18* (1), 35-40.
10. Smyth, H. F.; Carpenter, C. P.; Weil, C. S., The toxicology of the polyethylene glycols. *Journal of the American Pharmaceutical Association* **1950,** *39* (6), 349-354.
11. Wang, H.; Su, L.; Li, R.; Zhang, S.; Fan, J.; Zhang, F.; Nguyen, T. P.; Wooley, K. L., Polyphosphoramidates That Undergo Acid-Triggered Backbone Degradation. *ACS Macro Letters* **2017,** *6* (3), 219-223.
12. Steinbach, T.; Alexandrino, E. M.; Wahlen, C.; Landfester, K.; Wurm, F. R., Poly(phosphonate)s via Olefin Metathesis: Adjusting Hydrophobicity and Morphology. *Macromolecules* **2014,** *47* (15), 4884-4893.
13. Schöttler, S.; Becker, G.; Winzen, S.; Steinbach, T.; Mohr, K.; Landfester, K.; Mailänder, V.; Wurm, F. R., Protein adsorption is required for stealth effect of poly (ethylene glycol)-and poly (phosphoester)-coated nanocarriers. *Nature nanotechnology* **2016,** *11* (4), 372-377.
14. Holmberg, K.; Jönsson, B.; Kronberg, B.; Lindman, B., *Surfactants and polymers in aqueous solution*. Wiley Online Library: 2002.
15. Steinbach, T.; Ritz, S.; Wurm, F. R., Water-Soluble Poly(phosphonate)s via Living Ring-Opening Polymerization. *ACS Macro Letters* **2014,** *3* (3), 244-248.
16. Wolf, T.; Steinbach, T.; Wurm, F. R., A Library of Well-Defined and Water-Soluble Poly(alkyl phosphonate)s with Adjustable Hydrolysis. *Macromolecules* **2015**.
17. Ujhelyi, Z.; Fenyvesi, F.; Váradi, J.; Fehér, P.; Kiss, T.; Veszelka, S.; Deli, M.; Vecsernyés, M.; Bácskay, I., Evaluation of cytotoxicity of surfactants used in self-micro

emulsifying drug delivery systems and their effects on paracellular transport in Caco-2 cell monolayer. *European Journal of Pharmaceutical Sciences* **2012,** *47* (3), 564-573.
18. Partearroyo, M. A.; Ostolaza, H.; Goñi, F. M.; Barberá-Guillem, E., Surfactant-induced cell toxicity and cell lysis. *Biochemical Pharmacology* **1990,** *40* (6), 1323-1328.
19. Grant, R. L.; Yao, C.; Gabaldon, D.; Acosta, D., Evaluation of surfactant cytotoxicity potential by primary cultures of ocular tissues: I. Characterization of rabbit corneal epithelial cells and initial injury and delayed toxicity studies. *Toxicology* **1992,** *76* (2), 153-176.
20. Partearroyo, M. A.; Ostolaza, H.; Goñi, F. M.; Barberá-Guillem, E., Surfactant-induced cell toxicity and cell lysis: A study using B16 melanoma cells. *Biochemical Pharmacology* **1990,** *40* (6), 1323-1328.
21. Miyazawa, K.; Ogawa, M.; Mitsui, T., The physico-chemical properties and protein denaturation potential of surfactant mixtures. *International Journal of Cosmetic Science* **1984,** *6* (1), 33-46.
22. Elzoghby, A. O.; Samy, W. M.; Elgindy, N. A., Albumin-based nanoparticles as potential controlled release drug delivery systems. *Journal of Controlled Release* **2012,** *157* (2), 168-182.
23. Strutz, W., Exploring Protein Stability by NanoDSF. *Biophysical Journal 110* (3), 393a.
24. Baran, J.; Penczek, S., Hydrolysis of polyesters of phosphoric acid. 1. Kinetics and the pH profile. *Macromolecules* **1995,** *28* (15), 5167-5176.
25. del Real, R. P.; Padilla, S.; Vallet-Regí, M., Gentamicin release from hydroxyapatite/poly(ethyl methacrylate)/poly(methyl methacrylate)composites. *J Biomed Mater Res* **2000,** *52* (1), 1-7.
26. Bettencourt, A.; Almeida, A. J., Poly(methyl methacrylate) particulate carriers in drug delivery. *Journal of Microencapsulation* **2012,** *29* (4), 353-367.
27. Changerath, R.; Nair, P. D.; Mathew, S.; Nair, C. P. R., Poly(methyl methacrylate)-grafted chitosan microspheres for controlled release of ampicillin. *Journal of Biomedical Materials Research Part B: Applied Biomaterials* **2009,** *89B* (1), 65-76.
28. Carter, D.; He, X.; Munson, S.; Twigg, P.; Gernert, K.; Broom, M.; Miller, T., Three-dimensional structure of human serum albumin. *Science* **1989,** *244* (4909), 1195-1198.
29. Fasano, M.; Curry, S.; Terreno, E.; Galliano, M.; Fanali, G.; Narciso, P.; Notari, S.; Ascenzi, P., The extraordinary ligand binding properties of human serum albumin. *IUBMB Life* **2005,** *57* (12), 787-796.
30. Alyautdin, R. N.; Petrov, V. E.; Langer, K.; Berthold, A.; Kharkevich, D. A.; Kreuter, J., Delivery of Loperamide Across the Blood-Brain Barrier with Polysorbate 80-Coated Polybutylcyanoacrylate Nanoparticles. *Pharmaceutical Research* **1997,** *14* (3), 325-328.
31. Hamberger, A.; Landfester, K., Influence of size and functionality of polymeric nanoparticles on the adsorption behavior of sodium dodecyl sulfate as detected by isothermal titration calorimetry. *Colloid and Polymer Science* **2011,** *289* (1), 3-14.
32. Mohr, K.; Sommer, M.; Baier, G.; Schöttler, S.; Okwieka, P.; Tenzer, S.; Landfester, K.; Mailänder, V.; Schmidt, M.; Meyer, R. G., Aggregation behavior of polystyrene-nanoparticles in human blood serum and its impact on the in vivo distribution in mice. *Journal of Nanomedicine & Nanotechnology* **2014,** *5* (2).
33. Macfarlane, R., An enzyme cascade in the blood clotting mechanism and its function as a biochemical amplifier. *Nature* **1964,** *202* (4931), 498-499.
34. Song, S.; Ravensbergen, K.; Alabanza, A.; Soldin, D.; Hahm, J.-i., Distinct Adsorption Configurations and Self-Assembly Characteristics of Fibrinogen on Chemically Uniform and Alternating Surfaces including Block Copolymer Nanodomains. *ACS Nano* **2014,** *8* (5), 5257-5269.

35. Kendall, M.; Ding, P.; Kendall, K., Particle and nanoparticle interactions with fibrinogen: the importance of aggregation in nanotoxicology. *Nanotoxicology* **2011,** *5* (1), 55-65.
36. Langer, K.; Anhorn, M. G.; Steinhauser, I.; Dreis, S.; Celebi, D.; Schrickel, N.; Faust, S.; Vogel, V., Human serum albumin (HSA) nanoparticles: Reproducibility of preparation process and kinetics of enzymatic degradation. *International Journal of Pharmaceutics* **2008,** *347* (1), 109-117.
37. Rausch, K.; Reuter, A.; Fischer, K.; Schmidt, M., Evaluation of Nanoparticle Aggregation in Human Blood Serum. *Biomacromolecules* **2010,** *11* (11), 2836-2839.
38. Phosphonic acid phostones. Google Patents: 1960.
39. Ziegler, A.; Landfester, K.; Musyanovych, A., Synthesis of phosphonate-functionalized polystyrene and poly(methyl methacrylate) particles and their kinetic behavior in miniemulsion polymerization. *Colloid and Polymer Science* **2009,** *287* (11), 1261.
40. Dreis, S.; Rothweiler, F.; Michaelis, M.; Cinatl, J.; Kreuter, J.; Langer, K., Preparation, characterisation and maintenance of drug efficacy of doxorubicin-loaded human serum albumin (HSA) nanoparticles. *International Journal of Pharmaceutics* **2007,** *341* (1), 207-214.

Chapter 5

Active targeting of mannose-receptor presenting cells with nanocarriers coated with mannosylated biodegradable polyphosphoester-surfactants

Foreword

The following project was accomplished in cooperation with Johanna Simon[1] (MPIP), who did the biological evaluation of the prepared nanoparticle dispersions. The preparation and analysis of the mannose-derivatives **(2)** and **(3)** was performed by Jens Langhanki[2] from the working group of Prof. Dr. Till Opatz[2]. MALDI-ToF analysis was performed by Dr. Elena Berger-Nicoletti.[2]

[1]*Max Planck Institute for Polymer Research, Ackermannweg 10, 55128 Mainz, Germany*
[2]*Institute of Organic Chemistry, University of Mainz, Duesbergweg 10–14, 55128 Mainz, Germany*

Abstract

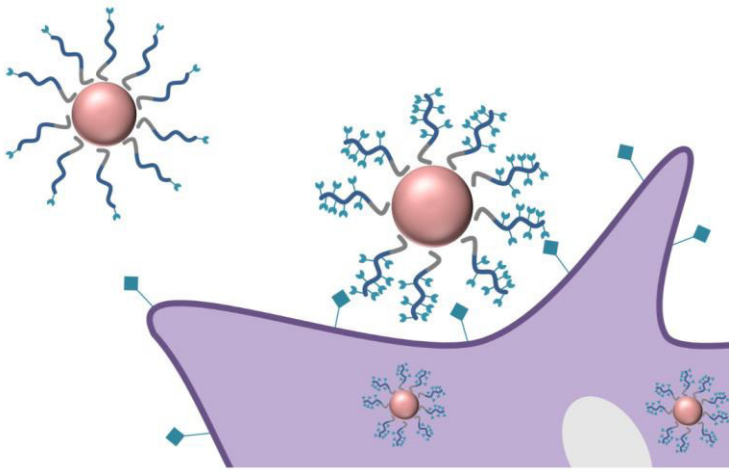

Functional mannose-containing PPE-surfactants for the surface modification of nanocarriers were prepared. The surfactants were designed in order to guarantee targeted delivery of the modified nanocarriers to mannose-receptor presenting cells. Various targeting surfactants

containing mannose moieties were prepared in a two-step synthesis starting with the ring-opening polymerization of cyclic phosphoester monomers and following mannosylation by thiol-Michael addition. In the first approach a targeting surfactant containing one terminal mannose moiety was prepared and assembled on the surface of polystyrene nanoparticles. Cellular uptake studies against mannose-receptor presenting murine macrophages and immature dendritic cells showed no enhanced cellular uptake compared to polystyrene particles coated with mere PPE-surfactant. In the second approach, targeting surfactants were prepared with various amounts and location of mannose and were assembled on the surface of poly(methyl methacrylate particles) and HES nanocapsules. Cellular uptake studies against murine macrophages showed significantly enhanced uptake depending on the structure of the targeting surfactant.

1 Introduction

In recent years, the application of nanocarriers for medicine and more specifically for drug delivery has increased rapidly. The perfect drug delivery system fulfills four key requirements - (i) retaining the cargo, (ii) evading the immune cells to avoid rapid blood clearance, (iii) targeting the site of affection and finally (iv) releasing the cargo at the place of action.[1-2] However, today's nanomedicine typically fulfills these requirements only in part.

Here, we have focused on the targeted delivery of nanocarriers by noncovalent attachment of mannosylated surfactants on the surface of nanoparticles. The main mechanism behind active targeting is the recognition of a ligand that is installed on the carrier by its targeted substrate (on the surface of certain cell types).[3] Many strategies have been developed to target nanocarriers to specific receptors in certain cells, and these typically involve covalent binding the surface of nanoparticles with proteins, antibodies, sugars, or other biomolecules.[4-6] Covalent attachment of targeting moieties to nanocarriers often requires high synthetic efforts and furthermore is often plagued by low degrees of functionalization.[7-8] Another approach towards surface modification of nanoparticles is the coating of the surface with amphiphilic polymers or surfactants respectively.[9-11]

The objective of the current study was the preparation of structurally different mannosylated polyphosphoester-based surfactants for the non-covalent surface modification of any nanocarrier.

Poly(phosphoester)s (PPEs) have gained attention in the past years due to their potential biodegradability and biocompatibility making them interesting materials especially for

biomedical applications.[12-13] Here, several polymeric surfactants were prepared by ring-opening polymerization of cyclic phosphoester monomers which were subsequently functionalized with mannose. The mannosylated surfactants were used for coating of nanocarriers and their ability to target immature dendritic cells and murine macrophages were evaluated *in vitro*. Due to the amphiphilic character of surfactants, they typically enrich at the interphase between particle and surrounding continuous phase upon solution in nanoparticle dispersions. Thus, surfactants can be used for a straightforward surface modification of nanoparticles by coating-techniques. A further benefit of surfactants is their potential compatibility with nanoparticles consisting of different materials providing a universal strategy for nanoparticle modification.

We selected targeting of the mannose receptor that is expressed on the surface of cells of the immune system, i.e. typically macrophages and immature dendritic cells (iDCs).[14-15] The mannose receptor is known to bind to mannose- and fucose-containing microorganisms by carbohydrate recognition domains.[16] Recent strategies for developing preventing and therapeutic vaccines have focused on the ability to deliver antigen to dendritic cells.[17-18] DCs are the most effective antigen-presenting cells and have a crucial role in initiating T-cell mediated immunity.[19] Therefore, targeting DCs with an antigen-delivery system provides tremendous potential in developing new vaccines.

2 Results & Discussion

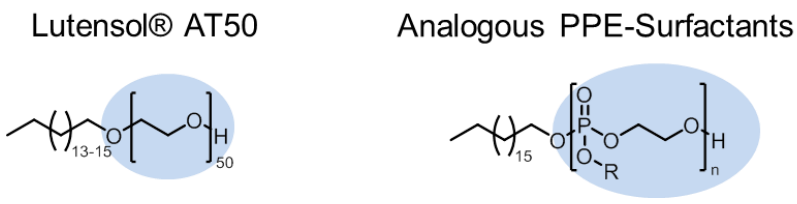

Figure 5.1. General structure of surfactants of the Lutensol® AT series and analog PPE-surfactants.

The mannosylated surfactants were designed in analogy to Lutensol® AT50 that is a well-established polymeric surfactant (Figure 5.1). Surfactants of the Lutensol AT® series consist of a fatty alcohol (C_{16}-C_{18}) as the hydrophobic part and a hydrophilic PEG segment. PPE surfactants with an analogous structure were prepared by replacing the hydrophilic PEG-part by hydrophilic PPEs. Two different approaches to integrate the targeting mannose units into the surfactant structure were studied. In the first approach, one single mannose unit is attached to the hydrophilic PPE-part via a terminal linker (**Figure 5.2**, left). In contrast, in the second

approach PPE (co)polymers were prepared carrying a reactive methacrylate group in the pendant chain allowing the introduction of several mannose units along the hydrophilic chain of the surfactant (**Figure 5.2**, right).

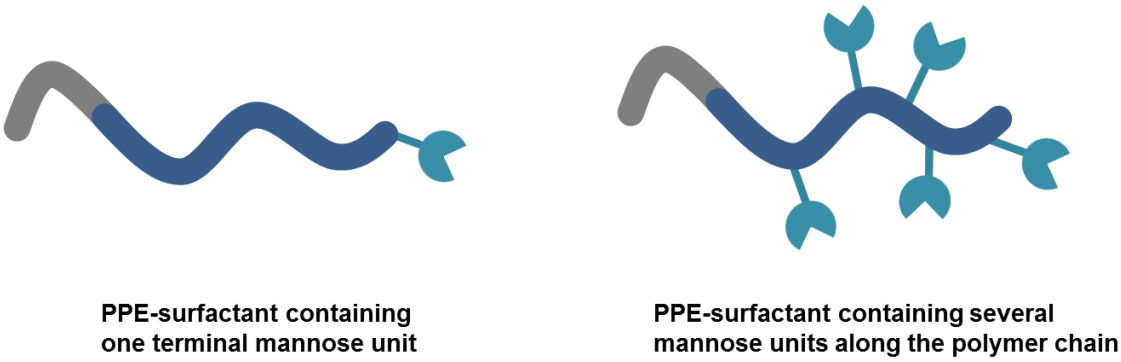

Figure 5.2. Schematic depiction of the mannose-containing targeting surfactants.

All targeting surfactants prepared in this study were prepared by a two-stage protocol: the first step comprises the preparation of a precursor (**P**) containing methacrylate groups, which is subsequently transferred into a targeting surfactant (**TS**) by functionalization with mannose. The functionalization was accomplished by thiol-Michael addition (Scheme 5.1) with thiolated mannose. The thiol-Michael addition has been developed in the 1960s by Allen et al.[20] and typically proceeds in quantitative yield under mild conditions. The thiol-Michael addition is ranked among the 'click' reactions and has proven to be a powerful tool for polymer modification.[21]

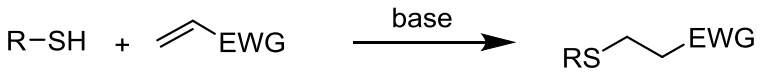

Scheme 5.1 . General scheme of the thiol-Michael addition

For the applicability of the thiol-Michael addition for the modification of the precursors containing attackable methacrylate groups, the mannose was transferred into a thiol-derivative (Scheme 5.2). The preparation and analysis of compounds **(2)** and **(3)** depicted in Scheme 5.2 were performed by Jens Langhanki from the working group of prof. Dr. Till Opatz.

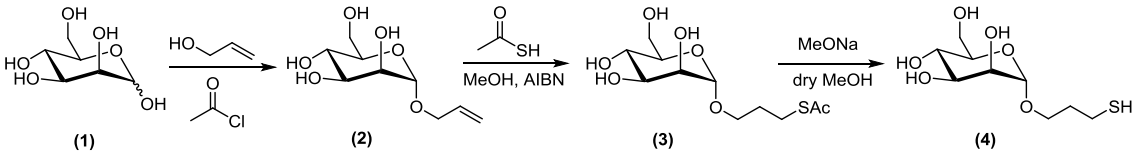

Scheme 5.2. Preparation of the thiol-mannose derivative (4) via a three-step synthesis. (*The preparation and analysis of compounds* (2) *and* (3) *were performed by Jens Langhanki from the working group of Prof. Dr. Till Opatz.)*

α-D-mannopyranoside **(1)** was modified in the anomeric position to guarantee further recognition of the modified sugar by the lectins.[22-23] In the first step, α-D-mannopyranoside **(1)** was modified at the anomeric hydroxyl-group by allylation with allyl alcohol and acetyl chloride and was subsequently transferred into acetylthiopropyl-α-D-mannopyranoside **(3)** by radical addition of thio acetic acid to the terminal double bond using α,α'-azoisobutyronitrile (AIBN) as radical initiator. In the last step the thioacetic acid ester is cleaved by sodium methylate in methanol[24] leading to a mannose-derivative containing a terminal thiol group **(4)** which can be used as nucleophile in thiol-Michael addition. For each polymer modification the thiopropyl-α-D-mannopyranoside was prepared freshly prior to use due to the tendency of thiols to form disulfides lowering the yield of the thiolated sugar acting as nucleophile in the thiol-Michael-addition.

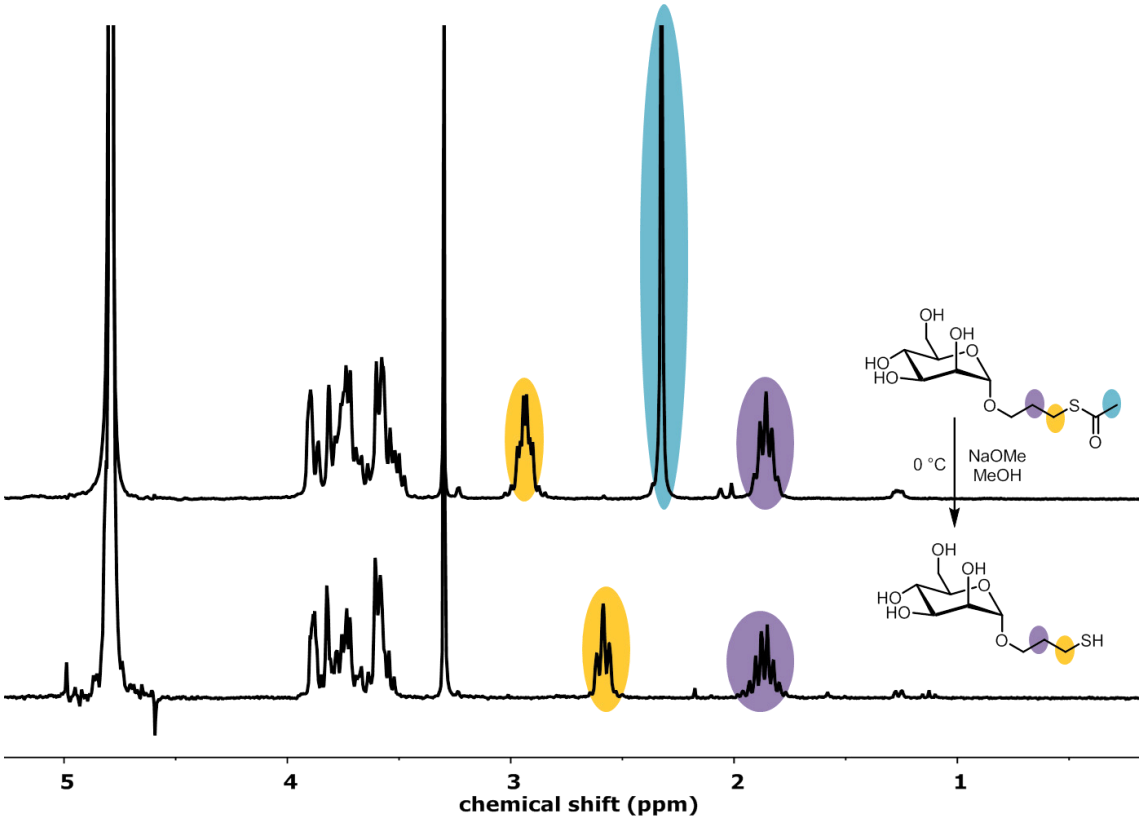

Figure 5.3. ^{1}H NMR (250 MHz, D_2O, 298 K) spectra of the thioester cleavage. The thioester was cleaved using NaOMe in dry methanol at 0 °C over a period of 3 h. Complete ester cleavage was indicated by the disappearance of the signal at 2.32 ppm.

Successful cleavage of the thioester was indicated by the disappearance of the signals of the methyl group of the thioacetic ester at 2.32 pm. Furthermore, the signals of the methylene group adjacent to the sulfur atom shifted from 2.93 ppm to 2.51 ppm upon thiol formation. Depending on the reaction conditions disulfide formation was already observed during the preparation of thiopropyl-α-D-mannopyranoside. The formation of disulfide can be suppressed when the temperature of the cleavage of the thioester is performed at 0°C and reaction times of 2-3 h are not exceeded. As the disulfide cannot be used for the thiol-Michael addition, it needs to be avoided. However, when disulfide formation was observed a reduction agent, namely tris(2-carboxyethyl)phosphine (TCEP), was added to the thiol-Michael addition to regain the thiol in situ.

The first approach to mannose-containing targeting surfactant (**TS(1)**) comprises the preparation of a PPE-based surfactant were one single mannose unit is attached to the hydrophilic PPE-part via a terminal linker group (Figure 5.2 (left)).

Methyl ethylene phosphate (MEP) was used as the hydrophilic monomer. PMEP contains a short hydrophilic methoxy side chain and shows no temperature dependent solubility in water. In order to achieve the Lutensol-like structure, 1-ocatadecanol was used as the initiator in the organocatalytic ring-opening polymerization of MEP. Typically, ring-opening polymerizations of cyclic phosphoester monomers are conducted in dry dichloromethane at low temperatures and high monomer concentrations to avoid unwanted side reactions such as transesterification or cyclization. However, the usage of 1-octadecanol complicates the ROP of MEP due to its low solubility in DCM at 0 °C. Partially precipitation of the initiator at 0°C leads to a lower number of chains starting the polymerization and therefore higher molecular weights are obtained. Using THF as solvent guarantees a better solubility of 1-octadecanol but led to a precipitation of the polymer within the polymerization. To avoid initiator precipitation at 0°C a mixture of DCM and THF (3:0.8) was used. For the incorporation of mannose units into the surfactant structure a precursor was synthesized with a terminal methacrylate group (Scheme 5.3).

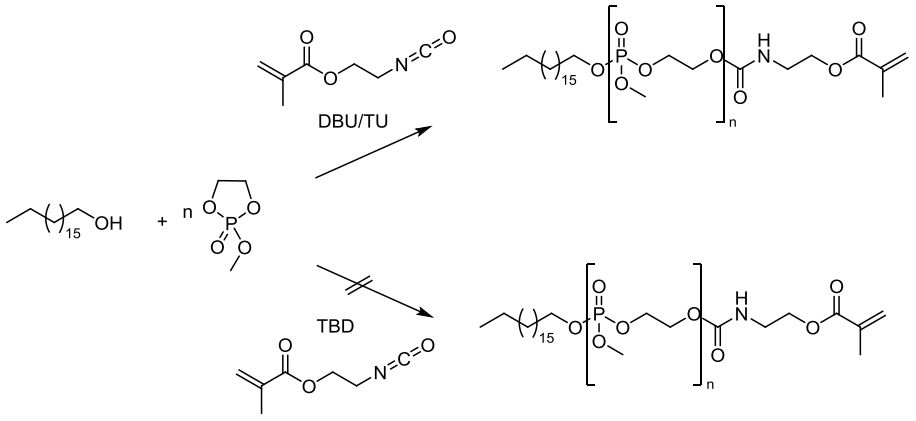

Scheme 5.3. Synthesis of the precursor of the targeting surfactant containing one terminal mannose unit.

The introduction of a terminal linker group was achieved by terminating the ring-opening polymerization of MEP by rapid addition of an excess (5 equivalents compared to the initiator) of the commercially available 2-isocyanatoethyl methacrylate. It was found that the usage of 1,5,7-Triazabicyclo[4.4.0]dec-5-ene (TBD) as catalyst prohibits the introduction of the linker group while the change of the catalyst to a combination of 1-(3,5-bis(trifluoromethyl)phenyl)-3-

phenylthiourea (TU) and 1,8-Diazabicyclo[5.4.0]undec-7-en (DBU) led to a reliable introduction of the linker. The incorporation of the terminal linker was proven by ^{1}H NMR spectroscopy. ^{1}H NMR spectra after three-times precipitation from diethyl ether showed clearly the introduction of the linker group by the appearance of the signals of the double bonds at 6.11 ppm and 5.57 ppm respectively (Figure 5.4). The number of repeat units was calculated from the ^{1}H NMR spectra of the polymers. The signal of the methyl group of the initiator appearing at 0.86 ppm was integrated and set as 3 and compared either with the integrals of the pendant methyl groups or the methylene groups of the backbone to calculate the M_n. The results from NMR and SEC results for the prepared precursors (**P(1)**) containing one terminal methacrylate functionality are listed in Table 5.1.

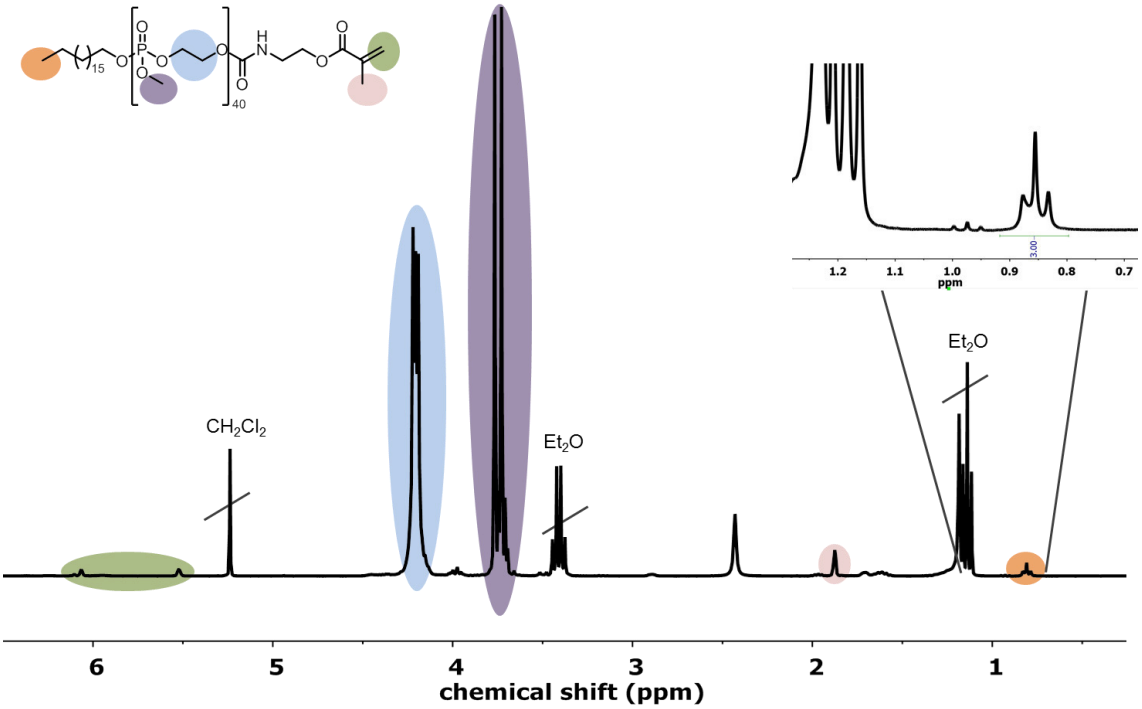

Figure 5.4. ^{1}H NMR (300 MHz, $CDCl_3$ at 298K) spectrum of $PMEP_{40}$ with terminal methacrylate group

The terminal acrylate group always harbours the possibility of spontaneous crosslinking by free radical addition. Therefore, the prepared precursors (Table 5.1) were only purified by repeated precipitation from diethyl ether and subsequently stored at -80°C until further usage.

Table 5.1. Overview of the NMR and SEC data for the precursors with terminal methacrylate group.

sample[a]	solvent	$M_{n,theo}$ / g mol^{-1} [a]	M_n / g mol^{-1} [b]	Đ[c]
P(1)-1	THF	5800	5200	1.26
P(1)-2	THF	5800	6500	1.28
P(1)-3	THF/DCM	5800	5800	1.32

[a]*:* According to monomer feed ratio. [b]*:* Determined via ^{1}H NMR. [c]*:*Determined via SEC in DMF.

The modification of the surfactant was performed by thiol-Michael addition with an excess of freshly prepared thiopropyl-α-D-mannopyranoside. The thiol-Michael addition was conducted in methanol due to the limited solubility of the mannose derivative in organic solvents at ambient temperature. After 24 h, the reaction was terminated and the polymer was charged into a dialysis tube with a molecular weight cut off (MWCO) of 3,500 g mol^{-1} and dialyzed against water for further 24 h to remove excess of thiopropyl-α-D-mannopyranoside.

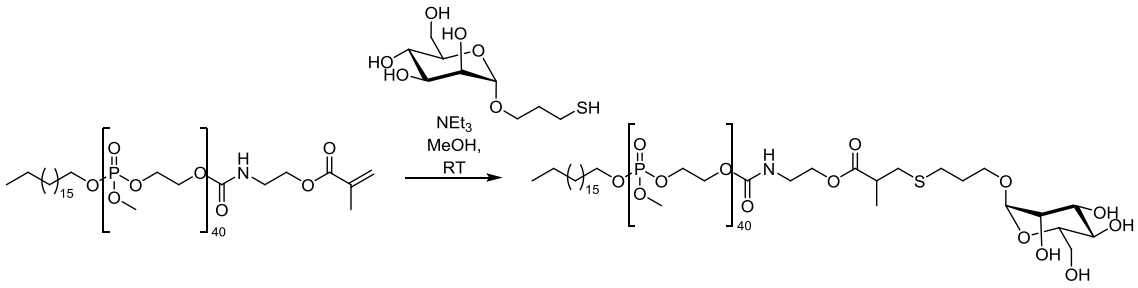

Scheme 5.4. Synthesis of the targeting surfactant TS-1 by thiol-Michael addition.

After modification, the ^{1}H NMR spectrum (Figure 5.5) showed only minimal signals at 6.11 ppm and 5.57 ppm that can be ascribed to residual double bonds of the terminal methacrylate group indicating successful modification of the terminal methacrylate group. Furthermore, signals at 2.5-2.75 ppm emerged that can be ascribed to the methanetriyl group as well as to the methylene groups on both sides adjacent to the thioether (Figure 5.5) formed upon thiol-Michael addition. At 1.82 ppm the signals of the second methylene group (-S-CH_2-***CH*****$_2$**-CH_2-) in the thiopropyl spacer are visible. The signal of this methylene group was integrated, set as two and compared to the integral of the signal at 2.5-2.75 ppm showing the expected ratio of 2:5

indicating a successful modification of **P(1)-3**. However, comparing these integrals with the integral of the initiator methyl group indicated an incomplete modification of the precursor.

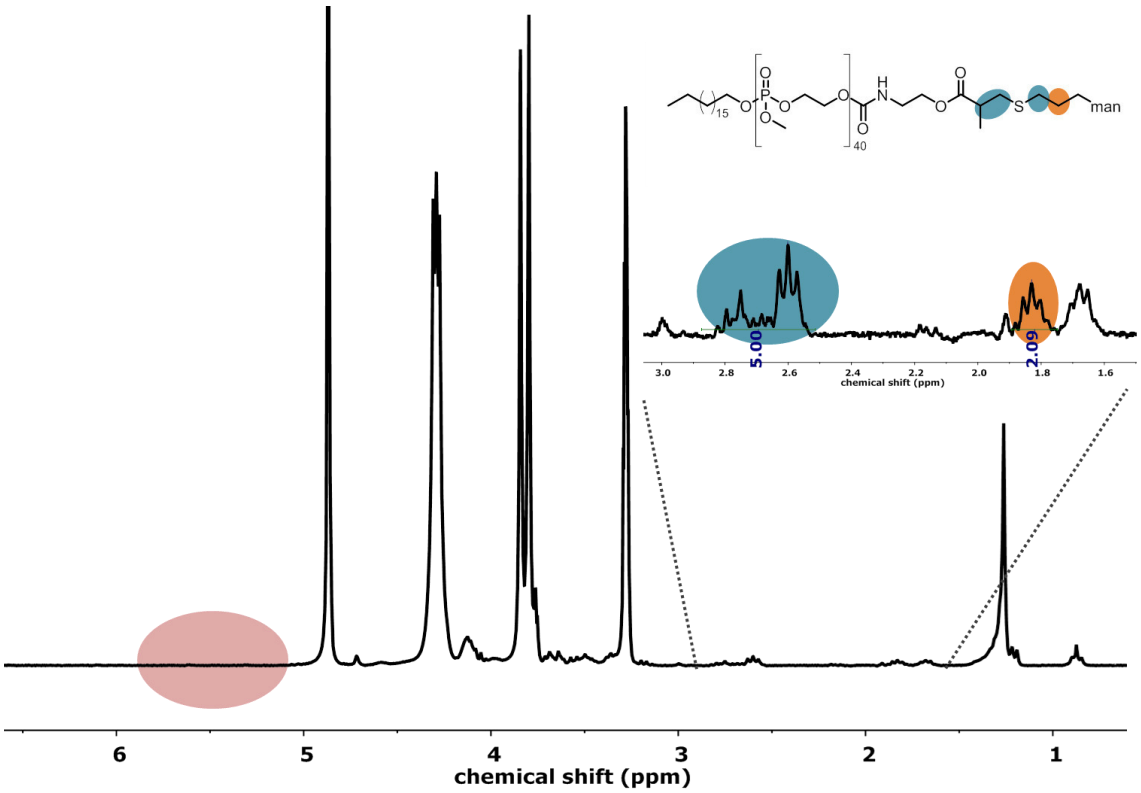

Figure 5.5. ^{1}H NMR (250 MHz, MeOD at 298K) of TS(1)-1. TS(1)-1 was prepared from P(3) by thiol Michael addition with (4) in methanol at ambient temperature.

However, the size of the mannose signals in the ^{1}H NMR spectra of the targeting surfactant **TS(1)-1** makes it difficult to judge whether the mannose is attached to the precursor or if it is residual mannose that could not be removed during the purification by dialysis. Thus, a MALDI-TOF spectrum (Figure 5.6) was recorded as further proof of the successful mannosylation of the precursor.

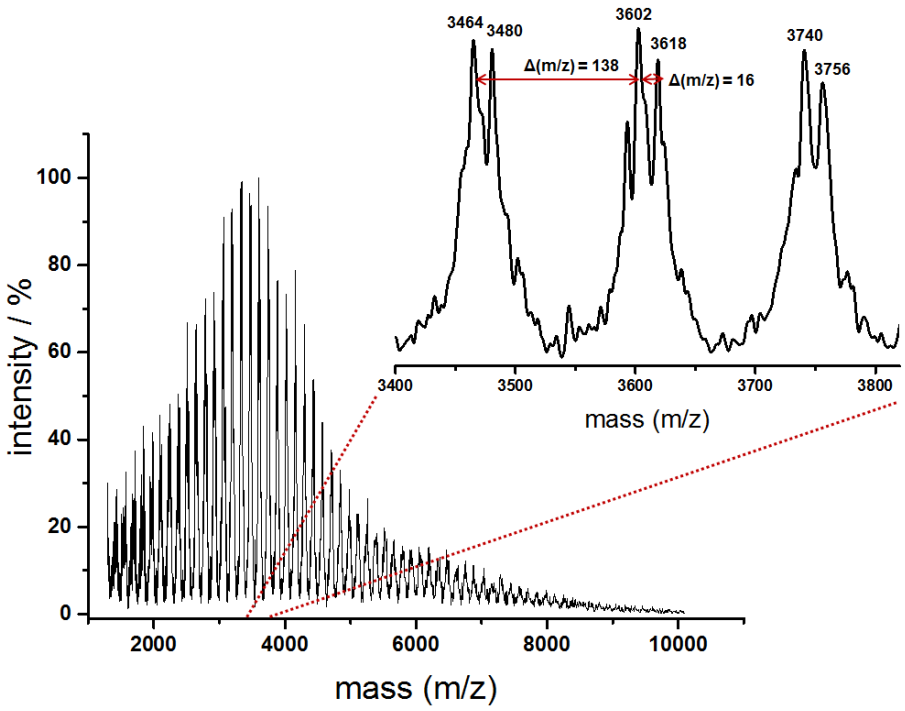

Figure 5.6. MALDI-ToF spectrum of TS(1)-1 with 2-(4'-hydroxybenzeneazo)benzoic acid as matrix

.

Table 5.2. Overview over calculated and found masses for TS(1)-1.

n(repeat units)	TS(1)-1	TS(1)-1+Na	TS(1)-1+K	found	found
19	3303	3326	3342	3327	3342
20	3441	3464	3480	3465	3480
21	3579	3602	3618	3602	3756
22	3717	3740	3756	3740	3756
23	3855	3878	3894	3879	3894

Figure 5.6 shows the recorded MALDI-ToF spectrum of **TS(1)-1** using 2-(4'-hydroxybenzeneazo)benzoic acid as matrix. The molecular weight distribution is centered at ~3,500 g mol^{-1} that is below the expected molecular weight of 6,100 g mol^{-1} and can be ascribed to a discrimination of higher molecular weights during the measurement. The resolved repeat units are separated by 138 mass units corresponding to the mass of one repeat unit of MEP. Magnification of the region m/z = 3,400-3,800 g mol^{-1} (Figure 5.6) showed that the signals are

split in two main signals. These two main peaks are separated by 13 mass units and the right peak matches the mass of **TS(1)-1**+Na and the left peak matches the mass of **TS(1)-1**+K indicating a successful mannosylation of precursor **P(3)-1**. However, the mass peak ascribed to **TS(1)-1**+Na also matches the precursor-mass without mannose. Nevertheless, the peak pattern indicates a successful mannosylation of the precursor. As the resolution of the mass spectrum could not be enhanced, not isotopic resolution was possible to rule out the latter option. However, together with the NMR results a conversion of the methacrylates most likely to the desired product was achieved.

To evaluate the targeting ability of the synthesized surfactant, polystyrene nanoparticles (PS-NPs) were coated with the mannosylated surfactant TS(1)-1 and the cellular uptake was evaluated against macrophages and dendritic cells both exhibiting mannose receptors on the cell surface. The applied PS-NPCs were prepared by miniemulsion polymerization with sodium dodecyl sulfate (SDS). For the particle coating the PPE-surfactant was dissolved in the 2wt% PS-NPs dispersion and the mixture was charged into a dialysis tube with MWCO = 3,500 g mol^{-1}, that is permeable for the small SDS but impermeable for the PPE-surfactant leading to an exchange of the surfactant. The particles were dialyzed for 24 h.

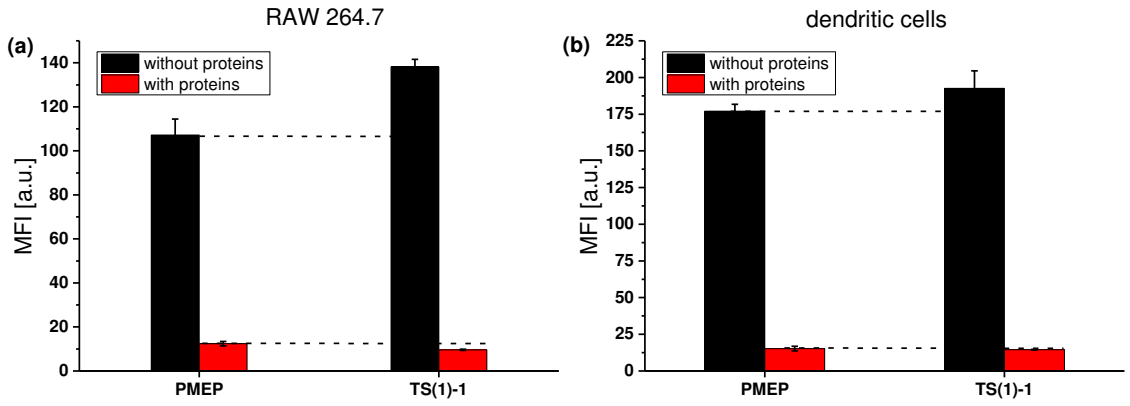

Figure 5.7. Flow cytometry analysis of RAW264.7 cells and immature dendritic cells incubated with differently coated PS-NPs for 2 h. As refrence, PS-NPs coated with a PMEP$_{65}$-surfactant containing no terminal mannose moiety were used. Cellular uptake studies were conducted in the absence and presence of proteins where human blood plasma was used as protein source.

The PS-NPs were coated with two different surfactants, one with a terminal mannose unit and the other one consisting exclusively of PMEP (presented in Chapter 4). The stability of the coated nanoparticles in plasma was evaluated by DLS measurements and showed no aggregation

(Figure 5.33). The cellular uptake studies against macrophages and DCs were conducted in the absence of proteins as well as in the presence of proteins using 10% human blood serum as protein source.

Figure 5.7 shows a slightly increased cellular uptake for the PS-NPs coated with the mannose-containing surfactant **TS(1)-1** in absence of proteins for both cell lines. However, in the presence of proteins the cellular uptake decreased significantly for the PS-NPs coated with both PPE-surfactants and no enhanced cellular uptake was observed for the particles coated with the mannose containing surfactant compared to the PMEP-surfactant without mannose. Therefore, in the presence of proteins the introduction of a terminal mannose unit did not lead to an increased receptor mediated cellular uptake against macrophages and dendritic cells. However, these results may have different reasons. On the one hand, the targeting unit density per nanoparticle may be too low for surfactants bearing only one terminal mannose-moiety since it was described earlier that the interaction of mannosylated nanocarriers with lectins depends strongly on the density of mannose moieties on the surface.[25-26] On the other hand, the presence of proteins may lead to shielding of the targeting units by the adsorption of serum proteins, which was described earlier by Dawson *et al.* for transferrin-functionalized nanoparticles.[4] Taking these results into account further studies were conducted including two alterations: (i) surfactants containing a higher number and density of mannose-moieties per surfactant molecule were prepared and applied to (ii) nanocarriers showing reduced protein adsorption compared to polystyrene nanoparticles, i.e. poly (methyl methacrylate) nanoparticles (PMMA-NPs) and hydroxyl ethyl starch nanocapsules (HES NCs). To achieve a higher mannose concentration per surfactant molecule 2-(2-oxo-1,3,2-dioxaphospholoyloxy)ethyl methacrylate (OPEMA) was used either as single monomer or as a comonomer during the surfactant synthesis. OPEMA was prepared by esterification of 2-chloro-1,3,2-dioxaphospholane 2-oxide (COP) with HEMA according to a literature procedure (Scheme 5.5).[27]

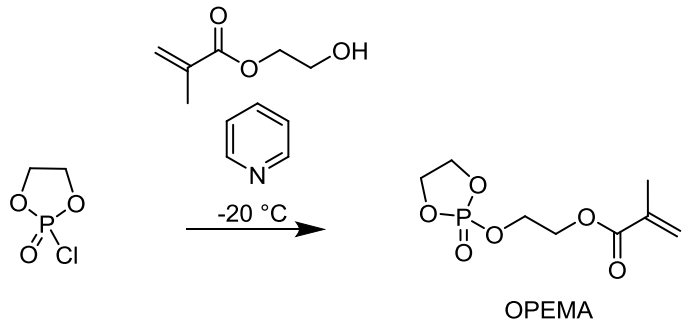

Scheme 5.5. Synthesis of 2-(2-oxo-1,3,2-dioxaphospholoyloxy)ethyl methacrylate (OPEMA).[27]

The usage of OPEMA as monomer for the synthesis of precursors with multiple methacrylate moieties (**P(2)**) allowed the introduction of a high and precisely adjustable number of pendant methacrylate groups along the hydrophilic chain of the surfactant that can be used as working point for further modification with mannose by thiol-Michael addition. Three different precursor structures were synthesized using either a combination of MEP and OPEMA or exclusively OPEMA as monomers. The simplest precursor structure is a homopolymer of POPEMA, which allows the introduction of a maximum number of mannose units per surfactant molecule (Table 5.3, Entry 1-4). As further precursor structure copolymers with MEP as comonomer were synthesized leading to a statistical distribution of pendant methacrylate chains and mannose units respectively along the polymer chain (Table 5.3, Entry 5,6). Finally block copolymers with the first block PMEP and the second block POPEMA were prepared (Table 5.3, Entry 7,8). Scheme 5.6 provides an overview over the preparation of precursors (**P(2)**) with multiple methacrylate moieties.

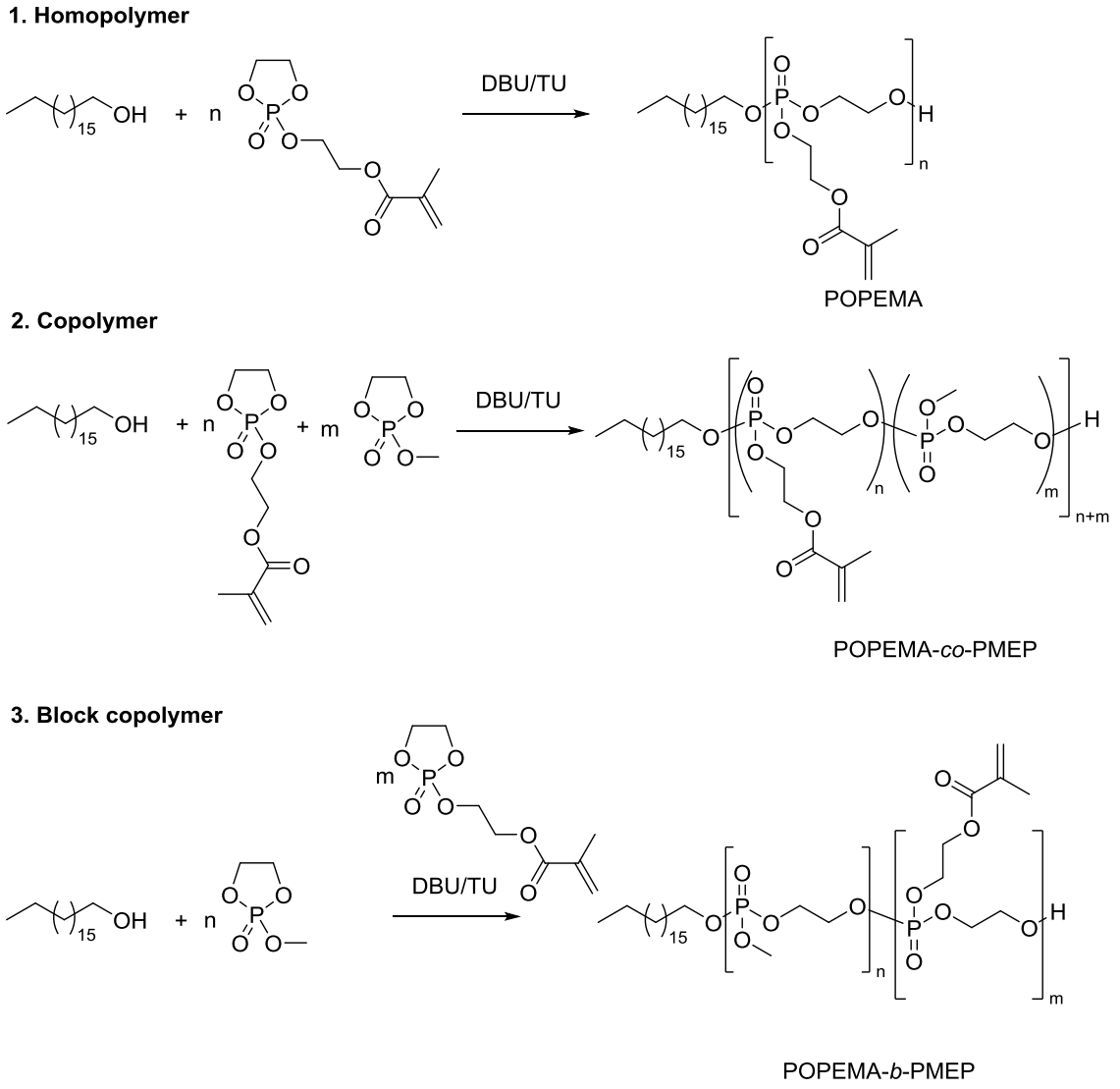

Scheme 5.6. Synthesis of the precursors P(2) by anionic ring opening polymerization of cyclic phosphates.

The prepared surfactants were analyzed by size exclusion chromatography (SEC) and NMR spectroscopy. SEC analysis was used to determine the molecular weight distribution and ^{1}H NMR spectroscopy was employed to determine the amount of repeating units of each monomer in the precursors and the molecular weight. Table 5.3 gives an overview over the SEC and NMR data of the prepared precursors. In Figure 5.8 one representative ^{1}H NMR spectrum of each precursor type is presented.

Table 5.3. Overview of the NMR and GPC data for precursors P(2) with multiple methacrylate units.

#	precursor	n(OPEMa)/n(MEP)[a]	n(OPEMA)/n(MEP)[b]	$M_{n,theo}$ [a] / g mol^{-1}	M_n [b] / g mol^{-1}	Đ[c]
1	**P(2)-1**	20/-	18/-	5,000	4,500	1.45
2	**P(2)-2**	40/-	37/-	9,700	9,000	1.27
3	**P(2)-3**	40/-	36/-	9,700	8,800	1.23
4	**P(2)-4**	80/-	75/-	19,200	18,000	1.23
5	**P(2)-5**	20/20	18/22	7,800	8,000	1.29
6	**P(2)-6**	40/20	35/23	10,100	11,700	1.26
7	**P(2)-7**	20/20	15/23	7,800	7,000	1.59
8	**P(2)-8**	20/30	19/20	10,100	7,500	1.50

[a]According to monomer feed ratio. [b]Determined via ^{1}H NMR. [c]Determined via SEC in DMF

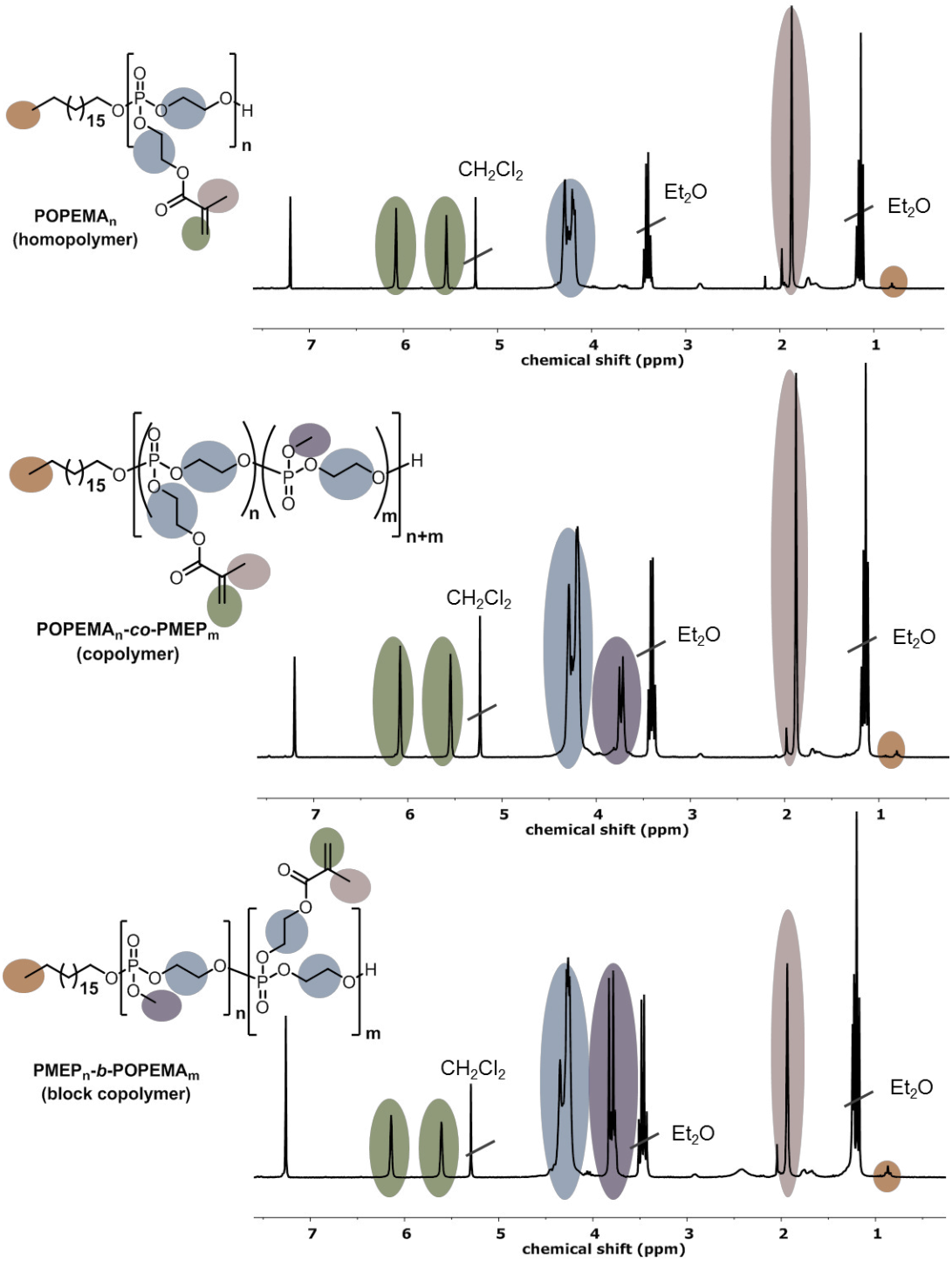

Figure 5.8. Representative ^{1}H NMR spectra (300 MHz, $CDCl_3$, 298 K) of each precursor structure; homopolymer (top), copolymer(middle) and block copolymer bottom.

The number of OPEMA units represents at the same time the maximum number of introducible mannose units. ^{1}H NMR spectra of precursors with the hydrophilic part consisting exclusively of POPEMA (Figure 5.8 top) show signals at 5.67 ppm and 6.16 ppm respectively that can be ascribed to the double bonds of the pendant methacrylate groups while the signal of the neighboring methyl group appears as singlet at 1.9 ppm. The signals of the backbone as well as of the ethylene glycol spacer in pendant chain appear as a broad signal at 4.4 - 4.1 ppm. The amount of OPEMA units and therefore, the amount of maximum insertable mannose units was determined by comparison of the integrals of the double bond signals with the integrals of the methyl group of the initiator that appears as typical triplet at 0.86 ppm. To evaluate if crosslinking of the terminal methacrylate groups of the OPEMA units occurred during the polymerization the integrals of the double bonds were compared to the integrals of the adjacent methyl group. The precursors **P(2)-5,6** and **P(2)-7,8** contain additionally MEP units or a MEP block respectively. The signals of the pendant methoxy group appear at 3.8-3.6 ppm (Figure 5.8 middle and bottom) and were used to determine the number of MEP repeat units by comparison with the initiator signals. As mentioned previously, the final targeting surfactants were prepared by mannosylation of the precursors by thiol-Michael addition (Table 5.4). When the targeting surfactants are coated on the particle surface, the mannose units are supposed to form the outer sphere around the particle and are therefore in the best position to guarantee targeting of the mannose receptor (Figure 5.9). Polymer modifications were conducted at ambient temperature using 4-(dimethylamino)pyridine (DMAP) as catalyst and an excess of 5 eq of thiol-α-D-mannopyranoside per methacrylate unit. Due to the limited solubility of the thiol-α-D-mannopyranoside in organic solvents the reaction was performed in methanol.

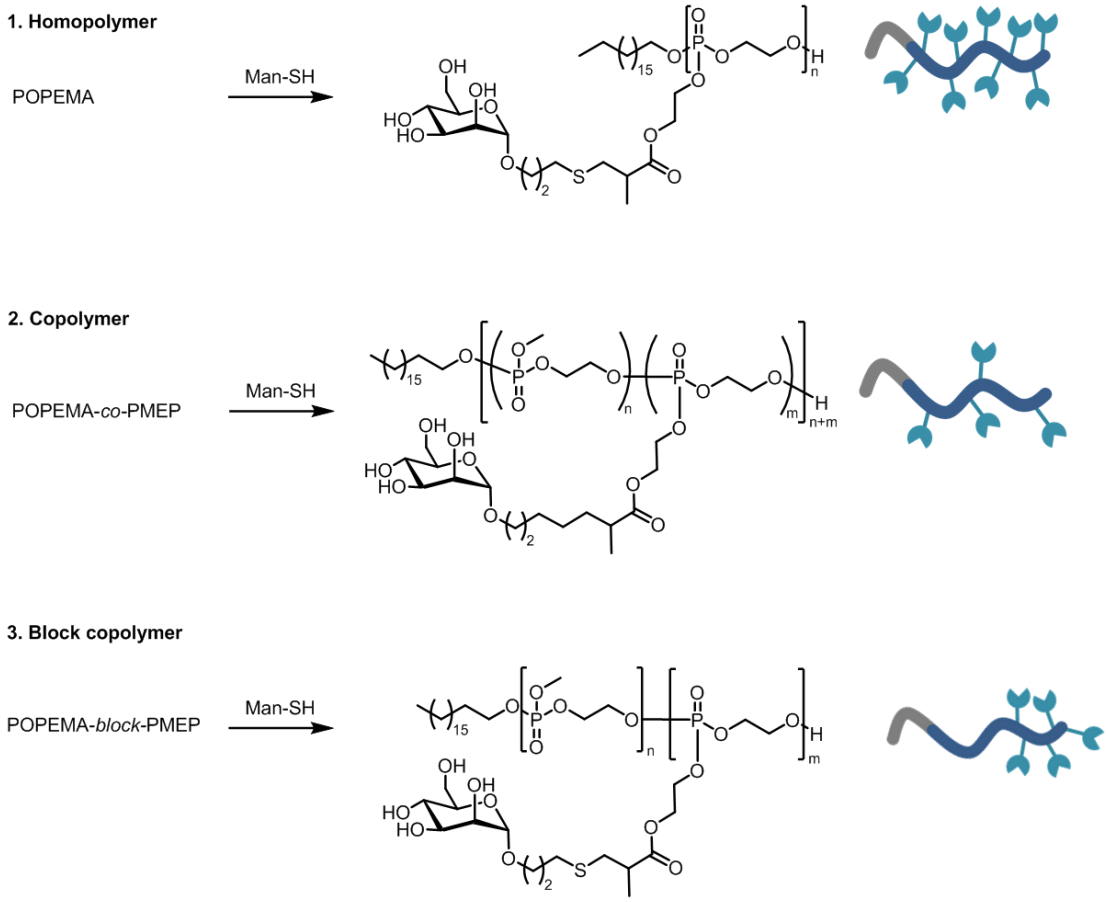

Figure 5.9. Preparation of the targeting surfactants TS(2) by mannosylation of the methacrylate containing precursers by thiol Michael addition.

As mentioned above the thiopropyl-α-D-mannopyranoside tend to form disulfides that are inactive in thiol-Michael additions. In order to reduce the disulfide, TCEP was added to the reaction mixture. The progress of the reaction was followed by ^{1}H NMR spectroscopy. Figure 5.10 shows the ^{1}H NMR spectra recorded within the course of a representative mannosylation. In case of residual double bond signals in the NMR spectra further DMAP and TCEP were added to avoid too long reaction times that can lead to crosslinking of the methacrylate groups. The disappearance of the double bonds in the ^{1}H NMR spectra (Figure 5.10) indicated the end of the reaction. Furthermore, the shape of the signal of the ethylenglycol backbone of the polymer changed throughout the reaction indicating successful mannosylation of the precursors.

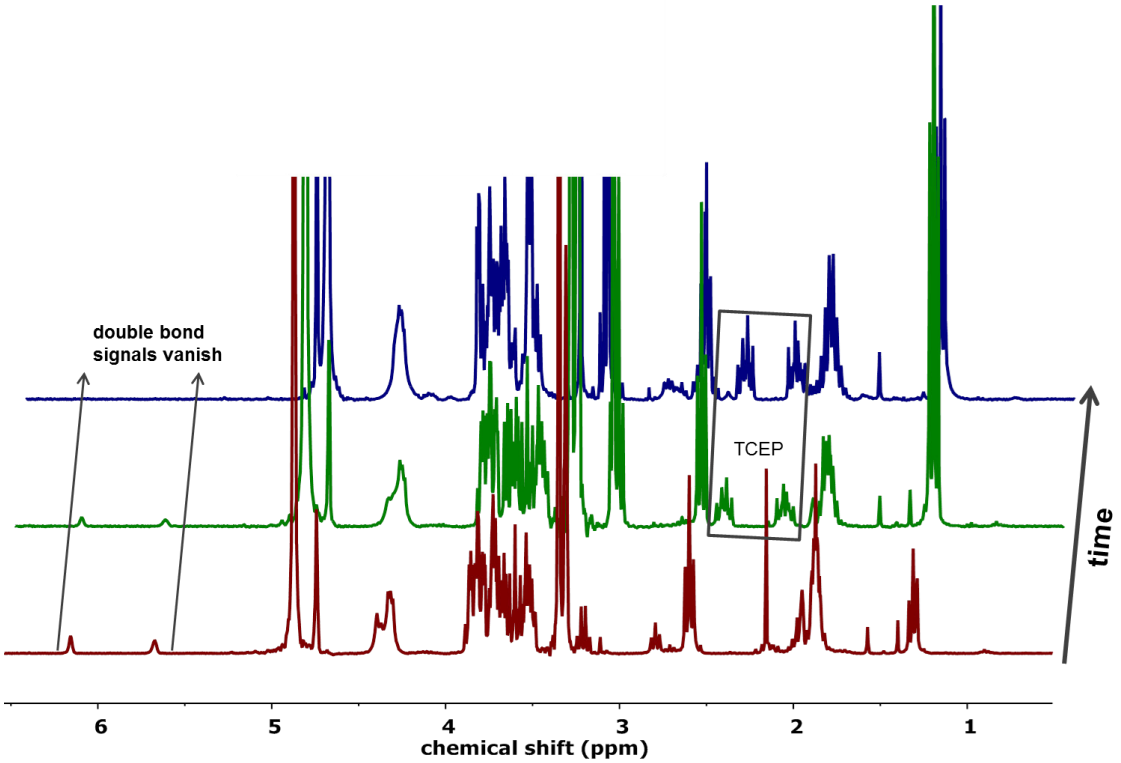

Figure 5.10. Progress of the mannosylation of PC(2)-8 with thiol-α-D-mannopyranoside, DMAP and TCEP by monitored by ^{1}H NMR spectroscopy (250 MHz, D_2O or MeOD, 298K).

The surfactants were purified by dialysis against deionized water using a dialysis tube with a MWCO of 3.5 kDa. The dialysis tube thus, is permeable for DMAP and the excess of thiopropyl-α-D-mannopyranoside but impermeable for the mannosylated surfactant. A representative ^{1}H NMR spectrum of the purified targeting surfactant **TS(2)-1** is depicted in Figure 5.11. The spectrum shows the signals of the polymer backbone at 4.37 ppm that lost its typical splitting pattern upon mannosylation. The signals of the hydrogen atoms of α-D-mannopyranoside remained in the range of 3.95 - 3.45 ppm and stayed unaffected upon mannosylation. In contrast, the signals of the methyl group adjacent to the modified double bond shifted from 1.9 ppm to 1.22 ppm upon mannosylation. Furthermore, the methyl signal shows a slight splitting that can be attributed to coupling with the neighboring methanetriyl-hydrogen. The newly emerged signal at 2.78 ppm can be ascribed to the methylene group next to the sulfide indicating a successful introduction of mannose into the surfactant structure.

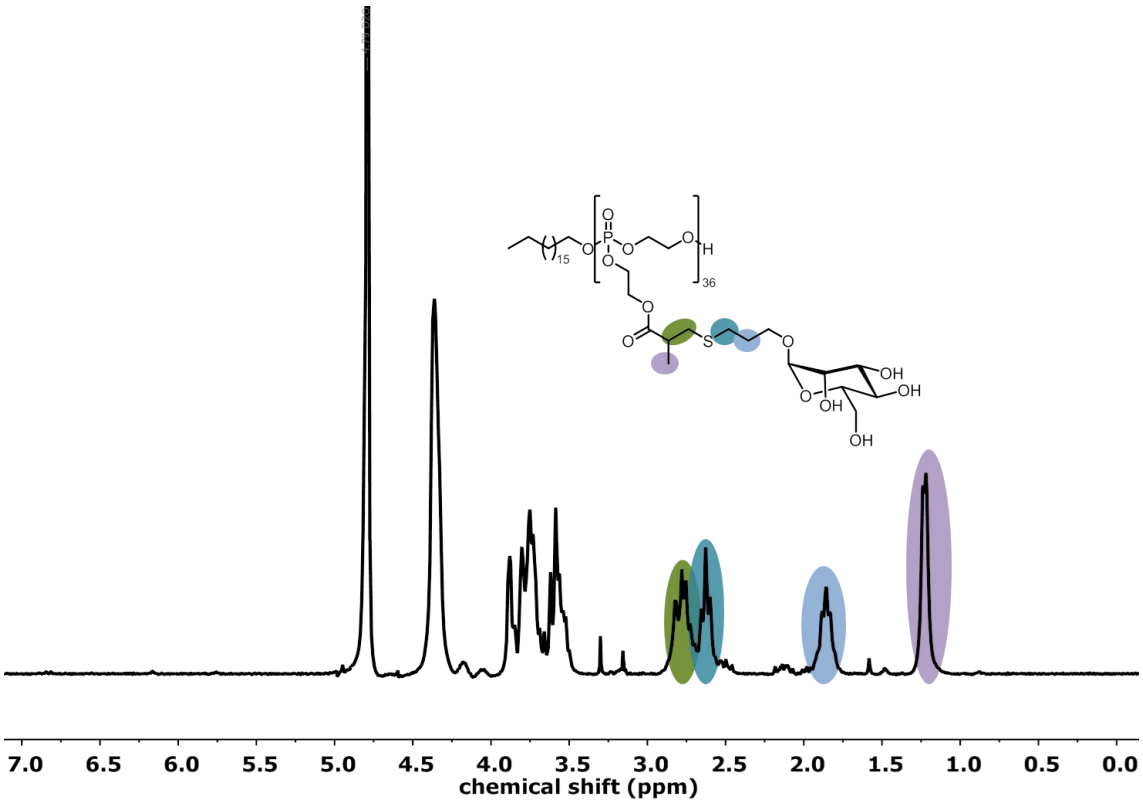

Figure 5.11. ^{1}H NMR spectrum (250 MHz, D_2O, 298K) of mannosylated TS(2)-1.

The assignment of the newly emerged signals in the ^{1}H NMR spectra was accomplished by H,H correlation spectroscopy (COSY). Figure 5.12 shows the correlation spectrum of **TS(2)-2** in deuterium oxide.

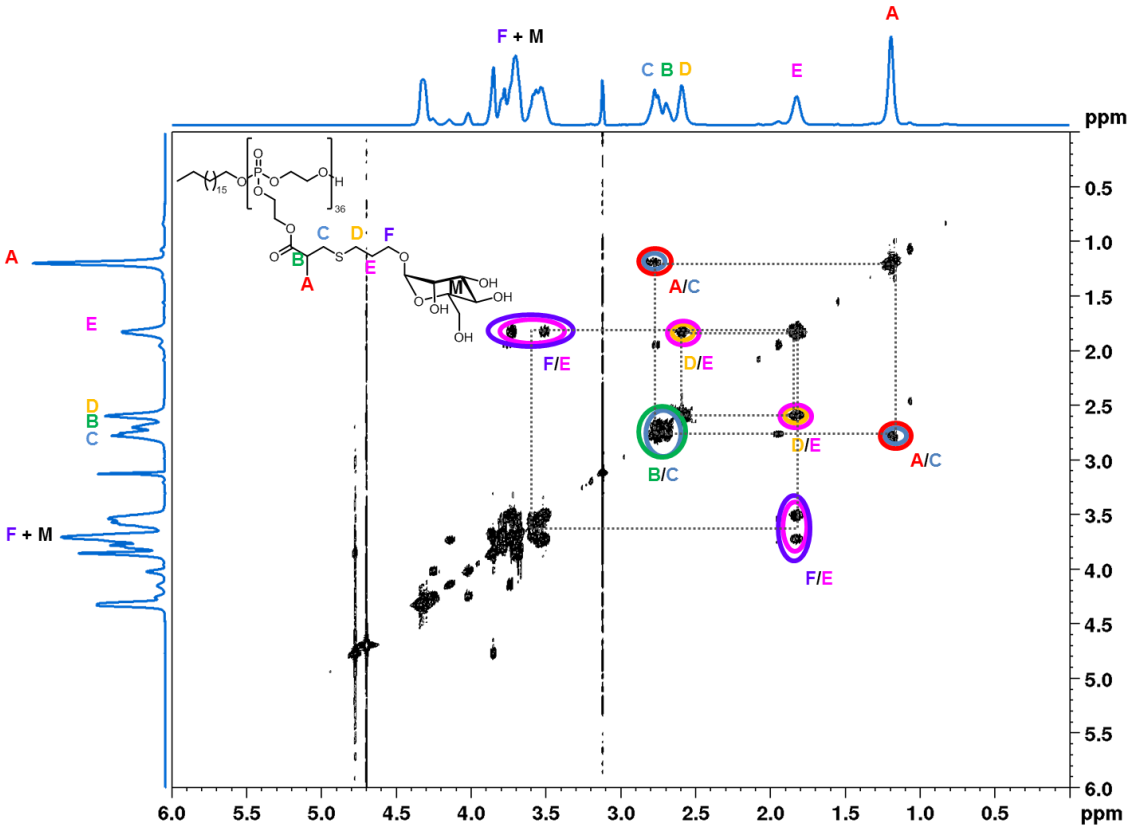

Figure 5.12. H,H COSY spectrum (500 MHz, D_2O, 298K) of mannosylated targeting surfactant TS(2)-2.

However, ^{1}H NMR spectra of the final targeting surfactants showed no initiator signals that can probably be attributed to self-assembly of the surfactants in deuterium oxide where the hydrophobic initiator is located in the center of the micelle to reduce contact with surrounding deuterium oxide. Due to the disappearance of the initiator signals, a determination of the number of introduced mannose units is not possible by ^{1}H NMR spectroscopy. Thus, the determined number of methacrylate groups in the respective precursor was equated with the number of introduced mannose units since no residual double bonds were observed. Table 5.4 provides an overview over the prepared targeting surfactants.

Table 5.4. Overview of the NMR data for the mannosylated targeting surfactants TS(2) containing multiple mannose units.

#	precursor	n(mannose)[a]	M_n[a]/ g mol^{-1}	M_w/M_n[b]

TS(2)-1	**P(2)-3**	36	18,000	3.22
TS(2)-2	**P(2)-4**	75	37,000	2.49
TS(2)-3	**P(2)-6**	18	12,600	n.d.
TS(2)-4	**P(2)-8**	19	12,300	2.33

[a] :determined by ^{1}H NMR spectroscopy of the respective precursor. [b]: determined by SEC in water at 30°C

Mannoslyation of the surfactant precursors led to drastically changed solubility properties. The precursors are readily soluble in common organic solvents such as dichloromethane or DMF and the SEC elugrams were standardly measured in DMF. However, the introduction of mannose led to insolubility of the final surfactants in DMF thus SEC measurements of the targeting surfactants were conducted in water at 30 °C. In order to proof successful modification of the precursors diffusion-ordered spectroscopy (DOSY) was applied. Diffusion-ordered spectroscopy allows a separation of NMR signals of different species contained in one sample according to their diffusion coefficient. In case of separated precursor and mannose their ^{1}H NMR signals would lead to two different diffusion signals with a distinctly lower diffusion coefficient for mannose compared to the precursor due its lower molecular weight. In Figure 5.13 a representative ^{1}H DOSY spectrum of a mannosylated surfactant is depicted showing that the signals of the polymer backbone and the mannose are in line belonging to the same diffusion coefficient range. However, due to self-assembly of the final targeting surfactants in deuterium oxide the signals were rather broad.

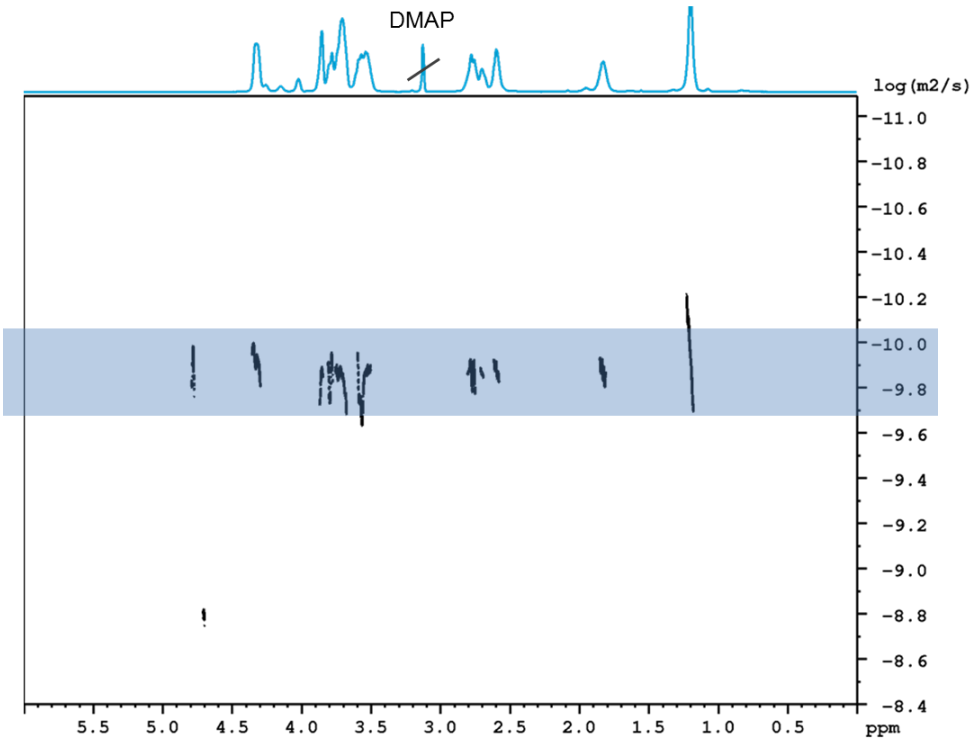

Figure 5.13. 1H DOSY (500 MHz, D2O, 298K) of TS (2)-2 (Table 5.4 entry 2). The ^{1}H DOSY spectrum shows that the signals of the polymer backbone and the signals of the mannose are in one line indicating that the mannose is attached to the polymer backbone.

To evaluate the targeting ability of the prepared surfactants, nanocarriers were decorated with the different surfactants and the cellular uptake of the surfactant modified particles was evaluated against macrophages. In the first approach polystyrene nanoparticles were coated with the **TS(1)-1** and no increased cellular uptake was observed, which might be attributed the protein corona formed upon plasma incubation shielding the mannose moieties. Thus, in addition also poly(methyl methacrylate) (PMMA) and hydroxyl ethyl starch (HES) nanocapsules were investigated, which generally show lower protein adsorpion.

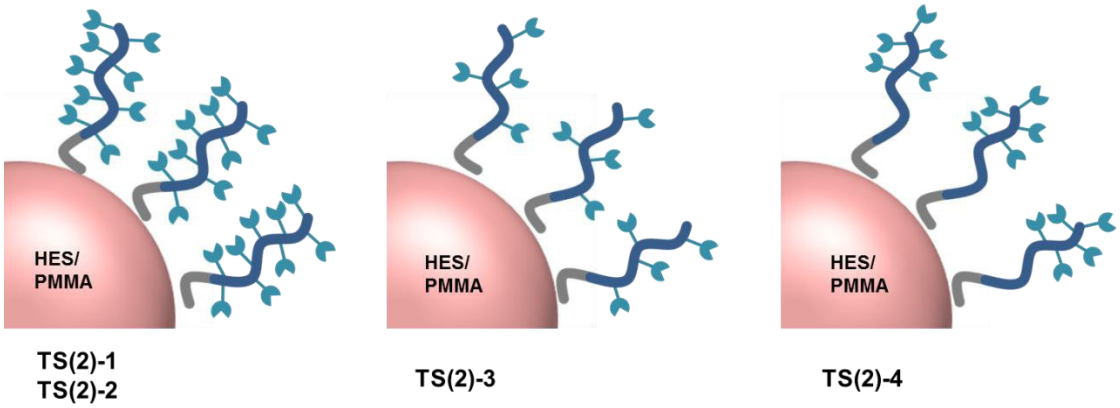

Figure 5.14. Schematic depiction of nanocarriers decorated with targeting surfactants with altered mannose content and location.

In recent years hydroxyethyl starch nanocapsules (HES-NCs) have been studied intensively by our group.[23] HES is a derivative of starch and possesses high biocompatibility as well as improved stability against enzymatic degradation.[28] HES-NCs are prepared by a well-established inverse miniemulsion via the polyaddition reaction at the interface of water nanodroplets dispersed in cyclohexane.[29] This method allows precise adjustment of the particle size and the incorporation of hydrophilic cargo into the hollow nanocapsule.[23, 30] Previous studies concerning HES nanocapsules covalently modified with mannose proved an increased affinity to dendritic cells both in the presence and absence of the plasma protein corona.[23] Therefore, HES NCs are supposed to be suitable for the evaluation of the targeting ability of the prepared targeting surfactants.[23] Additionally PMMA particles were used. PMMA is a well-established material in biomedical applications especially in the field of bone cements[31] and particles can prepared analogously to the PS-NPs by miniemulsion polymerization with precisely adjustable diameters.[32] For the coating, the particles at a concentration of 1wt% were centrifuged, the supernatant was removed and the particles were redispersed in the respective surfactant solution with a concentration of 10 mg mL^{-1} and incubated for 24 h. The cellular uptake of the coated particles was evaluated against macrophages (RAW 264.7). Table 5.5 provides an overview over ζ-potential and diameter of the particles used in the cellular uptake studies.

Table 5.5. ζ-Potential and diameter of HES nanocapsules used in the cellular uptake studies.

	HES	+ $PMEP_{35}$	+TS(2)-1	+TS(2)-2	+TS(2)-3	+TS(2)-4
ζ-Potential[a] / mV	-4.6 ± 3.1	-8.4 ± 3.7	-5.5 ± 4.5	-5.6 ± 2.9	-16.7 ± 3.9	-17.8 ± 3.2
	PMMA	**+ $PMEP_{35}$**	**+TS(2)-1**	**+TS(2)-2**	**+TS(2)-3**	**+TS(2)-4**
ζ-Potential[a] / mV	-35.1 ± 8	-29 ± 7	-25 ± 6	-37 ± 8	-36 ± 8	-28 ± 6
Ø[b] / nm	114 ± 15	115 ± 33	108 ± 11	116 ± 30	117 ± 37	119 ± 22

[a] Determined by electrophoresis. [b] Determined by DLS (diameters were only determined for the surfactant coated PMMA particles since the dye, incorporated in the HES-NCs, showed interference with the laser).

Cellular uptake of the nanoparticles coated with the mannosylated surfactants **TS(2)-1–TS(2)-4** towards macrophages (RAW 264.7) was evaluated. Therefore, cells were incubated with the respective particles for 2 h and subsequently cellular internalization was analyzed by flow cytometry. Data is presented as the relative amount of cells taking up particles ("positive cells") and as the mean fluorescence intensity ("MFI"). Nanoparticles coated with the non-targeting surfactant PMEP (presented in Chapter 4) were used as reference.

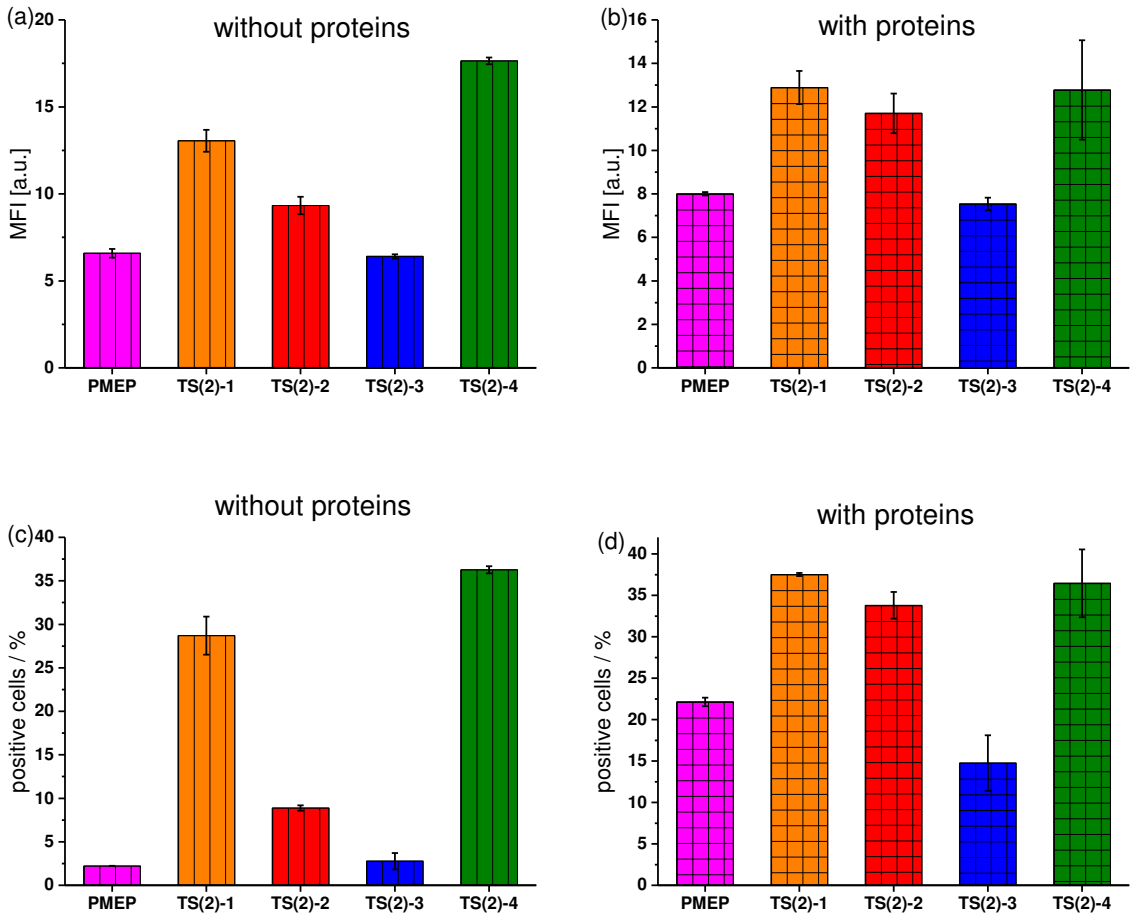

Figure 5.15. Flow cytometry analysis of RAW264.7 cells incubated with differently coated HES nanocapsules for 2 h. Cellular uptake studies were conducted in the absence and presence of proteins where human blood plasma was used as protein source. (*Experiments depicted in this figure were conducted by Johanna Simon*)

Cellular uptake of HES-NCs coated with the mannosylated targeting surfactants **TS(2)-1**, **TS(2)-2** and **TS(2)-4** was increased compared to HES-NCs coated with PMEP-surfactant (Figure 5.15 (a)-(d)) in the presence and absences of proteins. In contrast, coating with the targeting surfactant **TS(2)-3** did not alter uptake behavior. In the absence of proteins (Figure 5.15 (a)), the highest cellular uptake was observed for HES-NCs coated with the block copolymer **TS(2)-4**, which led to a 2.7 fold higher uptake compared to the PMEP coated HES-NCs. In general, due to the presences of proteins the interactions of HES-NCs and cells are favored resulting in an increased unspecific uptake for all HES-NCs (Figure 5.15 (d)). Hence, coating HES-NCs with mannosylated surfactants **TS(2)-1**, **TS(2)-2** or **TS(2)-4** was still enhanced compared to PMEP and **TS(2)-3** coated nanocapsules hereby proofing the targeting ability.

Furthermore, PMMA particles were coated with the targeting surfactants **TS(2)-1–TS(2)-4** and the cellular uptake was evaluated towards murine macrophages and compared to PMMA-NPs coated with PMEP (Figure 5.16). In case of the PMMA particles, 10% human blood serum was used as protein source. Colloidal data for the surfactant coated PMMA-particles presented in Table 5.5 showed similar diameters for the PPE-surfactant coated nanoparticle as for the SDS-stabilized nanoparticle indicating that the PPE-surfactants are suitable for stabilizing PMMA particles.

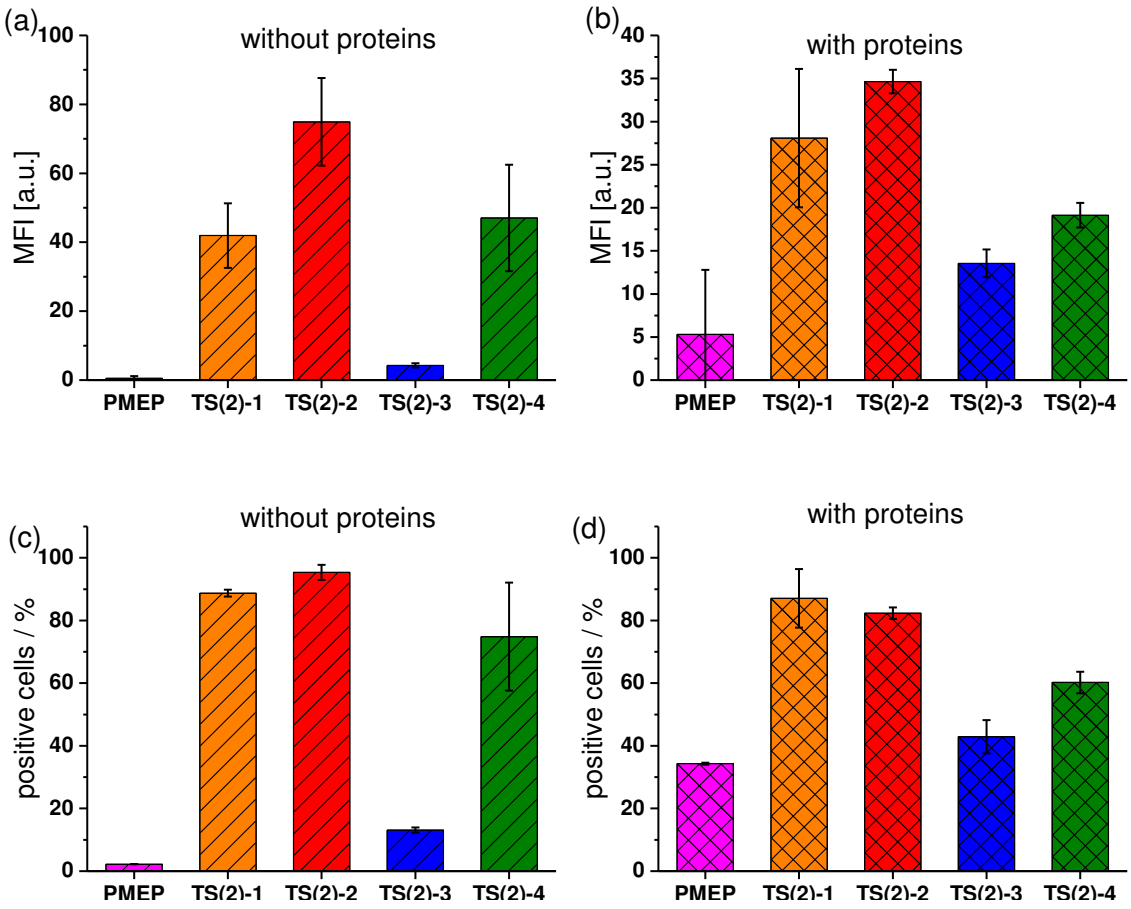

Figure 5.16. Flow cytometry analysis of RAW264.7 cells incubated with differently coated PMMA nanoparticles for 2 h. Cellular uptake studies were conducted in the absence and presence of proteins where 10% human blood serum was used as protein source. (*Experiments depicted in this figure were conducted by Johanna Simon*)

Compared to PMEP coated PMMA-NPs, cellular uptake was dramatically increased upon coating with targeting surfactants **TS(2)-1, TS(2)-2** and **TS(2)-4** in the presence and absences of

proteins (Figure 5.16 (a)-(d)). The strongest cellular interaction was observed for NPs coated with homopolymer **TS(2)-2** , while coating with **TS(2)-3** caused minor effects. As observed for HES-NCs the presences of proteins enhanced cellular interactions for all PMMA-particles (Figure 5.16 (d)). However, for PMMA-particles coated with the targeting surfactants still a significantly increased uptake was observed indicating that the presence of proteins did not lead to complete shielding of the mannose units.

Cellular uptake studies conducted for HES-NCs and PMMA-NPs coated with mannosylated targeting surfactants showed the highest cellular uptake for coating with homopolymer surfactants **TS(2)-1** and **TS(2)-2** and block copolymer surfactant **TS(2)-4**, respectively. In contrast, coating with the copolymer surfactants **TS(2)-3** slightly elevated uptake for PMMA-NPs, while coating of HES-NCs with **TS(2)-3** did not alter uptake behavior. Thus, it can be concluded that the structure of the surfactant is critical for the targeting ability of the coated nanocarrier. Homopolymers **TS(2)-1** and **TS(2)-2** exhibit a mannose moiety on every repeat unit hereby achieving the maximum number and density of mannose moieties per surfactant molecule. In case of the block copolymer, a high density of mannose units is provided at the end of the surfactant molecule, that is supposed to form the outer sphere of the nanocarrier and therefore enables the interaction with the receptor presented on the cell surface. It was reported earlier, that the number of mannose functionalities presented by nanocarriers significantly influences the recognition by macrophages and that the binding affinity increases with increasing mannose density.[33] Similar results were obtained in the here presented study. The copolymer surfactant, in contrast, contains randomly distributed mannose functionalities and therefore exhibit a lower density of mannose functionalities. Furthermore, the different nanocarrier materials need to be considered. In general, similar results were obtained for nanocarriers based on HES or PMMA - in both cases, the highest cellular uptake was observed for targeting surfactants with a high number and density of mannose moieties. However, compared to PMEP coated NPs the targeting effect caused by the mannose surfactants was stronger for PMMA-NPs compared HES-NCs. This can probably be attributed to the different binding affinities of the surfactants to the nanocarrier materials. HES is more hydrophilic than PMMA and thus a weaker interaction of the hydrophobic surfactant tail with HES is expected compared to PMMA. Therefore, the surface modification is more efficient for PMMA-NPs.

3 Summary & Outlook

In this study, a facile strategy towards non-covalent surface modification of nanocarriers with mannose for active targeting of lectins (presented by cells of the immune system) by using mannosylated PPE-surfactants is presented. A library of surfactants was prepared by a two-step protocol, including the polymer preparation by ring-opening polymerization of cyclic phosphates and subsequent mannosylation by thiol-Michael addition. Within this study, surfactants with altered mannose content and position were prepared. The prepared surfactants were characterized in detail by size exclusion chromatography and NMR spectroscopy. The surfactants were assembled on the surface of nanocarriers consisting of different materials and the targeting ability of the modified nanocarriers was evaluated by cellular uptake studies against lectin presenting cells. It was found, that the targeting ability of the surfactants is strongly dependent on the mannose content and density. Polystyrene nanoparticles coated with **TS(1)-1** containing one terminal mannose moiety showed no enhanced uptake by macrophages and dendritic cells. In contrast, coating of nanocarriers with the targeting surfactants **TS(2)**, exhibiting multiple mannose moieties, led to a significantly increased cellular uptake by murine macrophages depending on the surfactant structure.

The highest cellular uptake was observed for nanocarriers coated with surfactants containing a high number and density of mannose moieties, i.e. homopolymer surfactants **TS(2)-1** and **TS(2)-2** as well as the block copolymer surfactant **TS(2)-4,** which is in agreement with earlier studies. Furthermore, slightly distinct results were found for nanocarriers consisting of different materials which can probably be attributed to material-dependent interactions with the surfactants. However, in further studies it need to be proven that the increased cellular uptake of the targeting surfactant coated nanocarriers is receptor-mediated. Thus, experiments need to be done where the mannose-receptor is blocked by presaturation for example with mannan, before incubation with the surfactant coated nanocarriers. If the cellular uptake of the surfactant coated nanocarriers decreases upon receptor-blocking, the receptor-mediated uptake provided by the mannosylated PPE-surfactants is proven.

To conclude, for PMMA and HES nanocarriers coated with mannosylated targeting surfactants exhibiting a high density of mannose moieties a significantly increased cellular uptake was detected compared to nanocarriers coated with PMEP surfactant. Thus, the prepared PPE-based targeting surfactants provide a facile strategy towards functional surface modification of nanocarriers composed of different materials.

4 Experimental

4.1 General information

All chemicals and solvents were purchased from Sigma-Aldrich, Acros Organics or Fluka and used as received unless otherwise stated. Deuterated solvents were purchased from Sigma-Aldrich and used as received. The eluents for column chromatography (cyclohexane and ethyl acetate) were distilled prior to use. Deuterochloroform was stored over alumina (Brockmann activity I).Whole human blood was obtained form 10 healty donors. Sodium citrate was added as anticoagualant to generate human blood plasma. For serum preparation, blood from 6 healty donors was taken and allowed to clot overnight according to the standard procedure.

4.2 Instrumental Techniques

NMR. NMR spectra of the mannose derivatives **(2)** and **(3)** were recorded on an *Avance II 400* (400 MHz ^{1}H NMR, 101 MHz ^{13}C NMR, COSY, HSQC, HMBC; *Bruker*), using a 5 mm probe head at a temperature of 23°C. The ^{13}C-NMR spectra are ^{1}H broadband decoupled. The HSQC sepctra are phase-sensitive (opposite signs for CH/CH_3 and CH_2).The ^{1}H and ^{13}C chemical shifts (δ) were referenced to the residual solvent signal as internal standard (DMSO-d_6: δ = 2.50 ppm and 39.52 ppm, CD_3OD: δ = 3.31 ppm and 49.00 ppm for ^{1}H and ^{13}C NMR, respectively).[34] Coupling constants (*J*) are reported in Hz (splitting abbreviations: s, singlet; d, doublet; t, triplet; q, quartet; m, multiplet; br, broad; and combinations thereof). ^{1}H, ^{13}C and ^{31} P NMR spectra of mannose derivative **(3)** and all polymers were recorded using a Bruker Avance III 250, a Bruker Avance 300, a Bruker Avance III 500 and processed with MestReNova. All ^{31}P NMR spectra were recorded decoupled from protons. All spectra were referenced internally to residual proton signals of the deuterated solvent. 2D spectra were processed with the topspin 3.5 software.
For the diffusion measurements (DOSY)[35] a 5 mm triple resonance BBFO ^{1}H/X probe equipped with a z-gradient on the 500 MHz Bruker AVANCE III system was used. For the diffusion measurements a 2D sequence (DOSY, dstebpgp3s) with a stimulated echo was used.[36] The temperature was kept at 298.3 K and regulated by a standard ^{1}H methanol NMR sample using the topspin 3.1 software (Bruker). The control of the temperature was realized with a VTU (variable temperature unit) and an accuracy of +/- 0,1K. The diffusion time was 30-70 ms and the gradient length to 1.4 ms. The relaxation delay between scans was 1.5-2 s. The gradient strength was calibrated by analysis of a sample of $2H_2O/1H_2O$ at a defined temperature and comparison with the theoretical diffusion coefficient of $2H_2O/1H_2O$.

SEC. For the size exclusion chromatography (SEC) measurements two different methods were used. ***Method a***: SEC measurements of standard polymers were performed in DMF (containing 1 gL^{-1} of lithium bromide as an additive) at 60 °C and a flow rate of 1 mL min^{-1} with a PSS SECurity as an integrated instrument, including a set of 3 PSS GRAM columns (porosity of 100 Å and 1000 Å) and a refractive index (RI) Detector. Calibration was carried out using polyethylene glycol standards provided by Polymer Standards Service. ***Method b***: SEC measurements were performed in DMF (containing 1 gL^{-1} of lithium bromide as an additive) at 50 °C with an Agilent 1100 Series as an integrated instrument, including a HEMA column (300/100/40) from MZ Analysentechnik, a UV (275 nm), and a refractive index (RI) detector. Calibration was carried out using poly(ethylene glycol) standards provided by Polymer Standards Service. ***Method c:*** For the targeting surfactants **TS(2)** SEC measurements were performed in 0.1 M aqueous $NaNO_3$ solution at 30 °C and a flow rate of 1 mL min^{-1} with a PSS SECurity as an integrated instrument including a PSS Suprema linear S column. and a refractive index (RI) Detector. Calibration was carried out using polyethylene glycol standards provided by Polymer Standards Service.

Chromatography. Thin-layer chromatography (TLC) was carried out on silica gel 60 F254 plates (*Merck*) or RP silica gel RP-18 F_{254s} plates (*Merck*). Compounds were visualized by immersion in a solution of of *m*-methoxyphenol (0.1 mL) in ethanol (95 mL) and sulfuric acid (2 mL) followed by heating. Chromatography was performed using flash chromatography of the indicated solvent system on 35-70 µm silica gel (*Acros Organics*) unless otherwise noted.

Mass Spectrometry. HPLC-ESI-MS^n was performed on a *1200 series* HPLC system with a UV diode array detector coupled with a *LC/MSD trap XCT* mass spectrometer (*Agilent Technologies*). Mixtures of water (with 0.1% formic acid) and acetonitrile were used as eluents at a total flow rate of 0.5 to 1.0 mL/min. An *Ascentis Express C18* column (pore size: 2.7 µm, length: 3 cm, diameter: 2.1 mm; *Supelco*) was used at a temperature of 40 °C. High-resolutionmasses (ESI) were recorded on a *Q-ToF-Ultima 3* instrument (*Waters*) with LockSpray® interface and a suitable external calibrant.

MALDI-ToF. For the matrix assisted laser desorption/ionization time of flight (MALDI ToF) mass spectrometry measurement a Shimadzu Axima CFR mass spectrometer equipped with a nitrogen laser with a pulse rate of t=3 ns at a wave length of λ=337 nm was used. 2-(4'-hydroxybenzeneazo)benzoic acid was used as matrix

DLS. The average size and the size distribution of the nanoparticles were measured by DLS at 25 °C using a PSS NicompTM Submicron Particle Sizer 380 (Nicomp Particle Sizing Systems) equipped with a detector for a scattering angle of 90° to the incident beam. The samples were diluted in demineralized water to be slightly cloudy.

For evaluation of the stability of surfactant-coated nanoparticles in human blood plasma the method by Rausch *et al.*[37] was applied.

ζ-Potential. The zeta potential of the dispersion was determined with a Zeta Sizer Nano Series (Malvern Instruments, U.K.) at 25 °C by diluting 10 µL of a 2wt% dispersion in 1 mL of 10^{-3} M potassium chloride solution.

Flow Cytometry. For cellular uptake analysis, 150.000 cells per well (RAW 264.7) were seeded out in 24-well plates. After overnight incubation at 37°C, cells were washed with PBS and kept in cell culture medium additional proteins. Prior to cellular uptake experiments, nanoparticles were incubated with plasma/serum (see protein corona preparation in the experimental section of Chapter 4) and added to cells at a concentration of 75 µg/mL for 2h. Further, cells were washed wit PBS to remove free nanoparticles and detached with 2.5% trypsin (Gibco, Germany). Measurements were conducted on a CyFlow ML Cytometer and data analysis was analyzed with FCS Express V4 software. Cells were selected on a forward/sideward scatter plot, eluding cell debris and gated events were as median fluorescence intensity (MFI) or percentage of fluorescent positive cells (%).

DC Preparation. Dendritic cells were prepared according to method by Freichels *et al.*[38]

Particle coating. For coating of polystyrene nanoparticles **TS(1)-1** was dissolved at a concentration of 3 mg mL^{-1} in the particle dispersion (2wt%) and charged into a dialysis tube with MWCO of 1 kDa and dialyzed against deionized water for 24 h. For coating of PMMA-NPs and HES-NCs the dispersion was centrifuged, the supernatant was removed and the obtained nanoparticle pellet was redispersed in 1wt% solution of the respective surfactant.

4.3 Synthetic procedures

Allyl α-D-mannopyranose *(2).* A solution of α-D-mannopyranose (**1**, 5.00 g, 27.8 mmol, 1 eq.) in allylalcohol (48.4 g, 56.9 mL, 833 mmol, 30 eq.) was treated with acetyl chloride (5.41 g, 4.92 mL, 69.4 mmol, 1.5 eq.) under stirring at room temperature. The reaction mixture was heated to 100 °C and stirred at that temperature 16 hours. Subsequently the reaction mixture was cooled to room temperature and treated with solid $NaHCO_3$ until pH = 7. The mixture was filtered over a bed of Celite, which was washed thoroughly with toluene. The solvents were

removed under reduced pressure and the residue was purified by flash column chromatography (ethyl acetate/ methanol, 10:1) to give the title compound (4.75 g, 21.6 mmol, 78%) as a colorless viscous oil.

R_f = 0.32 (silica gel, ethyl acetate/ methanol, 10:2).

^{1}H-NMR, COSY (400 MHz, CD_3OD) δ (ppm) = 5.94 (dddd, ^3J = 17.3 Hz, ^3J = 10.7 Hz, ^3J = 6.0 Hz, ^3J = 5.1 Hz, 1H, Man–O–CH_2–C*H*), 5.30 (*pseudo* dq, ^2J = 17.2 Hz, J = 1.7 Hz, 1H, O–CH_2–CH=C$H_{2,a}$), 5.17 (*pseudo* dq, ^2J = 10.4 Hz, J = 1.5 Hz, 1H, O–CH_2–CH=C$H_{2,b}$), 4.97 (d, ^3J = 1.7 Hz, 1H, H_{Man}-1), 4.22 (*pseudo* ddt, ^2J = 13.1 Hz, ^3J = 5.1 Hz, ^4J = 1.6 Hz, 1H, O–C$H_{2,a}$–CH=CH_2), 4.00 (*pseudo* ddt, ^2J = 13.1 Hz, ^3J = 5.9 Hz, ^4J = 1.4 Hz, 1H, O–C$H_{2,b}$–CH=CH_2), 3.86–3.78 (m, 2H, H_{Man}-2, H_{Man}-6_a), 3.72–3.67 (m, 2H, H_{Man}-3, H_{Man}-6_b), 3.61 (*pseudo* t, ^3J = 9.5 Hz, 1H, H_{Man}-4), 3.53 (ddd, ^3J = 9.8 Hz, ^3J = 5.8 Hz, ^3J = 2.3 Hz, 1H, H_{Man}-5).**^{13}C-NMR, HSQC, HMBC** (100.6 MHz, CD_3OD) δ (ppm) = 135.5 (Man–O–CH_2–*C*H), 117.3 (O–CH_2–CH=*C*H_2), 100.7 (C_{Man}-1), 74.7 (C_{Man}-5), 72.6 (C_{Man}-3), 72.2 (C_{Man}-2), 68.8 (Man–O–*C*H_2–CH), 68.6 (C_{Man}-4), 62.9 (C_{Man}-6).

IR (ATR) λ_{max}/cm^{-1} 3344, 2923, 1453, 1422, 1412, 1261, 1129, 1096, 1053, 1024, 975, 925, 879, 810.

$[\boldsymbol{\alpha}]_{\boldsymbol{D}}^{\mathbf{24}}$ = +62.5° (c = 1.00, H_2O).

ESI-MS: *m/z* (%) = 243.1 (100) $[M + Na]^+$, 244.2 (11) $[M + Na]^+$.

The spectral data are in accordance with literature.[39]

Acetylthiopropyl-α-D-mannopyranoside (3). A solution of allyl α-D-mannopyranose (**2**, 4.24 g, 19.3 mmol, 1 eq.) in thoroughly degassed methanol (100 mL, four freeze-pump-thaw cycles) was treated with thioacetic acid (8.30 g, 7.83 mL, 109 mmol, 6 eq.) and AIBN (40 mg, cat.). The reaction mixture was heated under reflux for 3 days and subsequently the solvent was removed under reduced pressure. The residue was coevaporated with toluene (3 × 60 mL) and purified by flash column chromatography (dichloromethane/ methanol, 10:1.5) to give the title compound (1.83 g, 6.18 mmol, 32%) as a colorless viscous oil. Some of the starting material could be recovered (2.75 g, 12.5 mmol, 65%).

R_f = 0.40 (silica gel, dichloromethane/ methanol, 10:1.5).

^{1}H-NMR, COSY (400 MHz, CD_3OD) δ (ppm) = 4.73 (d, ^3J = 1.7 Hz, 1H, H_{Man}-1), 3.86–3.76 (m, 3H, H_{Man}-2, H_{Man}-6_a, Man–O–C$H_{2,a}$), 3.74–3.67 (m, 2H, H_{Man}-3, H_{Man}-6_b), 3.60 (*pseudo* t, ^3J = 9.5 Hz, 1H, H_{Man}-4), 3.54–3.43 (m, 2H, H_{Man}-5, Man–O–C$H_{2,b}$), 3.03–2.90 (m, 2H, CH_2–SAc), 2.31 (s, 3H, CH_3), 1.89–1.81 (m, 2H, Man–O–CH_2–CH_2). **^{13}C-NMR, HSQC, HMBC**

(100.6 MHz, CD_3OD) δ (ppm) = 197.4 (C=O), 101.6 (C_{Man}-1), 74.7 (C_{Man}-5), 72.6 (C_{Man}-3), 72.2 (C_{Man}-2), 68.6 (C_{Man}-4), 66.9 (Man–O–CH_2), 62.9 (C_{Man}-6), 30.7 (Man–O–CH_2–CH_2), 30.5 (CH_3), 26.9 (CH_2–SAc).

IR (ATR) λ_{max}/cm^{-1} 3354, 2920, 1688, 1414, 1354, 1321, 1129, 1086, 1051, 1022, 958, 915, 810.

$[\boldsymbol{\alpha}]_{\boldsymbol{D}}^{\mathbf{24}}$ = +51.5° (c = 1.00, MeOH).

ESI-MS: *m/z* (%) = 319.1 (100) $[M + Na]^+$, 320.2 (9) $[M + Na]^+$.

HRMS (ESI): Calculated for $[C_{11}H_{20}O_7S + Na]^+$: 319.0827 found: 319.0830.

Representative procedure for the synthesis of thiopropyl-α-D-mannopyranoside (4). Thiopropyl-α-D-mannopyranoside was synthesized freshly prior to use to avoid the formation of disulfide. Acetylthiopropyl-α-D-mannopyranoside (1 g, 3.37 mmol, 1 eq) was dissolved in dry methanol and cooled down to 0 °C. Sodium methylate solution 5.4 M (1 mL, 5.06 mmol, 1.5 eq) in dry methanol was added and the solution was stirred for 2 h where a colorless solid precipitated. Subsequently, cation exchanger Amberlite® IR-120 was added, stirred for several minutes until the supension became a clear solution. The cation exchanger was filtered and the solvent was removed at reduced pressure. 860 mg of thiopropyl-α-D-mannopyranoside was obtained as colorless viscous oil in qunatitative yield. **^{1}H NMR** (250 MHz, Deuterium Oxide) δ 3.91 – 3.34 (m, 9H), 2.49 (t, *J* = 7.1 Hz, 2H), 1.95 – 1.62 (m, *J* = 7.5 Hz, 2H). ^{13}C NMR (75 MHz, Deuterium Oxide) δ 118.15, 99.71, 72.78, 70.58, 70.04, 66.74, 65.80, 60.91, 48.86, 32.49, 20.49.

2-((2-Oxido-1,3,2-dioxaphospholan-2-yl)oxy)ethyl methacrylate **(OPEMA).**The compound was synthesized according to a literature procedure. 2-hydroxyethyl methacrylate (HEMA) (22.84 g, 175.5 mmol, 1eq) and triethylamine (17.76 g, 175.5 mmol, 1eq) were transferred into a 500 mL round-bottom flask equipped with a dropping funnel, dissolved in 200 ml of dry THF and cooled down to -20°C. 2-chloro-1,3,2-dioxaphospholane-2-oxide (COP) (25.00 g, 175.5 mmol, 1eq) was transferred into the dropping funnel and added droppwise to the stirred reaction mixture within the course of one hour. Subsequently, the reaction mixture was cooled down to -30°C and stirred for several hours. The precipitated salt was filtered under argon, washed with dry THF and the solvent was removed at reduced pressure. Diethylether was added, precipitated salt was filtered, and the solvent was removed under reduced pressure. OPEMA was obatined as

a colorless viscous oil (31 g, 131.3 mmol, 74.8%). **^{1}H NMR** (300 MHz, Chloroform-*d*) δ 6.27 – 5.97 (m, 1H), 5.57 (p, *J* = 1.6 Hz, 1H), 4.64 – 4.08 (m, 8H), 1.91 (t, *J* = 1.5 Hz, 3H). **^{31}P NMR** (121 MHz, Chloroform-*d*) δ 17.67.

2-Methoxy-1,3,2-dioxaphospholane-2-oxide (MEP). A flame-dried three-neck flask, equipped with a dropping funnel, was charged with a solution of dry methanol (11.24 g, 0.35 mol) and dry triethylamine (39.1 g, 0.39 mol, 1.1 eq) in dry THF (250 mL) and cooled down to 0 °C. A solution of 2-chloro-2-oxo-1,3,2-dioxaphospholane (50 g, 0.35 mol, 1 eq) dissolved in dry THF (50 mL) was added to the trimethylamine/methanol mixture under constant stirring. After complete addition of COP the reaction mixture was stirred for 2 more hours at 0 °C. The precipitated salt was removed by filtration and the filtrate concentrated *in vacuo*. The residue was purified by distillation under reduced pressure . The product was obtained as colorless, liquid (37.3g, 0.27mol, yield: 77%, bp.: 83°C, 10^{-2} mbar). **^{1}H NMR** (300 MHz, Chloroform-*d*) δ 4.54 – 4.26 (m, 4H,-O-***CH$_2$-CH$_2$***-O-), 3.82 (d, 3H, *J* = 11.7 Hz,- ***CH$_3$***). **^{31}P {H} NMR** (121 MHz, Chloroform-*d*) δ 18.57.

Representative procedure for the synthesis of precursor (P(1)). All Schlenk-tubes were flame-dried prior to use. 1-octadecanol was used as initiator and DBU/TU as catalyst. TU (376 mg, 1.02 mmol, 5 eq) and 1-octadecanol were introduced into separate flame-dried Schlenk-tubes, dissolved in dry benzene and dried by lyophilization. MEP (1.12 g, 8.08 mmol, 40 eq) was introduced into the TU-tube. A stock solution of the initiator in dry THF was prepared (240 µmol mL^{-1}). 0.82 mL (55 mg, 203 µmol, 1 eq) of initiator stock solution and 3 mL of dry DCM were added to the MEP/TU mixture. The mixture was cooled down to 0°C and the reaction was started by rapid addition of DBU. The reaction was stirred for 1h at 0°C and terminated by rapid addition of 2-isocyanatoethyl methacrylate (158 mg, 1.02 mmol, 5 eq). The ice bath was removed and the mixture was stirred for 10 minutes at ambient temperature. The polymer was obtained as a colorless viscous oil in quantitative yield by three times precipitation from diethyl ether and subsequent centrifugation and decantation. It was desisted from further purification to avoid crosslinking of the terminal methyl methacrylate groups and the polymer was stored at -85°C until further usage. **^{1}H NMR** (300 MHz, Chloroform-*d*) δ 6.06 (s, double bond terminal methacrylate), 5.52 (s, double bond terminal methacrylate), 4.31 – 4.10 (m, -O-C***H$_2$***-C***H$_2$***-O-, backbone), 3.84 – 3.67 (m, -O-C***H$_3$***, side chain), 1.88 (m, -C***H$_3$***, terminal methacrylate), 1.18 (s, initiator, CH$_3$-(C***H$_2$***)$_{15}$-), 0.86 – 0.76 (m, -C***H$_3$***, initiator). **^{31}P{H} NMR** (121 MHz, Chloroform-d) δ 1.09, -0.20,

Synthesis of targeting surfactant TS(1)-1. Precursor **P(1)-3** (400 mg, 0.07 mmol, 1 eq) and an excess of thiopropyl-α-D-mannopyranoside (450 mg, 1.75 mmol, 25 eq) were dissolved in 25 mL DMSO/MeOH (1:1) at ambient temperature. 0.1 mL trimethylamine were added and the reaction mixture was stirred for 24 h at ambient temperature. After 24 h the reaction mixture was transferred into a dialysis tube with MWCO = 3,500 g mol^{-1} and was dialyzed against deionized water to remove the excess of thiopropyl-α-D-mannopyranoside. The dialysis water was exchanged three times every 2 h. The product was obtained by lyophilization. NMR spectroscopy of the obtained product showed signals belonging to residual disulfide. In order to remove the residual amount of disulfide in the product, it was again dialyzed against water for 24 h together with 1,4-dithiothreitol as reducing agent. The product was obtained by lyophilization in quantitative yield. **^{1}H NMR** (250 MHz, Methanol-d_4) δ 4.50 – 4.19 (m, -O-C***H*****$_2$**-C***H*****$_2$**-O-, backbone), 3.82 (d, J = 11.2 Hz, -O-C***H*****$_3$**, side chain), 3.73 – 3.42 (m), 2.84 – 2.53 (m), 1.86 (m), 1.26 (s, CH_3-(C***H*****$_2$**$)_{15}$- initiator), 0.86 (m, C***H*****$_3$**, initiator). **^{31}P{H} NMR** (121 MHz, DMSO-d_6) δ 1.11, -0.12.

Representative procedure for the synthesis precursors P(2)-1 – P(2)-4. All Schlenk-tubes were flame-dried prior to use. 1-octadecanol was used as initiator and DBU/TU as catalyst. TU (376 mg, 1.02 mmol, 5 eq) and octadecanol were introduced into separate flame-dried Schlenk-tubes, dissolved in dry benzene and dried by lyophilization. OPEMA (823 mg, 3.49 mmol, 40 eq) was added to the cocatalyst. The initiator stock solution was prepared at a concentration of 10 mg mL^{-1}. 2.35 mL (23.5 mg, 1 eq) were added to the TU/OPEMA mixture and cooled down to 0 °C. The reaction was started by rapid addidtion of DBU to the reaction mixture. The reaction was stirred for 1.75 h at 0 °C and terminated by rapid addition of an excess of acetic acid dissolved in DCM (20 mg mL^{-1}). The ice bath was removed and the mixture was stirred for 10 minutes at ambient temperature. The polymer was obtained in quantitative yield as colorless viscous oil by precipitation from diethyl ether, subsequent centrifugation and decantation.

Representative NMR data

^{1}H NMR (300 MHz, Chloroform-*d*) δ 6.14 (s, double bond terminal methacrylate), 5.60(s, double bond terminal methacrylate), 4.57 – 4.00 (m, -O-C***H*****$_2$**-C***H*****$_2$**-O- backbone and side chain),

1.93 (s, -C***H₃*** methacrylate), 1.18 (s, CH_3-(C***H₂***)$_{15}$- initiator), 0.86 (t, -C***H₃*** initiator). **^{31}P{H} NMR** (121 MHz, Chloroform-*d*) δ -1.29.

Representative procedure for the synthesis of precursors P(2)-7,8. All Schlenk-tubes were flame-dried prior to use. 1-octadecanol was used as initiator and DBU/TU as catalyst. TU (376 mg, 1.02 mmol, 5 eq) and 1-octadecanol were introduced into separate flame-dried Schlenk-tubes, dissolved in dry benzene and dried by lyophilization. MEP (416 mg, 3.02 mmol, 20 eq) was added to the TU cocatalyst. A stock solution of the initiator in dry DCM was prepared at a concentration of 148 µmol mL^{-1} (40 mg mL^{-1}). 1.02 mL (40.8 mg, 151 µmol, 1 eq) of initiator stock solution and 2 mL of dry DCM were added to the MEP/TU mixture. The reaction mixture was cooled down to 5 °C and the polymerization was started by rapid addition of DBU. Subsequently, the temperature was adjusted to 0 °C. The reaction was stirred for 1.5 h at 0 °C. After 1.5 h 0.1 mL of the reaction mixture was withdrawn for SEC analysis. 1.07 g OPEMA (4.52 mmol, 30 eq) was added and the reaction was stirred further for 1 h. The polymerization was terminated by rapid addition of an excess of acetic acid dissolved in DCM (20 mg mL^{-1}). The ice bath was removed and the mixture was stirred for 5 minutes at ambient temperature. The polymer was obtained in quantitative yield as colorless viscous oil by precipitation from diethyl ether, subsequent centrifugation and decantation.

Representative NMR data

^{1}H NMR (250 MHz, Chloroform-*d*) δ 6.14 (s, double bond terminal methacrylate), 5.60(s, double bond terminal methacrylate), 4.52 – 4.09 (m,-O-***CH₂-CH₂***-O- backbone and side chain), 3.80 (dd, *J* = 11.2, 4.8 Hz, -O-C***H₃*** side chain), 1.94 (s, -C***H₃*** methacrylate), 1.24 (s, -(C***H₂***)$_{15}$-CH_3 initiator), 0.86 (t, -C***H₃***initiator). **^{31}P{H} NMR** (121 MHz, Methylene Chloride-d_2) δ -0.16, -1.27.

Representative procedure for the synthesis of precursors **P(2)-5,6.** All Schlenk-tubes were flame-dried prior to use. 1-octadecanol was used as initiator and DBU/TU as catalyst. TU (376 mg, 1.02 mmol, 5 eq) and octadecanol were introduced into seperate flame-dried Schlenk-tubes, dissolved in dry benzene and dried by lyophilization. MEP (1.12 g, 8.08 mmol, 40 eq) was introduced into the TU-tube. A stock solution of the initiator in dry THF was prepared (240 µmol mL^{-1}). 0.82 mL (55 mg, 203 µmol, 1 eq) of initiator stock solution and 3 mL of dry DCM were added to the MEP/TU mixture. The mixture was cooled down to 0°C and the reaction was started by rapid addition of DBU. The reaction was stirred for 1h at 0°C and terminated by rapid

addition of 2-isocyanatoethyl methacrylate (158 mg, 1.02 mmol, 5 eq). The ice bath was removed and the mixture was stirred for 10 minutes at ambient temperature. The polymer was obtained as a colorless viscous oil in quantitative yield by three times precipitation from diethyl ether and subsequent centrifugation and decantation. It was desisted from further purification to avoid crosslinking of the terminal methyl methacrylate groups and the polymer was stored at -85°C until further usage.

Representative NMR data

^{1}H NMR (300 MHz, Methylene Chloride-d_2) δ 6.14 (s, double bond terminal methacrylate), 5.60(s, double bond terminal methacrylate), 4.52 – 4.09 (m, -O-C***H*****$_2$**-C***H*****$_2$**-O- backbone and side chain), 3.79 (d, J = 11.2 Hz,-O-C***H*****$_3$**), 1.94 (s, -C***H*****$_3$** methacrylate), 1.24 (s, -(C***H*****$_2$**)$_{15}$-CH_3 initiator), 0.86(t, -C***H*****$_3$** initiator). **^{31}P{H} NMR** (121 MHz, Chloroform-d) δ -0.16, -1.33.

***General procedure for the mannosylation of the precursors* P(2).** The respective precursor and thiopropyl-α-D-mannopyranoside were dissolved in methanol. DMAP was added as catalyst and the reaction was stirred at ambient temperature. The progress of the reaction was monitored by ^{1}H NMR spectroscopy. When the signals of the double bond in the ^{1}H NMR spectrum have disappeared the reaction was completed and methanol was removed under reduced pressure. The residue was dissolved in water and charged into a dialysis tube (MWCO = 3,500 kDa). The crude product was dialyzed against water where the water was exchanged four times to remove DMAP and TCEP. The products were obtained as white solids by lyophilization and

Representative NMR data for homopolymer surfactants **TS(2)-1** *and* **TS(2)-2**

^{1}H NMR (500 MHz, Deuterium Oxide) δ 4.42 – 4.19 (m, -O-C***H*****$_2$**-C***H*****$_2$**-O- backbone and side chain), 3.95 – 3.44 (m), 2.86 – 2.52 (m, -CR_3***H***, -S-C***H*****$_2$**-CH-), 1.82 (h, J = 7.0 Hz, -S-C***H*****$_2$**-CH_2-O-), 1.20 (s, -C***H*****$_3$**). ^{13}C NMR (126 MHz, Deuterium Oxide) δ 99.78, 72.75, 70.69, 70.14, 67.10, 66.52, 66.04, 66.01, 63.58, 60.85, 40.22, 34.52, 28.63, 16.46. **^{31}P{H} NMR** (202 MHz, Deuterium Oxide) δ 0.39, -0.00, -0.99 – -1.64

NMR data for targeting surfactant **TS(2)-3**

^{1}H NMR (500 MHz, Methanol-d_4) δ 4.36 (m, -O-***CH*****$_2$**-***CH*****$_2$**-O- backbone and side chain), 3.92 – 3.47 (m, -O-C***H*****$_3$**), 2.91 – 2.59 (m, -C***H***, -S-C***H*****$_2$**-CH-), 1.87 (m, -S-C***H*****$_2$**-CH_2-O-), 1.28 (m, -C***H*****$_3$**), 0.92 (t, -C***H*****$_3$** initiator). **^{31}P{H} NMR** (202 MHz, Methanol-d_4) δ 0.62, -0.33, -1.76.

NMR data for targeting surfactant **TS(2)-4**

^{1}H NMR (500 MHz, Deuterium Oxide) δ 4.66 – 4.27 (m, 18H), 4.01 – 3.52 (m, 15H), 2.96 – 2.57 (m, 5H), 1.91 (s, 2H), 1.37 (d, J = 81.4 Hz, 7H). ^{13}C NMR (126 MHz, Deuterium Oxide) δ

99.77, 72.76, 70.71, 70.16, 67.07, 66.51, 66.01, 64.38, 63.57, 60.86, 60.45, 55,25, 40.22, 34.51, 29.85, 28.61, 16.32.**^{31}P{H} NMR** (202 MHz, Deuterium Oxide) δ 1.48, -0.10, -1.44.

4.3.1 Particle preparation

Poly(methyl methacrylate) (PMMA)/polystyrene (PS) nanoparticles. A macroemulsion was prepared with a continuous phase containing sodium dodecyl sulfate (SDS) (60 mg, 0.21 mmol) as surfactant in 24 g Milli-Pore water and a dispersed phase containing distilled styrene (6 g, 57.6 mol), hexadecane (250 mg, 0.9 mmol) as ultrahydrophobe, Bodipy methacrylate (6 mg, $1.3 \cdot 10^{-5}$ mol) as fluorescent dye and azoisobutyronitrile (AIBN) (100 mg, 0.6 mmol) as oil soluble initiator. For the synthesis of PMMA particles styrene was replaced by methyl methacrylate (MMA) (6 g, 59.9 mmol) as monomer, while all other components remained the same. In both cases, both phases were homogenized by mechanical stirring and subsequently, the organic phase was added slowly to the stirring aqueous phase. The macroemulsion was stirred for 1h at highest speed. Subsequently, the macroemulsion was ultrasonicated with a Branson Sonifier (1/2“ tip, 6.5 nm diameter) for 3 min (programm: 10 s puls and 3 s pause) at 70% amplitude under ice cooling to obtain a miniemulsion. The miniemulsion was directly transferred into a 50 mL flask, heated to 72°C and stirred overnight.

Table 5.6. Size and ζ-potebntial of nanoparticles prepared by miniemulsion polymerization.

#	Ø / nm	ζ / mV
PS	101 ± 12	-52 ± 13
PMMA	114 ± 15	-46 ± 12

Synthesis of hydroxyethyl starch nanocapsules (HES). HES nanocapsules were synthesized as previously described via by polyaddition reactions at the miniemulsion droplet interfaces.[29] Briefly, HES solution (10 wt%, 1.4g), 20 mg NaCl, 100 µL Cy5Oligo solution and 150µL CellTracker was added to 7.5 g cyclohexane containing 100 mg of P(E/B-*b*-EO) and stirred for 1h. The emulsion was further sonicated under ice-cooling with a Branson W450-D sonifier. TDI

(100 mg) and P(E/B-b-EO) (30 mg) was dissolved in 5 g cyclohexane, added dropwise to the miniemulsion and stirred for 24h at RT. The nanocapsules were purified by centrifugation and redispersion in cyclohexane (2x). Further, the nanocapsules were transferred into aqueous medium using 0.1wt% SDS solution. The dispersion was slowly added to the SDS solution in a sonication bath and stirred overnight to evaporate cyclohexane. To remove excess SDS, nanocapsules were dialyzed for 24h, centrifuged and redispersed in water (1x).

4.4 SEC

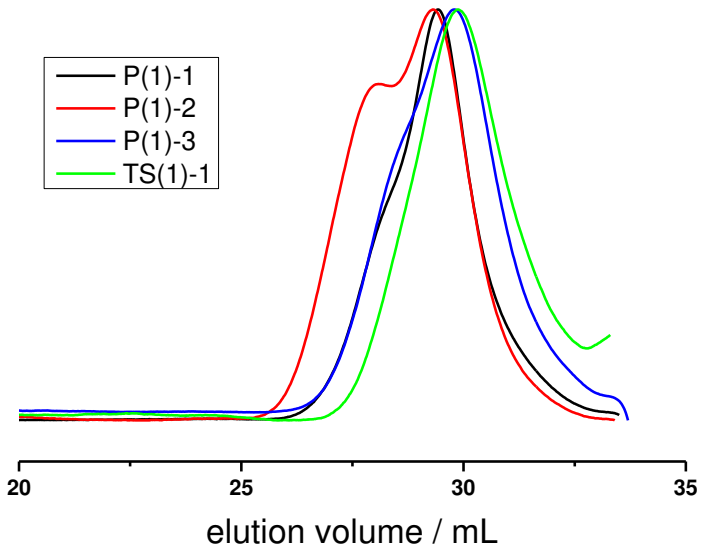

Figure 5.17. SEC-elugrams of precursors P(1)-1, P(1)-2, P(1)-3 and targeting surfactant TS(1)-1 in DMF at 60 °C (Method a).

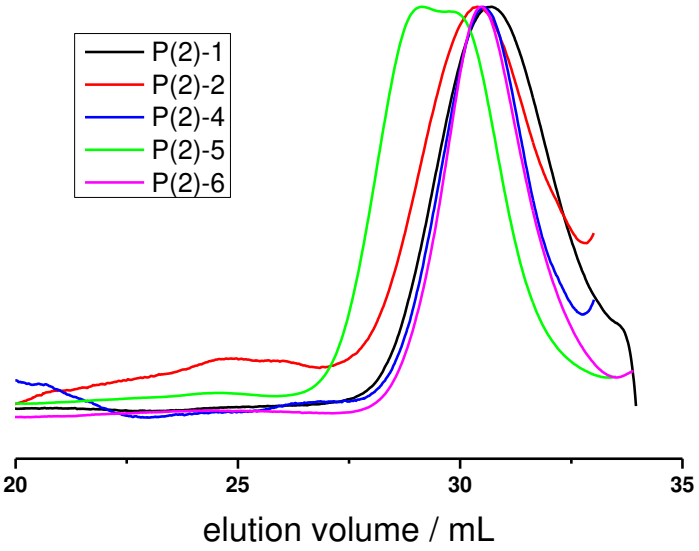

Figure 5.18. SEC-traces of precursors P(2)-1, P(2)-2, P(2)-4, P(2)-5, P(2)-6 in DMF at 60 °C (Method a).

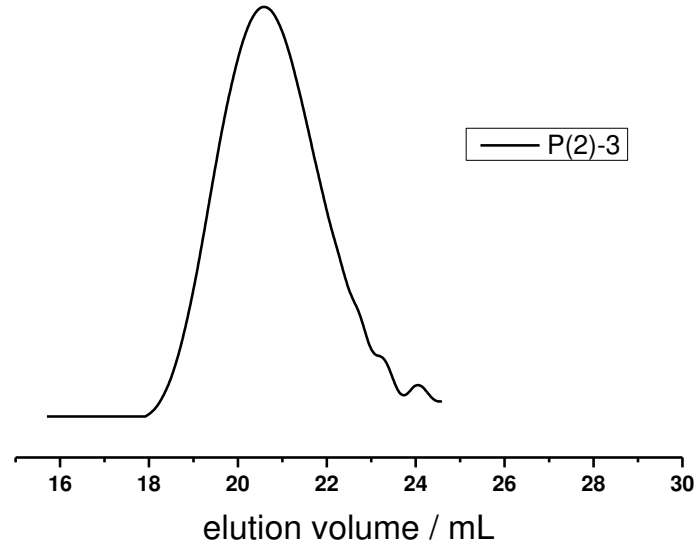

Figure 19. SEC-elugrams of precursor P(2)-3 in DMF at 50 °C (*Method b*).

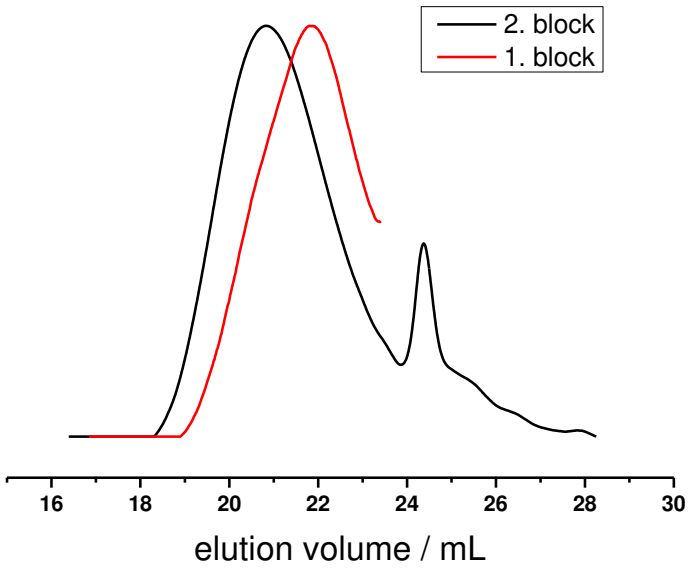

Figure 5.20. SEC-elugrams of P(2)-7 in DMF at 50 °C (*Method b*).

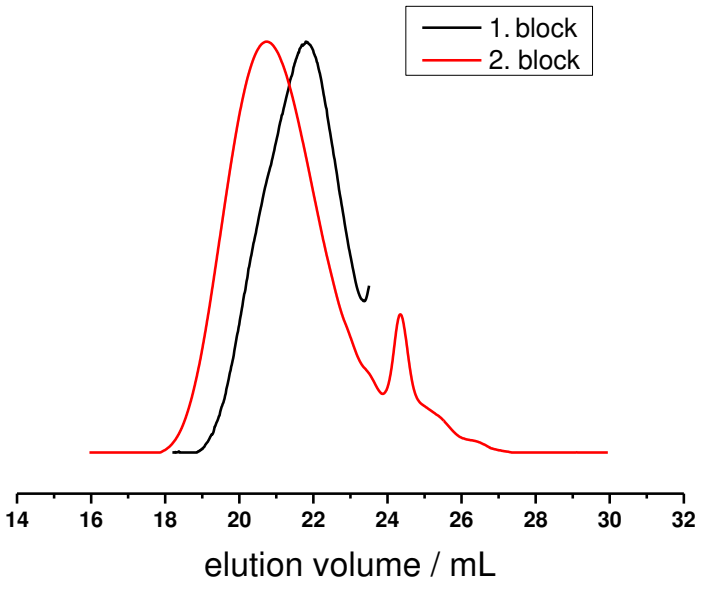

Figure 5.21. SEC-elugrams of P(2)-8 in DMF at 50 °C.

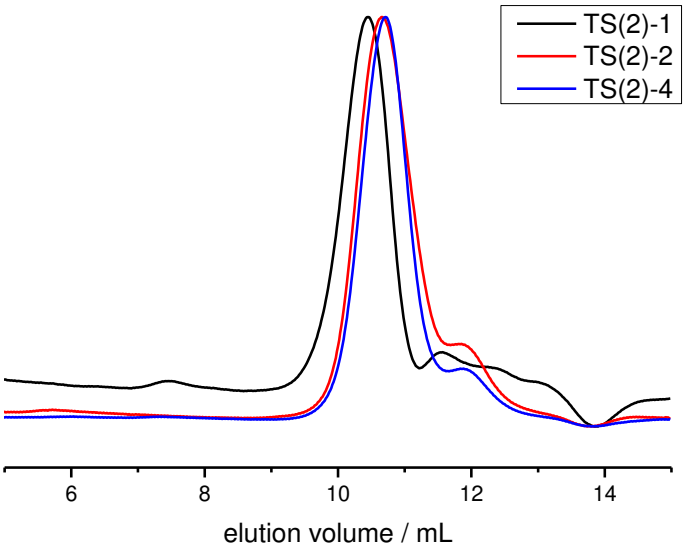

Figure 5.22. SEC-elugrams of TS(2)-1, TS(2)-2 and TS(2)-4 in water at 30°C (Method c).

4.5 Spectra

4.5.1 ^{1}H NMR Spectra

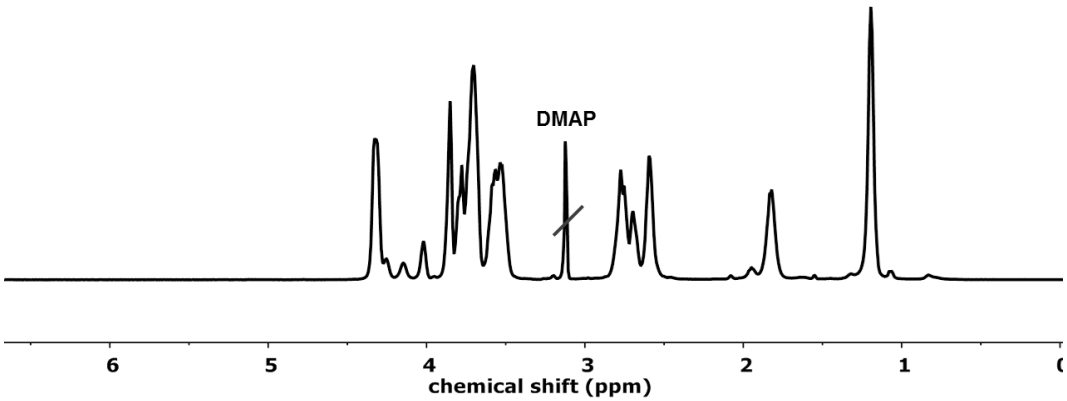

Figure 5.23. ^{1}H NMR spectrum of TS(2)-2 (500 MHz, 298 K, D_2O) (KRB331)

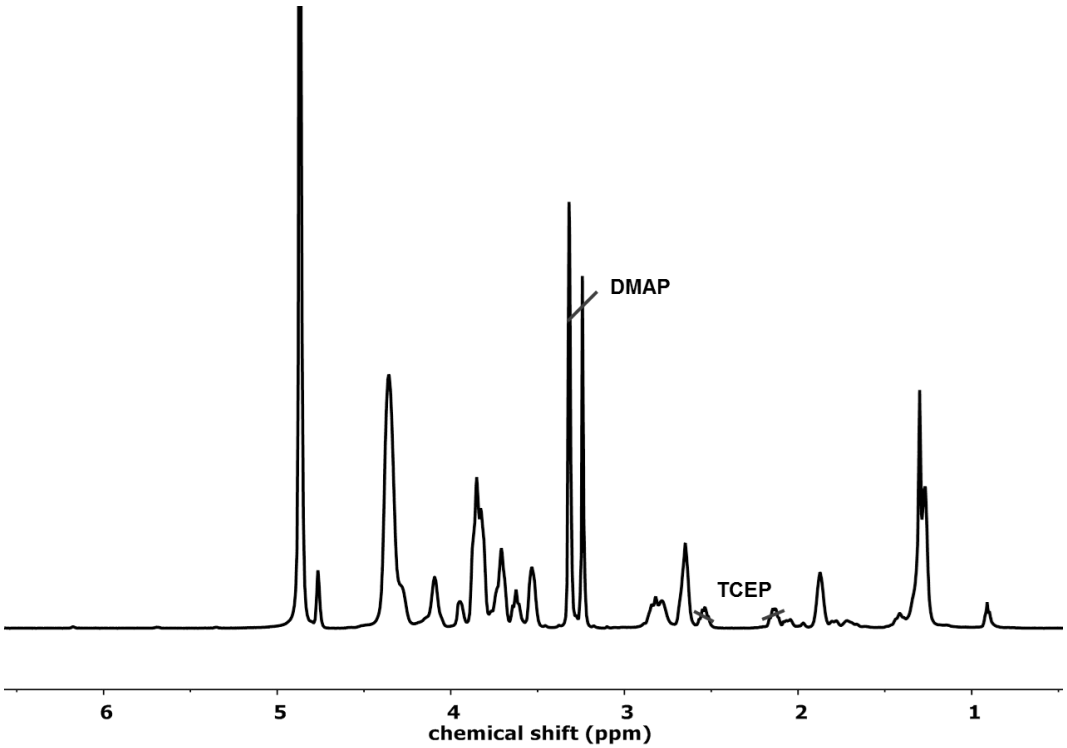

Figure 5.24. ^{1}H NMR spectrum of TS(2)-3 (500 MHz, 298 K, D_2O) (KRB344)

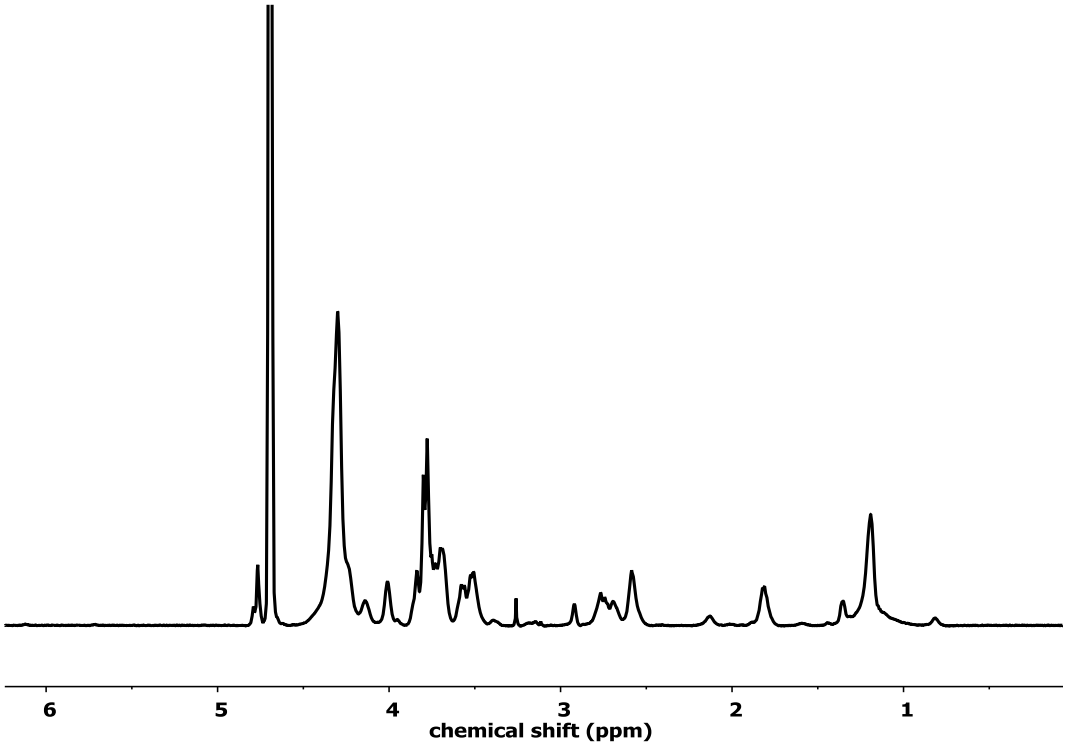

Figure 5.25. ^{1}H NMR spectrum of TS(2)-4 (500 MHz, 298 K, D_2O) (KRB330)

31P NMR spectra

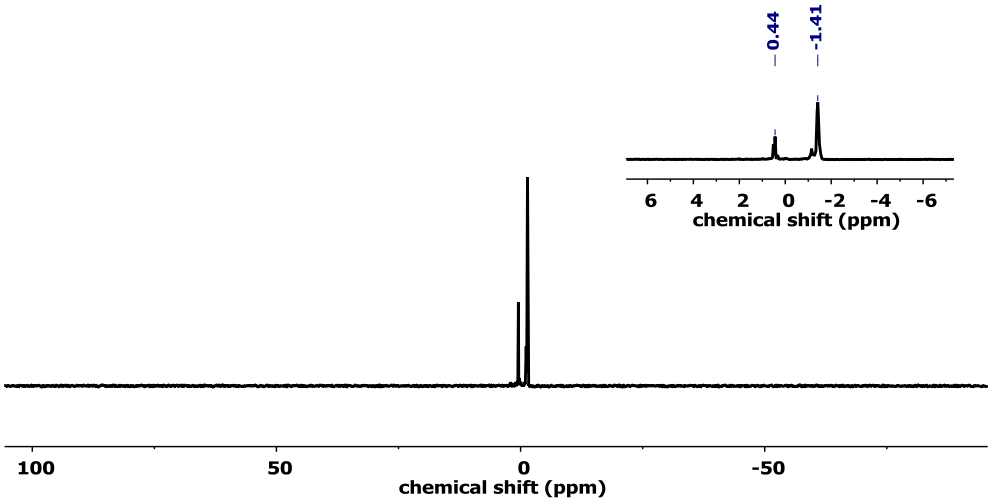

Figure 26. $^{31}P\{H\}$ NMR (202 MHz, MeOD, 298 K) of TS(2)-2

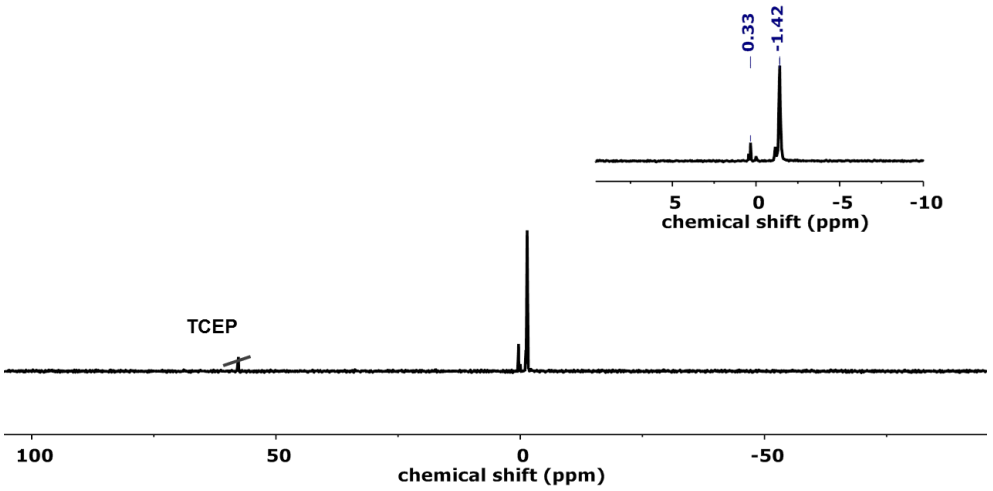

Figure 5.27. $^{31}P\{H\}$ NMR (202 MHz, D_2O, 298 K) of TS(2)-1

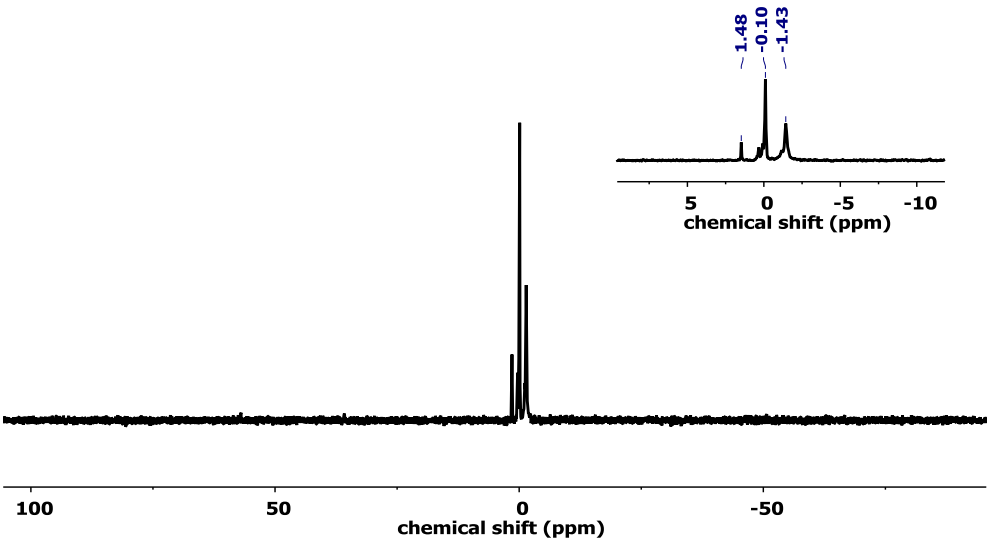

Figure 5.28. $^{31}P\{H\}$ NMR (202 MHz, D_2O, 298 K) of TS(2)-4.

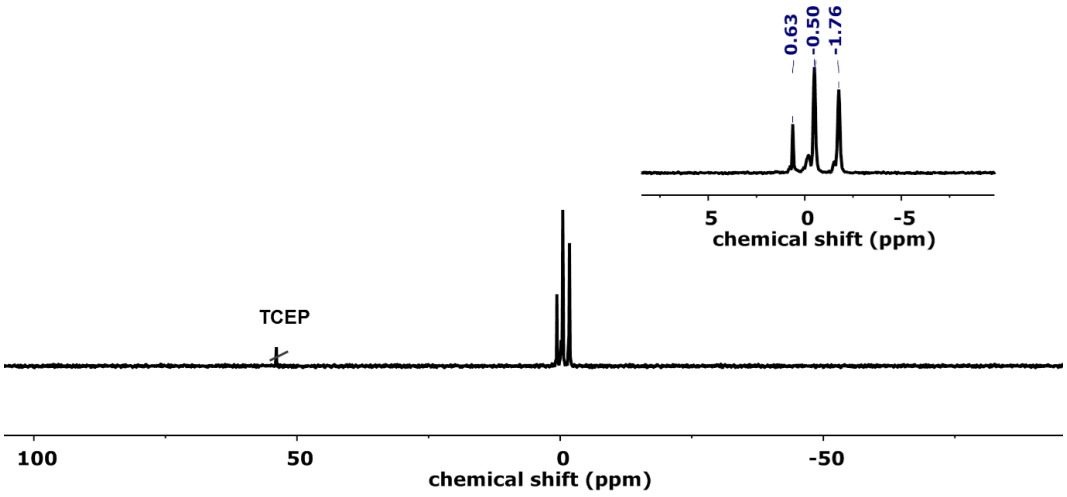

Figure 5.29. $^{31}P\{H\}$ NMR (202 MHz, MeOD, 298 K) of TS(2)-3.

4.5.2 DOSY spectra

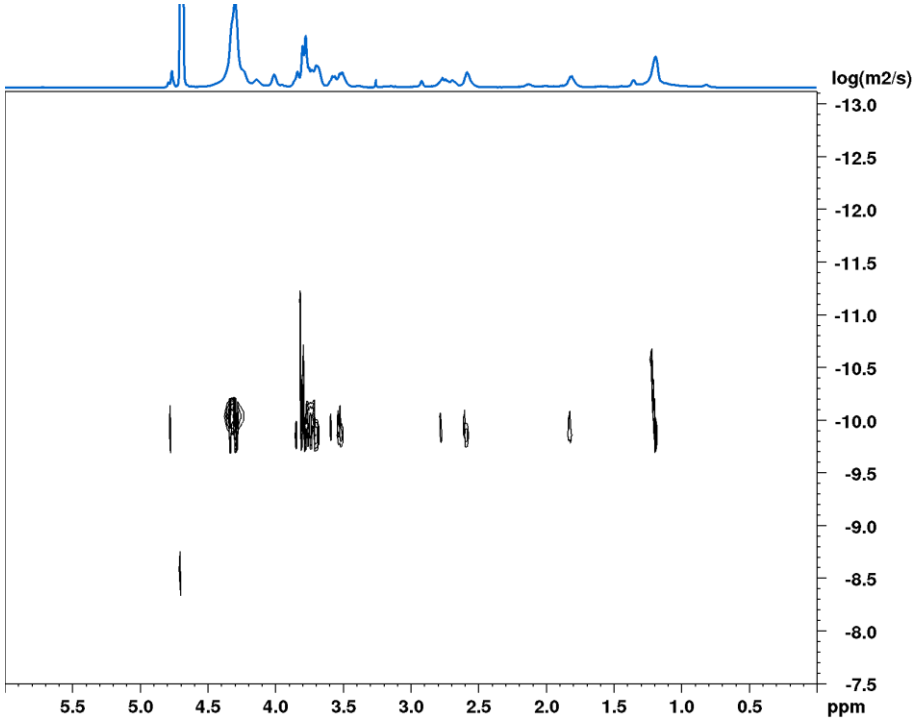

Figure 5.30. ^{1}H DOSY NMR spectrum of TS(2)-4 (500 MHz, 298 K, D_2O).

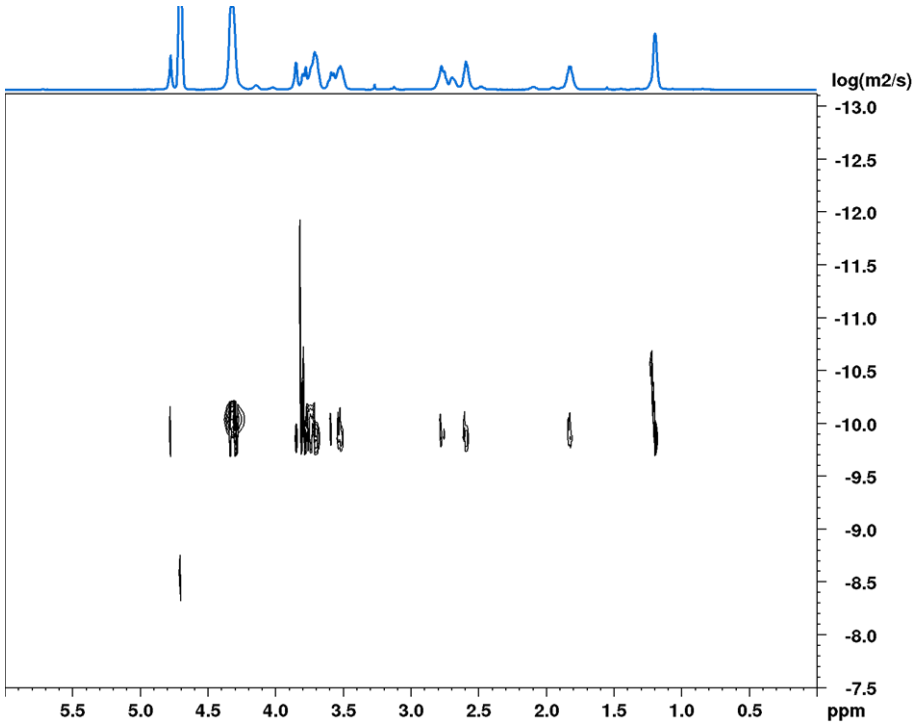

Figure 5.31. ^{1}H DOSY NMR spectrum of TS(2)-1 (500 MHz, 298 K, D_2O).

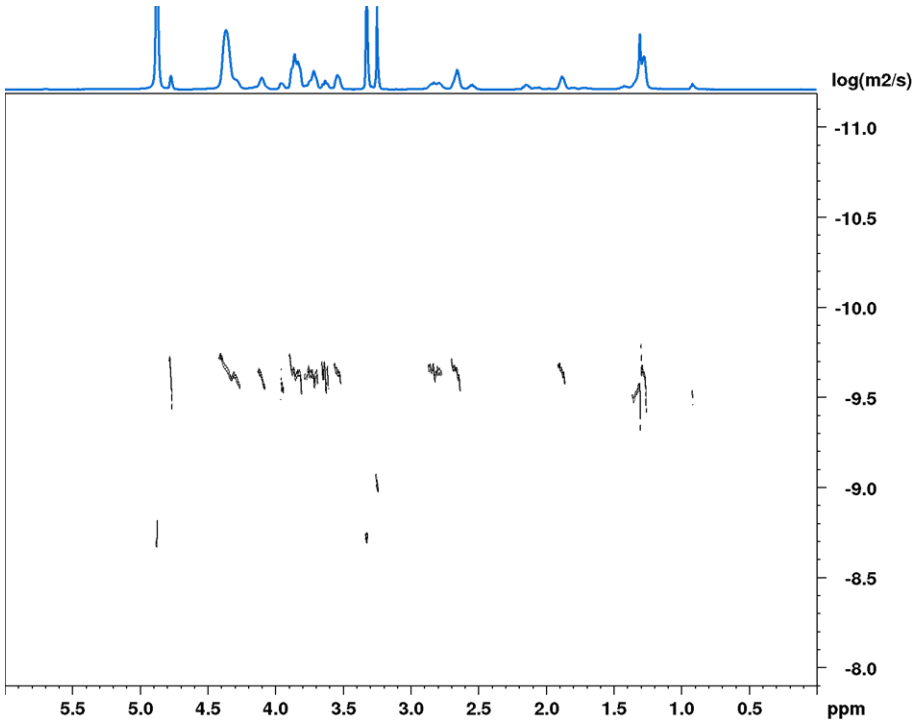

Figure 5.32. ^{1}H DOSY NMR spectrum of TS(2)-3 (500 MHz, 298 K, MeOD).

4.6 DLS measurements in human plasma

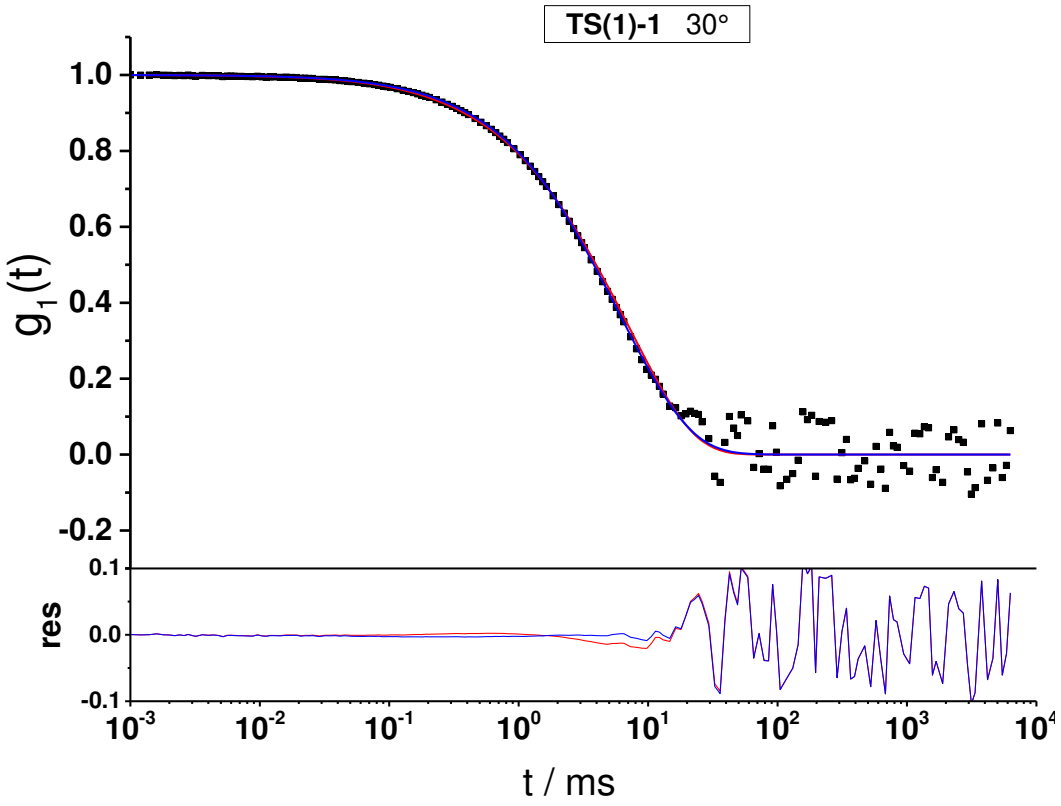

Figure 5.33. Autocorrelation functions (ACFs) for PS-NPs coated with TS(1)-1. Upper graphs: ACF $g_1(t)$ (black dots) for a scattering angle of 30 ° with a forced fit consisting of the sum of the two individual components (red line −) and a fit with an additional aggregate function where necessary (blue line −). Lower graphs: Residuals resulting from the difference of the data and the corresponding fits.

5 References

1. Mills, J. K.; Needham, D., Targeted drug delivery. *Expert Opinion on Therapeutic Patents* **1999,** *9* (11), 1499-1513.
2. Bae, Y. H.; Park, K., Targeted drug delivery to tumors: myths, reality and possibility. *Journal of Controlled Release* **2011,** *153* (3), 198.
3. Bertrand, N.; Wu, J.; Xu, X.; Kamaly, N.; Farokhzad, O. C., Cancer nanotechnology: The impact of passive and active targeting in the era of modern cancer biology. *Advanced Drug Delivery Reviews* **2014,** *66* (Supplement C), 2-25.
4. Salvati, A.; Pitek, A. S.; Monopoli, M. P.; Prapainop, K.; Bombelli, F. B.; Hristov, D. R.; Kelly, P. M.; Aberg, C.; Mahon, E.; Dawson, K. A., Transferrin-functionalized nanoparticles lose their targeting capabilities when a biomolecule corona adsorbs on the surface. *Nat Nano* **2013,** *8* (2), 137-143.
5. Ulbrich, K.; Hekmatara, T.; Herbert, E.; Kreuter, J., Transferrin- and transferrin-receptor-antibody-modified nanoparticles enable drug delivery across the blood–brain barrier (BBB). *European Journal of Pharmaceutics and Biopharmaceutics* **2009,** *71* (2), 251-256.
6. Zhang, Y.; Li, J.; Lang, M.; Tang, X.; Li, L.; Shen, X., Folate-functionalized nanoparticles for controlled 5-Fluorouracil delivery. *Journal of Colloid and Interface Science* **2011,** *354* (1), 202-209.
7. Nobs, L.; Buchegger, F.; Gurny, R.; Allémann, E., Surface modification of poly(lactic acid) nanoparticles by covalent attachment of thiol groups by means of three methods. *International Journal of Pharmaceutics* **2003,** *250* (2), 327-337.
8. Juillerat-Jeanneret, L., The targeted delivery of cancer drugs across the blood–brain barrier: chemical modifications of drugs or drug-nanoparticles? *Drug Discovery Today* **2008,** *13* (23), 1099-1106.
9. Kreuter, J.; Ramge, P.; Petrov, V.; Hamm, S.; Gelperina, S. E.; Engelhardt, B.; Alyautdin, R.; von Briesen, H.; Begley, D. J., Direct Evidence That Polysorbate-80-Coated Poly(Butylcyanoacrylate) Nanoparticles Deliver Drugs to the CNS via Specific Mechanisms Requiring Prior Binding of Drug to the Nanoparticles. *Pharmaceutical Research* **2003,** *20* (3), 409-416.
10. Gulyaev, A. E.; Gelperina, S. E.; Skidan, I. N.; Antropov, A. S.; Kivman, G. Y.; Kreuter, J., Significant Transport of Doxorubicin into the Brain with Polysorbate 80-Coated Nanoparticles. *Pharmaceutical Research* **1999,** *16* (10), 1564-1569.
11. Alyautdin, R. N.; Petrov, V. E.; Langer, K.; Berthold, A.; Kharkevich, D. A.; Kreuter, J., Delivery of Loperamide Across the Blood-Brain Barrier with Polysorbate 80-Coated Polybutylcyanoacrylate Nanoparticles. *Pharmaceutical Research* **1997,** *14* (3), 325-328.
12. Wang, H.; Su, L.; Li, R.; Zhang, S.; Fan, J.; Zhang, F.; Nguyen, T. P.; Wooley, K. L., Polyphosphoramidates That Undergo Acid-Triggered Backbone Degradation. *ACS Macro Letters* **2017,** *6* (3), 219-223.
13. Du, J.-Z.; Du, X.-J.; Mao, C.-Q.; Wang, J., Tailor-Made Dual pH-Sensitive Polymer–Doxorubicin Nanoparticles for Efficient Anticancer Drug Delivery. *Journal of the American Chemical Society* **2011,** *133* (44), 17560-17563.
14. Ezekowitz, R. A.; Sastry, K.; Bailly, P.; Warner, A., Molecular characterization of the human macrophage mannose receptor: demonstration of multiple carbohydrate recognition-like domains and phagocytosis of yeasts in Cos-1 cells. *The Journal of Experimental Medicine* **1990,** *172* (6), 1785-1794.
15. Banchereau, J.; Steinman, R. M., Dendritic cells and the control of immunity. *Nature* **1998,** *392* (6673), 245-252.

16. Taylor, M. E.; Conary, J. T.; Lennartz, M. R.; Stahl, P. D.; Drickamer, K., Primary structure of the mannose receptor contains multiple motifs resembling carbohydrate-recognition domains. *Journal of Biological Chemistry* **1990,** *265* (21), 12156-62.
17. Hsu, F. J.; Benike, C.; Fagnoni, F.; Liles, T. M.; Czerwinski, D.; Taidi, B.; Engleman, E. G.; Levy, R., Vaccination of patients with B–cell lymphoma using autologous antigen–pulsed dendritic cells. **1996,** *2*, 52.
18. Condon, C.; Watkins, S. C.; Celluzzi, C. M.; Thompson, K.; Falo Jr, L. D., DNA–based immunization by in vivo transfection of dendritic cells. **1996,** *2*, 1122.
19. Apostolopoulos, V.; McKenzie, I. f. c., Role of the Mannose Receptor in the Immune Response. *Current Molecular Medicine* **2001,** *1* (4), 469-474.
20. Allen, C. F. H.; Fournier, J. O.; Humphlett, W. J., THE THERMAL REVERSIBILITY OF THE MICHAEL REACTION: IV. THIOL ADDUCTS. *Canadian Journal of Chemistry* **1964,** *42* (11), 2616-2620.
21. Hoyle, C. E.; Bowman, C. N., Thiol–Ene Click Chemistry. *Angewandte Chemie International Edition* **2010,** *49* (9), 1540-1573.
22. Feinberg, H.; Mitchell, D. A.; Drickamer, K.; Weis, W. I., Structural Basis for Selective Recognition of Oligosaccharides by DC-SIGN and DC-SIGNR. *Science* **2001,** *294* (5549), 2163-2166.
23. Kang, B.; Okwieka, P.; Schöttler, S.; Winzen, S.; Langhanki, J.; Mohr, K.; Opatz, T.; Mailänder, V.; Landfester, K.; Wurm, F. R., Carbohydrate-Based Nanocarriers Exhibiting Specific Cell Targeting with Minimum Influence from the Protein Corona. *Angewandte Chemie International Edition* **2015,** *54* (25), 7436-7440.
24. Ondera, T. J.; Hamme Ii, A. T., Magnetic-optical nanohybrids for targeted detection, separation, and photothermal ablation of drug-resistant pathogens. *Analyst* **2015,** *140* (23), 7902-7911.
25. Rieger, J.; Freichels, H.; Imberty, A.; Putaux, J.-L.; Delair, T.; Jérôme, C.; Auzély-Velty, R., Polyester Nanoparticles Presenting Mannose Residues: Toward the Development of New Vaccine Delivery Systems Combining Biodegradability and Targeting Properties. *Biomacromolecules* **2009,** *10* (3), 651-657.
26. Feinberg, H.; Castelli, R.; Drickamer, K.; Seeberger, P. H.; Weis, W. I., Multiple Modes of Binding Enhance the Affinity of DC-SIGN for High Mannose N-Linked Glycans Found on Viral Glycoproteins. *Journal of Biological Chemistry* **2007,** *282* (6), 4202-4209.
27. Lv, Y.; Yang, B.; Li, Y.-M.; Wu, Y.; He, F.; Zhuo, R.-X., Crosslinked triblock copolymeric micelle for redox-responsive drug delivery. *Colloids and Surfaces B: Biointerfaces* **2014,** *122* (Supplement C), 223-230.
28. Yoshida, M.; Yamashita, T.; Matsuo, J.; Kishikawa, T., Enzymic Degradation of Hydroxyethyl Starch. Part I. Influence of the Distribution of Hydroxyethyl Groups on the Enzymic Degradation of Hydroxyethyl Starch. *Starch - Stärke* **1973,** *25* (11), 373-376.
29. Baier, G.; Baumann, D.; Siebert, J. M.; Musyanovych, A.; Mailänder, V.; Landfester, K., Suppressing Unspecific Cell Uptake for Targeted Delivery Using Hydroxyethyl Starch Nanocapsules. *Biomacromolecules* **2012,** *13* (9), 2704-2715.
30. Kang, B.; Opatz, T.; Landfester, K.; Wurm, F. R., Carbohydrate nanocarriers in biomedical applications: functionalization and construction. *Chemical Society Reviews* **2015,** *44* (22), 8301-8325.
31. Ramakrishna, S.; Mayer, J.; Wintermantel, E.; Leong, K. W., Biomedical applications of polymer-composite materials: a review. *Composites Science and Technology* **2001,** *61* (9), 1189-1224.

32. Ziegler, A.; Landfester, K.; Musyanovych, A., Synthesis of phosphonate-functionalized polystyrene and poly(methyl methacrylate) particles and their kinetic behavior in miniemulsion polymerization. *Colloid and Polymer Science* **2009,** *287* (11), 1261.
33. Yeeprae, W.; Kawakami, S.; Yamashita, F.; Hashida, M., Effect of mannose density on mannose receptor-mediated cellular uptake of mannosylated O/W emulsions by macrophages. *Journal of Controlled Release* **2006,** *114* (2), 193-201.
34. Fulmer, G. R.; Miller, A. J. M.; Sherden, N. H.; Gottlieb, H. E.; Nudelman, A.; Stoltz, B. M.; Bercaw, J. E.; Goldberg, K. I., NMR Chemical Shifts of Trace Impurities: Common Laboratory Solvents, Organics, and Gases in Deuterated Solvents Relevant to the Organometallic Chemist. *Organometallics* **2010,** *29* (9), 2176-2179.
35. Stejskal, E. O.; Tanner, J. E., Spin Diffusion Measurements: Spin Echoes in the Presence of a Time-Dependent Field Gradient. *The Journal of Chemical Physics* **1965,** *42* (1), 288-292.
36. Jerschow, A.; Müller, N., Suppression of Convection Artifacts in Stimulated-Echo Diffusion Experiments. Double-Stimulated-Echo Experiments. *Journal of Magnetic Resonance* **1997,** *125* (2), 372-375.
37. Rausch, K.; Reuter, A.; Fischer, K.; Schmidt, M., Evaluation of Nanoparticle Aggregation in Human Blood Serum. *Biomacromolecules* **2010,** *11* (11), 2836-2839.
38. Freichels, H.; Wagner, M.; Okwieka, P.; Meyer, R. G.; Mailander, V.; Landfester, K.; Musyanovych, A., (Oligo)mannose functionalized hydroxyethyl starch nanocapsules: en route to drug delivery systems with targeting properties. *Journal of Materials Chemistry B* **2013,** *1* (34), 4338-4348.
39. Winnik, F. M.; Brisson, J.-R.; Carver, J. P.; Krepinsky, J. J., Syntheses of model oligosaccharides of biological significance.Synthesis of methyl 3,6-DI-O-(α-d-mannopyranosyl)-α-d-mannopyranoside and the corresponding mannobiosides. *Carbohydrate Research* **1982,** *103* (1), 15-28.

Chapter 6

Hydrolytic degradation: poly(phosphate)s *vs.* poly(phosphonate)s

Abstract

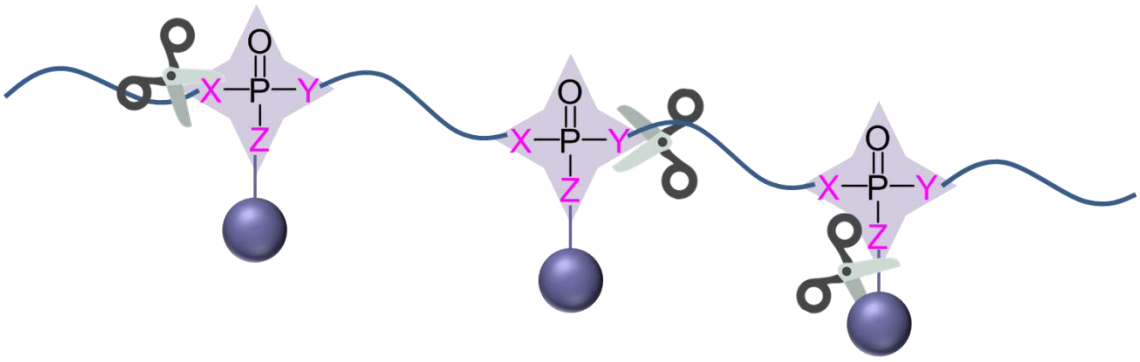

The degradation of three different PPE-classes, i.e. poly(phosphate)s, in-chain and side-chain poly(phosphonate)s, exhibiting different binding patterns around the central phosphorus atom were studied to evaluated the influence of the binding pattern on the degradation profiles. The degradation studies were conducted in aqueous media under acidic and basic conditions and the degradation process was followed by NMR spectroscopy. Under acidic conditions no degradation was observed. In contrast under basic conditions degradation was observed for all considered polymers with distinct different degradation profiles. Detailed investigation of the degradation by NMR spectroscopy indicated a degradation mechanism proceeding by backbiting of the terminal alcohol group similar to the mechanism proposed for the degradation of poly(lactic acid) (PLA) to be most likely. Moreover, it was found that the aggregation behavior in aqueous media play a key role in the hydrolytic degradation of the considered polymers.

1 Introduction

Polymeric materials have been used for a long time in biomedical applications and can be divided in two classes: biostable and biodegradable polymers. Biodegradable polymers are especially appealing for temporary therapeutic applications.[1] Many types of surgical implants and drug delivery systems that are needed *in vivo* only temporarily can be made from polymers that are eliminated from the body by a combination of hydrolytic and enzymatic degradation after fulfilling the intended task.[2]

Most biodegradable polymers contain linkages such as esters or amides along the polymer chains that are susceptible of enzymatic and hydrolytic cleavage.[3] The pre-evaluation of enzymatic degradation *in vivo* is difficult, due to varying enzyme concentrations at different sites in the body. However, dissolved aliphatic polyesters with flexible polymer chains usually fit into the active site of an enzyme and are therefore readily degraded enzymatically. Furthermore, they are attractive materials due to their adjustable biodegradability and versatile physical and chemical properties.[4] Hydrolytic degradation is affected by a number of parameters such as the polarity and molecular weight of the polymers as well as the pH.[5] For the hydrolytic degradation of polymer agglomerates their size, shape and surface to volume ratio are crucial parameters that affect their degradation rates significantly.[6-8]

For a few years, PPEs containing the phosphorus atoms within the polymer backbone are tipped promising candidates as degradable materials for biomedical applications. Although the potential biodegradability and biocompatibility is emphasized in most publications about PPEs, only a few deal with a more detailed investigation of the degradation kinetics of PPEs.[9-10] First studies on the kinetics of PPE hydrolysis were presented by Penczek in the 1990s.[11] They evaluated the hydrolysis of poly(methyl ethylene phosphate) (PMEP) at different pH-values ranging from 2 to 12. They suggested two different mechanisms for hydrolysis under basic and acidic conditions. Under basic conditions they proposed a direct nucleophilic attack of the OH^- ion on the phosphorus atom leading to an intermediate five-binding phosphorus with a trigonal bipyramidal geometry in which the axial position is preferably shed. Due to comparable probabilities for main and side chain to occupy this position, side and main chain should be cleaved with the same probability taking the statistical factor into account. Under acidic conditions, however, they proposed a nucleophilic attack of H_2O on the α-carbon, after protonation.

Recently, we established the side-chain and in-chain poly(phosphonate)s as potentially degradable materials for future bioapplications. In contrast to the poly(phosphate)s, they are based on phosphonic acid, either with one or two phosphonate esters in the main chain. These in-chain or side-chain polyphosphonate exhibit a strongly altered hydrolysis profile compared to the polyphosphates, which is discussed herein (Figure 6.1). Due to the different binding patterns around the central phosphorus atom of each repeating unit, the polymers are expected to differ in their degradation behavior and time, especially. As a first approach the hydrolytic degradation of the different PPE-classes under basic and under acidic conditions were evaluated.

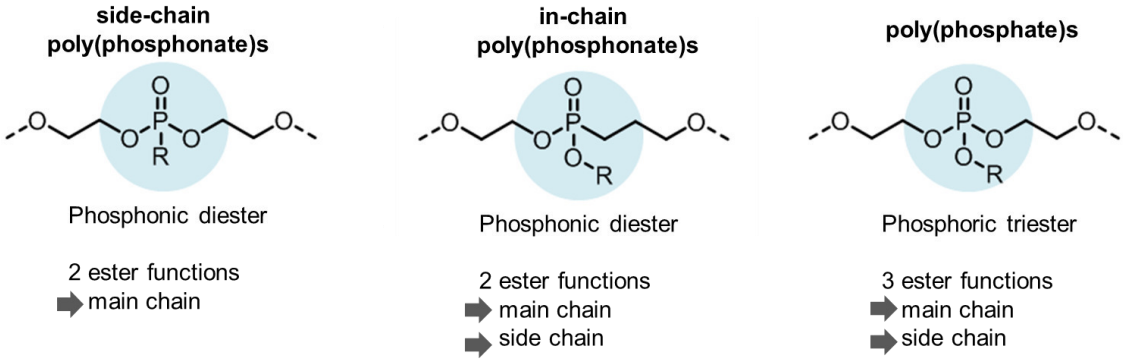

Figure 6.1. Structures of the polyphosphoester classes used for the degradation study (R= methyl or ethyl).

2 Results & Discussion

For studying the influence of different binding patterns on the hydrolytic degradation of PPEs, four water-soluble polymers of the three different PPE-classes were used. To exclude steric effects, polymers with similar pendant chains were used (Figure 6.1). As representative of the side-chain poly(phosphonate)s, poly(ethyl ethylene phosphonate) (PEEPn, Figure 6.2, top left) with an ethyl side chain was used (Figure 6.2, top left). Poly(ethyl propylene phosphonate) (PEPP, Figure 6.2, top right) with an ethoxy side chain was used as representative of the in-chain poly(phosphonate)s. In case of the poly(phosphate)s two different polymers were chosen, i.e. poly(methyl ethylene phosphate) (PMEP, Figure 6.2, bottom left) containing a methoxy side chain and poly(ethyl ethylene phosphate) (PEEP, Figure 6.2, bottom right) containing an ethoxy side-chain.

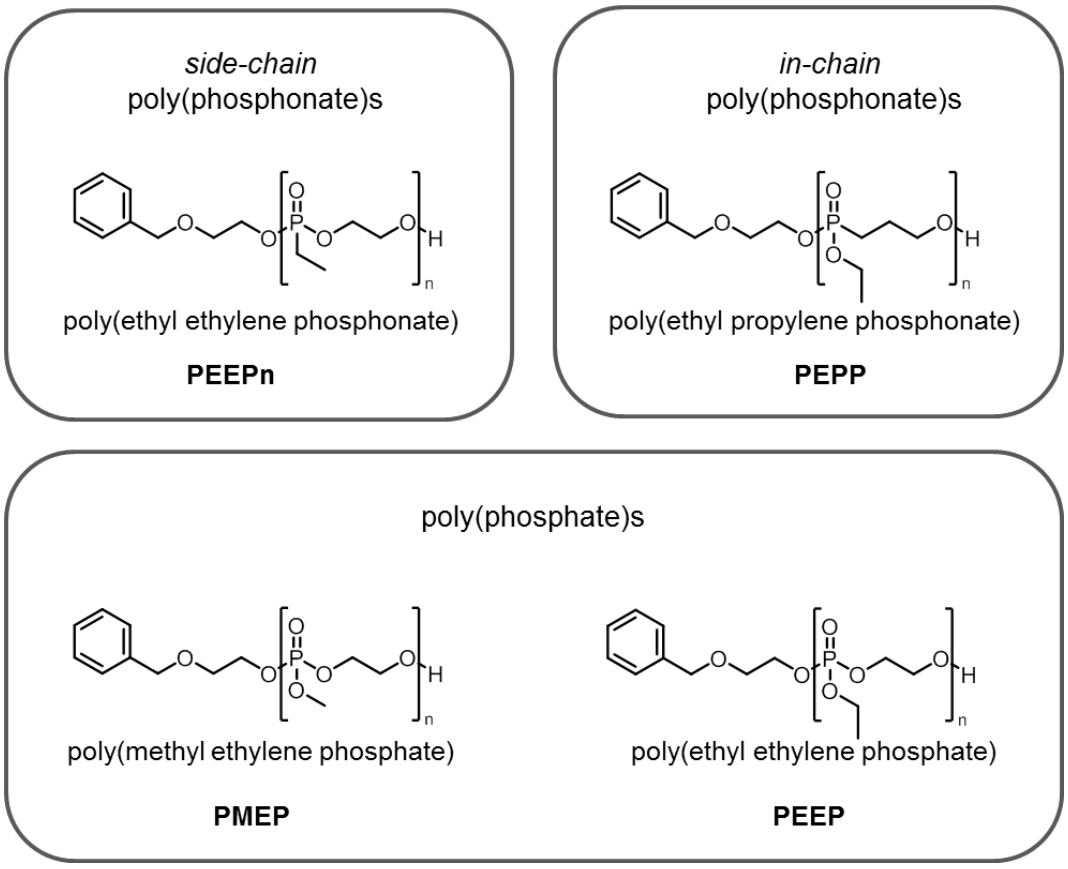

Figure 6.2: Structures of the different poly(phosphoester)s used in the degradation study.

The degradation of the polymers was evaluated at pH 11 and 1. For the degradation at pH 11, a $NaHCO_3$/NaOH buffer was chosen to guarantee a constant basic pH throughout the degradation time. For the degradation at pH 1 a 0.1 M HCl solution was used. The degradation was followed by ^{1}H and ^{31}P NMR spectroscopy, allowing quantification of residual polymer and degradation products respectively as well as the identification of the degradation products. For all considered polymers, scission of the main chain can occur randomly at any ester linkage within the polymer chain or at the last ester linkage at the polymer terminus. Scission of the last ester linkage of the polymer chain would result in the release of one monomeric repeat unit and a polymer with n-1 repeat units. In contrast, scission of a random ester linkage, for example in the middle of a polymer chain, would lead to the formation of two polymeric degradation products.

2.1 Degradation under basic conditions

Side-chain polyphosphonates. As the cleavable phosphonic acid esters are located only in the polymer backbone, the side-chain poly(phosphonate)s represents the easiest degradation pathway of the three PPE classes used in this study. Thus, any cleavage of an ester bond will lead to a scission of the polymer backbone and thus results in a reduction of the molecular weight of at least one repeating unit.

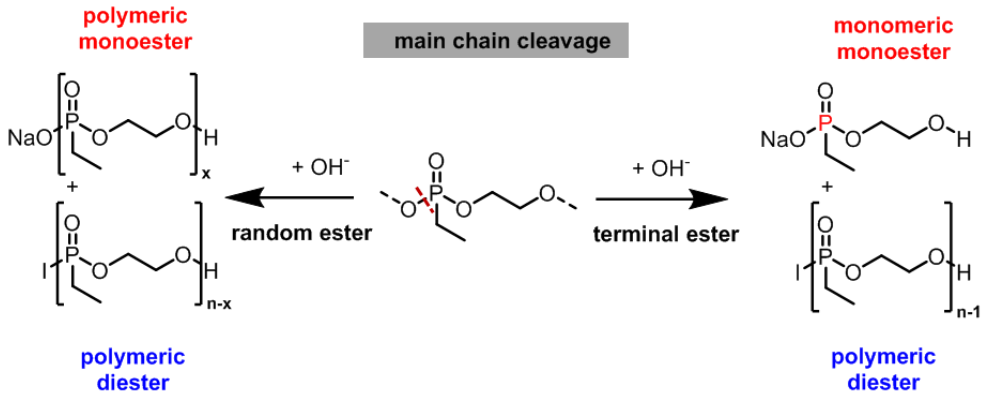

Figure 6.3. Possible degradation products upon ester cleavage in PEEPn.

The degradation was followed continuously over a period of 4.5 h via ^{1}H and ^{31}P NMR spectroscopy. In the ^{31}P NMR spectra, the phosphonic acid diesters were detected at 38.29 ppm, while the degradation product (i.e. a phosphonic acid monoester) appeared at 31.07 ppm (Figure 6.5 (B)). In addition, ^{1}H NMR spectroscopy showed the evolution of signals at 3.80 ppm and 3.64 ppm that could be assigned to the methylene group next to the phosphonic acid diester and the terminal alcohol group, respectively. Furthermore, upon ester cleavage the signals of the

pendant alkyl chain in the monoester are shifted to higher field from 1.86 ppm to 1.49 ppm for the methylene group and from 1.06 ppm to 0.95 ppm for the methyl group. For quantification the signals of the methylene group attached to the diester and monoester respectively were used. As final breakdown product of the cleavage of both ester linkages contained in every repeating unit ethyl phosphonic acid was expected. However, under these conditions no signals in the NMR spectra were observed that can be assigned to formation of ethyl phosphonic acid over the investigated time period. Instead, 2-hydroxyethyl ethylphosphonate was identified as the only degradation product after 4 h. After cleavage of the first ester linkage, the electron density in the degradation product at the phosphorus atom is probably too high for a second nucleophilic attack of an OH^- ion under these conditions.

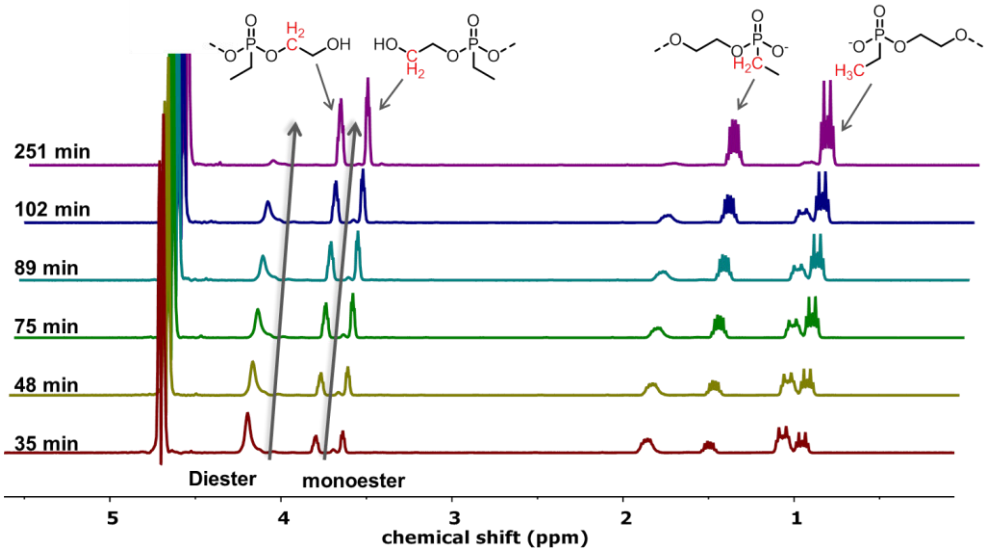

Figure 6.4. ^{1}H NMR spectra (500 MHz, D_2O/H_2O 1:9, 298 K) of the degradation of PEEPn at pH 11 at different time points.

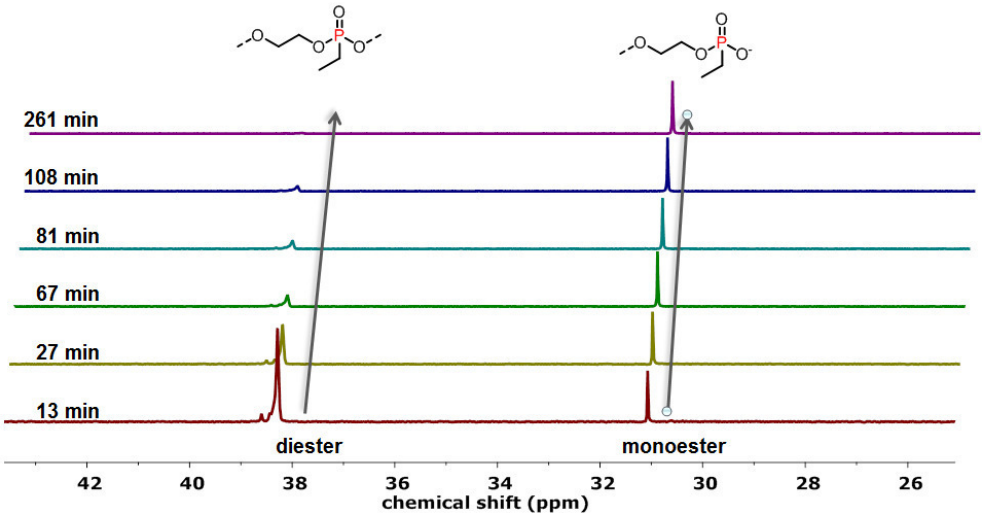

Figure 6.5. ^{31}PNMR spectra (202 MHz, D_2O/H_2O 1:9, 298 K) of the degradation of PEEPn at pH 11 at different time points.

For quantitative determination of the amount of degraded polymer by ^{31}P NMR spectroscopy the signals for the phosphonic diester and monoester were integrated and the sum was normalized to 1. The values of the integrals are plotted as a function of the degradation time (Figure 6.6). For quantitative determination of PEEPn hydrolysis by ^{1}H NMR spectroscopy the signals of the methylene group in the pendant chain attached to a phosphonic diester or monoester were integrated and also plotted as function of the degradation time (Figure 6.6).

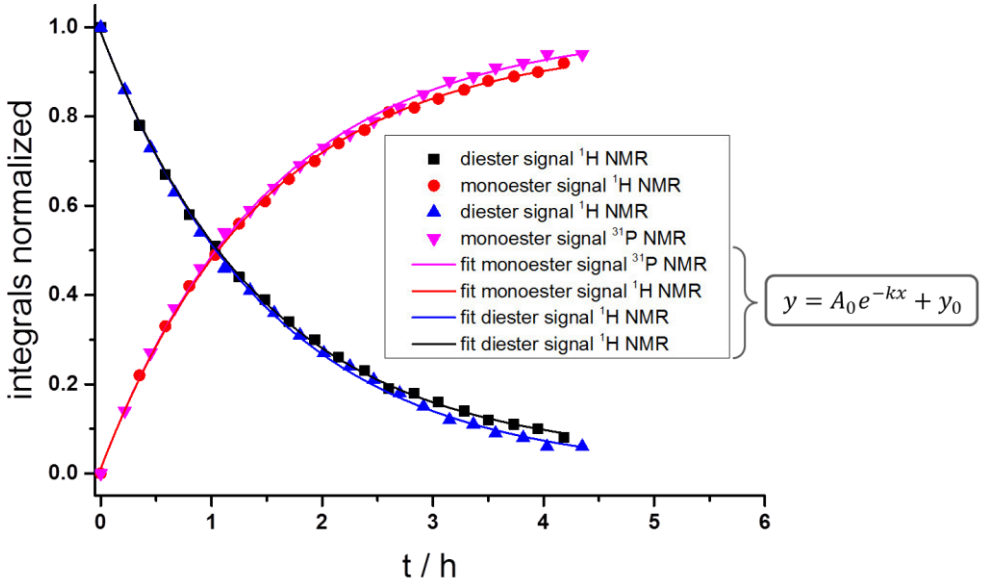

Figure 6.6. Quantitative analysis of the basic hydrolysis of PEEPn at pH 11 (in $NaHCO_3$/NaOH buffer 0.2 mol L^{-1}). Phosphonic diester/monoester signals in the ^1H and ^{31}P NMR spectra were integrated and the sum was normalized to 1. The values for the integrals are plotted.

Quantitative analysis of the ^1H and ^{31}P NMR spectra recorded during the degradation of PEEPn showed a degradation of 95% within 4.5 h at pH 11 with a half life (τ) of ~ 1h. The degradation curves derived from ^1H and ^{31}P NMR spectroscopy proved to be almost identical values, which followed an exponential decay (equation (6.1)). The values for the parameters are summarized in Table 6.1.

$$y = A_0 e^{-kx} + y_0 \qquad \textbf{(6.1)}$$

Table 6.1. Summary of the parameters of the exponential fit curves derived from the monoester and diester signals by ^{1}H and ^{31}P NMR spectroscopy.

	^{31}P NMR		^{1}H NMR	
	diester	**monoester**	**diester**	**monoester**
y_0	0.00239 ± 0.008	0.99761± 0.008	0.03404 ± 0.006	0.96596 ± 0.006
A_1	0.98659± 0.008	-0.98659 ± 0.007	0.95486 ± 0.006	-0.95486 ± 0.006
t_1	1.52178± 0.035	1.52178 ± 0.035	1.47789 ± 0.028	1.47789 ± 0.028
k	0.65713± 0.015	0.65713 ± 0.015	0.67664 ± 0.013	0.67664 ± 0.013
τ	1.05482± 0.024	1.05482 ± 0.024	1.0244 ± 0.019	1.0244 ± 0.019

In-chain poly(phosphonate)s. In contrast to the side-chain poly(phosphonate)s, the in-chain counterparts exhibit only one of the ester linkages in the polymer backbone, while the second one is located in the pendant chain. Therefore, only the cleavage of the ester bond located in the polymer backbone leads to a scission of the polymer chain, with reduction of the molecular weight. The scission of an ester linkage located in the polymer side chain leads to the formation of a polymeric anion accompanied by the release of ethanol. In case of statistical ester cleavage, as reported by Penczek for polyphosphates, a 1:1 ratio of side to main chain scission would be expected (Figure 6.7).

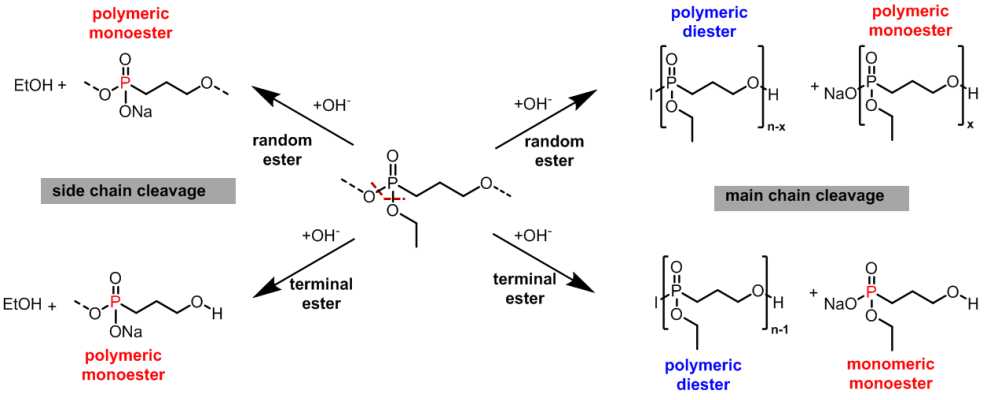

Figure 6.7. Degradation products of in-chain polyphosphonates.

The cleavage of an ester bond located in the polymer backbone leads to the formation of two polymeric breakdown products - one polymeric phosphonic acid diester, carrying a terminal

alcohol group, and the other one a terminal phosphonic monoester group. ^{31}P NMR spectroscopy allows a differentiation between the phosphonic diester (intact polymer) and monoester and therefore a quantification of the ratio of cleaved to intact ester bonds by integration of the phosphonic diester (34.69 ppm, Figure 6.9) and monoester (28.28 ppm, Figure 6.9) signals, respectively. However, a differentiation between phosphonic diesters formed upon side or main chain scission is not possible by the ^{31}P spectra, but can be determined form ^{1}H NMR spectroscopy. The cleavage of the side chain can exclusively be followed by ^{1}H NMR spectroscopy (Figure 6.8) by the evolution of signals that can be assigned to ethanol released within the degradation process. The methyl group in ethanol appears at 1.07 ppm and was used for the quantification of side chain scission. The formation of a terminal phosphonic monoester upon main chain scission shifts the signals of the attached pendant chain to the high field in the ^{1}H NMR spectra. The signal of the methyl group in the pendant chain shifts to 1.14 ppm (from 1.24 ppm) upon ester cleavage and was used for the quantification of the amount of cleaved main chain. By comparing the integrals of the three different methyl groups (pendant chain diester : pendant chain monoester : ethanol) the ratio of cleaved to intact ester can be determined and allows a differentiation between side and main chain scission.

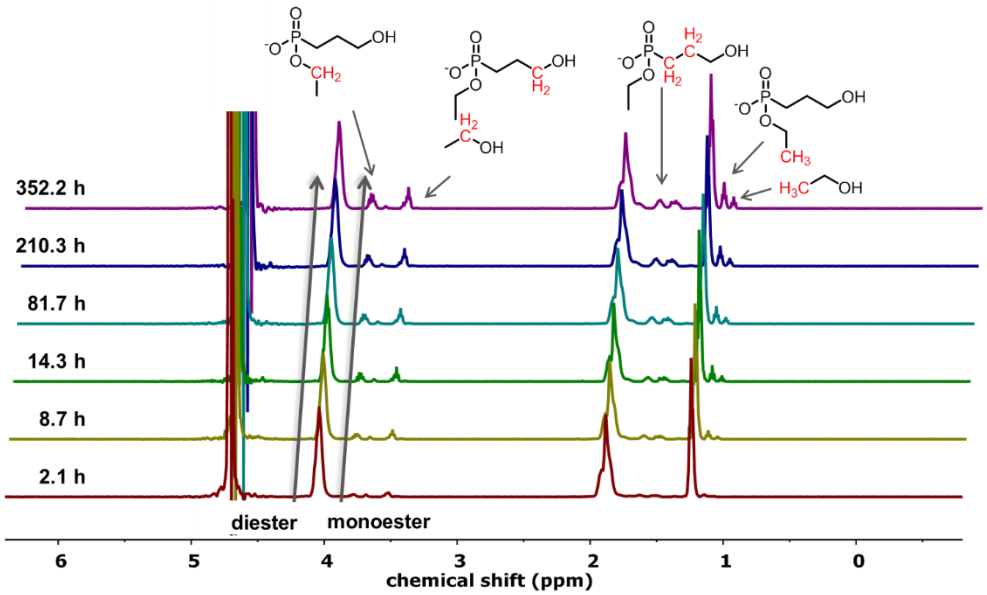

Figure 6.8. ^{1}H NMR spectra (500 MHz, D_2O/H_2O 1:9, 298 K) of the degradation of PEPP at pH 11 at different time points.

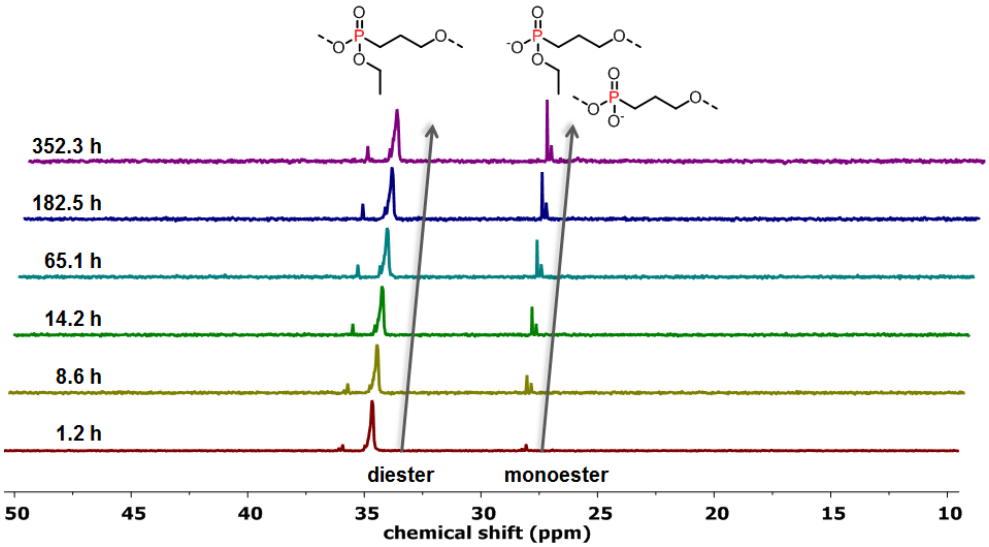

Figure 6.9. ^{31}PNMR spectra (202 MHz, D_2O/H_2O 1:9, 298 K) of the degradation of PEPP at pH 11 at different time points.

Interestingly, evaluation of the ^{1}H-^{31}P correlation spectra of the degradation of PEPP (Figure 6.10) showed that the methylene signal adjacent to the terminal alcohol group correlates

exclusively with the monoester. In case of a random ester cleavage leading to the formation of polymeric degradation products, a correlation of the methylene group adjacent to the terminal alcohol with the diester is expected. Thus, the missing correlation indicates that mainly the monomeric degradation product was built. The formation of mainly monomeric product is further indicated by DOSY NMR (Figure 6.25) spectra, showing beside the signal of the polymer only one further signal with a significantly lower diffusion coefficient, that can be attributed to a low molecular weight species.

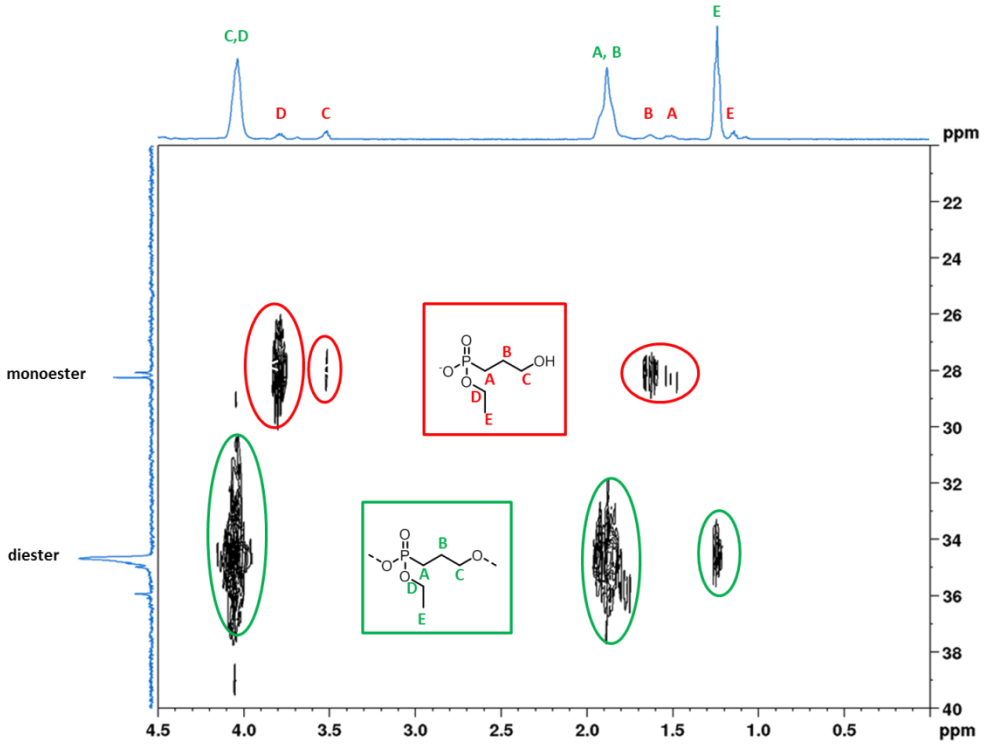

Figure 6.10. ^{1}H-^{31}P HMBC NMR spectrum (500, 202 MHz, H_2O/D_2O (9:1), 298 K) of the degradation products of PEPP. The spectrum shows a correlation of the methylene group (C) with the monoester indicating the formation of mainly monomeric degradation product.

For quantitative determination of the amount of degraded polymer from the ^{31}P NMR spectra, the signals for the phosphonic diester and monoester were integrated and the sum was normalized to 1. The values of the integrals are plotted as a function of the degradation time (Figure 6.7). As mentioned above, ^{1}H NMR spectroscopy can be further used for the differentiation between side and main chain cleavage. Scission of the pendant chain leads to the release of ethanol. The signal of the methyl group in ethanol was used for the quantification of side chain scission. The methyl group in the pendant chain attached to the phosphonic diester was used for the quantification of main chain scission and the methyl group in the pendant chain

of intact phosphonic diester was used for quantification of residual polymer. The signals of the three different methyl groups were integrated, the sum was normalized to 1 and the integral values were also plotted as function of the degradation time (Figure 6.7). The sum of main and side chain scission (derived from ^{1}H NMR spectra) can be summarized and represents the amount of built phosphonic diester.

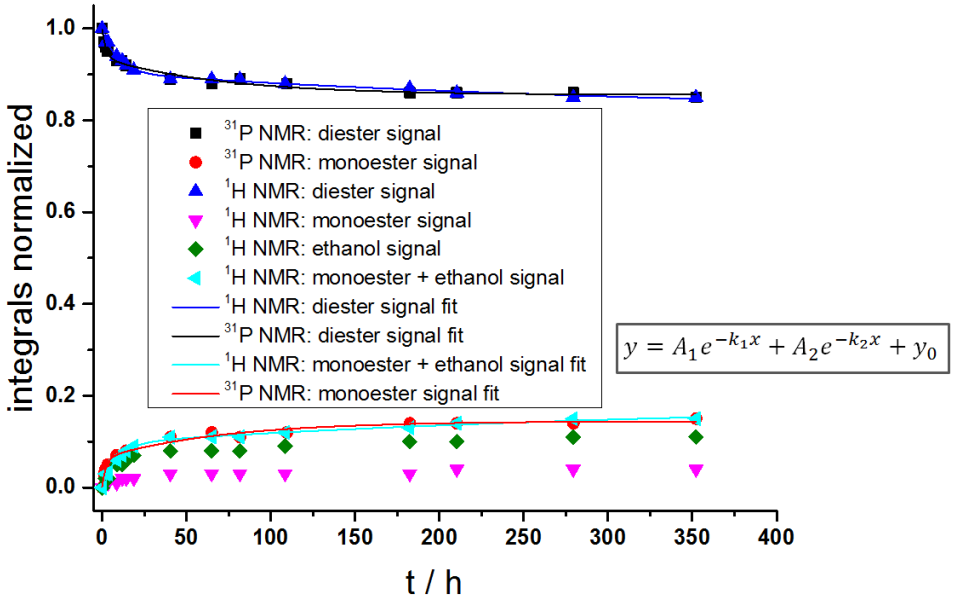

Figure 6.11. Quantitative analysis of the basic hydrolysis of PEPP at pH 11 (in $NaHCO_3$/NaOH buffer 0.2 mol L^{-1}). The degradation curve derived from ^{31}P NMR spectroscopy was obtained by integration of the phosphonic diester and monoester signal and normalizing the sum to 1. The degradation curve derived from ^{1}H NMR spectroscopy was obtained by integration of the methyl group signals of the different degradation products and the sum was normalized to 1. The values for the integrals are plotted as a function of the degradation time.

Quantitative evaluation of the NMR spectra over a period of 15 days (352 h) led to almost identical results for ^{1}H and ^{31}P NMR spectroscopy. For the in-chain polyphosphonate, PEPP, a two stage degradation pathway was observed, which fits to a biexponential decay (equation (6.2)) with an initial rapid degradation and a second phase of significantly slower degradation.

$$y = A_1 e^{-k_1 x} + A_2 e^{-k_2 x} + y_0 \quad \textbf{(6.2)}$$

$$k = \frac{1}{t} \quad \textbf{(6.3)}$$

Table 6.2. Summary of the parameters of the biexponential fit curves derived from the monoester and diester signals by ^{1}H and ^{31}P NMR spectroscopy.

	^{31}P NMR		^{1}H NMR	
	diester	**monoester**	**diester**	**monoester**
y_0	0.855 ± 0.005	0.145 ± 0.005	0.813 ± 0.047	0.187 ± 0.047
A_1	0.063 ± 0.008	-0.063 ± 0.008	0.093 ± 0.007	-0.093 ± 0.007
t_1	2.384 ± 0.664	2.384 ± 0.664	9.449 ± 1.394	9.449 ± 1.394
k_1	0.419 ± 0.117	0.419 ± 0.117	0.106 ± 0.016	0.106 ± 0.016
A_2	0.081 ± 0.006	-0.081 ± 0.006	0.090 ± 0.042	-0.090 ± 0.042
t_2	71.166 ± 15.482	71.166 ± 15.482	354.622± 309.396	354.622± 309.396
k_2	0.014 ± 0.003	0.014 ± 0.003	0.003 ± 0.002	0.003 ± 0.002
τ_1	1.653 ± 0.005	1.653 ± 0.005	6.549 ± 0.966	6.549 ± 0.966
τ_2	49.328 ± 10.731	49.328 ± 10.731	245.805 ± 214.457	245.805 ± 214.457

The first rapid phase led to a degradation of ca. 9% within 19 h. Subsequently the degradation rate decreases dramatically and reaches a maximum degradation of 15% within the following 14 days. Furthermore, evaluation of the amount of cleaved side chain showed a significantly lower amount of side chain scission of maximum 4% within the considered 15 days compared to 11% main chain scission. Based on a statistical degradation the same extent of side and main chain scission was expected. The significantly higher amount of main chain scission indicates that hydrolysis of the differently located ester bonds does not occurs statistically under these conditions (pH 11, $NaHCO_3$/NaOH buffer, 0.2 mol L^{-1}, 21°C).

Poly(phosphate)s. In case of the poly(phosphate)s, the degradation behavior of two different polymers was investigated (PMEP and PEEP). In contrast to the poly(phosphonate)s, the phosphorus atoms in poly(phosphate)s are surrounded by three ester linkages, i.e. two in the polymer backbone and the third in the pendant chain. Upon scission of the main-chain, two polymeric breakdown products are formed one containing an alcohol as terminal group and the other one containing a phosphoric acid diester. Cleavage of the last ester linkage in the polymer chain leads to the formation of a monomeric breakdown product, where the terminal alcohol is

attached to a diester and a polymer with n-1 repeat units. Scission of the side chain leads to the formation of a polymeric phosphoric diester and the release of the corresponding alcohol (Figure 6.12).

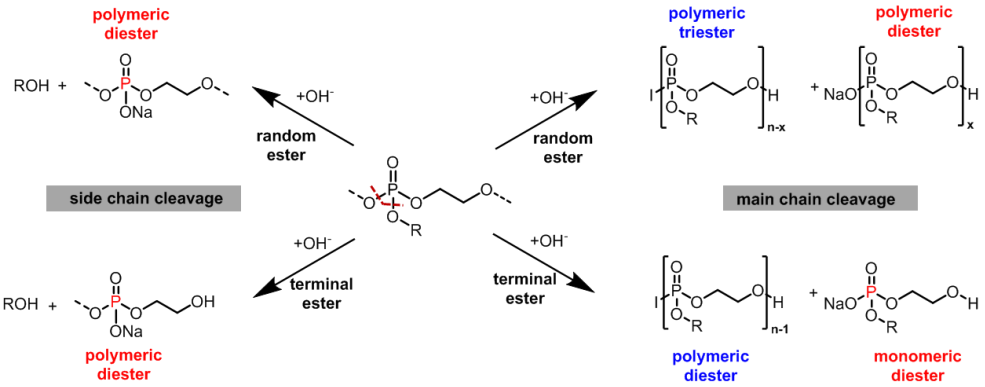

Figure 6.12. Degradation products upon hydrolysis of ester linkages located in the polymer backbone or side chain.

PMEP. In case of PMEP, the evolution of methanol signals in the ^{1}H NMR (Figure 6.13) indicated the scission of the side chain. Upon main chain scission a terminal alcohol group is formed, that can be identified by the signals of the adjacent methylene group appearing at 3.67 ppm and the methoxy side chain attached to the phosphoric diester shifting to 3.50 ppm. For the quantitative evaluation of the degradation the methyl signal of methanol (OH-C$\boldsymbol{H_3}$ 3.34 ppm) and the side chain attached to the phosphoric diester was used. In the ^{31}P NMR spectra the evolving signal at 1.92 ppm (Figure 6.14) indicated the formation of phosphoric diester either by side or main chain scission and was compared to the triester signal for quantification.

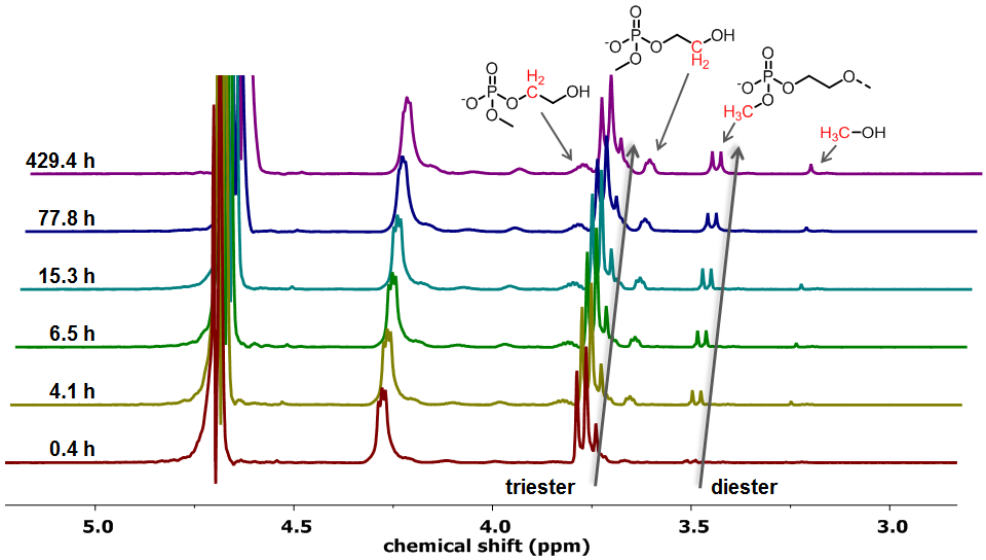

Figure 6.13. ^{1}H NMR spectra (500 MHz, D_2O/H_2O 1:9, 298 K) of the degradation of PMEP at pH 11 at different time points.

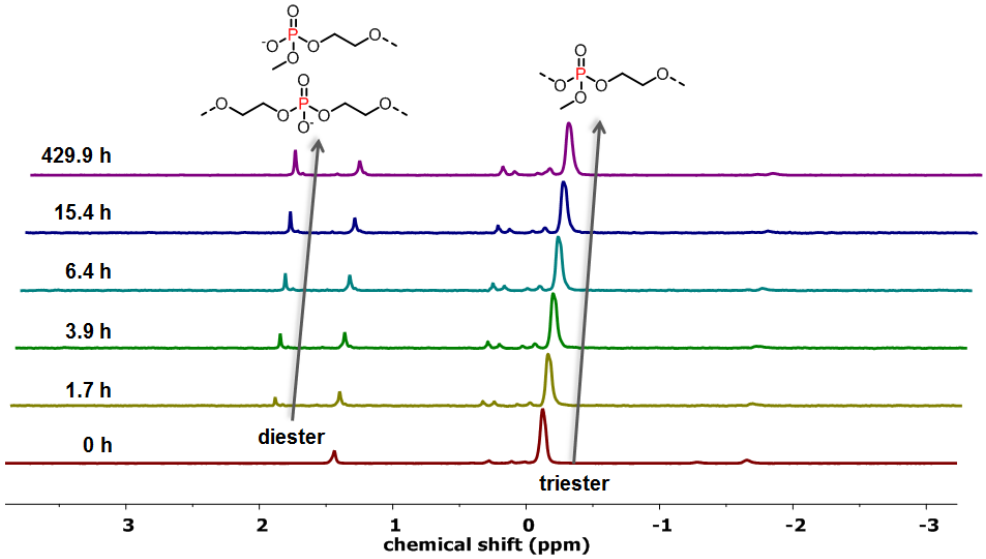

Figure 6.14. ^{31}PNMR spectra (500 MHz, D_2O/H_2O 1:9, 298 K) of the degradation of PMEP at pH 11 at different time points.

Quantitative evaluation of the NMR spectra recorded over a period of 20.5 days showed a similar degradation progress as observed for the degradation for PEPP with following a double exponential decay (Figure 6.15). Within the first 15 h 10% of ester linkages were cleaved that rose to 13% until day 20. Furthermore, only slight evolution of methanol of maximum 2% within 20 days was observed indicating only small extent of side chain scission. With maximum 11% of main chain scission this is the predominant degradation pathway in PMEP. However,

after 44 h the amount of cleaved ester bonds almost stagnated though control of the pH still showed basic conditions.

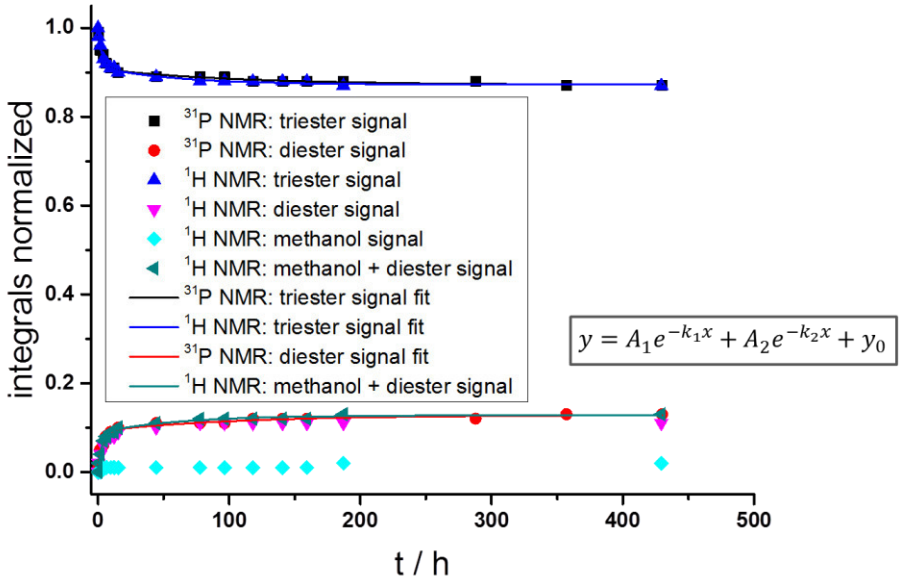

Figure 6.15. Quantitative analysis of the basic hydrolysis of PMEP at pH 11(in $NaHCO_3$/NaOH buffer 0.2 mol L^{-1}). The degradation curve derived from ^{31}P NMR spectroscopy was obtained by integration of the phosphoric triester and diester signal and normalizing the sum to 1. The degradation curve derived from ^{1}H NMR spectroscopy was obtained by integration of the methyl group signals of the different degradation products and the sum was normalized to 1. The values for the integrals are plotted as a function of the degradation time.

Table 6.3. Summary of the parameters of the biexponential fit curves derived from the monoester and diester signals by ^{1}H and ^{31}P NMR spectroscopy for the degradation of PMEP.

	^{31}P NMR		^{1}H NMR	
	triester	**diester**	**triester**	**diester**
y_0	0.872 ± 0.003	0.128 ± 0.003	0.872 ± 0.003	0.128 ± 0.003
A_1	0.084 ± 0.005	-0.084 ± 0.005	0.084 ± 0.004	-0.084 ± 0.004
t_1	3.486 ± 0.543	3.486 ± 0.543	3.204 ± 0.389	3.204 ± 0.389
k_1	0.287 ± 0.045	0.287 ± 0.045	0.312 ± 0.038	0.312 ± 0.038
A_2	0.036 ± 0.004	0.036 ± 0.004	0.039 ± 0.004	-0.039 ± 0.004

t_2	104.058 ± 33.043	104.058 ± 33.043	60.914 ± 17.440	60.914 ± 17.440
k_2	0.010 ± 0.003	0.010 ± 0.003	0.016 ± 0.005	0.016 ± 0.005
τ_1	2.416 ± 0.376	2.416 ± 0.376	2.221 ± 0.269	2.221 ± 0.269
τ_2	72.127 ± 22.904	72.127 ± 22.904	42.222± 12.089	42.222± 12.089

PEEP. Analogously to the degradation of PEPP or PMEP, the evolution of signals in the ^{1}H NMR spectra (Figure 6.16) that can be assigned to released ethanol indicated the scission of the side chain (1.06 ppm HO-CH_2-C***H*****$_3$** and 3.54 ppm HO-C***H*****$_2$**-CH_3). The amount of cleaved side chain during the degradation of PEEP was evaluated by integration of the methyl group at 1.06 ppm. The amount of main chain scission was evaluated by the methyl signal (1.16 ppm) of the pendant chain attached to the built phosphoric diester upon main chain cleavage. During the degradation process of PEEP a second signal appears in the ^{31}P NMR spectra (Figure 6.17) at 0.79 ppm that can be attributed to the formation of phosphoric diester. By integration of both signals the ratio of intact triester to diester was determined.

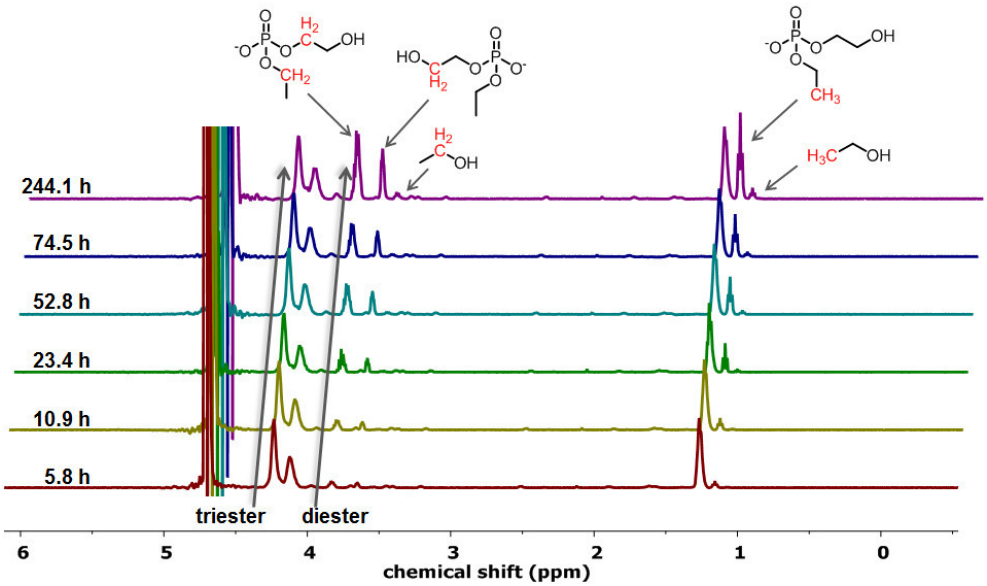

Figure 6.16. ^{1}H NMR spectra (500 MHz, D_2O/H_2O 1:9, 298 K) of the degradation of PEEP at pH 11 at different time points.

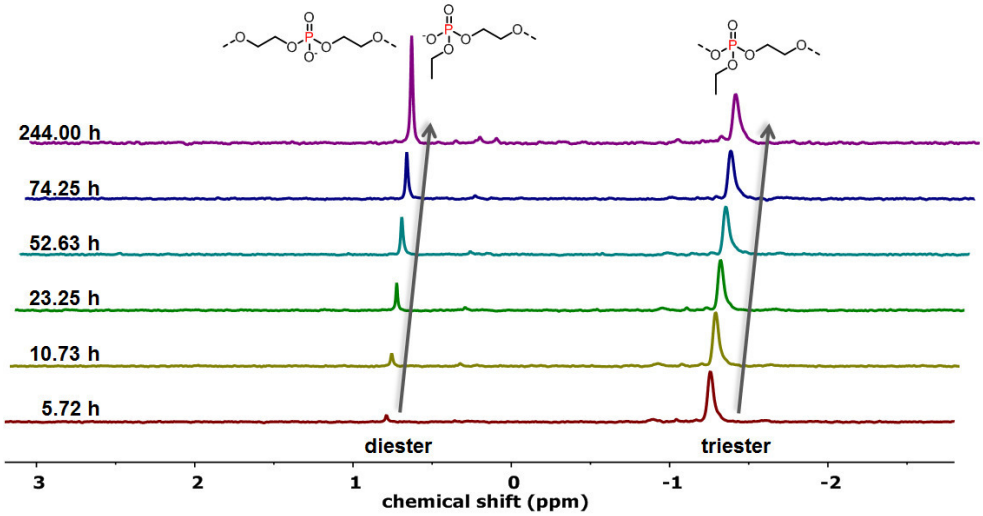

Figure 6.17. ^{31}PNMR spectra (500 MHz, D_2O/H_2O 1:9, 298 K) of the degradation of PEEP at pH 11 at different time points.

The degradation of PEEP was observed over a period of 13 days and was found to follow the same biphasic slope like PMEP and PEPP with an initial rapid degradation which slowed down distinctly in the second phase. However, in contrast to PMEP with an almost stagnating degradation after the initial phase the degradation of PEEP proceeds clearly visible in the second phase. Furthermore, quantitative analysis of the ^{1}H NMR spectra showed a maximum side chain cleavage of 5% after 13 days and a maximum main chain scission of 42% in the same time, indicating again a preference for main chain ester cleavage. As seen for the degradation of PEPP and PMEP, evaluation of the ^{1}H-^{31}P correlation spectrum (Figure 6.23) indicated also for the degradation of PEEP the formation of monomeric ethyl (2-hydroxyethyl) phosphate as main degradation product.

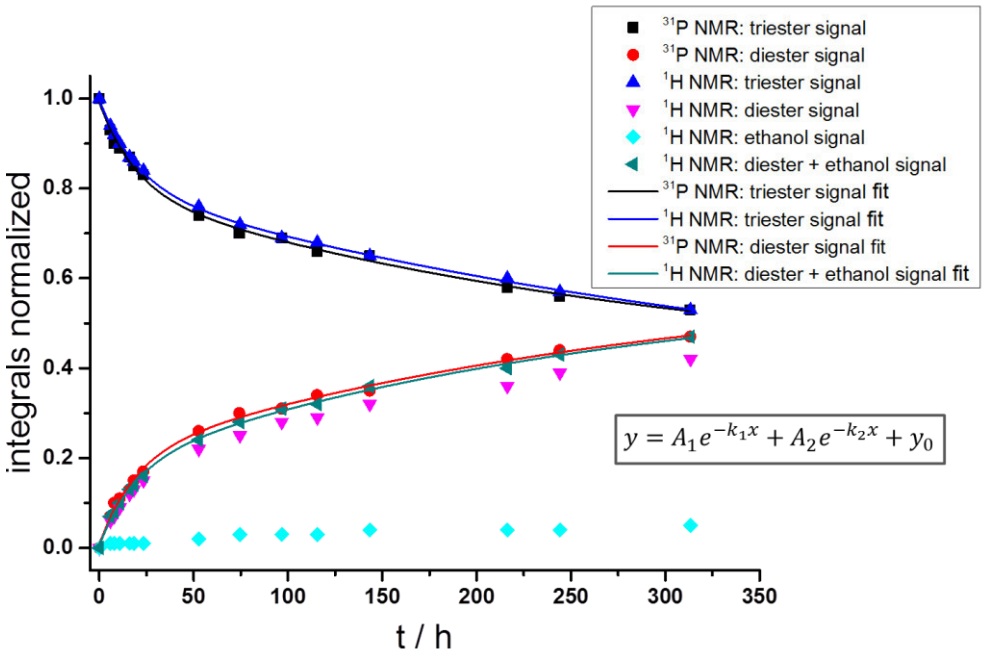

Figure 6.18. Quantitative analysis of the basic hydrolysis of PEEP at pH 11(in $NaHCO_3$/NaOH buffer 0.2 mol L^{-1}). The degradation curve derived from ^{31}P NMR spectroscopy was obtained by integration of the phosphoric triester and diester signal and normalizing the sum to 1. The degradation curve derived from ^{1}H NMR spectroscopy was obtained by integration of the methyl group signals of the different degradation products and the sum was normalized to 1. The values for the integrals are plotted as a function of the degradation time.

Table 6.4. Summary of the parameters of the biexponential fit curves derived from the monoester and diester signals by ^{1}H and ^{31}P NMR spectroscopy for the degradation of PEEP.

	^{31}P NMR		^{1}H NMR	
	triester	**diester**	**triester**	**diester**
y_0	0.384 ± 0.120	0.616 ± 0.120	0.3120 ± 0.106	0.688 ± 0.106
A_1	0.193 ± 0.030	-0.193 ± 0.030	0.193 ± 0.015	-0.193 ± 0.015
t_1	18.785 ± 3.764	18.785 ± 3.764	20.243 ± 2.014	20.243 ± 2.014
k_1	0.053 ± 0.011	0.053 ± 0.011	0.054 ± 0.008	0.054 ± 0.008
A_2	0.415 ± 0.093	-0.415 ± 0.093	0.492 ± 0.052	-0.492 ± 0.052
t_2	294.135± 160.242	294.135 ± 160.242	386.861 ± 136.461	386.861 ± 136.461

k_2	0.003 ± 0.002	0.003 ± 0.002	0.003 ± 0.001	0.003 ± 0.001
τ_1	13.021 ± 2.610	13.021 ± 2.610	14.031 ± 1.396	14.031 ± 1.396
τ_2	203.877 ± 111.071	203.877 ± 111.071	245.805 ± 214.457	245.805 ± 214.457

As found for the degradation of PEPP, evaluation of the ^{1}H -^{31}P correlation spectra of the degradation of PEEP (Figure 6.23) and PMEP (Figure 6.29) showed that the methylene signals adjacent to the terminal alcohol group correlates exclusively with the diester. This observation indicated the presence of mainly monomeric degradation products. The presence of predominantly monomeric degradation products was further confirmed by DOSY NMR spectroscopy. DOSY NMRs recorded within the degradation of PMEP (Figure 6.31) and PEEP (Figure 6.22) showed significantly lower diffusion coefficients for the degradation product indicating the presence of only low molecular weight degradation products. Species with diffusion coefficients between the initial polymer and the "monomer" were not observed. Furthermore, the correlation spectra showed no correlation of the polymeric triester with the methylene group adjacent to the terminal alcohol in the ^{1}H NMR spectrum at all. The identification of almost exclusively monomeric degradation product indicated that degradation occurred from the alcohol-terminus. Furthermore, ^{1}H-^{31}P correlation spectra showed no correlation of the terminal alcohol group with the polymer. The missing correlation might indicate, that the terminal hydroxyl group did not exist as hydroxyl group but reacts with a phosphorus atom within the polymer chain leading to cyclic structures. Figure 6.19 gives an overview over possible and identified degradation products.

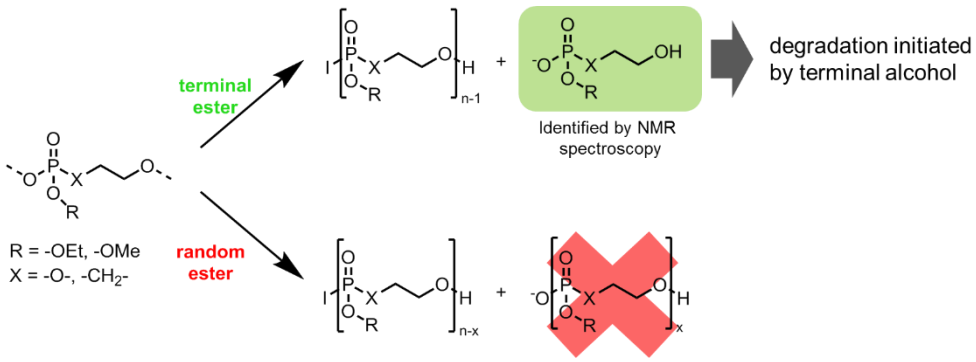

Figure 6.19. Overview over possible and identified degradation products for the degradation of poly(phosphate)s and in-chain poly(phosphonate)s.

The formation of predominant monomeric degradation products and the missing correlation of the terminal hydroxyl group with the polymer signal indicate a degradation of the poly(phosphoester)s by alkaline catalyzed intramolecular transesterfication ('backbiting') of the terminal alcohol group and elimination of one repeat unit similar to the hydrolysis mechanism proposed for PLA.[12-14] Upon backbiting of the terminal alcohol group a trigonal bipyramidal coordinated phosphorus atom is proposed where the five-membered cycle can be either located in the equatorial or equatorial/axial position (Figure 6.20). Within the degradation of the poly(phosphate)s, (PMEP and PEEP) a small signal at 18 ppm (Figure 6.31) was observed in both cases. Furthermore, the ^{1}H NMR spectra recorded within the degradation process of both polymers showed a characteristic doublet at 4.25 ppm (Figure 6.30). ^{1}H-^{31}P correlation spectrum of the degradation of PMEP (Figure 6.32) showed a correlation of both signals. Most likely, these signals can be asigned to the five-fold coordinated, cyclic phosphorus at the end of the polymer chain formed upon backbiting of the terminal alcohol on the adjacent phosphorus atom where the doublet can be attributed to the methylene groups located within the ring structure.[15] This assumption was further confirmed by ^{1}H NMR predictions conducted with ChemDraw Professional 16.0 software. The signal, at 18 ppm observed in the ^{31}P NMR spectra is in the same region like the signals of the five-membered cyclic phosphate monomers and therefore an attribution of this signal to the five-fold coordinated cyclic phosphorus atom is most likely.

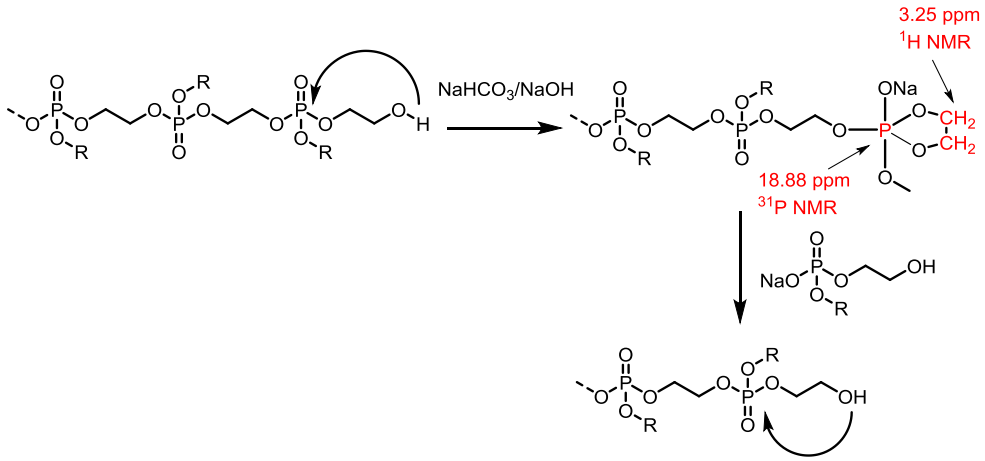

Figure 6.20. Proposed mechanism for the degradation of polyphosphoesters by backbiting of the terminal hydroxyl group on the neighboring phosphorus atom.

Thus, degradation of poly(phosphate)s initiated by the terminal alcohol group is most likely under the considered conditions. For the in-chain polyphosphonate, correlation spectra also

indicate an analogous degradation mechanism as proposed for the poly(phosphate)s though a five-fold coordinated phosphorus was not identified by NMR spectroscopy. However, the degradation of the side-chain polyphosphonate, PEEPn, was exclusively followed by ^{1}H and ^{31}P NMR spectroscopy and therefore prediction of the degradation mechanism is not possible.

Although similar observations were made for the considered polymers concerning their degradation products, distinct different degradation profiles were observed. In hydrolytic degradation under basic conditions, there are a number of parameters that affect the rates of degradation. OH^- ions are the agents that cause or catalyze hydrolysis. Therefore, the accessibility of the cleavable sites in the polymer by the OH^--ions is a crucial parameter. Upon molecular solution degradation is controlled by reactivity.[16] In contrast, in the presence of polymer aggregates, the accessibility of the polymer by the hydrolizing agent is a key parameter.[17] Cleavable sites located in in the center of the aggregate can be inaccessible or at least harder to reach for OH^--ions. Thus, a significantly slower degradation is supposed in presence of aggregates, where degradation is supposed to occur predominantly from the surface of the aggregate (similar to surface erosion). Cleavable polymer sites on the aggregate surface are easily accessible while for degradation of the inner part penetration by the hydrolysis agents is required.[18] Therefore, the penetration rate that depends among others on the structure of the aggregate is supposed to have a pronounced effect on the degradation kinetics.[7, 19] The significantly different degradation behavior of the analyzed polymers indicated that more aspects than simply the binding pattern around the phosphorus atom have to be taken into account. Especially, the almost stagnating degradation of PEPP and PMEP after an initial rapid degradation phase might point to the formation of aggregates in aqueous media where the easily accessible ester linkages on the aggregate surface are rapidly cleaved while the inner ester linkages are hard to reach and are therefore only slowly cleaved. A further indication for the influence of aggregate formation on the degradation behavior is the structure of the fit curve. For PMEP, PEEP and PEPP the experimental data fit a biexponential function indicating the superposition of two separate degradation processes – one with fast kinetics and the second one with distinctly slower kinetics. This points out to a superposition of different mechanisms occurring during the degradation of the polymers, besides the differences of main- and side-chain hydrolysis. This might be attributed to the cleavage of ester linkages located on the aggregate surface and cleavage of internal ester linkages which is associated with the penetrativeness of the polymer aggregate. However, to evaluate if aggregation has to be taken

into account for the degradation behavior of the examined polymers, dynamic light scattering was measured for the polymers dissolved in water and the results are presented in Table 6.5.

Table 6.5. Dynamic light scattering results for the polymers dissolved in MilliQ water.

polymer	R_{h1} / nm	R_{h2} / nm
PEEPn	2	-
PEEP	2	410
PMEP	1.3	240
PEPP	-	190

Indeed, dynamic light scattering measurements of the polymers used in this degradation study showed significantly different results. For PEEPn up to high concentration of 10 mg mL^{-1} exclusively small structures with hydrodynamic radii of 2 nm were found indicating that the polymers are unimolecularly dissolved. PEEPn was also the polymer (from the herein investigated PPEs) with the fastest degradation, following a monoexponential decay. In contrast, for PEPP exclusively large structures with hydrodynamic radii of 190 nm were detected by DLS after "solution" in water. The formation of aggregates is consistent with its degradation behavior – during the initial rapid degradation phase the readily accessible ester linkages on the aggregate surface are cleaved. When the outer ester linkages are cleaved, the degradation slows down due to the limited accessibility of the inner ester linkages. For PMEP aggregates with similar size ($R_{h,agg}$ = 240nm) were found matching the resembling degradation kinetics of PEPP and PMEP. However, for PEEP significantly larger aggregates were found with R_h = 410 nm compared to the ones found for PMEP and PEPP. Furthermore, the degradation behavior of PMEP and PEEP, though belonging to the same PPE-class, differed significantly. For PEEP degradation proceeded faster compared to PMEP, in spite of its higher hydrophilicity. This difference might be attributed to the larger size of the aggregates allowing a better penetration of the OH^--ions and thus leading to a constantly faster cleavage of the inner ester linkages.[7]

Degradation under acidic conditions

For the degradation under acidic conditions the polymers were dissolved in 0.1 M HCl solution at pH 1 and the progress of degradation was followed by ^1H and ^{31}P NMR spectroscopy. Within

the considered time frame of 10 days for all polymers no hydrolysis, which is in agreement with the degradation studies conducted by Penczek *et al.* reporting a significantly slower degradation profile for PMEP under acidic conditions compared to alkaline hydrolysis. Thus, to evaluate the degradation behavior of PPEs under acidic conditions longterm studies need to be conducted.

3 Conclusion

All observed PPEs degraded under the investigated basic conditions, while they remained stable under acidic conditions during the time of the experiment. However, distinct differences concerning the degradation time and overall amount of cleaved ester bonds were found for all PPEs. The easiest degradation pathway was expected for the side-chain polyphosphonate, PEEPn, due to the location of the ester linkages within the polymer backbone, which was confirmed by the experimental results. 95% PEEPn were degraded within 4.5 hours and the degradation curve determined by ^{1}H as well as by ^{31}P NMR spectroscopy showed monoexponential decay. ^{1}H NMR spectroscopy furthermore showed the formation 2-hydroxyethyl ethylphosphonate as single degradation product indicating that at each repeating unit only one ester linkage is cleaved. However, as the only polymer used in this degradation study PEEPn showed no aggregation in MilliQ water. For the poly(phosphate)s a significant slower degradation was observed when compared to PEEPn. The degradation curves obtained from quantitative analysis of the NMRs showed, in contrast to PEEPn, slopes which fit biexponential decay. For both polymers exponential degradation was observed with an initial rapid degradation which slows down distinctly in the second phase. Though degradation of PEEP slowed down in the second phase degradation proceeded further. In contrast, for PMEP degradation almost stagnated after 44 h and showed after 20 days an overall degradation of 13%. Similar results were found for the main chain polyphosphonate PEPP which showed a degradation of 9% in the initial phase and an overall degradation of 15% after 15 days. Evaluation of the NMR spectra recorded within the degradation process indicated for PEPP, PMEP, and PEEP degradation by alkaline catalyzed intramolecular transesterification initiated by the terminal hydroxyl group. Furthermore, the significantly different degradation of PEEP, PMEP and PEPP can probably be attributed to the formation of aggregates upon dissolution in aqueous medium. In the aggregates the concentration of catalyzing OH^- -ion is lower compared to the concentration in the surrounding medium leading to a slower degradation of the polymers located within the aggregate compared to the polymers located in the outer sphere of the aggregates. Thus, the different OH^- -ion concentrations lead to different degradation rates

resulting in a biexponential degradation curves for the aggregating poly(phosphoester)s compared to the monoexponential degradation curve of the molecular dissolved PEEPn.
In conclusion, all PPEs can be degraded under basic conditions, but further *in vivo* studies are essential to assess their potential for future bioapplications, as the presence of enzymes and other additives under *in vivo* conditions will govern the degradation behavior.

4 Outlook

The conducted studies on the degradation of different poly(phosphoester)s led two major findings. Firstly, all polymers were considered to be water-soluble and had been previously investiagtad for aqueous applications (PEEP and PMEP). PEEPn and PEPP are novel polymers prepared recently in our group. However, their hydrophilicity differs to a certain degree, which leads to altered solubility. The aggregation behavior of the PPEs in water strongly influences their degradation kinetics and secondly, degradation of PEPP, PEEP and PMEP followed mainly an intramolecular transesterification ('backbiting'), mainly from the terminal hydroxyl group.
However, further studies need to be conducted to finally proof these observations from NMR and DLS. In order to prove that the presence of aggregates strongly influences the degradation kinetics, further studies need to be conducted in the absence of aggregates. Thus, to guarantee the absence of aggregates, concentration dependent DLS measurements need to be conducted to evaluate a critical aggregate concentration (CAC) and further degradation studies thus need to be conducted below the CAC. If the presence of aggregates influences the degradation rate, below the CAC a faster degradation rate is expected similar to the degradation of PEEPn. Furthermore, in order to prove that degradation occurred mainly via intramolecular transesterification (backbiting) initiated by the terminal hydroxyl group, the terminal hydroxyl group need to be blocked (Figure 6.21). Degradation studies need to be conducted with polymers bearing a free terminal hydroxyl group and with polymers bearing a blocked one. If the polymer with the blocked hydroxyl group shows slower degradation, the critical influence of the terminal hydroxyl group is proven. Similar, experiments have been conducted for PLA and showed significantly attenuated degradation rates compared to polymers with a terminal hydroxyl group.[14]

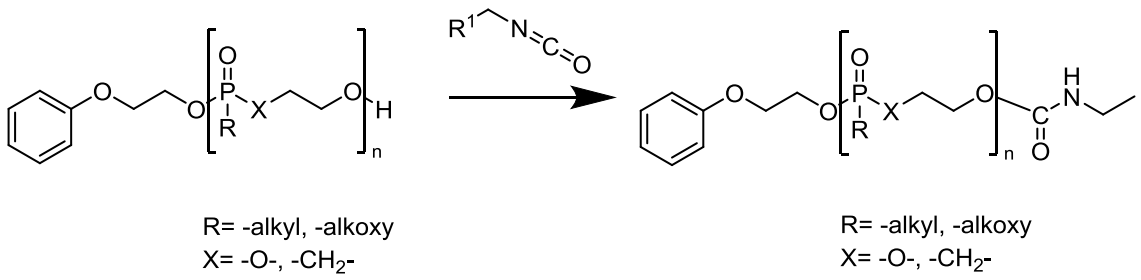

Figure 6.21. Blocking of the terminal hydroxyl group by treatment with isocyanates.

So far, degradation by backbiting of the terminal hydroxyl group was only indicated for the degradation of poly(phosphate)s and in-chain poly(phosphonate)s. The degradation of PEEPn was followed exclusively by ^{1}H and ^{31}P NMR spectroscopy, which allowed no evaluation of the degradation mechanism. In order to gain detailed insight into the degradation mechanism of PEEPn, correlation spectra need to be recorded throughout the degradation process.

5 Experimental

NMR. ^{1}H and ^{31}P NMR spectra were recorded using a Bruker Avance 300 and a Bruker Avance III 500. All spectra were referenced internally to residual proton signals of the deuterated solvent. 1D spectra were analyzed using MestReNova and for the alnalysis of the 2D spectra topspin was used.

For the diffusion measurements (DOSY)[20] a 5 mm triple resonance BBFO $^{1}H/X$ probe equipped with a z-gradient on the 500 MHz Bruker AVANCE III system was used. For the diffusion measurements a 2D sequence (DOSY, dstebpgp3s) with a stimulated echo was used.[21] The temperature was kept at 298.3 K and regulated by a standard ^{1}H methanol NMR sample using the topspin 3.1 software (Bruker). The control of the temperature was realized with a VTU (variable temperature unit) and an accuracy of +/- 0,1K. The diffusion time was optimised at 70 ms and the gradient length to 1.4 ms. The relaxation delay between scans was 2 s. The gradient strength was calibrated by analysis of a sample of $2H_2O/1H_2O$ at a defined temperature and comparison with the theoretical diffusion coefficient of $2H_2O/1H_2O$.

DLS. Dynamic light scattering (DLS) measurements were performed on an ALV spectrometer that consists of a goniometer and an ALV-5004 multiple-tau full-digital correlator(320 channels) allowing measurements over an angular range from 30° to 150. A He-Ne Laser (wavelength of 632.8 nm) is used as light source. For temperature controlled measurements the light scattering instrument is equipped with a thermostat from Julabo.

5.1 Degradation kinetics

5.1.1 Alkaline hydrolysis

10 mL of Buffer solution with pH 11.08 were prepared by adding 5.6 mL of 0.4 M $NaHCO_3$-solution with 2.05 mL of 1 M NaOH solution and 1.35 mL H_2O and 1 mL D_2O to achieve a H_2O: D_2O ratio of 9:1. The pH of the buffer was determined with a pH electrode.

The degradation studies of all polymers under basic conditions were conducted with 3.5 mg (0.03 mol L^{-1} (repeat unit)) of polymer dissolved in 0.75 mL of $NaHCO_3$/NaOH (0.2 mol L^{-1}) buffer at pH 11.08. The first 12 h of each degradation were observed constantly by recording alternating ^{1}H and ^{31}P NMR spectra.

5.1.2 Acidic hydrolysis

The degradation studies of all polymers under acidic conditions were conducted with 5 mg of polymer dissolved in 0.75 mL of 0.1 M HCl (pH 1). Degradation was followed by ^{1}H and ^{31}P NMR spectroscopy.

5.2 Synthetic procedures

Synthesis of poly(ethyl ethylene phosphate) ($PEEP_{33}$). All Schlenk-tubes were flame-dried prior to use. 2-(benzyloxy) ethanol was used as initiator and DBU/TU as catalyst. TU (1.3g) and EEP (5.0 g, 36.7 mmol) were introduced into a flame-dried Schlenk-tube, dissolved in dry benzene, and dried by lyophilization. 6 mL of dry DCM were added and 112 mg (734.8 µmol) initiator dissolved in 1 mL of dry DCM. The temperature was adjusted to 0°C and the polymerization was started by rapid addition of DBU (560 mg) to the reaction mixture. The polymerization was quenched after 1.5 h by addition of 2 mL of 2 M formic acid in dry DCM. The polymer was obtained as a colorless viscous liquid (1.4 g, 88%) and purified by precipitation into diethyl ether and subsequent dialysis.
^{1}H NMR (300 MHz, Chloroform-*d*) δ 7.36 (d, *J* = 3.7 Hz), 4.58 (s), 4.43 – 4.06 (m), 1.37 (td, *J* = 7.1, 1.0 Hz). $^{31}P\{H\}$ NMR (121 MHz, Chloroform-*d*) δ -1.08, -1.28.

Synthesis of poly(methyl ethylene phosphate) ($PMEP_{54}$). All Schlenk-tubes were flame-dried prior to use. 2-(benzyloxy) ethanol was used as initiator and DBU/TU as catalyst. TU (1.1g, 2.90 mmol) was introduced into a flame-dried Schlenk-tube, dissolved in dry benzene, and dried by lyophilization. Subsequently, EEP (4.0 g, 36.7 mmol), 5 mL of dry DCM and 88 mg (579.46 µmol) initiator dissolved in 1 mL of dry DCM were added. The temperature was adjusted to 0°C and the polymerization was started by rapid addition of DBU (432 mg) to the reaction mixture. The polymerization was quenched after 1.25 h by addition of an excess of formic acid in dry DCM. The polymer was obtained as a colorless viscous liquid (2.67 g, 67%) and purified by precipitation into diethyl ether and subsequent dialysis.
^{1}H NMR (300 MHz, Chloroform-*d*) δ 7.35 (m, 5H), 4.58 (s, 2H), 4.29 (q, *J* = 4.9, 4.4 Hz), 3.81 (dd, *J* = 11.2, 6.2 Hz).$^{31}P\{H\}$ NMR (121 MHz, Chloroform-*d*) δ 1.12, -0.18, -1.49.

Synthesis of poly(methyl ethylene phosphate) ($PEPP_{54}$). All Schlenk-tubes were flame-dried prior to use. 2-(benzyloxy) ethanol was used as initiator and DBU/TU as catalyst. TU (122 mg,

328 µmol) was introduced into a flame-dried Schlenk-tube, dissolved in dry benzene and dried by lyophilization. EPP (585 mg, 3.94 mmol), 1 mL of dry toluene and 10 mg of initiator (734.8 µmol) dissolved in 0.5 mL of dry toluene were added. The temperature was adjusted to 0°C and the polymerization was started by rapid addition of DBU (121.67 mg, 328.53 µmol) to the reaction mixture. The polymerization was quenched after 24 h by addition of 2 mL of acetic acid (20 mg mL^{-1}) in dry toluene. The polymer was obtained as a colorless viscous liquid (380 mg, 65%) and purified by precipitation into diethyl ether and subsequent dialysis.

^{1}H NMR (300 MHz, Methylene Chloride-d_2) δ 7.27 (d, J = 3.9 Hz), 4.47 (s), 3.99 (ddtd, J = 9.6, 8.0, 6.9, 4.1 Hz), 1.94 – 1.65 (m), 1.23 (t). **^{31}P{H} NMR** (121 MHz, Methylene Chloride-d_2) δ 31.21, 30.80

Synthesis of poly(ethyl ethylene phosphonate) (PEEPn$_{48}$). All Schlenk-tubes were flame-dried prior to use. 2-(benzyloxy) ethanol was used as initiator and DBU as catalyst. EEPn (1.5 g, 11.02 mmol) was introduced into a flame-dried Schlenk-tube, dissolved in dry benzene, and dried by lyophilization thrice. 1.6 mL of dry DCM and 33.5 mg (220.45 µmol) initiator dissolved in 0.5 mL of dry DCM were added. The temperature was adjusted to 25°C and the polymerization was started by rapid addition of DBU (100.68 mg 661.34 µmol) dissolved in 1 ml of dry DCM to the reaction mixture. The polymerization was stirred overnight and quenched by addition of 1 mL of 2 M formic acid in dry DCM. The polymer was obtained as a yellowish viscous liquid (1.33 g, 89%) and purified by precipitation into diethyl ether and subsequent dialysis.

^{1}H NMR (300 MHz, Chloroform-*d*) δ 7.35 (d, J = 4.9 Hz), 4.58 (s), 4.43 – 4.03 (m), 1.98 – 1.65 (m), 1.20 (dtd, J = 15.4, 8.3, 7.7, 3.3 Hz). **^{31}P{H} NMR** (121 MHz, Chloroform-*d*) δ 35.82, 35.18.

5.3 NMR spectra

2D spectra of the degradation of PMEP, PEEP and PEPP were recorded to identify the degradation products. For the degradation of PEEPn no 2D spectra were recorded, since the ^{1}H and ^{31}P NMR spectra showed the formation of one single degradation product.

5.3.1 Spectra of the degradation of PEEP

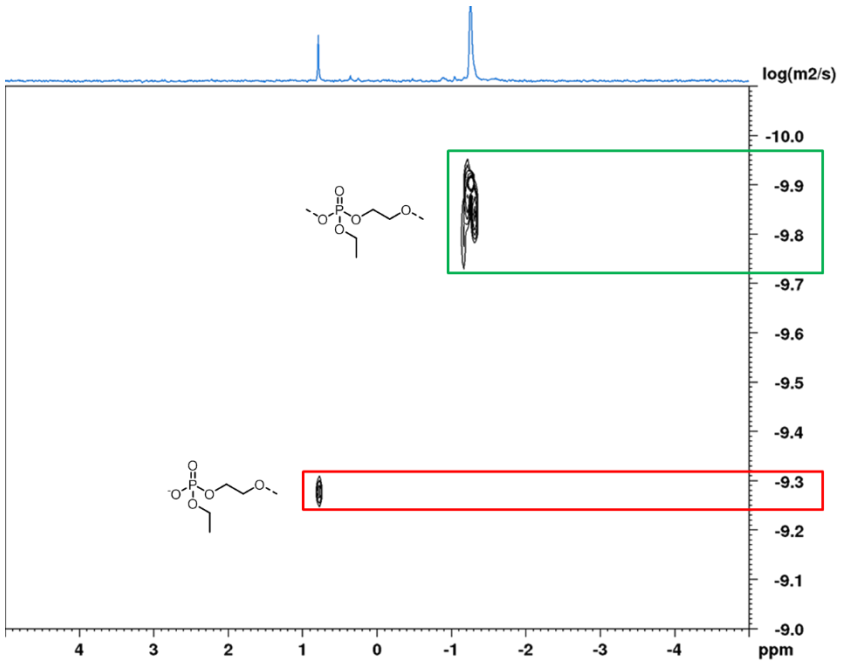

Figure 6.22. ^{31}P DOSY NMR of PEEP (202 MHz, H_2O/D_2O (9:1), 298 K) of the degradation products of PEEP. The spectrum shows two different diffusion coefficients for the triester and the diester signals indicating a significantly lower molecular weight of the diester.

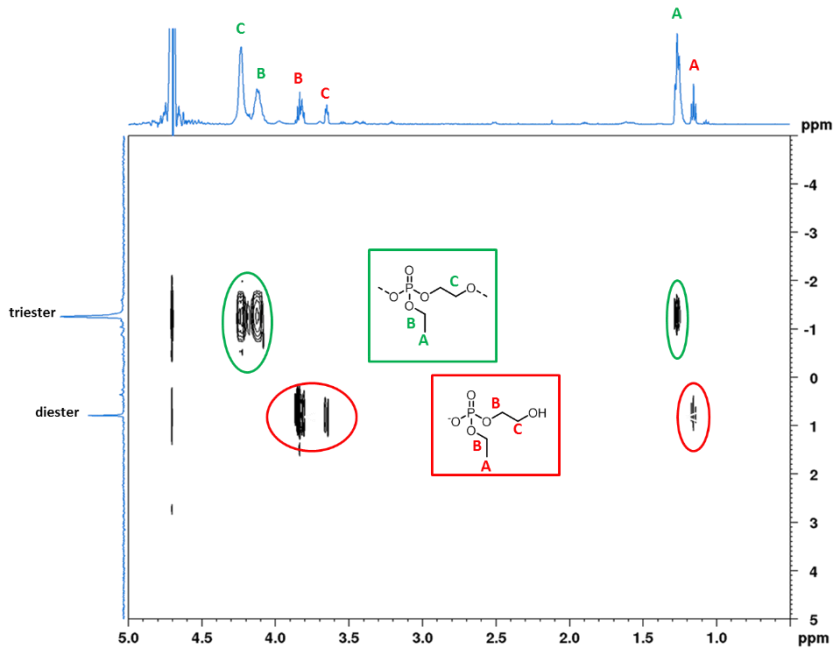

Figure 6.23. ^{1}H-^{31}P HMBC NMR spectrum (202 MHz, H_2O/D_2O (9:1), 298 K) of the degradation products of PEEP.

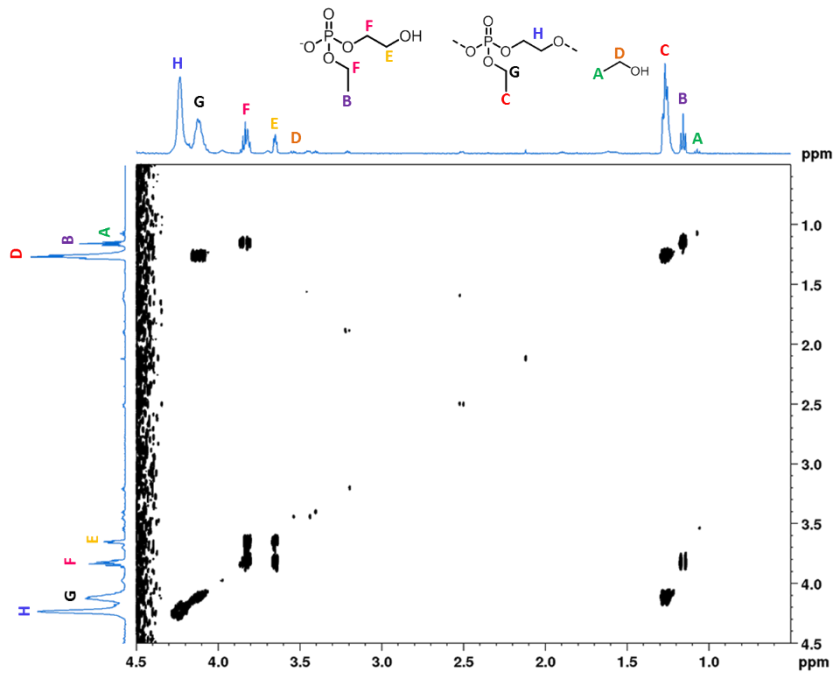

Figure 6.24 . ^{1}H COSY NMR spectrum (500 MHz, H_2O/D_2O (9:1), 298 K) of the degradation products of PEPP.

5.3.2 Spectra of the degradation PEPP

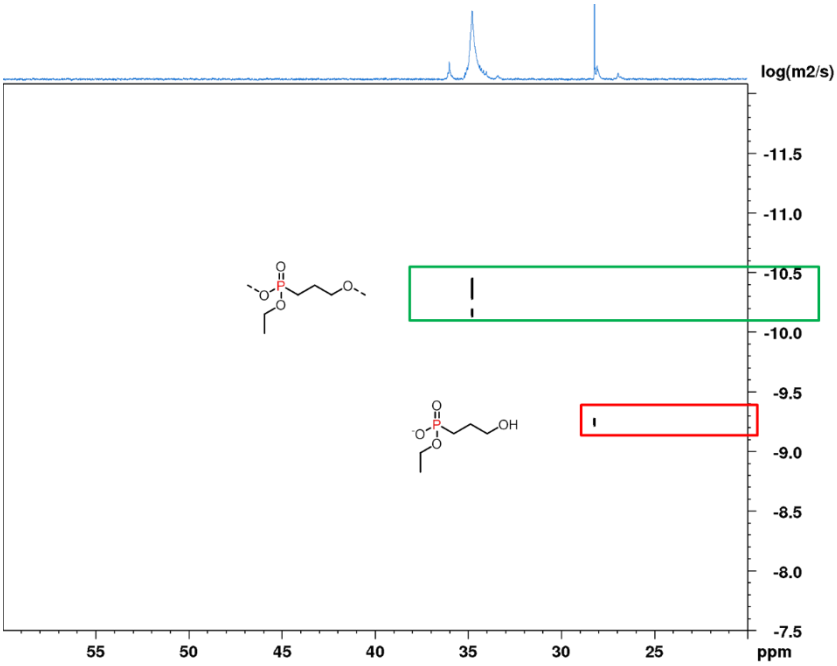

Figure 6.25. ^{31}P DOSY NMR of PEPP (202 MHz, H_2O/D_2O (9:1), 298 K) of the degradation products of PEEP. The spectrum shows two different diffusion coefficients for the diester and the monoester signals indicating a significantly lower molecular weight of the monoester

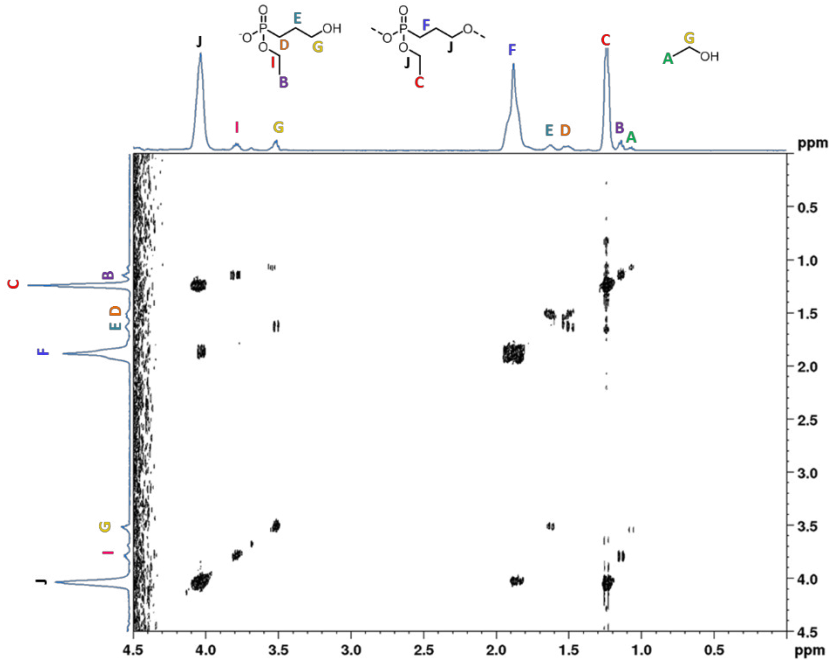

Figure 6.26. ^{1}H-^{1}H COSY NMR spectrum (500 MHz, H_2O/D_2O (9:1), 298 K) of the degradation products of PEPP.

5.3.3 Spectra of the degradation of PMEP

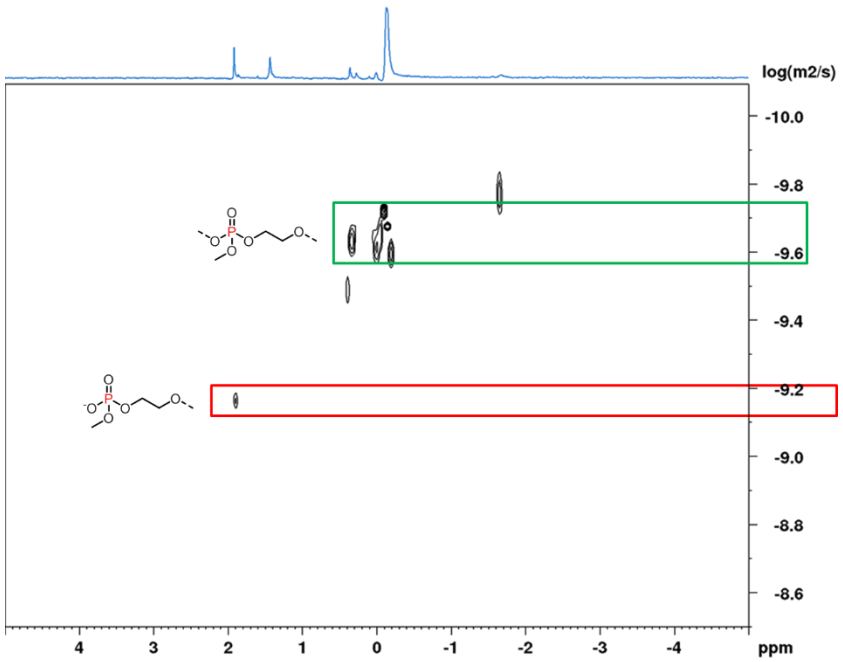

Figure 6.27. ^{31}P DOSY NMR (202 MHz, H_2O/D_2O (9:1), 298 K) of the degradation products of PMEP. The spectrum shows two different diffusion coefficients for the triester and the diester signals indicating a significantly lower molecular weight of the diester.

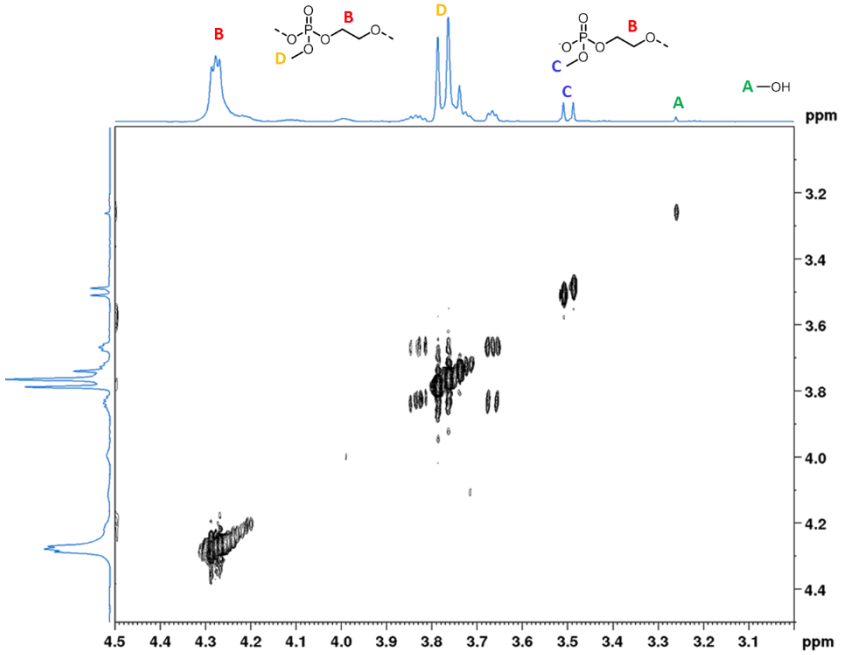

Figure 6.28. ^{1}H-^{1}H COSY NMR spectrum (500 MHz, H_2O/D_2O (9:1), 298 K) of the degradation products of PMEP.

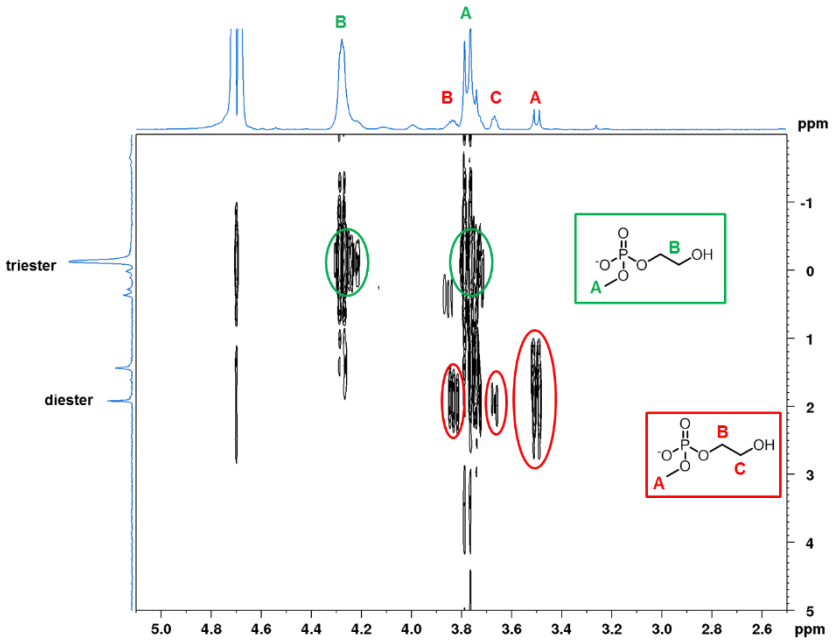

Figure 6.29. ^{1}H-^{31}P HMBC NMR spectrum (500, 202 MHz, H_2O/D_2O (9:1), 298 K) of the degradation products of PMEP.

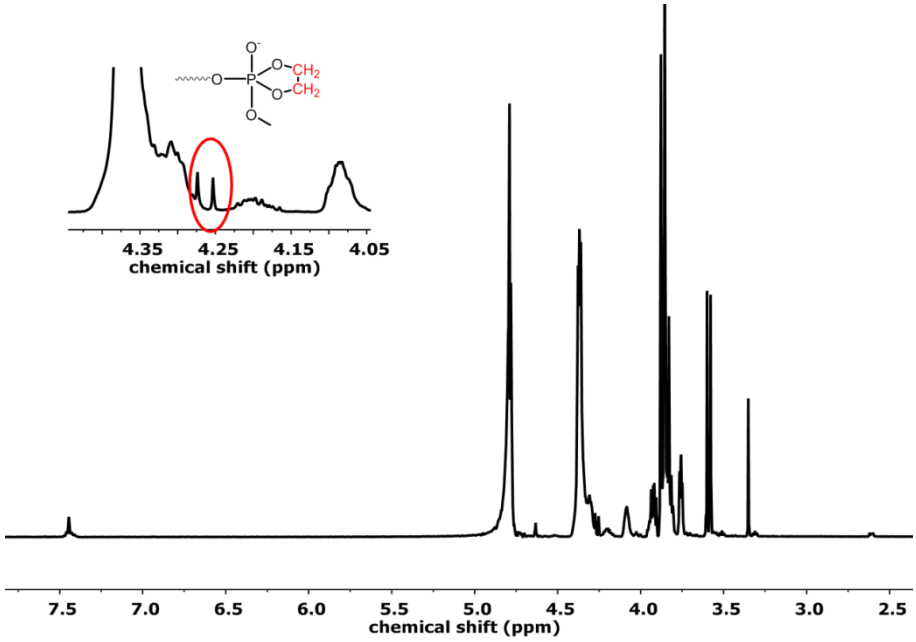

Figure 6.30. ^{1}H NMR spectrum (500 MHz, H_2O/D_2O (9:1), 298 K) of the degradation products of PMEP after 70 days.

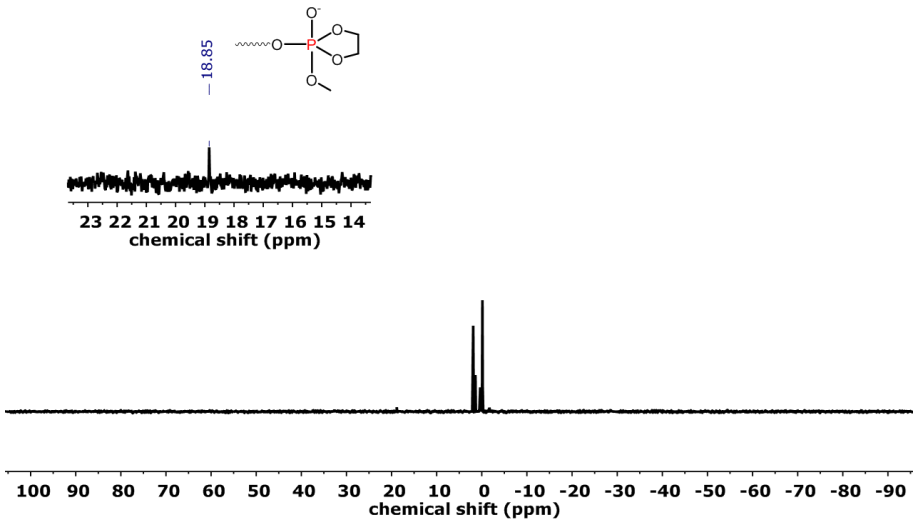

Figure 6.31. ^{31}**P NMR spectrum (202 MHz,** H_2O/D_2O **(9:1), 298 K) of the degradation products of PMEP after 70 days.**

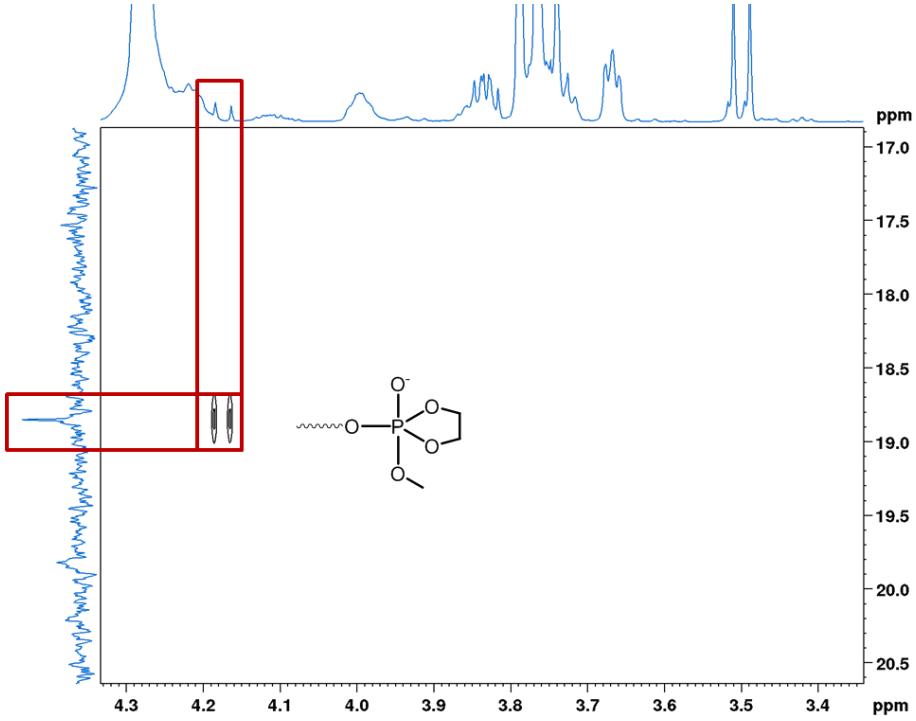

Figure 6.32. ^{1}**H-**^{31}**P HMBC NMR spectrum (500, 202 MHz,** H_2O/D_2O **(9:1), 298 K) of the degradation products of PMEP after 78 days.**

6 References

1. Amass, W.; Amass, A.; Tighe, B., A review of biodegradable polymers: uses, current developments in the synthesis and characterization of biodegradable polyesters, blends of biodegradable polymers and recent advances in biodegradation studies. *Polymer International* **1998,** *47* (2), 89-144.
2. Böstman, O.; Pihlajamäki, H., Clinical biocompatibility of biodegradable orthopaedic implants for internal fixation: a review. *Biomaterials* **2000,** *21* (24), 2615-2621.
3. Huang, S. J.; Bitritto, M.; Leong, K. W.; Pavlisko, J.; Roby, M.; Knox, J. R., The Effects of Some Structural Variations on the Biodegradability of Step-Growth Polymers. In *Stabilization and Degradation of Polymers*, AMERICAN CHEMICAL SOCIETY: 1978; Vol. 169, pp 205-214.
4. Engelberg, I.; Kohn, J., Physico-mechanical properties of degradable polymers used in medical applications: A comparative study. *Biomaterials* **1991,** *12* (3), 292-304.
5. Leong, K. W.; Brott, B. C.; Langer, R., Bioerodible polyanhydrides as drug-carrier matrices. I: Characterization, degradation, and release characteristics. *J Biomed Mater Res* **1985,** *19* (8), 941-955.
6. Grizzi, I.; Garreau, H.; Li, S.; Vert, M., Hydrolytic degradation of devices based on poly(dl-lactic acid) size-dependence. *Biomaterials* **1995,** *16* (4), 305-311.
7. Dunne, M.; Corrigan, O. I.; Ramtoola, Z., Influence of particle size and dissolution conditions on the degradation properties of polylactide-co-glycolide particles. *Biomaterials* **2000,** *21* (16), 1659-1668.
8. Keles, H.; Naylor, A.; Clegg, F.; Sammon, C., Investigation of factors influencing the hydrolytic degradation of single PLGA microparticles. *Polymer Degradation and Stability* **2015,** *119*, 228-241.
9. Kaczorowska, M. A.; Cooper, H. J., Characterization of Polyphosphoesters by Fourier Transform Ion Cyclotron Resonance Mass Spectrometry. *Journal of the American Society for Mass Spectrometry* **2009,** *20* (12), 2238-2247.
10. Chaubal, M. V.; Su, G.; Spicer, E.; Dang, W.; Branham, K. E.; English, J. P.; Zhao, Z., In vitro and in vivo degradation studies of a novel linear copolymer of lactide and ethylphosphate. *Journal of Biomaterials Science, Polymer Edition* **2003,** *14* (1), 45-61.
11. Baran, J.; Penczek, S., Hydrolysis of polyesters of phosphoric acid. 1. Kinetics and the pH profile. *Macromolecules* **1995,** *28* (15), 5167-5176.
12. Wiggins, J. S.; Hassan, M. K.; Mauritz, K. A.; Storey, R. F., Hydrolytic degradation of poly(d,l-lactide) as a function of end group: Carboxylic acid vs. hydroxyl. *Polymer* **2006,** *47* (6), 1960-1969.
13. Xu, L.; Crawford, K.; Gorman, C. B., Effects of Temperature and pH on the Degradation of Poly(lactic acid) Brushes. *Macromolecules* **2011,** *44* (12), 4777-4782.
14. de Jong, S. J.; Arias, E. R.; Rijkers, D. T. S.; van Nostrum, C. F.; Kettenes-van den Bosch, J. J.; Hennink, W. E., New insights into the hydrolytic degradation of poly(lactic acid): participation of the alcohol terminus. *Polymer* **2001,** *42* (7), 2795-2802.
15. Kumara Swamy, K. C.; Burton, S. D.; Holmes, J. M.; Day, R. O.; Holmes, R. R., CYCLIC OXYPHOSPHORANES. *Phosphorus, Sulfur, and Silicon and the Related Elements* **1990,** *53* (1-4), 437-455.
16. Lyu, S.; Untereker, D., Degradability of Polymers for Implantable Biomedical Devices. *International Journal of Molecular Sciences* **2009,** *10* (9), 4033.
17. Göpferich, A., Mechanisms of polymer degradation and erosion. *Biomaterials* **1996,** *17* (2), 103-114.

18. Langer, R.; Chasin, M., Biodegradable polymers as drug delivery systems. *Informa Health Care* **1990**.
19. Champion, J. A.; Katare, Y. K.; Mitragotri, S., Particle shape: A new design parameter for micro- and nanoscale drug delivery carriers. *Journal of Controlled Release* **2007,** *121* (1), 3-9.
20. Stejskal, E. O.; Tanner, J. E., Spin Diffusion Measurements: Spin Echoes in the Presence of a Time-Dependent Field Gradient. *The Journal of Chemical Physics* **1965,** *42* (1), 288-292.
21. Jerschow, A.; Müller, N., Suppression of Convection Artifacts in Stimulated-Echo Diffusion Experiments. Double-Stimulated-Echo Experiments. *Journal of Magnetic Resonance* **1997,** *125* (2), 372-375.